



**HAL**  
open science

# Dynamic flexibility of protein prenyltransferase activities

Quentin Chevalier

► **To cite this version:**

Quentin Chevalier. Dynamic flexibility of protein prenyltransferase activities. *Vegetal Biology*. Université de Strasbourg, 2020. English. NNT : 2020STRAJ088 . tel-03738058

**HAL Id: tel-03738058**

**<https://theses.hal.science/tel-03738058>**

Submitted on 25 Jul 2022

**HAL** is a multi-disciplinary open access archive for the deposit and dissemination of scientific research documents, whether they are published or not. The documents may come from teaching and research institutions in France or abroad, or from public or private research centers.

L'archive ouverte pluridisciplinaire **HAL**, est destinée au dépôt et à la diffusion de documents scientifiques de niveau recherche, publiés ou non, émanant des établissements d'enseignement et de recherche français ou étrangers, des laboratoires publics ou privés.



**UNIVERSITÉ DE STRASBOURG**



**ÉCOLE DOCTORALE DES SCIENCES DE LA VIE (ED 414)**

**Institut de Biologie Moléculaire des Plantes (UPR 2357 CNRS/Unistra) Laboratoire  
d'Innovation Thérapeutique (UMR 7200 CNRS/Unistra)**

# THÈSE

présentée par :

**Quentin CHEVALIER**

soutenue le : **16 Novembre 2020**

pour obtenir le grade de : **Docteur de l'université de Strasbourg**

Discipline/ Spécialité : Biochimie et Biologie Moléculaire

## **Dynamic Flexibility of Protein Prenyltransferase Activities**

**THÈSE dirigée par :**

**HEMMERLIN Andréa**

**VONTHRON-SÉNÉCHEAU Catherine**

Chargé de recherche CNRS, Université de Strasbourg

Maître de conférence (HDR), Université de Strasbourg

**RAPPORTEURS :**

**M. DÖRMANN Peter**

**M. DUVAL Romain**

Professeur, Rheinische Friedrich-Wilhelms-Universität Bonn

Chargé de recherche CNRS, Université Paris V

**AUTRES MEMBRES DU JURY :**

**Mme. DAVIOUD-CHARVET Elisabeth**

**M. DAVID Bruno**

Directeur de recherche CNRS, Université de Strasbourg

Docteur (HDR), Laboratoires Pierre Fabr

Mine are not the years,  
that time has taken away  
Mine are not the years,  
that would have something come  
The present is mine,  
and I take heed  
That He is mine,  
who made time and eternity.

*Andreas Gryphius (1616-1664)*

# Remerciements

Tout d'abord, merci à la famille : merci, Papa, merci, Maman, d'avoir semé vos graines et entretenu votre jardin pendant tant d'années. Merci aux frères Martin, Julien et Yann Chevalier qui ont grandi avec moi et partagé les nutriments, mais également cette expérience familiale unique au goût tant appréciable. Je remercie également mes grands-parents qui ont chapeauté la famille et inculqué une curiosité pour les plantes et le bricolage que l'on retrouve finalement au cœur de cet ouvrage. Un énorme merci à ma femme Mercedes qui m'a épaulée et soutenue sans relâche depuis le début de ce doctorat. Par ailleurs, Félix, Antoine, Ben, Wallid, Maximilien, Lisa, Robin, Arnaud, Loïc, Pierre, Olivier, Jey, Joanna et de nombreux autres, merci d'exister et d'avoir partagé tous ces moments qui ont contribué à ma créativité et mon épanouissement personnel.

Également, merci au support et à l'enseignement de qualité fourni par l'université de Strasbourg et les enseignants de la licence Biologie Cellulaire et Physiologie des Organismes et du master Biologie et Valorisation des Plantes – Valorisation des Ressources Végétales. Après 10 ans d'études dans vos mains, je vous dois plus de 90% de mes connaissances scientifiques. Elles sont les bases qui ont fait de cette thèse le fruit unique de notre travail.

Un grand merci aux collaborateurs : Dr. Mourad Elhabiri et Valérie Mazan (LIMA Strasbourg) pour leur expertise sur l'étude des propriétés physico-chimiques et particulièrement optiques des composés fluorescents. Philippe Hamman, Laurianne Kuhn, Johana Chicher de la Plateforme Protéomique de Strasbourg (IBMC, Strasbourg). Dimitri Heinz, Claire Villette et Julie Zumsteg de la Plateforme d'analyse métabolomique (IBMP, Strasbourg). Christine Schaeffer-Reiss du Laboratoire de Spectrométrie de Masse BioOrganique (LSMBO, Strasbourg). Philippe Schaeffer et Pierre Adam du laboratoire de Biogéochimie moléculaire (Institut de Chimie, Strasbourg).

Également merci Pierre Mercier et Chloé Groh pour vos trois années de soutien au laboratoire. Une attention particulière à ceux qui m'ont encadré ou conseillé au cours des stages Dr. Mélanie Bourjot, Dr. Felix Kregel, Dr. Ricardo Reyes-Chilpa et dans cette thèse Dr. Andréa Hemmerlin, Dr. Catherine Vonthron-Sénécheaux, Dr. Hubert Schaller. Pr. Thomas. J. Bach. Ils ont réussi année après année à faire fructifier ce qu'il y a de plus beau dans la recherche à mon estime, la passion d'identifier et de comprendre un phénomène.

Enfin, merci à vous membres du jury pour évaluer ce travail de thèse.

“There are experiences about which most of us are hesitant to speak, because they do not conform to everyday reality and defy rational explanation. These are not particular external events, but rather occurrences in our inner lives, which are generally dismissed as figments of the imagination and then barred from memory.” ...“The questions that children ask: “Daddy, where does the world end?... When did loving God create the world?... Why must we all die?...” and others like them show that we are born philosopher. These are questions to which we have yet to find any answers, despite all of the many philosophical treatises...even though they constitute the fundamental questions of our very existence.” Albert Hofmann, *LSD My Problem Child*

# TABLE DES MATIÈRES

<b>1 Preface</b> .....	<b>19</b>
<b>2 General introduction</b> .....	<b>21</b>
<b>2.1 Post-Translational Modifications</b> .....	<b>23</b>
<b>2.2 Isoprenoids</b> .....	<b>25</b>
2.2.1 Diversity of Isoprenoids in Yeast and Animals .....	29
2.2.2 Diversity and Functions of isoprenoids in Plant .....	33
2.2.3 Diversity and Functions of Isoprenoids in Apicomplexa .....	41
<b>2.3 Insight Into Protein Prenylation</b> .....	<b>47</b>
2.3.1 Generalities .....	47
2.3.2 Function of Protein Prenylation in Animals.....	52
2.3.3 Specific Function of Protein Prenylation in Plants .....	58
2.3.4 Protein Prenyltransferase Activities and Selectivity.....	65
<b>2.4 Deep Into The Flexibility of Plant Protein Prenylation Machinery</b> .....	<b>71</b>
2.4.1 Lethality in Animals and Fungi Protein Prenyltransferase Mutants.....	71
2.4.2 How Do Plant Mutants of Protein Prenyltransferase Survive? .....	74
2.4.3 Isoprenoids Crosstalk, a Keystone in the Flexibility of Protein Prenylation in Plants .....	77
<b>2.5 Purification and Analysis of Prenylated Proteins: a 40-years old story</b> .....	<b>81</b>
2.5.1 The Bitter Taste of the Original Recipes in Animals and Yeast Studies .....	81
2.5.2 Does it Taste Better With Plants Studies?.....	87
2.5.3 After 20 Years, Wouldn't it Be the Time to Change the Kitchen? .....	89
2.5.4 10 More Years to Deal with the New Kitchen .....	93
<b>2.6 Inhibition of Protein Prenylation in Human Pathologies</b> .....	<b>94</b>
2.6.1 Cancer, When Simple Words Got Complicated.....	94
2.6.2 Protein Prenylation Inhibitors: a Problem to All your Needs .....	95
<b>2.7 Inhibition of Protein Prenylation in Malaria</b> .....	<b>97</b>
2.7.1 Conventional Treatments and Resistances .....	97
2.7.2 Protein Prenylation Inhibitors vs <i>P. falciparum</i> .....	100
<b>2.8 Here Are our Warrants and our Mission</b> .....	<b>104</b>
2.8.1 Crop Fields in a no Freshwater's Land.....	104
2.8.2 Plant factory Twisted for Valuable Isoprenoids .....	104
2.8.3 To Recognize Target in Order to Cure Different Ailments .....	105
2.8.4 Problems in Inhibitor Conception. The RAS Model .....	106
2.8.5 Limits in Studying Protein Prenylation .....	107
<b>2.9 I'm Taking my Labpack</b> .....	<b>109</b>
<b>2.10 What Do I Feature?</b> .....	<b>111</b>
2.10.1 Condition Inducing Flexibility of PPTs and Analysis of Prenylated Proteins in Plants .....	111
2.10.2 Driving Isoprenoids Production <i>via</i> Protein Prenylation Inhibitors.....	111
2.10.3 Screening of Protein Prenylation Inhibitors: Anticancer and Antimalarial Compounds .....	112
2.10.4 Characterization of Prenylated Anthranoids Fluorescence <i>In Vivo</i> .....	112
<b>3 Modulation of protein-prenyltransferase substrate specificities</b> .....	<b>113</b>
<b>3.1 Introduction</b> .....	<b>115</b>
<b>3.2 Phytohormonal Regulation of Protein Prenylation in Plants</b> .....	<b>119</b>

3.2.1	Flexibility of Protein Prenyltransferases in BY-2 Expressing GFP-CVIL.....	119
3.2.2	MeJA-induced Flexibility of PFT in <i>ggb2</i> Mutant Expressing GFP-CVIL .....	123
<b>3.3</b>	<b>Sucrose Modulates Protein Prenylation in Plants .....</b>	<b>125</b>
3.3.1	Impact of Sucrose on Capacity of Protein Prenylation in Tobacco Plants.....	125
3.3.2	Impact of Sucrose on PPTs Loss-of-Function Mutation in Arabidopsis .....	129
3.3.3	Conclusion .....	133
<b>4 Developing a Protocol for Purification and Analysis of Prenylated Proteins Modified In Vivo.....</b>		<b>135</b>
<b>4.1</b>	<b>Introduction.....</b>	<b>137</b>
<b>4.2</b>	<b>Purification of Prenylated GFP Sensor Proteins .....</b>	<b>141</b>
4.2.1	Immunoprecipitation of the GFP Sensor Proteins .....	141
<b>4.3</b>	<b>Consideration for Cheap and Efficient GFP-Trap Development.....</b>	<b>144</b>
4.3.1	How Do I Get Spherical Magnetic Particles? .....	144
4.3.2	Key Parameters to Handle Preparation of Microparticles Using W/O Process.....	145
4.3.3	What Kind of Polymer to Use For Cheap and Multivalent Support?.....	147
4.3.4	Cross-Linking and Functionalization of the Support.....	149
4.3.5	A First Sketch to Design our GFP-Trap .....	151
<b>4.4</b>	<b>Synthesis of a GFP-Trap v1.....</b>	<b>152</b>
4.4.1	Synthesis of MAPs Using W/O Emulsion Process.....	152
4.4.2	Functionalization of MAPs and Immobilization of Nb@GFP .....	155
4.4.3	Comparison of Efficiency Between GFP-Trap_MA and GFP-Trap v1.....	157
4.4.4	Digestion of GFP-Sensor by BY-2 Cells Endoproteases.....	159
<b>4.5</b>	<b>Consideration for Proteomics of Prenylated Proteins .....</b>	<b>161</b>
4.5.1	Analysis of Prenylated Proteins.....	161
4.5.2	Parameters for LC-MS/MS Analysis of Immunoprecipitated Prenylated Proteins.....	162
4.5.3	Trypsin On-Beads Digestion .....	165
<b>4.6</b>	<b>Proteomic Analysis of Immunoprecipitated Prenylated Proteins.....</b>	<b>167</b>
4.6.1	Comparison of In-Gel and In-Solution Digestion Methods for Proteomics.....	167
4.6.2	Proteomics for the Identification of Protein Interacting with Prenylated GFP-Sensor.....	171
<b>4.7</b>	<b>GC-EI-MS Analysis of S-prenyl-L-Cysteine Methyl Ester .....</b>	<b>177</b>
<b>4.8</b>	<b>Targeted Metabolomics Study of Prenylated Proteins using HPLC-TQ-MS/MS.....</b>	<b>183</b>
<b>4.9</b>	<b>Optimization of a GFP-Trap v2 for Non-Targeted Metabolomics .....</b>	<b>187</b>
4.9.1	To Remove Lipids Contamination and Reduce Loss of Material .....	187
4.9.2	Improve Selectivity and Capacity of the GFP-Trap .....	191
4.9.3	Evaluation of the New Optimized GFP-Trap Systems .....	193
<b>4.10</b>	<b>Comparative Non-Targeted Metabolomics Using UPLC-QTOF-MS/MS.....</b>	<b>195</b>
<b>4.11</b>	<b>Synthesis of S-Prenyl-L-Cysteine Methyl Ester .....</b>	<b>199</b>
<b>4.12</b>	<b>Identification of S-Farnesyl-L- Cysteine in GFP-CVIM Purified from Tobacco Leaves ....</b>	<b>201</b>
<b>4.13</b>	<b>Conclusion .....</b>	<b>201</b>
<b>5 Screening for Protein Prenylation Inhibitors and Applications.....</b>		<b>203</b>
<b>5.1</b>	<b>Introduction.....</b>	<b>205</b>
<b>5.2</b>	<b>Screening for Protein Prenylation Inhibitors.....</b>	<b>207</b>
5.2.1	Rhodophytes Extracts and Subfractions .....	207

5.2.2	Synthetic Compounds Interacting with Prohibitins.....	211
5.2.3	Vismiones: Antimalarial Prenylated Anthranoids .....	219
<b>5.3</b>	<b>Application of Protein Prenylation Inhibition in Metabolite Engineering .....</b>	<b>225</b>
5.3.1	Elicitation and Inhibition of Protein Prenylation .....	225
5.3.2	Analysis of Metabolites from Tobacco Leaves .....	228
5.3.3	Analysis of Metabolites from the Culture Medium.....	232
<b>5.4</b>	<b>Conclusion .....</b>	<b>239</b>
<b>6 Observation and Analysis of Anthranoids in Living Cells using Spectral Imaging Coupled to Mass-Spectrometry..... 241</b>		
<b>6.1</b>	<b>Introduction.....</b>	<b>243</b>
<b>6.2</b>	<b>Evaluation of Anthranoids Cytotoxicity using Spectral Imaging .....</b>	<b>245</b>
<b>6.3</b>	<b>Visualization of Anthranoids in Living Cells using Spectral Imaging.....</b>	<b>250</b>
6.3.1	Abstract .....	250
6.3.2	Introduction .....	250
6.3.3	Materials and Methods for publication .....	254
6.3.4	Results and Discussion .....	258
6.3.5	Conclusion .....	284
6.3.6	Acknowledgments.....	285
<b>6.4</b>	<b>Identification of anthranoids subcellular localization.....</b>	<b>287</b>
6.4.1	ER Localization of Anthranoids.....	287
6.4.2	Golgi Localization of Anthranoids .....	291
6.4.3	Lipid Droplets Localization of Anthranoids .....	295
<b>6.5</b>	<b>Comparison of the vismiones and synthetic dihydroanthracenones fluorescence.....</b>	<b>299</b>
6.5.1	To Study Relationship Between Localization-Structure-Activity of Anthranoids using SImaging.....	299
6.5.2	Prenylated DHA are Not Metabolized and Transported into the Vacuole of Living Cells .....	300
<b>6.6</b>	<b>Conclusion .....</b>	<b>303</b>
<b>7 Discussion .....</b>		
<b>7.1.1 Philosophical Note for a New <i>Philosophiae Doctor</i>..... 317</b>		
<b>8 Materials &amp; Methods .....</b>		
<b>8.1 Biological Material .....</b>		
8.1.1	BY-2 cell Suspension.....	321
8.1.2	Tobacco Plants .....	321
8.1.3	Arabidopsis Plants.....	322
8.1.4	The <i>dxs</i> Deletion Mutant DY329 .....	322
<b>8.2</b>	<b>Chemicals.....</b>	<b>323</b>
8.2.1	Screening of Protein Prenylation Inhibitors .....	323
8.2.2	Inhibition of DY329 Strain .....	324
8.2.3	Plant Material Treatments .....	324
8.2.4	Synthesis of S-Prenyl-L Cysteine Methyl Ester References .....	325
<b>8.3</b>	<b>Synthesis of a Homemade GFP-Trap.....</b>	<b>327</b>
8.3.1	Synthesis of Magnetic Agarose Particles (MAPs) .....	327
8.3.2	Functionalization of MAPs in a GFP-Trap .....	328
8.3.3	Production of @GFP Nanobodies.....	329
<b>8.4</b>	<b>Biochemistry and Analytical Methods .....</b>	<b>332</b>
8.4.1	Immunoprecipitation (IP) .....	332



8.4.2	IN2-Agarose Affinity Purification.....	332
8.4.3	SDS-PAGE .....	333
8.4.4	Silver Nitrate Staining.....	333
8.4.5	Western Blot .....	334
8.4.6	Digestion of Purified GFP-Sensors.....	334
8.4.7	Proteomics and Metabolomics .....	335
<b>8.5</b>	<b>Cell biology methods .....</b>	<b>340</b>
8.5.1	Classical Confocal Microscopy.....	340
8.5.2	Viability of BY-2 treated cells .....	341
8.5.3	Localization with Fluorescent Proteins CVIL, ER, Golgi and Nile Red .....	341
8.5.4	Spectral Imaging Data Analysis .....	342
8.5.5	RT-qPCR.....	343
<b>9</b>	<b>References.....</b>	<b>345</b>
<b>10</b>	<b>Annexes.....</b>	<b>375</b>
<b>11</b>	<b>Résumé de Thèse en français.....</b>	<b>389</b>
<b>11.2</b>	<b>Context générale.....</b>	<b>391</b>
<b>11.3</b>	<b>Problématique et stratégies .....</b>	<b>392</b>
	Axe 1. Conditions induisant la flexibilité de l'activité des PPTs et analyse des protéines prénylées dans les plantes 392	
	Axe 2. Criblage d'inhibiteurs de la prénylation des protéines et applications .....	393
	Axe 3. Caractérisation de la fluorescence <i>in vivo</i> et de la métabolisation de composés anthracéniques prénylés 394	
<b>11.4</b>	<b>Conditions induisant la flexibilité de l'activité des PPTs et analyse des protéines prénylées dans les plantes .....</b>	<b>394</b>
11.4.1	Flexibilité de l'activité des PPTs.....	394
11.4.2	Analyse des protéines prénylées dans les plantes .....	398
<b>11.5</b>	<b>Criblage d'inhibiteurs de la prénylation des protéines et applications .....</b>	<b>401</b>
<b>11.6</b>	<b>Caractérisation de la fluorescence <i>in vivo</i> et de la métabolisation de composés anthracéniques prénylés .....</b>	<b>403</b>
<b>11.7</b>	<b>Conclusion générale .....</b>	<b>407</b>

# TABLE DES FIGURES

Figure 1	Survey of protein lipidation in eukaryotes and bacteria reviewed by Hang et al. 2011 .....	24
Figure 2	Early steps of isoprenoids biosynthesis pathways.....	26
Figure 3	Isoprenoid downstream of the MVA and MEP pathways.....	28
Figure 4	Current view of the subcellular localization of isoprenoid biosynthesis in mammalian cells.....	30
Figure 5	Carotenoids in WT and albino mutants of <i>T. urticae</i> .....	31
Figure 6	Subcellular compartmentalization of isoprenoid biosynthesis in plants. ....	34
Figure 7	Snapshot of Plant MVA-derived isoprenoids diversity. ....	34
Figure 8	Snapshot of Plant MEP-derived isoprenoids diversity.....	36
Figure 9	Carotenoids and tocopherol biosynthesis pathways in <i>A. thaliana</i> .....	36
Figure 10	ABA metabolic pathways.....	38
Figure 11	Selected hormonal crosstalk events related to stress response in plants.....	38

Figure 12 The malaria parasite life cycle involves two hosts.....	42
Figure 13 Model for apicoplast evolutionary history. ....	44
Figure 14 Isoprenoid metabolism in apicomplexan parasites. ....	44
Figure 15 Overview of prenylation reactions.....	48
Figure 16 Evolution of protein prenylation. ....	48
Figure 17 Overview of Ykt6 prenylation by PGGT-III, a new orphan protein prenyltransferase. ....	50
Figure 18 Enzymatic pathway for the modification of prenylated proteins. ....	54
Figure 19 Exocytic pathway of palmitoylated Ras proteins through REs to PM. ....	54
Figure 20 Overview of Rho functions in animals.....	56
Figure 21 Regulation of Rho GTPases by lipid modifications.....	56
Figure 22 Observation of GFP-CaM53 in plant material.....	62
Figure 23 Prediction of prenylated proteins in <i>A. thaliana</i> (2017). ....	64
Figure 24 Structures of the CaaX prenyltransferases. ....	66
Figure 25 Structures along the protein farnesyltransferase (FTase) reaction path.....	66
Figure 26 CDC42 splice variants in the regulation of mTOR. ....	70
Figure 27 Global labeling of prenylated proteins using novel alkyne-tagged isoprenoid analogues. ....	70
Figure 28 Overview of <i>A. thaliana</i> protein prenyltransferases mutants <i>era1</i> , <i>ggb-2</i> and <i>plp</i> (reconstitution from different articles).....	75
Figure 29 Topology of the prenyltransferase genes within the isoprenoid pathway of <i>A. thaliana</i> . ....	78
Figure 30 Overview of protocols for the analysis of prenylated proteins <i>in vitro</i> and <i>in vivo</i> at a molecular level. ....	83
Figure 31 p21 <sup>N-RAS</sup> protein incorporate label from Mevalonic Acid into the Processed Forms as a Polyisoprenoid.....	84
Figure 32 SDS/PAGE analysis of $\alpha$ -factor farnesyltransferase activity in <i>E. coli</i> extracts with p21 <sup>NRAS</sup> . ....	84
Figure 33 Identification of the isoprenoid transferred to RAS2CT1.....	85
Figure 34 Analysis of the geranylgeranylated peptide from protein copurified with lamin B ....	86
Figure 35 Exemple of reaction with Raney Ni. ....	86
Figure 36 Localization of GFP-CaM61 and GFP-CVIL in BY-2 Cells.....	90
Figure 37 MVA and GGol rescued prenylation of GFP-CVIL inhibited by fosmidomycin and mevinolin.....	90
Figure 38 Plasmodium's life cycle and its relationship to drug resistance.....	97
Figure 39 Molecular targets of and mechanisms of resistance to major antimalarial drugs.....	99
Figure 40 Study of the dynamic flexibility of protein prenyltransferase activities in plants, key issues for the treatment of human diseases and global warming. ....	108
Figure 41 MeJA rescues prenylation of GFP-CVIL under inhibition by fosmidomycin (FOS). ....	120
Figure 42 The MVA pathway supply prenyl precursor under MeJA-induced stress in the presence of fosmidomycin (FOS), a protein prenylation inhibitor. ....	120
Figure 43 Induced-MeJA response is influenced by synergism and antagonism with other hormones in protein prenylation.....	122
Figure 44 Flexibility of PFT activity is induced by MeJA and MVA in leaves of <i>A. thaliana ggb2::GFP-CVIL</i> mutant lacking of PGGT-I activity. ....	124
Figure 45 Influence of tissue damage on protein prenylation in plant.....	126
Figure 46 Influence of sugar on protein prenylation in tissue damaged tobacco leaves. ....	126
Figure 47 GFP-CVIL prenylation is impacted in both <i>ggb-2</i> and <i>era1.9 A. thaliana</i> KO mutants.....	130
Figure 48 GFP-CVIM prenylation is only affected in <i>era1.9 A. thaliana</i> KO mutant.....	130
Figure 49 Tissue damages does not impact protein prenylation of GFP-sensor in <i>A. thaliana era1-9</i> mutant. ....	132
Figure 50 GGol rescue GFP-CVIM in the PFT <i>A. thaliana</i> KO mutant ( <i>era1-9</i> ).....	132
Figure 51 Farnesol does not rescue protein prenylation in <i>era1.9 A. thaliana</i> KO mutant lacking the PFT activity. ....	134
Figure 52 Proposed rules to study protein prenylation mechanisms. ....	138
Figure 53 General procedure for purification of GFP-sensor protein from plant by using IP and analysis with mass spectrometry.....	142
Figure 54 Immunoprecipitation of GFP-CVIL from BY-2 cells. ....	142
Figure 55 Structure of the three different magnetic particles types described. ....	144
Figure 56 Overview of the characteristics influenced by physical (yellow pill) and chemical factors (red pill). ....	148

Figure 57 Example of linkers used to cross-link or/and functionalize MAPs for proteins or ligands immobilization. ....	150
Figure 58 Overview of the MAPs cross-linking and functionalization process steps using divinylsulfone (DVS) .....	150
Figure 59 Overview of MAPs prepared according to reported procedure (Gu et al., 2017). ....	152
Figure 60 Confocal microscope observation of MAPs after calibration. ....	154
Figure 61 Calibrated F3 MAPs < 73 $\mu$ m. ....	154
Figure 62 Peptide sequence of the Nb-tRFPCh@GFP. ....	155
Figure 63 Development process for our GFP-Trap using MAPs. ....	156
Figure 64 GFP-Trap grafted with Nb-tRFP@GFP. ....	156
Figure 65 GFP-CVIL immunoprecipitated on the GFP-Trap v1. ....	158
Figure 66 Comparison of GFP-Trap v1 and commercialized GFP-Trap_MA (Chromotek). ....	158
Figure 67 Specific digestion of GFP-CVIL by BY-2 cells endoproteases. ....	160
Figure 68 Protease inhibitors reduce degradation of GFP-CVIL in BY-2 cells. ....	160
Figure 69 Procedures for the preparation of GFP-sensor immunoprecipitated samples for proteomic analysis. ....	163
Figure 70 Peptidic sequence of the His-GFP-CVIL protein. ....	163
Figure 71 On-beads digestion with trypsin promotes C-ter unstructured domain degradation. ....	166
Figure 72 NanoLC-Orbitrap-MS/MS analysis of His-GFP-CVIL after in-gel digestion with AspN (LSMBO). ....	168
Figure 73 NanoLC-Q-Orbitrap-MS/MS analysis of His-GFP-sensor after in-solution digestion with trypsin (IBMC). ....	170
Figure 74 Detection of GFP-sensors from plant after immunoprecipitation with the GFP-Trapv1 and In-gel digestion with AspN (IBMC). ....	170
Figure 75 The prenylated GFP-sensor are immunoprecipitated with putative specific proteins in plant. ....	174
Figure 76 Putative Ionization of S-farnesyl-L-cysteine methyl ester (S-Far-L-cys OMe) and CVIM tetrapeptides. ....	175
Figure 77 Tetrapeptides reference MS spectra and separation by NanoLC-QTOF-MS/MS. ....	175
Figure 78 Analysis of S-Far-L-cys by GC-EI-MS. ....	178
Figure 79 Hypothetical fragmentation mechanisms of S-Far-L-cys OMe. ....	179
Figure 80 GC-EI-MS analysis of protein samples processed by on-beads tryptic digestion method. ....	182
Figure 81 HPLC-TQ-MS/MS stacked chromatograms from the MRM analysis of tetrapeptides. ....	184
Figure 82 Comparative study of S-Far-L-cys OMe and CVIM tetrapeptides by using targeted metabolomics. ....	186
Figure 83 SVIL tetrapeptides released from GFP-SVIL after on-beads tryptic digestion. ....	187
Figure 84 Comparison of surfactant ratio for MAPs synthesis using Toluene/H <sub>2</sub> O emulsion. ....	188
Figure 85 Size of MAPs produced by Toluene/H <sub>2</sub> O emulsion is dependent of surfactant ratio. ....	189
Figure 87 New GFP-Trap without RFP signal as compared to the GFP-Trap v1. ....	192
Figure 86 Peptidic sequence of the bivalent nanobodies (NbD@GFP). ....	192
Figure 88 The final GFP-Trap v2 is equivalent to the commercially available GFP-Trap_MA (Chromotek). ...	194
Figure 89 Comparison of efficacy for GFP-Trap v2 prototypes to bind GFP-sensors. ....	194
Figure 90 Scheme of S-farnesyl L-cysteine methyl ester (S-Far-L-cys OMe) synthesis and TLC of degraded/pure products. ....	200
Figure 91 S-Prenyl-L-cysteine were successfully synthesized. ....	200
Figure 92 Antiplasmodial rhodophyte <i>M. stellatus</i> , <i>P. cartillagineum</i> and <i>D. carnosus</i> extracts-induced inhibition of protein prenylation. ....	209
Figure 93 Prohibitin ligands evaluated in protein prenylation inhibition assay. ....	212
Figure 94 IN2 inhibits protein geranylgeranylation of GFP-CVIL. ....	214
Figure 95 IN2 does not target the PGGT-I. ....	214
Figure 96 IN2 does not target MEP pathway enzymes. ....	215
Figure 97 Capsidiol production is not depleted by IN2. ....	216
Figure 98 Low selectivity of IN2-agarose affinity purification support for elucidation of target proteins. ....	216
Figure 99 Phenotypes observed in vismiones treated BY-2 cells expressing GFP-CVIL. ....	220
Figure 100 Vismiones does not inhibit the prenylation of GFP-CVIL in BY-2 cells. ....	222
Figure 101 Vismiones decrease GFP-labelled cells. ....	222
Figure 102 Vismiones does affect the translation of GFP-CVIL but not transcription. ....	223
Figure 103 <i>De novo</i> synthesis of MVA-derived lipids in S-carvone treated leaf discs. ....	226

Figure 104 <i>De novo</i> synthesis of a putative carotenoid containing endoperoxide in 5-carvone treated leaf discs. ....	227
Figure 105 Influence of light and inhibitor of protein prenylation on tobacco leaf metabolite profiles. ....	229
Figure 106 Protein prenylation inhibition and MVA complementation induce changes in metabolites from tobacco leaves culture media. ....	235
Figure 107 Light does not affect most metabolites found in culture medium after treatments. ....	236
Figure 108 Blue light influence abundant metabolite 12 culture medium content. ....	237
Figure 109 Protein prenylation inhibitors and MVA influence metabolites founds in the culture medium. ...	238
Figure 110 Anthranoids exhibit low cytotoxicity in BY-2 cells after 24h of treatment. ....	246
Figure 111 Spectral imaging allows observation of cell viability markers and anthranoids. ....	248
Figure 112. State of the art on the biosynthesis and structures of anthranoids (orange) and other phenolic compounds (black) studied. ....	252
Figure 113. Normalized excitation/emission and absorption spectra. ....	261
Figure 114. Normalized mean spectra and images from SImaging analysis of cells treated with 25 $\mu$ M. ....	265
Figure 115. PCA of the normalized mean spectra obtained by SImaging analysis of BY-2 cells. ....	268
Figure 116. Vismione H vh photophysical properties are influenced by metal cations complexation. ....	274
Figure 117. Hypothetical metabolization pathways according to reference and related metabolites only detected in ESI/UPLC-QTOF- MS <sup>2</sup> analysis. ....	277
Figure 118 Vismiones colocalize with the ER rather anthraquinones being mostly localize in other structures. ....	289
Figure 119 VH does label medial Golgi and other vesicles. ....	293
Figure 120 VD/anthrone label medial Golgi vesicles. ....	293
Figure 121 Madagascine-like anthraquinones label lipid droplets. ....	296
Figure 122 Prenylated DHA are not metabolized and transported into the primary vacuole. ....	302
Figure S1. UV-Vis. absorption spectrophotometric titrations versus pH of most of the compounds considered in this work (Left). ....	262
Figure S2. Fluorescence emission/excitation spectra from species studied. ....	263
Figure S3. Normalized mean spectra and images from SImaging analysis of Lapachol treated cells. ....	268
Figure S4. Normalized mean spectra and images from SImaging analysis of cells treated with 50 $\mu$ M. ....	270
Figure S5. Distant matrix of normalized mean spectra obtained by SImaging analysis of cells treated or not with 25 $\mu$ M of phenolic compounds. ....	271
Figure S6. PCA of normalized mean spectra obtained by SImaging analysis of BY-2 cells treated or not with 50 $\mu$ M of phenolic compounds. ....	271
Figure S7 Distant matrix of normalized mean spectra obtained by SImaging analysis of cells treated or not with 50 $\mu$ M of phenolic compounds. ....	272
Figure S8 UV-Vis. absorption titration of vismione H by Ca(II). ....	274
Figure S9 UV-Vis. absorption titration of vismione H by Mg(II). ....	275
Figure S10 Non targeted metabolomic analysis using ESI/UPLC-QTOF- MS2 analysis of MeOH extracts from BY-2 cells treated 15 min and 18 h with 50 $\mu$ M lapachol Lap. ....	279

## TABLE DES TABLEAUX

Table 1 Prenylated proteins reported in plant in 2020. ....	59
Table 2 Characteristics of protein prenyltransferase mutants described in yeast, animal and plant. ....	72
Table 3 Advantages and limits of analytical methods used to characterize protein prenylation <i>in vitro</i> and <i>in vivo</i> . Examples of references in which these analytical methods have been used. ....	138
Table 4 Overview of GFP-CaaX samples for proteomic analyses. ....	168
Table 5 Proteomics on GFP-CVIM processed by on-beads tryptic digestion. ....	172
Table 6 Proteins interacting with GFP-CVIM in tobacco leaves. ....	172
Table 7 GC-EI-MS result for compounds varying between GFP-CVIM digested sample and controls. ....	182
Table 8 Analysis of the tetrapeptides SVIL, CVIL, CVIM and S-Far-L-cys OMe by HPLC-TQ-MS/MS. ....	184

Table 9 Conditions used to prepare samples for metabolomic analysis by UPLC-TQ-MS/MS of immunoprecipitated GFP-sensors. ....	184
Table 10 Cross-linking and functionalization for the GFP-Trap optimization. ....	192
Table 11 Overview of the non-targeted metabolomic analysis. ....	197
Table 12 Identification of S-farnesyl-L-cysteine in GFP-CVIM prenylated in plants. ....	202
Table 13 Inhibition of protein prenylation by rhodophyte EtOAc extracts and subsfractions. ....	209
Table 14 Prohibitin ligands as anticancer agents. ....	212
Table 15 Structure and antiprotozoal activity of vismiones and synthetic anthranoids used in the GFP-CVIL prenylation inhibition assay. ....	220
Table 16 Overview of metabolites from tobacco leaves influenced by light and/or protein prenylation inhibition. ....	230
Table 17 Compounds detected in GC-EI-MS and influenced by treatments tested. ....	233
Table 18 compounds used for SImaging proof of concept of vismiones and related compounds metabolization. ....	246
Table 19 Main photophysical characteristics evaluated for the pure compounds investigated in this work. ....	263
Table 20 Overview of vismiones and related anthranoids subcellular distribution in living BY-2 cells. ....	298
Table 21 NW0184 is not metabolized in anthraquinone in BY-2 cells. ....	303
Table S 1 pKa values of pure compounds measured in solution. <sup>a</sup> ....	259
Table S2. Metabolites identified in metabolomic analysis of MeOH extracts from BY-2 cells treated with 50 $\mu$ M Lap. ....	279
Table S3. Metabolites identified in metabolomic analysis of MeOH extracts from BY-2 cells treated with 50 $\mu$ M Fra. ....	279
Table S 4. Metabolites identified in metabolomic analysis of MeOH extracts from BY-2 cells treated with 50 $\mu$ M Qui. ....	281
Table S 5. Metabolites identified in non-targeted metabolomic analysis of MeOH extracts from BY-2 cells treated with 50 $\mu$ M Emo, Mad and VH. ....	281

## TABLE DES ANNEXES

Annexe 1 Compounds and molecular formula of the 346 compounds investigated in non-targeted metabolomic analysis by HPLC-QTOF-MS/MS ....	377
Annexe 2 Examples of proteins found to be immunoprecipitated with our GFP-sensor expressed in tobacco plant or BY-2 cells. ....	379
Annexe 3 <sup>1</sup> H NMR spectrum of farnesyl bromide in CDCl <sub>3</sub> (400 Mhz) ....	381
Annexe 4 <sup>1</sup> H NMR spectrum of geranylgeranyl bromide in CDCl <sub>3</sub> (400 Mhz) ....	382
Annexe 5 <sup>1</sup> H NMR spectrum of phytyl bromide in CDCl <sub>3</sub> (400 Mhz) ....	383
Annexe 6 <sup>1</sup> H NMR spectrum of S-farnesyl-L-cysteine methyl ester in CDCl <sub>3</sub> (400 Mhz) ....	384
Annexe 7 <sup>1</sup> H NMR spectrum of S-geranylgeranyl-L-cysteine methyl ester in CDCl <sub>3</sub> (400 Mhz) ....	385
Annexe 8 <sup>1</sup> H NMR spectrum of S-phytyl-L-cysteine methyl ester in CDCl <sub>3</sub> (400 Mhz) ....	386
Annexe 9 Map of the plasmid pETGG #2 used for the cytoplasmic production of the Nb-tRFP@GFP in <i>E. Coli</i> ....	387
Annexe 10 Map of the plasmid used for the periplasmic production of the NbD@GFP in <i>E. Coli</i> ....	388

# Abbreviations

AA	Amino acids
AACT	Acetoacetyl-CoA thiolase
ABA	Abscisic acid
ACTs	artemisinin-based combination therapies
AGG1	G-protein gamma-subunit 1
A IPL1	Aryl-hydrocarbon-interacting protein-like 1
ANJ1	DnaJ protein homolog ANJ1
ARF	ADP ribosylation factors
ASG2	Protein altered seed germination 2
ATP	Adenosine triphosphate
Aux	Auxine induced protein
AVD	Acetyl vismione D
BP	Biphosphonates
BR	Brassinosteroids
BY-2	Bright yellow 2 tobacco cells
C-ter	C-terminus end
CaM	Calmodulin
CGN	<i>cis</i> -Golgi network
CK	Cytokinins
CMK	1-deoxy-d-xylulose-5-phosphate synthase
CMS	MEP cytidyltransferase
CoA	Coenzyme A
Co-IP	Co-immunoprecipitation
DCM	Dichloromethane
DD	DVS crosslinked and activated MAPs
Dex	Dexamethasone
DG	DVS crosslinked-glyoxyl activated MAPs
DHA	Dihydroanthracenones
DIC	Differential interferential contrast
DIEA	N, N-diisopropylethylamine
DMA	Dimethylallyl
DMAPP	Dimethylallyl diphosphate
DMF	Dimethylformamide
DMSO	Dimethylsulfoxide
DTT	Dithiothreitol
DVS	Divinylsulfone
DX	1-deoxy-D-xylulose
DXP	1-deoxy-D-xylulose-5-phosphate
DXR	DOXP reductoisomerase
DXS	DOXP synthase
ED	Epichlorhydrin crosslinked-DVS activated MAPs
EG	Epichlorhydrin crosslinked-glyoxyl activated MAPs
Emo	Emodin
ER	Endoplasmic reticulum

era1	Enhanced response to ABA 1
ET	Ethylene
Ethep	Ethephon
EtOAc	Ethyl acetate
EtOH	Ethanol
FDA	Fluorescein diacetate
FDS	Farnesyl diphosphate synthase
Fol	Farnesol
Fra	Fraxetin
FRET	Fluorescence resonance energy transfer
Gol	Geraniol
GGol	Geranylgeraniol
FAB	Fast atom bombardment
FBXL2	F-box/LRR-repeat protein 2
FOS	Fosmidomycin
FPP	Farnesyl diphosphate
FT	Flow through
FTase	Protein farnesyltransferase
FTI	Farnesyltransferase inhibitors
G3P	Glyceraldehyde-3-phosphate dehydrogenase
GA	Gibberellins
GAPs	GTPase-activating proteins
GC-EI-MS	Gas chromatography-Electronic impact-mass spectrometry
GC-FID	Gas chromatography-flame ionization detection
GDP	Guanosine diphosphate
GDS	Geranyl diphosphate synthase
GFP	Green fluorescent protein
GFPP	Geranylgeranyl diphosphate
ggb	Geranylgeranyltransferase type-1 beta subunit
GGDR	Geranylgeranyl diphosphate reductase
GGDS	Geranylgeranyl diphosphate synthase
GGPP	Geranylgeranyl diphosphate
GGTase I	Protein geranylgeranyltransferase type-1
GGTase II	Protein geranylgeranyltransferase type-2
GGTase III	Protein geranylgeranyltransferase type-3
GGTI	Geranylgeranyltransferase inhibitors
GPI	Glycerophosphatidylinositol
GPP	Geranyl diphosphate
GST	Glutathione S-transferase
GTP	Guanosine triphosphate
HAD	Haloacide deshydrogenase
HDL	High-density lipoproteins
HDR	HMBDP reductase
HDS	HMBDP synthase
His-GFP	His tagged green fluorescent protein
HLB	Hydrophobic-liphophilic balance
HMBDP	( <i>E</i> )-4-Hydroxy-3-methyl-but-2-enyl pyrophosphate

HMGR	Hydroxymethylglutaryl CoA reductase
HMGS	Hydroxymethylglutaryl CoA synthase
HPLC	High performance liquid chromatography
HPTLC	High performance thin layer chromatography
HPV	Human Papillomavirus
HR	High resolution
Hsp	Heat shock proteins
IAA	Indole-3-acetic acid
ICMT	Protein-S-isoprenylcysteine O-methyltransferase
IDI	Isopentenyl-diphosphate delta-isomerase
IgG	Immunoglobuline G
IMAC	Immobilized metal ion chromatography
Inbox	Induction of protein in petri dishes
IP	Immunoprecipitation
IPP	Isopentenyl diphosphate
IPT3	Isopentenyltransferase 3
JA	Jasmonates
KAN	Kanamycin
Kin	Kinetin
KO	Knock-out
$\lambda_{405}$	Excitation at 405 nm and acquisition from 415 nm to 664 nm
$\lambda_{488}$	Excitation at 488 nm and acquisition from 498 nm to 664 nm
$\lambda_{Ex}$	Excitation maximum
$\lambda_{Em}$	Emission maximum
Lap	Lapachol
LB	Lysogeny broth medium
LC	Liqui chromatography
LDL	Low-density lipoproteins
LOD	Limit of detection
Mad	Madagascine
MAPs	Magnetic agarose particles
MCS	2-C-methyl-D-erythritol 2,4-cyclodiphosphate synthase
MeJA	Methyl-jasmonate
MeOH	Methanol
MEP	Methylerythritol phosphate
MIAs	Monoterpene indole alkaloids
MK	Mevalonate kinase
MS	Murashig and Skoog medium
MS/MS	Tandem mass spectrometry
MUB	Membrane-anchored Ub-fold proteins
MV	Mevinolin
MVA	Mevalonate
MPDC	Diphosphomevalonate decarboxylase
NAP	Nucleosome assembly proteins
N-ter	N-terminus end
NbD@GFP	Bivalent nanobodies targeting GFP protein
Nb@GFP	Nanobodies targeting GFP protein



Nb-tRFP@GFP	RFP tagged nanobodies targeting GFP protein
NMR	Nuclear magnetic resonance
NR	Nile red
PCA	Principal component analysis
PCR	Polymerization chain reaction
PDE $\delta$	cGMP phosphodiesterase
PEX19	Peroxisomal biogenesis factor 19
PFK9	Phosphofructokinase 9
PFT	Protein farnesyltransferase
PfCPT	<i>Plasmodium falciparum</i> cis-polyprenyl transferase
PGGT-I	Protein geranylgeranyltransferase type-1
PGGT-II	Protein geranylgeranyltransferase type-2
PGGT-III	Protein geranylgeranyltransferase type-3
PHB	Prohibitins
PhPP	Phytyl diphosphate
PI	Propidium iodide
PKA	Protein kinase A
PLCP	Papain-like cysteine proteases
pLDH	<i>Plasmodium falciparum</i> lactate deshydrogenase
plp	Pluripetala
PMK	Phosphomevalonate kinase
PPT	Protein prenyltransferases
PreOH	Prenols
PTAR1	Protein prenyltransferases alpha subunit repeat containing 1
PTM	Post-Translational Modifications
Q-Orbitrap	Quadripole-Q Extractive Orbitrap
QTOF	Quadripole-Time of flight
Qui	Quinizarin
RabGDI	Rhab GDP dissociation inhibitor
RAC	Ras-related cytosolic proteins
RAN	Ras related nuclear proteins
RAS	Ras GTPase protein
Raney Ni	Raney nickel reagent
RCE	CaaX endoprotease/Ste24 endopeptidase
R <sub>f</sub>	Retardation factor
RHO	Rho family of GTPases
REP	Replication-associated protein
RFP	Red fluorescent protein
RT-qPCR	Reverse transcriptase quantitative polymerase chain reaction
S-Far-L-cys OMe	S-farnesyl-L-cysteine methyl ester
S-GG-L-cys OMe	S-geranylgeranyl-L-cysteine methyl ester
S-Phy-L-cys OMe	S-Phytyl-L-cysteine methyl ester
SAM	S-adenosylmethionine
SEC	Size exclusion chromatography
SDS-PAGE	Sodium dodecyl sulphate-polyacrylamide gel electrophoresis
SImaging	Spectral imaging
S <sub>N</sub> 2	Nucleophilic substitution type-2

SNARE	Soluble N-ethylmaleimide-sensitive-factor attachment protein receptor
SQ%	Sequence coverage
TGN	<i>trans</i> -Golgi Network
TLC	Thin layer chromatography
UPLC	Ultra performance liquid chromatography
UV	Ultraviolet
VD	Vismione D
VH	Vismione H
W/O	Water-in-oil
WT	Wild-type
YKT6	Synaptobrevin homolog YKT6

## Oral communications

January 2020	Talk (1h) - Seminar at the Institute of Plant Molecular Biology (IBMP), Strasbourg "Visualization of metabolites in living cells using spectral imaging"
	Short talk (15 min) - Institute of Plant Molecular Biology (IBMP), Strasbourg "Insight into prenylated protein analysis: comparison between proteomics and metabolomics approaches"
	Talk (30 min) - Seminar at the Laboratory for Therapeutic Innovation (LIT), Illkirch-Graffenstaden "Visualization of metabolites in living cells using spectral imaging"
July 2019	Short talk (15 min) - 12 <sup>th</sup> Congress of the French Society of Plant Biology (SFBV), Strasbourg "Regulation of plant hormone signalling via the modulation of protein lipidation"
June 2019	Talk (1h) - Seminar at the Institute at Plant Molecular Biology (IBMP), Strasbourg "IBeadsMP the cheap and powerful GFPTrap system you've always dreamt of"
April 2019	Short talk (12 min) - 7 <sup>th</sup> Brazilian Symposium on Molecular Plant Genetics (SBGMP), Sao Paulo "Regulation of plant hormone signaling <i>via</i> the modulation of protein lipidation"
June 2018	Talk (30 min) - Workshop organized by the Working Group of Plant Imaging (GDRImabio), Strasbourg "Spectral Imaging for the discrimination of fluorescent markers and cytotoxicity"
May 2018	Talk (1h) - Pint of Science Festival 2018, Strasbourg "An original solution to treat addictions", ibogaine as an alternative remedy.
March 2018	Blitz Presentation (5 min) - Doctoral School Days of Life and Health Sciences (ED 414), Strasbourg "Dynamic flexibility of protein-prenyltransferase activities"
February 2018	Short talk (15 min) - Institute of Plant Molecular Biology (IBMP), Strasbourg "Incidence of stress on protein post-translational modifications with prenyl groups"

## Posters

Août 2019	<b>TERPNET, 14<sup>e</sup> International congress on the biosynthesis, function and biology of isoprenoids, Halle</b> Visualization of prenylated anthranoids in living cells using spectral imaging
July 2019	<b>12<sup>th</sup> congress of French Society of Plant Biology (SFBV), Strasbourg</b> Visualization of prenylated anthranoids in living cells using spectral imaging

# 1 PREFACE

The emergence of life on earth is due to peculiar conditions that fostered the biodiversity of organisms whose structure, organization and physiology depends so far on the chemistry of carbon, oxygen and the presence of water. The cell, which is defined as the fundamental unit of life emerged from the membrane formation, this hydrophobic layer enclosing intracellular environments from the external one. Although the plasma membrane is pictured as a double layer of lipids, the fact remains that this former is composed of about 50% lipids and 50% proteins (Harayama and Riezman, 2018; Cooper, 2019). Remarkably, the evolution has selected a fascinating tangle of mechanisms intrinsically connecting lipids and proteins within cells in order to perceive the external environment as a matter of self-preservation. What kind of physiological mechanisms involving both lipids and proteins do organisms use to live, preserve homeostasis and evolve within unpredictable environment? In this respect, some threads have been unraveled offering not only a sketch of protein-lipid interactions in living organisms, but also a showcase of human pathologies related to disorders of such interactions. Considering the perpetual quest for survival invested by every organism, Humans should carefully consider the question afford mentioned. As a matter of fact, my thesis brings some new elements collected from the perilous investigation of protein prenylation mechanisms, a post-translational modification involving a group of lipids so-called isoprenoids.



## 2 GENERAL INTRODUCTION



## 2.1 POST-TRANSLATIONAL MODIFICATIONS

In eukaryotes, proteins are characterized by interaction between amino acids (AA) and post-translational modifications (PTMs), offering rapid changes in protein conformation, functionality, localization and regulation (Millar et al., 2019). PTMs are reaction catalyzed by enzymes that covalently attach chemical groups onto electron acceptor (COOH, OH) or donor (NH<sub>3</sub>, SH) functions from AA. The chemical moieties transferred consist in small chemical groups (< 100 g.mol<sup>-1</sup>) such as phosphate (phosphorylation), methyl (methylation), acetyl moieties (acetylation) or bigger molecules like sugars (glycosylation), lipids (lipidation) or even peptides like ubiquitin (ubiquitination). Phosphorylation or ubiquitination have been well investigated, while lipidation were much less well characterized, likely because lipidated proteins are more hydrophobic and methods for purification and analysis differ from that of usual soluble proteins (Hang et al., 2011).

The main role of protein lipidation is to improve their hydrophobicity for membrane targeting or protein-protein interaction with hydrophobic domains (Jiang et al., 2018). For instance, some proteins are modified on the N-terminus (N-ter) by N-myristoylation or N-palmitoylation, while others occur on the C-terminus (C-ter) such as with phosphatidylethanolamine, isoprenoids or glycosylphosphatidylinositol (GPI) (**Figure 1**). Glypiation, also known as GPI anchoring, refers to the transfer of GPI onto proteins being involved in cell trafficking and mostly found in the Trans-Golgi-network (TGN) (Zurzolo and Simons, 2016). By the way, changes can occur within the protein itself as described for S-palmitoylation or O-palmitoylation. In comparison, prokaryotes do also modify their proteins by acetylation (Christensen et al., 2019), adding a diacylglycerol with fatty acids on the N-ter or in some bacteria by acylation within the sequence (**Figure 1**) (Buddelmeijer, 2012; Noland et al., 2017).

So far, protein prenylation also concerns public health as many proteins involved in primordial processes of eukaryotes depend on membrane targeting. For instance, a mutation in prenylated protein from the RAS family is found in 30 % of cancer (Prior et al., 2012). Also, protein prenylation inhibitors arrest the growth of *Plasmodium falciparum*, which is responsible for over 200 million cases of malaria infections and about 400 000 deaths (OMS, 2019). Hence, the study of protein prenylation address critical challenges for the development of new antimalarial and anticancer drugs.



Three major types of protein prenylation have been outlined in eukaryotes: farnesylation, type I geranylgeranylation (Schafer and Rine 1992) and type II geranylgeranylation involving two geranylgeranyl groups (Alory and Balch 2000; Leung et al. 2006) and the type III protein geranylgeranylation (Shirakawa et al., 2020). However, protein prenylations with cholesterol also occur, as reported for the HEDGEHOG protein in *Drosophila* (Porter et al. 1997), or polyprenols in animals, apicomplexans and plants (Hjertmann et al. 1997; Gutkowska et al. 2004; D'Alexandri et al. 2006). Although the prenylation of cyclic pheromones or peptides in bacteria has been described (Okada et al. 2004; Okada et al. 2008; Tsuji et al. 2012), this thesis is dedicated to the study of protein prenylation mechanisms in eukaryotes and especially in Plant, which is a masterpiece of isoprenoid metabolism.

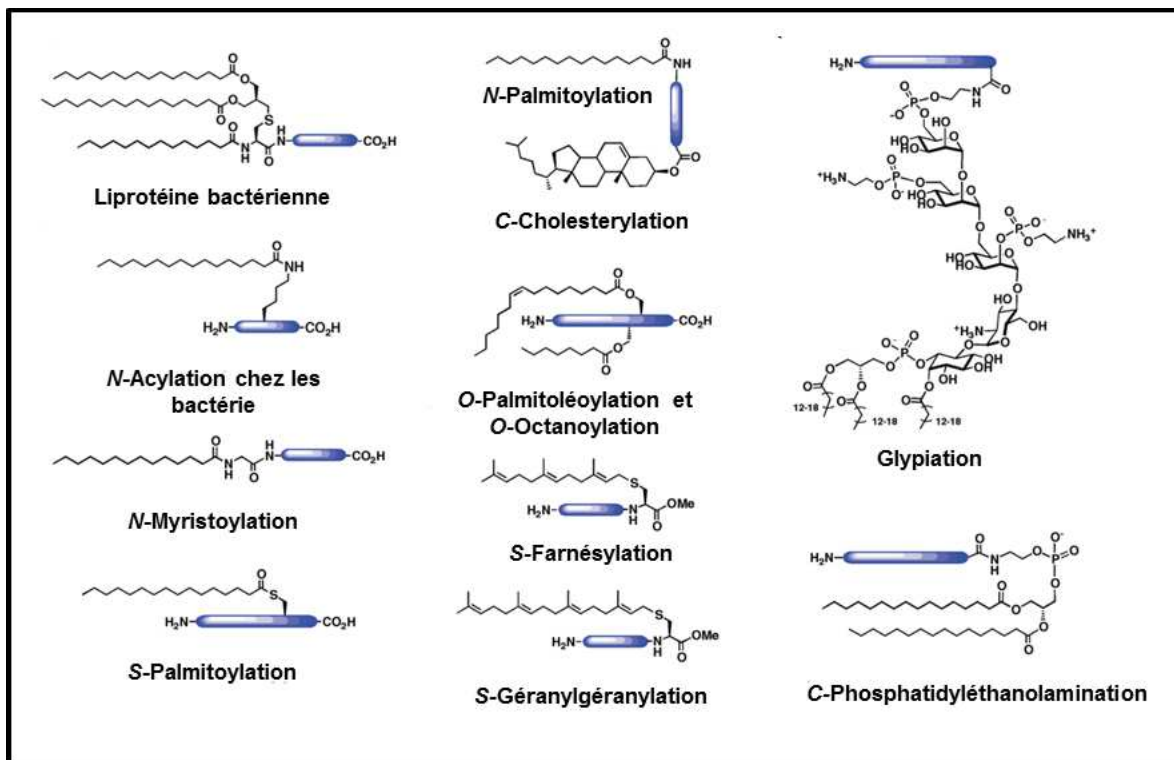
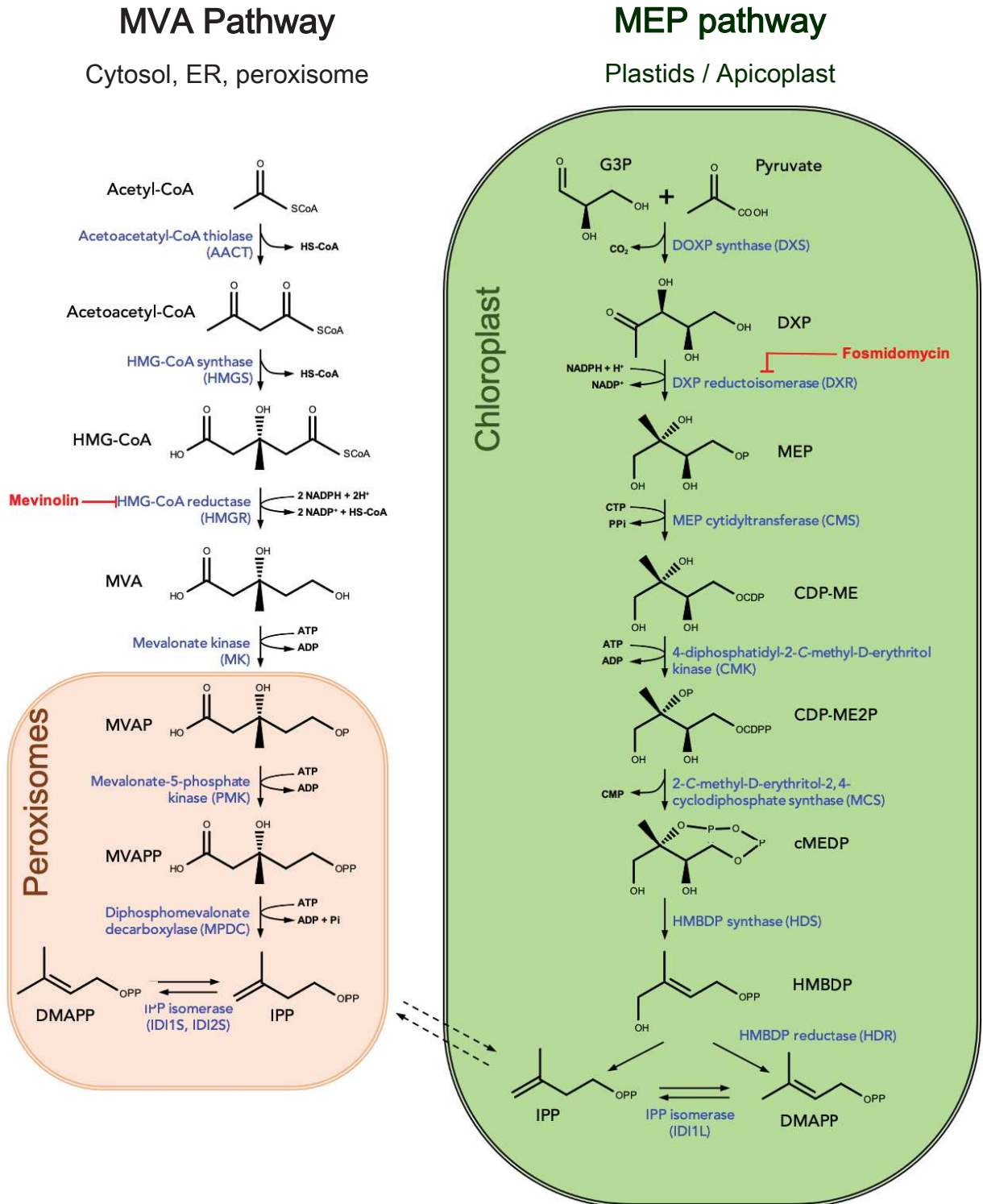


Figure 1 Survey of protein lipidation in eukaryotes and bacteria reviewed by Hang et al. 2011

## 2.2 ISOPRENOIDS

Isoprenoids or terpenes are hydrocarbon organic compounds belonging to the class of lipids. These molecules are widely distributed within eukaryotes. More than 80,000 isoprenoids have been described, representing one of the most diverse classes of metabolites in plants, in terms of structure and biological role (Holstein and Hohl, 2004; Christianson, 2017). Isoprenoids are classified as a function of the number of carbon atoms in their backbone structure: hemiterpenes (C<sub>5</sub>), monoterpenes (C<sub>10</sub>), sesquiterpenes (C<sub>15</sub>), diterpenes (C<sub>20</sub>), triterpenes (C<sub>30</sub>), tetraterpenes (C<sub>40</sub>), etc (Kumari et al., 2013). The biosynthesis of isoprenoids is achieved by the oligomerization of elemental units with five carbon atoms (C<sub>5</sub>) known as isopentenyl diphosphate (IPP) and its isomer dimethylallyl diphosphate (DMAPP). The supply of these precursors was initially characterized by substrates and enzymes involved within the mevalonate pathway (MVA) in yeast as well as animal models (Ruzicka, 1953; Rudney, 1957; Lynen et al., 1958; Bloch et al., 1959; Ferguson et al., 1959; Ferguson and Rudney, 1959; Rudney and Ferguson, 1959). This pathway is initiated by the Acetoacetyl-CoA thiolase (AACT1, EC 2.3.1.9, AACT2, 2.3.1.16) which transform Acetyl-CoA in Acetoacetyl-CoA. Then the key enzymes HMG-CoA synthase (HMGS: EC 2.3.3.10) and HMG-CoA reductase (HMGR: EC 1.1.1.88) catalyze the conversion of acetoacetyl-CoA into MVA, a molecule used for IPP biosynthesis in all eukaryotic cells, archaea and some eubacteria such as *Staphylococcus aureus* (**Figure 2**).

It has been reported that the MVA pathway occurs in the cytoplasm and peroxisomes in all eukaryotes (Breitling and Krisans, 2002; Simkin et al., 2011). The HMGR is inhibited by lovastatin, originally called mevinnolin (MV), which is the first member of the statins, a family of molecules used as hypocholesterolemic agents (Endo et al., 1976; Alberts et al., 1980). During the nineties, experiments using <sup>13</sup>C labeled precursors in bacteria evidenced that MVA pathway was not exclusively responsible for the biosynthesis of isoprenoids (Flesch and Rohmer, 1988; Zhou and White, 1991; Rohmer et al., 1993). Accordingly, this alternative pathway was called MEP pathway as IPP/DMAPP derived from the 2-C-methylerythritol-4-phosphate (MEP) and does supply prenyl precursors in eubacteria (Rohmer et al., 1996; Rohmer, 2003), in alga (Schwender et al., 1996; Disch et al., 1998) and in vascular plants as it was extensively reviewed (Hemmerlin et al., 2012).



Other experiments indicated that DXP synthase (EC: 2.2.1.7), DXP reductoisomerase (EC: 1.1.1.267) and likely the HDR (EC: 1.17.7.1) and HDS (EC: 1.17.7.2) do play key regulatory function in this pathway (Rodríguez-Concepción and Boronat, 2015; Pamanes, 2017). Accordingly, the DXS catalyzes the first step of the MEP pathway by condensation of glyceraldehyde 3-phosphate (G3P) and pyruvate into 1-deoxy-D-xylulose 5-phosphate (DXP). The Fosmidomycin (FOS) isolated from *Streptomyces sp.* inhibit the DXS enzyme, depleting therefore the MEP pathway (Kuzuyama et al., 1998; Zeidler et al., 1998; Mueller et al., 2000). Unlike the MVA pathway, it is well established that the MEP pathway is exclusive to bacteria such as *Mycobacterium spp.* or *E. coli* and plants whose plastids have been inherited by endosymbiosis of cyanobacteria (Rockwell et al., 2014). The IPP and DMAPP precursors are then used downstream for the biosynthesis of different prenyl intermediates such as geranyl diphosphate (GPP), farnesyl diphosphate (FPP) or geranylgeranyl diphosphate (GGPP) which are not only precursors for a large number of primary and specialized metabolites, but also used in protein prenylation (**Figure 3**). Consistent is the fact that a part of the IPP/DMAPP produced is not only used for the biosynthesis of other prenyl intermediates, but also for the methylthioisoprenylation, which stabilize the interaction between tRNA and the mRNA ribosome complex to promote translation (Imlay and Odom, 2014). Although non-photosynthetic eukaryotes generally exhibit only the MVA pathway, the phylum Apicomplexa including Human parasites of the genera *Plasmodium*, *Toxoplasma* or *Eimeria* biosynthesize isoprenoids *via* the MEP pathway (Petersen et al., 2014). In fact, phylogenetic studies have shown the relationship between plants and the phylum Apicomplexa whose apicoplast was inherited from a red algae (Boucher and Yeh, 2019). In this respect, it can be proposed that plants embracing both MVA and MEP pathways, represent a suitable model for the study of the isoprenoid's regulation. Why do cells conserve, diversified biosynthesis pathways and developed tight mechanisms for regulation of isoprenoids through billions of years?

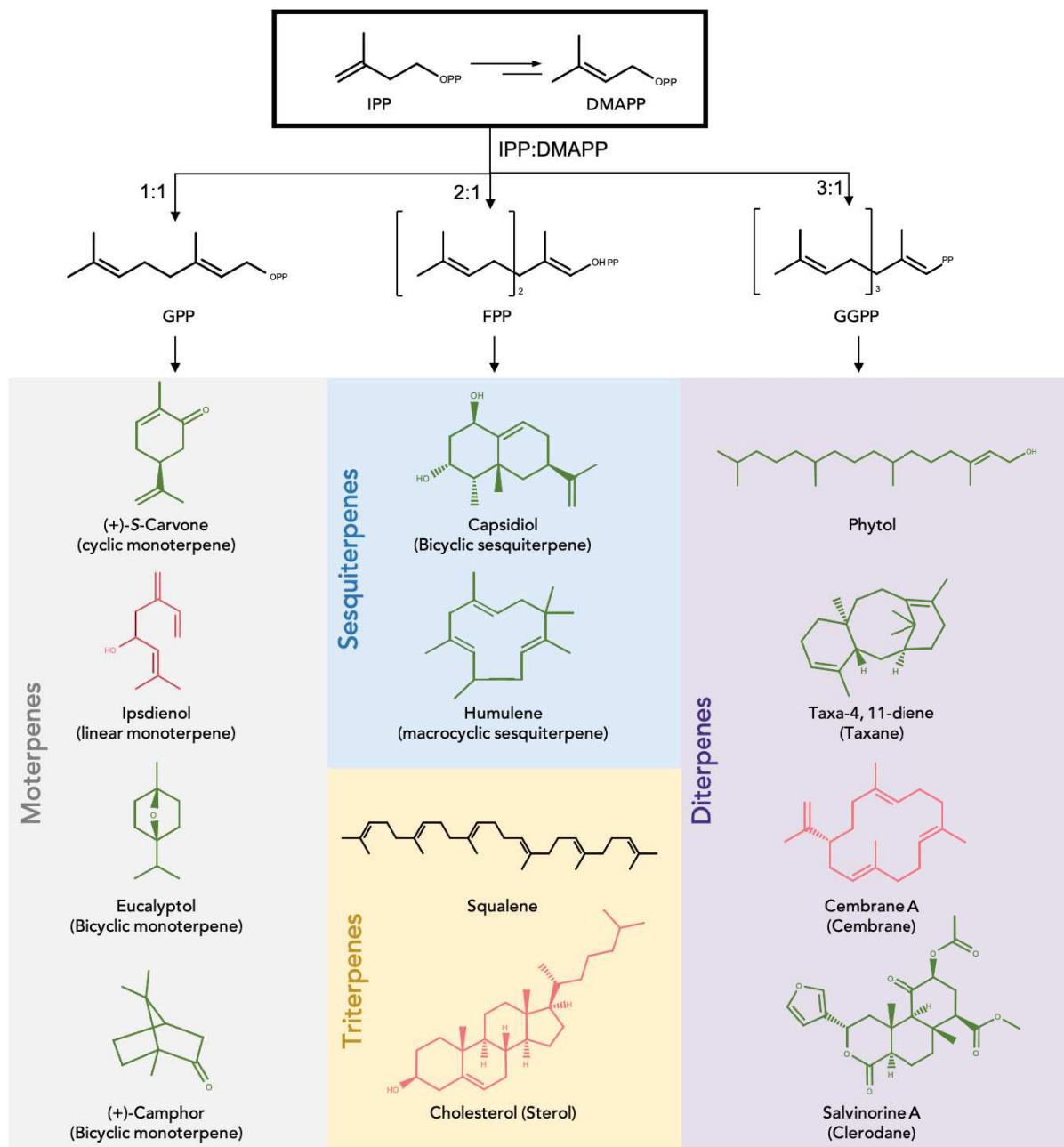


**Figure 3 Isoprenoid downstream of the MVA and MEP pathways.**

Early precursors IPP and DMAPP are condensed by prenyltransferases into intermediate prenyls known as geranyl diphosphate (GPP), farnesyltransferase diphosphate (FPP) and geranylgeranyl diphosphate (GGPP). Ratio of precursors used by prenyltransferase are indicated (IPP:DMAPP). Intermediate prenyls are used for the biosynthesis of more than 80 000 isoprenoids including several monoterpenes (grey box), sesquiterpenes (blue box), diterpenes (purple box), and triterpenes (yellow box) compounds with diverse structures and function. Plants isoprenoids structures (green), animal isoprenoids structures (pink), isoprenoids structures found both in animal and plants (black)

### 2.2.1 Diversity of Isoprenoids in Yeast and Animals

First of all, the IPP from the MVA pathway in yeast and animals is basically condensed with DMAPP in a ratio (2:1, IPP/DMAPP) to form farnesyl diphosphate (FPP) by a farnesyl diphosphate synthase (FDS: EC 2.5.1.29), which localize in the cytosol, peroxisomes and mitochondria (Poulter et al., 1981; Breitling and Krisans, 2002; Szkopińska and Płochocka, 2005) (**Figure 4**). Thereafter, FPP is used to build sterols in the ER compartment or into ubiquinone in mitochondria. The critical role of sterols in cell membrane and signaling was a prominent reason for the initiation of studies on isoprenoids. Actually, studies on the biosynthesis and cholesterol regulation in animals were fundamental for the treatment of man-made diseases such as hypercholesterolemia, therefore being rewarded with several Nobel prizes in medicine and chemistry with for instance to K. Bloch and F. Lynen in 1964 and M.S. Brown and J.L. Goldstein in 1985. Similarly, it has been found that several mitochondrial diseases such as cerebella ataxia, severe infantile multisystemic disease, nephrotic syndrome or myopathy does involve deficiencies of ubiquinone that require a hydrophobic polyprenyl for mitochondrial membrane anchoring (Quinzii and Hirano, 2010). In addition, some studies evidenced the role of FPP in the biosynthesis of sesquiterpenes for fungi and insects defense or communication (Camazine et al., 1983; Francis et al., 2005; Ditengou et al., 2015)

Exceptionally, part of the IPP used in some insects is also dedicated to geranyl diphosphate (GPP) being produced either by a geranyl diphosphate synthase (GDS) or by the FDS like in *Aedes Aegypti* mosquito (Rivera-Perez et al., 2015). In animals GPP is mostly an intermediate of FPP synthesis, but some studies evidenced that bark beetle genera (Coleoptera: Scolytidae) produce monoterpenes that function in intraspecific chemical communication as aggregation and dispersion of pheromones (Gilg et al., 2005). Moreover, the elongation of DMAPP with three IPP by a unique geranylgeranyl diphosphate synthase (GGDS: EC 2.5.1.10) leads to geranylgeranyl diphosphate (GGPP) (Koyama, 1999; Kavanagh et al., 2006). It also appears that FPP can be converted directly into GGPP (Kuzuguchi et al., 1999; Zhang and Li, 2014; Ding et al., 2019), which mostly contributes to cell signaling. In the 1990s, the role of isoprenoids in post-translational modifications was evidenced in yeast (Kamiya et al., 1977; Kamiya et al., 1978), then in animals and was so-called protein prenylation (Farnsworth et al., 1989; Goodman et al., 1990; Casey, 1992).

Although the latter process only requires a small portion of FPP or GGPP, it appears to be essential for membrane targeting of proteins being involved in developmental and adaptation processes within eukaryotes. Apparently, GGPP does also act as a regulator of HRD-dependent HMGR degradation pathway, as reported in yeast (Garza et al., 2009). Anecdotally, some species of aphids and spider mites use plant prenyls content for the production of carotenoids in diapause (Figure 5), involving carotenoid-synthase-carotenoid-cyclase loci inherited from fungi (Moran and Jarvik, 2010; Bryon et al., 2017). Nevertheless, the diversity of structure and function of isoprenoids is far more important in the plant kingdom, emphasizing the role and evolution of the inherited MEP pathway.

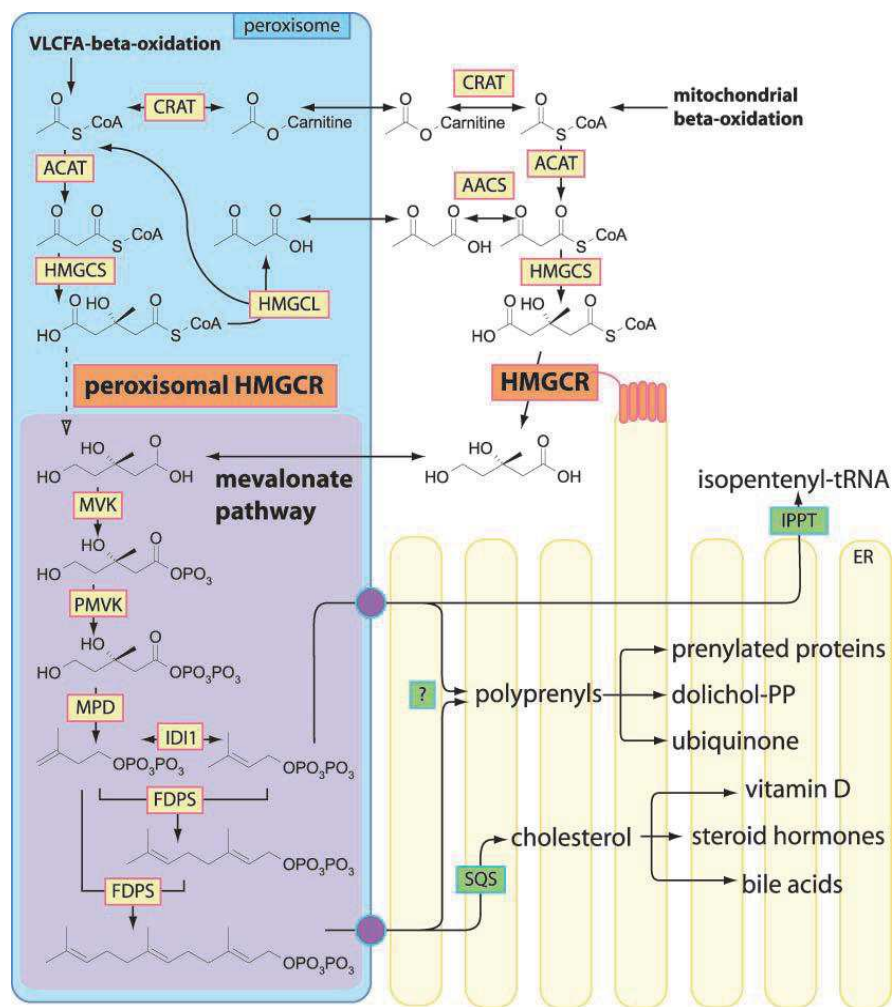


**Figure 4 Current view of the subcellular localization of isoprenoid biosynthesis in mammalian cells.**

Reactions between mevalonate and farnesyl diphosphate are assumed to be almost exclusively peroxisomal (purple shading). Several reactions downstream of farnesyl diphosphate are omitted for clarity. Enzyme names are abbreviated as follows: AACS, acetoacetyl-CoA synthase; ACAT, acetoacetyl-CoA lyase; CRAT, carnitine acetyltransferase; FDPS, farnesyl diphosphate synthase; HMGCL, HMG-CoA lyase; HMGCR, HMG-CoA reductase; HMGCS, HMGCoA synthase; IDI1, isopentenyl diphosphate isomerase; IPPT, isopentenyl tRNA transferase; MPD, mevalonate diphosphate decarboxylase; MVK, mevalonate kinase; PMVK, phosphomevalonate kinase; SQS, squalene synthase; VLCFA, very long chain fatty acid. **Breitling and Krisans, 2002**

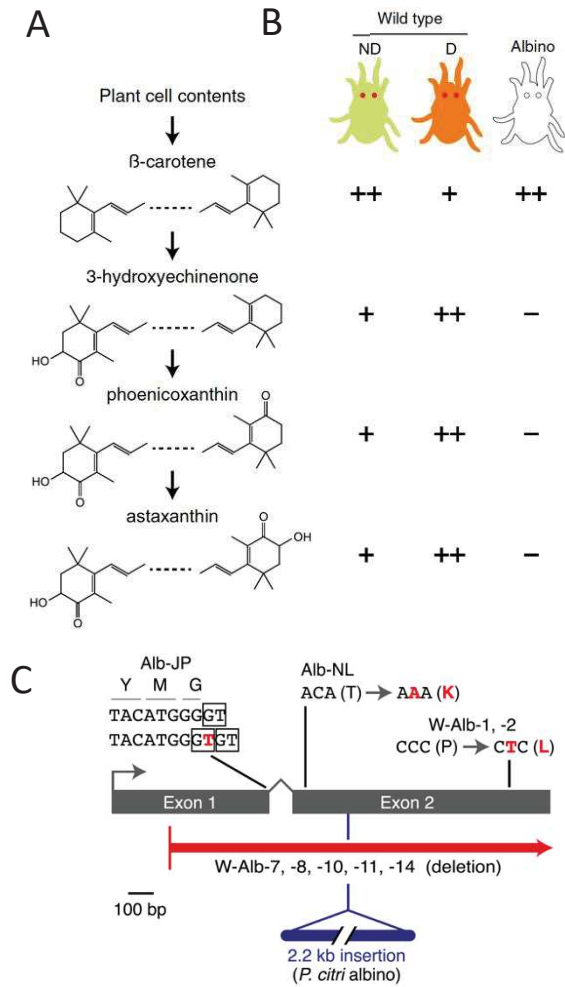


**Figure 5 Carotenoids in WT and albino mutants of *T. urticae*.**

(A) Carotenoids observed in females of Tetranychus mite species as reported in earlier studies. The previously proposed pathway from presumptive dietary  $\beta$ -carotene to the terminal *keto*-carotenoid astaxanthin is shown; intermediates, minor carotenoid species, and carotenoid esters are not indicated. (B) Carotenoid profiles in nondiapausing (ND) and diapausing (D) WT *T. urticae* females, and in nondiapausing albino mutants (compare with A). Plus, or minus signs indicate relative levels, with the ketocarotenoids undetectable in albino mites. Schematics of WT and mutant mites are given at the top; for display, the eyes have been enlarged. (C) Mutations in the scaffold 1 phytoene desaturase in *T. urticae* and *P. citri* albino strains. Coding exons for tetur01g11270 (carotenoid-synthase-carotenoid cyclase loci) are represented as rectangles. WT sequences are indicated in black, with mutations shown in red (*T. urticae*) or blue (*P. citri*); where single nucleotide substitutions are observed, the impact on the coding potential is shown. For the Alb-JP mutation, boxes indicate the exon 1 splice donor in WT (at the top) with two out-of-frame splice donors created by the "T" insertion shown underneath. **Byron et al., 2017**





## 2.2.2 Diversity and Functions of isoprenoids in Plant

As far as isoprenoids are concerned, except for bacteria such as *Enterococcus spp.* or *Streptomyces spp.* plants are the only organisms that exhibit both MVA and MEP biosynthetic pathways (Vranová et al., 2013). Since plants remain predominantly sessile organisms, they benefited from the use of isoprenoids to deal with the multiple pressures exercised by different biotopes (Kumari et al., 2013; Pichersky and Raguso, 2018). In plants, the MVA pathway supplies IPP for phytosterols, triterpenes, sesquiterpenes and polyprenols biosynthesis (**Figure 6**). In contrast to animals and fungi, many other valuable compounds emerged exclusively in plants for hormone signaling pathway and for defense against biotic, abiotic stresses or attraction of pollinators (Tetali, 2019). For example, studies from the past decades evidenced the biosynthesis of brassinosteroids (BRs) from campesterol, and its role in plant germination and growth (Nolan et al., 2020). Besides, various triterpenes of steroid genuine such as cardenolides or saponin type have been described for their role in defense against herbivores and nematodes (Agrawal et al., 2012; D'Addabbo et al., 2020). Thus, the investigation of triterpenes is an important field for medical research as well as for agronomy and agri-food industries (Miettinen et al., 2018).

Similarly, several linear sesquiterpenes (e.g. farnesene) or cyclic ones (e.g.  $\beta$ -caryophyllene or capsidiol in Solanaceae) play a role as phytoalexins, due to their antifungal and antibacterial properties (**Figure 7**). Thus, pharmaceutical preparations or essential oil containing such molecules can be used to treat animal diseases. Other more atypical plant sesquiterpenes are of particular interest but their structure complexity involving high degree of asymmetric carbon makes the chemical synthesis challenging. For instance, the total synthesis of the artemisinin isolated from *Artemisia annua* and used to cure malaria was so far investigated, but the total synthesis is relatively long (> 8 steps) and complicated with overall yield from 20 to 42 % (Maude et al., 2009; Wang et al., 2014c; Wang et al., 2019a). Other partial syntheses were proposed with higher yields but plant production remain the main source (Ikram and Simonsen, 2017). Although these molecules are biologically active for plant defense, they exhibit cytotoxicity on the plant too, which sequestrates them into specific structures such as trichomes (Morimoto et al., 2007; Chaimovitsh et al., 2017; Tissier et al., 2017). The latter also represents a storage site as *de novo* synthesis of specialized metabolites cost energy and resources, therefore limiting plant growth.

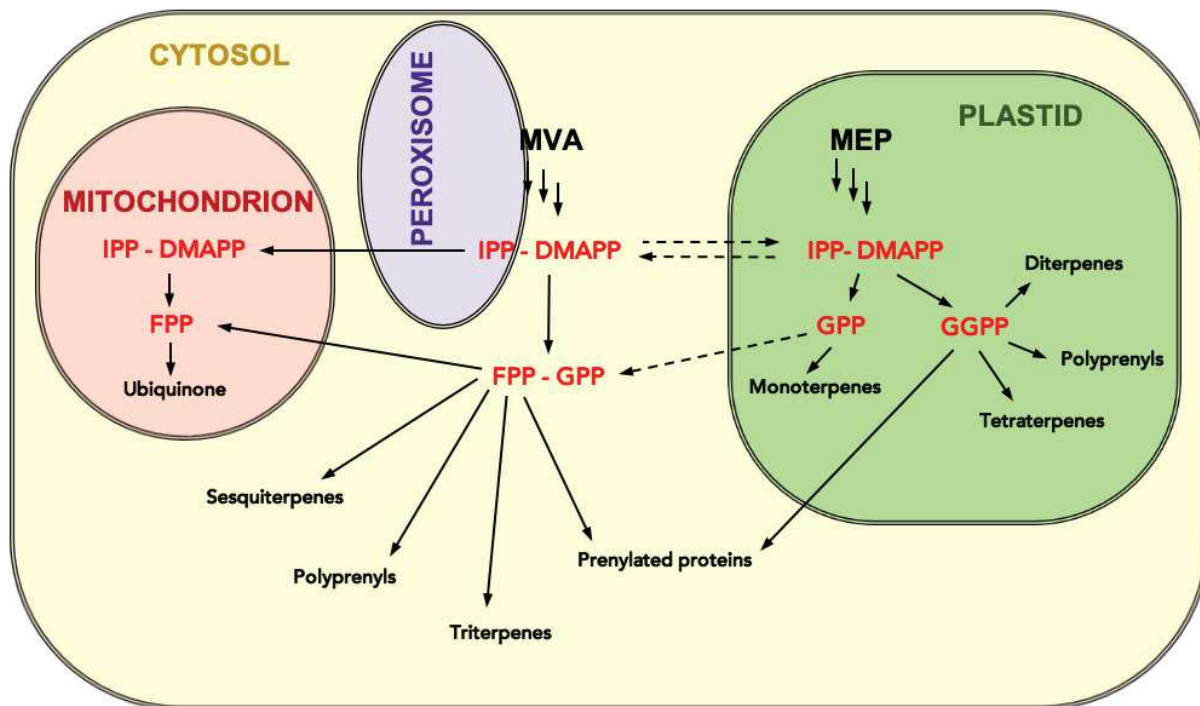


**Figure 6 Subcellular compartmentalization of isoprenoid biosynthesis in plants.**

The mevalonate (MVA) pathway is located in the cytosol and peroxisomes. The methylerythritol phosphate (MEP) pathway is localized exclusively in the plastids. The prenyl diphosphates IPP, isopentenyl diphosphate; DMAPP, dimethylallyl diphosphate; GPP, geranyl diphosphate; FPP, farnesyl diphosphate; GGPP; geranylgeranyl diphosphate) are displayed in red. Adapted from **Huchelmann, 2013**

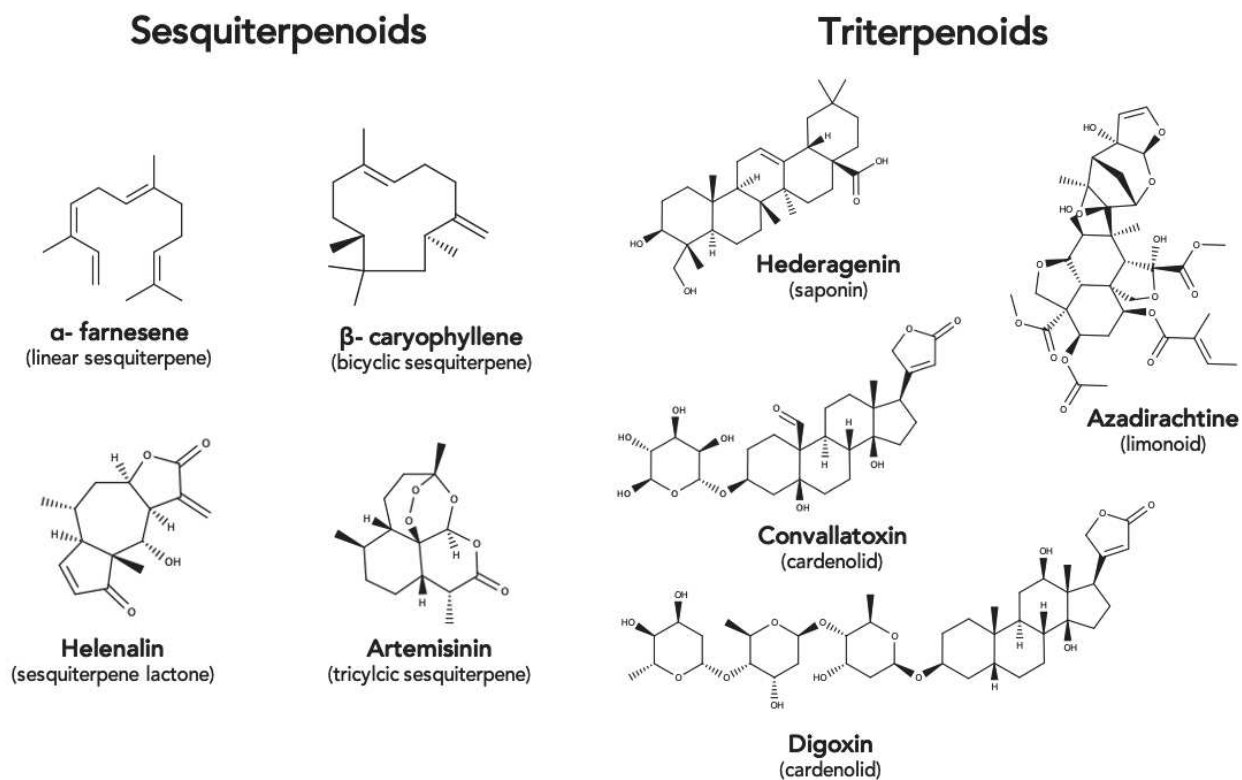


**Figure 7 Snapshot of Plant MVA-derived isoprenoids diversity.**

Example of structures for sesquiterpenoids and triterpenoids derived from the FPP being mostly supplied by the MVA pathway

Remarkably, plants have developed a whole isogenic family coding for several HMGR isoforms unlike yeast which has two forms and solely one gene exists in animals (Hemmerlin, 2013; Vranová et al., 2013). The HMGR-1 in plant is constitutively expressed and supplies IPP for primary metabolites under standard conditions (Hemmerlin, 2013; Vranová et al., 2013). Under stress conditions, the level of HMGR-2 expression is strongly increased, reinforcing the production of MVA also needed for the biosynthesis of specialized metabolites such as capsidiol in *N. tabaccum* (Huchelmann et al., 2014).

Another point is that plants have inherited of the MEP pathway which takes place in plastids and provides IPP/DMAPP (5:1) for the biosynthesis of GPP by the GDS and GGPP by the geranylgeranyl diphosphate synthase (GGDS) (**Figure 6**). Although these enzymes were initially characterized in plastids, in *Arabidopsis* twelve isozymes of GGDS have been described, from which two locates in plastids, five are inactive *in vitro* and five other are in fact geranylgeranyl diphosphate synthase (GFDS), producing C<sub>25</sub> rather than C<sub>20</sub> (Okada et al., 2007; Nagegowda, 2010; Nagel et al., 2015; Nagel et al., 2019)s. Recently, an enzyme closely related to the cytosolic FDS was found to produce GPP in *Lithospermum erythrorhizon* and therefore called cytosolic GDS (Ueoka et al., 2020). It was suggested that this GDS provide substrates for prenylation of meroterpenoids like shikonin, but no information about *in vivo* activity was afforded. In plant, the GPP produced in plastids is mostly transformed into monoterpenes (Phillips et al., 2008a; Banerjee and Sharkey, 2014; Frank and Groll, 2017). Most monoterpenes exert activities such as antibacterial, antifungal, insecticidal and play a key role in long-distance attraction of pollinators including humans (Pichersky and Raguso, 2018). These valuable small volatiles like carvacrol or neral are appreciated for their smell and are thus widespread not only in the field of cosmetics and agri-foods but also in hospital to limit nosocomial infection (**Figure 8**) (Horváth et al., 2016). In contrast, many diterpenes have strong anticancer, anti-inflammatory, neuroprotective or even psychoactive activities like salvinorin A from *Salvia divinorum* (Butelman and Kreek, 2015; González, 2015; Islam, 2017; Jin et al., 2019). For instance, *Taxus spp.* synthesize taxane-type anticancer diterpenes such as paclitaxel which has been approved by the U.S Food and Drug Administration in 1991 and is available as Taxol® (Khanna et al., 2015) (**Figure 8**).

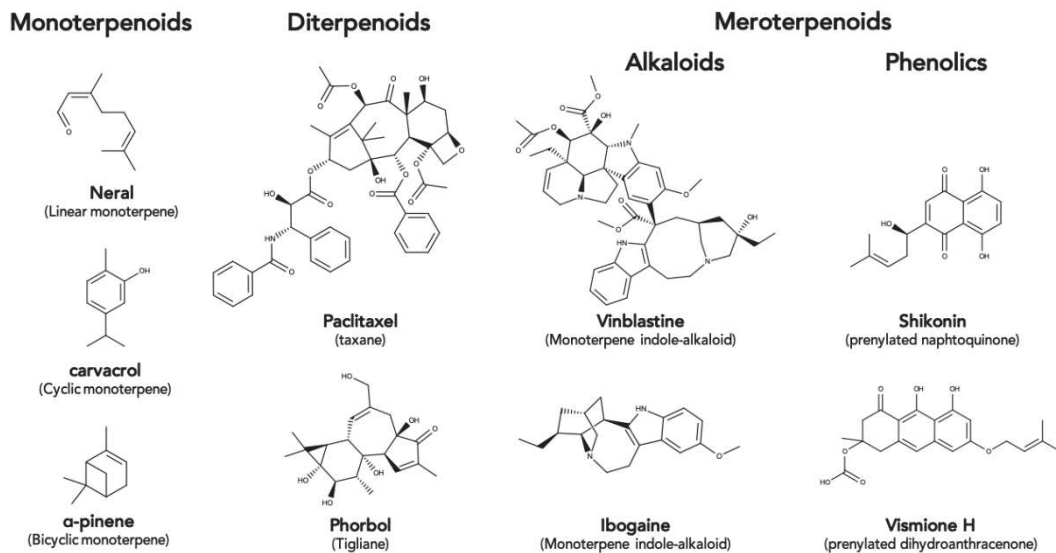


**Figure 8 Snapshot of Plant MEP-derived isoprenoids diversity.**

Example of structures for monoterpenoids, diterpenoids and molecules so called meroterpenoids, originating from both isoprenoids and alkaloids or phenolics. The MEP pathway supply GPP and GGPP for the biosynthesis of most of these natural compounds.

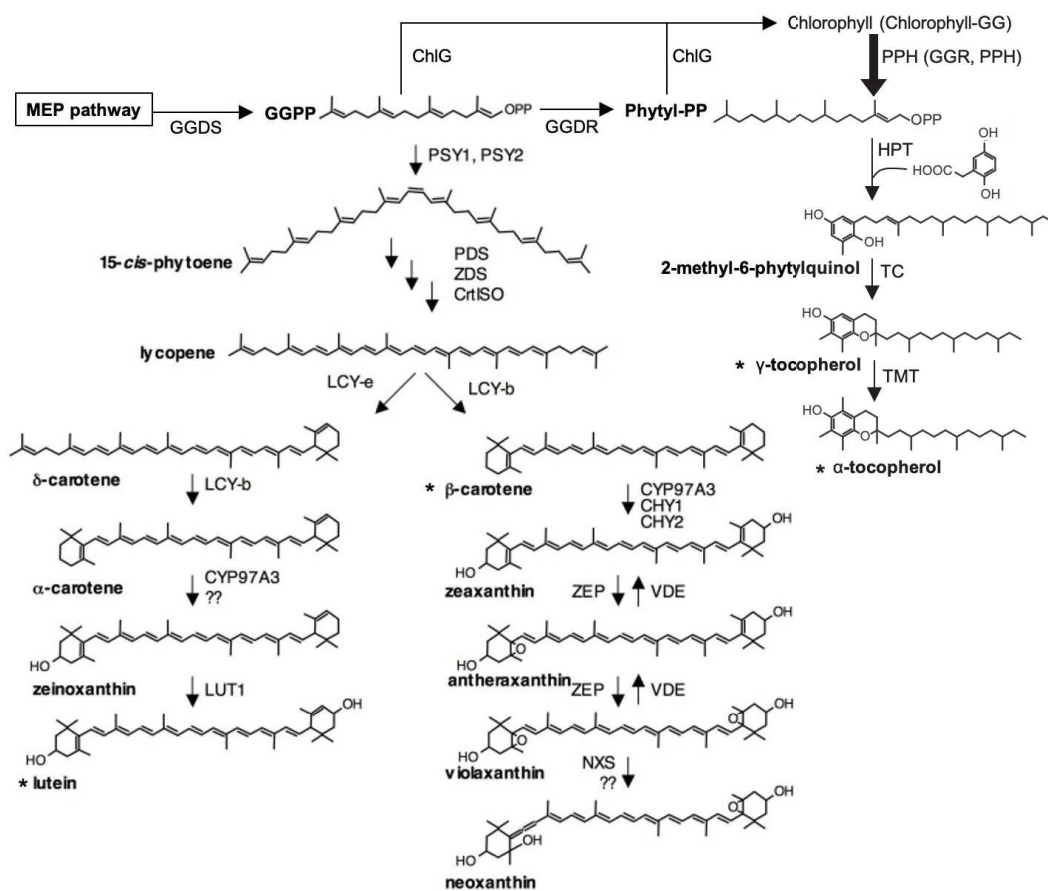


**Figure 9 Carotenoids and tocopherol biosynthesis pathways in *A. thaliana*.**

The asterisks indicate the carotenoid compounds identified and characterized by HPLC and mass spectrometry in intraerythrocytic stages of *P. falciparum*. Adapted from Tonhosolo et al., 2009; Sussmann et al., 2011.

Similarly, several labdane were identified in Asteraceae and Cistaceae or lathyrane-type diterpenes from *Euphorbia lathyrys* have been described for their anticancer and anti-inflammatory properties (Chinou, 2005; Zhang et al., 2019), while some tiglanes like phorbol from *Euphorbia sp* act just as toxics (Hohmann and Molnár, 2004). By the way, as artemisinin, it is such a nightmare to think about total synthesis of most of these molecules. For instance, the synthesis of phorbol is achievable in 19 steps, that of paclitaxel has required hundreds of chemists over decades (Kawamura et al., 2016; Kanda et al., 2020).

In fact, the main uses of GGPP remain for protein prenylation and for the biosynthesis of long chain isoprenoids, to build up hydrophobic lateral chain of chlorophylls or carotenoids (Ruiz-Sola et al., 2016) (**Figure 9**). Although, the GGPP supply directly the biosynthesis of phytoene for carotenoids and phytol for tocopherols, it was found that the latter are mostly produced *via* the recycling of chlorophyll prenyl chain (Gutbrod et al., 2019). Carotenoids play an essential role in protecting photosystems against photooxidation (Tracewell et al., 2001) as well as for abscisic acid (ABA) hormone biosynthesis. For instance, ABA is a sesquiterpenoid derived from the catabolism of violaxanthin into xanthoxin by NECD enzyme family in plastids, then exported into the cytoplasm to be converted into ABA aldehyde and ABA, or into ABA-Glc for storage into the primary vacuole or ER (Finkelstein, 2013) (**Figure 10**). Many reports on ABA evidenced its key role in abiotic stress response and stomatal regulation as well as in plant developmental step such as seed maturation, germination, growth, flowering and senescence (Finkelstein, 2013; Fernando and Schroeder, 2016; Yoshida et al., 2019). In this regard, GA are also derived from GGPP, this family of hormones control the plant growth and development (Brian et al. 1954; Borrow et al. 1955; Stowe and Yamaki 1957; Koornneef and van der Veen 1980; Hedden and Phillips 2000), as well as seed dormancy (Kahn 1959; Burns and Coggins 1969; Groot and Karssen 1987). Their biosynthesis begins in the plastid by cyclisation into *ent*-kaurene from GGPP, being then exported in the cytosol to be converted into different GAs (Graebe et al. 1965; Jefferies et al. 1974; Hedden and Phillips 2000). In plants the hormonal system is extremely dynamic, and hormones act synergistically or antagonistically to integrate multiple environmental parameters. The ABA/GA balance plays a key role in the regulation of the whole plant hormone machinery for plant growth with cytokinins (CK), auxins, BRs, while defense reactions are mostly associated with JA and ethylene (Vanstraelen and Benková, 2012; Kohli et al., 2013; Yang et al., 2019) (**Figure 11**).

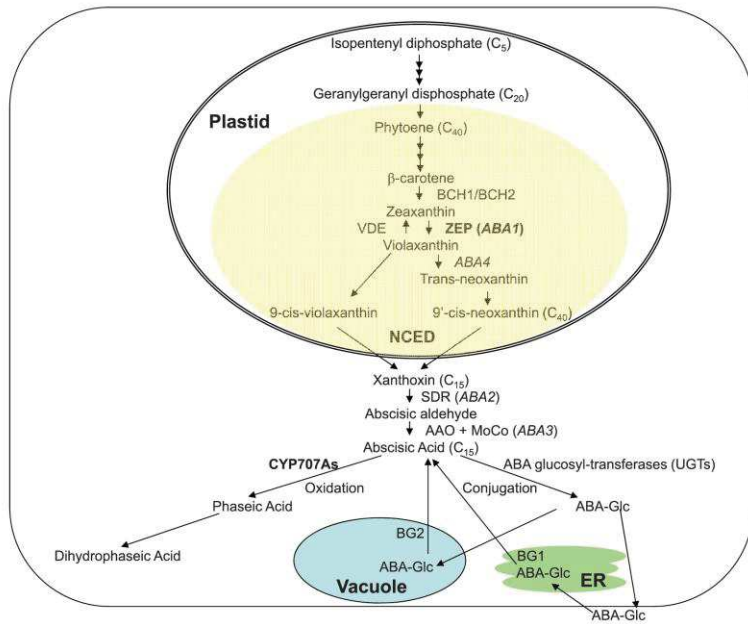


**Figure 10 ABA metabolic pathways.** ABA biosynthesis, degradation and conjugation pathways are shown in relation to the cellular compartments where these events occur. Carotenoid intermediates are highlighted in yellow. Enzymes regulating key regulatory steps are shown in bold. Individual loci identified based on ABA deficiency are shown in italics. **Finkelstein, 2013**

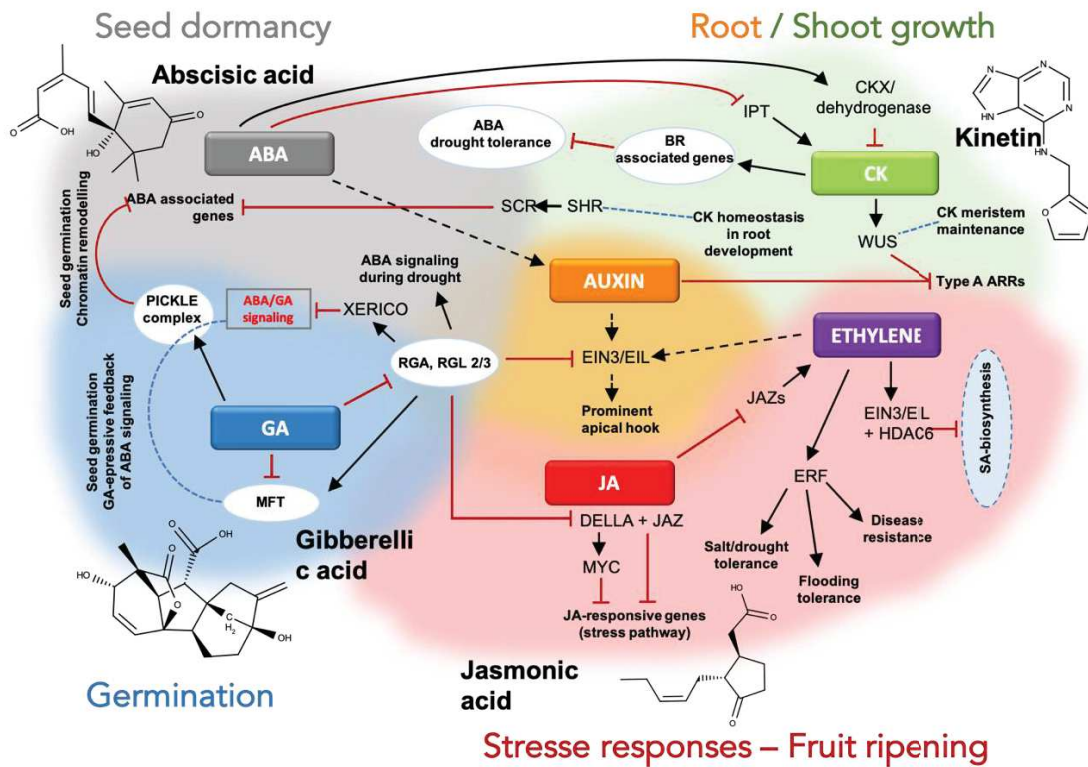


**Figure 11 Selected hormonal crosstalk events related to stress response in plants.**

The central roles played by abscisic acid (ABA) and gibberellins (GA) in regulating the stress responses are evident from the interactions surrounding DELLA repressors. The DELLA proteins establish important crosstalk with auxin, ethylene and jasmonates (JA) as well. While ABA and cytokinin crosstalk, they also interact with auxins and brassinosteroids (BR) to mutually influence stress responses in plants. The interaction map shown is only a portion of the intricate web of signal crosstalk occurring in plants subjected to stress. This is further highlighted by the modulation of biosynthesis of salicylic acid (SA) by ethylene. Various other crosstalk points are being discovered continually, and these can provide valuable strategies for genetic improvement of crop plants in the future. The various plant hormones and their respective signaling intermediates forming the network are shaded differently. Arrows indicate positive effects (accumulation of transcript and/or protein and hormone level, respectively; activation through interaction, etc.), dashed arrows precise that one or more proteins are not represented, blocked arrows indicate negative effects, and dashed lines indicate other forms of interaction. Redesigned from **Kohli et al., 2013**

Interestingly, ABA and GA are also present in *Plasmodium* where they play a similar role in the dormancy and activation of the parasite metabolism (Toyama et al., 2012; Duvalsaint and Kyle, 2018). Since carotenoid biosynthesis correlates with the diapause of some insects (Bryon et al., 2017), it can be speculated that these insects produce hormones like ABA via carotenoids degradation. To note, as strigolactones are also derived from the degradation of carotenoids (Al-Babili and Bouwmeester, 2015), CK which has a moiety that issued from DMAPP (Kieber and Schaller, 2014), and BRs deriving from phytosterols (Bajguz et al., 2020), five out of the nine major phytohormones are directly dependent on the metabolism of isoprenoids. Thus, it is not very surprising that isoprenoid biosynthesis inhibitors interfere with plant development.

Considering these studies, the pre-existing MEP pathway in cyanobacteria has been preserved to sustain first the development and photosynthetic machinery in supplement of the MVA, already stormed by sterols and quinones biosynthesis (Hemmerlin et al., 2012; Banerjee and Sharkey, 2014; Hoshino and Gaucher, 2018).

Also, it is amazing to see that the plant cell has adopted a pre-existing system to develop its own factory for an extended set of defense and communication metabolites. Thus, the expression of the key enzymes HMGR in the MVA pathway, and at least DXS and DXR in the MEP pathway is regulated by stress factors or at specific developmental stage (Lois et al., 2000; Estévez et al., 2001; Rodríguez-Concepción et al., 2001; Kishimoto and Ohmiya, 2006; Okada et al., 2007; Harada et al., 2009). It needs mentioning that three isoforms of DXS occur in most higher plants, whereas a single DXR has been characterized (Carretero-Paulet et al., 2002). The type-I DXS-1 is expressed constitutively and involved in developmental and photosynthetic processes, while type-II DXS-2 and three isoforms are more related to specialized metabolites (Walter et al., 2002; Paetzold et al., 2010; Cordoba et al., 2011). For example, AaDXS-2 from *Artemisia annua* is expressed in trichomes and likely helping in the biosynthesis of specialized metabolites like artemisinin (Zhang et al., 2018). By the way, artemisinin is a typical example of sesquiterpenes biosynthesized from both MVA and MEP precursors (Schramek et al., 2010). Besides, studies with melon evidenced that the expression of type-II DXS isoforms CmDXS-2a and CmDXS-2b is induced in flowers and ripening fruit of orange-fleshed varieties for  $\beta$ -carotene accumulation (Saladié et al., 2014).



Different molecules such as FOS or 5-ketoclozazole are inhibitors of DXR and DXS respectively (Okuhara et al., 1980; Kuzuyama et al., 1998; Mueller et al., 2000; Han et al., 2013), they induce plant bleaching in neosynthesized tissues by depletion of chlorophyll and carotenoids biosynthesis (Kamuro et al., 1986; Zeidler et al., 1998; Mueller et al., 2000). In *Catharanthus roseus* these inhibitors do not exhibit the same activity, supporting difference between isoprenoid metabolism of plant species (Han et al., 2013).

In contrast to the situation in other eukaryotes, the dual origin of IPP/DMAPP in plants appears to be perfectly adapted to equilibrate growth and stress responses. From these two building blocks plants succeed in synthesizing thousands of isoprenoids. GPP and GGPP are predominantly synthesized from the MEP pathway in plants, studies evidenced that monoterpenes or diterpenes such as GA can be derived from IPP produced in both MVA and MEP pathways (Kasahara et al., 2002), outstanding a complexity of isoprenoids metabolism.

Numerous complementation experiments have been performed which have demonstrated that substrates of the MEP pathway such as DX can reverse the effects of mevinolin (Hemmerlin et al., 2003), whereas MVA is able to rescue albino phenotype in the *Clu 1-1 A. thaliana* mutant knock-out in *dxs* (Nagata et al., 2002). More recently, it has been proved that this dual origin of prenyl substrates is involved in the adaptation of protein prenylation mechanisms in plants (Gerber et al., 2009; Huchelmann, 2013) and likely in *Plasmodium* with an import of host isoprenoids.

### 2.2.3 Diversity and Functions of Isoprenoids in Apicomplexa

The Apicomplexa phylum contains only metazoan parasites, including *Plasmodium* genera responsible for malaria, *Toxoplasma* causing toxoplasmosis, or other organisms involved in coccidiosis. In our study we were especially interested by mechanisms occurring in *Plasmodium falciparum* responsible for the Top 1 parasitosis in the world.

#### 2.2.3.1 Malaria: a booster shot

Malaria is a parasitic illness caused by protozoan from the genus *Plasmodium*, including over 100 species parasites of metazoan such as reptiles, birds and mammals. Five species are parasite of Human: *P. falciparum*, *P. vivax*, *P. ovale*, *P. malariae* and *P. knowlesi*. These parasites are transmitted by the bite of *Anopheles* mosquito. The most common and dangerous species are *P. falciparum* and *P. vivax*, they are found throughout the tropics and intertropics areas. *P. falciparum* is responsible for more than 90% of malaria cases in Africa, with about 80% of deaths in the 5-year-old population. According to WHO, about 230 millions cases have been recorded in 2018 with about 400 000 deaths, ranking malaria at the first place of human parasitosis and this for several decades (OMS, 2019).

The parasite has a heteroxenous cycle implying two different hosts (**Figure 12**). The female *Anopheles* is the definitive host involved in the sexual reproduction (gamogony) and the vertebrate intermediate host is used as a nursery for asexual reproduction (schizogony). The asexual cycle is initiated by the inoculation of the sporozoite form at the bite of the female *Anopheles* blood-meal. Then, the parasite undergoes three distinct stages: the liver-stage in hepatocytes, the blood-stage in erythrocytes and the mosquito stage in the *Anopheles* host cells (**Figure 12**). An exponential growth is observed at each of these steps, multiplying the number of parasite cells over  $10^{12}$  for a complete cycle of infection by less than 100 sporozoites (Blasco et al., 2017). The asexual cycle is fundamental for the massive multiplication of the parasite until lysis occur, provoking anemia in infected human. During blood-stage, the parasite degrades actively the hemoglobin to ensure its own protein biosynthesis. The heme-related toxicity is decreased by metabolization into hemozoin evacuated towards the parasitophoric vacuole, provoking fever attacks. Belonging to Apicomplexa, *P. falciparum* is characterized by the presence of an apicoplast, a unique chloroplast-like organelle essential for growth and pathogenesis of the malaria parasite.

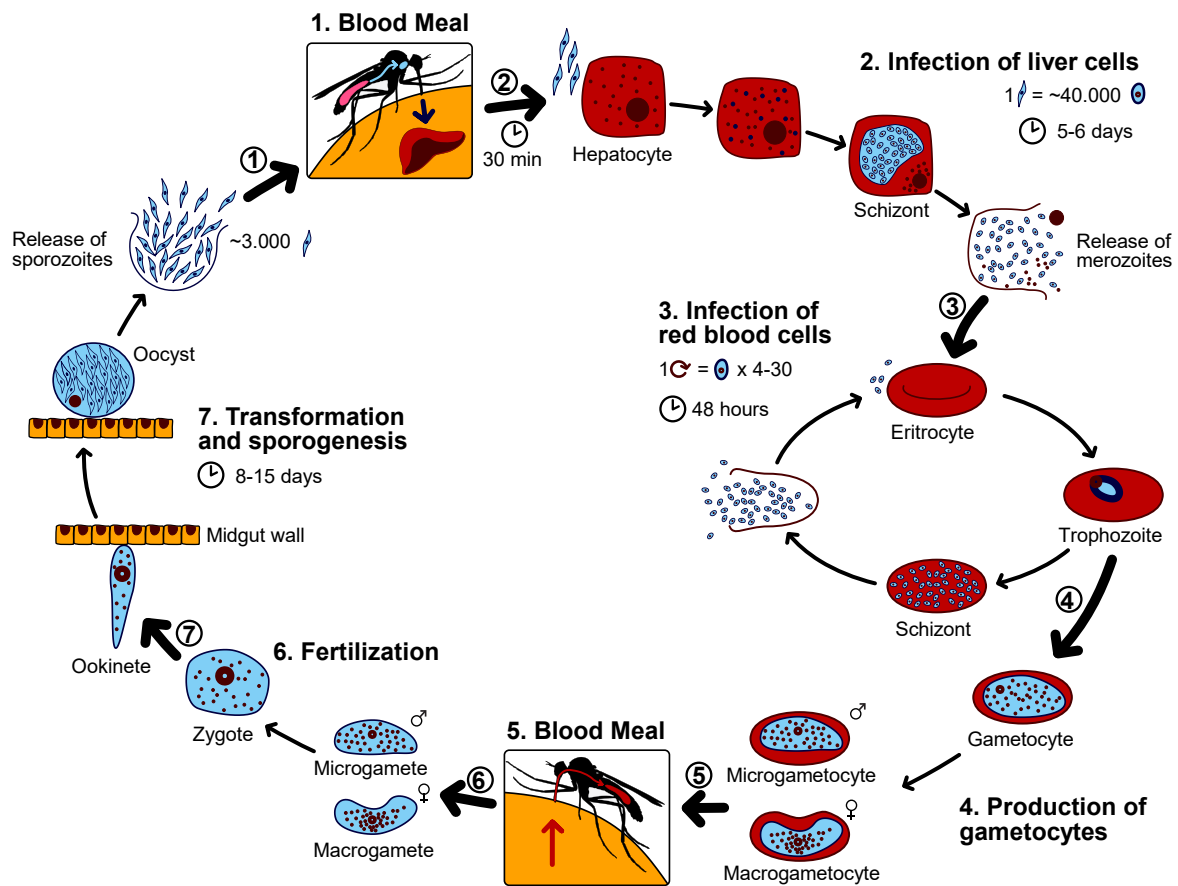


**Figure 12** The malaria parasite life cycle involves two hosts.

A mosquito causes an infection by a bite (1). The sporozoites enter the bloodstream, and migrate to the liver. They infect liver cells, where they multiply into merozoites, rupture the liver cells, and return to the bloodstream (2). The merozoites infect red blood cells, where they develop into ring forms, trophozoites and schizonts that in turn produce further merozoites (3). Sexual forms (gametocytes) are also produced (4), which, if taken up by a mosquito with the blood (5), mature in the mosquito gut to gametes. The male and female gametes fuse (6) and form an ookinete—a fertilized, motile zygote able to cross the midgut wall as Oocyst. Oocyst develop new sporozoites that migrate to the insect's salivary glands (7), ready to infect a new vertebrate host. Made available by Bbkkk (User:OgreBot/Uploads by new users/2018 June 28 13:30) [https://upload.wikimedia.org/wikipedia/commons/2/24/Life\\_Cycle\\_of\\_the\\_Malaria\\_Parasite.svg](https://upload.wikimedia.org/wikipedia/commons/2/24/Life_Cycle_of_the_Malaria_Parasite.svg).

### 2.2.3.2 The Apicoplast, the Isoprenoids Factory of Apicomplexans

The apicoplast is an organelle involved in heme biosynthesis, Fe-S cluster assembly, fatty acids biosynthesis and of course the biosynthesis of isoprenoids *via* the MEP pathway. The origin of this four-membrane organelle has long been discussed between the inheritance after secondary endosymbiosis of a red alga or a green alga, according to circular genomic DNA. Nevertheless, the sequence comparison of apicoplast DNA with that found in the photosynthetic organelle of the protozoan *Chromera velia*, which also has four membranes, definitively confirmed that the apicoplast was inherited from a red alga (Boucher and Yeh, 2019) (**Figure 13**). Apicomplexans also biosynthesize FPP, GPP and GGPP (**Figure 14**), but these reactions are catalyzed by a single bifunctional FDS/GGDS in *Plasmodium* and *Toxoplasma gondii* (Ling et al., 2007; Jordão et al., 2013), as compared to most organisms expressing two distinct enzymes. Other longer isoprenoids are synthesized downstream, until now the octaprenyl synthase (Tonhosolo et al., 2005), and another *cis*-prenyltransferase (PfcPT) of *P. falciparum* have been characterized and contributes to the dolichol biosynthesis through reduction by polyprenol reductase (Zimbres et al., 2020). As in other eukaryotes, the biosynthesis of isoprenoids in apicomplexans is essential for the membrane anchoring of ubiquinone and menaquinone or proteins *via* GPI-anchoring. In contrast, apicomplexans do not use their own FPP pool for sterol biosynthesis as sterol biosynthesis enzymes are absent. In fact, it appears that cholesterol is mainly imported from the host cell membranes' *de novo* synthesis, and by degrading the host High-density lipoproteins (HDL) and low-density lipoproteins (LDL) (Imlay and Odom, 2014).

Surprisingly, although most isoprenoids occurring in algae are absent in apicomplexans, some of them remain well preserved. For instance, studies have highlighted the biosynthesis of metabolites such as carotenoids with all-*trans*- $\beta$ -carotene, all-*trans*-lutein or the vitamin E likely for the prevention of oxidative stress as plants (Tonhosolo et al., 2005; Tonhosolo et al., 2009; Sussmann et al., 2011) (**Figure 9**). Oddly, it seems that abscisic acid (ABA) also plays a role in apicomplexans signaling such as in calcium releases in *Toxoplasma spp.* and dormancy in *P. falciparum* (Duvalsaint and Kyle, 2018). Moreover, the inhibition of ABA and gibberellin (GA) biosynthesis with fluconazole, fluridone or inabenfide induces cell death of different apicomplexans (Toyama et al., 2012; Liu et al., 2019). Also, ABA appears to regulate the parasite transmission/growth in mammals and in host mosquitos, and *T. gondii* development (Nagamune et al., 2008; Glennon et al., 2016; Glennon et al., 2016; Glennon et al., 2017).

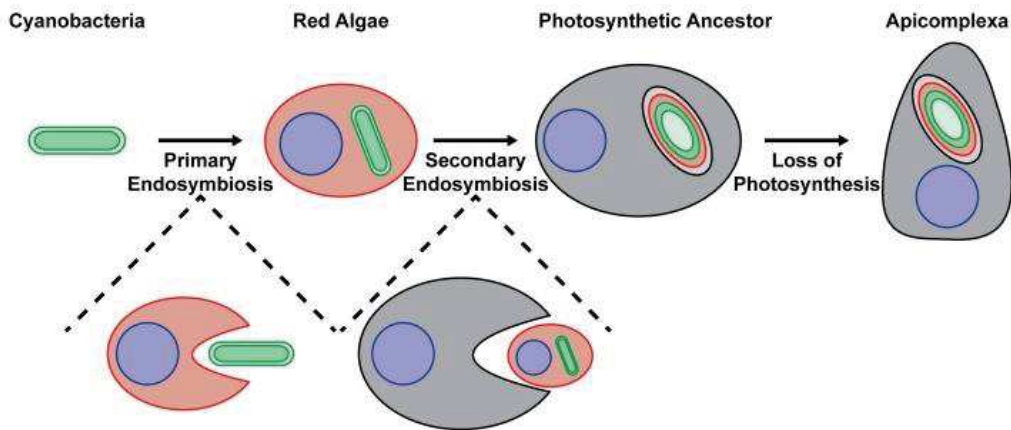


**Figure 13 Model for apicoplast evolutionary history.**

Red algae (rose) following primary endosymbiosis, during which a eukaryotic cell engulfed a photosynthetic cyanobacterium that underwent evolutionary reduction to become a chloroplast. The ancestors of the Apicomplexa emerged following secondary endosymbiosis, during which another eukaryotic cell engulfed a red alga, which then underwent evolutionary reduction to become a four-membraned, photosynthetic secondary plastid. During evolution of the Apicomplexa, the secondary plastid lost its photosynthetic machinery but retained components of key metabolic pathways to become what we now know as the apicoplast. Note that this model is simplified and that the precise evolutionary events that gave rise to the apicoplast (e.g., vertical plastid inheritance from a common chromalveolate ancestor versus acquisition by tertiary endosymbiosis) are not yet resolved.

**Boucher and Yeh, 2019**

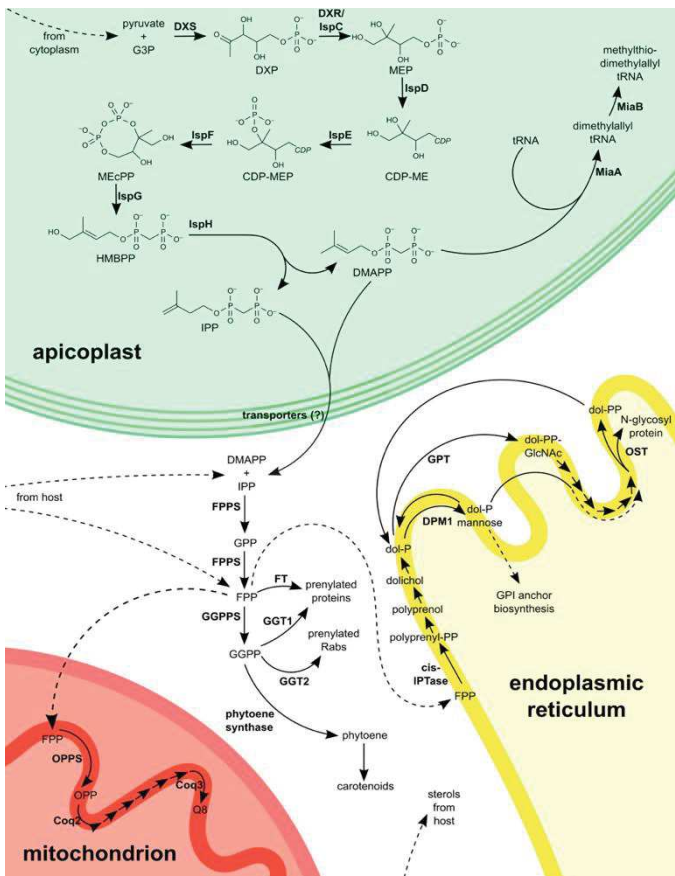


**Figure 14 Isoprenoid metabolism in apicomplexan parasites.**

Some enzymes and processes are not conserved in all Apicomplexa. In *Plasmodium* and *Toxoplasma* spp., FPP and GGPP are synthesized by a single bifunctional enzyme; in *Cryptosporidium* spp., NPPPS (nonspecific polyprenyl pyrophosphate synthase) synthesizes products with a wide range of chain lengths.

Abbreviations: G3P, glyceraldehyde-3-phosphate; DXP, 1-deoxy-D-xylulose-5-phosphate; MEP, 2-C-methyl-D-erythritol-4-phosphate; CDPME, 4-diphosphocytidyl-2-C-methyl-D-erythritol; CDP-MEP, 4-diphosphocytidyl-2-C-methyl-D-erythritol 2-phosphate; MEcPP, 2-C-methyl-D-erythritol 2,4-cyclodiphosphate; HMBPP, 1-hydroxy-2-methyl-2-buten-4-yl 4-diphosphate; IPP, isopentenyl pyrophosphate; DMAPP, dimethylallyl pyrophosphate; GPP, geranyl pyrophosphate; FPP, farnesyl pyrophosphate; GGPPS, geranylgeranyl pyrophosphate synthase; FT, protein farnesyltransferase; GGT1, type I protein geranylgeranyltransferase; GGT2, type II (Rab) protein geranylgeranyltransferase; OPP, octaprenyl pyrophosphate; OPPS, octaprenyl

pyrophosphate synthase; Q8, ubiquinone-8; cis-IPTase, cisopentenyltransferase; polyprenyl-PP, polyprenyl pyrophosphate; dol-P, dolichol phosphate; DPM1, dolichol phosphate mannosyltransferase; GPT, dolichol phosphate N-acetylglucosamine-1-phosphotransferase; dol-P mannose, dolichol phosphate mannose; dol-PP-GlcNAc, dolichol pyrophosphate N-acetylglucosamine; OST, oligosaccharyltransferase; dol-PP, dolichol pyrophosphate Imlay and Odom, 2014

It is noteworthy that apicomplexans regulation with hormones does not appear to be restricted to ABA, as melatonin modulate intraerythrocytic cycle in *P. falciparum* (Koyama et al., 2013). Actually, this molecule is structurally similar to auxin, which is a phytohormone controlling among others, root branching and elongation, and acts in plants as a plant growth regulator under stress conditions (Arnao and Hernández-Ruiz, 2014). Lastly, it appeared that the treatment of *P. falciparum* and *T. gondii* with thiazuron a synthetic analog of cytokinins inhibits the parasite growth by downregulation of cyclin gene (Andrabi et al., 2018).

Several studies evidenced the role of isoprenoids in PTMs of proteins. For instance, it has been shown that the synthesis of dolichols in *Plasmodium* and especially *Toxoplasma spp.* and *Cryptosporidium spp.* is required for the N-glycosylation and biosynthesis of GPI anchor for membrane localization of proteins involved in the parasite survival (de Macedo et al., 2003; Debierre-Grockiego and Schwarz, 2010). Also, protein prenylation plays a key role in the growth of *Plasmodium*, which is inhibited by FOS or protein prenyltransferase inhibitors (Lell et al., 2003; Ha et al., 2015). In comparison, FOS is poorly effective against organisms from the other genera, proposing that protein prenylation and metabolism of isoprenoids differ between apicomplexans (Clastre et al., 2007; Nair et al., 2011). Also, it was found that *P. falciparum* as *E. coli* actively absorb FOS unlike *T. gondii*, mycobacterium and many other organisms. However, the FOS rapidly lose its efficacy against *P. falciparum* as outlined by the characterization of resistant strains (Armstrong et al., 2015; Guggisberg et al., 2018). In these studies, it was proposed that in FOS-resistant *Plasmodium* strains, the prenyl pool might not be provided through the MEP pathway. Although no mechanisms for the import of host cell prenyl substrates were characterized, experiments revealed that the growth of *Plasmodium* in the host cell is altered by statins, which could potentially inhibit the MVA pathway. In addition, complementation experiments with IPP reverses death following treatment with chloramphenicol, clindamycin, or doxycycline that cause loss of the apicoplast in *P. falciparum* by specific inhibition of apicoplast gene expression (Yeh and DeRisi, 2011).

Very recently, a viable *P. falciparum* strain was transformed to express cytosolic MVA pathway enzymes (MK, PMK, MPDC, IDI (**Figure 2**)), resulting in mutant PfMev parasite line (Swift et al., 2020). With this respect, feeding of the PfMev line with MVA allow parasite survival in the absence of the apicoplast disrupted by azithromycin or after loss of *dxr* function, which normally leads to parasite death.

Nevertheless, it was noticed that a minimum of 10  $\mu$ M MVA is required for bypass in PfMev, while the serum level is about 200 nM. Besides, proteomics studies have pointed out a lack of host isoprenoids biosynthesis in erythrocytes (Kakhniashvili et al., 2004; Goodman et al., 2007). Taken together these results support the hypothesis that precursors from the host MVA pathway can be used by *Plasmodium* to survive under protein prenylation inhibitors treatment, but the crosstalk of precursors and adaptation mechanisms remain unknown.

Given that protein prenylation occur in animals and apicomplexan parasites, also considering the crosstalk between host MVA and apicoplast MEP pathways in *P. falciparum* as mechanism of resistance, it becomes essential to provide a better description of adaptation mechanisms driving exchange of isoprenoid precursors and protein prenylation *in vivo*. In this regard, the study of protein prenylation mechanisms in a plant model becomes clearly relevant as somehow it encompasses both MVA pathway found in Human and MEP pathway in Apicomplexa

## 2.3 INSIGHT INTO PROTEIN PRENYLATION

### 2.3.1 Generalities

Protein prenylation can be considered as a rather prevalent post-translational modification, with up to 1-2% of a total proteome that might represent potential substrate candidates (Ochocki et al., 2014; Qureshi et al., 2018; Suprun, 2019). However, only four PPTs have been described in eukaryotes, a modest number compared to other classes of enzymes dedicated to post-translational modifications, such as protein kinases, phosphatases or methyltransferases (Walsh et al., 2005). All enzymes modify exclusively cysteinyl residues leading to chemically stable thioether linkages with a prenyl group. Modifications of RAS and related proteins (RHO, RAC, etc) refers to type-I protein prenylation between a single C-ter cysteinyl residue denoted by a CaaX motif and a farnesyl (F) or a geranylgeranyl (GG) hydrophobic prenyl group (**Figure 15**). The catalysis implies two enzymes: the protein-farnesyltransferase (PFT: EC 2.5.1.58) and the protein-geranylgeranyltransferase type I (PGGT-I: EC 2.5.1.59). Both are heterodimeric enzymes resulting from a common  $\alpha$ -subunit and a unique  $\beta$ -subunit, which holds substrate specificity. Indeed, the  $\beta$ -subunit functions in the recognition of a protein substrate and its so-called CaaX motif localized at the C-terminus side (**Figure 15**).

A second class of enzymes (PGGT-II; EC 2.5.1.60) catalyze the modification of RAB proteins in the presence of a RAB escort protein (REP). The enzymology refers to the transfer of two geranylgeranyl moieties onto two C-ter localized cysteinyl residues (Leung et al., 2006; Guo et al., 2008). The process is achieved when a RAB GDP dissociation inhibitor (RabGDI) recycles the prenylated RAB between the membrane and the cytosol. Based on enzymes structures and mechanistic analyses, an evolutionary origin premise has been proposed and suggests that PFT preceded PGGT-I and PGGT-II (Nguyen et al., 2010) (**Figure 16**). Lastly, but very recently, two studies revealed a third type of PPT (PGGT-III) catalyzing the transfer of geranylgeranyl onto farnesylated proteins such as YKT6 (UniProtKB-O15498) or FBXL2 (UniProtKB-Q9UKC9) both including an additional cysteine forming a CCaaX motif (Kuchay et al., 2019; Shirakawa et al., 2020). PGGT-III consists of orphan prenyltransferase  $\alpha$ -subunit repeat containing 1 (PTAR 1) and the  $\beta$ -subunit of PGGT-II (Kuchay et al., 2019; Shirakawa et al., 2020) (**Figure 17**).



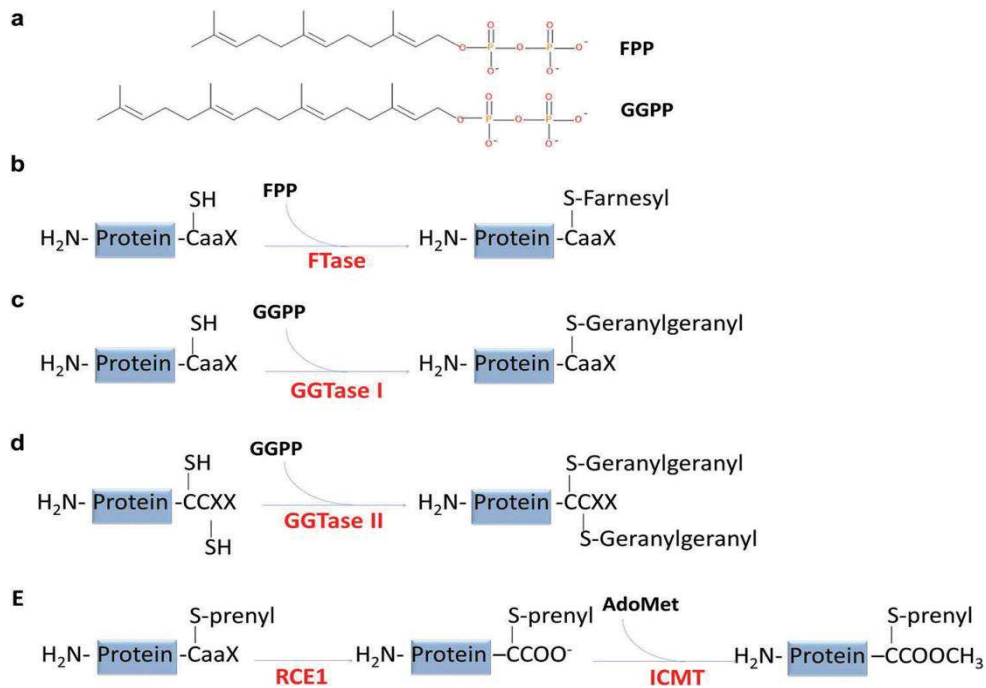


**Figure 15 Overview of prenylation reactions.**

(A) Isoprenoids substrates for prenylation (FPP, farnesyl diphosphate, Structure 1; GGPP, geranylgeranyl diphosphate, Structure 2). (B-D) Mechanism of action of farnesyltransferase (FTase) (panel B), geranylgeranyltransferase I (GGTase I) (panel C), and Rab geranylgeranyltransferase (RabGGTase or GGTase II) (panel D). (E) Processing of farnesylated or geranylgeranylated CAAX-proteins catalyzed by RAS-converting CAAX endopeptidase 1 (RCE1), which removes the -AAX residues, followed by isoprenylcysteine carboxyl methyltransferase (ICMT), which adds a methyl group from S-adenosylmethionine (AdoMet) to the carboxy-terminal isoprenoid-modified Cys residue. **Brioschi et al., 2017**

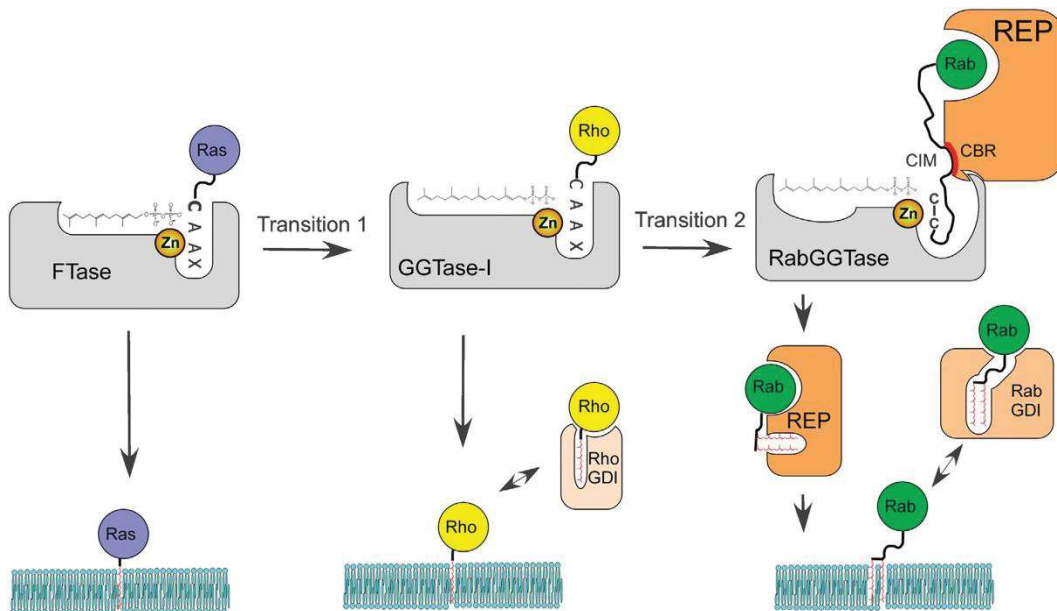


**Figure 16 Evolution of protein prenylation.**

Transition 1 represents expansion of the lipid-binding site of the ancestral FTase. Transition 2 represents invasion of the ancestral GGase-I by the bifunctional REP/GDI molecule. **Guo et al., 2008**

Accordingly, different combinations of farnesyl and/or geranylgeranyl moieties decorate prenylated proteins in eukaryotes. Nonetheless, the co-existence of at least four different enzymes captures the complexity associated to the need of modifying specific proteins in eukaryotes cells with specific prenyl groups or a special combination of molecules. Once prenylated, most protein substrates of type I PPTs undergo a necessary CaaX processing taking place in the endoplasmic reticulum (Hancock et al., 1991; Yalovsky, 2011). It has been proposed that prenylation of the protein is needed to provide enzyme's substrates on site (Choy et al., 1999). First, the three AA at the S-prenylated carboxyl-terminal are proteolytically cleaved by a metal-dependent CaaX endoprotease/Ste24 endopeptidase (RCE, EC 3.4.24.84). Then, the remaining isoprenyl cysteinyl residue at the new C-ter is methylated by a protein-S-isoprenylcysteine O-methyltransferase (ICMT, EC 2.1.1.100). Methylation neutralizes the negatively charged and hydrophilic cysteinyl residue to an uncharged, hydrophobic group, increasing membrane affinity by 2 to 10-fold (Parish et al., 1996; Bhatnagar and Gordon, 1997). This methylation step is the only reversible step within the whole process, calling isoprenylcysteine  $\alpha$ -carbonyl methyltransferase (ICME, EC 3.1.1.n2) for its demethylation to decrease protein hydrophobicity. Depending on the protein, the maturation steps are required for proper protein targeting, or not (Michaelson et al., 2005).

Regulatory mechanisms must take place after protein prenylation to adjust releasing and recycling of prenylated proteins, such as RAS proteins being involved in vesicular trafficking processes. For example, methylation considerably influences the prenylated proteins affinity for neutral interfaces. The former becomes effective specially for farnesylated proteins whose prenyl motif is very short and may not be hydrophobic enough to offset the charge from deprotected carboxyl function of the cysteinyl residue. A turnover has been observed, indicating that a cycle of methylation/demethylation would likely regulate prenylated proteins. Another hypothesis considers that carrier proteins could hide the prenyl moiety and thereby decrease the hydrophobicity of prenylated proteins. It has been evidenced that maturation steps can be shunted due to some CaaX motifs found to be "resistant" to post-isoprenylation events (Hildebrandt et al., 2016). Also, in a splice variant of *cdc42* (bCdc42), a CCIF motif appears to be prenylated, but postprenylation steps are bypassed, and therefore the protein is palmitoylated at the second cysteine (Nishimura and Linder, 2013).

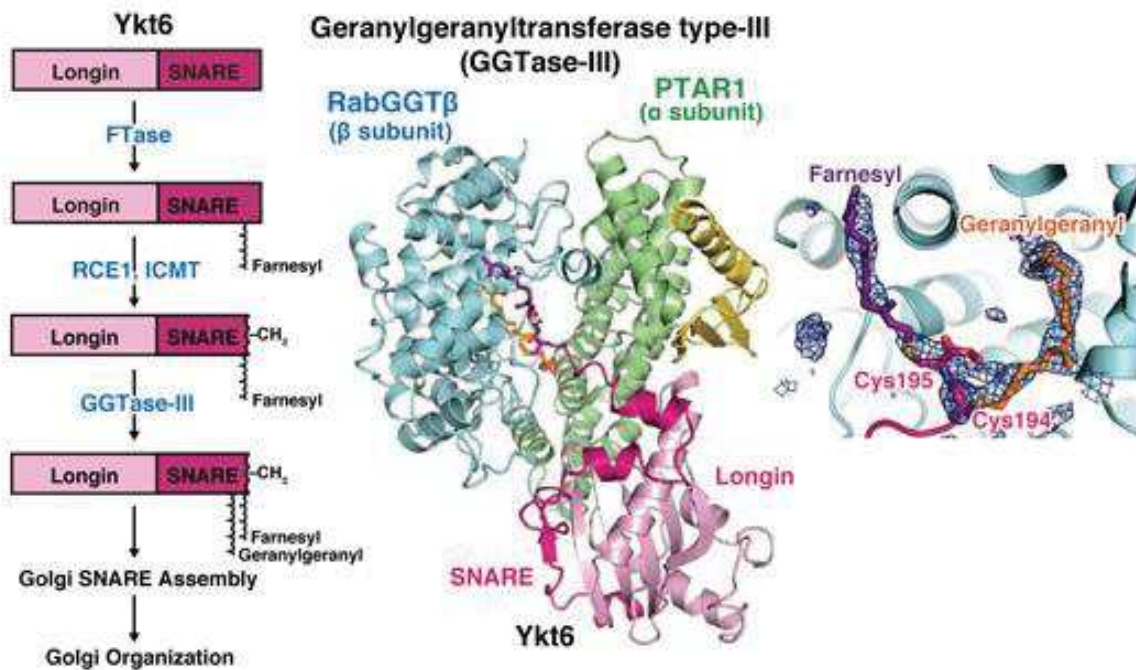


**Figure 17 Overview of Ykt6 prenylation by PGGT-III, a new orphan protein prenyltransferase.**

First, the Ykt6 protein which has a C<sub>2</sub> end is farnesylated on the first cysteine by the protein farnesyltransferase (FTase). Then, Ykt6 undergoes to the post-prenylation steps of proteolysis and carboxymethylation catalyzed by RCE1 and ICMT respectively. PGGT-III consists of PGGT-II B subunit (RabGGTB) and the orphan PTAR1  $\alpha$ -subunit. The PTAR1 subunit recognize the farnesylated Ykt6 and ensure the geranylgeranylation of the second cysteine. Finally, the prenylated Ykt6 is released from the PGGT-III active site prior to Golgi SNARE assembly. **Shirakawa et al., 2020**

Under those conditions, the protein does no longer interact with RhoGDI $\alpha$ , increasing its affinity especially for the plasma membrane as compared to ER and Golgi endomembranes. The authors also acknowledged that the absence of carboxymethylation of the prenyl and palmitoyl form of bCdc42 may contribute to its reduced affinity for RhoGDI $\alpha$  (Nishimura and Linder, 2013).

These examples definitely pictured how far maturation steps are part of the regulation processes for protein prenylation *in vivo*. Why does evolution conserved such a number of mechanisms to regulate the protein prenylation *in vivo*? How far organisms depend of prenylated proteins?

### 2.3.2 Function of Protein Prenylation in Animals

Prenylation promotes specific features to modified proteins including membrane anchoring, protein-protein interactions or modification of biological activities (Resh, 2006; Jeong et al., 2018). Many of those proteins are involved in signaling pathways coordinating cellular actions such as proliferation, differentiation, survival, metabolites biosynthesis and trafficking according to intracellular and extracellular environments (Jeong et al., 2018; Hála and Žárský, 2019). In this way, to be active, some enzymes require prenylation.

For instance, farnesylation is required for the binding of complexes as it was demonstrated for the recruitment of the human mitotic checkpoint protein Spindly to kinetochores (Moudgil et al., 2015). Taken together, it can be proposed that through protein interactions, not only the modified protein is associated with specific membranes, but also presumably participating in a whole protein complex. Besides, it has been evidenced that prenylation is also involved in protein conformational changes. The farnesylated PEX19 protein, serves as a chaperone and peroxisomal import receptor. For the biogenesis of peroxisomes, the modification is required to recognize cargo peroxisomal membrane proteins. Interestingly, in the 3D-structure of the farnesylated human protein, the prenyl group is not accessible for interaction with membranes suggesting other functions (Emmanouilidis et al., 2017). In other words, farnesylation induces a stiffening and compaction of the PEX19 C-ter domain that stabilizes the C-ter region, but also locks the arrangement of helix  $\alpha 1$  and the lid providing a hydrophobic binding surface needed for interactions with peroxisomal membrane proteins (Emmanouilidis et al., 2017). Likewise, YKT6, a SNARE protein, plays a critical role in membrane-trafficking processes through undergoing conformational changes, in which farnesylation make the SNARE domain unreachable for interaction with SNARE partners membrane fusion processes (Dai et al., 2016). Finally, it is believed that the localization of some proteins in the plasma membrane can be considered as an elegant way to store “ready to use” proteins (Yalovsky et al., 1999). Accordingly, the protein is awaiting specific cellular signals, which purports a relocalization into different subcellular compartments such as nuclei, where it can be quickly operational. It remains however unquestionable that many prenylated proteins are tethered to specific membrane structures likely related to other modifications (Aicart-Ramos et al., 2011; Nishimura and Linder, 2013; Jeong et al., 2018).

In fact, protein prenylation can only be considered as one of many different post-translational modifications regulating a protein activity and the specific subcellular localization needed for. A typical example including other post-prenylation lipidation is the starring farnesylated oncogene protein family p21RAS (Casey et al., 1989; Rocks, 2005). The K-RAS 4A, N-RAS and H-RAS proteins are subsequently palmitoylated *in vivo* (Hancock et al., 1989; Aicart-Ramos et al., 2011) (**Figure 18**). It is the use of this lipid combination that drives the accurate subcellular localization of the targeted protein. In this respect, the palmitoyl chains (C<sub>16</sub> saturated fatty acid) rather associate with the saturated chains of lipids and cholesterol molecules, reducing lipid lateral fluidity in lipid rafts (Zhang et al., 2018).

The lipid raft hypothesis proposes that cholesterol and saturated lipids have the ability to pack tightly into “liquid-ordered” domains (raft-like domains) in which lipids have a low diffusion rate, whereas unsaturated lipids constitute “liquid-disordered” domains (nonrafts domains) in which lipids are more fluid (Brown and London, 2000). In this respect, prenylated proteins are excluded from lipid rafts, while palmitoylated proteins make part of (Melkonian et al., 1999). Thus, the lipidation of RAS does not only favor membrane anchoring, but also alters dynamics between different cellular membrane compartments (Gelb et al., 2006). At first sight, palmitoylation enables membrane association in the absence of farnesylation (Booden et al., 1999). It was later clarified that while prenylation remains a critical and necessary step, the specific subcellular distribution of H- and N-RAS is generated by a constitutive deacylation cycle that operates on palmitoylated proteins, switching between the plasma membrane, recycling endosome and the Golgi apparatus (Rocks, 2005; Misaki et al., 2010) (**Figure 19**).

However, plasma membrane targeting is not only due to protein lipidation such as palmitoylation, myristoylation, but candidates’ proteins are also very often substrates for other type of modifications including, but not restricted to phosphorylation or nitrosylation (Khan and Singh, 2019). With this respect, it has been described that signaling events can affect the modification of protein by a prenyl moiety. For instance, the Rap11B protein, known to promote the formation and maintenance of adherent junctions in epithelial cells, is also substrate of protein kinase A (PKA) specifically phosphorylating two serine residues located at the C-ter polybasic region (Ntantie et al., 2013). The consequence is a delay of the prenylation process thus avoiding its plasma membrane localization (Ntantie et al., 2013).

**Figure 18 Enzymatic pathway for the modification of prenylated proteins.**

PFT attaches a farnesyl group to the C-terminal CaaX motif of specific cytosolic proteins. The farnesylated protein undergoes C-terminal aaX removal by the endoprotease Rce1p, and this is followed by S-adenosylmethionine (SAM)-dependent methylation of the COOH terminus by Imct; both modifications occur in the endoplasmic reticulum. Some proteins, such as N-Ras and H-Ras, are further modified after transfer to Golgi membranes by palmitoylation on one or two cysteines near the prenylated cysteine in a reaction catalyzed by DHHC9 and GCP16 in mammals (Erf2 and Erf4 in yeast endoplasmic reticulum membranes) and using palmitoyl coenzyme A (CoA) as the fatty-acid donor. After palmitoylation, fully lipidated N-Ras and HRas are transferred to the plasma membrane probably by vesicle transport. Other proteins, such as KRas, contain a polybasic region (KKKKKSKTK) next to the prenylated C terminus that is thought to bind the protein to the cytosolic face of the plasma membrane through electrostatic interactions with acidic phospholipids. PPO, pyrophosphate. Farnesyl groups are shown in blue and palmitoyl groups are red. **Gelb et al., 2006**

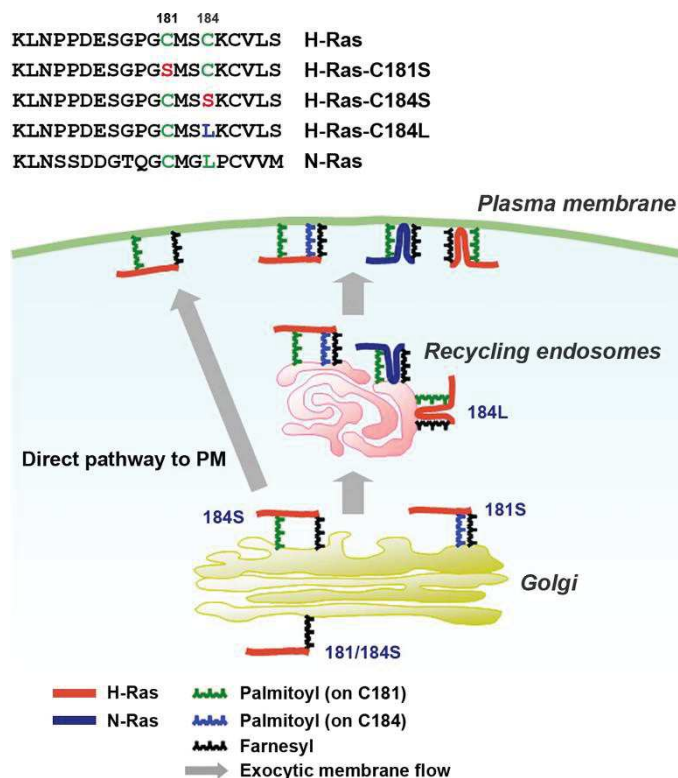
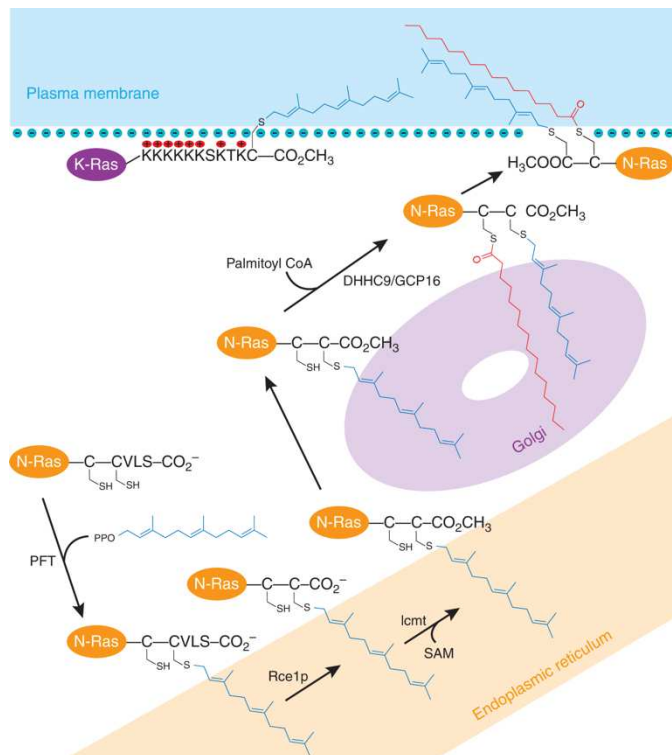


**Figure 19 Exocytic pathway of palmitoylated Ras proteins through REs to PM.**

The sequences of C-terminal 20-amino acid stretch of Ras proteins and palmitoylation deficient mutants used in this study are shown. After the exit from Golgi, H-Ras is first transported to recycling endosomes, then to PM. A palmitoyl group on C181 (green) is required to exit Golgi. Without the palmitoyl group on C184 (blue) upon the exit, mutant H-Ras (H-Ras-C184S) is directly transported to PM. L184 can substitute the palmitoyl group on C184 (H-Ras-C184L can access REs), which explains N-Ras residency on REs. **Misaki et al., 2010**

Even though protein post-translational modification contributes to the membrane targeting, the protein primary structure itself can also affect the location as exemplified by the polybasic domain contained at the C-ter of K-RAS (Hancock et al., 1990). Actually, some lipidated proteins contain such C-ter clusters of cationic AA residues dedicated for interaction with anionic lipid-rich domains, but also for sequestration of those lipids into membrane domains (Epanand, 2008; Janosi and Gorfe, 2010).

Commonly, RAS refers to a RAS superfamily of small GTPase comprising RAB, RAN, ARF and RHO (RAS homologous) proteins (Wennerberg, 2005). For example, RHO GTPases are important in the regulation of cellular functions such as cytoskeletal dynamics, cell motility, cell polarity, axonal guidance, vesicular trafficking, and cell cycle control (Jaffe and Hall, 2005; Hodge and Ridley, 2016; Phuyal and Farhan, 2019) (**Figure 20**). In the RHO geranylgeranylated CDC42 protein, the specific di-arginine motif within the polybasic C-ter domain is reported to bind specifically phosphatidylinositol 4,5-bisphosphate (PIP<sub>2</sub>) a major component of the inner leaflet of human cell plasma membrane (Johnson et al., 2012) (**Figure 21**). In addition, as all small GTPases, they require the loading of GTP and the effect of prenylation on this GTP loading process is well recognized. As a matter of fact, unprenylated Rho-GTPases accumulate in the GTP-bound form, suggesting that the rate of nucleotide exchange exceeds the rate of hydrolysis of GTP to GDP (Dunford et al., 2006; Golding et al., 2019). Although unprenylated Rho and Rac hydrolyze GTP, they are unable to interact with GTPase activating proteins (GAPs) *in vitro* resulting in GTP hydrolysis at uncatalyzed rates as compared to the prenylated counterpart which does not hydrolyze GTP (Molnár et al., 2001). Finally, to be biologically active, monomeric RAS associates first to the plasma membrane, in which its diffusion enables the formation of an active dimer, oligomer or nanocluster such as RAS-RAF, influencing its mobility within the membrane (Nussinov et al., 2019). Although the size of RAS multimeric forms decreases its lateral diffusion speed as compared to the monomeric form, it was argued that these variations may not play important function for the biological activity at this scale.



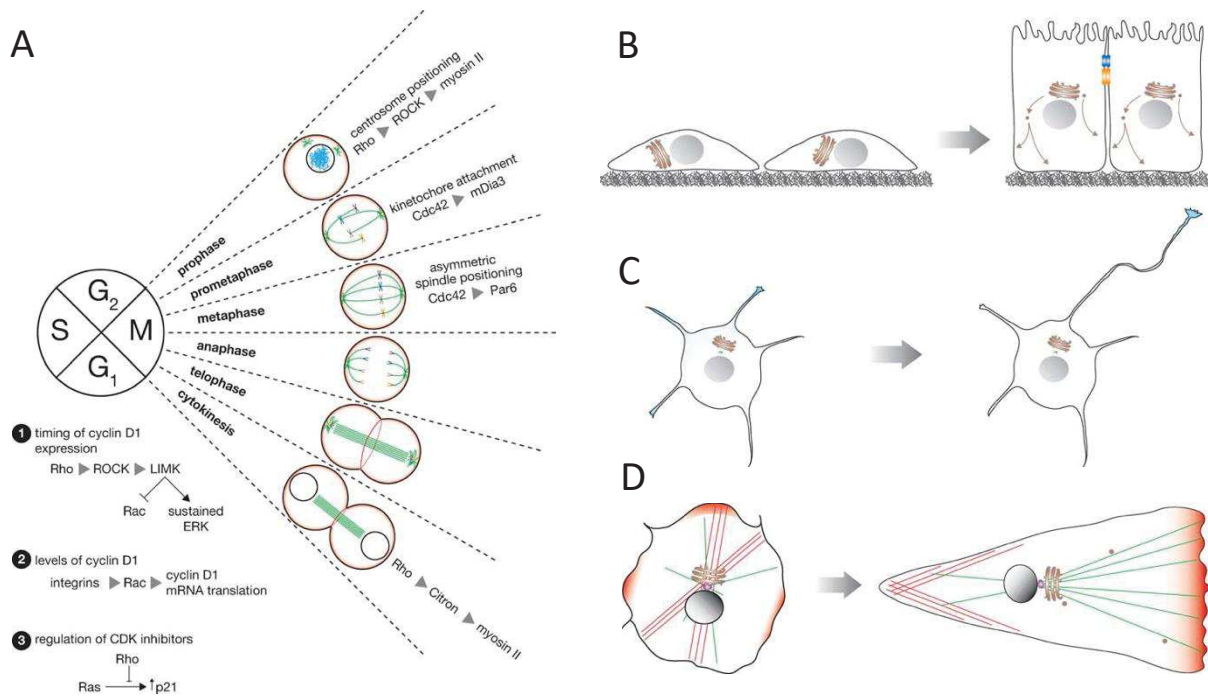
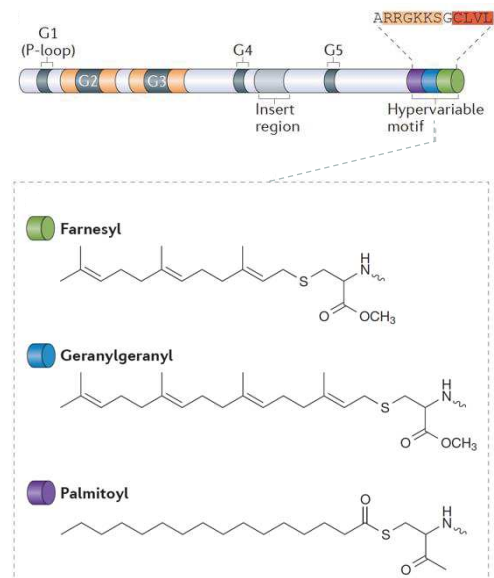


**Figure 20 Overview of Rho functions in animals.**

Rho GTPases and the cell cycle (A). Rho GTPases control multiple aspects of M phase and G<sub>1</sub> progression. The signaling pathways are shown for the relevant stages. Microtubules, (green); actin, (red); condensed chromosomes, (blue). Rho GTPases and Morphogenesis (B and C). Epithelial morphogenesis (B) involves cell-cell interactions leading to the formation of apical and basolateral domains (B), separated by tight junctions (blue) and adherens junctions (orange). Cell polarity is reinforced through the directed trafficking of vesicles from the Golgi (brown). Neuronal morphogenesis (C) begins with the establishment of axonal and somato-dendritic compartments. Rho GTPases and cell migration. Rho GTPases and cell migration (D). Cell migration requires actin-dependent protrusions at the front (red) and contractile actin:myosin filaments (red) at the rear. In addition, microtubules (green) originating from the centrosome (purple) are preferentially stabilized in the direction of migration allowing targeted vesicle trafficking from the Golgi (brown) to the leading edge. **Jaffe and Hall, 2005**

**Figure 21 Regulation of Rho GTPases by lipid modifications.**

General schematic diagram of Rho GTPase domain architecture and prenyl substrates. The G domain in Rho GTPases is highly conserved and is responsible for binding to guanine nucleotides. The G domain contains a variety of amino acid motifs responsible for GTP and GDP binding and coordinating conformational changes. The P-loop (phosphate-binding loop), also known as the G1 domain, is a conserved GXXXXGKS/T motif that is responsible for binding to the β<sub>γ</sub>-phosphate of the guanine nucleotide. Rho GTPase specificity is imparted through the hypervariable domain at the carboxyl terminus, which contains several important sequences (and shows the highest level of variability between Rho proteins). The highlighted sequence shown is taken from RhoA as an example. The CAAX motif (red) at the C terminus undergoes a variety of post-translational lipid modifications that are crucial for membrane targeting. They consist of isoprenylation, including farnesylation (green), geranylgeranylation (blue) and palmitoylation (purple). The lipid moiety tethers the Rho GTPase to the membrane and prevents free diffusion through the cytoplasm. Some Rho GTPases also contain a C-terminal polybasic region (orange) that immediately precedes the CAAX motif, containing several Lys and Arg residues, which provide a positively charged interface for membrane association. **Hodge and Ridley, 2016**



These examples emphasize the diversity of regulation mechanisms for protein prenylation, which is essential to the function of many prenylated proteins involved in critical step for the development, communication and adaptation of animal cells. The genome analysis of various animals suggests that a large number of prenylated proteins exist, including over 170 RAS proteins (*Colicelli, 2004*), but their functional characterization remains poorly investigated. The situation is even more critical in plants lacking RAS and in which only a dozen prenylated proteins have been characterized, whereas more than 800 proteins are potentially prenylable in *A. thaliana*.

### 2.3.3 Specific Function of Protein Prenylation in Plants

In the 90s, radiolabeling experiments using [5-<sup>3</sup>H]-mevalonolactone evidenced the presence of a 23 kDa labeled protein associated to thylakoids in spinach leaves (Swiezewska et al., 1993). Interestingly, it was found that prenylated proteins are not only modified with farnesol or geranylgeraniol, but also with polyprenols. Other experiments using spinach confirmed these results and precised the distribution of prenylated proteins in different subcellular fractions (Shipton et al., 1995; Parmryd et al., 1997; Parmryd et al., 1999). The cytosolic and microsomal fractions contained low levels of radiolabeled proteins as compared to nuclear, mitochondrial, plastids and plasma membrane fractions. Besides, a level of protein prenylation of 0.5 % was estimated, being similar to results obtained with yeast and mammals (Epstein et al., 1991; Shipton et al., 1995). Similarly, feeding of [<sup>14</sup>C]-MVA to tobacco BY-2 cells, demonstrated that membrane but also soluble fractions are labeled (Randall et al., 1993). Nevertheless, radioactivity was not totally recovered in those fractions as compared to the whole cell extract, proposing that other prenylated proteins were lost by proteolysis or associated to cell debris and thus discarded. Although, none of these proteins was characterized, comparison of protein sizes with human features suggested that lamin (about 55-66 kDa) as well as ras-like GTP binding proteins (about 21-31 kDa) were part of prenylated proteins in plants too (Randall et al., 1993; Shipton et al., 1995).

ANJ1 (UniProtKB-P42825) from *Atriplex numularia* was the first prenylated protein identified in plants (Yalovsky et al., 1999; Crowell, 2000) (**Table 1**). It is a farnesylated chaperone homologous to bacterial DnaJ regulating the Hsp70 chaperone activity. Hsp70 members are involved in the protein folding, the assembly of protein complexes or heat-shock responses, but the exact role of ANJ1 remains unknown. The farnesylation of ANJ1 is required for membrane targeting and function at high temperature, as shown by studies on the yeast homolog YDJ1 mutant (Zhu et al., 1993; Yalovsky et al., 1999). As reported, heat-shock increases prenylation of DnaJ, which localizes to the membrane of glyoxysome and likely in that of mitochondria (Preisig-Muller et al., 1994). The expression of ANJ1 in the yeast YDJ1 mutant rescued the default of protein import in ER and mitochondria (Randall and Crowell, 1999; Crowell, 2000). Recently, a quite complete study supported that farnesylation of Hsp40 chaperone J2 (=ANJ1), J3 (UniProtKB-Q94AW8) homologs influence the AGO1 association with rough ER membranes to act in small RNA-mediated gene regulation (Sjögren et al., 2018). Nonetheless, no molecular proof of the farnesyl moiety was afforded in this study.

**Table 1 Prenylated proteins reported in plant in 2020.**The protein prenylation and/or function was described by *in-vitro* or *in vivo* prenylation study.

Accession number	Function / Homology	CaaX	Prenyl	Function	Publication
<b>Transcription factor</b>					
A0A1P8AMJ8	AP1	CFAA	F	MADS box transcription (Inflorescence shoot to floral meristem transition,	Yalovsky et al., 2000
Q39081	CAULIFLOWER	CYAA	F	development of petals and sepals	Kempin et al., 1995
P33077	AUX2-11	CGGL	GG	Transcription factor (Repressor of early auxin response genes)	Caldelari et al., 2001
<b>Cell cycle regulators</b>					
Q9SZI2	NAP1-1	CKQQ	F	Cell expansion	Galichet et al., 2006
Q9ZUP3	NAP1-2	CKQQ	F		
Q94K07	NAP1-3	CKQQ	F	Growth response to ABA and salt	Liu et al., 2009
Stress tolerance					
Q94AW8	ATJ3/ Hsp40	CAQQ	F	Chaperone (Abiotic stress and RNAi regulation)	Sjögren et al., 2018
P42825	ATJ2/ANJ1	CAQQ	F		Zhu et al., 1993
<b>Plant hormones</b>					
Q94BQ3	ASG2	CTQS	F	Stress tolerance	Dutilleul et al., 2016
Q93WC9	AtIPT3	CLVA	F	Hormone (Biosynthesis of Isopentenyl-type cytokinin)	Galichet et al., 2008
Q940V4	CYP85A2	CSPY	F	Hormone biosynthesis (convert castasterone into brassinolide)	Northey et al., 2016 Jamshed et al., 2017
<b>Metal ion binding proteins</b>					
Q9C5D3	ATFP3	CTVM	F	Metal ion-binding protein	Dykema et al., 1999
<b>GTP-Binding proteins</b>					
Q38912	ROP6/RAC3	CSIL	GG (F)	Cell polarity	Sorek et al., 2011
O82480	ROP9/RAC7	CTAA	F (GG)	Modulator of auxin and abscisic acid	Lavy et al., 2002 Nibau et al., 2013
Q9FDX9	AGG1	CLIL	GG	GTP binding (defense response, auxin transport)	Zeng et al., 2007
Q93V47	AGG2	CSIL	GG		Sorek et al., 2010
<b>Other proteins</b>					
Q9MAB9	AtMUB1	CSVM	F		
Q9SW27	AtMUB3	CTIL	GG (F)		
Q9LSD8	AtMUB4	CTIM	F (GG)	Autophagy recycling, Vesicular trafficking	Downes et al., 2006
Q9SH14	AtMUB5	CCIL	GG (F)		
Q8GWJ6	AtMUB6	CTIL	GG		
P27164	PhCaM53	CTIL	GG	Ca <sup>2+</sup> signaling (sugar-sensing and sugar mediated transduction)	Manuel Rodriguez coneccion et al., 1999
Q40642	OsCaM61	CVIL	GG	Ca <sup>2+</sup> signaling	Dong et al., 2002
Q9SRQ3	PEX19	CCIM	GG (F)	Peroxisome organization, protein import into peroxisome membrane	McDonnell et al., 2016

Although, the loss of J2/J3 farnesylation does not impair the RISC assembly process, it appears to result in translocation of membrane-associated miRNAs towards the polysome-bound fraction. In this context, protein prenylation regulates some abiotic stress-response processes and part of the plant RNAi machinery.

Other prenylated proteins were so far reported, but only about 24 were more or less characterized *in vivo* (**Table 1**). For instance, a screening *in vitro* of isoprenylated proteins encoded by *A. thaliana*, *N. tabacum* and *Glycine max* cDNAs revealed the plant specific existence of a unique family of proteins containing metal-binding M/LXCXXC motifs (Dykema et al., 1999). Among those, NtGP4 (UniProtKB-M1CEC4) emphasizes the putative role of protein prenylation in the plant defense response to pathogen attacks. This geranylgeranylated protein contains two of three GTPase motifs and exhibits 42 % identity with *A. thaliana* AIG1 (UniProtKB-Q67Y39), which is thought to be involved in the resistance of *A. thaliana* to pathogens carrying the avirulence gene *avrRpt2* (Reuber and Ausubel, 1996; Dykema et al., 1999). Interestingly, a YopT and AvrPphB cysteine protease family were reported in some phytopathogenic bacteria such a *Yersinia sp* and *Pseudomonas sp*. These proteins inactivate prenylated Rho-GTPases like RhoAL63, RacL61 and Cdc42L61, by proteolysing near the C-terminus, releasing them from the membrane (Shao et al., 2002). This confirms the role of Rho-GTPases in plant defense against phytopathogen bacteria. In contrast, the geranylgeranylated AtGP1 (UniProtKB-Q9ZRD6) and NtGP1 (UniProtKB-M0ZUC8) exhibit significant homologies with the yeast v-SNARE protein Ykt6p, suggesting function related to intracellular docking and fusion of vesicles from the ER to Golgi apparatus (Dykema et al., 1999; Dai et al., 2016).

As in animals, the Rho protein Rop6/Rac3 is also described in plants and the homolog Rho1Ps protein from *Pisum sativum* is geranylgeranylated and involved in the calcium-mediated signal transduction to control the organization of the actin cytoskeleton in the movement of generative cell and growth of pollen tube tip (Crowell, 2000; Sorek et al., 2011). Several other small GTP-binding proteins were characterized *in vitro*, which likely indicate prenylation *in vivo* too (Randall and Crowell, 1999; Yalovsky et al., 1999). Nevertheless, at the beginning of 2000's, only prenylation of ANJ1, AP1 and CaM53 were confirmed to occur *in vivo* (**Table 1**). The MADS-box transcription factors from *A. thaliana* (AP1, CAULIFLOWER), *Antirrhinum majus* (SQUAMOSA), and silver birch (MADS3) are farnesylated and ensure not only the transition from inflorescence shoot to floral meristems, but also the development of sepals and petals. It

has been proposed that farnesylation of AP1 is required for an optimal binding of the transcription factor to DNA, and for the assembly of the active heterotetrameric form in the *A. majus* SQUAMOSA mutant (Yalovsky et al., 2000). Nonetheless, this hypothesis is still a matter of debate. In contrast, the petunia calmodulin CaM53 and the rice CaM61 are constitutively expressed and are involved in the regulation of calcium signaling (Rodríguez-Concepcion, 1999). Accordingly, the ectopic expression of CaM53 in *Nicotiana benthamiana* leads to necrosis and stunting unless the non prenylable CaM53, pinpointing the critical role of protein prenylation in the inactivation of calmodulin. Interestingly, the geranylgeranylation of CaM53 offset a nuclear C-ter tag, allowing membrane targeting of the protein rather than the nuclear targeting (**Figure 22**). Although the former is required for membrane targeting indeed, a polybasic domain drives the specific interaction of CaM53 with plasma membrane lipids (Caldelari et al., 2001). It was later shown that this behavior is also true for CaM61 and that carboxymethylation contribute to membrane localization too (Rodríguez-Concepción et al., 2000; Gerber, 2005; Gerber et al., 2009a). The plant members of the Membrane-anchored Ub-fold (MUB) proteins family illustrated by Related to Ub-1 (RUB1 or NEDD8), Small-Ub-like Modifier (SUMO), Autophagy (ATG)-8 and -12 and other (Downes et al., 2006) showed similar “switch-on” mechanism. Although the function of the AtMUB1 to 6 was not identified, it was demonstrated that AtMUB1 and AtMUB4 are farnesylated and AtMUB3, -5 and 6 are geranylgeranylated, while AtMUB2 is likely palmitoylated (Dowil et al., 2011; Park et al., 2011; Lu et al., 2016). Most of the time protein prenylation increases hydrophobicity and allows anchoring into different cell membranes. However, some proteins such as PEX19 and metal binding proteins or enzymes involved in biosynthesis of metabolites are localized in the cytosol or the nucleus even after prenylation (Dykema et al., 1999; Galichet et al., 2008; McDonnell et al., 2016).

Protein prenylation functions also as a regulator of hormones isopentenyl-type cytokinins biosynthesis (Galichet et al., 2008). Indeed, the farnesylated protein AtIPT3 (UniProtKB-Q93WC9) responsible for the first step of cytokinin biosynthesis is localized in plastids in the absence of prenylation. At the opposite, the farnesylated form is located in the cytoplasm/nucleus even if the 55 first AAs of AtIPT3 are described to function as transit peptide signal (Kasahara et al., 2004)

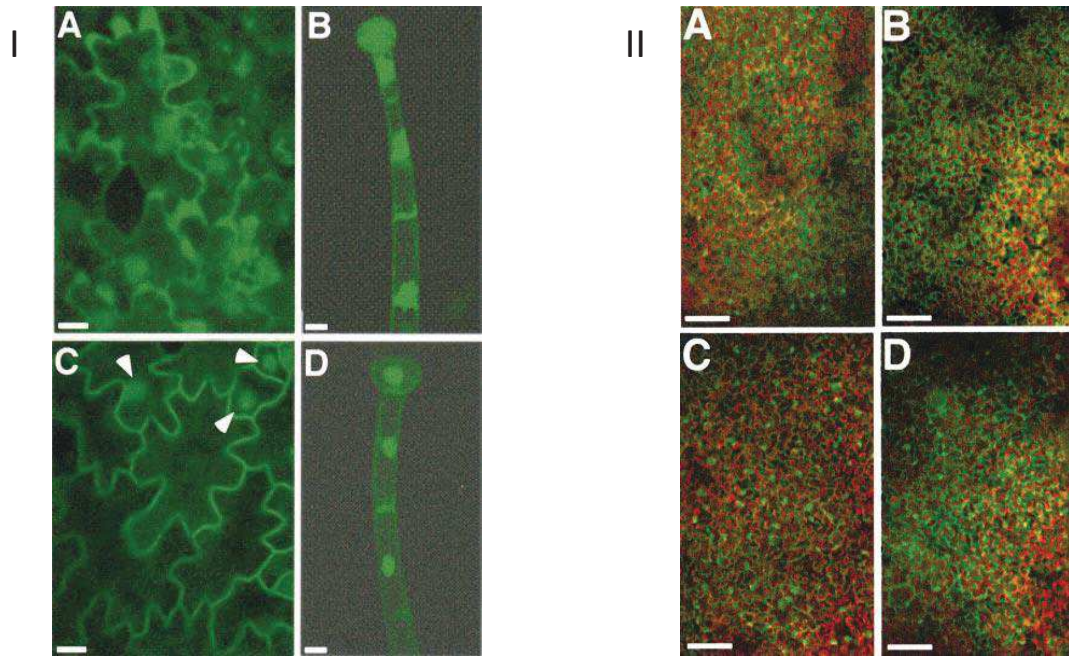


**Figure 22 Observation of GFP-CaM53 in plant material.**

(I) The CaM53 basic domain is important for subcellular localization in plants. Leaves from the *N.benthamiana* plants shown in Figure 4C were observed directly using CSLM. (A and B) Plant expressing sGFP-CTIL. (A) Leaf epidermis; (B) trichome. (C and D) Plant expressing sGFP-BDCaM53. (C) Leaf epidermis; the arrows indicate the position of nuclei. (D) Trichome. Bars indicate 10 mm. (II) Distribution of sGFP-BDCaM53 in leaf explants. Leaf explants from the *N.benthamiana* plants shown in Figure 4C were observed using CSLM after incubation for 72 h in the following conditions: (A) light, MS medium with 2% mannitol; (B) light, MS medium with 2% sucrose; (C) dark, MS medium with 2% mannitol; (D) dark, MS medium with 2% sucrose. Green fluorescence corresponds to sGFP-BDCaM53, and red fluorescence corresponds to chloroplasts. Bars correspond to 100 mm. **Rodriguez-Concepcion, 1999**

Interestingly, it appeared that the farnesyl acceptor cysteine-333 is involved in the catalytic activity, as AtIPT3 expressed in bacteria increased by 3-fold the IPP in the medium, while AtIPT3<sup>C333S</sup> was inactive. Accordingly, these results suggest that protein prenylation may not only act on protein localization and protein-protein interaction, but also directly on the active site of an enzyme (Galichet et al., 2008). Another example of hormone-biosynthesis prenylated enzyme is CYP85A2, a cytochrome P450 monooxygenase catalyzing the formation of brassinolide. This enzyme requires an ER localization to catalyze the formation of this plant steroid hormone from a membrane-localized sterol (campesterol), which then functions as a growth stimulator and stress tolerance actor (Northey et al., 2016). Besides, it has been proposed that this enzyme might initiate the formation of a metabolon allowing an efficient substrate channeling of the whole pathway within the ER, on which brassinosteroids would be synthesized (Vukašinović and Russinova, 2018).

A last example is illustrated with the ASG2 protein, which is putatively involved in ABA hormone signaling. The sequence of this Small GTPase contains a WD40 domain, tetratricopeptides repeats, a CaaX motif and a bipartite NLS signal (Dutilleul et al., 2016). The ASG2 protein DWD-box interacts with the DDB1 protein as substrate adapter in the E3 ubiquitin ligase complex. The subcellular localization of ASG2 has been shown to be dependent on the bipartite NLS signal and protein farnesylation. Actually, the results suggested that farnesylation of ASG2 does not enable an appropriate 3D conformation of the protein necessary to connect the bipartite NLS signal. Thus, the cytosolic farnesylated protein is relocated into the nucleus in the absence of prenylation, a situation similar to the CaM53 protein. Surprisingly, the ASG2 mutant showed ABA-related phenotype involving ABA, osmotic and salt sensitivities similarly to the *A. thaliana* *era1* mutant defective in PFT activity. In conclusion, it turns out that a number of functions of protein prenylation activities and prenylated proteins described in animals and yeast are valid in plants too. Although growth, reproduction, stress response, communication are common rules to live, each organism evolved with its own lifestyle, thus pushing up the diversity of prenylated proteins. Nevertheless, according to genomic and protein sequences recorded for *A. thaliana*, about 800 proteins have a CXXX signal, but only 200 are predicted to be prenylated using PrePS *in silico* analysis (**Figure 23**). Although the number of predicted proteins is likely insufficient, this analysis did not take into account the whole flexibility of PPTs protein substrate and every possible CaaX formation by alternative splicing, pointing the hidden face of the protein prenylation iceberg.



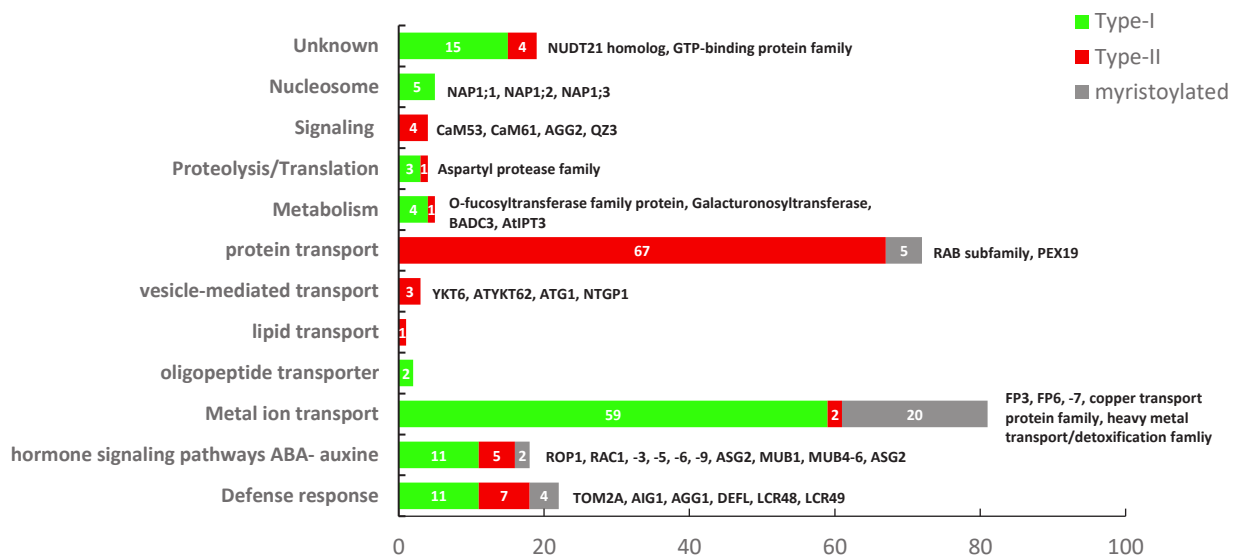


**Figure 23 Prediction of prenylated proteins in *A. thaliana* (2017).**

Sequences of about 800 proteins with a CXXX box were obtained from genomic databases. The set of data was refined using the PrePS algorithm (Maurer-Stroh et al., 2005) for Type I farnesylation and geranylgeranylation or Type-II geranylgeranylation. A total of 205 proteins were positive, of which 110 prenylated proteins were associated with Type-I prenylation (green) and 95 with Type-II geranylgeranylation (red). In addition, the myristoylation site being well characterized the latter was also include in the prediction model with the data subset (grey). Finally, the sequences of the 205 proteins were analysed using GPS-lipid prediction tool (Xie et al., 2016) to refine PrePS identification. Protein transport annotations were considered as Type-II geranylgeranylation by both PrePS and GPS-lipid. Nevertheless, Type-II geranylgeranylation within the other proteins was only associated to GPS-lipid prediction. Finally, a high variability was observed for Type-I prenylated proteins, illustrating the challenge of predicting protein prenylation site based on the current knowledge of canonical CaaX motifs. Sided, some unexhaustiv examples of genes or families annotated (Black bold). **A. Hemmerlin**

However, only homologs to PRL-1, Hsp40 and Pfykt6.1 proteins were characterized in the Apicomplexa phylum, illustrating a lack of visibility on all functions of prenylated proteins and prenylation mechanisms that occur *in vivo* (Pendyala et al., 2008; Ayong et al., 2011; Mathews et al., 2019). In fact, it appears that the consensus established for PPTs substrates in other eukaryotes differs from that of apicomplexans, limiting the prediction of prenylated proteins. Actually, in *Plasmodium* it has been shown that some sequences encode more than one protein, hence it is difficult to predict the cleavage of the primary sequence alone. Furthermore, routine molecular biology techniques such as PCR, vector expression is unappropriated to Plasmodium's genome, which DNA bas composition is really low in GC, making complicated the study of *P. falciparum* proteins in heterologous system. Taken together, these studies highlight a lack of knowledge not only about protein prenylation including PPTs activities and substrates selectivity, but also mechanism of protein prenylation adaptation to environmental conditions. The following section discusses the current knowledge available on the structure, activity and selectivity of PPTs in eukaryotes, calling the need to update the paradigm established more than 20 years ago.

### 2.3.4 Protein Prenyltransferase Activities and Selectivity

The biochemistry of type I protein prenylation has been carefully investigated and is well documented since decades (Casey, 1992; Gelb, 1997; Long et al., 2002; Scott Reid et al., 2004; Lane and Beese, 2006; Wang and Casey, 2016). Still, this research area is booming so far reflecting the constant interest for protein prenylation mechanisms. Both PFT and PGGT are metalloenzymes requiring  $Zn^{2+}$  and  $Mg^{2+}$  to be active (Reiss et al., 1992; Hightower and Fierke, 1999; Lane and Beese, 2006). The  $Zn^{2+}$  ion is bound close to the surface of the  $\beta$ -subunit by coordination with three strictly conserved residues D297 $\beta$ , C299 $\beta$ , and H362 $\beta$  in FTase and D269 $\beta$ , C271 $\beta$ , and H321 $\beta$  in GGTase-I (**Figure 24**). Besides, it was evidenced that the  $Zn^{2+}$  bication is involved in the catalytic activity to coordinate the cysteine thiol of the CaaX substrate. In contrast,  $Mg^{2+}$  binds to the D297 $\beta$  in FTase and D311 $\beta$  in GGTase for stabilization of the prenyl diphosphate as the bond breaks between the  $\alpha$ -phosphate and the C1 atom of the prenyl group, improving the PFT activity by up to 700-fold (Lane and Beese, 2006). The resolution of PFT and PGGT-I 3D-structures emphasize a substrate preference of PFT for FPP and PGGT-I for GGPP, providing a clear molecular picture of how prenyls are transferred (details reviewed Lane and Beese, 2006; Jiang et al., 2018). Accordingly, the prenyl diphosphate initially forms a PPT-prenyl diphosphate complex, then the CaaX protein gets into the active site at which the prenyl transfer onto cysteine is catalyzed (**Figure 25**). Once the prenylation reaction is ended, an inorganic pyrophosphate molecule is released, whereas the intake of a new prenyl diphosphate ejects the prenylated protein from the PPT active site (Long et al., 2002). The binding pocket for FPP has a well-defined length, and binding of GGPP at this site would leave the electrophilic carbon too far from the attacking sulfhydryl group of the prenyl acceptor (Park, 1997). Consistent with this idea is the fact that FTase binds FPP only 30 times as tight as it does for GGPP. In contrast, PGGT-I binds GGPP 300 times better than FPP, pinpointing the relative affinity of PPTs for their prenyls *in vitro*. Nonetheless it appeared that these specificities are relative to cellular context as under restrictive conditions, alternative prenylation occurs *in vivo*. For instance, inhibition with specific PFT inhibitors induces geranylgeranylation of RAS proteins to preserve a biologically active form (Whyte et al., 1997). Other resistance acquisitions have been described in *P. falciparum* involving Y837C substitution in the  $\beta$ -subunit of the PFT, affecting both affinity for the CaaX substrate and the tetrahydroquinoline inhibitor (Eastman et al., 2005).

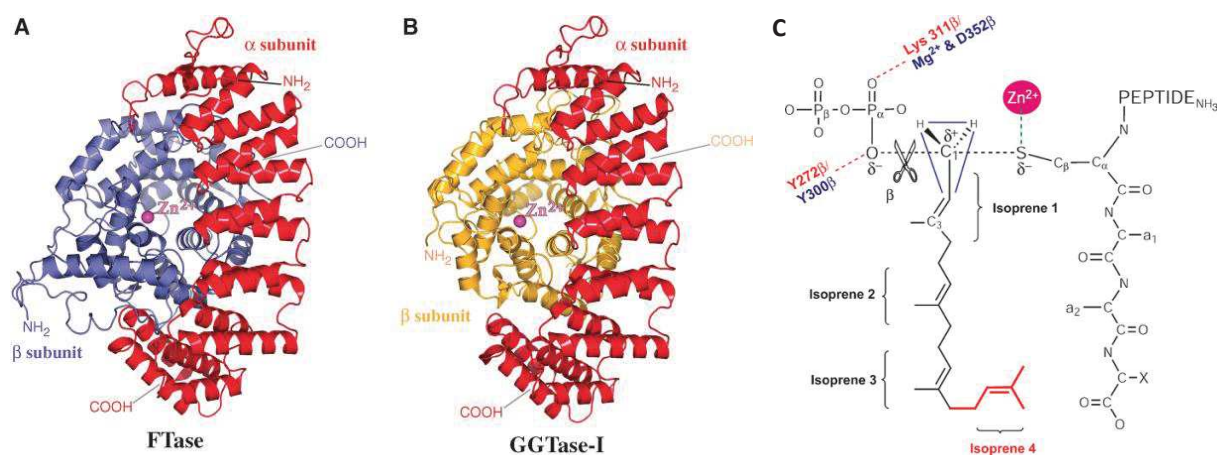


**Figure 24 Structures of the CaaX prenyltransferases.**

Overall structures of (A) FTase and (B) geranylgeranyltransferase type I (GGTase-I), with the  $\alpha$  subunit in red, the  $\beta$ -subunit in blue and yellow, respectively, and the catalytic zinc ion in magenta. (C) Proposed transition state model for the CaaX prenyltransferases. The scissile phosphoether bond between the diphosphate and prenyl groups and the nascent thioether bond between the CaaX cysteine and the prenyl group are shown as black dotted lines. Hydrogen bonds predicted to stabilize the phosphate in the transition state are shown as red dotted lines (residues of FTase are labeled in blue, GGTase-I in red). In this model, the magnesium ion, in turn coordinated by D352b, in FTase is replaced by K311b in GGTase-I. Lys, lysine.) **Lane and Beese, 2006**

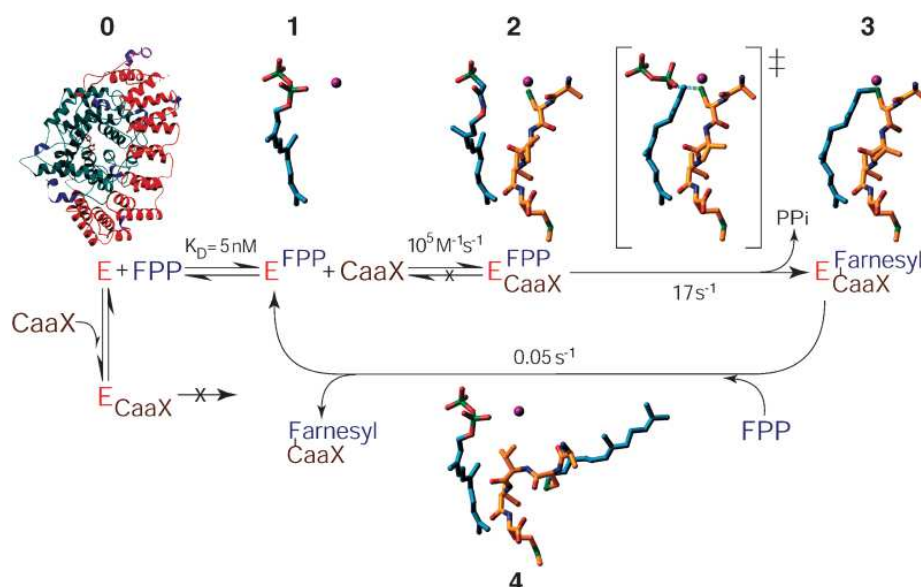


**Figure 25 Structures along the protein farnesyltransferase (FTase) reaction path.**

Crystallographic studies have produced structures representing the major steps along this path. In each of these complexes, the enzyme acts as a rigid scaffold; therefore, for clarity, only the substrates and products are shown as they bind in the active site. The path begins with the unliganded (apo) enzyme (0) [Protein Data Bank identifier (PDB ID) 1FT1], with the  $\alpha$ - subunit shown in red and the  $\beta$ -subunit in blue. The FPP molecule binds to form a binary substrate complex (1) (PDB ID 1FT2), followed by binding of the CaaX substrate to form a ternary substrate complex (2) (PDB ID 1D8D). The resulting farnesylated product remains bound in the active site (3) (1KZP). Excess substrate, particularly FPP, facilitates product displacement, demonstrated by a complex in which the new FPP molecule and the partially displaced product are bound simultaneously (4) (1KZO). The double dagger symbol indicates a modeled transition state along the reaction coordinate between 2 and 3 (see Fig. 12 for a more detailed view of the transition state). Throughout this figure, the isoprenoid is shown in blue, the CaaX in yellow, and the catalytic zinc ion in magenta. Also shown are the kinetic parameters determined for this reaction. **Lane and Beese, 2006**

Altogether, such observations provide a hint to metabolic flexibility of protein prenylation, but the exact mechanisms remain unknown. As suggested by the original paradigm, PPTs are supposed to catalyze reaction according to AA (X) of the CaaX box, driving the prenyl preference (F or GG) with respect of PFT and PGGT-I. First Ca<sub>1</sub>a<sub>2</sub>X motifs were defined as “C” corresponding to a prenyl-modified cysteine, “a1 and a2” to aliphatic AA (P, A, L, V or I) and X driving the nature of the prenyl group transferred onto the protein. Thus, when X corresponds to M, S, D, A, the protein substrate is recognized by PFT, while PGGT-I recognizes the substrate if X corresponds to L or P (Lamphear, 2012; Berger et al., 2018; Blanden, 2018). In addition, it has been shown that FTase discriminates between peptide substrates based on both hydrophobicity and steric volume of the side chain at the a<sub>2</sub> position (Houglund et al., 2009). Accordingly, several predictive algorithms were designed and successively refined to ascertain that a protein sequence may potentially be prenylated by type-I or type-II PPTs (Maurer-Stroh and Eisenhaber, 2005; Maurer-Stroh et al., 2007; Hussain et al., 2019) (our example: **Figure 23**).

Several studies were carried out to validate substrate prediction *in silico*, using an *in vitro* prenylation assays with purified recombinant PPTs and CaaX-protein substrates produced in heterologous systems. For instance, the farnesylation of metal binding protein ATRP, NTRP and GMFP homologs have been identified using cDNA libraries of *A. thaliana*, *N. tabacum* and *G. max* (Dykema et al., 1999). Similarly, a screening using Swiss-Prot and TrEMBL databases with PROSITE syntax “C-[DEHKR]-[DEHKR]-[LIFV]->” leads to the prediction of 200 putative proteins including FBL2, which was characterized as a geranylgeranylated protein being involved in the replication of Hepatitis V virus (Wang et al., 2005). Another example using Prenylation Prediction Suite (PrePS, (Maurer-Stroh and Eisenhaber, 2005; Maurer-Stroh et al., 2007)) is offered by the characterization of cGMP phosphodiesterase (PDE $\delta$ ) as a small G protein from the Ras family, contributing to the phototransduction process in animals (Baehr, 2014).

Nonetheless, most of these predictions were established on the pattern of Ca<sub>1</sub>a<sub>2</sub>X but ignoring the flexibility of PPTs. Although type-I protein prenylation is documented as calling for Ca<sub>1</sub>a<sub>2</sub>X motif-containing protein substrates, this paradigm evolved over time. Furthermore, the PTMs were not taken into account as PPT and substrates were produced in bacteria.



Not surprisingly, alternative splicing seems to be a way to insert CaaX motifs into some proteins (Endo et al., 2020) (**Figure 26**). Moreover, recent studies highlighted an alteration of the CaaX consensus rules when analogs to FPP were used as prenyl donors (Jennings et al., 2016). As a matter of fact, the PFT selectivity can be tuned *in vivo* by expressing PFT active-site mutations generating enzyme variants (Hougland et al., 2012). With this respect, it can be speculated that natural selection could select similar variants under the pressure of inhibitors as observed for DXR with FOS (Armstrong et al., 2015). This, raises the issue of how important are modifications of the protein in adjusting enzyme activities and selectivity? More recently, bio-orthogonal chemistry has frequently been used to identify PPTs protein substrates and sketch prenylomes of organisms (Charron et al., 2013; Wang et al., 2014b; Dutilleul et al., 2016; Palsuledesai et al., 2016; Suazo et al., 2016; Suazo et al., 2018; Storck et al., 2019) (**Figure 27**). Despite the advantages offered by the purification of “clicked” prenylated protein *in vivo*, the matrix selectivity of the system is not absolute, and this method induce some artefacts. In fact, all those observations were made in a biased context, as only farnesyl or geranylgeranyl were considered as co-substrates to PPT. Besides, protein prenylation is dependent on the prenyl substrate level, hence feeding with alkyne-prenyl or epoxy-prenyl substrates analogs could induce prenylation of proteins not prenylated under physiological conditions (Hemmerlin et al., 2003; Hemmerlin et al., 2012). Still, this is of particular interest to study protein prenylation mechanisms and PPTs *in vivo* under physiological conditions as they are regulated by cells indeed. Altogether, these studies expanded the listing of possible protein substrates in a cellular context, increasing number of possible substrate proteins. To note, some proteins are substrates of a least two PPTs types demonstrating already a flexibility in adapting the possibility to modify a specific protein. Accordingly, RAB8 has been shown to be modified by both type I and type II GGTase (Wilson et al., 1998). Furthermore, it may be an open question finding out to what extent the nature of the prenyl diphosphate is restricted to FPP and GGPP as electrophilic alkyl donors? Are CaaX proteins and prenyl diphosphate exclusive substrates for PPTs? Several studies argue against this statement. In a quite early study, DTT has been identified as a plant PFT substrate on which FPP can be transferred *in vitro* (Parmryd et al., 1995). An investigation on thiol specificity, using the DTT and the glutathione in PFT assays, confirmed this observation but highlighted a much less efficiency (Hightower et al., 2001). This means, that while a thiol group is required, protein substrates are not indispensable for PFT to be active and opens new questions on unanticipated functions of PFT *in vivo*.



## 2.4 DEEP INTO THE FLEXIBILITY OF PLANT PROTEIN PRENYLATION MACHINERY

Plants developed compensatory mechanisms to modify protein with lipid entities (section 2.3.4). The question arising is to understand how important is it for the proteins' function to be modified with a specific molecule? Even though many articles describe protein prenylation and substrate specificities, only few of them focus on biophysical properties conferred by lipid moieties to proteins. Remarkably, specific lipid modifications are sufficient to sequester proteins into membrane microdomains of unique lipid composition or organization (Thissen and Casey, 1993).

### 2.4.1 Lethality in Animals and Fungi Protein Prenyltransferase Mutants

From the dawn of the first studies on protein prenylation, particular phenotypes have been characterized in yeast, animal and plant mutants loss of PPTs functions (Table 2). As early as the 90's, each yeast KO mutant of the PFT  $\beta$ -F (RAM1), PGGT-I  $\beta$ -GG (CDC43) and the  $\alpha$ -PPT (RAM2) were described (Goodman et al., 1990; He et al., 1991; Ohya et al., 1991; Ohya et al., 1996). The viable RAM1 mutant is thermosensitive, while the RAM2 and CDC43 mutants are lethal. At the opposite, the mutant RAM1 in *Cryptococcus neoformans* is lethal, and the equivalent of CDC43 null mutant in *Candida albicans* is viable but morphologically abnormal (Kelly et al., 2000; Vallim et al., 2004). Besides, the study of CaCDC43 mutant not only evidenced cross-prenylation by the CaPFT, but also supported the poor efficacy of a PGGT-I inhibitor (Kelly et al., 2000). To some extent, these findings argue for the flexibility of PPTs and divergence of prenylated proteins despite conserved process within eukaryotes.

Concurrently, the proximity between yeast and mammalian PPTs has been stated and the expression of cDNA from Rat homologue confirmed these data (Chen et al., 1991; Kohl et al., 1991). Nevertheless, the PFT and PGGT-I mutants were characterized post-2000 in mice by engineering PFT KO *Fntb*-mice and PGGT1b KO mouse cell lines (Mijimolle et al., 2005; Sjogren et al., 2007). The absence of PFT lead to early lethality, as crosses between PFT<sup>+/-</sup> failed to yield PFT<sup>-/-</sup> *Fntb*-mice mutant (Mijimolle et al., 2005; Lee et al., 2010).



**Table 2 Characteristics of protein prenyltransferase mutants described in yeast, animal and plant.**

The mutants are classified according to the mutated subunit, as  $\beta$ -subunit of protein farnesyltransferase (grey), protein geranylgeranyltransferase (green) and  $\alpha$ -subunit of protein prenyltransferase (blue). Mutations leading to a lethal phenotype have been highlighted in red.

Mutant	Phenotype	Reference
Fntb KO <i>M. musculus</i>	<b>Lethal but not in conditional line induced at 10d-old</b>	(Mijimolle et al., 2005)
RAM1 KO <i>S. cerevisiae</i>	Viable temperature sensitive	(He et al., 1991)
RAM1 KO <i>C. neoformans</i>	<b>Lethal</b>	(Vallim et al., 2004)
ERA1 KO <i>A. thaliana</i>	Viable growth delay, ABA phenotype	(Cutler et al., 1996)
GGtb KO <i>C. albicans</i>	Viable morphologically abnormal	(Kelly et al., 2000)
CDC43 KO <i>S. cerevisiae</i>	<b>lethal</b>	(Ohya et al., 1991; Ohya et al., 1996)
SR2-2 <i>D. melanogaster</i>	<b>lethal</b>	(Therrien et al., 1995)
PGGT1b <sup>fl/fl</sup> <i>M. musculus</i> fibroblasts	Not lethal Disruption of actin cytoskeleton, proliferation arrest and reduced migration	(Sjogren et al., 2007)
<i>ggb</i> <i>A. thaliana</i>	Viable ABA phenotype	(Johnson et al., 2005)
RAM2 KO <i>S. cerevisiae</i>	<b>lethal</b>	(He et al., 1991)
<i>plp</i> <i>A. thaliana</i>	Viable strong growth delay, ABA phenotype	(Running et al., 2004)

As a result, early embryogenesis processes such as cell proliferation, cell adhesion etc. were critically affected by the absence of PFT, inducing abortion of the embryos latest after 6 days. The absence of PFT had no effect on tumorigenesis of H-RAS and K-RAS cancer cell lines, but it reduced tumor progression these mice (Mijimolle et al., 2005; Lee et al., 2010). Consistent is the fact that compensatory mechanisms involving PGGT-I also exist in animal cancer cells, but this flexibility is indeed limited under standard conditions and does not balance the lack of the prenylation of all prenylatable proteins involved in animals' embryogenesis or cancer. Despite these results, the conditional PFT<sup>-/-</sup>;RERT<sup>ert/ert</sup> mice, in which the  $\beta$ -PFT gene was disrupted by inducible activation of CreERT2 recombinase (Cre-Lox recombination) during post-natal development (10-d-old) succeeded to live for over 18 months. However, PFT<sup>-/-</sup>;RERT<sup>ert/ert</sup> lines displayed delayed wound healing and maturation defects in erythroid cells, confirming the key role of prenylated proteins in cell proliferation and differentiation. Furthermore, the lack of PGGT-I activity in a PGGT1b KO fibroblast cell line disrupted the actin cytoskeleton, reduced cell migration, and blocked the proliferation of fibroblasts expressing oncogenic K-RAS (Sjogren et al., 2007). Although, KO mutant of PGGT-I in mammalian are lethal as in *Drosophila melanogaster* (Therrien et al., 1995), the conditional inactivation of PGGT1b improved survival and reduced lung tumor formation and myeloproliferation in conditional K<sup>LSL</sup>LC mice expressing mutated K-RAS<sup>G12D</sup> after Cre-Lox recombination (Sjogren et al., 2007). Remarkably, the cell proliferation was not arrested in PGGT1b KO lung tumor cells and bone marrow as compared to fibroblast, supporting the fact that other mutations or an alternative prenylation by PFT might compensate for the absence of PGGT-I activity.

Overall, the significant lethality induced by the absence of any of the PPTs emphasizes not only the importance of protein prenylation in the development, differentiation and stress responses of animal, but also the flexibility of protein prenylation mechanisms that occur in tumor cells or specific cell type. Nevertheless, no detailed report of the mechanisms involved in the flexibility of PPTs activities has been described, leaving a blank in this fascinating puzzle. In contrast, viable KO mutants of PPTs have been described in *A. thaliana*, showcasing the flexibility of protein prenylation in plants too, enabling to study this biochemical process.

## 2.4.2 How Do Plant Mutants of Protein Prenyltransferase Survive?

There are three kinds of viable *A. thaliana* KO mutants affected in protein prenylation (**Table 2**). First, *era1* (Enhanced Response to ABA 1), in which the  $\beta$ -F subunit of the PFT is inactivated either by deletion, chemical mutation, silenced gene expression or insertion of a T-DNA (Cutler et al., 1996; Caldelari et al., 2001; Johnson et al., 2005; Galichet et al., 2008; Goritschnig et al., 2008; Dutilleul et al., 2016; Sjögren et al., 2018). Hence, *era1* expresses only PGGT as an active type 1 enzyme. Similarly, the unique mutant *ggb-2* is mutated within the  $\beta$ -GG of the PGGT-I and expresses only the PFT (Johnson et al., 2005). Finally, in *plp* both PFT and PGGT-I genes are disrupted inactivating the common  $\alpha$ -subunit of PPTs (Running et al., 2004). To some extent, the latter shows a rather sick phenotype, but it can be handled to growth and reproduction under mild conditions (light quality and photoperiod). For instance, phenotypes are enhanced under short-day growth conditions (Yalovsky et al., 2000), and blue light promotes stomatal opening in the *era1* mutant as compared to red light (Jalakas et al., 2017).

In plants, stomata are key interfaces for gas exchange including CO<sub>2</sub> uptake necessary for photosynthesis as well as water loss for thermic and hydric regulation by evapotranspiration (Long et al., 2002; Buckley, 2019). All three Arabidopsis mutant plants exhibit an enhanced response to ABA as outlined by permanent stomatal closure without any water deficit. In comparison to *ggb-2* (Johnson et al., 2005), the *era1* mutant is definitely more affected in growth, flowering and displays different sensibilities towards environmental factors (Pei, 1998; Yalovsky et al., 2000; Brady et al., 2003; Andrews et al., 2010; Wu et al., 2017; Sjögren et al., 2018) (**Figure 28**). From this can be concluded that PFT (the enzyme remaining in *ggb* but absent in *era1*) should be the most flexible enzyme. Andrews *et al.* characterized enzyme protein substrate specificity *in vitro* using recombinant *Arabidopsis* enzymes (Andrews et al., 2010). In this study, PFT exhibits little specificity for the terminal AA of the CaaX motif and PGGT-I exclusively modifies CaaX protein acceptors with a leucine in the terminal position (Andrews et al., 2010). Moreover, it also supports that substrate specificities are determined primarily by reactivity rather than binding affinity. Furthermore, it was proposed that prenylation of AGG1 and AGG2 in *A. thaliana* may be indifferently prenylated by PFT or PGGT-I as shown by effective prenylation in *ggb-2* mutant and earlier with AP1 (Yalovsky et al., 2000; Zeng et al., 2007).

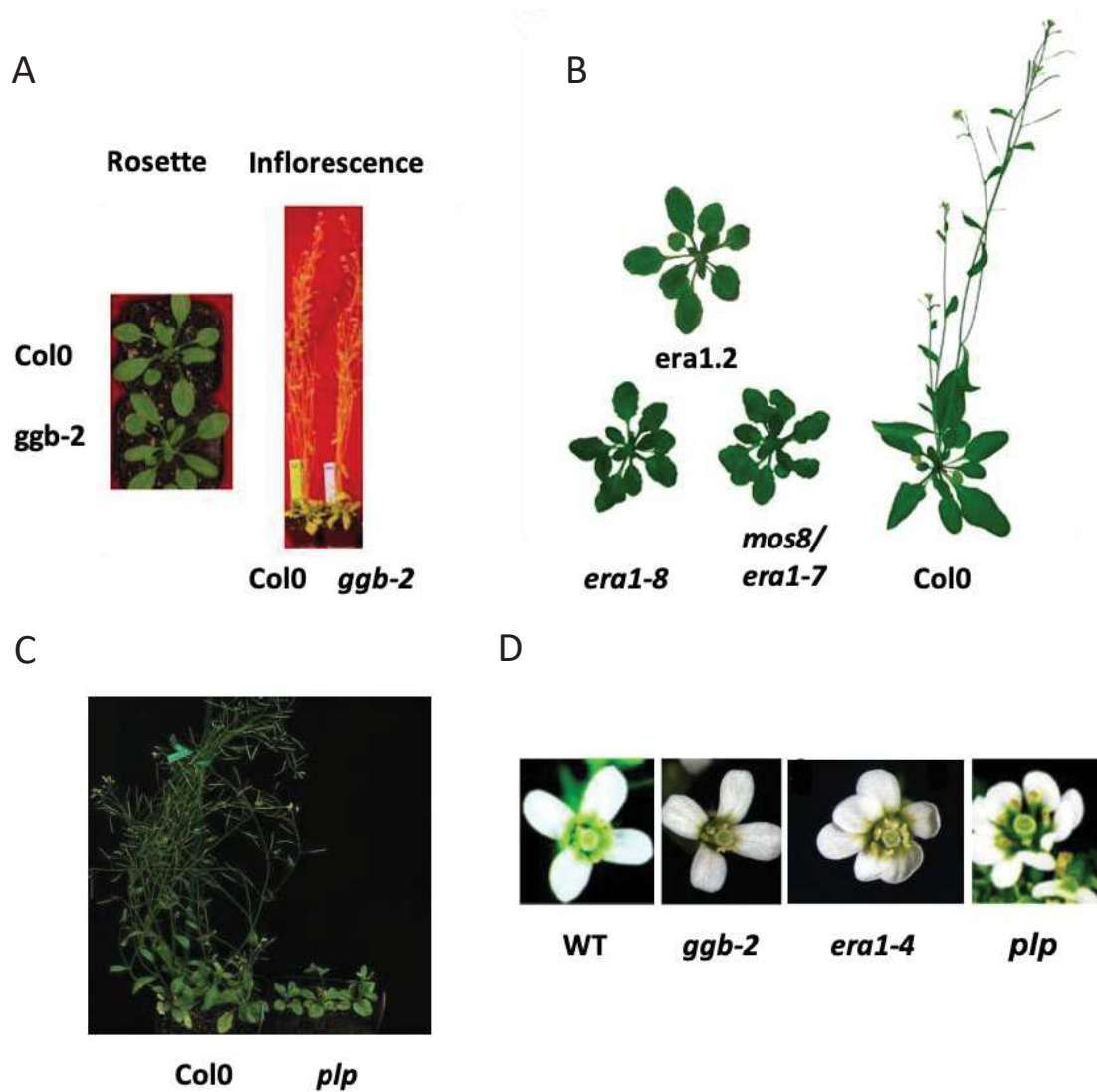


**Figure 28 Overview of *A. thaliana* protein prenyltransferases mutants *era1*, *ggb-2* and *plp* (reconstitution from different articles).**

Growth and morphology of wildtype and *ggb-2* mutants of Arabidopsis. (A) Rosettes, inflorescences, and flowers of Col0, and *ggb-2* are shown **Johnson et al., 2005**. (B) Two additional alleles of *era1* display the same late-flowering phenotype as the *mos8* (*era1-7*) single mutant. Pictures were taken at 7 weeks after planting **Goritschnig et al., 2008**. (C) Wild-type Arabidopsis plants (Left) and *plp-1* plants (Right) 38 days after stratification **Running et al., 2004**. Comparison of flowers from Wild-Type (WT) and arabidopsis mutant *ggb-2*, *era 1-4* and *plp* (D). Based on **Running et al., 2004 and Johnson et al., 2005**.

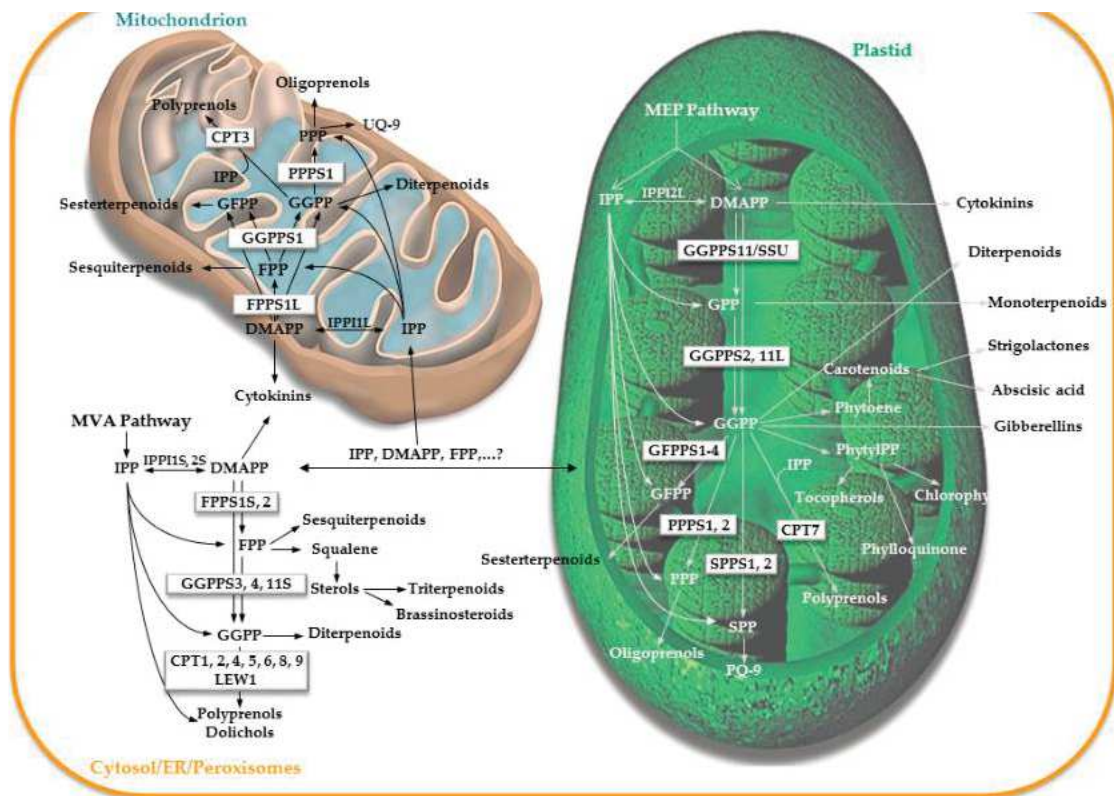
It turns out that the PGGT-I might also be flexible because unless the growth delay, *era1* exhibit a much weaker phenotype than *p/p* mutant (Johnson et al., 2005).

Interestingly, the  $\beta$ -GG subunit of PGGT-I was still detected in the *p/p* mutant as compared to the  $\beta$ -F of the PFT, supporting that PGGT-I subunit is not destabilized by the absence of an  $\alpha$ -subunit, and therefore could complement the lack of PFT activity in these conditions (Running et al., 2004; Johnson et al., 2005). Still, mystery surrounds the fact that other  $\alpha$ -subunit are reported raising the question: is another  $\alpha$ -subunit able to form active PGGT-I? Subsequently, what  $\alpha$ -subunit could be associated to the PGGT-I and how plant cells manage to build this recovery engine?

Although the dynamic flexibility of PPTs activities remain fuzzy, important features about isoprenoids crosstalk have afforded and propose that MVA and MEP pathways allow plant to adapt PPT substrate selectivity depending on precursors available.

### 2.4.3 Isoprenoids Crosstalk, a Keystone in the Flexibility of Protein Prenylation in Plants

A particular metabolic dynamic occurs in plants: as sessile organisms, they have to adapt continuously and quickly to their environment. With this respect, an example of adaptation is the supplying of isoprenoid precursors *via* the MVA and MEP pathways (Hemmerlin et al., 2012; Vranová et al., 2013). The unusual organization of IPP biosynthesis in plants has several advantages. First, it allows to study the enzyme involved in the process of protein prenylation by using the viable PPTs mutant's loss-of-function characterized. Second, as far as FPP is biosynthesized by the MVA pathway and GGPP by the MEP pathway, it is possible to study origin of prenyl substrates for protein prenylation using MV (MVA inhibitor) and FOS (MEP inhibitor). The Incorporation of radiolabeled-MVA or mevalonolactone was the main approach used to prove protein prenylation leading to the believe that in plants, like in yeast or animals, the MVA pathway was the unique source to provide precursors (Kamiya et al., 1978; Hancock et al., 1989; Randall et al., 1993). These hasty conclusions were offset at the beginning of 2000s, as proteins were found to be labeled following feedings of tobacco cells with radioactive 1-deoxy-D-xylulose (DX), a precursor of the MEP pathway (Hemmerlin et al., 2003). When DX vs MVA incorporations were compared, DX was found to be a better substrate than MVA. Another technical artefact was an almost systematic utilization of statins, such as MV before addition of labeled MVA to plant tissues or cells. It was wrongly expected to thereby avoid some endogenous dilution, omitting the crosstalk with MEP precursors induced by inhibition of MVA pathway (Hemmerlin et al., 2012). The involvement of the plastidial MEP pathway to provide prenyl diphosphates used as PPTs substrates was proven latter ([Gerber et al., 2009](#); [Hemmerlin et al., 2012](#)). In fact, the biosynthesis of prenyl diphosphate substrates in plants depends upon the activity of FDS and GGDS enzymes encoded by gene families and expressed in different subcellular compartment presumably in multienzyme complexes (Kopcsayová and Vranová, 2019) (**Figure 29**). In contrast, in animals and fungi, the activity of short chain prenyltransferases is restricted to a unique FDS and GGDS (**section 2.2.1**).



Enzyme				
Acronym	Name	EC Number	AGI	Gene Model
GPPS	Geranyl diphosphate synthase <sup>b</sup>	EC 2.5.1.1	At4g36810	GGPPS11L <sup>a</sup> / /At4g38460
			At5g47770	FPPS15 <sup>a</sup> FPPS1L <sup>a</sup>
FPPS	Farnesyl diphosphate synthase	EC 2.5.1.10	At4g17190	FPPS2
			At1g49530	GGPPS1
GGPPS	Geranylgeranyl diphosphate synthase	EC 2.5.1.29	At2g18620	GGPPS2
			At2g18640	GGPPS3
			At2g23800	GGPPS4
			At4g36810	GGPPS11S <sup>a</sup> At4g36810
GFPPS	Geranylfarnesyl diphosphate synthase	EC 2.5.1.81	At3g14530	GFPPS1
			At3g14550	GFPPS2
			At3g29430	GFPPS3
			At3g32040	GFPPS4
PPPS	Polyprenyl diphosphate synthase	EC 2.5.1.91	At2g34630	PPPS1
SPPS	Solanesyl diphosphate synthase	EC 2.5.1.85	At3g20160	PPPS2
			At1g78510	SPPS1
CPT	cis-Prenyltransferase	EC 2.5.1.87	At1g17050	SPPS2
			At1g11755	LEW1
			At2g23410	CPT1
			At2g23400	CPT2
			At2g17570	CPT3
			At5g60510	CPT4
			At5g60500	CPT5
			At5g58780	CPT6
			At5g58770	CPT7
			At5g58782	CPT8
At5g58784	CPT9			

Abbreviations: EC, Enzyme Commission; AGI, The Arabidopsis Genome Initiative.

<sup>a</sup> Alternative transcription start site.

<sup>b</sup> Heterodimeric GPP synthase.

**Figure 29 Topology of the prenyltransferase genes within the isoprenoid pathway of *A. thaliana*.**

Based on the isoprenoid pathway network constructed by Vranová et al. 2011.

Abbreviations of the enzymes in boxes are given in the table.

MVA, mevalonate;

MEP, 2-C-methyl-D-erythritol 4-phosphate;

IPPI, isopentenyl diphosphate (IPP, C5)

isomerase; IPPI1S, 2S, short IPPI variants;

IPPI1L, 2L, long IPPI variants;

DMAPP (C5), dimethylallyl diphosphate;

GPP (C10), geranyl diphosphate;

FPP (C15), farnesyl diphosphate;

GGPP (C20), geranylgeranyl diphosphate;

GFPP (C25), geranylfarnesyl diphosphate;

PPP (C30), polyprenyl diphosphate;

SPP (C45), solanesyl diphosphate;

PQ-9, plastoquinone 9;

UQ-9, ubiquinone 9.

Adapted from (Kopcsayová and Vranová, 2019).

Unfortunately, despite 40 years of knowledge on protein prenylation and prenylomes in different organisms, conditions and mechanisms operating in the flexibility of PPTs have not yet been elucidated. It remains a challenge for the development of effective prenylation inhibitors. Discrepancies between the paradigm established initially and the reality, raise critical issues in the perception of the PPTs activities. In this context, a priority is to rethink the simplistic sketch offered by *in vitro* studies and to redesign approaches depicting the reality of protein prenylation mechanisms occurring *in vivo*, this under physiological conditions. Obviously, the perception of any phenomenon always depends on the frame of reference used to observe it, in this case on the tools deployed to characterize protein prenylation. What tools have been used to characterize protein prenylation at the molecular level? Why did they lead us to an inaccurate vision of protein prenylation? Ultimately in the interest of Man, what are the consequences for validation of prenylation inhibitors currently being developed?

The following sections address these aspects, leading to the problematic of this thesis and the proposed solutions to fill some historical gaps.





## 2.5 PURIFICATION AND ANALYSIS OF PRENYLATED PROTEINS: A 40-YEARS OLD STORY

### 2.5.1 The Bitter Taste of the Original Recipes in Animals and Yeast Studies

The first prenylated proteins reported in yeast and animal cells were RAS proteins and lamin B (Schafer and Rine, 1992). Typically, purified protein produced in bacteria or animal cell expressing prenylated protein were incubated with [<sup>3</sup>H] or [<sup>14</sup>C]-MVA, -FPP or -GGPP one hour after inhibition with MV to (Casey et al., 1989; Farnsworth et al., 1989; Hancock et al., 1989; Maltese and Erdman, 1989; Farnsworth et al., 1990b). Since different types of protein prenylation were described, it became necessary to adapt methods for the characterization of the protein and its prenyl moiety after both prenylation *in vitro* and *in vivo*. Very early, protocols were described for specific cleavage of protein-bound prenyl compounds and their analysis by thin layer chromatography (TLC), high-performance liquid chromatography (HPLC), gas chromatography (GC) coupled to a radioactivity flow detector, or GC coupled to mass spectrometry (GC-MS) (Farnsworth et al., 1990a) (**Figure 30**). The former concept was to cleave the thioether bond between cysteine and prenyl to release the prenyl moiety.

Thus, two methods were reported, using iodomethane which releases prenyl alcohols or Raney Nickel (Raney Ni), yielding allyle or alcane if hydrogenation over platinum is performed. As reported, the hydrogenation over platinum is usually carried prior to Raney Ni indeed, as several side reactions such as cyclisation or elimination can occur in unsaturated lipids. Even though these approaches can be used on the total protein fraction, purification, digestion with proteases and alkaline or acid hydrolysis were recommended to enrich protein or peptides of interest and limit contamination by non-covalently bound lipids. Then, if feeding experiments with radiolabeled precursors or substrates was performed, the lipids released after cleavage were generally extracted with organic solvents prior to analysis by HPLC or GC-FID radiometry. Another solution proposed was GC-MS, which enables differentiation of volatile lipids with respect to fragmentation spectra of references. For instance, the protein p21<sup>N-RAS</sup> produced in T15<sup>+</sup> cell (NIH-3T3 cell line murine expressing human N-ras proto-oncogene) to treated with [<sup>3</sup>H]MVA was immunoprecipitated and separated on SDS-PAGE gel. The radiolabeled p21<sup>N-RAS</sup> was then collected and digested with a mixture of endoproteases (Pronase). After digestion and freeze-drying, the prenylated peptides were extracted with hexane and then separated by TLC.

As compared to references (geraniol, farnesol, squalene, solanesol, dolichol), it was assumed that geranyl and farnesyl were mainly transferred on the p21<sup>N-RAS</sup> protein (**Figure 31**) (Hancock et al., 1989). However, a weak signal was observed likely at the dolichol level, suggesting uses of alternative substrate in protein prenylation. Although, the use of MV can be justified for the incorporation of [<sup>3</sup>H]MVA, it may be contested as it turns on mechanisms of protein prenylation dependent on the [<sup>3</sup>H]MVA concentration used being likely different from that at physiological levels. Unfortunately, the molecular analysis of prenyls was not thorough, for instance GGPP or alternative prenyls were not tested, and the authors did not have protein prenylation inhibitors to assess the flexibility of PPTs either. Thereafter, studies of the *ram1* mutant in yeast were published, revealing the ability of yeast control protein extracts to transfer [<sup>3</sup>H]FPP onto the recombinant p21<sup>N-RAS</sup> protein unlike the mutants (He et al., 1991) (**Figure 32**). It was found that the *ram1* mutant had lost the farnesylation ability. Regrettably, it was not shown that the viable *ram1 mutant* was unable to transfer alternative prenyl substrate on p21<sup>N-RAS</sup>.

Meanwhile, the protein prenylation *in vitro* of purified recombinant RAS2 was assessed with yeast soluble crude extract from the WT and the mutant *ram1* in the presence of [<sup>3</sup>H]MVA (Goodman et al., 1990). The analysis by GC-FID radiometry of prenyl released after Raney Ni cleavage of radiolabeled protein confirmed that RAS2 is farnesylated in the WT, unlike the *ram1* mutant (**Figure 33**). Furthermore, prenylation of Lamine B and a copurified protein was featured by the analysis of purified fragments from tryptic digestion of radiolabeled proteins from HeLa cells fed with [<sup>3</sup>H]MVA (Farnsworth et al., 1989; Farnsworth et al., 1990b). Accordingly, the purified radiolabeled fragments were cleaved by iodomethane or Raney Ni and analyzed using GC-FID coupled to radioactivity flow detector and GC-MS. To some extent, the results prone that lamin B is farnesylated (Farnsworth et al., 1989), while the fragment of copurified protein (Peak A 1000 Da) is geranylgeranylated (**Figure 34**) (Farnsworth et al., 1990b). Several other prenylated proteins were characterized following similar protocol (Farnsworth et al., 1990a). Prenyl moieties from purified proteins were detected and identified indeed, but in all these studies feeding with MVA may have altered protein prenylation, especially as no control without MVA was shown. Although Raney Ni with and without hydrogenation over catalytic platinum were compared, both steps may induce artifacts.

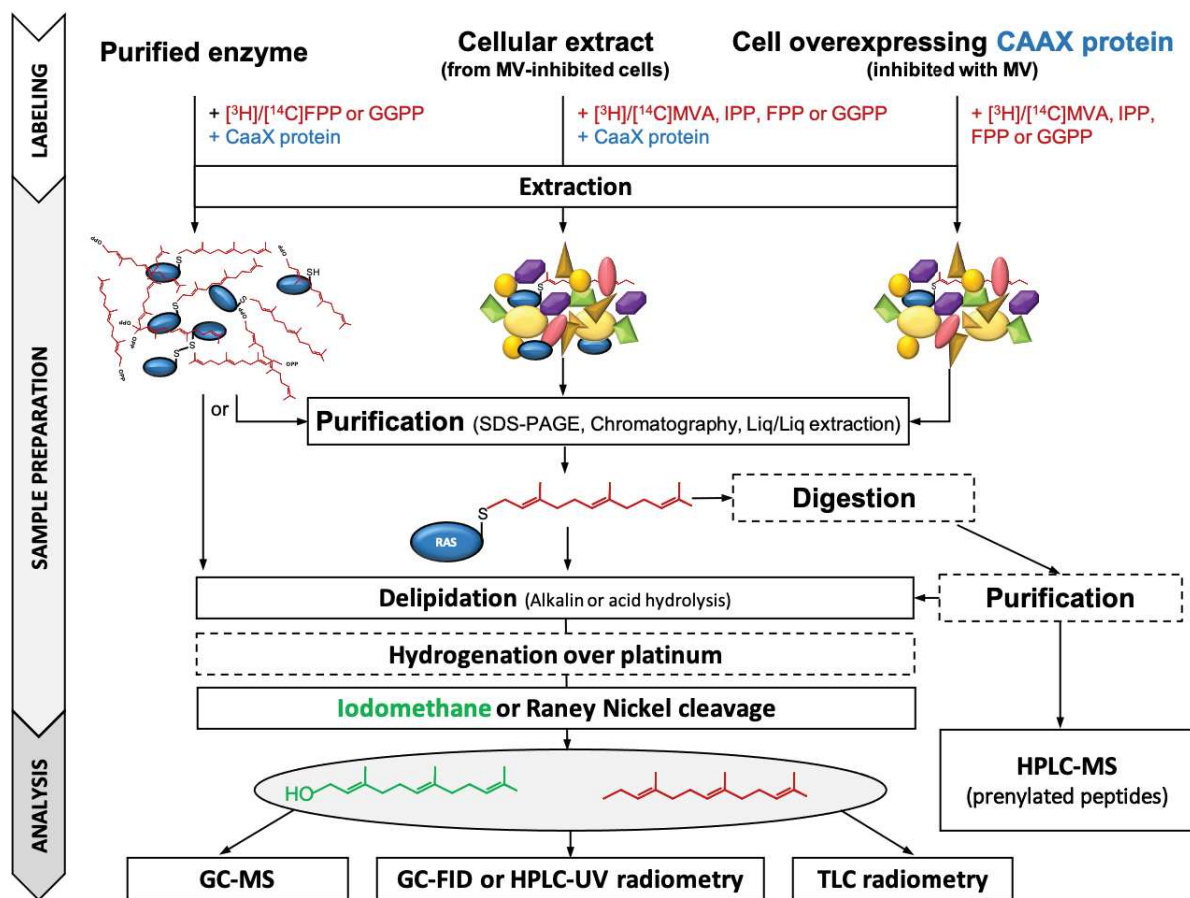


**Figure 30 Overview of protocols for the analysis of prenylated proteins *in vitro* and *in vivo* at a molecular level.**

Before 2000s, strategies characterized were using cell extracts containing native PPTs, cells overexpressing CaaX proteins or purified native and recombinant PPTs. Incorporation experiments were usually performed with CaaX protein (blue) and incubation with  $[^{14}\text{C}]$  or  $[^3\text{H}]$  mevalonate (MVA), isopentenyl diphosphate (IPP), farnesyl diphosphate (FPP) or geranylgeranyl diphosphate (GGPP) prenyl substrates (red) to visualize low abundant prenylated proteins. An inhibition with 5 to 50  $\mu\text{M}$  mevinoline (MV) 1 to 3 h was usually performed before feeding cells with radiolabeled substrates to limit dilution induced by endogenous prenyls. After extraction, the proteins were purified and analyzed either by SDS-PAGE alone or in combination with a thorough analysis of the prenyls by GC-MS or TLC, HPLC-UV and GC-FID radiometry or fluorometry. Accordingly, a delipidation was recommended to avoid non-covalently bound prenyls. The prenyl alcohols were released from the protein by iodomethane (green) or the prenyl allyle and alkane by Raney Nickel cleavage after or not hydrogenation on platinum. Finally, prenyls were extracted by an organic solvent and then analyzed. Variations between protocols are observed including protease digestion, other purification and after 2000 *de novo* analysis with HPLC-MS/MS started for the analysis of prenylated and peptides. Essential steps (solid line box), variable step (dashed line),

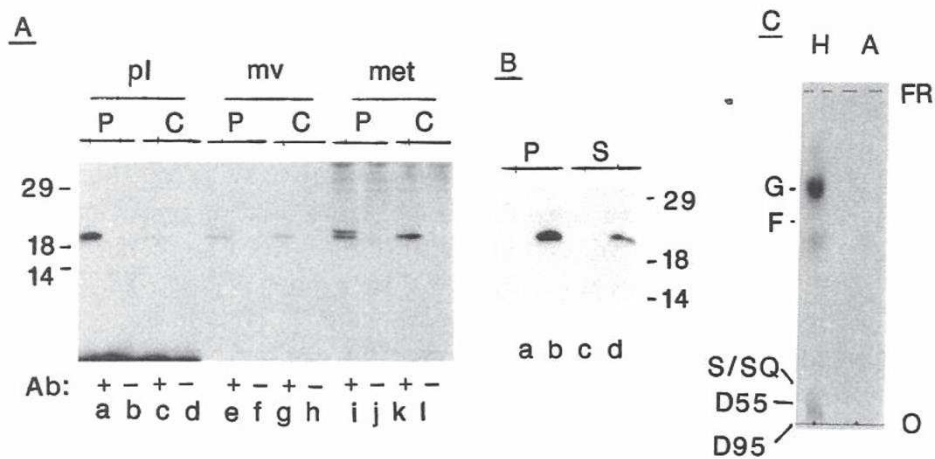


**Figure 31 p21<sup>N-RAS</sup> protein incorporate label from Mevalonic Acid into the Processed Forms as a Polyisoprenoid.**

(A) T<sup>15+</sup> cells were pretreated for 1 hr with mevinolin and pulse-labeled with [<sup>3</sup>H]mevalonate (mv) for 3 hr (p = pulse, lanes e + f) followed by a 3 hr chase with cold medium (c = chase, lanes g + h). Cultures untreated with mevinolin were labeled with [<sup>3</sup>H]palmitic acid (pl) as above (p = pulse, lanes a + b; c = chase, lanes c + d). To show the positions of pro-p21 and the processed forms c-p21 and m-p21 (not resolved in this gel), cells were labeled with [<sup>35</sup>S]methionine (met) for 10 min (P = pulse, lanes i + j, shows pro-p21) followed by a 3 hr chase (C = chase, lanes k + l, shows processed p21). Immunoprecipitations with antibody (+) or controls without (-) were resolved by SDS-PAGE and fluorographed for 7 days. (B) T<sup>15+</sup> cells pretreated with mevinolin (lanes b + d) or not treated (lanes a + c) were labeled for 6 hr with [<sup>3</sup>H]mevalonic acid and fractionated into S100 (s) and P100 (p) before immunoprecipitation and analysis as above. (C) [<sup>3</sup>H]mevalonic acid labeled p21<sup>N-RAS</sup> was immunoprecipitated from T<sup>15+</sup> cells and digested with pronase. The hexane (H) and aqueous (A) phases were analyzed by reverse-phase TLC followed by fluorography. Standards are listed in Experimental Procedures. O = origin, FR = solvent front, G = geranial (C10), F = farnesol (C15), SQ = squalene, S = solanesol, D = dolichol. **Hancock et al., 1989**

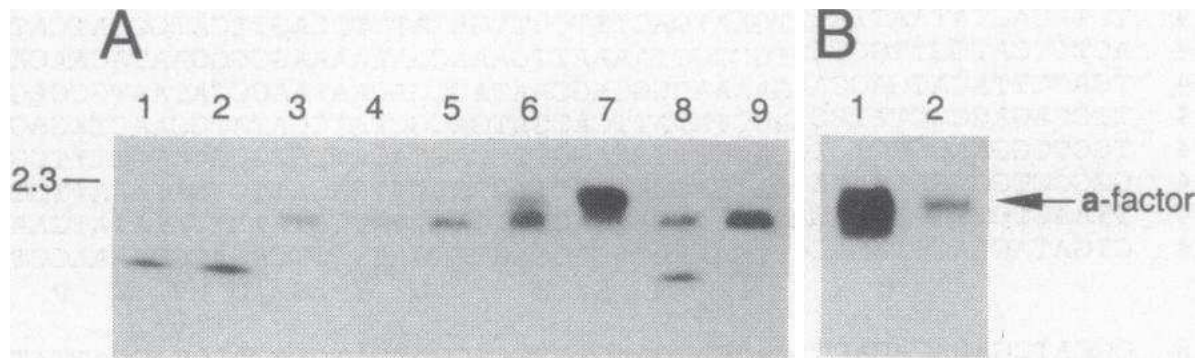


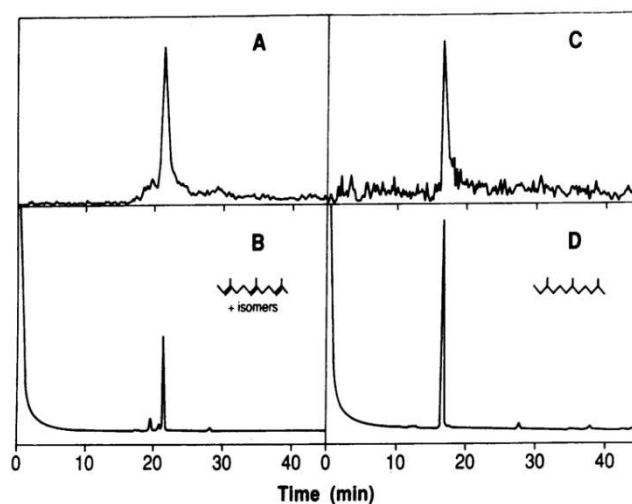
**Figure 32 SDS/PAGE analysis of  $\alpha$ -factor farnesyltransferase activity in *E. coli* extracts with p21<sup>N-RAS</sup>.**

(A) Farnesylation assays with the  $\alpha$ -factor quindecapptide substrate were performed (see text) and analyzed by SDS/PAGE and fluorography. Unless otherwise stated, all reaction mixtures contained buffer, [<sup>3</sup>H]FPP, the  $\alpha$ -factor 15-mer substrate, and an *E. coli* extract. Mock reactions are shown in which the *E. coli* extract and peptide substrate (lane 1) or *E. coli* extract only (lane 2) is absent. Lanes 3-7 display complete reactions containing extract from the control *E. coli* strain BHE-1 (lane 3), extract from BHE-2, which expresses RAM1 alone (lane 4), extract from BHE-3, which expresses RAM2 alone (lane 5), a mixture of extracts from BHE-2 and BHE-3 (lane 6), and extract from BHE-4, which coexpresses RAM1 and RAM2 (lane 7). Lanes 8 and 9 represent control reactions identical to that shown in lane 7 but with substitution with the 12-mer  $\alpha$ -factor substrate (lane 8) or no peptide substrate (lane 9). (B) Comigration of in vitro farnesylated  $\alpha$ -factor and authentic  $\alpha$ -factor. Lane 1, same reaction mixture as in lane 7 of A. Lane 2,  $\alpha$ -factor that was immunoprecipitated from the culture supernatant of a MATa strain that had been radiolabeled with [<sup>35</sup>S]cysteine. **He et al., 1991**

In fact, cyclisation and/or isoprenoids oligomerization may occur in a complex mixture containing AA, but also other molecules copurified with proteins (**Figure 35**)(Gregg, 1968; Croizy, 1987; Luo, 1995; Holte et al., 2012). Still, this step prevents secondary reactions between Raney Ni and prenyl unsaturations, it implies a risk of explosion with H<sub>2</sub> and autoinflammation with dry Raney Ni. On the top of that Raney Ni would not allow discrimination of phytyl and geranylgeranyl residues in plants, as both may be converted into phytane. Actually, one critical issue, namely the fact that neither iodomethane nor Raney Ni cleavage allow to identify prenyl and protein moieties. It is therefore hard to believe in unambiguous identification of the covalent attachment to the C-ter cysteine. Authors argued that no radioactivity was detected in organic solvent after mild base hydrolysis. In this respect, this does not mean that prenyls detected were not stuck onto protein or into protein aggregates, first being not extracted by pentane, then released during Raney Ni. Consistent with this idea is the fact that simultaneous treatment of Raney Ni with guanidine-HCl helped to solubilize protein and improved its yield of released radioactivity (Farnsworth et al., 1990b). Unfortunately, these methods were employed as standards to characterize prenylated proteins and conclude on protein prenylation mechanisms in animals and plants (Sorek et al., 2013).

**Figure 33 Identification of the isoprenoid transferred to RAS2CT1.**

The farnesyltransferase reaction was catalyzed by UC100 extracts and RAS2CT1 protein. The radioactivity incorporated into RAS2CT1 protein was identified on a 12.5% polyacrylamide gel containing SDS. The radioactivity was eluted from the gel and was analyzed by GC. (A) Nonhydrogenated <sup>3</sup>H-labeled material released from RAS2CT1. (B) Authentic all-*trans*-2,6,10-trimethyl-2,6,10-dodecatriene with trace amounts of other *cis/trans* isomers (23). (C) [<sup>3</sup>H]MVA labeled material released from RAS2CT1, which had been hydrogenated over platinum. (D) Authentic farnesane. No C20 isoprenoid was observed (all-*trans*-2,6,10,14-tetramethyl-2,6,10,14-hexadecatetraene, tR = 43.9 min; phytane, tR = 38.3 min). **Goodman et al., 1990**



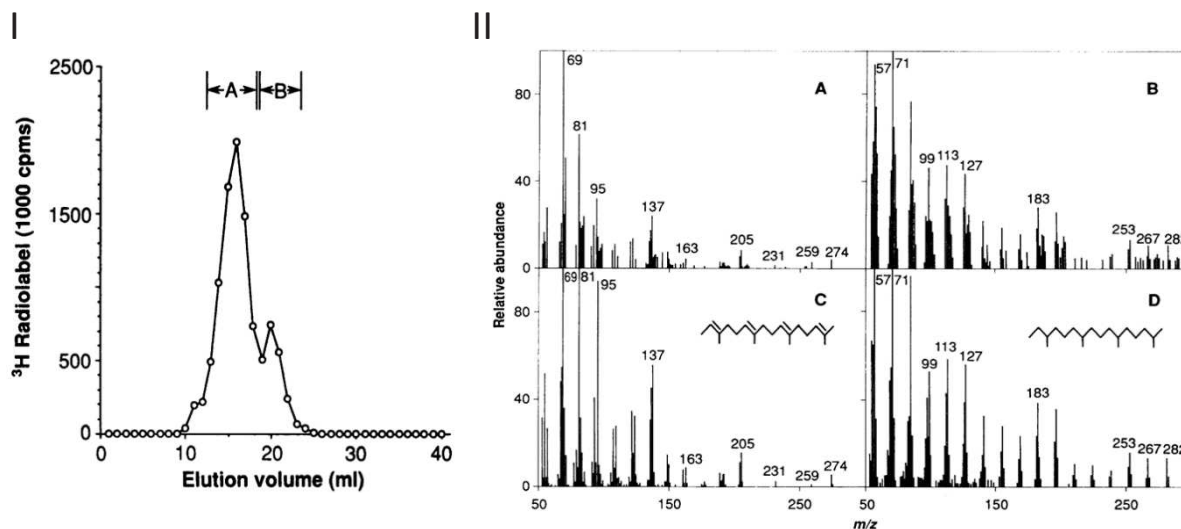


**Figure 34 Analysis of the geranylgeranylated peptide from protein copurified with lamin B**

(I) Size-exclusion chromatography of proteolytic hydrolysates of HeLa cell total proteins on Sephadex LH-20. Cells were labeled for 36 hours with [5<sup>3</sup>H]mevalonic acid in the presence of 30  $\mu$ M mevinolin, harvested, washed with phosphate-buffered saline, and extracted with lipid solvents. Cell pellets were then successively digested with proteases, and labeled digestion products were concentrated and purified by step elution from DEAE Sephacel. The eluted material was then passed through Sephadex LH-20 in 20% formic acid in ethanol at a flow rate of 0.25 ml/min, and 1.0-ml fractions were collected. Peak A, which corresponded to 1000-dalton material, contained 74% of the recovered label. Peak B, which corresponded to 500-dalton material, contained 22% of the recovered label. Recovery of the total applied label was 78%. Comparable chromatograms were obtained in six separate experiments. (II) Electron ionization spectra of Raney nickel-released material from proteolytic fragments of HeLa cell proteins. Samples were prepared from 3 liters of cultured cells as described in Figs. 1 and 2, then analyzed by GC-MS on a 30-m DB-5 column, before or after hydrogenation (3). (A) Nonhydrogenated, peak A-derived material corresponding to the major peak of radioactivity in Fig. 2A. (B) Hydrogenated, peak A-derived material corresponding to the peak of radioactivity in Fig. 2B. (C) All-trans 2,6,10,14-tetramethyl-2,6,10,14-hexadecatriene. (D) Phytane. All spectra have been background corrected, and the spectra in (A) and (C) have been enhanced. Minor differences between spectra of protein-derived samples and standards are likely due to the much smaller amounts of naturally derived materials analyzed. **Farnsworth et al., 1990b**

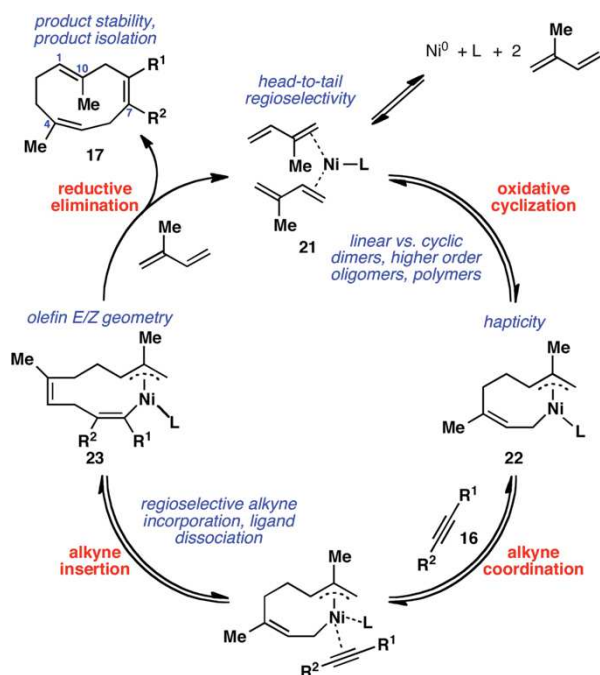


**Figure 35 Example of reaction with Raney Ni.** Catalytic Cycle as Proposed by Wilke, and Difficulties (blue) Associated with the Cooligomerization of Isoprene and Alkynes **Holte et al., 2012**

### 2.5.2 Does it Taste Better With Plants Studies?

Meanwhile, by extrapolation from animal and yeast studies, first experiments were carried out with spinach leaves or tobacco BY-2 cells (Randall et al., 1993; Swiezewska et al., 1993; Shipton et al., 1995; Parmryd et al., 1997). In spinach leaves analyzed, it was primarily concluded that plants accumulated more mevalonate-derived lipids in proteins than do animal cells (Swiezewska et al., 1993). Furthermore, the authors suggested that not only farnesyl and geranylgeranyl residues were transferred to proteins, but also other polyisoprenes and likely phytol too. Even if these results are interesting from the alternative-substrates point of view, analytical procedures were heavily skewed. In fact, from spinach leaves, lipidated proteins were successively extracted and purified with  $\text{CHCl}_3/\text{MeOH}$  (2:1) and  $\text{CHCl}_3/\text{MeOH}/\text{H}_2\text{O}$  (1:1:0.3). Then radiolabeled proteins were analyzed by SDS-PAGE or hydrolyzed extracts for lipids detection were analyzed by HPLC coupled to radioactivity flow detection. However, only one radiolabeled-band could be detected on the SDS-PAGE Gel, while at least four different prenyls were identified after acid hydrolysis, alkaline hydrolysis and reaction with iodomethane (Swiezewska et al., 1993).

Considering the chlorophyll spinach leaves richness and that of MVA is mostly needed for the biosynthesis of sterols and its intermediates. There is reason to be puzzled by these results as purified isoprenoids detected could be stuck to the proteins by hydrophobic interactions. Then, each of the protein denaturation due to acid, alkaline hydrolysis or with iodomethane may have released them. Accordingly, the most accurate estimation might be the Fol and GGol released with iodomethane, which is more specific of the thioether bond. In any case, the SDS-PAGE analysis being decoupled from the lipid analysis does not allow to conclude definitively on the relationship between radiolabeled proteins and lipids detected. Furthermore, the absence of consideration for alternative substrates has so far conditioned the experimentation but also the interpretation of results. Recent studies conducted with plants have provided critical information on the importance of MVA/MEP crosstalk to supply precursors for prenyl substrates biosynthesis, inextricably relied to PPTs activities (Gerber et al., 2009a; Hemmerlin et al., 2012).



Other incorporation of [<sup>3</sup>H]-MVA into spinach leaves were performed in combination with MV inhibition. The radioactivity was evidenced in several proteins within different subcellular fractions (Shipton et al., 1995; Parmryd et al., 1997). As before, the analysis by HPLC-radiometry of lipids after alkaline hydrolysis or iodomethane revealed that radioactivity was incorporated into Fol, but mostly found in GGol, supporting the hypothesis that the use of MV acts as a switches to use one or the other pathway. Similar results were found with proteins extracted from different chloroplasts compartments, it was even shown that thylakoids extract exhibit farnesyl transferase activity on DTT (Cleland's reagent), while PFT is reported as cytosolic (Parmryd et al., 1997; Parmryd et al., 1999; Bracha-Drori et al., 2004). Since, PGGT-I localization was not determined and assuming the current elements on the flexibility of PPTs activities, it might be considered that in the presence of MV, the PFT activity observed may involve the PGGT-I. Nevertheless, at that time data were not robust enough, letting such free gaps for hasty conclusion skewed by the use of MV, sample preparation steps and analysis, which by the way did not allow direct relation between PPTs, prenylated proteins and lipids analyzed.

In BY-2 cells, the analysis of prenylated proteins was performed both by incorporation of [<sup>14</sup>C]-MVA followed by SDS-PAGE with radiolabeled proteins prenylated *in vivo* or *in vitro*, and also measuring incorporation of [<sup>3</sup>H]FPP or [<sup>3</sup>H]GGPP in cell protein extracts (Randall et al., 1993). Interestingly, in this study, the effect of MV onto the incorporation of [<sup>14</sup>C]MVA was evaluated at different concentration (0-50 uM). Although MV did not appears to affect the total protein content, again it increased the incorporation of radioactivity into proteins, especially those pelleted at 70 000g. As with spinach, these results claimed the effect of MV on the protein prenylation *in vivo*, influencing the isoprenoids crosstalk as well as flexibility of PPTs (Hemmerlin et al., 2012). Meanwhile, it was proved *in vitro* that BY-2 cell protein extract only transfers [<sup>3</sup>H]FPP onto ras-CAIM, while [<sup>3</sup>H]GGPP is transferred onto both *ras*-CAIM and -CAIL (Randall et al., 1993). It was therefore assumed that PFT activity is specific of [<sup>3</sup>H]FPP and CaaM, but PGGT-I is more flexible as it transfers [<sup>3</sup>H]GGPP onto both CaaM and CaaL. Unfortunately, these experiments were not done with MV-treated BY-2 cells, omitting the regulation of PPTs activity under inhibition of MVA pathway (Gerber et al., 2009a). Many other experiments were done with animal and plant cells or purified enzymes, but artifacts were induced by either *in vitro* or analytical setups, which did not allow to define properly the nature of both PPTs and prenyl transferred *in vivo*.

### 2.5.3 After 20 Years, Wouldn't it Be the Time to Change the Kitchen?

The characterization of PPTs mutants in *A. thaliana*, the development of fluorescent markers and analytical techniques for the study of prenylated proteins *in vivo* raised inconsistencies in the paradigm established during the 1990s. The characterization of viable *era1*, *ggb* and *plp A. thaliana* mutants was a real revolution in the field, because for the first time, a single model organism allowed to observe the impact of the absence of PPTs *in vivo*. Although the first studies of *era1* as *ram1* only considered the incorporation of [<sup>3</sup>H]FPP (He et al., 1991), the characterization of the Arabidopsis *plp* mutant evidenced that an absence of the  $\alpha$ -subunit can be somehow compensated (Running et al., 2004; Johnson et al., 2005). First, a GFP fusion protein has been developed with CaM53 calmodulin, which localizes to the plasma membrane if prenylated or to the nucleus if not (**Figure 22**). This tool has proven that in *plp*, the CaM53 protein mostly localizes in the nucleus (Running et al., 2004). In addition, the prenylation assays of AtNAP1.1 and [<sup>3</sup>H]FPP or CaM53 and [<sup>3</sup>H]GGPP *in vitro* with WT or *plp* plant protein extracts confirmed the absence of prenylation under normal conditions. However, the reverse combination and other alternative substrates were not tested.

Since the *plp* mutant is viable and the resolution of images were low, it can be speculated that the residual signal of CaM53 observed in the membrane of the *plp* mutant is modified by another substrate. One may wonder: Why did not the authors extract and purify the GFP-CaM53 protein expressed in the *plp* mutant to directly analyze the prenyl and compare their results to *in vitro* assays? One explanation emphasize that it might not be trivial and that the amount of protein produced in plants is regulated, and despite a strong promoter, it remains much less important than in bacteria or yeasts. Also, at this time the equipment and proteomics approaches were not yet adapted for the analysis of prenylated proteins limiting the choice to iodomethane and Raney nickel cleavages or TLC analysis of prenylated radiolabeled peptides. From this study we can only assume that the modification of AtNAP1.1 and CaM53 in *plp* should be different of the WT.

It was only in 2005 that studies started to characterize the flexibility of PPTs and the relation with isoprenoids crosstalk in plants. Different proteins were evaluated to design a prenylatable sensor not only devoid of biological activity, but also offering a clear view on prenylation state. In this respect, following traces of CaM53 studies, a GFP-sensor of protein prenylation had been developed with OsCaM61 (**Figure 36**, Gerber, 2005).

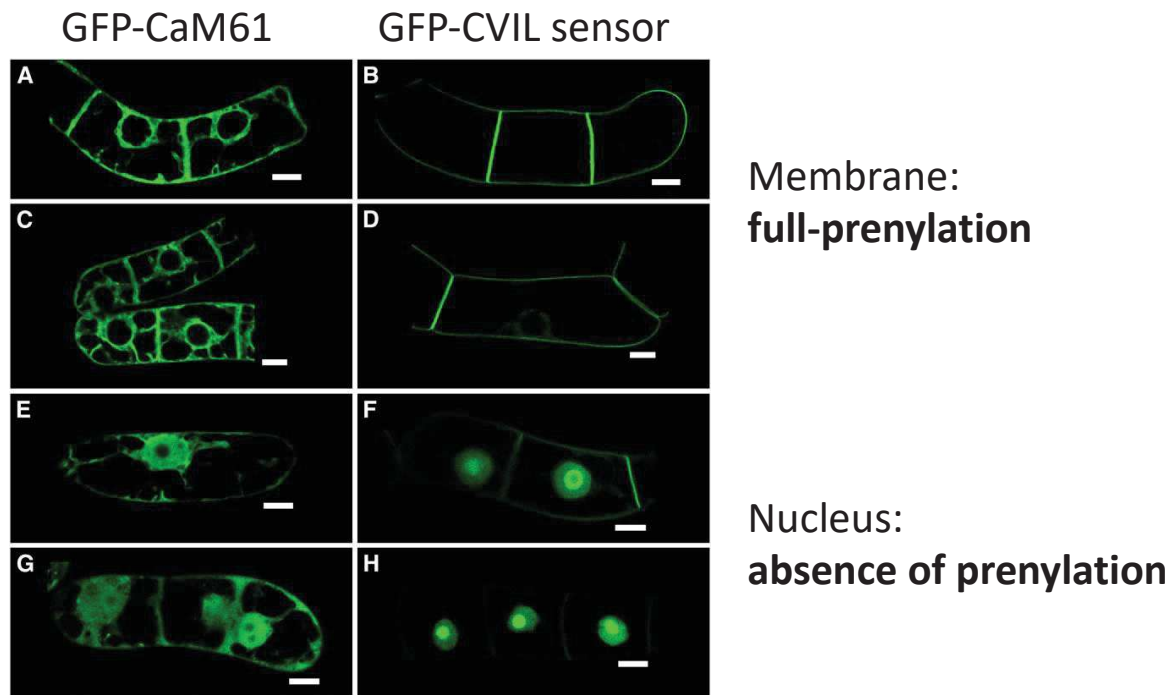


**Figure 36 Localization of GFP-CaM61 and GFP-CVIL in BY-2 Cells.**

(A) Localization of GFP-CaM61 in BY-2 cells, showing GFP fluorescence associated with ER and perinuclear membranes, plasma membrane, and cytoplasmic strands. (B) Localization of GFP-CVIL in BY-2 cells, showing GFP fluorescence associated exclusively with the plasma membrane. (C) Localization of GFP-CaM61 in BY-2 cells treated with MV as described by Dong et al. (2002), showing GFP fluorescence associated with ER and perinuclear membranes, plasma membrane, and cytoplasmic strands. (D) Localization of GFP-CVIL in BY-2 cells treated with MV as described by Dong et al. (2002), showing GFP fluorescence associated with the plasma membrane (faint fluorescence is also seen in the nucleus). (E) Localization of GFP-CaM61 in BY-2 cells treated with Fos, showing partial translocation of GFP fluorescence to the nucleus, but not the nucleolus. (F) Localization of GFP-CVIL in BY-2 cells treated with Fos, showing translocation of GFP fluorescence to the nucleus and nucleolus. (G) Localization of GFP-CaM61 in BY-2 cells treated with MV and Fos, showing increased translocation of GFP fluorescence to the nucleus. (H) Localization of GFP-CVIL in BY-2 cells treated with MV and Fos, showing almost complete translocation of GFP fluorescence to the nucleus and nucleolus. Bars = 10 mm. **Gerber et al., 2009**

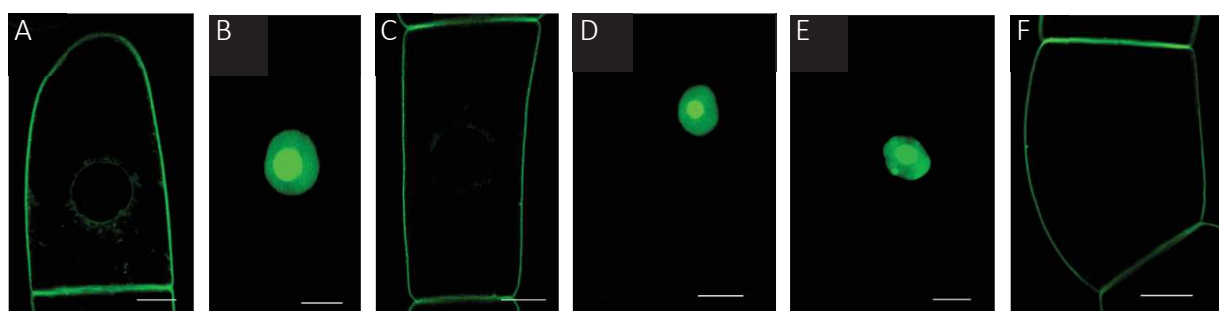


**Figure 37 MVA and GGol rescued prenylation of GFP-CVIL inhibited by fosmidomycin and mevinolin.**

(A) Treatment of cells expressing GFP-CVIL protein without treatment, (B) with 5  $\mu$ M mevinolin and 40  $\mu$ M fosmidomycin, (C) complemented by 3 mM MVA or different prenyl alcohols at 20  $\mu$ M ((D) Farnesol, (E) Geraniol, (F) geranylgeraniol). confocal microscopy images are representative of the GFP-CVIL protein cellular distribution under the effect of the different treatments (x63 objective); the white bar represents 10  $\mu$ m; DIC, differential interferential contrast. Adapted from results in **Gerber, 2005**

The latter consists of a GFP fused with the basic domain of rice CaM61 followed by the farnesylation motif (GFP-CVIM), the geranylgeranylation motif (GFP-CVIL) or non-prenylable protein (GFP-SVIL) (Gerber, 2005; Gerber et al., 2009a) (**Figure 36**). Quite practically, the expression of GFP-CaaX sensors has to be under the control of an inducible promoter (dexamethasone, DEX), which allows the expression of the protein under various conditions. Therefore, inhibition with MV and/or FOS can be performed prior to induction of the GFP-sensor, allowing to study how the MVA or MEP biosynthesis pathway provide precursors for the protein prenylation. Several experiments were performed such as *in vitro* prenylation of GFP-CaaX and a Ras-CaaX protein by tobacco cell-free extracts, a study of the GFP-CaaX subcellular localization in BY-2 cells according to MVA and MEP pathway inhibitors, and proteomic analysis of the purified GFP-CVIL protein from BY-2 cells inhibited or not with FOS. Thus, *in vitro*, GGPP was transferred to both CaaM and CaaL proteins, while FPP was mostly transferred to the protein with a CaaM signal, but also weakly to the CaaL protein. These results were in contradiction with the results observed by Randall et al. (Randall et al., 1993).

In addition, pharmacological approaches employed with MV or/and FOS to treat BY-2 cells have stated that both MVA and MEP provide prenyl substrates for protein prenylation in plants. Indeed, the inhibition of GFP-CVIL prenylation by FOS and MV was reversed in the presence of MVA (**Figure 37**), while the total inhibition of GFP-CVIM prenylation in BY-2 cells was only achieved by using high MV concentrations in combination with FOS (Gerber, 2005). On the top of that, a proteomics approach using HPLC-MS/MS evidenced each of the geranylgeranylated, non-carboxymethylated and non-prenylated peptides of His-GFP-CVIL in induced BY-2 cells, while prenylated form was not found in FOS-inhibited cells (Gerber et al., 2009a). Although, proteins being prenylated under induced-flexibility of PPTs were not analyzed, it was proven that under physiological condition BY-2 cells transfer geranylgeranyl onto CVIL proteins (Gerber et al., 2009).

As a result, it appears that the characterization of this GFP-sensor prenylated *in vivo* can be achieved by affinity chromatography purification and proteomic analysis of prenylated peptides released after AspN digestion. However, it was noticed that the GFP-CVIL protein from BY-2 remained largely bound to the purification support even after elution by 1 M imidazol (Data not published). Accordingly, combination of polar (Basic domain) and hydrophobic (GFP and prenyl) physicochemical properties of prenylated proteins may not be suitable for these affinity purification support. Besides, the signal detected in HPLC-MS/MS was extremely low, and the experiment was performed just once, letting some space to false positive signals. Like a boomerang, few years later, the analysis of PPTs substrate specificities was achieved using recombinant *A. thaliana* PFT and PGGT-I incorporation assay with [<sup>3</sup>H]FPP, [<sup>3</sup>H]GGPP and multiple GFP-CaaX substrates (Andrews et al., 2010). It appeared that recombinant AtPFT transfers not only FPP onto CaaM and CVIL, CAIL, CTIL substrates with a clear preference for CaaM, but also in a significant way the GGPP onto CaaM and CAIQ substrates (Andrews et al., 2010). In contrast, the AtPGGT-I was very specific of CaaL substrates and GGPP but it also transferred FPP onto CaaL substrates

Altogether, these findings exposed whether protein prenylation mechanisms are flexible and differ between *in vitro* and *in vivo* studies. Although many biases were generated by *in vitro* studies and it is still a matter of debate whether enzymatic assays drive PPTs activities, these studies gave a picture of the intrinsic flexibility of PPTs activities without any post-translational modifications. Consistent is the fact that *in vivo*, this flexibility also exists and is clearly adjusted to the metabolism of isoprenoids in plants. In 2010, all elements were available to characterize at a molecular level the flexibility of PPTs activities in plants and animals. Why in 2020 no matter which organism being concerned, any model could clearly define the physiological conditions inducing the flexibility, the substrates involved and PPTs responsible for the prenylation of a model protein under these conditions?

#### 2.5.4 10 More Years to Deal with the New Kitchen

To sum up, assuming that what has been studied *in vitro* does not reflect the reality of protein prenylation, the criteria to be considered as essential to understand and characterize the dynamic flexibility of PPTs are:

- **To study prenylated proteins in vivo**
- To study the prenylation in vivo by subcellular localization of a reporter protein
- To perform assays with and without inhibitors of protein prenylation and KO mutants of PPTs
- To perform complementation assays with different prenyl or precursor substrates
- To characterize by SDS-PAGE the proteins in every condition
- **In a single analysis characterize at a molecular level the nature of the prenyl transferred *in vivo* and/or the related protein moiety in each of the physiological, inhibition, mutants, complementation with prenyl substrates conditions.**

To conclude, in 2017, at the initiation of this thesis, several tools had been developed for the purification of prenylated proteins by immunoprecipitation, bio-orthogonal chemistry, but also for proteomic analysis by HPLC-MS/MS. Although these tools have been progressively imposed and several prenylated proteins have been characterized, many studies still followed traces from the past. A good example is the bio-orthogonal chemistry, which facilitates the accurate analysis of proteins prenylated with modified prenyls and thus the identification of the prenyl transferred by HPLC-MS/MS. However, since protein prenylation is highly sensitive to isoprenoid precursor pools within cells, the simple addition of a PPTs substrate will affect the status of protein prenylation. More than 150 papers address the theme of prenylated proteins or protein prenylation, but to date only 2 studies provide sufficient evidences to get to the identification of the prenyl transferred *in vivo* onto a specific protein under physiological conditions (Mohamed et al., 2018; Wilkins et al., 2020). Very recently, a new reproducible method to analyze prenylated proteins from a physiological point of view was reported with brain mouse cells using thiopropyl-based capture technic ([Wilkins et al., 2020](#)).

With regard to the role of prenylated proteins in human pathologies or parasitosis, the widespread of resistances to current treatments, hundreds of PPTs inhibitors have been developed regardless of the physiological context and the flexibility of PPTs. What are these inhibitors and how do they work? Why do so many inhibitors failed?

## 2.6 INHIBITION OF PROTEIN PRENYLATION IN HUMAN PATHOLOGIES

### 2.6.1 Cancer, When Simple Words Got Complicated

The interest in protein prenylation stems from the identification of mutated RAS prenylated proteins involved in various cancers. In 2014 1,665,540 suffered from cancer and 585,720 of them died, and the American Cancer Society estimates 1,806,590 new cancer cases and 606,520 cancer deaths by 2020 (Hassanpour and Dehghani, 2017; Siegel et al., 2020). Actually, cancer refers to 277 different types of cancer disease rooting from gene mutations responsible for abnormal cell proliferation. Although six Human papillomavirus (HPV)-associated cancers were characterized and responsible for 15% cancer (Bansal et al., 2016), most cancer are derived from inherited mutations or appearing naturally through chromosomal translocation, point mutation, deletion, amplification and insertion activation depending on environmental factors (Hassanpour and Dehghani, 2017). Early, several molecules were identified and used to fight cancer widespread. The antimetabolites are the oldest anticancer drugs described. They interfere with essential biosynthesis pathways such as purine and pyrimidine bases with antifollics (methothrexate, pemetrexed) or DNA synthesis with antipurines (mercaptopurine, fludarabine) and antipyrimidines (Fluorouracil, cytarabine). DNA interacting agents were discovered later and exhibit a variety of mechanisms of action. For instance, in this group there are alkylating (dacarbazine, temozolomide), cross-linking (cisplatin, oxaliplatin), intercalating (doxorubicin, actinomycin-D) and cleaving agents (bleomycin) that latter induce different types of DNA damage. Also, topoisomerase inhibitors (topotecan, mitoxantrone) represent an important class of DNA interacting agents that interfere with the enzymes responsible for the regulation of the DNA-structure in replication, transcription and other primordial processes. Famous and still widely used is the group of antimitotic agents divided into spindle poison (vinblastine, colchicine) and spindle stabilizer (paclitaxel, docetaxel) preventing microtubule dynamic. Although antimetabolites, DNA interacting and antimitotic agents are very potent, they affect stages of primary metabolism and lack of selectivity causing such side effects (Mehrmohamadi et al., 2017). In addition, many resistances have been reported and limit the efficacy of these molecules for some cancer therapies (Kruh, 2003; Mansoori et al., 2017). Research is still active to discover new analogs, but other strategies such as protein prenylation inhibition, tyrosine kinase inhibitors or immunotherapy were suggested through decades of studies on anticancer drugs.

## 2.6.2 Protein Prenylation Inhibitors: a Problem to All your Needs

In the middle of the 80s, the statement of mutations within RAS family proto-oncogene in a third of tumors opened new perspectives in the cancer therapy associated with prenylated proteins dysfunction (Prior et al., 2012). The RAS genes are among the earliest, if not the first, genes mutated in a variety of cancers and often result from a single point mutation leading to permanent activation and thus downstream signaling pathway. With this respect RAS is converted from an inactive GDP-bound state to an active GTP-bound state by RAS guanine nucleotide exchange factors (GEFs) recruited to the plasma membrane (Li et al., 2018). GTP-bound RAS adopts a new conformation that binds effectors through their RAS binding domain (RBD). Several effectors have been described including Mitogen-activated protein kinases (MAPK) like PI3K, RAL GEFs, which trigger signaling through successive activation by phosphorylation to induce pro-proliferative signals among other. Signaling is terminated by the association with RAS GTPase-activating proteins (GAPs), which accelerate the GTPase activity of RAS, returning RAS to the inactive GDP-bound state.

Furthermore, the prenylation of the lamin B involved in progeria was quickly evidenced and one thing leading to another, other prenylated proteins were discovered and associated with immune deficiency or psychologic disorder or Alzheimer's disease (Hooff et al., 2010; Pinner et al., 2020). Massive studies have been carried out to develop inhibitors of protein prenylation for cancer, progeria and other human pathologies diseases (Dai et al., 2020; Manaswiyoungkul et al., 2020).

However, early studies depicting protein prenylation in *in vitro* models with labelled prenyl precursors or substrates triggered the development of protein prenylation inhibitors towards inhibitors of prenyl biosynthesis enzymes and PPTs. The blockbuster bisphosphonate (BP) inhibitors Tiludronate, Pamidronate, Alendronate, Risedronate inhibiting the FDS and/or GGDS are widely used against bone resorption disorder (Coxon et al., 2000; Russell, 2011; Wills et al., 2015; Wills et al., 2017; Manaswiyoungkul et al., 2020), have been so far investigated by pharmaceutical companies. Most of them target the active site s1, s2 or the allosteric site s3 of FDS or GGDS. Similarly, *in vitro* assays have rapidly demonstrated the efficacy of prenyl substrates (FPP-mimicking analogs) or CaaX peptides (peptidomimetics) analogs.



Accordingly, chemo-informatic with molecular docking and other computer modeling tools erupted in this field taking advantage of the structural data and activities reported by studies published before 2010. In fact, hundreds of natural and synthetic analogs have been screened on *in vitro* assays with purified recombinant enzymes (Lobell et al., 2001; Guida et al., 2005; Berndt et al., 2014; Ho et al., 2014; Subramani et al., 2015).

Actually, Tipifarnif, Lonafarnib and BMS-214662, L-778123 have reached the clinical trial phase, but only the first two got through the Phase III, while the others are still pending or were rejected (Berndt et al., 2014; Wang et al., 2017). One reason suggest that some studies did not considered enough the RAS-type involved in patient selected for clinical trials. In a pathological scenario, for cell survival, it can be speculated that the *in vivo* regulation of PPTs activities would induce conformational changes to promote binding of protein substrate or another prenyl rather than the inhibitor. Since better results were observed with combination of FTIs and GGTIs in (Lobell et al., 2001; Berndt et al., 2014)), the PGGT-I may likely rescue protein prenylation if the PFT is inhibited and vice-versa. Finally, Ras proteins are prenylated and palmitoylated, perhaps this or other modifications enable non-prenylated Ras protein to maintain a minimal function in cancer cells.

As a matter of fact, the efficacy of protein prenylation inhibitors in the treatment of cancer has been challenged (Holstein and Hohl, 2012), or even dropped in favor of other strategies such as the development of immunotherapy or tyrosine kinase inhibitors. However, is this really the case or is it a hasty but predictable conclusion after building our perception of protein prenylation on simplistic models? Other trials have been carried out in the context of parasitosis induced by apicomplexan, what are their results?

## 2.7 INHIBITION OF PROTEIN PRENYLATION IN MALARIA

### 2.7.1 Conventional Treatments and Resistances

Antimalarial drugs mainly focused on inhibition at intraerythrocytic and liver stages (Figure 38)

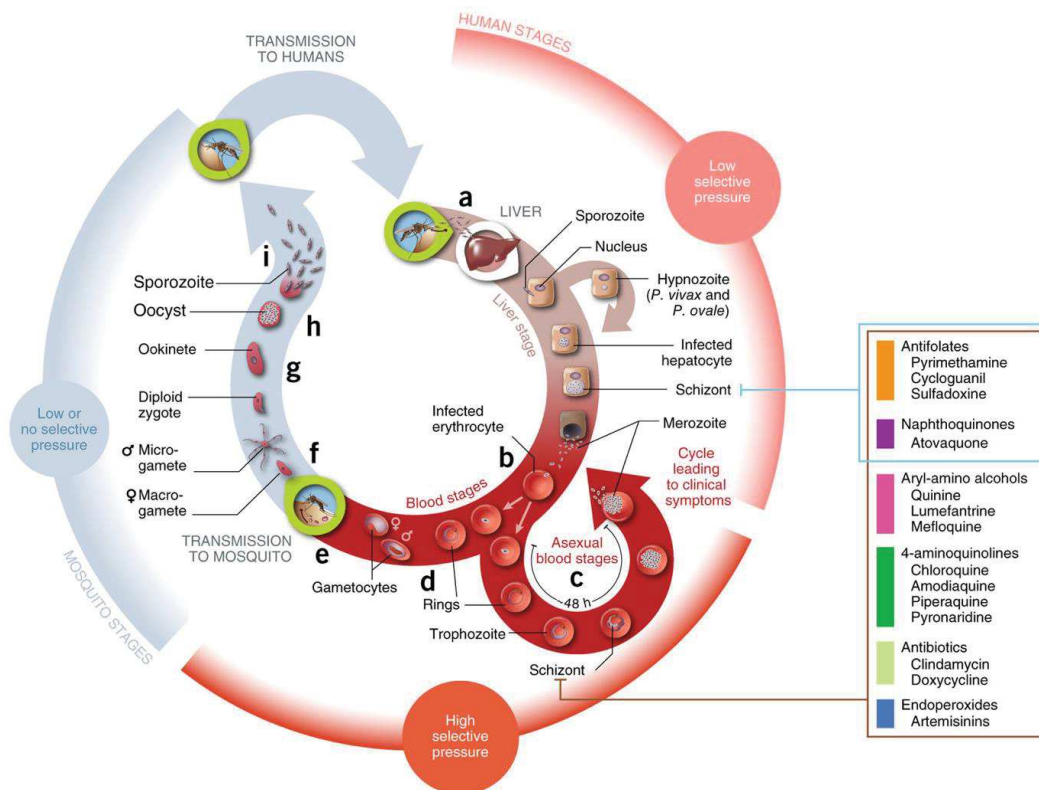


**Figure 38 Plasmodium's life cycle and its relationship to drug resistance.**

(a) Human infection begins when infective female Anopheles mosquitoes deliver fewer than 100 sporozoites into the dermis during blood feeding. These motile forms migrate rapidly into the bloodstream and to the liver, where they invade hepatocytes. A prodigious phase of replication over a week results in an estimated 10,000–30,000 merozoite progeny per intracellular parasite. (b) Liberated merozoites ( $\sim 10^5$ – $10^6$  in total) then invade human mature red blood cells (RBCs), developing inside a parasitophorous vacuole and initiating  $\sim 48$ -h cycles of asexual blood stage (ABS) parasite growth, egress and reinvasion. (c) ABS parasites, typically  $10^8$ – $10^{12}$ , are responsible for disease manifestations. (d) About 1–2% of intra-erythrocytic parasites enter an alternative program of sexual development, a process that over  $\sim 10$ – $12$  d produces mature male and female gametocytes that are transmissible to Anopheles mosquitoes. (e) An estimated  $10^3$ – $10^4$  mature gametocytes are taken up during a blood meal. (f–i) These gametocytes then form male and female gametes ( $\sim 10^2$ – $10^3$ ) that undergo sexual recombination (f), forming ookinetes ( $< 100$ ; g) and then oocysts (typically 1–2; h) before completing their life cycle by forming  $10^3$  to  $10^4$  sporozoites that migrate to salivary glands (i), ready for further human infection. In acute cases, ABS parasites can infect up to 10–20% of all erythrocytes (i.e.,  $> 10^{12}$ ). Primary causes of death include severe malaria anemia, or cerebral malaria that causes brain herniation and respiratory arrest. Immunity is acquired slowly and is nonsterilizing; its maintenance is dependent on continued infection. Selective forces that drive the emergence and spread of drug resistance differ throughout the life cycle. Important factors include the parasite numbers and drug pressure at different stages, stage specificity of drug action, the essentiality of the targeted pathways in the mosquito vector and vertebrate host, host immunity, multiplicity of infection, and local factors that affect therapeutics use and compliance. The pathogenic ABS reproduction cycle experiences the highest parasitemias and drug pressure, whereas the lower numbers of clinically silent liver-stage parasites provide much less fertile ground for the emergence of resistance. Human-to-mosquito transmission is possible only if sufficient densities of mutant gametocytes are produced, which can be triggered in some instances by drug treatment. **Blasco et al., 2017**

Many natural and synthetic molecules have been identified and used for more than 200 years to treat malaria. The bark of red cinchona (*Q. pubescens* or *Q. succirubra*) was traditionally used by populations in the Andes and served as raw material to extract and isolate quinine and quinidine, the first antimalarial active substances identified in 1817 by Pelletier and Caventou. Chloroquine was synthesized later during the Second World War and therefore in 1955, the first WHO global program to fight malaria was initiated. Unfortunately, chloroquine-resistant *P. falciparum* strains progressively emerged triggering so far research for new anti-malarial drugs.

In the approved drugs there are the synthetic derivatives of quinine comprising amino alcohols (mefloquine, lumefantrine), 4-aminoquinolines (chloroquine, naphthoquine, piperazine) and the 8-aminoquinolines (primaquine, tafenoquine). The main target of quinine and synthetic analogs is the heme detoxification, including biocrystallization into hemozoin, transport towards vacuole. Nevertheless, other mechanisms less described do involve perturbation of endocytosis and mitochondrial processes. As with cancer, antifolics are also used to inhibit the replication and transcription of the parasite. Nevertheless, prodrugs form (Proguanil, Chlorproguanil) were developed to limit side effects on human DNA. Furthermore, artemisinin isolated from *Artemisia annua* has opened the field to a new class of antimalarial drugs. Even though the mechanisms of action are not completely known, the presence of an endoperoxide bond on the molecular scaffold enable its reaction with heme iron, resulting into radical species inducing alkylating stress in the parasite. Artemisinin derivatives (artemether, artesunate) are very effective and drastically reduce the parasitic charge, hence artemisinin-based combination therapies (ACTs) were developed to limit the risk of resistance as observed in monotherapy (Blasco et al., 2017)(**Figure 39**). Scarcely, since 2008 cases of resistances appeared in Southeast Asia, suggesting that even ACT will not stop the parasite forever. Thus, the search for antimalarial molecules is constant and requires fighting the parasite with new molecular scaffold involving other mechanisms of action. For example, naphthoquinones such as atovaquone, which is used in combination with Proguanil®, acts on the mitochondrial electron transport chain and inhibit ATP synthesis. Also, phase II Clinical trials are in progress with KAF156 (unknown mechanism), Cipargamin et SJ173 (inhibitors of plasma membrane Na<sup>+</sup> transporter), DSM 225 (dihydroorotate deshydrogenase inhibitor). Since the MEP pathway has been identified in *Plasmodium*, protein prenylation inhibitors were investigated too.

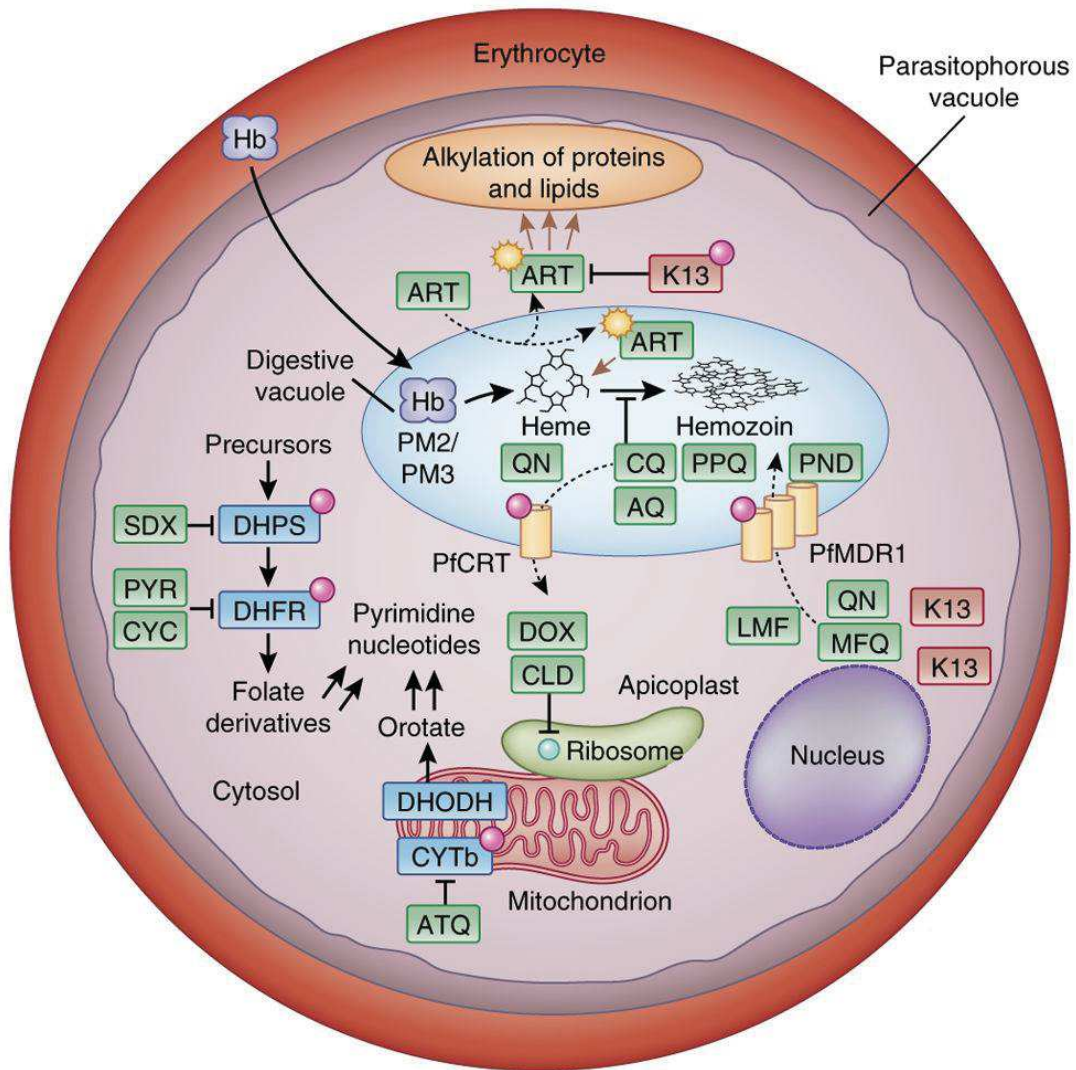


**Figure 39 Molecular targets of and mechanisms of resistance to major antimalarial drugs.**

Frequently targeted biological pathways include heme detoxification in the digestive vacuole, folate and pyrimidine biosynthesis in the cytosol, and electron transport in the mitochondrion. The 4- aminoquinolines, including CQ and AQ, as well as PPQ, the Mannich base pyronaridine (PND), and to some degree the aryl-amino alcohol quinine (QN), are all thought to concentrate in the digestive vacuole, where they bind reactive heme and interfere with its detoxification through incorporation into chemically inert hemozoin. Ferrous ( $\text{Fe}^{2+}$ ) iron-heme liberated after parasite protease-mediated degradation of imported host hemoglobin (Hb) can cleave and thereby activate the endoperoxide bridge of ART derivatives (star symbol). Point mutations (pink circles) in the transporters PfCRT and PfMDR1 are important determinants of resistance to 4-aminoquinolines. Resistance to PPQ is associated with increased expression of the hemoglobins plasmepsin 2 and 3 (PM2/PM3, in the digestive vacuole), and might in some instances involve mutant PfCRT. Copy-number changes in *pfmdr1*, as well as PfCRT and PfMDR1 sequence variants, also affect the parasite's susceptibility to the aryl-amino alcohols quinine (QN), lumefantrine (LMF) and mefloquine (MFQ) and can modulate ART potency. Variant forms of K13, thought to localize at the ER and in vesicular structures, are the primary mediator of ring-stage parasite resistance to ART. Mutations in two key enzymes of the folate biosynthesis pathway, dihydropteroate synthetase (DHPS) and dihydrofolate reductase (DHFR), can confer resistance respectively to the antifolates sulfadoxine (SDX) and both pyrimethamine (PYR) and cycloguanil (CYC). Atovaquone (ATQ) inhibits mitochondrial electron transport, and a single point mutation in the cytochrome b subunit (CYTb) of the bc1 complex can confer resistance to this drug. The ETC is important in ABS parasites because of its role in providing electrons for the ubiquinone-dependent dihydroorotate dehydrogenase (DHODH), an enzyme essential for de novo pyrimidine biosynthesis. Antibiotics such as clindamycin (CLD) and doxycycline (DOX) inhibit protein translation inside the apicoplast. CLD resistance is mediated by a point mutation in the apicoplast-encoded 23S rRNA. **Blasco et al., 2017**

### 2.7.2 Protein Prenylation Inhibitors vs *P. falciparum*

In 1999, the *P. falciparum* DXR gene was identified by homology with plants and some bacteria in which MEP pathway was reported (Jomaa, 1999). In addition, the GFP-DXR fusion protein expressed in the parasite localized in the apicoplast. Accordingly, it was evidenced that the inhibition of isoprenoid biosynthesis by FOS and its more permeable analog FR-900098 induces death of blood-stage HB3, A2 and Dd2 (chloroquine resistant) *P. falciparum* strains. Since the MEP pathway is absent in animals, the FOS was therefore used in clinical trials and considered as an effective and safe antimalarial drug (Missinou et al., 2002; Borrmann et al., 2006). Nevertheless, It was noticed that repeated treatment with FOS even in combination resulted into a high rate of recrudescence malaria in children (Armstrong et al., 2015). In fact, FOS is effective against blood-stage *P. falciparum*, but its charged nature results in impermeability, poor pharmacokinetics and therefore low efficacy against other pathogens such as *T. gondii* or *Mycobacterium tuberculosis*. Although these studies emphasized the key role of MEP-derived isoprenoids for the parasite survival, it was also shown that IPP but not DMAPP could rescue inhibition caused by FOS resulting in a delayed death of the parasite. Since *P. falciparum* does not inherit the MVA pathway and expression of the latter has not been detected in red blood cells, it has been suggested that the parasite imports IPP from the external environment *via* an unknown mechanism (Yeh and DeRisi, 2011).

Few years later, a screening of FOS-resistant *P. falciparum* strains shed the light on mutations of haloacid dehalogenase (HAD)-like sugar phosphatase (pfHAD1), the first regulator of MEP pathway discovered in *Plasmodium* (Guggisberg et al., 2014). Interestingly, the loss of PfHAD1 function, especially by Y148C or A60E, increased the level of MEP pathway intermediates in a FOS-resistant strain, allowing competition between DXP substrate and FOS. In addition, mutation of the S222T in PfDXR was found to confer resistance to FOS *in vitro* and *in vivo* but also to its more permeable analog FR-900098 (Armstrong et al., 2015).

Very recently, other *Plasmodium* FOS-resistant mutants were isolated, proposing new mechanism of resistance *via* regulation by HAD2 (Guggisberg et al., 2018). Although, HAD2 is a homolog of HAD1, they appeared to act on the regulation of MEP pathway by different manner. Interestingly, different suppressors mutated in the phosphofructokinase 9 (PFK9) within the *Pfhad2<sup>R157X</sup>* FOS-resistant strains appeared spontaneously during routine culturing. These suppressors were mostly found after 79 days without FOS, suggesting that FOS-resistance

induced by mutation of *Pfhad2*<sup>R157X</sup> has a fitness cost which is offset by spontaneous mutation of PFK9. Consistent is the fact that inhibition of the MEP irremediably leads to the adaptation of the parasite, which shunt prenyl substrate from the host producer or adopt spontaneous mutations to up-regulate MEP pathway enzymes.

As in animals, other assays were performed to inhibit downstream steps by using various BP inhibitors. Thus, the bifunctional FDS/GGDS of different *Plasmodium sp* has been targeted. First, zoledronate and risedronate BPs were studied *in vitro* on *P. vivax* or *P. falciparum* FDS/GGDS enzymes and *in vivo* on intraerythrocytic *P. falciparum* ring, trophozoite and schizont stages, but their efficacy was disputable as variability was observed between studies (Singh et al., 2010; Artz et al., 2011; Jordão et al., 2011). Interestingly, it was noticed that the incorporation of [<sup>3</sup>H]FPP and [<sup>3</sup>H]GGPP into proteins of *P. falciparum* differ between the different development stages (Jordão et al., 2011). For instance, under risedronate inhibition, only proteins at 7kDa were labeled in trophozoite stage with [<sup>3</sup>H]FPP as compared to several proteins > 27 kDa labeled by [<sup>3</sup>H]GGPP, while both rescued parasite growth after 48h treatment. Hence, it was proposed that risedronate modulates in an opposite manner the incorporation of FPP and GGPP into proteins, converging to the idea of some flexibility in protein prenylation mechanisms. Surprisingly, it was concluded that risedronate inhibit protein prenylation, but according to their protocol, only prenols released by inhibited *P. falciparum* fed with [<sup>14</sup>C]IPP have been analyzed on TLC after phosphatase alkaline treatment, which is truly nonsense (Jordão et al., 2011). On the top of that, the control for TLC samples consisted of non-infected red blood cells, while the treated cells were infected. Even though other experiments may have been considered such as rescue with [<sup>3</sup>H]DMAPP or [<sup>3</sup>H]GPP, the TLC experiment did not allow to conclude as to the effect of risedronate on protein prenylation.

In contrast, the lipophilic diphosphate substrate analogs BPH-942, -943 and particularly BPH-715 showed promising results against the liver stage and blood-stage forms of *P. berghei* (Singh et al., 2010). All BP inhibitors exhibit similar efficacy on the resistant chloroquine strain W2mef. Furthermore, a screening of 560 compounds on *P. vivax* allowed the identification of other lipophilic analogs (No et al., 2012). BPH-703 and BPH-811 were good candidates as PvFDS/GGDS enzyme was inhibited at Ki values comprised between 270 and 570 nM, respectively. Also, a significant decrease in the parasitemia of about 80 % at 3 mg.kg<sup>-1</sup> and 92 % with BPH-703 at 10 mg.kg<sup>-1</sup> were observed in mice infected by *P. chabaudi* 14-d post treatment.

Even though lipophilic BP inhibitors are good candidates for malaria therapy and therefore still investigated (G. Ricci et al., 2016), it can be speculated that resistance may appear that balance the lack of isoprenoids and ensure cell survival as it was the case with MEP pathway inhibitors. Accordingly, it has been found that the overexpression of PfFDS/GGDS induce resistance to risedronate of *P. falciparum* blood stage (Gabriel et al., 2018).

Along with the inhibition of prenyls supplying pathways, the inhibition potential of FTIs and GGIs were investigated on *P. falciparum* (Chakrabarti et al., 2002; Glenn et al., 2006; Clapp et al., 2013; Ha et al., 2015)). In 1998, PGGT-I inhibitors L-741,177 and PFT inhibitors L-745,631, L-744,832 were tested *in vitro* on the purified PfPPTs and *in vivo* on the *P. falciparum* Dd2 chloroquine-resistant strain (Chakrabarti et al., 1998). All inhibitors arrested parasite growth with an IC<sub>50</sub> of about 5 μM, outlining once again the role of protein prenylation in the development of *P. falciparum*. Next, other PPTs inhibitors were tested by the same lab and complementary results were provided, including incorporation of [<sup>3</sup>H]FPP into proteins at different blood stages (Chakrabarti et al., 2002). As for the L-series, growth arrest with similar IC<sub>50</sub> values was observed with FTI-277 and GGTI-298, the methyl ester forms of FTI-276 and GGTI-297.

Noteworthy, the comparison of proteins labelled by [<sup>3</sup>H]FPP or [<sup>3</sup>H]GGPP in different parasite blood-stages also evidenced differences between profile of ring, trophozoite and schizont forms. Actually, it appeared that the ring stage did not transfer [<sup>3</sup>H]FPP onto proteins as compared to [<sup>3</sup>H]GGPP, outlining the key role of protein geranylgeranylation and likely that of PfPGGT-I. Furthermore, the incorporation of [<sup>3</sup>H]FPP and [<sup>3</sup>H]GGPP into proteins was greatly reduced with 25 μM of FTI-277 or GGTI-298 (Chakrabarti et al., 2002). Interestingly, the same trend was observed *in vivo* between both inhibitors while the activity measured for GGTI-297 with purified PfPFT *in vitro* was six times lower than that of FTI-276. Besides, the TLC analysis of prenyls derived from [<sup>3</sup>H]Fol radiolabeled proteins suggests that proteins are mostly geranylgeranylated as only ¼ of protein analyzed released Fol.

To some extent, without any inhibitors, *P. falciparum* would transfer GGPP rather than FPP onto proteins, supporting either one or both hypothesis on the dynamic flexibility of PPTs activities and/or the crosstalk of isoprenoids in *Plasmodium* too. In general, FTIs tested on *P. falciparum in vitro* exhibit IC<sub>50</sub> values ranging from 0.7 to 1000 nM (Nallan et al., 2005). More recently, Tipifarnib® (R115755, Zanestra) revealed a very good efficacy *in vivo* on *P. falciparum*

3D7 strain ( $IC_{50} = 0.1 \mu\text{M}$ ) and *in vitro* ( $IC_{50} 0.01 \text{ nM}$ ) (Ha et al., 2015). Interestingly, treatment of *P. falciparum* human-infected cells with FTIs appeared to disrupt specifically the function of malarial mitochondria through an increase in the production of ROS. Although, no study on prenylated proteins was performed, these findings suggest that they are involved in the regulation of the mitochondrial electron transport chain or ROS signaling. In spite of the fact that research pursue investigations for inhibitors mimicking isoprenoids precursors or PPTs substrates, other studies claim new activities with other molecular structures (Jahnke et al., 2010; Durrant et al., 2011; Gisselberg et al., 2017). Accordingly, this novel family of non-bisphosphonate inhibitors including MMV019313 or MMV008138 inhibit PfFDS/GGDS *via* another site than bisphosphonate inhibitors (Gisselberg et al., 2017). MMV019313 exhibit  $IC_{50} = 0,33 \mu\text{M}$  for FPP synthesis *in vitro* and  $2 \mu\text{M}$  for FPP or  $9.8 \mu\text{M}$  for GGPP in the presence of high substrate level. In fact, *P.falciparum* treated with  $5 \mu\text{M}$  of MMV019313 was rescued with  $200 \mu\text{M}$  of IPP and mutation of PfFDS/GGDS (S228T) induced resistance. Remarkably, according to the enzyme 3D-structure, this position is located close to the IPP site and at the base of a putative allosteric site, suggesting a novel mechanism of action for MMV019313.

All in all, for cancer such as against malaria the inhibition of prenylation has shown promising results *in vitro*. However, *in vivo* results are still very patchy and reflect the lack of knowledge on protein prenylation mechanisms. Although highly effective inhibitors have been identified, acting on the active sites of prenyl substrate biosynthesis pathways or PPTs, they also induce cell resistance to balance the absence of prenyl precursors or PPT activities under inhibition (Eastman et al., 2005). Recent studies have also shown that indeed, it is possible to improve results in some cancers by combination of FTI and GGTI. To some extent, is there any future for protein prenylation inhibitors? Is it reasonable to pursue this approach with limited knowledges on the flexibility of protein prenylation mechanisms? Wouldn't it be more judicious to describe the dynamic flexibility of PPT activities *in vivo*?



## 2.8 HERE ARE OUR WARRANTS AND OUR MISSION

Today, we are not only facing such mistakes as outlined in **section 0**, but we are also offering explanations and solutions. Different aspects related to protein prenylation must be clarified in order to understand and interact with the protein prenylation for applications in the pharmaceutical, agronomic and cosmetic fields.

### 2.8.1 Crop Fields in a no Freshwater's Land

Considering the global warming and repeated droughts over the last years, the management of water resources for field crops became a key factor for the future. Also, intensive farming and varietal selection have so far fostered widespread of phytopathogens (Andow, 1983; Lundgren et al., 2009; Yahya et al., 2017). Thus, how can we feed a blooming population with dwindling freshwater resources? Raising the fact that pests develop resistances to pesticides (Khan et al., 2015), the latter being also a matter of debate. Can we limit damages caused by some phytopathogens without increasing pesticide treatments? Addressing these questions, the study of protein prenylation in plant offers promising prospects. Accordingly, the *A. thaliana* PPTs mutants exhibit ABA phenotype as observed by a reduced stomatal aperture, conferring them a remarkable drought and salt resistance (Chinnusamy et al., 2005). Although the *plp* mutant is rather sick and *era1* shows growth delay, the growth rate of *ggb* mutants is similar to the WT. Also, it was evidenced that stomatal enclosure in *era1* decreases susceptibility of plant to pathogens bacteria. While prenylated proteins such as AGG1 and 2, CYP85A2, ROP9, ASG2 are involved in ABA signaling and stress response (**section 2.3.3**), our vision of protein prenylation mechanism and prenylated proteins engaged in PPT mutants is still limited. In this context, to understand protein prenylation in *A. thaliana* mutant address new perspectives for plant breeding of naturally drought tolerant and pest resistant cultivars.

### 2.8.2 Plant factory Twisted for Valuable Isoprenoids

Isoprenoids have shown to be induced in response to stress in plants. For example, it has been shown that capsidiol (C15) in tobacco is induced in response to elicitation with cellulase. In consequence, the plant arrests sterol synthesis from FPP (Chappell and Nable, 1987), meanwhile the HMGR remains stimulated increasing the concentration of FPP precursor

available for the capsidiol production. Moreover, previous studies have evidenced that induced-capsidiol production is abolished by the treatments with protein prenylation inhibitors such as FOS or GGT-2133 (Huchelmann et al., 2014). At the opposite, the HMGR is still highly expressed under these conditions, raising the question of: what tobacco plants do with the MVA if both sterol and capsidiol biosynthesis are impaired? Could we use this hypothetical pool to drive the biosynthesis of specialized metabolites? With this respect, several other valuable molecules such as artemisinin (antimalarial), mono indole terpene alkaloids (anticancer) or carotenoids (dietary supplement) can be biosynthesized from both MVA and MEP precursors (Camara et al., 1992; Courdavault et al., 2009; Schramek et al., 2010; Vranová et al., 2013; Kumar et al., 2020). Is it possible to increase or diversify the production of molecules with a high-added value by using protein prenylation inhibitors?

### **2.8.3 To Recognize Target in Order to Cure Different Ailments**

The PPTs and MVA/MEP biosynthesis enzymes have been proposed as possible targets for the design of new efficient drugs interfering with their activity (Ochocki and Distefano, 2013). Although, cancer, malaria, progeria are investigated since decades, other studies are interested by interfering in host-pathogen interactions with viruses or bacteria (Brioschi et al., 2017). Also, other studies revealed a decrease in  $\alpha$ -subunit of PFT,  $\beta$ -GG of PGGT-I and PGGT-II in schizophrenia, supporting a putative abnormal protein–protein interactions and protein localization in schizophrenia (Pinner et al., 2020). Finally, several other applications in nonalcoholic fatty liver disease, cardiac and vascular, neurodegenerative pathologies have been suggested (Hooff et al., 2010; Xu et al., 2015; Yang et al., 2016). What are the targets? How does protein prenylation works in all these cell-types? To some extent, is there any perspective to interact specifically with mutated prenylated proteins?

#### 2.8.4 Problems in Inhibitor Conception. The RAS Model

In general, targeting protein-protein interactions, cellular localization or species-specific signaling pathways are prime targets for inactivation of cell proliferation. In this context, farnesylated-RAS proteins are relevant as mutations in *ras* oncogenes are globally found in ~30% of malignant tumor cells (Prior et al., 2012). It causes a constitutive activation of those GTP-binding proteins regulating signal transduction pathways leading to cell proliferation *via* MAP kinases (Gelb, 1997), with K-RAS most often point-mutated (McCormick, 2019). Unfortunately, it turned out that the biological inactivation of RAS is a very challenging task (Khan et al., 2020). Intense work was and still is ongoing to isolate drugs interfering with the proper location of RAS, and thus with protein lipidation. In the presence of specific PFT inhibitors, RAS proteins have been found to be modified by geranylgeranyl allowing Ras to stay biologically active (Whyte et al., 1997). This cross-reactivity can be considered as a resistance acquisition.

Thus, alternative, promising strategy to block RAS activity have been undertaken to isolate a clinically effective inhibitor, while this observation opens new biological questions in the field of protein prenylation studies: why an unspecific lipidation is possible? How is unspecific prenylation regulated? What are the borders for unspecific prenylation?

At first sight, it can appear very surprising that such basic questions are not considered as a priority and solved yet, but to answer such questions, modification of proteins in a cellular environment has to be considered. Most of studies dealing with these questions are made *in vitro* adding substrates, using recombinant proteins and in the best cases cell extracts, which cannot respond to physiological stimuli and therefore cell regulation. Nevertheless, at the present time and despite considerable efforts, one of the major limits in studying protein prenylation remains a lack of basic understanding of its biochemical regulation process *in vivo*.

### 2.8.5 Limits in Studying Protein Prenylation

Thus, understanding the regulation of protein prenylation *in cellula*, at a molecular level, still needs to be addressed as only one recent example is relevant (Wilkins et al., 2020). Here are the questions: why type-I protein prenylation does involve two prenyl-substrate, which differ only by one isoprene unit? Also, why it requires two distinct enzymes, which at the same time must be linked through the use of a common  $\alpha$ -subunit? Moreover, how critical is it that a dedicated protein is modified by a F group rather than by a GG group, or *vice versa*? Is protein prenylation in eukaryotes only limited to those substrates? To address those questions, we propose to use plants as a universal model (**Figure 40**). In this context, this thesis will focus on how plants support a gain of knowledges of this subject with many applications in medical research.

As a consequence, several limits in studying regulation of protein prenylation have to be considered. A non-exhaustive list can be enumerated as follows:

- (a) Substrate specificities are exclusively studied *in vitro* without considering possible regulation of activities in a cellular context, in which the enzyme does not occur as an isolated entity.
- (b) Technical challenges to study regulation of prenylated protein *in vivo* due to their hydrophylic-lipophylic character, a very low abundance *in cellula* (1 – 2 %) and their physicochemical properties.
- (c) What modification occurred *in cellula*? FPP and GGPP were defined as the prenyl diphosphate donors used for protein prenylation, but GPP, phytylPP, polyprenylPP are also synthesized in organisms of interest. In addition, post-prenylation processing event such as CaaX proteolysis and carboxymethylation were proposed as regulation point for membrane targeting. How to distinct between the use of FPP, GGPP, other hypothetical prenyl substrate and post-prenylation stage of protein prenylated *in vivo*?

Therefore, this entire thesis pictures a young researcher exploring the protein prenylation's far side to report the dynamic flexibility of PPTs and other pieces related to isoprenoid metabolism in living plants.

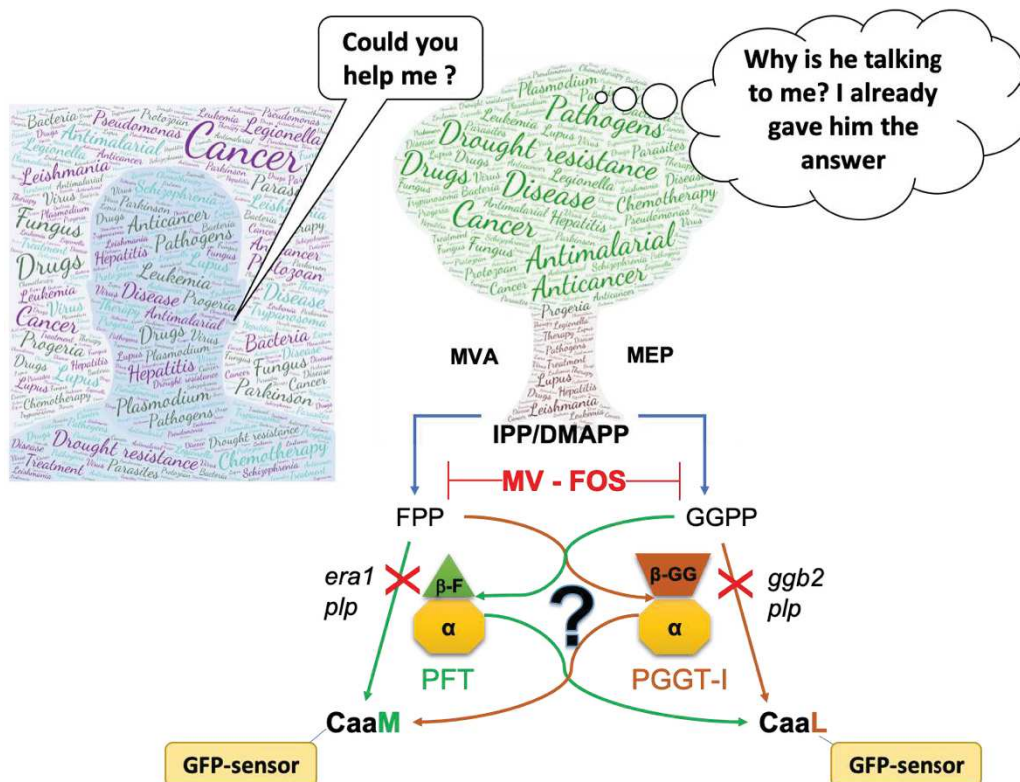


**Figure 40 Study of the dynamic flexibility of protein prenyltransferase activities in plants, key issues for the treatment of human diseases and global warming.**

Here is a caricature of a human calling for Plant help to treat various pathologies affecting millions of people by cancers and various parasitic diseases including malaria (words displayed on Human). The plant that does not speak the same language has already warned of solutions (words displayed on plants). In fact, plants already proposed to humans some of its secrets, humans only have to pay interest to it. In a caricatural way, the plant confronts the human being with the fact that it is necessary to clarify some concepts on the mechanisms of protein prenylation occurring in living organisms.

Thus, the plant likes to remind that protein prenylation depends on protein prenyltransferases (1), the **PFT** and **PGGT-I** transfer FPP and GGPP respectively onto proteins with a CaaX Box at C-ter end. In this context, it also reveals that it is possible to ethically and precisely follow these mechanisms *in planta*. Therefore, the **X** of the CaaX motif can be replaced by **M** to study farnesylation or by a **L** to study geranylgeranylation *in vivo* with a fluorescent GFP-sensor protein. In the plant, the FPP and GGPP substrates are supplied by the MVA and MEP pathway respectively. It is therefore possible to use inhibitors such as mevinoline (MV) or fosmidomycin (FOS) to inhibit each or both type of protein prenylation. With this respect, the plant has a considerable advantage, namely, mutant congeners that survive in the absence of active PFT (*era1*), PGGT-I (*ggb2*) or both prenyltransferase proteins (*plp*). While these cases are lethal in other kingdoms and especially animals. How is this possible? At what level does flexibility take place? At the prenyl donor substrates, the protein acceptor substrates, or both? This is the most prominent point proposed by studying these mechanisms in a plant model.

## 2.9 I'M TAKING MY LABPACK

Ensuring a biological model that allows an easy biochemical characterization is critical for *in vivo* study. Here we argue in favor of plant models that have several positive properties as compared to other organisms and that will allow to solve some of the problems (**section 2.4**). Indeed, previous studies with PPTs mutants in *A. thaliana* have clearly demonstrated the advantage of the plant model in the study of protein prenylation flexibility (**section 2.4.2, 2.4.3**) In addition, tools have been developed to observe the localization and *statu quo* of prenylated proteins *in vivo*. Accordingly, investigations carried out by the Isoprenoid Biology Laboratory (IBMP, Strasbourg) have led to the development of a GFP-CaaX from the CaM61 inspired by previous reports of CaM53 (Gerber, 2005; Gerber et al., 2009a). This sensor modified with the motifs -CVIM (farnesylation), -CVIL (geranylgeranylation), -SVIL (absence of prenylation) allows distinction between non prenylated state (nuclear localization) or prenylated state (plasma membrane). Consequently, pharmacological approaches allow the observation of the prenylation state in the presence of MVA or MEP pathways inhibitors or in *A. thaliana* mutants lacking PFT (*era1*), PGGT-I (*ggb-2*) or both (*plp*) (Andrews et al., 2010; Huchelmann, 2013). Treatment of tobacco BY-2 cells and leaves expressing GFP-CaaX sensors under inhibition of protein prenylation has revealed that plants use the MVA and MEP pathways for the biosynthesis of PPTs prenyl substrates (Hemmerlin et al., 2003; Gerber, 2005; Gerber et al., 2009a). In this respect, these findings provided a new backbone not only to support the existence of such flexibility in plants, but also to develop a screening system for inhibitors of protein prenylation *in vivo*, considering their efficacy in view of metabolic flexibility (Hartmann et al., 2015).

As a hit, the *S*-carvone shut down protein prenylation by inhibition of PPTs in BY-2 cells and tobacco leaves, resulting in a nuclear signal from the GFP sensor and inhibits the production of capsidiol, a phytoalexin produced in *N. tabacum* (Huchelmann, 2013; Huchelmann et al., 2014). Therefore, as an inhibitor of PPTs, the *S*-carvone has been used to evaluate the importance of the crosstalk in protein prenylation from a biological point of view. In this context, it was shown that feeding with prenyl precursors or elicitation of tobacco leaves by 0.5% cellulase can partially rescue the inhibition of protein geranylgeranylation by *S*-carvone (Huchelmann et al., 2014). Accordingly, it was concluded that geranylgeranylated proteins are involved in the defense signaling pathways.

The hypothesis supported that through “survival instinct”, the cell would be able to adjust the supply of prenyl substrates and the activity of PPTs to maintain prenylation of proteins involved in stress response induced by an inhibitor of protein prenylation.

Remarkably, the tales about protein prenylation inhibitors in plants, cancer cells and malaria offer similar morals. As a snake biting its own tail, the stress induced by protein prenylation inhibitor is sufficient to push down itself until its disappearance. At some point, as stress response has a fitness cost and every cell has to grow, thus other factors involved in stress might control the activity of PPTs to break the circle. What is the plan to catch the snake charmer?

## 2.10 WHAT DO I FEATURE?

### 2.10.1 Condition Inducing Flexibility of PPTs and Analysis of Prenylated Proteins in Plants

In the current situation, a priority is to understand the physiological conditions inducing the dynamic flexibility of prenyltransferase protein activities, but also to unambiguously identify the partners involved in protein prenylation. By using the prenylatable GFP-sensor established in the laboratory to study protein prenylation ([Gerber et al., 2009](#)), I identified conditions inducing *in vivo* changes in the substrate specificities of PPTs. Besides, to characterize the change in substrate specificity according to the environmental conditions, I developed a protocol for the purification and systematic analysis of prenyl and protein moieties allowing identification of prenylated proteins *in vivo*.

### 2.10.2 Driving Isoprenoids Production *via* Protein Prenylation Inhibitors

The stimulation of plant isoprenoid pathways after elicitation by biotic or abiotic stimuli is so far reported and they usually supply the needs for prenyl precursors for specialized metabolites biosynthesis. As a matter of fact, different prenylated proteins were reported to intervene in the biosynthesis of hormones, specialized metabolites and in their regulation. Thus, it was stated that *S*-carvone inhibits elicitation-induced capsidiol production by blocking protein prenylation (Huchelmann et al., 2014). In contrast, the production of MVA, its precursor, remains strongly stimulated (Huchelmann et al., 2014). This result suggests that controlling the prenylation of some proteins in plants could result in a pool of MVA available to produce molecules of interest. Is it possible to drive the flux of isoprenoids for specialized metabolites production by combining elicitation and inhibitors of protein prenylation? Thus, to understand the role of the crosstalk and PPTs in the production of high value-added isoprenoids, I compared the effect of light, *S*-carvone and its *R*-enantiomer on elicited tobacco plants grown under different conditions.



### **2.10.3 Screening of Protein Prenylation Inhibitors: Anticancer and Antimalarial Compounds**

Since protein prenylation was proposed as a key target for the development of new anticancer and antimalarial, I screened a set of synthetic and natural compounds on the plant cell model developed in the laboratory. Accordingly, a set of prohibitin (PHB) inhibitors which exhibit anticancer properties on different human cell lines was provided by L. Desaubry (LIT, Strasbourg). In fact, PHB are reported to act on prenylated proteins such as K-RAS and C-RAS (Polier et al., 2012; Moncunill-Massaguer et al., 2015; Yurugi et al., 2017), hence PHB or downstream protein may regulate the prenylation of protein *in vivo*. Furthermore, studies with red algae extracts have shown promising activity against intraerythrocytic *P. falciparum*. As the MEP pathway was identified in both red alga plastids and *P. falciparum* apicoplast, I screened red algae extracts studied by L. Margueritte (PhD 2018 – LIT ; (Margueritte, 2018)) to evaluate whether activity against *P. falciparum* may result from the inhibition of the MEP pathway. Finally, many inhibitors of PPTs are characterized by the presence of a prenyl moiety which fit in the active site of PPTs but cannot be transferred. Interestingly, a preliminary study with BY-2 cells expressing GFP-CVIL resulted in an atypic phenotype after inhibition with acetylvismione-D, a prenylated anthranoids (Hartmann et al., 2015).

In this respect, I pursued an investigation with vismiones extracted from *Psorospermum Glaberimum*, described by J.B. Galle (PhD 2015 - LIT; (Galle, 2015)) and dihydroanthracenone analogs synthesized by N. Wasser (PhD 2018 – LIT ; (Wasser, 2018))

### **2.10.4 Characterization of Prenylated Anthranoids Fluorescence *In Vivo***

A peculiar fluorescence was noticed specifically in BY-2 cells treated with prenylated anthranoids and therefore associated to autofluorescence. Although the fluorescence of anthranoids is reported, the vismiones fluorescence *in vivo* was never characterized. Moreover, the degradation of vismiones into anthrone, anhraquinones and dianthrone resulted in changes in fluorescence. Therefore, I developed an approach to observe the fluorescence of vismiones and related anthranoids *in vivo*, combining spectral imaging (Slmaging) microscopy and non-targeted metabolomic analysis by HPLC-MS/MS.

### 3 MODULATION OF PROTEIN- PRENYLTRANSFERASE SUBSTRATE SPECIFICITIES



### 3.1 INTRODUCTION

Many studies contributed to the characterization of PPTs in yeast and later in animals (Wang and Casey, 2016). Resolution of PPTs 3D structures emphasize a preference of PFT for FPP and PGGT-I for GGPP (Casey et al., 1991), but there is still no published report of 3D structures in plants. Besides, the crystallographic analysis of the PPTs with their substrate provided a clear molecular picture of the protein prenylation reaction kinetic (**section 2.3.4, Figure 25**) (Lane and Beese, 2006; Jiang et al., 2018). Furthermore, the canonical substrates of PPTs were confirmed with *in vitro* enzymatic assays using radiolabeled prenyl diphosphates and substrates bearing CaaX motifs (Goodman et al., 1990; Mitsuzawa et al., 1995; Gelb, 1997; Long et al., 2002; Scott Reid et al., 2004; Yokoyama et al., 2008; Wang and Casey, 2016).

Although PFT preference for FPP was confirmed in plants, the latter also seemed able to transfer GGPP onto -CVIM farnesylation substrate (Randall et al., 1993; Huchelmann, 2013). Moreover, PGGT-I was highly selective for the GGPP, but was also able to ensure its transfer onto substrates with CVIL geranylgeranylation motif or -CVIM. It was found that the prenylation inhibitors developed as anti-cancer drugs did not reach the expected results despite their efficacy *in vitro* (Whyte et al., 1997; Holstein and Hohl, 2012; Wang et al., 2017). Actually, PPTs used in *in vitro* studies were produced in heterologous system, and therefore did not take into account possible regulations *in vivo*. Accordingly, it became more suspicious that the activity of the PFT is versatile and might be regulated by eukaryotic cell mechanisms such as PTMs or protein-protein interactions.

Experiments performed with acellular extracts isolated from BY-2 cells showed that protein bearing a CVIL geranylgeranylation motif can be labelled with [<sup>3</sup>H]FPP (Randall et al., 1993; Gerber et al., 2009a; Huchelmann, 2013). Interestingly, none of the purified enzymes, produced in *E. coli* could use this combination of substrates, evidencing a possible regulation of PPT activity in eukaryotic cells. Considering that plants produce FPP through the MVA pathway and GGPP via the MEP pathway (**section 2.4.3, 0**), the plant model seems particularly suitable to study protein prenylation mechanisms which occur in all eukaryotes (Yalovsky, 2011; Hemmerlin et al., 2012; Hemmerlin, 2013). On the top of that, viable *A. thaliana* KO mutants defective in the production of  $\beta$ -F (*era1*),  $\beta$ -GG (*ggb-2*) or  $\alpha$  (*plp*) subunits have been characterized and allow to investigate the implication of each PPTs in prenylating specific protein substrates (Cutler et al., 1996; Running et al., 2004; Johnson et al., 2005).

Thus, a plant cell model expressing GFP-sensor of protein prenylation has been used in the laboratory to evaluate the dynamic flexibility of protein prenyltransferase activities *in vivo* (**section 0**). First, experiments conducted with BY-2 cells expressing GFP-sensor inhibited by MV and FOS have shown that indeed, it is possible to complement protein prenylation of a GFP-CVIL, using external prenyl substrates such as Fol, GGol, or MVA precursor. Then, similar studies with tobacco leaf discs indicated that the line expressing GFP-CVIM contain prenylated (membrane) and unprenylated (nucleus) forms under standard growth conditions unless BY-2 cells where only the membrane is labeled (Huchelmann, 2013). At the opposite of tobacco roots and BY-2 cells, the prenylation of GFP-CVIM in tobacco leaves could not be hindered even with MV and FOS at concentrations up to 20 and 200  $\mu\text{M}$ , respectively. Moreover, although a full inhibition of GFP-CVIL prenylation was achieved with 300  $\mu\text{M}$  FOS, same results were obtained with combination of 5  $\mu\text{M}$  MV and 50  $\mu\text{M}$  FOS, proposing that MVA pathway must contribute to the protein prenylation of geranylgeranylated proteins too. Remarkably, complementation assays with phytol have demonstrated its ability to restore protein prenylation in tobacco leaves while in BY-2 cells this compound had no effect (Huchelmann, 2013). These findings are compatible with a hypothetical mobilization of phytol through chlorophyll catabolism as it is the case for tocopherol biosynthesis (Ischebeck et al., 2006; Gutbrod et al., 2019). It also suggests that phytol kinases required to activate phytol into phytol diphosphate may exclusively be functional in photosynthetic tissues. Likewise, the inhibition with 50  $\mu\text{M}$  FOS and 1  $\mu\text{M}$  MV of a GFP-CVIL protein substrate expressed in BY-2 cells could be reversed by elicitation with cellulase (Huchelmann, 2013; Huchelmann et al., 2014).

These results indicated that elicitation modulates not only the metabolic flow of isoprenoids through induction of MVA biosynthesis, but also protein prenylation capacity. Because elicitation of tobacco plants induces a *hmgr* expression (Chappell and Nable, 1987), it can be speculated that a rise of MVA concentrations provides such a signal that switch on the flexibility of the PFT activity (Huchelmann, 2013). Other experiments supported this hypothesis as GGTi-2133 alone did not lead to a total shutdown of cellulase-induced capsidiol production, being by the way fully suppressed with 2 mM *S*-carvone (Huchelmann et al., 2014). Accordingly, it has been suggested that PFT rescues the lack of PGGT-I activity and at least one geranylgeranylated protein is involved in the cellulase-induced signaling cascade.

For this reason, the flexibility of PFT activity could provide a backup when protein geranylgeranylation or the biosynthesis of GGPP are inhibited, for example under interaction between plant and FOS-synthesizing *Streptomyces spp.* This study pinpointed an interconnection between stress and protein prenylation, proposing that flexibility of PFT activities must be essential for biotic interactions involving protein prenylation inhibition. However, such physiological properties are still a matter of debate as the amount of product used to realize experiments could differ from the physiological concentrations. We were therefore interested to find stress signals triggering such flexibility in a cellular context.

Also, forasmuch as glycolysis provides precursors for isoprenoids biosynthesis, it can be speculated that the concentration of sucrose in the culture medium impacts protein prenylation. Moreover, it is well reported that addition of external sugar improves plant growth and chlorophyll content (Eckstein et al., 2012; Shah et al., 2019). In this context, is the protein prenylation already influenced in BY-2 cells cultivated in MS with sugar? Thus, tobacco leaves from plants grown on culture media enriched with sucrose or not were compared too, in order to evaluate the influence of sugar on protein prenylation capacity in plants.



## 3.2 PHYTOHORMONAL REGULATION OF PROTEIN PRENYLATION IN PLANTS

### 3.2.1 Flexibility of Protein Prenyltransferases in BY-2 Expressing GFP-CVIL

It has been reported that in plants, the response to cellulase is mediated by the jasmonates (JA) signaling pathway (Ranjan et al., 2015; Saravanakumar et al., 2016). Thus, we propose that JA signaling pathway, being activated by cellulase (Saravanakumar et al., 2016), can switch on the flexibility of PPTs activity *in vivo* to maintain a decent level of prenylated protein essential for the JA response itself. Therefore, we have evaluated the influence of MeJA on the protein prenylation using BY-2 cells inhibited with FOS or/and MV. In this context, inhibitors were added prior induction of the protein to control substrate origin and determine the FPP or GGPP substrate nature.

First, BY-2 cells expressing the GFP-CVIL protein were treated with 100  $\mu$ M FOS, inhibiting thus the MEP-derived GGPP biosynthesis. Under these conditions, the GFP-CVIL sensor undergoes in the nucleus because it cannot be prenylated indeed. Different concentration of MeJA ranging from 0.5 to 20  $\mu$ M were simultaneously added to address relocation of GFP-sensor in the membrane, meaning that MVA derived prenyl diphosphate would be used to modify GFP-CVIL. As a result, the observation by confocal microscopy confirmed that MeJA exhibits a dose-dependent effect on the prenylation capacity of the GFP-CVIL protein in BY-2 cells devoid of GGPP (**Figure 41**). At 0.5  $\mu$ M MeJA, 95% of BY-2 cells exhibit at least a part of the GFP fluorescence in the plasma membrane as compared to the 20% in the FOS-treated control cells. The increase in MeJA concentration gradually restored the proportion of cells with GFP-CVIL completely located in the plasma membrane, reaching an equivalent level to the negative control with 20  $\mu$ M MeJA.

As reported, the expression of *hmgr* and other terpenoid synthases are enhanced by MeJA treatment, improving the production of plant defense molecules such as terpene indole alkaloids in *Catharantus roseus* (Maldonado-Mendoza et al., 1994; Schluttenhofer et al., 2014). Since we inhibited the MEP biosynthesis pathway, we hypothesized that in MeJA treated cells, the MVA pathway takes over the supply of the prenyl group used to modify GFP-CVIL. To prove that under these conditions, MVA is a new precursor, MV was added at 10  $\mu$ M, a treatment that abolished the membrane localization (**Figure 42**).



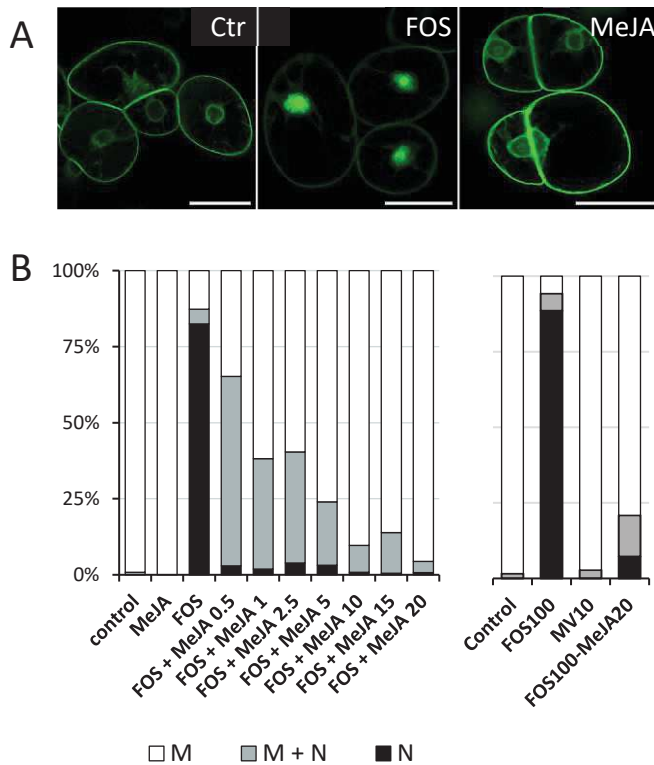


**Figure 41 MeJA rescues prenylation of GFP-CVIL under inhibition by fosmidomycin (FOS).**

(A) Tobacco BY-2 cells transformed with pTA-GFP-CVIL were treated with 100  $\mu\text{M}$  FOS and 20  $\mu\text{M}$  MeJA for 3 hours, before expression of GFP-CVIL induced with 15  $\mu\text{M}$  dexamethasone. Pictures are representative of the phenotype of a majority of cells in non-inhibited cells (Ctr), inhibited with 100  $\mu\text{M}$  FOS alone or supplemented with 20  $\mu\text{M}$  MeJA (MeJA). The white bar represents 50  $\mu\text{m}$ . (B) Dose-dependent effect of 0.5 to 20  $\mu\text{M}$  MeJA on the protein prenylation capacity of GFP-CVIL under inhibition with 50  $\mu\text{M}$  FOS in BY-2 cells induced 3h after treatments. Indicated, the proportion (%) of cells showing a GFP fluorescence phenotype localized in the plasma membrane only (white), in the plasma membrane and nucleus (grey) and in the nucleus only (black). The right histogram shows the absence of MV effect on prenylation of GFP-CVIL

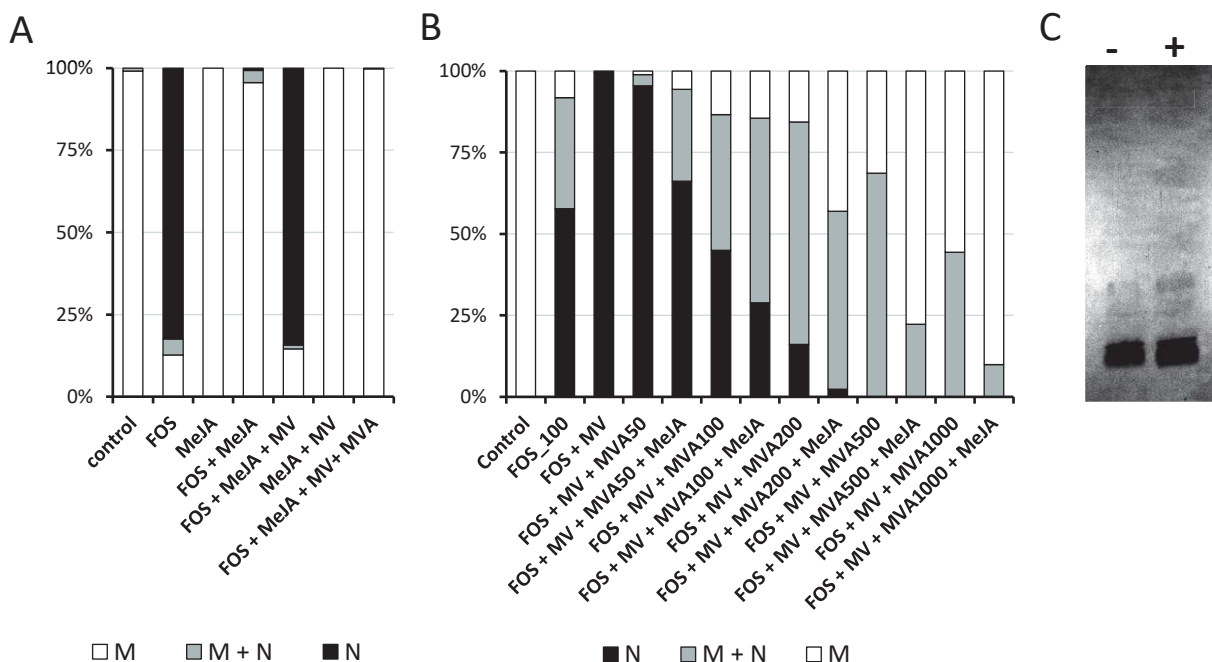


**Figure 42 The MVA pathway supply prenyl precursor under MeJA-induced stress in the presence of fosmidomycin (FOS), a protein prenylation inhibitor.**

(A) Tobacco BY-2 cells transformed with pTA-GFP-CVIL were treated as indicated with 50  $\mu\text{M}$  FOS and 20  $\mu\text{M}$  MeJA for 3 hours, before expression of GFP-CVIL induced with 15  $\mu\text{M}$  dexamethasone. The protein labeling is avoided in the presence of 10  $\mu\text{M}$  mevinolin (MV) and reversed in the presence of 1 mM MVA. (B) Dose dependent effect of 50 to 1000  $\mu\text{M}$  MVA on the protein prenylation capacity of GFP-CVIL in BY-2 cells treated with 100  $\mu\text{M}$  FOS, 10  $\mu\text{M}$  MV and/or 20  $\mu\text{M}$  MeJA. (C) [ $^{14}\text{C}$ ]MVA incorporation into prenylated proteins of tobacco BY-2 cells treated with (+) or not (-) with 20  $\mu\text{M}$  MeJA during 24 hours.

Accordingly, the presence of MV with FOS maintained the inhibition of protein prenylation even in the presence of 20  $\mu\text{M}$  MeJA (**Figure 42**), supporting that the prenyl transferred derived from the MVA pathway. It is noteworthy that under the absence of FOS, MV does not inhibit protein prenylation in MeJA treated cells, indicating that the MEP pathway has to be inactive to allow a switch toward the MVA pathway (**Figure 42**). The adjunction of 50 to 1000  $\mu\text{M}$  MVA with MeJA restored protein prenylation at a dose-dependent level. Although no cell with a nuclear phenotype was observed with 1 mM MVA and MeJA, it appears that FOS prevents full complementation as the ratio of cells with full membrane phenotype never reached 100% as compared to the negative control. Finally, [ $^{14}\text{C}$ ]MVA feeding experiments using BY-2 cells under MeJA-induced flexibility of PPTs confirmed an incorporation of MVA into prenylated proteins (**Figure 42**).

MeJA induced the flexibility of PPTs activities indeed, but the regulation of such mechanism might depend of the plant hormone balance rather than individual hormone effect, as reported in plant development and stress responses (**section 0, Figure 11**). For instance, ethylene and JA hormones act in synergia to trigger plant defense (Xu et al., 1994; Liu et al., 2004; Yang et al., 2019). Besides, JA and ethylene signaling are integrated into auxin signaling in root development process (Xu et al., 2020). In contrast, JA signaling is antagonized by CK involved in plant growth, pointing out the dilemma of defense and growth in plant (Pieterse et al., 2012; Jang et al., 2017). In this regard, experiments were carried out under identical conditions with 20 to 250  $\mu\text{M}$  Ethephon (Ethep), 20  $\mu\text{M}$  kinetin (Kin) and 20  $\mu\text{M}$  indole acetic acid (IAA) alone or combined with MeJA at different concentrations. Accordingly, a decrease in the percentage of cells with full nuclear phenotype as compared to FOS-treated cells indicates that ethylene also increases the capacity for protein prenylation (**Figure 43**). Nevertheless, the effect of 1  $\mu\text{M}$  MeJA alone remains higher than that obtained with 50  $\mu\text{M}$  Ethep and slightly lower than 100  $\mu\text{M}$  Ethep. Interestingly, it appears that ethylene and JA acts in synergia because full nuclear phenotype represented only 6% in BY-2 treated with 50  $\mu\text{M}$  Ethep and 1  $\mu\text{M}$  MeJA as compared to each of 1  $\mu\text{M}$  MeJA (34%) or 100  $\mu\text{M}$  Ethep (13%). Furthermore, results obtained with MeJA combined to Kin were consistent with those expected, supporting that CK antagonizes JA-induced flexibility of PPTs activities, while ethylene act as a synergist of JA (**Figure 43**). As, different concentrations of IAA were not compared, it was only proved that IAA does not antagonize JA effect.

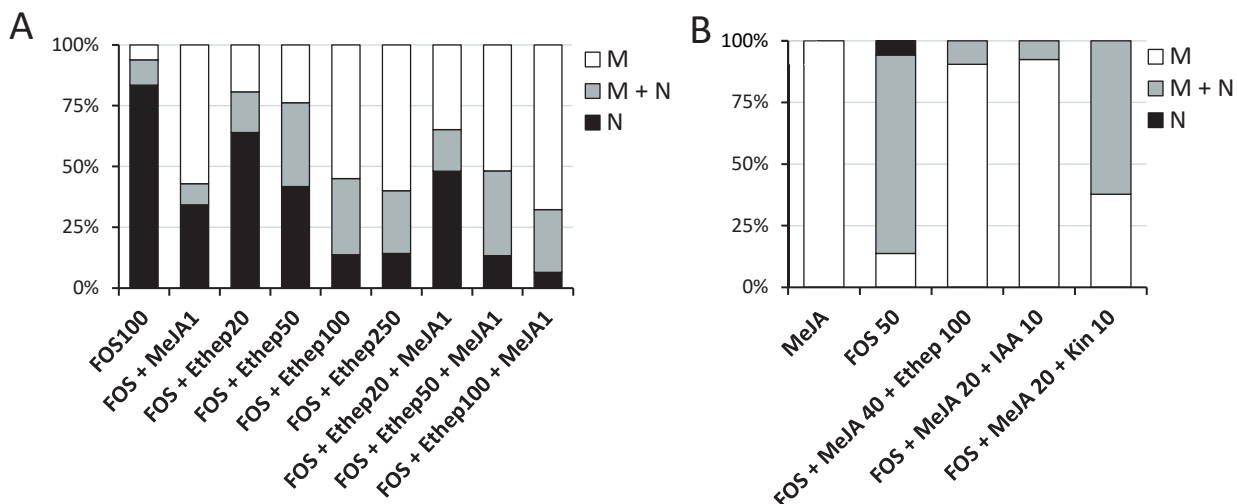


**Figure 43 Induced-MeJA response is influenced by synergism and antagonism with other hormones in protein prenylation.**

(A) Synergism between 1  $\mu$ M MeJA and 20 and 250  $\mu$ M Ethephon (Ethep) affects the protein prenylation capacity of GFP-CVIL in BY-2::GFP-CVIL cells inhibited by 100  $\mu$ M FOS induced 3h after treatments. (B) Influence of 20 or 40  $\mu$ M MeJA in combination with 10  $\mu$ M kinetin (Kin), 10  $\mu$ M Indole acetic acid auxin (IAA) or 100  $\mu$ M M Ethep. Indicated, the proportion of cells with a GFP fluorescence phenotype located in the plasma membrane only (white), in the plasma membrane and nucleus (grey) and in the nucleus only (black).

Altogether, complementation experiments with hormones reveal new information on the physiological conditions inducing flexibility of PTTs activities in plants. Actually, these results support that plant hormone balance is linked to protein prenylation as reported (Courdavault et al., 2009). This strongly suggests that the activity of PPTs is controlled by environmental conditions. Under stress conditions plants could ensure minimum levels of prenylation of proteins with geranylgeranylation specific motifs being involved in stress responses. We have demonstrated that part of the flexibility relies on changes in the pool of precursors used to synthesize prenyl substrates. However, in BY-2 cells, both PFT and PGGT are active and we cannot identify which enzyme catalyzes the MVA dependent prenylation. Also, it is stated that in plants an exchange may take place between the IPP forms produced in the cytoplasm and chloroplast (Hemmerlin et al., 2003; Laule et al., 2003; Rodríguez-Concepción et al., 2004; Phillips et al., 2008; Wang et al., 2019). Actually, protein prenylation was observed in the *ggb2* and *era1* mutant too, suggesting that flexibility could come from both enzymes (Caldelari et al., 2001; Lavy et al., 2002; Running et al., 2004; Sorek et al., 2011; Johnson et al., 2012). In this context, which enzyme catalyzes the reaction under our conditions? To answer this question, we reached the limits of pharmacological approach in BY-2 cells, proposing further studies on *A. thaliana*, in which mutant's loss of PPT functions exist.

With this respect, *era1*, *ggb2* and *plp* have been described, the GFP sensor can be expressed in these lines to evaluate the effect of each enzyme on protein prenylation. We therefore pursued our study with the *ggb2* line expressing the GFP-CVIL sensor as it cannot be prenylated under standard conditions. Thus, we could determine whether changes in PFT activity can take place. This mutant line was obtained by D.N. Crowell in the realm of a collaboration (Idaho State University, Pocatello, Etats-Unis).

### **3.2.2 MeJA-induced Flexibility of PFT in *ggb2* Mutant Expressing GFP-CVIL**

In *ggb2* mutant, in which the  $\beta$ -GG gene is defective, only the PFT is active. Interestingly, this mutant has a much lower growth delay than its *era1* congener, alluding that PFT plays a key role in the flexibility of PPTs activities as compared to PGGT-I. Thus, a *ggb2::GFP-CVIL* stable line was used to evaluate whether MeJA-induced flexibility can rescue the protein prenylation of GFP-CVIL in the absence of PGGT-I. Under standard growth conditions, GFP-CVIL is located in nuclei, corroborating the fact that PFT does not modify GFP-CVIL *in vitro* (Huchelmann, 2013). *ggb2::GFP-CVIL* plants were treated either with 20  $\mu$ M MeJA or 1 mM MVA together with induction of GFP-CVIL, then localization was compared to the untreated *ggb2::GFP-CVIL* control plants. When treated with MeJA or with MVA, the plants showed a GFP-sensor signal mostly in the plasma membrane while control plants exclusively express the protein in the nucleus (**Figure 44**). Even though some cells exhibited a membrane-nuclear signal phenotype, our results clearly demonstrated that under those conditions, PFT can modify the CaaL protein and that MeJA acts as a signal in this process.

Altogether, we proved that the PFT activity is flexible *in vivo* and can somehow overcome the absence of PGGT-I activity. Moreover, our results emphasize not only the essential role of plant defense hormones in the regulation of PFT activity, but also the importance of the crosstalk between MVA and MEP pathways. In this process, MVA was found to supply prenyl substrates under induced flexibility of PPT activities, but it was impossible to conclude on the nature of the prenyl group transferred onto GFP-CVIL by the PFT. Since MeJA boost the MVA pathway (Chappell and Nable, 1987), it turns out that the concentration of MVA may be critical to ignite the flexibility over a threshold.

This also means that in plant cells, somewhere, a sensing system must exist waiting for MVA increase up to a sufficient pressure to click on the MEP/MVA crosstalk button, remodeling thus the protein prenylation machinery according to the new conditions. Is there other condition able to induce similar process in plants? Accordingly, we were interested in evaluating the influence of sugar on protein prenylation capacity in *tobacco* and *A. thaliana* mutants.

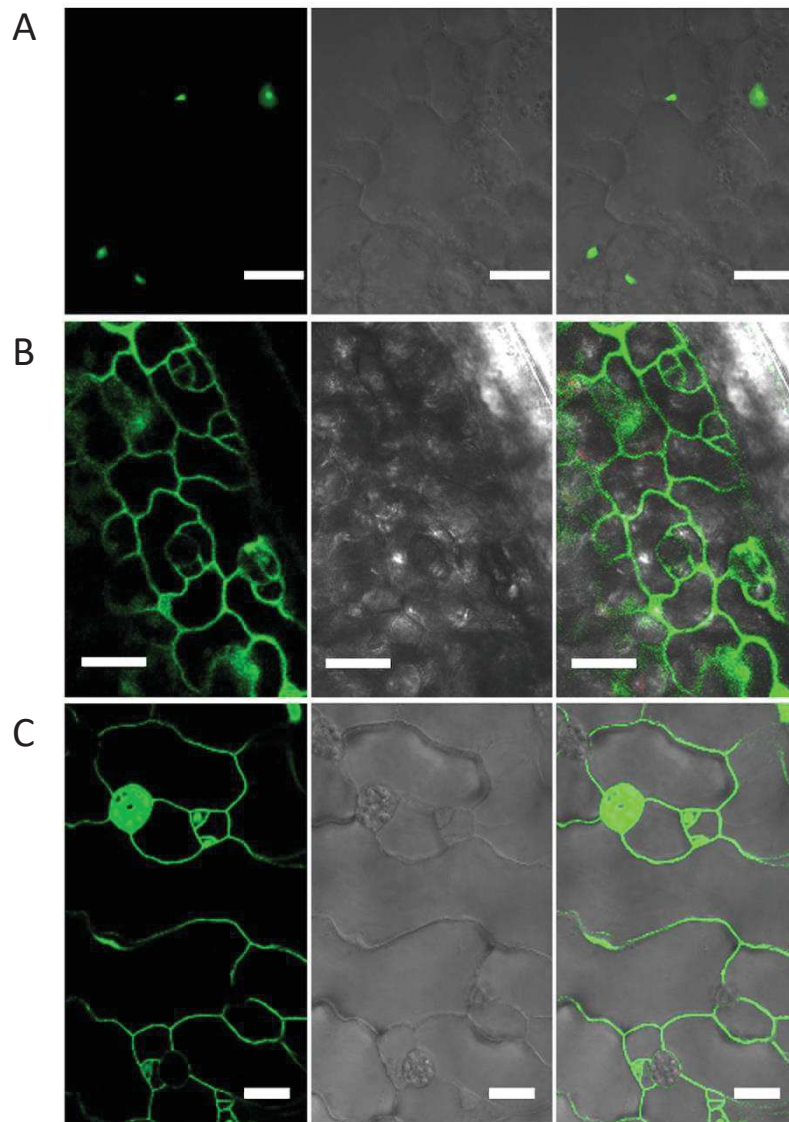


**Figure 44 Flexibility of PFT activity is induced by MeJA and MVA in leaves of *A. thaliana ggb2::GFP-CVIL* mutant lacking of PGGT-I activity.**

Subcellular localization of GFP-CVIL expressed in non-treated *ggb-2 Arabidopsis* mutant (A) transformed with pTA-GFP-CVIL, (B) treated with 20  $\mu$ M MeJA or (C) 1 mM MVA. The GFP fluorescence in the membrane hint that MeJA and MVA rescued protein prenylation in leaves of *ggb2 Arabidopsis* KO mutant plants. The white bar corresponds to 20  $\mu$ m

### 3.3 SUCROSE MODULATES PROTEIN PRENYLATION IN PLANTS

Isoprenoid biosynthesis depends on glycolysis through pyruvate produced by the Krebs cycle, which provide the MVA and the MEP, but also play a key role in the hormone signaling and adaptation to stress (Ruan et al., 2010; Ruan, 2014). Thus, we set up some experiments to test if sucrose influences protein prenylation in *N. tabacum* and *A. thaliana* WT and PPTs mutants expressing GFP-sensor proteins. Originally, the floating method was used for protein prenylation as a standard method in the lab. Nonetheless, the simple fact is that cutting plant leaves prior floating on liquid medium could be associated to wounding by an herbivore, triggering thus a stress response mediated by JA. Because JA modulates protein prenylation capacity (**section 0**), we worked with axenic undamaged and damaged plant material, that were grown for four weeks on MS<sup>1/2</sup> with or without 1% sucrose. Plantlets were watered with the treatment solution a single time directly in the Petri-dishes (InBox) or cut and transferred into treatment solution (Floating) 24h before observation.

#### 3.3.1 Impact of Sucrose on Capacity of Protein Prenylation in Tobacco Plants

Four-week-old tobacco plants induced with 60  $\mu$ M dexamethasone expressed GFP-CVI (M/L) proteins mainly in the plasma membrane (**Figure 45**). Nevertheless, some cells showed membrane and nuclear fluorescence for GFP-CVIL and in previous studies only GFP-CVIM line exhibited this phenotype with the floating method (Huchelmann, 2013). Surprisingly, this nuclear localization decreased with the use of the InBox rather than floating method, especially for the line expressing GFP-CVIM. These results confirmed that tissue damage of plantlets before treatment does affect to some extent, protein prenylation. Although lesions should promote PFT flexibility *in planta*, no difference was observed between Floating and InBox method plants expressing GFP-CVIL. The absence of an inhibitor as observed in BY-2 cells treated with MV alone or the amount of MeJA released by the tissue could have been too low to induce flexibility of PPT activities. Accordingly, where does changes in fluorescence phenotype could come from? To understand, why the localization was slightly different in experiments made by A. Huchelmann in 2013 and the one made more recently, we compared all experimental conditions. One important point is that the lab moved to another place with plant growth conditions that were different.

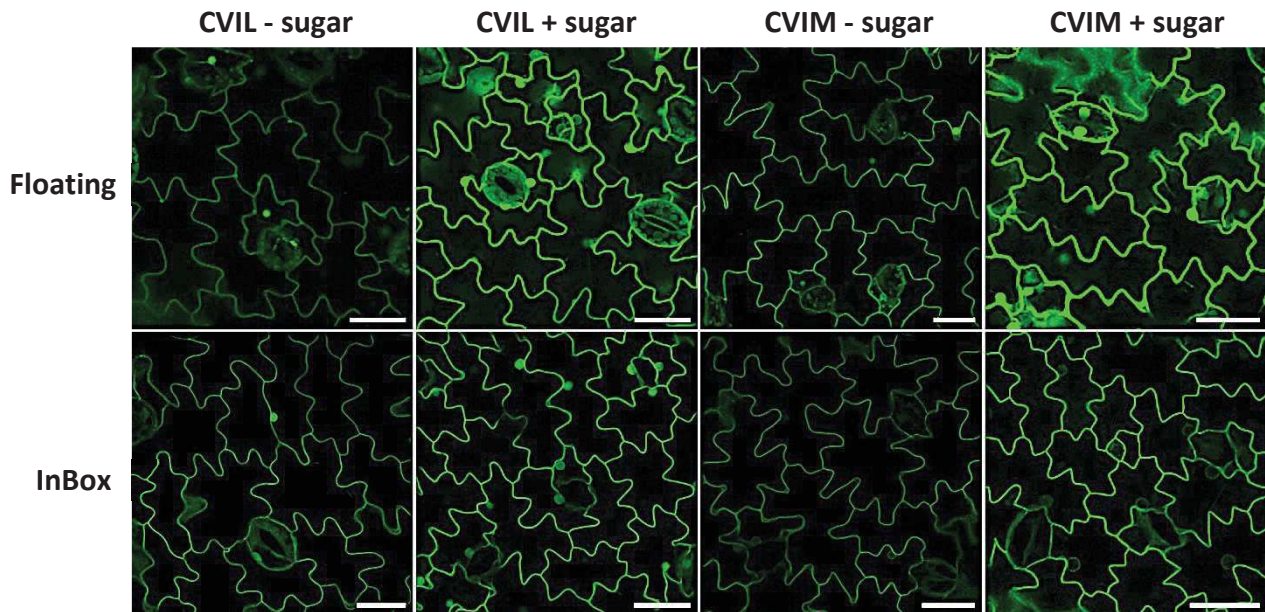


**Figure 45 Influence of tissue damage on protein prenylation in plant.**

Tobacco plants transformed with pTA-GFP-CVIL or pTA-GFP-CVIM were grown for 4 weeks on MS<sup>1/2</sup> with (+) or without sucrose (-), then watered with solution containing 60 μM dexamethasone (InBox) or cut and transfer into induction liquid medium (Floating) for 24h prior to observation by confocal microscopy. Pictures are representative of the phenotype of a majority of cells. The white bar represents 50 μm. The confocal microscope settings were kept for all observation to compare GFP-fluorescence intensity.

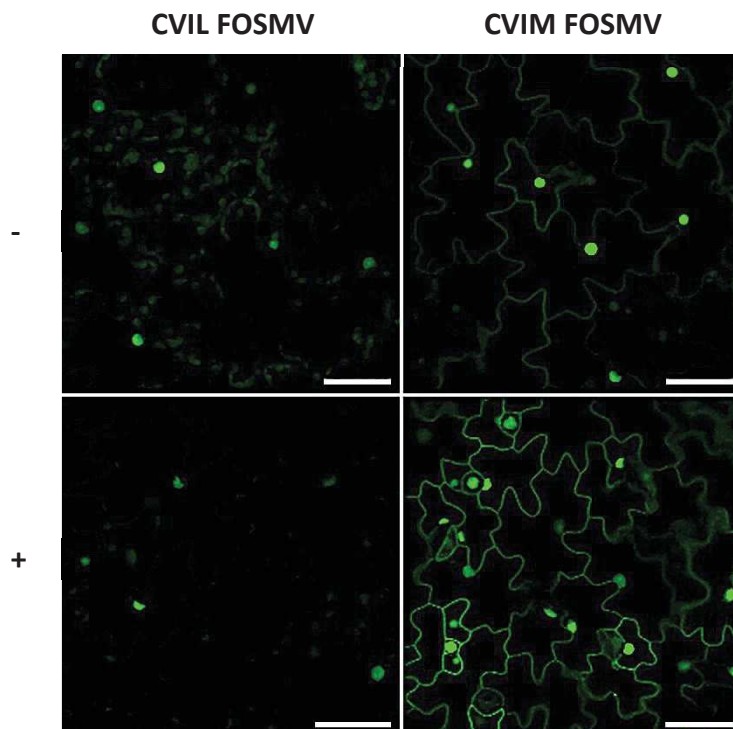


**Figure 46 Influence of sugar on protein prenylation in tissue damaged tobacco leaves.**

Tobacco plants transformed with pTA-GFP-CVIL or pTA-GFP-CVIM were grown for 4 weeks on MS<sup>1/2</sup> with (+) or without 1% sucrose (-).

Then, they were cut and transferred into liquid medium containing 100 μM fosmidomycin with 10 μM mevinolin (FOSMV) for 6h before induction with 60 μM dexamethasone and subsequent incubation for 24h prior to observation with confocal microscope.

Pictures are representative of the phenotype of a majority of cells. The white bar represents 50 μm. The confocal microscope settings were kept for all observations to compare GFP-fluorescence intensity.

Consistent is the fact that light period and quality is reported to be a key factor in the regulation of protein prenylation as reported for *era1* (Yalovsky et al., 2000; Yalovsky, 2011; Jalakas et al., 2017). With this respect, plants used in previous studies grew under light with a reddish spectrum, whereas in the current study, plants were grown under light with mostly blue component. Also, plant treated by floating were incubated in the dark, whereas IndBox plants were incubated under light. This detail could be significant, because the phenotype of *era1* is attenuated under blue light and long day as compared to red light and short day, evidencing the influence of the light quality on the protein prenylation (Yalovsky, 2011; Jalakas et al., 2017). Furthermore, the localization of the fluorescence was similar in plants grown in sucrose-enriched medium and those whose sugar was exclusively produced from the photosynthesis (**Figure 45**). Actually, the signal appeared to be stronger with external sugar inputs, but both fluorescence in plasma membrane and nuclei have been increased. Accordingly, sugar may have increases GFP-sensor protein biosynthesis rather than protein prenylation, otherwise GFP-signal in the nucleus would have decrease *vice-versa* in the membrane. Since the PPT flexibility occur only in the presence of protein prenylation inhibitor (**section 3.2.1**), we wanted to evaluate tissue damages as well as sucrose effect on leaves treated with FOS and MV.

Thus, additional experiments were performed using the floating method with GFP-CVI (M/L) tobacco leaves whose protein prenylation was inhibited with 100  $\mu$ M FOS and 10  $\mu$ M MV. Under these conditions, the GFP-CVIL protein was found in the nucleus (**Figure 46**), indicating that small tissue damages and the presence of sugar did not affect significantly the flexibility of PPTs activities in tobacco plants. Moreover, a difference between the phenotype of tobacco expressing GFP-CVIM was noticed between plant grown with and without 1% sucrose. The GFP-CVIM prenylation was almost totally inhibited by the FOS MV combo indeed, but plants grown with an external resource of sucrose showed a stronger membrane signal than the sugar-free control. Assuming that high sucrose-level improved the production of MVA, the inhibition by MV has likely been complemented, pushing part of the GFP-CVIM sensor into the membrane. Nevertheless, the nucleus-membrane phenotype remains the most prevalent. It was therefore not possible to conclude whether this effect resulted from sugar-enhanced protein biosynthesis, or if the prenylation capacity of GFP-CVIM protein was improved by a higher flux of MVA. For this reason, this study was pursued with *A. thaliana* plant model *ggb2* and *era1* mutants to compare the effect of these conditions on specific enzymes (PFT or PGGT-I).





### 3.3.2 Impact of Sucrose on PPTs Loss-of-Function Mutation in Arabidopsis

The *A. thaliana* WT and *era1.2* and *ggb2* lines expressing GFP-CVI (M/L) proteins have been generated by D.N. Crowell and characterized in a previous work (Huchelmann, 2013). However, the genotyping of the *era1.2* mutant (Cutler et al., 1996) failed. It turned out that this well used mutant we got from D.N. Crowell was in fact an Argonaute mutant (personal communication by Peter Brodersen who sequenced this line) and not a KO mutant of the  $\beta$ -F subunit. Therefore, a new *era1-9* line had been isolated in the lab (SALK\_110517) whose genotype was confirmed. I used this mutant to cross *Col0::GFP-CVI (M/L)* plants and obtain stable homozygous F2 lines. Next, we have addressed GFP-CVI (L/M) localization in both mutants following the same procedure afford mention for tobacco plants (**section 3.3.1**).

First, leaves were induced by the floating method with or without sucrose prior to observation by confocal microscopy. Background with previous report is the absence of GFP-CVIL prenylation in the *ggb-2* without sucrose suggesting that standard condition unable the PFT flexibility (Huchelmann, 2013), hence a nuclear location (**Figure 47**). Unexpectedly, although the *era1-9::GFP-CVIL* mutant showed a weak signal in the plasma membrane, most fluorescence was nuclear in the absence of sugar (**Figure 47**). As a matter of fact, the absence of PFT impacted the prenylation of GFP-CVIL too. One reason could be that in *era1* the PGGT-I activity is modulated to ensure prenylation of a low but sufficient level of prenylated protein no matter the CaaX signal. Another suggests that protein geranylgeranylation is regulated by farnesylated proteins otherwise GFP-CVIL would have been prenylated and mostly located in the plasma membrane. As in tobacco, the fluorescence intensity in the nucleus and plasma membrane ramped up in *Arabidopsis* plants expressing GFP-CVI (M/L) and grown with sucrose. Consequently, the presence of an external resource of sucrose might in fact induce a general increase of protein synthesis rather than real changes in PPTs activities.

Furthermore, leaf cells from both *WT::GFP-CVIM* and *ggb2::GFP-CVIM* induced on medium containing sugar showed a full plasma membrane phenotype (**Figure 48**), indicating the efficacy of GFP-CVIM prenylation in these lines as already reported (Huchelmann, 2013). The mutant *era1-9::GFP-CVIM* showed similar phenotype to its -CVIL homolog, no matter whether induction was performed with the floating or InBox method (**Figure 48**).

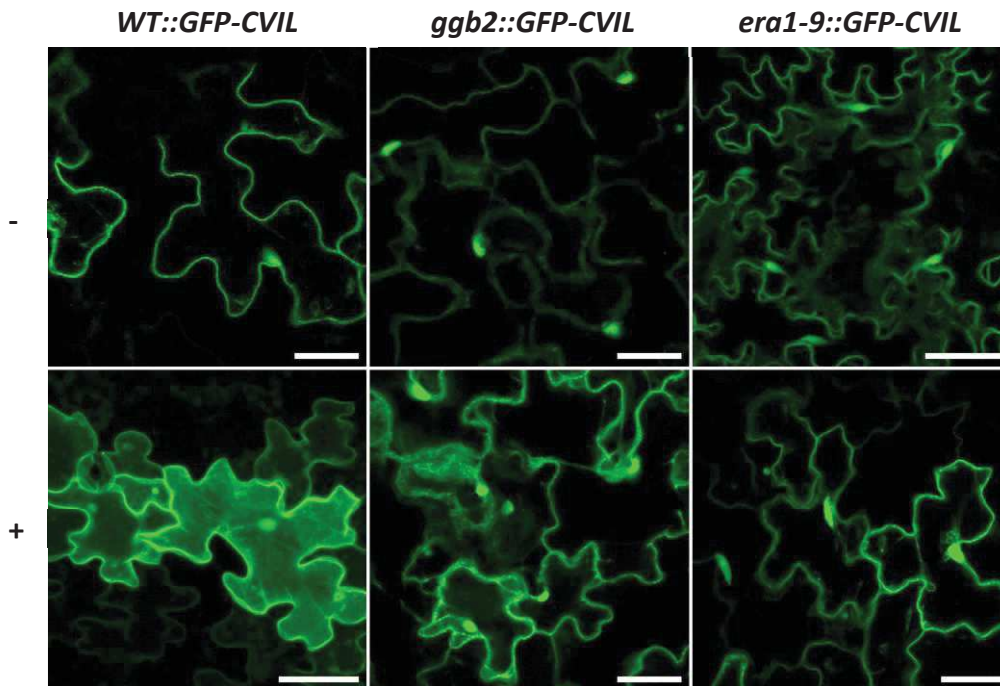


**Figure 47 GFP-CVIL prenylation is impacted in both *ggb-2* and *era1.9* *A. thaliana* KO mutants.**

*Arabidopsis* Col0 (WT), *ggb-2* and *era1.9* mutants were transformed with pTA-GFP-CVIL and grown for 4 weeks on MS<sup>1/2</sup> with (+) or without 1% sucrose (-), then cut and transfer into liquid medium containing 60  $\mu$ M dexamethasone for 24h. Pictures are representative of the phenotype of a majority of cells. The white bar represents 50  $\mu$ m. The confocal microscope settings were kept for all observation to compare GFP-fluorescence intensity.

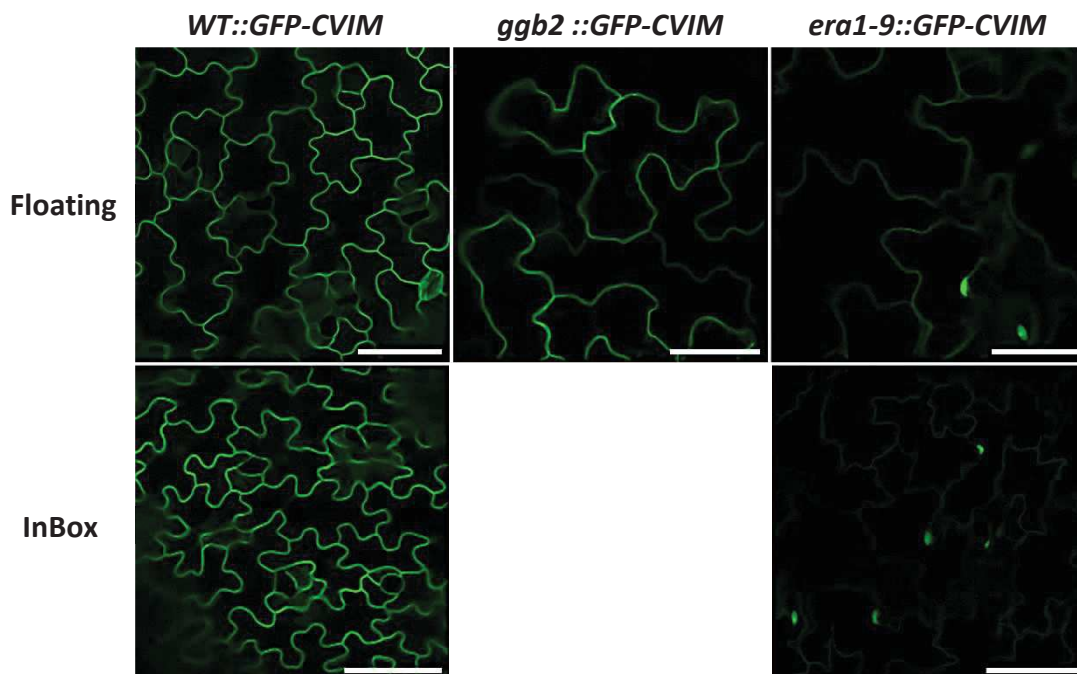


**Figure 48 GFP-CVIM prenylation is only affected in *era1.9* *A. thaliana* KO mutant.**

*Arabidopsis* Col0 WT, *era1-2* and *ggb-2* mutants were transformed with pTA-GFP-CVIM and grown 4 weeks on MS<sup>1/2</sup> with 1% sucrose, then watered with solution containing 60  $\mu$ M dexamethasone (InBox) or cut and transfer into induction liquid medium (Floating) for 24h. Pictures are representative of the phenotype of a majority of cells. The white bar represents 50  $\mu$ m. The confocal microscope settings were kept for all observation to compare GFP-fluorescence intensity.

In both cases a strong signal in the nucleus and a weaker one in the plasma membrane were observed, definitively highlighting an interconnection between PGGT and PFT on protein prenylation in plants. It is quite fair to notice that the homogeneity of the phenotype observed in *era1-9* turns out to be independent of the CaaX motif. It looks like in this mutant the rule is to maintain a low, but constant level of protein prenylation, no matter what kind of protein has to be modified. Our study contributes new knowledges to explain *era1* phenotype. The growth delay in *era1* appears to be the result of default in the whole protein prenylation machinery indeed. On the contrary, in *ggb2*, only protein geranylgeranylation is missing. These results not only emphasize with the crucial function of PFT activity in plants, but also that PGGT-I activity might be a minimum flexible, as GFP signal was low but detected in the membrane (**Figure 49**). The unanswered question remaining is which enzyme takes over prenylation functions in the absence of either PFT or PGGT-I? A simple view would be PGGT-I functions in the *era1* mutant and PFT in the *ggb2* mutant.

To evaluate the flexibility of PGGT-I, complementation assays with 40  $\mu$ M GGol were performed using the *era1-9::GFP-CVI (M/L)* lines following the floating or the InBox method. Confocal microscopy acquisitions of treated leaves revealed that the partial nuclear localization of GFP-CVIL was not complemented by GGol (**Figure 50**). However, the *era1-9::GFP-CVIM* treated with 40  $\mu$ M GGol showed a phenotype almost identical to that of the control *WT::GFP-CVIM* (**Figure 50**). In this respect, PGGT-I in the presence of high concentrations of its substrate may also be able to compensate the lack of PFT activity for GFP-CVIM prenylation. This would be in accordance with the *in vitro* results where PGGT-I is able to prenylate both GFP-CVIL and GFP-CVIM. Remarkably, this activity seems to be selective for GFP-CVIM as compared to its homolog *era1.9::GFP-CVIL* for which no difference was observed when compared to the control without GGol. Another complementation assay with 40  $\mu$ M Fol was performed in *era1.9::GFP-CVIM* to see if the prenylation of GFP-CVIM is affected. The results indicate that Fol has no influence on GFP-CVIM prenylation in *era1* as compared to the negative control without Fol (**Figure 51**).

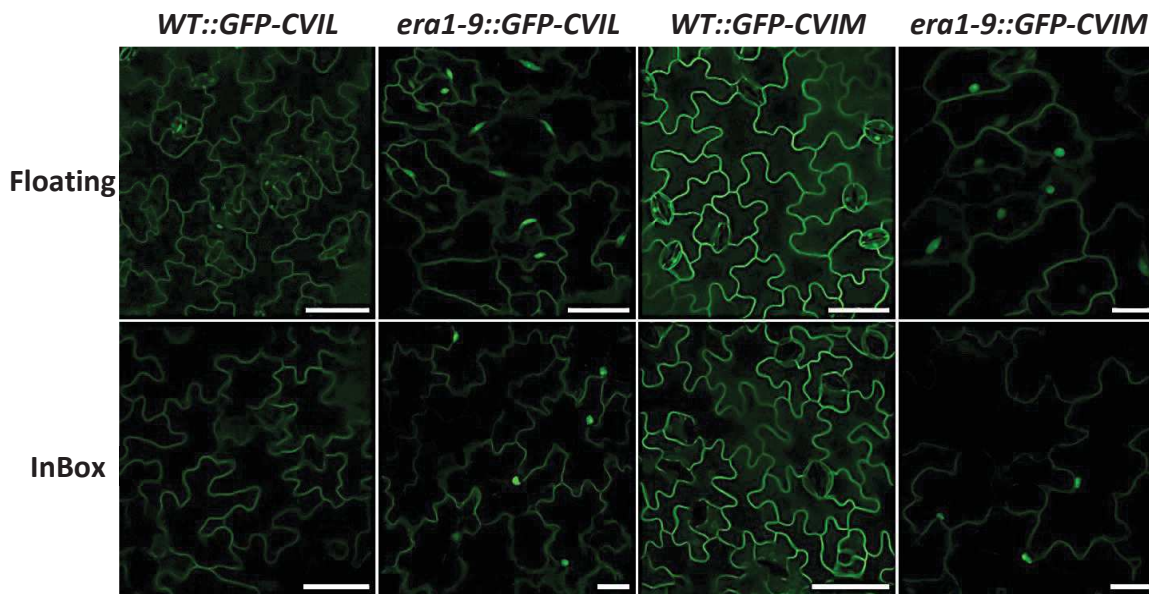


**Figure 49 Tissue damages does not impact protein prenylation of GFP-sensor in *A. thaliana era1-9* mutant.** Arabidopsis Col0 (WT), F2 *era1-9::GFP-CVIL* (EL) and *era1-9::GFP-CVIM* (EM) GFP mutants obtained after crosses between WT transformed with pTA-GFP-CVIL or pTA-GFP-CVIM and *era1-9*. Plants were grown for 4 weeks on solid MS<sup>1/2</sup> with 1% sucrose, then watered with solution containing 60 μM dexamethasone (InBox) or cut and transfer into induction liquid medium (Floating) for 24h. Pictures are representative of the phenotype of a majority of cells. The white bar represents 50 μm

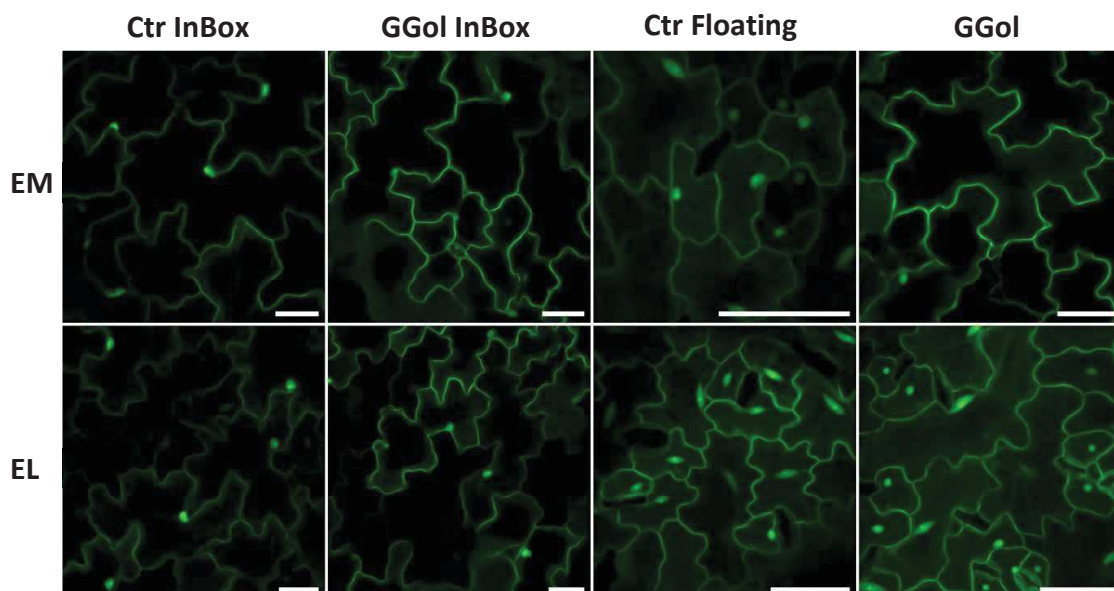


**Figure 50 GGol rescue GFP-CVIM in the PFT *A. thaliana* KO mutant (*era1-9*).** Arabidopsis Col0 (WT). F2 *era1-9::GFP-CVIL* (EL) and *era1-9::GFP-CVIM* (EM) GFP mutants obtained after crosses between WT transformed with pTA-GFP-CVIL or pTA-GFP-CVIM and *era1-9*. Plants were grown for 4 weeks on solid MS<sup>1/2</sup> with 1% sucrose, then watered with solution containing 60 μM dexamethasone (InBox) or cut and transfer into induction liquid medium (Floating) for 24h. 20 pictures from z-stack were superimposed and fluorescence was summed, the phenotype observed are representative of the phenotype of a majority of cells. The white bar represents 50 μm

### 3.3.3 Conclusion

This chapter showcases the flexibility of protein prenyltransferase activities *in planta*. It appeared that physiological mechanisms dependent on defense hormone signaling such as JA and ethylene induce PFT flexibility to overcome the absence of GGPP or PGGT-I activity in the prenylation of proteins with -CaaL motifs. Under these conditions, our results indicated that the MVA pathway is used to supply the prenyl substrate required for protein prenylation. Furthermore, the use of GFP-sensors in the *era1-9* mutant gave a snapshot of the protein prenylation process in the absence of PFT activity *in vivo*. By contrast to the *ggb2* mutant, *era1-9* allows a minimum but uniform level of protein prenylation regardless of the CaaX motif that has to be modified. It can be speculated that this homogeneous prenylation state is likely orchestrated by plant to ensure simultaneously at least the essential functions, involving prenylated proteins in development but also defense.

Although PFT plays a central role, it looks like PGGT-I can take over partially its function in the *era1* mutant. The prenylation capacity of the -CaaM sensor was enhanced by GGol while Fol could not, suggesting that the activity of PGGT-I is also flexible and may ensure the transfer of a GGPP-related substrate on protein with -CaaM motif rather than -CaaL. It would be interesting to conduct experiments where *era1-9::GFP-CVI (M/L)* lines are treated with MeJA. In such a context, we would be able to see whether the PGGT-I can promote the GFP-CVIL prenylation under stress conditions. Also, transformed Arabidopsis *plp* mutant lines might be critical to decipher the whole protein prenylation machinery, including the PFT, PGGT-I and other unknown partner triggering the dynamic flexibility of PPT *in vivo*. However, as *plp* mutant is quite hard to culture and *era1-9* lines expressing GFP-sensor were obtained late, these assays were not performed. Similarly, even if crosses were rigorously performed and *era1-9* genotype validated, sequencing the CaaX terminal sequence inserted in the genomic DNA was not done yet. Accordingly, it has to be performed in the future to make sure that no interconversion has been made in the handling of the lines.

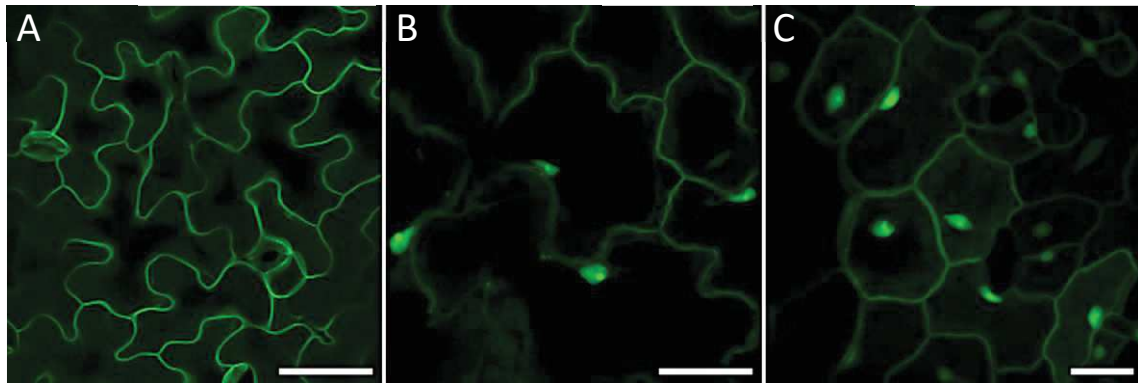


**Figure 51 Farnesol does not rescue protein prenylation in *era1.9 A. thaliana* KO mutant lacking the PFT activity.** (A) *Arabidopsis* Col0 and (B) F2 *era1-9::GFP-CVIM* mutant obtained after crosses between WT transformed with pTA-GFP-CVIM and *era1-9* were grown for 4 weeks on solid MS<sup>1/2</sup> with 1% sucrose. Then leaves were cut and transfer onto induction liquid medium containing (B) 60  $\mu$ M dexamethasone alone or (C) combined to 40  $\mu$ M farnesol. 20 pictures from z-stack were superimposed and fluorescence was summed, the phenotypes observed are representative of a majority of cells. The white bar represents 50  $\mu$ m

In conclusion, our results support the fact that the PGGT-I and the PFT activities are flexible *in vivo*. Nevertheless, without molecular characterization, none of our studies confirmed the nature of the prenyl transferred on the GFP-sensor *in planta*. Published data with our model has shown by HPLC-MS/MS analysis that in BY-2 cells the GFP-CVIL protein is geranylgeranylated. However, such characterizations need now to be performed with proteins modified under variable conditions where PPT substrate specificity has been adapted.

# 4 DEVELOPING A PROTOCOL FOR PURIFICATION AND ANALYSIS OF PRENYLATED PROTEINS MODIFIED *IN VIVO*





## 4.1 INTRODUCTION

Since the discovery of protein prenylation in 1975, and later the role of prenylated proteins such as RAS members in human cancer or the lamine B in progeria, several methods have been developed to purify and characterize prenyls carried by these proteins (**section 2.2.1**). Nevertheless, the evidence of flexibility in prenyl substrates as well as CaaX proteins pushed to reconsider the developed approaches to study protein prenylation *in vivo*. One reason was that many experiments were performed *in vitro* with purified substrates and recombinant PPTs, which could obviously not reflect the reality *in vivo*. Another reason was that inhibitors and/or radiolabeled substrates, or their precursors were added for experiments *in vivo*, inducing therefore adaptation of cellular mechanism to human-fixed conditions. Although analytical solutions were proposed in prenylated proteins studies, they exposed some limits (**Figure 52, Table 3**). For instance, Raney Ni and iodomethane were defined as standard to cleave prenyls before TLC, GC-FID, HPLC-UV radiometry or GC-MS analyses. First, these reactions involve explosion risks because H<sub>2</sub> is needed for hydrogenation over platinum before cleavage, and dried Raney Ni is auto-flammable as well. Then, these approaches allowed to release and detect prenyls indeed, but no direct correlation between protein and prenyls was afforded, especially *in vivo*. On the top that, if analysis was performed with plant material, phytol and GG would both result in phytane after hydrogenation step.

Accordingly, new protocols using HPLC-MS/MS or NMR were proposed to unambiguously determine prenylation state without cleavage of prenyls, but their use was restricted for a long time to proteins or peptides prenylated *in vitro*. Recently, supports for affinity purification, biorthogonal chemistry and analysis of tagged proteins provide new features on prenylome of some organisms (Chung et al., 2009; Hannoush and Sun, 2010; Onono et al., 2010). Still, most of these approaches call for feeding of cells with synthetic substrates for subsequent purification, resulting in putative artifactitious protein prenylation. Actually, the main challenge remains the analysis of prenylated proteins modified *in vivo* with prenyl substrates available under physiological condition. Even if overexpressed, the prenylated proteins remain low abundant as compared to ribosomal subunit or structural proteins such as actin, tubulin. Thus, other strategies were suggested for the purification of prenylated proteins without adding prenyl analogs.

**Table 3 Advantages and limits of analytical methods used to characterize protein prenylation *in vitro* and *in vivo*.** Examples of references in which these analytical methods have been used.

Analytical method	Advantages	Limits	Example of application
TLC-radiometry	<ul style="list-style-type: none"> <li>- Low cost</li> <li>- Availability</li> <li>- Small Peptides and prenyls</li> <li>- Medium sensitivity</li> </ul>	<ul style="list-style-type: none"> <li>- Radiolabeling</li> <li>- Resolution</li> <li>- References required</li> <li>- Low Molecular information</li> </ul>	(Hancock et al., 1989; Maltese and Erdman, 1989; Andres et al., 2002) (Benetka et al., 2006)
GC-FID radiometry	<ul style="list-style-type: none"> <li>- Medium cost</li> <li>- Resolution</li> <li>- Accurate quantification</li> <li>- High sensitivity</li> </ul>	<ul style="list-style-type: none"> <li>- Radiolabeling</li> <li>- Volatile compounds</li> <li>- References required</li> <li>- Low molecular information</li> <li>- Prenyls cleaved from the protein</li> <li>- thermolabile compounds</li> </ul>	(Farnsworth et al., 1989; Farnsworth et al., 1990a; Goodman et al., 1990)
LC-UV radiometry	<ul style="list-style-type: none"> <li>- Medium cost</li> <li>- Resolution</li> <li>- Peptides and prenyls</li> <li>- High sensitivity</li> </ul>	<ul style="list-style-type: none"> <li>- Radiolabeling</li> <li>- References required</li> <li>- Low molecular information</li> </ul>	(Casey et al., 1989; Farnsworth et al., 1989; Farnsworth et al., 1990; Epstein et al., 1991; FujiyamaSB et al., 1991)
GC-MS	<ul style="list-style-type: none"> <li>- Radiolabeling optional</li> <li>- Molecular information (mass + fragments)</li> <li>- High resolution available</li> <li>- Accurate quantification</li> <li>- Repeatability</li> <li>- NIST database</li> <li>- High Sensitivity</li> </ul>	<ul style="list-style-type: none"> <li>- Volatile compounds</li> <li>- Equipment and maintenance fees</li> <li>- Validation of prediction with references</li> <li>- Prenyls cleaved from the protein</li> <li>- thermolabile compounds</li> </ul>	(Kamiya et al., 1978; Farnsworth et al., 1990; Parmryd et al., 1999; Sorek et al., 2013)
*FAB- or MALDI-MS (MS/MS)	<ul style="list-style-type: none"> <li>- Molecular information (mass + fragments)</li> <li>- Peptides and prenyls</li> <li>- High resolution available</li> <li>- Accurate quantification</li> </ul>	<ul style="list-style-type: none"> <li>- *Pure compounds</li> <li>- Equipment and maintenance fees</li> </ul>	(Tuinman et al., 1991; Kassai et al., 2005; Hoffman and Kast, 2006; Gerber et al., 2009; Gillette et al., 2015)
HPLC-MS (MS/MS)	<ul style="list-style-type: none"> <li>- Radiolabeling optional</li> <li>- Peptides and prenyls</li> <li>- Molecular information (mass + fragments)</li> <li>- High resolution available</li> <li>- Accurate quantification</li> <li>- (Identification <i>de novo</i>)</li> <li>- High sensitivity</li> </ul>	<ul style="list-style-type: none"> <li>- Equipment and maintenance fees</li> <li>- Database dependent of analysis settings</li> </ul>	(Chung et al., 2009; Hannoush and Sun, 2010; Onono et al., 2010; Wotske et al., 2012; Gillette et al., 2015; Palsuledesai et al., 2016; Suazo et al., 2018; Storck et al., 2019)
NMR	<ul style="list-style-type: none"> <li>- Peptides and prenyls</li> <li>- Molecular details</li> <li>- Absolute identification</li> <li>- Accurate quantification</li> </ul>	<ul style="list-style-type: none"> <li>- Equipment and maintenance fees</li> <li>- Low sensitivity</li> <li>- Low suitability for complex extracts</li> </ul>	(Emmanouilidis et al., 2017; Bader et al., 2019)



DO NOT SNAPSHOT *IN VITRO* MODELS AS MODEL ORGANISMS

The prenyl is slipping, DO NOT DISTURB THE THIOETHER BOND

DO NOT FEED CELLS, it changes the dynamic of protein prenylation

**Figure 52 Proposed rules to study protein prenylation mechanisms.**

At least one of them is not respected in published studies and impaired unambiguous identification of prenyl from prenylated proteins

For instance, a model of farnesylated protein trap was proposed according to the affinity of protein Aryl Hydrocarbon-Receptor-interacting-protein-like-1 (AIP1) for the farnesyl moiety of the phosphodiesterase-6A subunit (Majumder et al., 2013). However, this approach might also be limited by the size, conformation and composition of prenylated proteins. Besides, phase partitioning using triton X-114 is quite well documented for the purification of acylated and prenylated proteins (Goalstone et al., 1999; Mohamed et al., 2012; Yang et al., 2016; Akula et al., 2019). But, this approach does not fit with the prospect of putative protein interacting with prenylated proteins as a variability in interactant proteins polarity would induce differential separation. Furthermore, a preliminary study was done with BY-2 cells expressing His-GFP-CVIL (Gerber et al., 2009a), but most of the GFP-protein was retained on the His-tag purification column (Data not published). In the end, some paper report affinity purification with GDP-dissociating inhibitors fused to glutathion-S-transferase (GST), but the amount of purified protein remains relatively low and specific of Small GTPases (Mohamed et al., 2018).

We are therefore interested to design a purification and analytical procedure for the unbiased analysis of protein prenylated *in vivo* under physiological condition of protein prenylation. Since several immunoprecipitation (IP) matrices for GFP-tag proteins are also available and reported (Fernandes et al., 2014), this strategy was implemented for the purification of the GFP-sensor proteins.



## 4.2 PURIFICATION OF PRENYLATED GFP SENSOR PROTEINS

### 4.2.1 Immunoprecipitation of the GFP Sensor Proteins

Among a large number of protein purification methods described in the literature, the IP or co-immunoprecipitation (Co-IP) of proteins prior to proteomics is a commonly used approach to purify and identify protein-protein interactions as well as PTMs in many organisms including plants (Kwon, 2006; Bontinck et al., 2018; Junková et al., 2018; Suprun, 2019).

As long as antibodies are specific of targeted proteins, IP offers simple procedure to purify protein of interest from a crude protein extract. Accordingly, the procedure consists in three steps: the extraction of proteins, the incubation of the extract with antibodies-coated matrix and washes before analysis of the purified proteins. Many types of resin are commercialized, depending on the monoclonal antibodies or nanobodies recognizing molecular tags such as HA, GFP, or Myc tags (Kimple et al., 2013). Also, the emergence of purification matrices in the form of magnetic beads made the development of fast and easy IP procedure possible. Accordingly, this technical innovation considerably reduces protein loss during the various steps. Since a preliminary trial with hydrophobic interaction (Sepharose CL-4B) purification did not succeed to purify our GFP sensor, we assessed IP procedure with commercial magnetic GFP-Trap (GFP-Trap\_M, Chromotek). Therefore, IP assays were carried out with the prenylated GFP-CVIL protein expressed in BY-2 cells and the recombinant reference protein His-GFP-CVIL produced in *E. coli* (**Figure 53**). Both ~35 kDa GFP-CVIL proteins have successfully been immunoprecipitated as shown by immunostaining using rabbit IgG raised against GFP-CVIL (**Figure 54**). The presence of another spot at ~30 kDa in the protein IP from BY-2 suggests that two forms of the protein are present and could be associated to the prenylated and non-prenylated GFP-CVIL. Nevertheless, the same spot was observed in the reference, so it might be a degradation product of GFP-sensor protein. Even though Immunostaining allowed detection of GFP-sensor, nothing was observed on the Coomassie blue stained gel performed in parallel. As average limit of detection (LOD) for immunostaining and NBT/BCIP revelation is 50 – 100 pg compared to 1 - 5 ng for Coomassie blue G-250, our results suggest that the amount of purified protein was very low (McDonald et al., 2008). These promising results support that IP seemed to be a suitable approach for the purification of our GFP-prenylated sensor. In this context, an optimization of this protocol was set up to rise amount of purified protein.

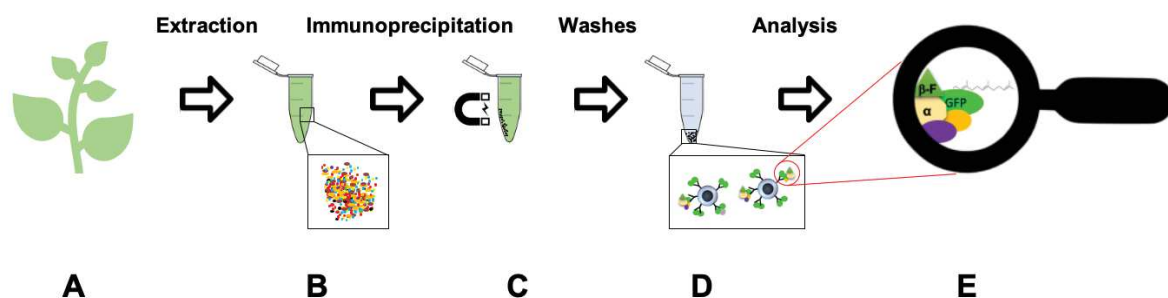


**Figure 53 General procedure for purification of GFP-sensor protein from plant by using IP and analysis with mass spectrometry.**

(A) Extraction of plant material expressing GFP-sensor with IPB buffer, (B) Immunoprecipitation of total protein extract after centrifugation and removal of pellets, (C) Magnetization of GFP-Trap with immunoprecipitated GFP-sensor prior to washes step with IPB, (D) Purified GFP-sensor with putative interacting proteins adsorbed on the GFP-Trap, (E) proteomics analysis of purified proteins after sample preparation and digestion with endoproteases.

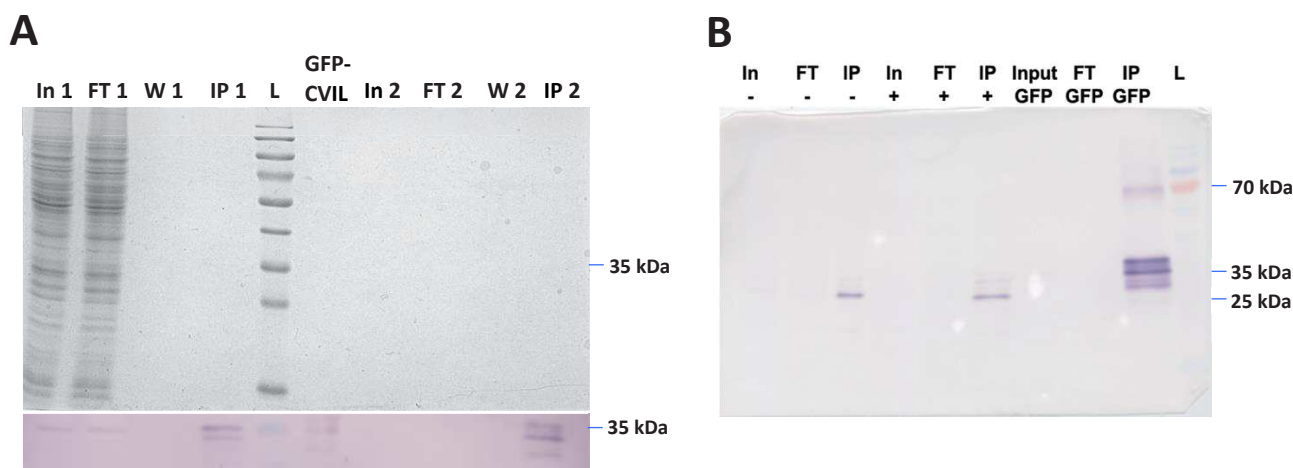


**Figure 54 Immunoprecipitation of GFP-CVIL from BY-2 cells.**

(A) Protein fractions obtained after IP with GFP-Trap\_M of the GFP-CVIL protein produced in BY-2 and the reference His-GFP-CVIL analysed by SDS-PAGE with coomassie blue staining (up), or Western blot using IgG @GFP-CaaX and NBT/BCIP staining (down). BY-2 cells: total protein extract (In1), flow through after IP (FT1), first wash(W1), immunoprecipitated proteins (IP1) ladder (L). Reference His-GFP-CVIL: solution 1/50 (GFP-CVIL), solution 1/500 (In2), flow through (FT2), first wash (W2). (B) Protein fractions obtained after IP with GFP-Trap\_M of the GFP-CVIL protein produced in BY-2 cells inhibited or not with 100  $\mu$ M FOS and the reference His-GFP-CVIL analysed by Western blot using IgG @GFP-CaaX.

Non FOS-inhibited BY-2 cells: total protein extract (In-), flow through after IP (FT-), immunoprecipitated proteins (IP-). FOS-inhibited BY-2 cells: total protein extract (In+), flow through (FT+), immunoprecipitated proteins (IP+). Reference His-GFP-CVIL: solution 1/500 (Input GFP), flow through (FT GFP), immunoprecipitated proteins (IP GFP). Ladder (L)

With this respect, the experiment was reproduced by doubling the amount of plant material extracted while maintaining the same volume of IPB buffer. Nevertheless, GFP-sensor seemed to be degraded in the process, according to our Western blot labelled by NBT/BCIP between BY-2 samples (~26 kDa) and the corresponding GFP reference (~35 kDa) (**Figure 54**). This protein degradation may result from the digestion of GFP-CVIL by endogenous proteases because no protease inhibitors had been added in the IPB buffer. As a result, the remaining 26 kDa protein coincides with the GFP, suggesting that the basic domain is more susceptible to proteases because less structured than the GFP. Besides, a spot at ~70 kDa was observed only in the His-GFP-CVIL, it was associated to the dimer of the protein, resulting likely from disulfide bridge formation between C-ter cysteines. However, the intensity of NBT/BCIP staining using 700 mg cell extracts was higher than the previous assay with 300 mg indeed, pinpointing an increase in purified GFP protein. Thus, if we want to analyze the prenyl group by GC-MS, 25 up to 100 µg of purified recombinant protein is required (Sorek et al., 2013). Since the capacity of the GFP-Trap\_M is limited to 0.5 µg/10 µl, around 500 µl GFP-Trap\_M would be needed to obtain 25 µg. This number raises a significant question: what is the budget for further optimization of purification method and analysis of prenylated proteins under many conditions? Actually, 500 µL of matrix cost 335 euros, what tops a budget for a routine chemical analysis.

Among the widely used suppliers of grafted matrices, there is Miltenyi with the µMACS™ (1335 € / 96 isolation) and Chromotek with the Dynabeads® (1900 € / 100 isolations) or the Nano-Trap® (1585 € / 100 isolation). At the same time, activated matrices alone are sold between 600 € and 900 € for the same number of reactions, which is by the way still expensive. To solve this problem, I reviewed literature on the synthesis of activated ferromagnetic microparticles for immobilization of proteins. Several protocols mentioned simple and fast syntheses of activated magnetic agarose microparticles (MAPs) for protein attachment by using cheap base materials. Starting from this, we had in mind to produce our own purification material.

Luckily, at the IBMP C. Ritzenthaler's team (Biology and Biotechnology of grapevine viruses, IBMP Strasbourg) is producing anti-GFP nanobodies (Nb@GFP) to detect plant viruses, and Vianney Pognavent (*Serendip innovations*, incubated within the SEMIA, Strasbourg) is running a startup based on this work. Thus, they could also supply huge amounts of pure Nb@GFP produced in *E. coli* strains. For this reason, a collaboration was set up to develop this cheap and efficient homemade version of GFP-Trap, we would use to purify and analyze our prenylated GFP-sensor proteins.



## 4.3 CONSIDERATION FOR CHEAP AND EFFICIENT GFP-TRAP DEVELOPMENT

### 4.3.1 How Do I Get Spherical Magnetic Particles?

Many procedures have been described to produce spherical magnetic particles and always requires compounds with supraparamagnetic properties. Typically iron oxide ( $\text{Fe}_3\text{O}_4$  or  $\text{Fe}_2\text{O}_3$ ) forms the core, which is embedded in an inorganic or organic matrix (Zucca and Sanjust, 2014; Zucca et al., 2016). Three type of ferromagnetic particles have been reported depending on the size, ratio and organization of ferromagnetic particles in the matrix (**Figure 55**). First there can be a single core in the particle or multi-cores with agglomerates of particulate cores. Two other types are the dispersing-type made of densified-powder uniformly dispersed in the matrix, and the integrity-type being a porous particle without polymer-coated layer (Zhao et al., 2009). The main advantage of core-type and integrity-type particles is their high mass transfer ( $1000$  to  $3000 \text{ cm.h}^{-1}$ ), allowing a fast and efficient magnetization unless dispersing type particles, in which this parameter is reduced by the presence of many pores. In contrast, the network and microstructure of pores in the dispersing-type particles increase the adsorption capacity by significantly rising the area within particles. The simplest and most commonly used process for preparing ferromagnetic microparticles consists to reverse-phase also called water-in-oil (W/O) suspension method. Accordingly, the polymer solubilized in the hot water phase with ferromagnetic particles is dispersed as droplets into the organic phase at  $70\text{-}85 \text{ }^\circ\text{C}$  (Zhao et al., 2009). The mixture is then cooled quickly for the polymerization of spherical droplets containing the matrix of polymer and magnetite microparticles. In this context, the W/O suspension method was chosen, and the type of matrix was selected according to the literature, by choosing the best compromise between the price, feasibility and efficiency.

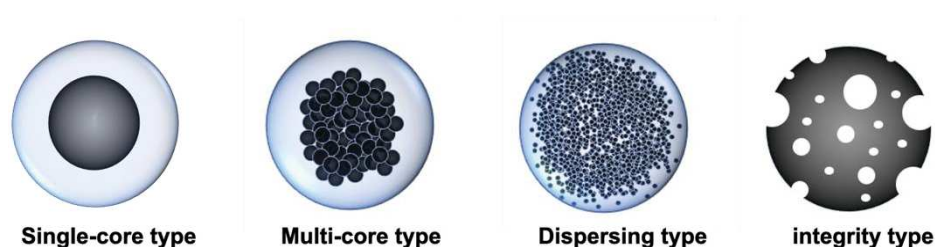


**Figure 55 Structure of the three different magnetic particles types described.**

Distribution of magnetite (black) into the matrix (blue) for core-type particles with single or multi-core, dispersing type while the integrity type particles are without polymer-coated layer. Adapted from **Zhao et al., 2009**

### 4.3.2 Key Parameters to Handle Preparation of Microparticles Using W/O Process

First of all, since shape and homogeneity of microparticles depend on the emulsion quality and stability, several parameters can be modulated to obtain the desired products. Thus, the homogeneity of MAPs can be adjusted by the type and ratio of organic phase and emulsifiers, which contribute to the stability of the emulsion (Kruglyakov, 1976; Tadros, 2013), but also by the dispersion method used to make the emulsion. Thus, the employed organic phase can be a pure solvent like toluene, or blended compounds such as oil, but it has to be non-miscible with water. Although, the oil viscosity promotes the emulsion stability, it remains questionable for products allowed to lipids analysis. Actually, as organic and mineral oils are often composed of several lipids (alkanes, alkynes), they represent an additional source of contaminants. In contrast, pure solvents such as toluene are found up to 99.9 % purity and can be easily detected, but they are more expensive and much less viscous.

For instance, procedure with water/cyclohexane or CCl<sub>4</sub>/toluene have been described to make microemulsions (Hjertén, 1964; Gelot et al., 1984; Davies et al., 1987; Gotch et al., 2008). Nevertheless, CCl<sub>4</sub> is described as highly toxic, it destroys the ozone layer and has been prohibited for industrial uses by the Montreal protocol since 1985. In the prospect of a possible industrial application considered by *Serendip innovation*, the H<sub>2</sub>O/oil or H<sub>2</sub>O/toluene combination must be considered rather than CCl<sub>4</sub>/toluene. As far as stability of the emulsion is concerned, changes of CCl<sub>4</sub> by water, or oil by toluene can cause emulsion breakdown, as they have different physicochemical properties. A common way to avoid emulsion breakdown is to adjust emulsifier content, but how?

To some extent, the hydrophilic-lipophilic balance (HLB) is a key and widely used parameter to define surfactant ratio for emulsion (Kruglyakov, 1976; Tadros, 2013). The HLB is available for many compounds and varies between 0 (most lipophilic) and 20 (most hydrophilic). Also, it is admitted that HLB of emulsifiers must be between 4 and 6 for W/O emulsions and must be adjusted with blend emulsifiers. Finally, as long as we are interested in magnetic particles, the dispersion method and ratio between magnetite, polymer and water phase will determine the type and magnetizing properties of particles indeed. For example, large magnetite particles (32-180 µm) usually result in single- or multi-core type particles, while magnetite fine powder (< 5 µm) rather leads to dispersing type (Zhao et al., 2009).

Moreover, larger the size of a droplet is, higher will be its mass diffusivity, decreasing the emulsion stability as droplets will collapse together faster (Zhao et al., 2009). Taken together, these basics allow the design and optimization of procedure for magnetic microparticles synthesis. Next, as particles involve polymer matrix, what polymer choose to synthesize versatile and low-cost magnetic particles for a GFP-Trap?

### 4.3.3 What Kind of Polymer to Use For Cheap and Multivalent Support?

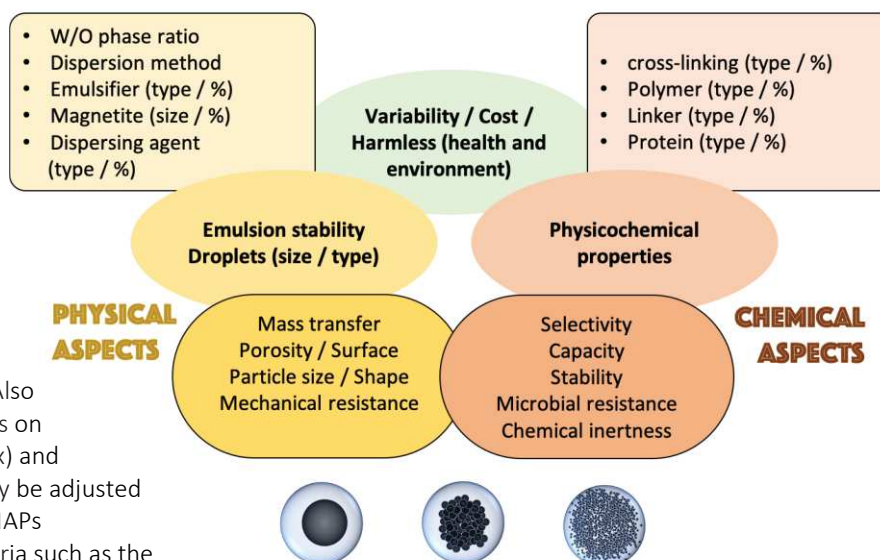
A critical component in the design of a GFP-Trap system is the type of matrix used to immobilize the Nb@GFP (dos Santos et al., 2015). Several parameters might be taken into account to prepare efficient support for protein attachment such as mechanical properties, area, porosity, particle size and also, the cost, environmental impact, toxicity, chemical and microbial inertness (**Figure 56**). It is stated that the type of polymer used influences the density, the grafting site type, the porosity, the rigidity of the support as well its polarity (Zucca and Sanjust, 2014; Santos et al., 2015; Zucca et al., 2016). For instance, matrices using inorganic materials such as Silica, Titania, Alumina or other oxide-based materials are considered as thermal, mechanical and microbial resistant. Besides, the stiffness of inorganic materials allows a total control and invariance in shape and pore size of the support.

At the opposite organic materials being very sensitive to pressure, pH as well as microbial degradation are responsible for variability in the volume, shape and pore size of the support itself (Zucca and Sanjust, 2014). Nevertheless, the amine or hydroxyl functions from organic materials are more suitable than inorganic materials for the support functionalization. Actually, the -OH groups from inorganic materials do not obey the octet rule, so no empty *d* orbital hosting the density of nucleophile such as water. Consequently, the support produced from inorganic materials requires an additional preparation step to avoid loss of function by S<sub>N</sub>2-type reactions, causing hydrolysis with heteroatoms in the conditions of subsequent enzyme immobilization (Zucca and Sanjust, 2014). In spite of the negative aspects mentioned before, supports using organic materials such as poly(vinyl alcohol), polyamides or polysaccharides are usual because they present outstanding physical properties and are easier to functionalize for covalent attachment of proteins (Zucca et al., 2016). Moreover, the diversity of organic molecules available for this application allows the physicochemical properties to be finely adjusted for hydrophilic/hydrophobic character of the support.

## SYNTHESIS OF MAPS: KEY ASPECTS

**Figure 56 Overview of the characteristics influenced by physical (yellow pill) and chemical factors (red pill).**

Main factors influencing the physical (yellow oval) and chemical (red oval) characteristics of MAPs prepared for the development of IP supports. Also represented, the key elements on which the physical (yellow box) and chemical (red box) factors may be adjusted depending on the expected MAPs characteristics and other criteria such as the variability, cost and toxicity.



Among the organic materials used, sugars especially agarose and dextran are by far the most popular, because natural (alga/bacteria) and highly hydroxylated. As a result, the density of grafting site can be finely adjusted according to the number of free hydroxyl functions of sugars. The agarose is generally preferred to dextran derivatives because cost-effective and has better mechanical resistance properties. Sugar-derived matrices can be easily cross-linked to reduce microbial sensitivity and be functionalized with various linkers for ligands and proteins immobilization too (Zucca et al., 2016). Although, the sugar-based matrices benefit to enzyme stability because very hydrophilic, this type of matrix can promote interaction with non-desired charged proteins by ionic or hydrogen bonds (Santos et al., 2015). Furthermore, as MAPs structure is submitted to variability, it involves a risk of non-desired proteins by retention in the microparticle pores (Zhao et al., 2009; Zucca and Sanjust, 2014; Zucca et al., 2016). However, the latter can be reduced by increasing sugar amount or percentage of crosslinking between sugar polymers in the matrix. Altogether, these elements indicate that despite its drawbacks, the agarose-based matrix is a good compromise not only for the cost, environment, but also by offering many alternatives for selective and adaptable protein attachment. With this respect, agarose was chosen as matrix and subsequently cross-linked and functionalized for protein attachment. How do I cross-link and functionalize MAPs for IP support?

#### 4.3.4 Cross-Linking and Functionalization of the Support

The cross-linking and functionalization are two key steps that drive the selectivity of the support and attachment of the antibodies or nanobodies needed to capture specifically GFP-Tag proteins. The molecules used for cross-linking and functionalization of the support are usually the same. The linkers available allow the cross-linking and grafting of ligands or proteins by their acid (Asp, Glu), amine (Lys, Arg, His) or thiol (Cys) functions (Zhao et al., 2009; dos Santos et al., 2015; Zucca et al., 2016) (**Figure 57**). Above all, it is important to consider that the type and size of the linker determine the polarity and reactivity of the support towards specific functions, but also the spatial conformation of protein immobilized and therefore their stability and activity (Santos et al., 2015; Zucca et al., 2016).

Linkers are composed of two moieties, a spacer which fix the distance between the attached molecules, and then reactive groups such as epoxide, vinyl, allyl or alkyne that react with the charged groups of molecules to be attached. Accordingly, linkers with short spacer are usually selected as cross-linking agents (cross-linker), as they reduce the penetration of proteins into microstructures within agarose particles. In contrast, molecules used for functionalization are short, long or even mixed and drive the density and conformation of grafted proteins. In our context, the latter have to be considered since too high density can result in a loss of selectivity from the support. At the opposite, too low density of grafting site can affect the capacity of our GFP-Trap, reducing the number of nanobodies to catch GFP-tagged proteins. Typically, epichlorohydrin with its epoxide groups and divinylsulfone (DVS) with vinyl groups are good cross-linker used between 3 and 12%. For example, up to 5% of DVS has been described to influence the gel stiffness proportionally to the % of cross-linking (Porath et al., 1975; Hjertén et al., 1987; dos Santos et al., 2015). In this case, an important step after cross-linking is the deactivation of free DVS vinyl groups with amine, thiol or hydroxyls rich compounds like AA or sugars. Interestingly, studies with DVS have shown that the higher the molecular weight of the sugar is, the smaller is the pore size (Hjertén et al., 1987). It is therefore possible to adjust the exclusion limit, which will be 45 kDa using Dextran T500 against 450 kDa with *D*-Mannitol (Hjertén et al., 1987) (**Figure 58**). Furthermore, an intense multipoint covalent attachment of protein at pH ~10 can be obtained with DVS due to its high reactivity with His and Cys, and less with Lys and Arg protein residues (dos Santos et al., 2015).

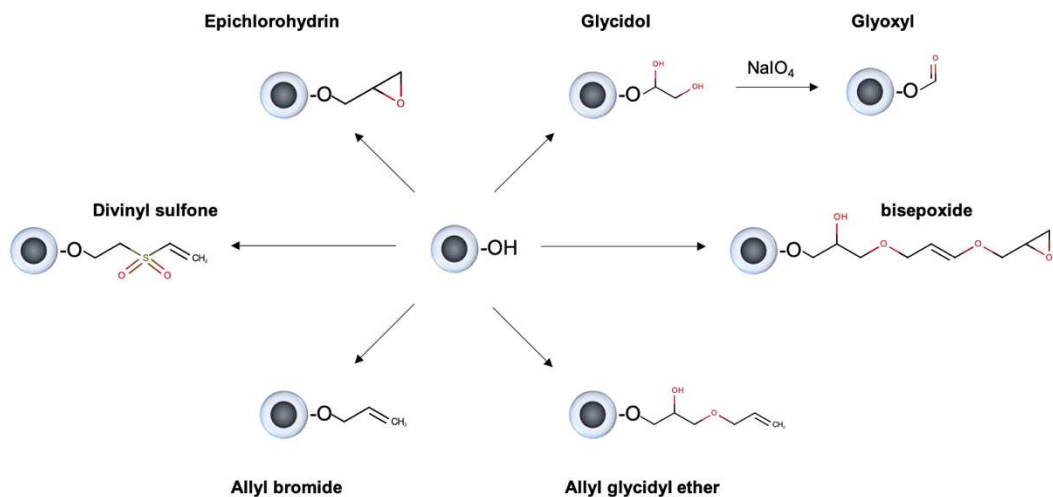


**Figure 57** Example of linkers used to cross-link or/and functionalize MAPs for proteins or ligands immobilization.

For functionalization, glyoxyl group reacts mostly with amine from Lys and Arg, while epoxide and vinyl groups are able to bind hydroxyl, acid (Asp, Glu), amine (His, Arg, Lys) and thiol (Cys) as well. Adapted from **Zhao et al., 2009**.

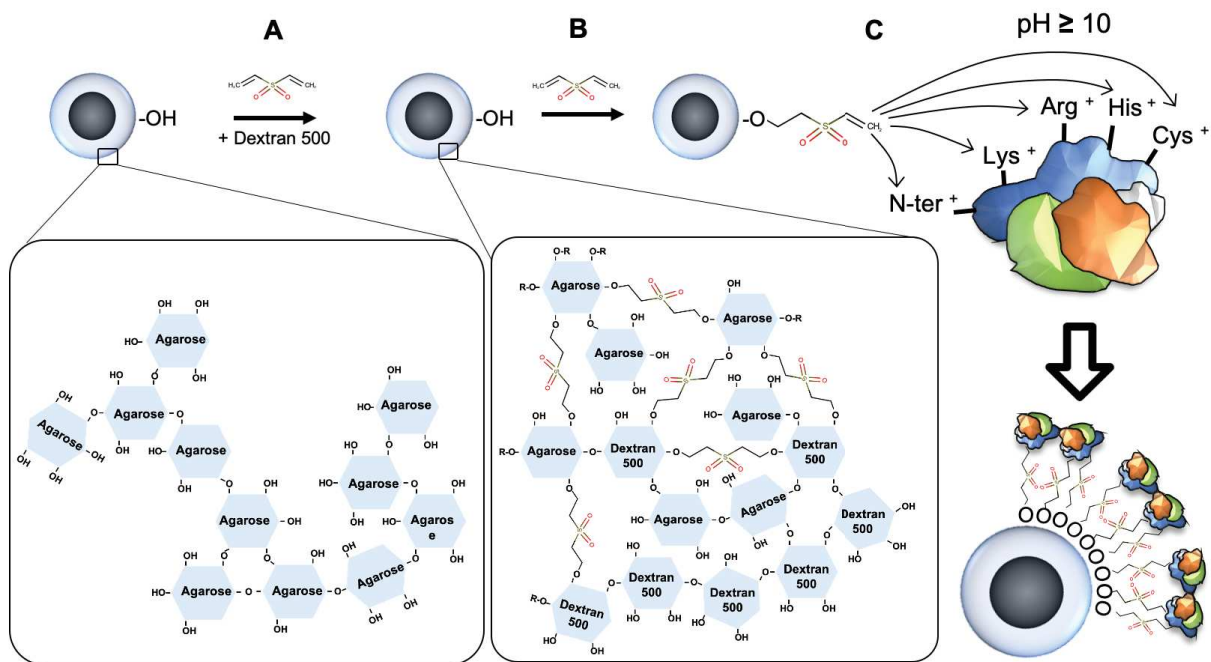


**Figure 58** Overview of the MAPs cross-linking and functionalization process steps using divinylsulfone (DVS) . (A) Cross-linking of agarose-matrix with DVS. (B) influence of coating step with Dextran T500 on the pore size. Functionalization of MAPs using DVS. (C) Immobilization of protein onto DVS-activated MAPs allows attachment of proteins by N-ter groups and Arg, Lys, His or Cys AA at pH >10

Other function such as glyoxyl provide more specific attachment of proteins by Arg and Lys AA only. Actually, the glyoxyl-agarose matrix is described as a simple and adaptable method to attach proteins *via* the N-ter function or the amines from Arg and Lys (Mateo et al., 2006; López-Gallego et al., 2013; Zucca et al., 2016). At pH 7 the glyoxyl function can only react with N-ter while at pH 10 the amine functions from Lys and Arg are charged and therefore can also react. It is reported that multipoint covalent attachment with Lys and Arg improves adsorption of the proteins as well as their stability and activity (Mateo et al., 2005; Mateo et al., 2006). Finally, glyoxyl-agarose is also a good intermediate for derivatizing the matrix into agarose-MANE or by the carboxy path for further carbodiimide or glutaraldehyde activation (Zucca et al., 2016).

Altogether, these examples illustrate all factors that might be taken into account for the production of MAPs and efficiency of our future GFP-Trap. What should I choose between all these possibilities?

#### **4.3.5 A First Sketch to Design our GFP-Trap**

Considering the elements discussed for the production of a cheap and versatile magnetic support, many options are available for the synthesis of our GFP-Trap. Being a beginner in the field, my first choice had been directed towards a simple but scalable protocol. Thus, I realized MAP synthesis following the protocol proposed in 2017 by Gu et al, which combines emulsion with vacuum pump oil and epichlorhydrin cross-linking (Gu et al., 2017). Then, glyoxyl-agarose functionalization of the support was considered because it offers an important flexibility in the protein attachment. Our collaboration with Vianney-Poignavent has enabled the production of nanobodies Nb-tRFP@GFP in *E. coli*. The sequences of the Nb-tRFP@GFP consisted of fusion between published GFP enhancer nanobodies which recognize different epitope (NbCh@GFP, Rothbauer et al., 2006; NbSF@GFP, Twair et al., 2014), and a tagRFP (Merzlyak et al, 2007). The use of Nb-tRFP@GFP was convenient since estimation of support saturation could be achieved by simple observation of residual fluorescence from RFP in the supernatant. Therefore, pure Nb-tRFPCh@GFP and Nb-tRFPsf@GFP from each GFP enhancer nanobodies have been produced and immobilized on the MAPs following reported procedure (López-Gallego et al., 2013).



## 4.4 SYNTHESIS OF A GFP-TRAP V1

### 4.4.1 Synthesis of MAPs Using W/O Emulsion Process

MAPs were synthesized according to the published protocol (Gu et al., 2017), by dispersing a heated 4% agarose aqueous solution containing 1% Fe<sub>3</sub>O<sub>4</sub> and 0.96% NaCl (w/w) in vacuum pump oil with a magnetic stirrer. Although dispersion by magnetic stirring caused some troubles due to the attraction of magnetic particles by the magnet, we successfully obtained MAPs. The observation using confocal microscope with differential interferential contrast (DIC) indicates that particles are spherical, and their size range from 5 μm to 200 μm containing from one to dozens of magnetite particles (Figure 59). As a result of magnetic stirring, the emulsion was not homogeneous. Also, we noticed that many washes had to be carried out to remove the vacuum pump oil. After washing and removing the large aggregates of MAPs, cross-linking was performed using 3% of epichlorohydrin (Gu et al., 2017).

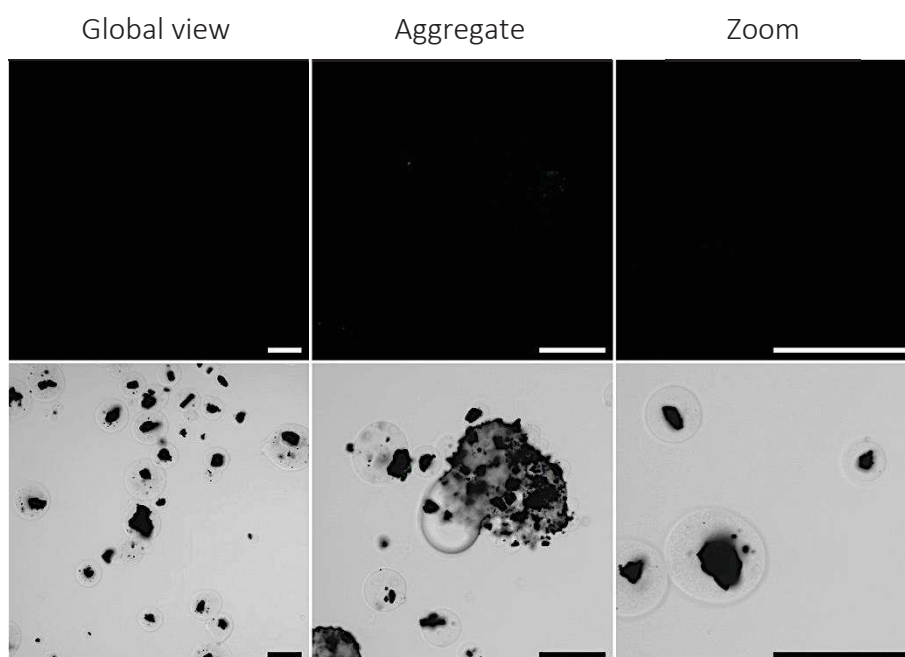


**Figure 59 Overview of MAPs prepared according to reported procedure (Gu et al., 2017).**

Global view, aggregates and a zoom on the MAPs prepared by W/O emulsion method and observed by confocal microscopy. Merged fluorescence of GFP channel and RFP channel (up), DIC view (down), scale bar = 50 μm

Considering relation between particle size and area, and that of commercial matrices are calibrated between 0.05  $\mu\text{m}$  ( $\mu\text{MACS}^{\text{TM}}$ , Miltenyi Bergisch Gladbach Germany) and 20-40  $\mu\text{m}$  (GFP-Trap\_MA, Chromotek), the finest particles might be the best one. Nevertheless, submicrometric particles have a low mass transfer and may require a special system for magnetization like  $\mu\text{MACS}^{\text{TM}}$  column (Miltenyi, Bergisch Gladbach Germany) to avoid loss of MAPs during IP procedure. Therefore, the cross-linked MAPs has been calibrated by successive filtration through sieve of  $\varnothing = 230 \mu\text{m}$  (F1), 120  $\mu\text{m}$  (F2) and 73  $\mu\text{m}$  (F3), yielding 94 mg (15%), 75 mg (12%) and 116 mg (18.5%) of dried MAPs, respectively (**Figure 60**). However, only the MAPs retained after 1 minute of magnetization were conserved to avoid the possible loss of MAPs during the IP process. The observation by confocal microscopy confirmed that the calibration was effective and the mean size of MAPs in F3 was around  $32.8 \pm 10.2 \mu\text{m}$  (**Figure 60**). Observation of MAPs using scanning electron microscopy (SEM) confirmed that F3 is homogeneous and except some non-coated magnetite particles, most MAPs are spherical or ellipsoidal (**Figure 61**). Furthermore, the total of each of the fractions suggests that 54.5% of the initial weight is wasted during the process of MAPs synthesis. Accordingly, fine and light-colored particles were observed after settling of the washing solutions, supporting the loss of MAPs poorly charged in magnetite particles. Another explanation comes from the formation of large aggregates removed before calibration. Despite these aspects, this method yields MAPs  $< 73 \mu\text{m}$  suitable for 4,6 ml of GFP-Trap at 2.5 % (dw/v). Therefore, it is cost-effective for preliminary study because 400 times cheaper as compared to the price of the commercial matrices (commercial value 2941 €, our cost 10 €). Thus, the MAPs F3 were functionalized prior to immobilization of Nb@GFP.

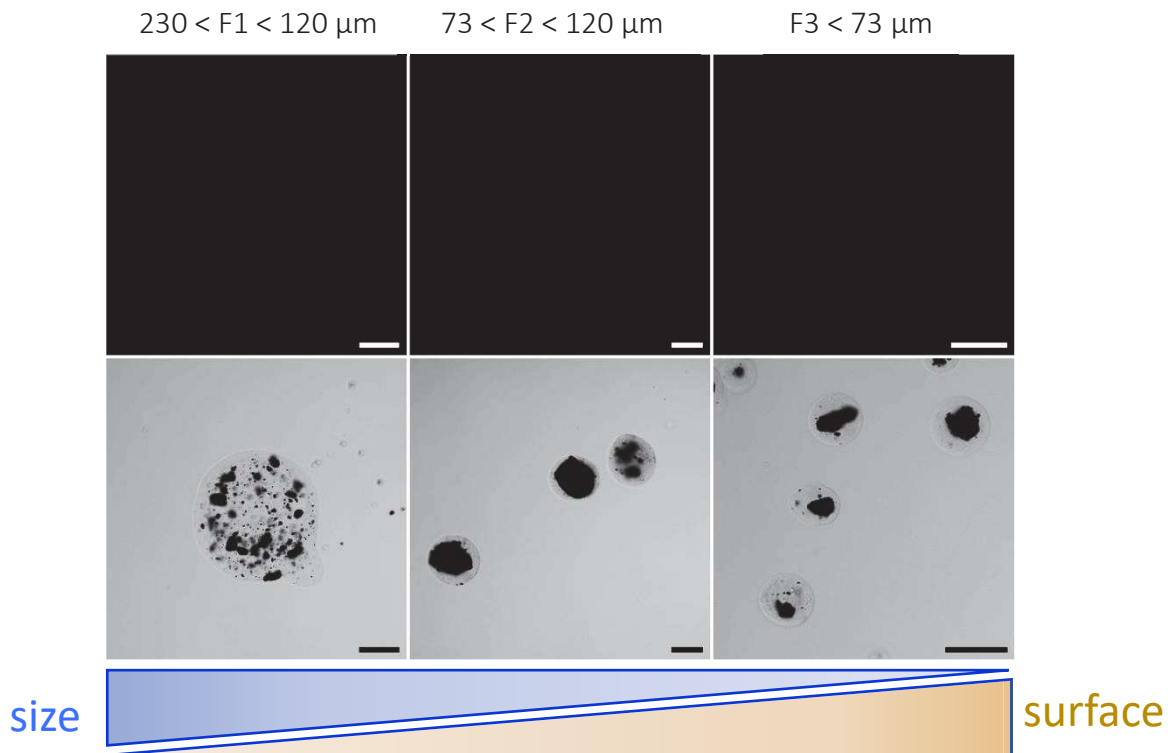


**Figure 60 Confocal microscope observation of MAPs after calibration.**

Washed MAPs were filtered through 230, 120 and 73  $\mu\text{m}$  sieves resulting in F1, F2 and F3 particles, respectively. Merged fluorescence of GFP and RFP channels (up), DIC view (down), scale bar = 50  $\mu\text{m}$ . At the bottom of the figure, a representation of the relation between size and adsorption surface of the MAPs.

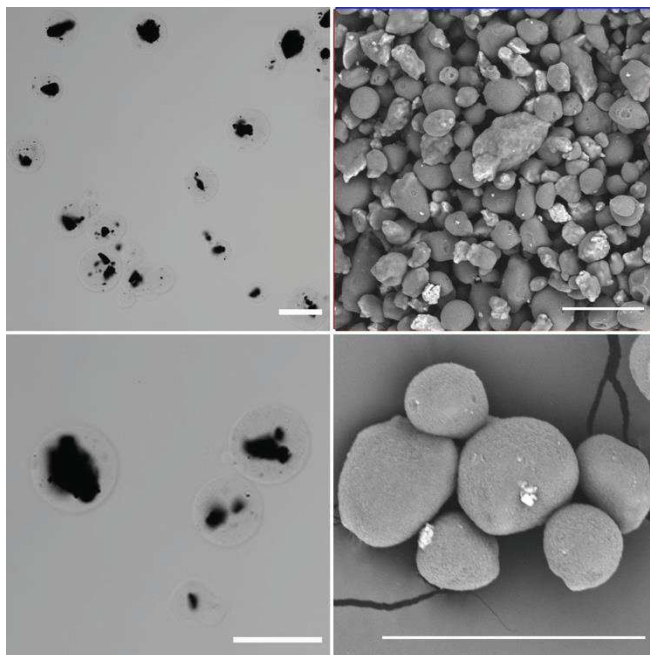


**Figure 61 Calibrated F3 MAPs < 73  $\mu\text{m}$ .**

Observation using confocal microscope (left) and SEM after dehydration by sublimation method (right). Global DIC (up left) and zoom (down left), global SEM view (up right), and zoom (down right). Scale bar = 50  $\mu\text{m}$

#### 4.4.2 Functionalization of MAPs and Immobilization of Nb@GFP

The functionalization of MAPs is essential to attach our Nb@GFP on the support. As reported (López-Gallego et al., 2013), we have functionalized our MAPs F3 batch into glyoxyl-agarose in order to compare N-ter monovalent attachment at pH 7, and multipoint covalent attachment with Arg and Lys from Nb-tRFP@GFP at pH 10 (Figure 62, Figure 63). Thus, in a PBS buffer at pH 7 alone or supplemented with 0.1 M H<sub>2</sub>CO<sub>3</sub> pH 10.6, nanobodies were incubated with glyoxyl-agarose MAPs until saturation of the support was reached (supernatant without red fluorescence).

Our results showed that saturation of the matrix at pH 7 was lower than 0.1:1 (Nb-tRFP@GFP:dried MAPs, m/m), whereas at pH 10 it was reached at 0.23:1 (Nb-tRFP@GFP:dried MAPs, m/m). This may be explained by the multipoint covalent attachment of charged Lys and Arg which increases the stability of the Nb-tRFP@GFP on the support. Moreover, 22 Lys and 18 Arg are present in our NB-tRFP@GFP (Figure 62). It was therefore suspected that the multipoint covalent attachment at pH 10 allows different conformation of Nb-tRFP@GFP, improving adsorption by decreasing the steric effect between each nanobody. The adsorption efficiency was confirmed using confocal microscopy to compare the intensity of red fluorescence from the Nb-tRFP@GFP immobilized, which was lower on with immobilization at pH 7 as compared to pH 10 (Figure 64).

MQVQLQESGGALVQPGGSLRLSCAASGFPVNRYSMRWYRQAPGKEREWVAGMSSAGDRSSYEDSVK  
GRFTISRDDARNTVYLQMNSLKPEDTAVYYCNVNVGFEYWGQGTQVTVSSGGSGGGSELIKENMHMKL  
YMEGTVNNHHFKCTSEGEGKPYEGTQTMRIKVVVEGGPLPFAFDILATSFMYGSRTFINHTQGIPDFFKQS  
FPEGFTWERVTTYEDGGVLTATQDTSLQDGLIYNVKIRGVNFPSNGPVMQKKT LGWEANTEMLYPAD  
GGLEGRSDMALKLVGGGH LICNFKTTYRSKPKAKNLKMPGVVYVDHRLERIKEADKETYVEQHEVAVARY  
CDLPSKLGHKGGSGHHHHHH

**NbCh@GFP** (12.8 kDa) **RFP** (25.3 kDa) **Total protein** = 40.34 kDa

**Figure 62 Peptide sequence of the Nb-tRFPCh@GFP.**

Protein was produced in *E. coli* and purified for immobilization on activated glyoxyl-agarose MAPs. Amino acids corresponding to the sequence of NbCh@GFP (blue), RFP (red), the whole protein includes the linker and C-ter His-Tag elements as well.

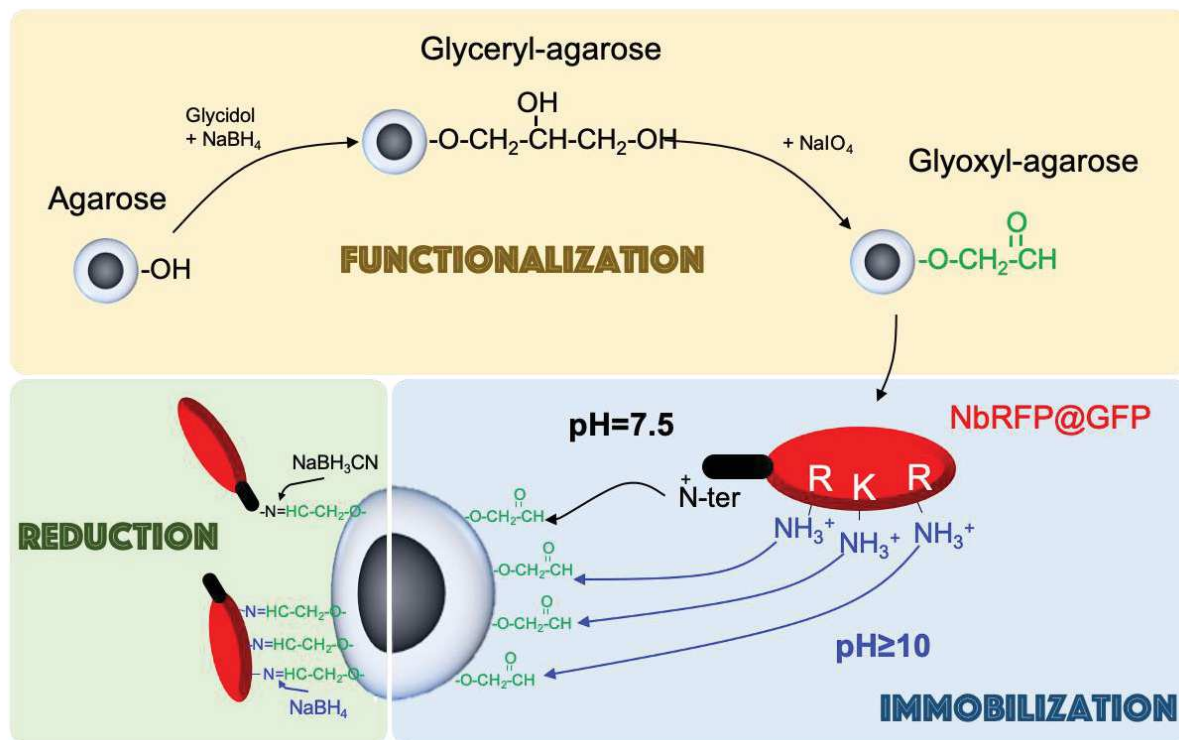


**Figure 63 Development process for our GFP-Trap using MAPs.**

First step is the functionalization of MAPs into glyoxyl-agarose (yellow box). Then, immobilization was achieved with a mix of Nb-tRFP@GFP (blue box) by single covalent attachment of the N-ter end at pH 7 (black) and multipoint covalent attachment with Arg and Lys at pH 10 (blue). The final step consists in the reduction of Schiff's base (green box) with  $\text{NaBH}_2\text{CN}$  at pH 7 and  $\text{NaBH}_4$  at pH 10 to allow stable and non-reversible binding of Nb-tRFP@GFP onto the support.

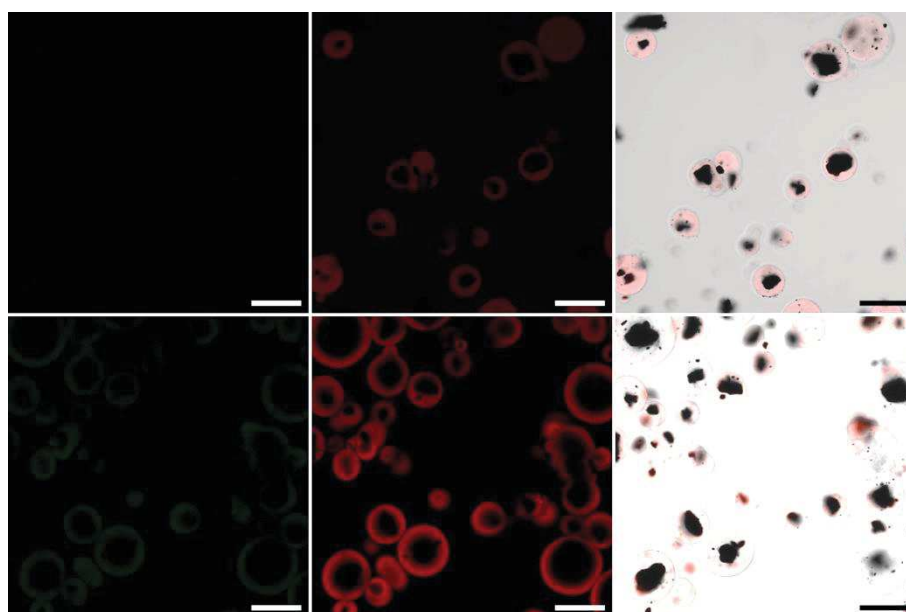


**Figure 64 GFP-Trap grafted with Nb-tRFP@GFP.**

Observation by confocal microscopy of the fluorescence from synthesized GFP-trap after immobilization of Nb-tRFP@GFP at pH 7 (up) and pH 10 (down). The GFP fluorescence channel GFP (left), RFP fluorescence channel (middle) and both fluorescence merged with DIC view (right). Scale bar = 50  $\mu\text{m}$

#### 4.4.3 Comparison of Efficiency Between GFP-Trap\_MA and GFP-Trap v1

The performance of the synthesized GFP-Trap 1<sup>st</sup> version (GFP-Trap v1) was evaluated and compared to that of GFP-Trap\_MA (Chromotek, Planegg, Germany) having a capacity of 8 µg/10 µl as compared to the GFP-Trap\_M (0.5 µg/ 10 µl). An IP assay was performed with His-GFP-CVIL reference and GFP-Trap v1 to validate the interaction between Nb-tRFP@GFP and GFP-sensor by confocal microscopy. The GFP fluorescence was only detected after IP and merged with the fluorescence of the RFP indeed, confirming the IP of the non-prenylated His-GFP-CVIL protein (**Figure 65**). Since IP efficiency is affected by the selectivity of the matrix for proteins, we performed trials with 5 µl of GFP-Trap\_MA or GFP-Trap v1 using the protein extract with prenylated GFP-CVIM from 700 mg of fresh tobacco leaves and the non-prenylated His-GFP-SVIL reference purified from bacteria. The analysis of the immunoprecipitated proteins by SDS-PAGE, western blot or staining with silver nitrate showed that both proteins GFP-CVIM and His-GFP-SVIL were well purified with GFP-Trap\_MA and our GFP-Trap v1 (**Figure 66**).

Nevertheless, the results indicate that the amount of GFP-CVIM protein is lower with our GFP-Trap v1 compared to the GFP-Trap\_MA, *vice-versa* for the His-GFP-SVIL protein. Besides, nonspecific proteins appear to be Co-IP with the GFP-CVIM protein more extensively with our GFP-trap v1 than with the GFP-Trap\_MA. Taken together, these results suggest that the GFP-Trap v1 capacity to bind GFP is higher than the GFP-Trap\_MA. But, the lack of GFP-Trap v1 selectivity may be responsible for the decrease of GFP-CVIM protein immunoprecipitated from plant extracts. Nonspecific proteins can be adsorbed on the very polar MAPs, but also by hydrophobic interaction with RFP from the Nb-tRFP@GFP, which literally coats the MAPs. Moreover, two intense spots at 40 kDa and 26 kDa were observed only in the fractions purified with our GFP-Trap v1 (**Figure 66**). Accordingly, the elution with the 1x Laemmli buffer at 85°C induces a considerable breakdown of Nb-tRFP@GFP (40kDa) partially fragmented in RFP alone (26 kDa). These first assays have shown that the synthesized GFP-Trap v1 is functional at a cost 400-time lower than commercial solutions. Although, purification with the commercial GFP-Trap\_MA remains more efficient than our system, we privileged uses of our cheaper GFP-Trap v1 for the development of a prenylated protein analysis protocol. Since GFP-CVIL degradation was suspected in BY-2 cells, we have controlled these aspects prior to other analysis.

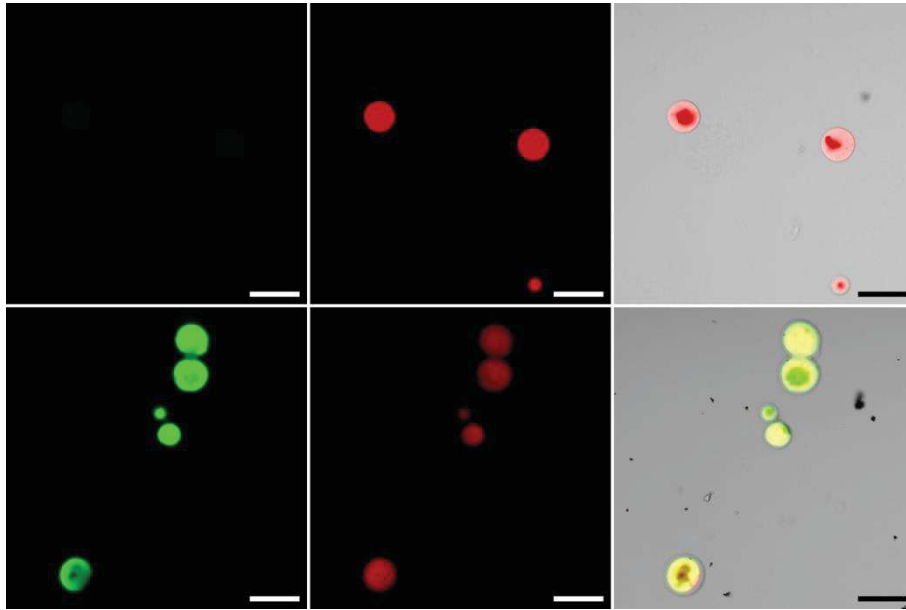
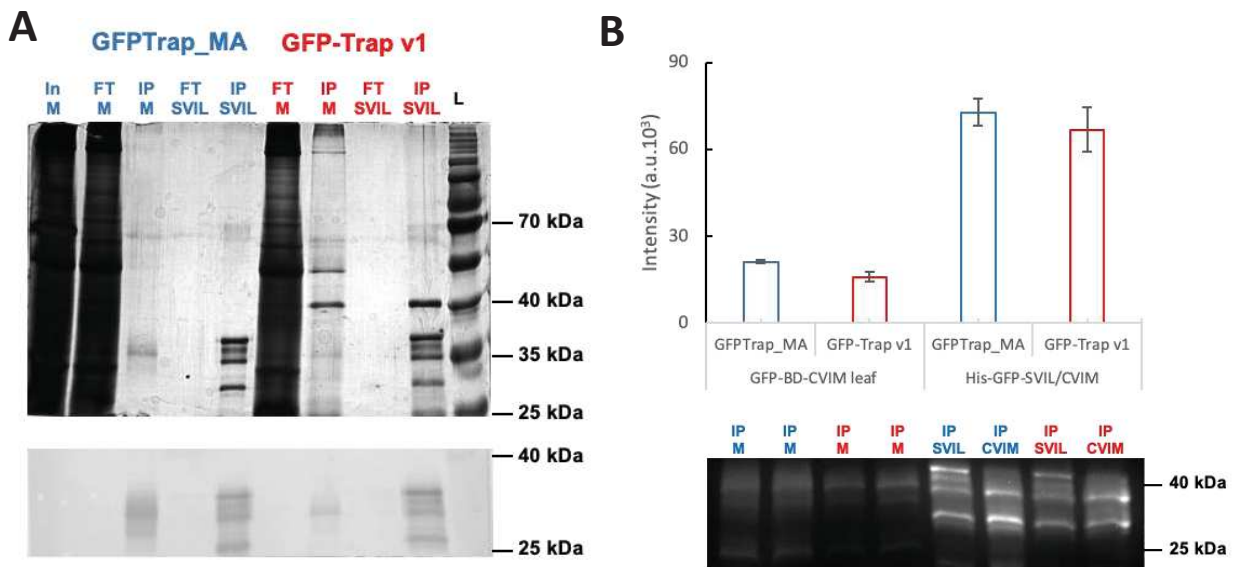


**Figure 65 GFP-CVIL immunoprecipitated on the GFP-Trap v1.**

Observation by confocal microscopy of the fluorescence from synthesized GFP-trap v1 before (up) and after IP of His-GFP-CVIL (down). Fluorescence in the GFP channel (left), RFP channel (middle) and both fluorescence merged with DIC view (right). Scale bar = 50  $\mu\text{m}$



#### 4.4.4 Digestion of GFP-Sensor by BY-2 Cells Endoproteases

First of all, a degradation of the GFP-CVIL protein was observed in the absence of proteases inhibitors during extraction BY-2 cells expressing GFP-CVIL (section 4.2.1). In addition, no difference was observed between the size of proteins supposed to be prenylated and those not prenylated. Therefore, this experiment was reproduced with the GFP-Trap v1 for IP and separation on 20 x 20 cm SDS-PAGE gel to improve resolution between proteins and determine accurately their size. Accordingly, GFP-CVIL from BY-2 cells inhibited or not with FOS and GFP-CVIL, -CVIM, -SVIL from tobacco leaves were immunoprecipitated and analyzed by SDS-PAGE. Surprisingly, our result confirmed the digestion of the GFP-sensor in BY-2 cells, but not in plant extracts (Figure 67). As a matter of fact, the western blot evidenced three different main digest products from the GFP-CVIL (35 kDa) at 32, 30 and 27 kDa. Accordingly, proteases might be specifically expressed in tobacco BY-2 cells and not in leaves. The addition of protease inhibitor cocktail (cOmplete®, Roche, Basel Switzerland) in the extraction buffer partially reduced this phenomenon (Figure 68). According to data available on the supplier website, cOmplete® cocktail of protease inhibitors inhibits > 95% even after 1h proteases such as pronase, pancreas-extract, metalloprotease such as thermolysine or serine protease like chymotrypsin. However, inhibition of trypsin is less efficient (89% after 1h) and cysteine protease like papain too (73% after 1h).

Interestingly, a prediction of cleavage site using PeptideCutter (Expasy tool, Swiss Institute of Bioinformatics, Lausanne Switzerland) including common proteases, suggest that enzyme with AspN or Proteinase K activity could be responsible for. Different proteases have been reported in exudates or intracellular washing fluid of tobacco such as subtilisin-like proteases, serine carboxypeptidases, papain-like cysteine proteases (PLCP) and homologs of the CND41 aspartic protease (Mandal et al., 2016). Furthermore, no apparent size differences were detected between the proteins GFP-CVIM and -CVIL. Whereas, it was noticed that GFP-SVIL always present a large smear between ~32 and ~35 kDa rather than a clear band at ~35 kDa appeared (Figure 67). It is stated that smear in SDS-PAGE often occurs in the case of DNA contamination or protein aggregation due to excessive heating. Since GFP-SVIL protein is exclusively located into the nucleus in tobacco leaves, the smear likely results from a DNA contamination. However, a nucleic acid precipitation before SDS-PAGE was not performed to test this hypothesis.



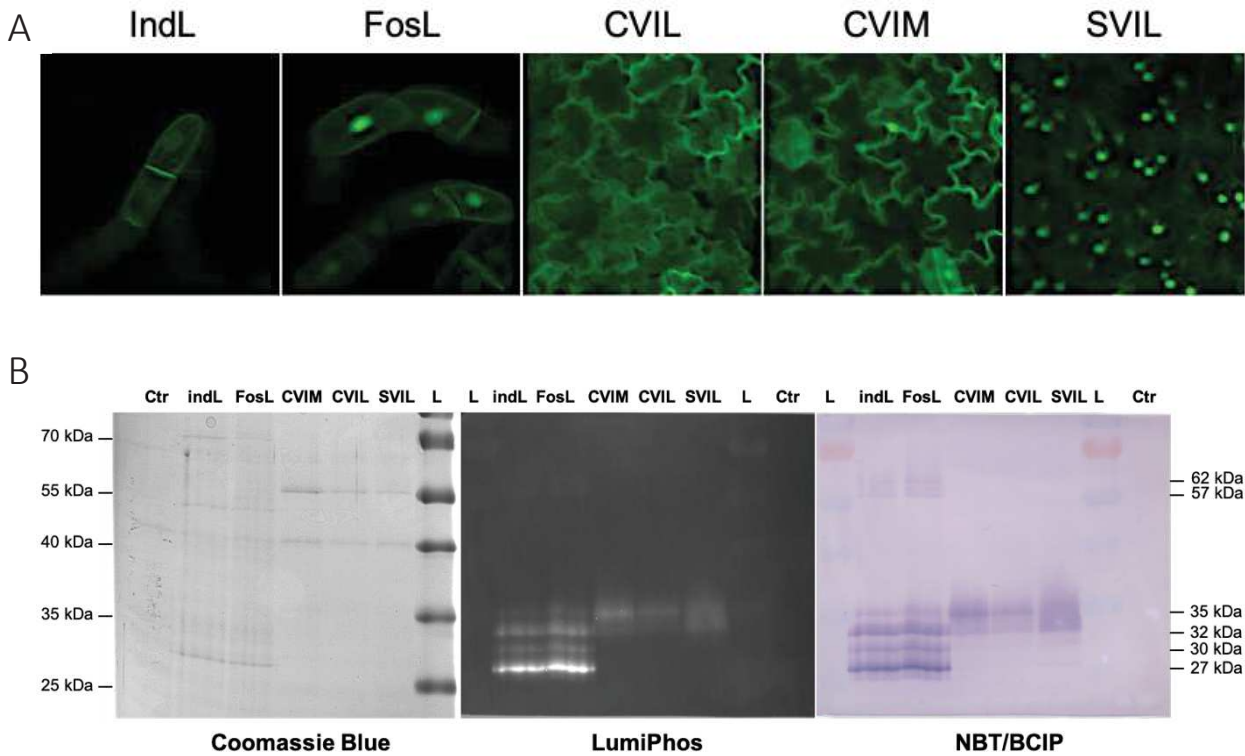


**Figure 67 Specific digestion of GFP-CVIL by BY-2 cells endoproteases.**

(A) GFP fluorescence observed by confocal microscopy of plant material: BY-2 cells expressing GFP-CVIL being prenylated in standard condition (IndL), with 100  $\mu$ M Fosmidomycin (FosL). *N. tabacum* leaves expressing GFP-CVIL (CVIL), GFP-CVIM (CVIM) which are prenylated unlike the GFP-SVIL (SVIL). (B) Protein immunoprecipitated without protease inhibitors from 2.5 g of plant material using the GFP-Trap v1. Proteins were analyzed by SDS-PAGE stained with Coomassie blue or western blot using rabbit IgG @GFP-CaaX revealed with NBT/BCIP.

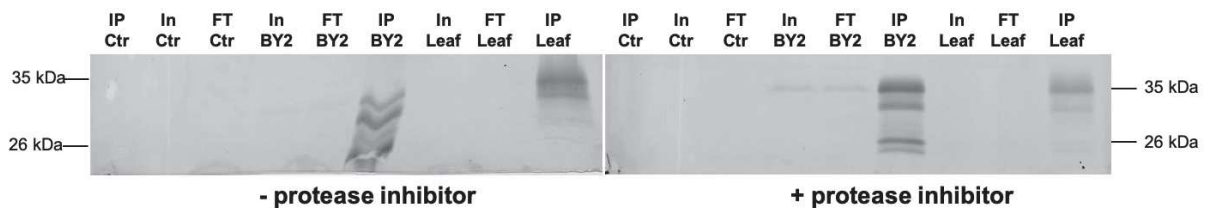


**Figure 68 Protease inhibitors reduce degradation of GFP-CVIL in BY-2 cells.**

Western blot analysis of GFP-CVIL immunoprecipitated with the GFP-Trap v1 from BY-2 cells (BY-2) and *N. tabacum* leaves (leaf) expressing GFP-CVIL or the negative control of BY-2 cells (Ctr). The IP was carried out without (left) or with cOmplete® protease inhibitor (right). Total protein extract (In), flow through after 1h of IP (FT) and the immunoprecipitated proteins (IP). The protein was degraded in BY-2 cells but not in plant, the absence of cOmplete inhibitor increased the abundance of GFP-CVIL degraded forms observed from 32 to 26 kDa.

## 4.5 CONSIDERATION FOR PROTEOMICS OF PRENYLATED PROTEINS

### 4.5.1 Analysis of Prenylated Proteins

Previously (**section 0**), we proposed that alternative substrates allow to reverse the inhibition of protein prenylation. Our hypothesis on the flexibility of PPTs activities suggest that PFT is the enzyme being able to transfer prenyl groups onto proteins supposed to be targeted by PGGT-I under standard conditions (**section 2.3**). That becomes our working hypothesis. Nonetheless, the cellular location of the GFP-sensor protein is insufficient by itself to identify unambiguously the nature of the transferred prenyl group. Therefore, a systematic method for identifying transferred prenyls is required to understand whether PFT uses alternative prenyl substrates when modifying GFP-CVIL proteins.

The identification of the prenyl moiety carried by proteins *in cellula* is not an easy task because prenylated proteins are not abundant in eukaryotic cells as compared to other proteins. As introduced, several methods have been published, but they do not consider enough *in vivo* factors (**section 0**).

Considering all our possibilities, the most sensitive, simplest and safest method is the proteomics approach analyzing a purified prenylated protein by HPLC-MS/MS after digestion by endoproteases.

#### 4.5.2 Parameters for LC-MS/MS Analysis of Immunoprecipitated Prenylated Proteins

Since the IP of the GFP sensor with a GFP-Trap was successfully achieved, it was conceivable to pursue with the proteomic analysis by HPLC-MS/MS. With this respect, the purification and digestion conditions, the separation of peptides by HPLC, and MS parameters such as the detection mode, charge  $z$ ,  $m/z$  detection range, ionization mode are critical points to be considered for sample preparation and proteomic analysis. Traditionally, proteins are separated by 1D or 2D SDS-PAGE before being isolated (**Figure 69**). After several washes, proteins are in-gel digested and peptides are eluted to be analyzed by HPLC-MS/MS (Deracinois et al., 2013). Despite high risks for sample contamination and the fact that the task is rather laborious, this approach was common and considered as sensitive and useful to concentrate final peptide samples. More recently, the development of technologies based on affinity purification *via* matrices and HPLC-MS/MS equipment allowed the emergence of new digestion protocols. Thus, in-solution or on-beads digestions are used in proteomic analysis of Co-IP proteins (**Figure 69**) (Bajczyk et al., 2020). This allows the identification of proteins interacting with the immunoprecipitated protein, so called interactome.

Although these protocols are faster and reduce the loss of protein during gel extraction, they are more sensitive to detergent traces that sometimes need to be adjusted or may not be compatible for some endoproteases. However, many proteases have been described to enable the digestion of proteins into peptides of different sizes. Among these proteases, trypsin (cleavage site: C-ter end of Arg and Lys residues) and AspN (cleavage site: N-ter end of Asp residue) are widely used alone or in combination for digestion protocols prior to proteomic analysis (Tsiatsiani and Heck, 2015; Dau et al., 2020). According to the GFP-sensor sequence, digestion with trypsin would be favorable to obtain small peptides especially on the C-ter end, as the former present a basic domain that is rich in Lys and Arg residues (**Figure 70**). On the contrary, digestion with AspN, already described for the analysis of the prenylated sensor (Gerber et al., 2009), would release larger peptides.

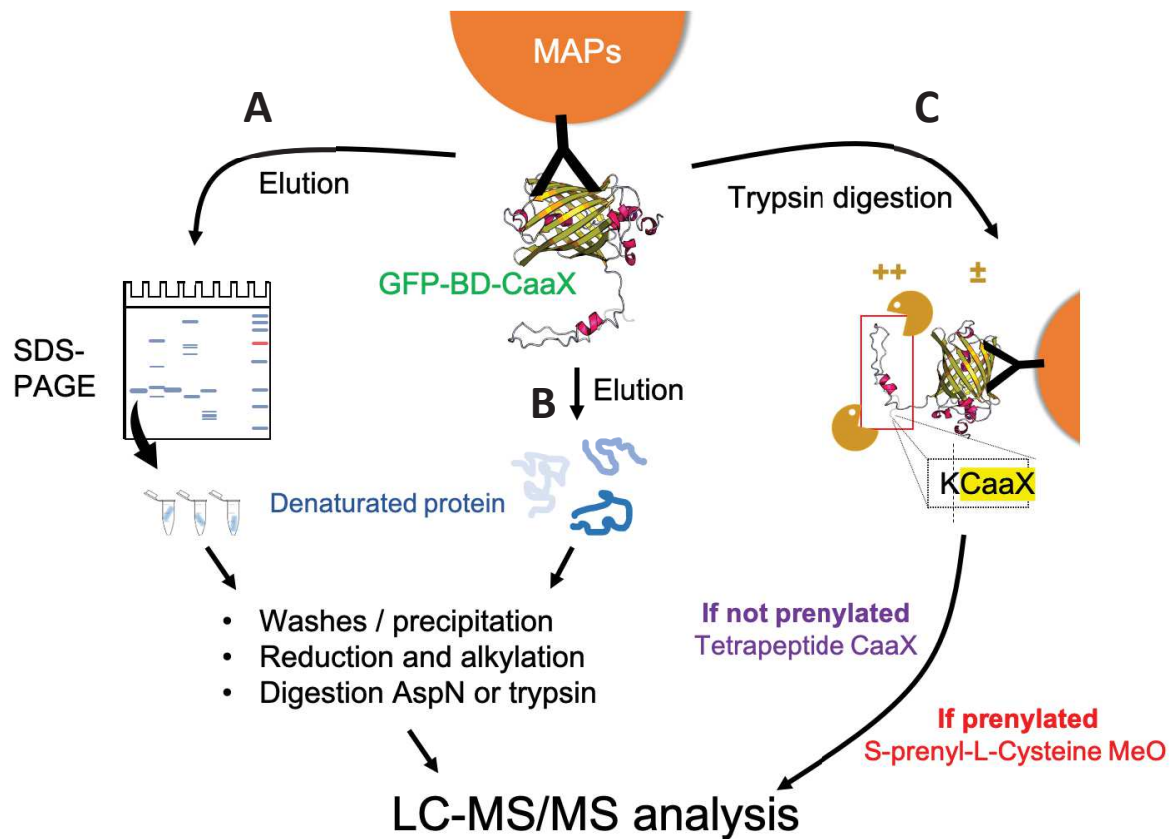


**Figure 69 Procedures for the preparation of GFP-sensor immunoprecipitated samples for proteomic analysis.**

(A) in-gel method, in which immunoprecipitated proteins are desorbed in Laemmli buffer to be separated on SDS-PAGE gel. After cutting the spots of interest and several washes, a reduction and alkylation of the proteins is performed before digestion by AspN or trypsin. (B) in-solution method which is similar to the in-gel method, but SDS-PAGE was replaced by precipitation steps using AcNH<sub>4</sub> in MeOH before being digested by proteases. (C) Native on-beads method in which the immunoprecipitated proteins are not desorbed, but digested without any denaturation/alkylation after three washes of the particles. This method is suitable for trypsin but not AspN digestion and offers a targeted digestion of the GFP-sensors C-ter domain.

MHHHHHHVSKGEELFTGVVPILVELDGDVNGHKFSVSGEGEGDATYGKLT**K**FICTTGKLPVPWPTLVTTFTY

GVQCFSRYPDHMKQHDFK**S**AMPEGYVQ**R**TIFFKDDGNYK**T**RAEVKFEGDTLVNRIELK**G**IDFKEDGNILG

HKLEYNYNshNVYIMADKQK**N**GIKVNF**K**IRHNIEDG**S**VQLADHYQQNTPIGDGPVLLP**D**NHYLSTQSALS**K**D

PNEKR**D**HMVLLFVTAAGITHGMDELVK**C**MMAK**K**RRKR**I**EEKR**D**H**D**GG**S**RTKSAGPSAAPASK**R**GQ**K**CVIL

His-Tag (0.8 kDa) GFP (26,47 kDa) Basic domain (4,78 kDa) CaaX (0,45 kDa)

**Figure 70 Peptidic sequence of the His-GFP-CVIL protein.**

The sequence elements are the His-tag (brown), the GFP (green), the basic domain (grey) and the CaaX motif (black). Trypsin (bold red) and AspN (blue) cleavage sites are indicated.

Although commercialized enzymes are considered to be very accurate and stable, some “miss-cleavages” or “preferred-sites” have been reported. They may arise from the presence of specific AA nearby the cleavage site, from non-adapted 3D conformation or eventually from modified AA (Siepen et al., 2007; Chiva et al., 2014; Šlechtová et al., 2015). For instance, it has been shown that trypsin favors Arg over Lys and that the presence of proline, acidic AA, methionine as well as Cys is unfavorable, especially if it is involved in S-bond formation close to the cleavage site (Chiva et al., 2014; Na et al., 2015; Šlechtová et al., 2015). In addition, other parameters such as the buffer, the presence of impurities or detergent traces may decrease the digestion efficiency (Kolsrud et al., 2012; León et al., 2013). In this regard, it can be speculated that without any denaturation, the unstructured C-ter would be more digested than the GFP being structured in barrel by  $\beta$ -sheets (**Figure 69**).

Accordingly, we were also interested to perform the on-beads digestion protocol without denaturing proteins in order to evaluate if trypsin digestion undergoes to unstructured C-ter end rich in Lys and Arg rather than to GFP being structured and likely stabilized by Nb@GFP (Steyaert and Kobilka, 2011). By considering all of these factors, the digestion of purified proteins was performed with trypsin and AspN using in-gel, in-solution and on-beads digestion. First, the feasibility of on-beads digestion with trypsin was evaluated using the GFP-CVIL protein immunoprecipitated with the GFP-Trap v1.

### 4.5.3 Trypsin On-Beads Digestion

Here we wanted to demonstrate that our digestion protocol is functional and allows selective digestion of the GFP-CaaX C-ter end. Therefore, the His-GFP-CVIL protein reference or the GFP-CVIL expressed in BY-2 cells were immunoprecipitated using our GFP-Trap v1 and were digested or not with trypsin (control). The His-GFP-CVIL before and after digestion was observed directly on-beads by confocal microscopy or eluted, then analyzed by Western blot using the IgG @GFP-CaaX. The confocal microscope images showed that following digestion, the fluorescent signal intensity decreased, suggesting that GFP was partly digested (**Figure 71**). Nevertheless, this signal persisted on the GFP-Trap even after 24 h of tryptic digestion and treatments with 2M urea, supporting the idea that GFP is well stabilized through the interaction with the nanobodies (**Figure 71**). However, by adding the denaturing Laemmli buffer, the whole fluorescence, including that of the Nb-tRFP@GFP attached to the matrix, is gone. We already observed in the (**section 4.4.3**), that GFP and part of the GFP-Trap v1 nanobodies are released in the presence of the Laemmli buffer (**Figure 66**). However, since nanobodies are normally covalently attached, it remains unclear if the loss of 3D conformation or loss of nanobodies themselves have shut down the RFP fluorescence on the GFP-Trap v1.

Furthermore, ~35 kDa spots observed on the western blot before digestion were not anymore detected after. Only one spot, at ~26 kDa, remained in all digested protein samples. This let us to propose that the C-ter end of the protein including the basic domain is digested and corresponds to the loss of ~9 kDa. Besides, spots observed with an apparent molecular mass of ~27 kDa are present only in the His-GFP-CVIL reference sample, suggesting that the His-tag was not digested. Our results confirmed that on beads digestion of the native GFP-CVIL with trypsin undergoes preferentially to the unstructured C-ter domain rather than the structured GFP molecule. This method, which is particularly suitable for C-ter peptide enrichment of GFP-sensors, was therefore included in our study to develop a systematic method for the analysis of prenylated proteins. To identify prenyl moieties adorning prenylated proteins, several assays were performed using samples containing protein GFP-CVI(L/M) or GFP-SVIL extracted and immunoprecipitated from BY-2 cells or tobacco leaves. The proteins were then analyzed using proteomics approach in collaboration with P. Hammann (IBMC, Strasbourg) and C. Schaeffer-Reiss (LSMBO, Strasbourg).

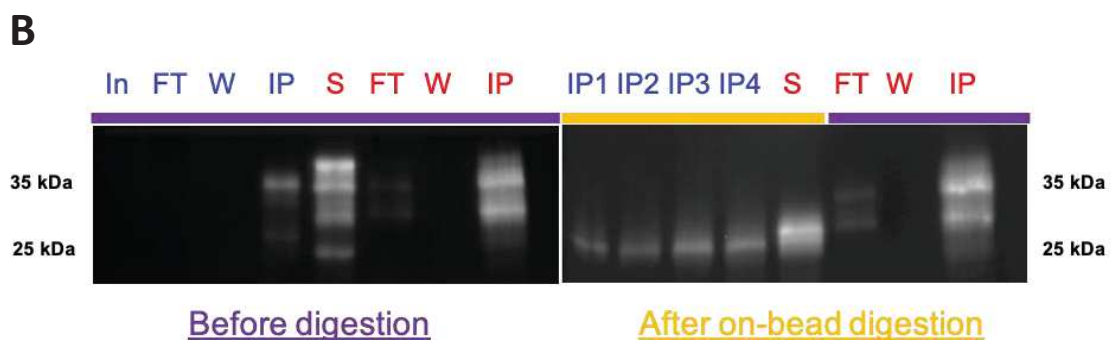
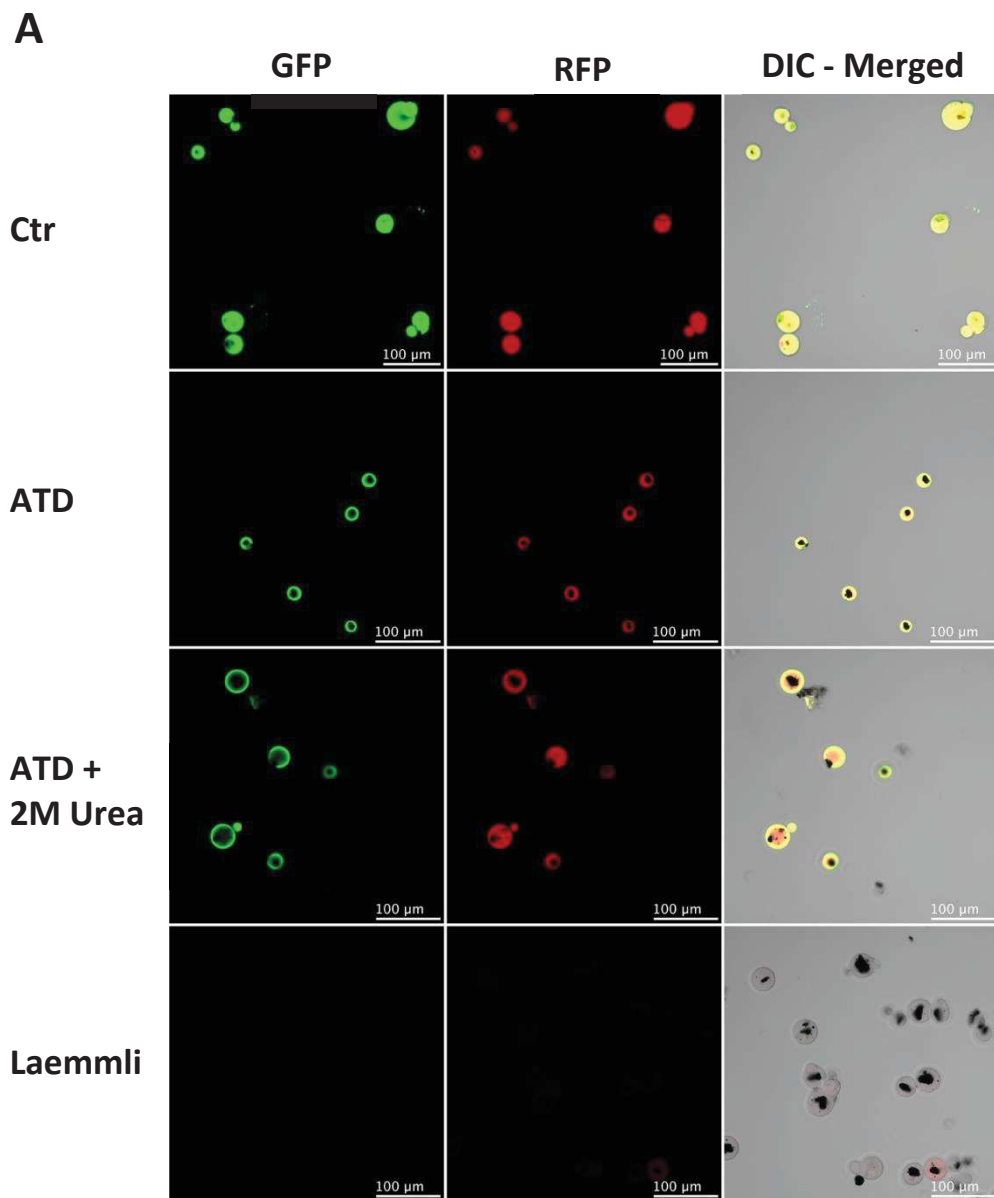


**Figure 71 On-beads digestion with trypsin promotes C-ter unstructured domain degradation.**

(A) Confocal microscope observation of His-GFP-CVIL immunoprecipitated protein on GFP-Trap v1 beads, before tryptic digestion (Ctr), after 24 h tryptic digestion (ATD), after 24 h tryptic digestion and 2M Urea (ATD + 2M Urea) and eluted by the Laemmli buffer (x1) at 85°C (Laemmli). (B) Western blot analysis using rabbit IgG @GFP-CaaX and LumiPhos chemoluminescence substrate for the detection of His-GFP-CVIL (red) and GFP-CVIL protein from BY-2 cells (Blue). Immunoprecipitated GFP-CVIL with the GFP-Trap v1, before digestion (purple) or after on-beads digestion (yellow). Total protein extract (In), flow through (FT), first wash (W), proteins immunoprecipitated by GFP-Trap with only Nb-tRFPCh@GFP (IP1, IP2) and the GFP-Trap v1 (IP, IP3, IP4). Complete™ protease inhibitor was used in these IP to limit the GFP-sensor degradation by BY-2 cells endoproteases.

## 4.6 PROTEOMIC ANALYSIS OF IMMUNOPRECIPITATED PRENYLATED PROTEINS

### 4.6.1 Comparison of In-Gel and In-Solution Digestion Methods for Proteomics

First, we analyzed samples of His-GFP-CaaX references as well as GFP-CVIL protein isolated from tobacco leaves or BY-2 cells that were immunoprecipitated using the GFP-Trap\_M beads. In-gel and in-solution digestion protocols with AspN and/or trypsin were applied on different protein samples (**Table 4**). First of all, the protein samples obtained from 700 mg of BY-2 cells (**section 4.2.1**) suspected of degradation were used for proteomic analysis using in-gel method and digestion with AspN (**Figure 54**). The digestion steps and the analysis by HPLC-Q-Orbitrap-MS/MS were performed at the LSMBO. Peptides corresponding to GFP and their  $\gamma$ -,  $\beta$ - ions were identified with a protein sequence coverage (SQ%) between 66 and 90%. Almost no peptides corresponding to the basic domain of GFP-CVIL were detected in the BY-2 samples at ~26, while they were observed for the protein at ~35 kDa (**Figure 72, Figure 73**). These results definitely confirmed the GFP-CVIL degradation occurring at the C-ter end in BY-2 cell extracts without any protease inhibitor. Unfortunately, the last eight AA (RGQKCVIL) are missing to fully identify the C-ter end of His-GFP-CVIL at ~32 and ~35 kDa (**Figure 72**). Interestingly, the analysis of the putative dimer at ~70 kDa improved the SQ%, but the two last AA were still lacking to get through the complete CaaX signal. Meanwhile, other trials were performed using in-solution AspN or tryptic digestion method on proteins purified from plant leaves, in which the GFP-sensor is not degraded. The analyses were carried out by P. Hamman (IBMC). Even though, these analyses allowed the detection of peptides associated to the GFP and basic domain with SQ% 53-85%, no additional information were obtained (**Table 4**). Once again, the five to seven AA at the C-ter end or prenylated peptides were missing. Also, it was noticed that the in-solution AspN digestion did not work out, therefore AspN digestion was reserved for in-gel procedure in further analysis.

A last attempt was carried out with 5 g of BY-2 cells and leaves using protease inhibitors. In this comparative study, we used plant material expressing prenylatable GFP-CVIL or unprenylatable GFP-SVIL in plants. As the BY-2 GFP-SVIL cell line was not available, we used GFP-CVIL from BY-2 cells, in which prenylation was inhibited with 100  $\mu$ M FOS. Proteins samples were prepared following in-gel AspN digestion and in-solution trypsin digestion.



**Table 4 Overview of GFP-CaaX samples for proteomic analyses.**

Are indicated, the parameters used for the preparation and proteomic analysis of GFP-sensors reference and immunoprecipitated from plant material (blue). Results obtained for protein prenylation markers expected (CaaX, S-Prenyl-L-cys OMe and PPTs motifs) in our proteomic analysis (white).

Location	Sample	Plant material (g)	GFP-Trap	Enzyme	Digestion type	GFP-sensor SQ%	CaaX	S-prenyl-L-cys OMe	PPTs
IBMC	His-GFP-Caax ref + GFP-CVIL leaf	0.35	Miltenyi	Trypsin	In solution	65-85	X	X	X
IBMC	His-GFP-Caax ref + GFP-CVIL leaf	0.35	Miltenyi	AspN + Trypsin	In solution	20 – 58			
LSMBO	His-GFP-CVIL ref + GFP-CVIL BY-2	0.7	GFP-Trap_M	AspN	In gel	66 - 90			
IBMC	His-GFP-CVI(M/L) ref	X	X	Trypsin	In solution	53 - 63			
IBMC	GFP-(C/S)VIL leaf + GFP-CVIL BY-2 cells induced and with FOS 100 µM	5	GFP-Trap v1	Trypsin	In solution	71 – 83			
	His-GFP-CVIM ref + GFP-CVIM leaf			AspN	In-gel	23 - 35			

Protein sequence coverage: 88 %

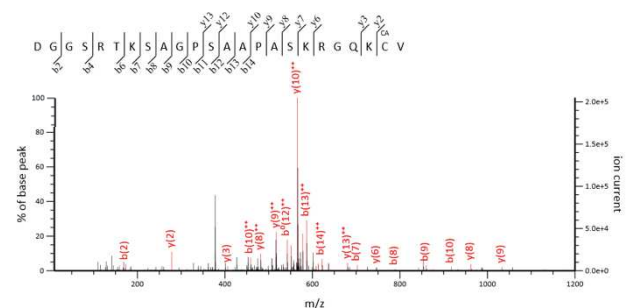
70 kDa

1 MHHHHH**HSVK** GEELFTGVVP ILVELDGDVN GHKFSVSGEG EGDATYCKLT  
 51 LKFICTTGKL PVPWPTLVTT FTYGVQCFSR YPDHMKQHDF FKSAMPEGYV  
 101 QERTIFFKDD GNYKTRAEVK FEGDTLVNRI ELKGIDFKED GNILGHKLEY  
 151 NYNSHNVYIM ADKQKNGIKV NFKIRHNIED GSVQLADHYQ QNTPIGDGPV  
 201 LLPDNHYLST QSALSKDPNE KRDMVLLLEF VTAAGITHGM DELVKCMMAK  
 251 KRRKRIEEKR DHDGGSRTKS AGPSAAPASK RGQKCVIM

Protein sequence coverage: 83 %

35 kDa

1 MHHHHH**HSVK** GEELFTGVVP ILVELDGDVN GHKFSVSGEG EGDATYCKLT  
 51 LKFICTTGKL PVPWPTLVTT FTYGVQCFSR YPDHMKQHDF FKSAMPEGYV  
 101 QERTIFFKDD GNYKTRAEVK FEGDTLVNRI ELKGIDFKED GNILGHKLEY  
 151 NYNSHNVYIM ADKQKNGIKV NFKIRHNIED GSVQLADHYQ QNTPIGDGPV  
 201 LLPDNHYLST QSALSKDPNE KRDMVLLLEF VTAAGITHGM DELVKCMMAK  
 251 KRRKRIEEKR DHDGGSRTKS AGPSAAPASK RGQKCVIL



Protein sequence coverage: 72 %

26 kDa

1 MHHHHH**HSVK** GEELFTGVVP ILVELDGDVN GHKFSVSGEG EGDATYCKLT  
 51 LKFICTTGKL PVPWPTLVTT FTYGVQCFSR YPDHMKQHDF FKSAMPEGYV  
 101 QERTIFFKDD GNYKTRAEVK FEGDTLVNRI ELKGIDFKED GNILGHKLEY  
 151 NYNSHNVYIM ADKQKNGIKV NFKIRHNIED GSVQLADHYQ QNTPIGDGPV  
 201 LLPDNHYLST QSALSKDPNE KRDMVLLLEF VTAAGITHGM DELVKCMMAK  
 251 KRRKRIEEKR DHDGGSRTKS AGPSAAPASK RGQKCVIM

**Figure 72 NanoLC-Orbitrap-MS/MS analysis of His-GFP-CVIL after in-gel digestion with AspN (LSMBO).**

Sequence coverage obtained in the proteomic analysis of the His-GFP-CVIL protein processed by the in-gel method after IP using the GFP-Trap\_M. Sequence coverage obtained in the 70 kDa (up left), 35 kDa (down left) and 26 kDa (down right) strips. Fragmentation spectrum associated with the C-ter peptide of the His-GFP-CVIL protein at 70 kDa (up right). To note, the analytical software confused the GFP-CVIM and GFP-CVIL for 70 and 26 kDa strips as the last amino acids are the only difference and they were not identified.

IP was successfully completed as shown by spots observed at 35 kDa on the Coomassie blue-stained gel, in all sample except the negative BY-2 control (**Figure 74**). Strips corresponding to the GFP-CVIL at  $35\pm 1$  kDa were cut off for each sample before being processed with the in-gel/AspN method. Meanwhile, samples were prepared with the in-solution/trypsin procedure and analyzed at the IBMC. The GFP protein was identified in all samples digested with AspN except in the negative control (**Figure 74**). Nevertheless, the SQ% 23-35% was much lower than that obtained with BY-2 cells samples analyzed previously at the LSMBO, indicating that the experimental conditions are definitely influencing the quality of AspN digestion. Other identified peptides corresponded to overrepresented protein such as 40S ribosomal protein S3a subunits or catalase (). In comparison, the in-solution method associated with tryptic digestion showed better results in intensity as well as SQ%, which was 71 up to 83%. Even if the GFP peptides were the most represented, a significant number of peptides have been associated to various proteins shared between tobacco leaves and particularly in between BY-2 cells samples, they were therefore considered as background from plant material.

This background highlights the lack of selectivity of the GFP-Trap v1. As a matter of fact, we could not detect the signal reported about 10 years ago that was just above background signals (Gerber et al., 2009a). Both methods did not lead to the identification of prenylated peptides or tetrapeptides while the amount of GFP-sensor purified was highly increased. However, the number of detected spectra correlated to GFP-CVIL remains relatively low and variable, especially in plant samples. One reason could be that the amount of immunoprecipitated protein was too low to detect the prenylated peptides and/or tetrapeptides. Another suggest that the signal may be hidden by the background.

Since on-beads trypsin method promotes the digestion of the C-ter rather than that of GFP, and the GFP-Trap\_MA being more effective than the GFP-Trap\_M for which production has in between been stopped. New assays have been performed following on-beads digestion method with GFP-CVIM produced in tobacco leaves and immunoprecipitated using GFP-Trap\_MA or GFP-Trap v1.

Protein sequence coverage: 87%

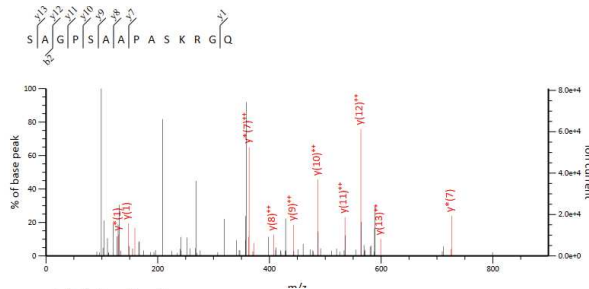
Matched peptides shown in **bold red**.

His-GFP-CVIL

```

1 MHHHHHHVSK GEELFTGVVP ILVELDGDVN GHKFSVSGEG EGDATYGKLT
51 LKFICTTGKL FVPWPTLVTT FTYGVQCFSR YPDHMQHDF FKSAMPEGYV
101 QERTIFFKDD GNYKTRAEVK FEGDTLVNRI ELKGIDFKED GNILGHKLEY
151 NYNSHNVIYM ADKQKNGIKV NFKIRHNIED GSVQLADHYQ QNTPIGDGPV
201 LLPDNHYLST QSALSQDPNE KRDMVLEF VTAAGITHGM DELVKCMMAK
251 KRRKRIEEKR DHDGGSRTKS AGPSAAPASK RGQKCVIL

```



Protein sequence coverage: 80%

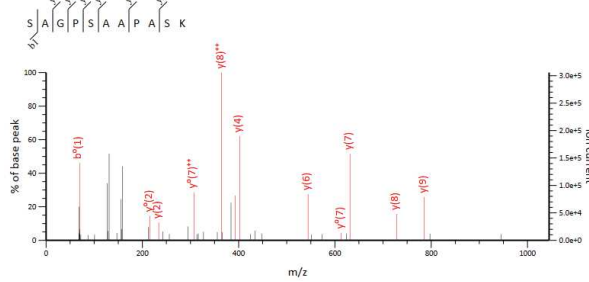
Matched peptides shown in **bold red**.

His-GFP-CVIM

```

1 MHHHHHHVSK GEELFTGVVP ILVELDGDVN GHKFSVSGEG EGDATYGKLT
51 LKFICTTGKL FVPWPTLVTT FTYGVQCFSR YPDHMQHDF FKSAMPEGYV
101 QERTIFFKDD GNYKTRAEVK FEGDTLVNRI ELKGIDFKED GNILGHKLEY
151 NYNSHNVIYM ADKQKNGIKV NFKIRHNIED GSVQLADHYQ QNTPIGDGPV
201 LLPDNHYLST QSALSQDPNE KRDMVLEF VTAAGITHGM DELVKCMMAK
251 KRRKRIEEKR DHDGGSRTKS AGPSAAPASK RGQKCVIM

```



Protein sequence coverage: 82%

Matched peptides shown in **bold red**.

His-GFP-SVIL

```

1 MHHHHHHVSK GEELFTGVVP ILVELDGDVN GHKFSVSGEG EGDATYGKLT
51 LKFICTTGKL FVPWPTLVTT FTYGVQCFSR YPDHMQHDF FKSAMPEGYV
101 QERTIFFKDD GNYKTRAEVK FEGDTLVNRI ELKGIDFKED GNILGHKLEY
151 NYNSHNVIYM ADKQKNGIKV NFKIRHNIED GSVQLADHYQ QNTPIGDGPV
201 LLPDNHYLST QSALSQDPNE KRDMVLEF VTAAGITHGM DELVKCMMAK
251 KRRKRIEEKR DHDGGSRTKS AGPSAAPASK RGQKSVIL

```

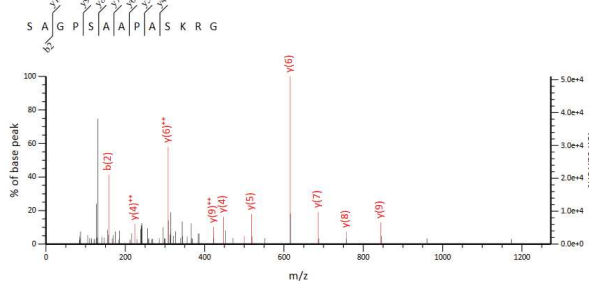


Figure 73 NanoLC-Q-Orbitrap-MS/MS analysis of His-GFP-sensor after in-solution digestion with trypsin (IBMC).

Sequence coverage and fragmentation spectra of peptides detected in the proteomic analysis of the His-GFP-CVIL, -CVIM and -SVIL reference proteins processed by in-solution method with tryptic digestion.

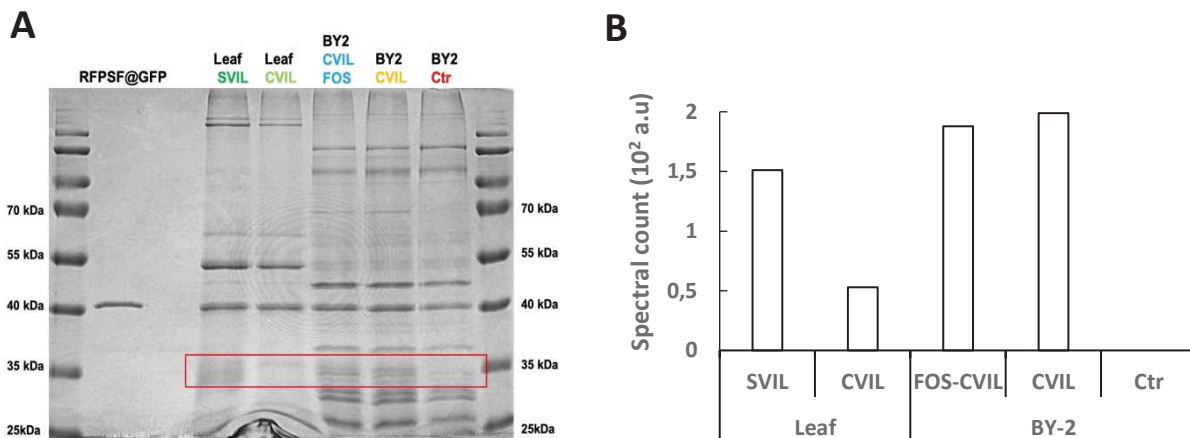


Figure 74 Detection of GFP-sensors from plant after immunoprecipitation with the GFP-Trapv1 and In-gel digestion with AspN (IBMC).

(A) Coomassie Blue-stained SDS-PAGE gel of the GFP-(C/S)VIL proteins immunoprecipitated from tobacco leaves (Leaf SVIL, Leaf CVIL) and GFP-CVIL from non-induced (BY-2 Ctr), induced BY-2 cells (BY-2 CVIL) alone or with 100  $\mu$ M fosmidomycin and 10  $\mu$ M mevinolin (BY-2 CVILFOS). At 35 kDa, bands were cut for proteomic analysis of the GFP-CaaX from each sample (red box), using in-gel digestion method with AspN. (B) Spectral count of GFP-sensor peptides analyzed by NanoLC-Q-Orbitrap-MS/MS (IBMC) after in-gel and AspN digestion.

#### 4.6.2 Proteomics for the Identification of Protein Interacting with Prenylated GFP-Sensor

The big issue here is to understand why we are unable to detect expected modified peptides. There are two possibilities: either the integrity of the GFP-CVIL protein is questionable or the analytical method is unappropriated. In these assays, tobacco leaves were used as a starting material to reduce the risk of endogenous proteolysis we faced using BY-2 cells (**Table 5**). Again, GFP was well represented, but the C-ter end including the prenylated cysteine was missing and several proteins were common to the negative control and considered as background. To note that in a GFP-CVIM sample, in which low background was detected, we were very astonished to identify, with 13 other proteins, both PFT subunits that coprecipitated with GFP-CVIM (**Table 6**). These findings suggest that PFT was still interacting with the membrane-bound prenylated protein under those specific conditions. This is surprising because of the reaction kinetic, in which theoretically this enzyme charges FPP just after releasing the enzyme product, what implies that the enzyme/product complex should not occur (**section 2.3**). Unfortunately, we could not reproduce these results a second time, so it remains a mystery why it worked out the first time. Nevertheless, this technique can be used for the identification of proteins interacting with GFP-CVIM *in vivo*. Surprisingly, although functional sites of calmodulin have been removed in GFP-sensor, some peptides were specifically detected in samples, in which prenylation was effective especially with the GFP-CVIM protein from tobacco leaves. These peptides were mostly associated to proteins of isoprenoid pathway such as the geranylgeranyl diphosphate reductase enzyme (GGDR, EC 1.3.1.83), several terpenoid synthase (**Figure 75**). In addition, peptides associated to photosynthetic system like chlorophyll a-b binding proteins or the protochlorophyllide reductase involved in the recycling system for chlorophyll were also detected (). It can thus be speculated that the 43 AA from CaM61 basic domain could be enough for protein-protein interactions. Since the GFP-CaaX localize in the plasma membrane why do proteins associated to chloroplast would be associated to it?

In conclusion, despite all methods applied, the proteomic analysis as we designed it, does not allow to characterize the prenyl substrate transferred onto our GFP-sensor *in vivo*. Although potential protein partners have been identified, the low abundance, variability and the lack of physiological function for GFP-CaaX proteins in tobacco does not allowed to confirm the relation between these proteins and the GFP-sensor.

**Table 5 Proteomics on GFP-CVIM processed by on-beads tryptic digestion.**

In green, parameters of the procedures used for the preparation and proteomic analysis of GFP-sensors reference from bacteria (ref) or immunoprecipitated from leaves (leaf). In white, the results obtained for markers of protein prenylation expected (CaaX, Prenyl-L-cys OMe and PPTs motifs) in our proteomic analysis. Sequence coverage of two analysis were not available (NA).

Location	Sample	Plant material (g)	GFP-Trap	Enzyme	Digestion type	GFP-sensor SC%	CaaX	S-prenyl-L-cys OMe	PPTs
IBMC	GFP-CVIM leaf	0.75	GFP-Trap_MA	Trypsin	On-beads	50 - 87	X	X	$\alpha, \beta$ -F
IBMC	GFP-CVI(M/L) ref + GFP-SVIL leaf	0.75	GFP-Trap_MA	Trypsin	On-beads	NA			X
IBMC	GFP-CVIM leaf	0.75	GFP-Trap v1 GFP-Trap_MA	Trypsin	On-beads	NA			X

**Table 6 Proteins interacting with GFP-CVIM in tobacco leaves.**

Annotation of proteins associated to peptides detected in the proteomic analysis of GFP-CVIM (Green) samples immunoprecipitated with GFP-Trap\_MA from 2016 tobacco leaves and digested following on-beads method with tryptic digestion. As summarized, the sequence number number of sequences (#sequences), number of different peptides detected for one annotation (#peptides) and the BASIC spectral count for peptides of each annotated

Accession	Description	Protein set score	#sequences	#peptides	BASIC Spectral count	
					Ctr	GFP-CVIM
GFP-CVIM	GFP-CVIM_QChevalier_IBMP	2362.95	23	29	0	1500
Niben101Scf01091g00036.1	farnesyltransferase subunit beta IPR008930	219.41	3	3	0	9
Niben101Scf03056g02008.1	50S ribosomal protein L15 IPR005749	122.99	1	2	0	5
Niben101Scf01339g04007.1	Protein farnesyltransferase/geranylgeranyltransferase type-1 subunit alpha IPR002088	106.51	2	2	0	4
Niben101Scf00705g06002.1	ATP-dependent Clp protease ATP-binding subunit ClpX IPR003959	100.37	1	1	0	2
Niben101Scf04410g09016.1	Chaperone protein ClpB IPR001270	95.33	2	2	0	2
Niben101Scf01116g01002.1	Protein RecA IPR013765	61.4	1	1	0	2
Niben101Scf01116g01002.1	soluble N-ethylmaleimide-sensitive factor adaptor protein 33 IPR000727	54.82	1	1	0	1
Niben101Scf02172g02008.1	Auxin response factor 18 IPR003311	46.5	1	1	0	1
Niben101Scf03206g01008.1	Cytochrome P450 superfamily protein IPR001128	44.6	1	1	0	1
Niben101Scf01694g10003.1	Heat shock 70 kDa protein IPR013126	331.27	5	5	2	48
Niben101Scf00449g06008.1	malate dehydrogenase IPR001557	380.43	7	7	1	22

protein.

In this context, characterization of protein partners using proteomics would be more suitable for other prenylated proteins reported and functional in the model organism studied. Therefore, it would be interesting to perform GFP fusions with ROP or Hsp40 proteins to validate the proteomic analysis method and extend this to Human Ras which is mutated in several forms of cancers.

To move the development of the protocol forward, we needed to review our strategy. Proteolysis of the protein C-terminus was a problem when working with tobacco BY-2 cells as a starting material. However, on the basis of our results, it becomes clear that we are facing other problems such as unexpected modifications or inappropriate HPLC-MS/MS settings rather than the loss of the last 7 AA by plant proteases. The ionization of hydrophobic peptides especially at the C-terminus can be a problem (Biniossek and Schilling, 2012). Tryptic digestions should release tetrapeptides or S-Prenyl-L-cys OMe, both being highly hydrophobic. Ionized, the charge of tetrapeptides or S-Far-L-cys OMe should be  $z = 1$ . Under those conditions, they would not be perceived in conducting the analysis with the NanoLC-Q-Orbitrap-MS/MS only by detection of ions with  $z \geq 2$  (**Figure 76**). Alternatively, these hydrophobic molecules may be adsorbed onto matrix of the HPLC column. To test these possibilities, tetrapeptides (CVIL, CVIM and SVIL) have been purchased and analyzed by MS infusion and NanoLC-Q-Orbitrap-MS/MS (**Figure 77**).

The mass and fragmentation spectra were obtained by infusion of a 10  $\mu$ M tetrapeptide solution. As expected, these molecules are ionized at  $z = 1$ , confirming the low ionization potential of hydrophobic CaaX tetrapeptides. Using 100 fmol of tetrapeptides by NanoLC-Q-Orbitrap-MS/MS,  $R_t$  could be determined and corresponded to 40.2, 44.42 and 38.01 min, for SVIL, CVIL and CVIM respectively. To note, the signal of CVI (L/M) was weaker than that of SVIL. As a matter of fact, these results demonstrated that the proteomic analytical method used was not suitable for the analysis of tetrapeptides and S-Pre-L-cys OMe obtained after tryptic digestion of GFP-CaaX proteins.

Therefore, we initiated a metabolomic study by using GC-EI-MS as well as HPLC-MS/MS analysis of metabolites resulting from tryptic digestion of GFP-CaaX proteins.

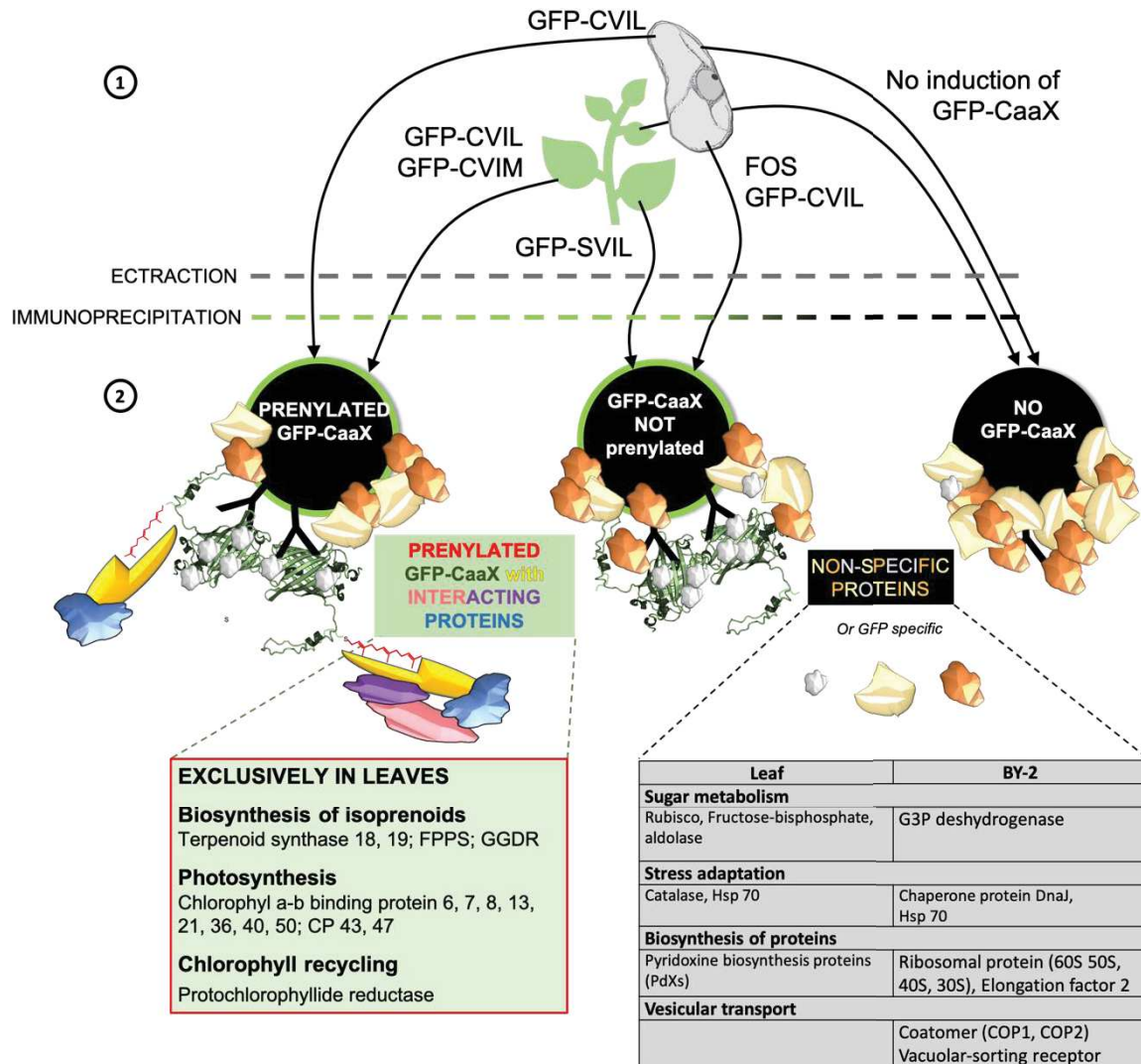


**Figure 75 The prenylated GFP-sensor are immunoprecipitated with putative specific proteins in plant.**

Representation of the pipeline used, (1) to produce prenylated GFP-sensor proteins (GFP-CVIM, GFP-CVIL) and unprenylated GFP-SVIL in tobacco plant or GFP-CVIL in BY-2 cells inhibited by 100  $\mu$ M fosmidomycin (FOS). The proteins were then extracted and purified by immunoprecipitation using GFP-Trap to enrich fraction in protein of interest. (2) Non-induced BY-2 cells/plant leaves or unprenylated GFP-SVIL and FOS GFP-CVIL were used as negative controls in proteomics to determine the proteins that bound non-specifically onto the GFP-Trap support or the GFP protein (grey, beige and orange). At the opposite, proteomics of immunoprecipitated prenylated GFP-CVIL and GFP-CVIM allowed the identification of putative proteins interacting with prenylated GFP-sensors found exclusively in plant cells (yellow, blue, pink, purple).

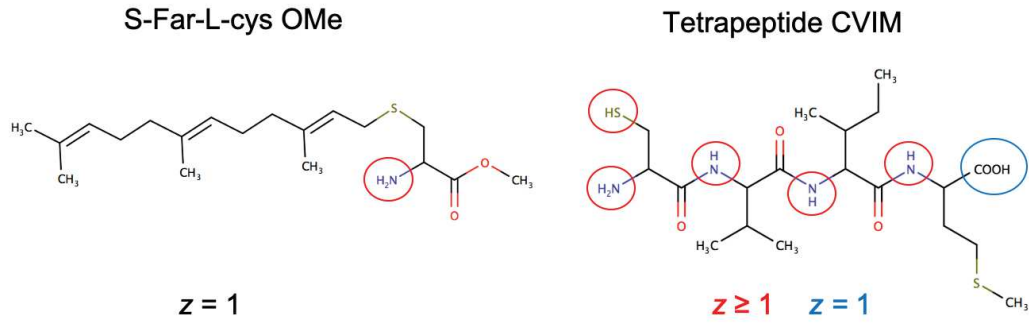


**Figure 76 Putative Ionization of S-farnesyl-L-cysteine methyl ester (S-Far-L-cys OMe) and CVIM tetrapeptides.** Structure of S-Far-L-cys OMe and CVIM tetrapeptide with their theoretical ionization sites in MS positive mode (red) and negative mode (blue).

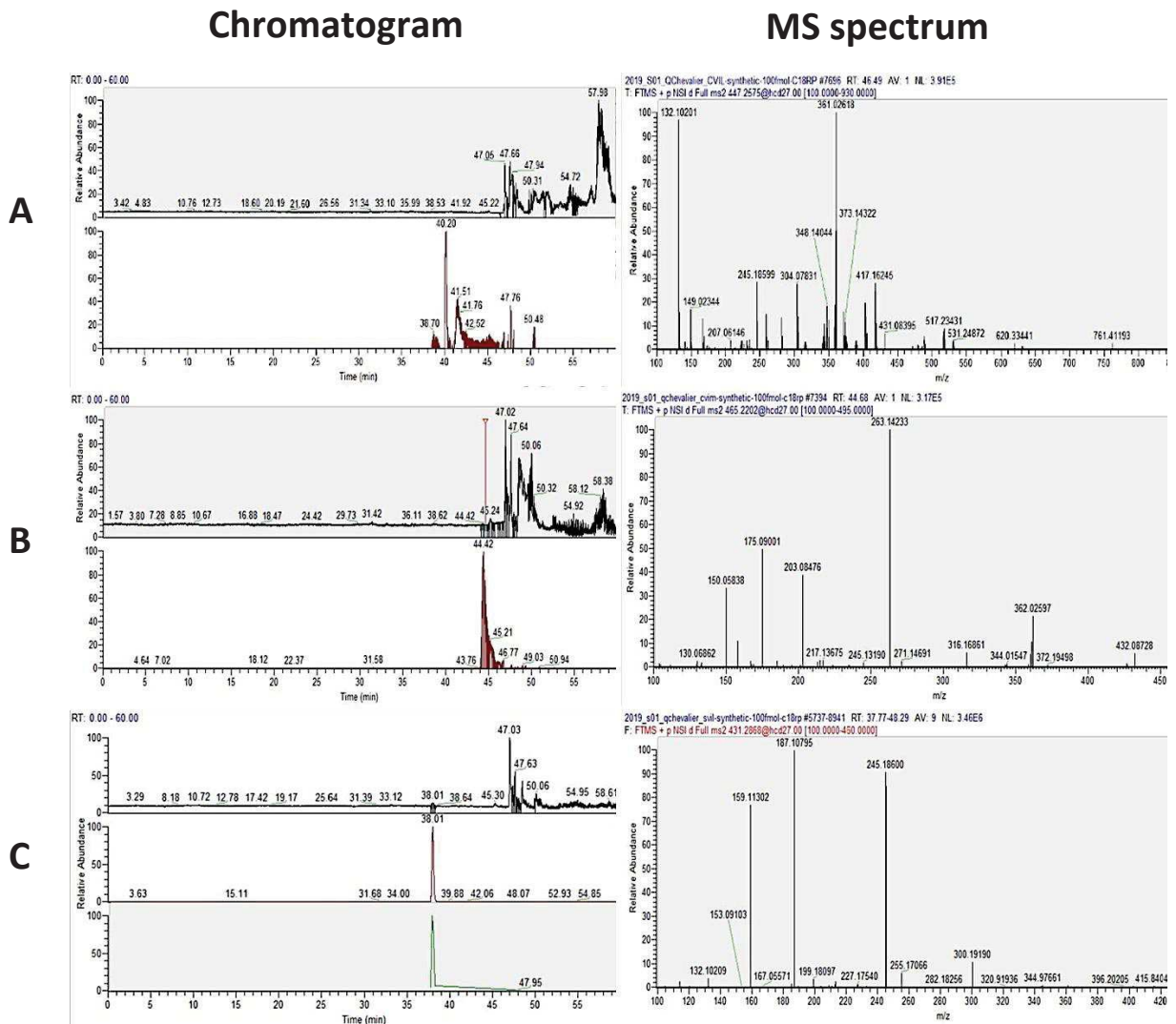


**Figure 77 Tetrapeptides reference MS spectra and separation by NanoLC-QTOF-MS/MS.**

CVIL (A), CVIM (B) and SVIL (C) tetrapeptides were analyzed by NanoLC-QTOF-MS/MS (left) and infusion (right) using 10  $\mu$ M or 100 fmol tetrapeptides solution, respectively. MS detection was fixed for a charge  $z = 1$

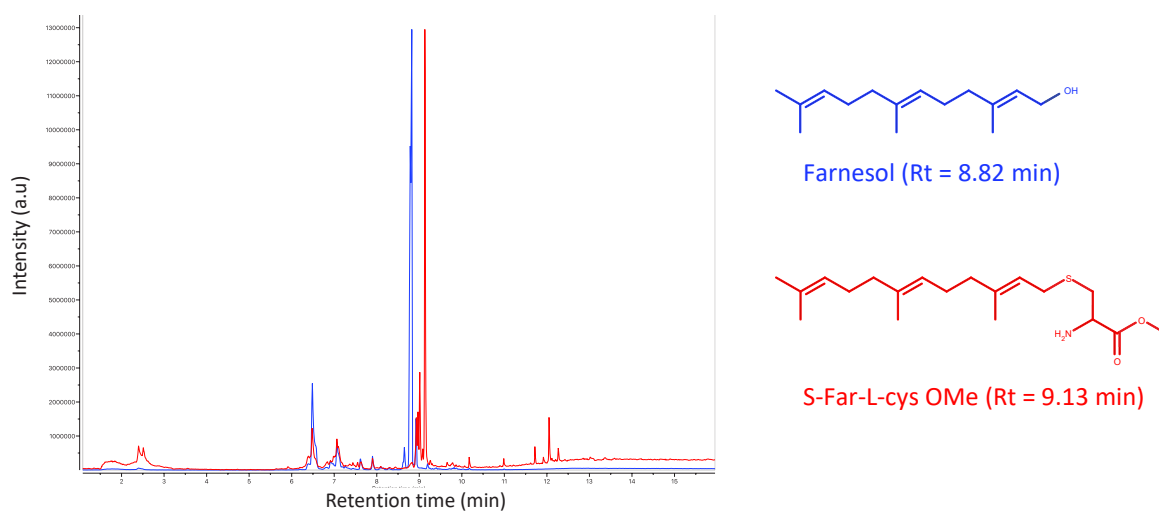
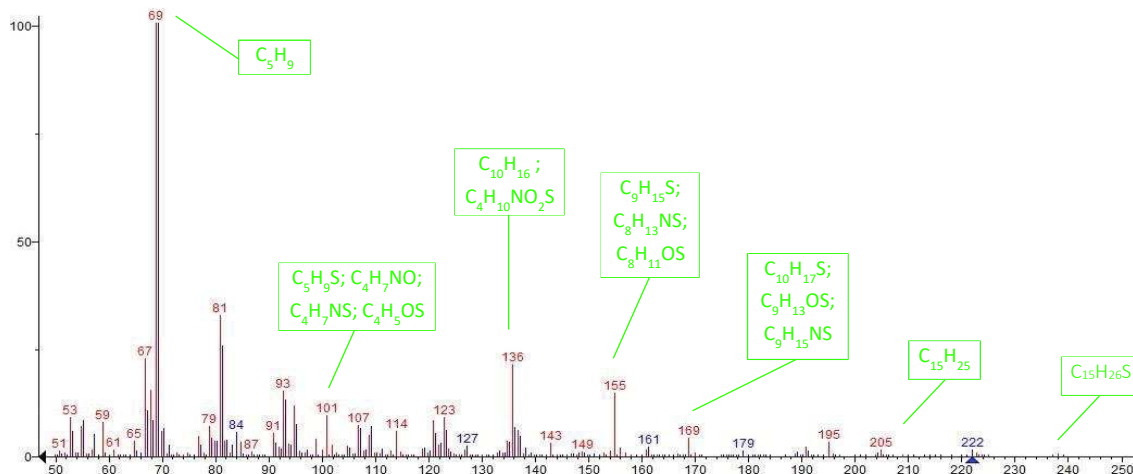
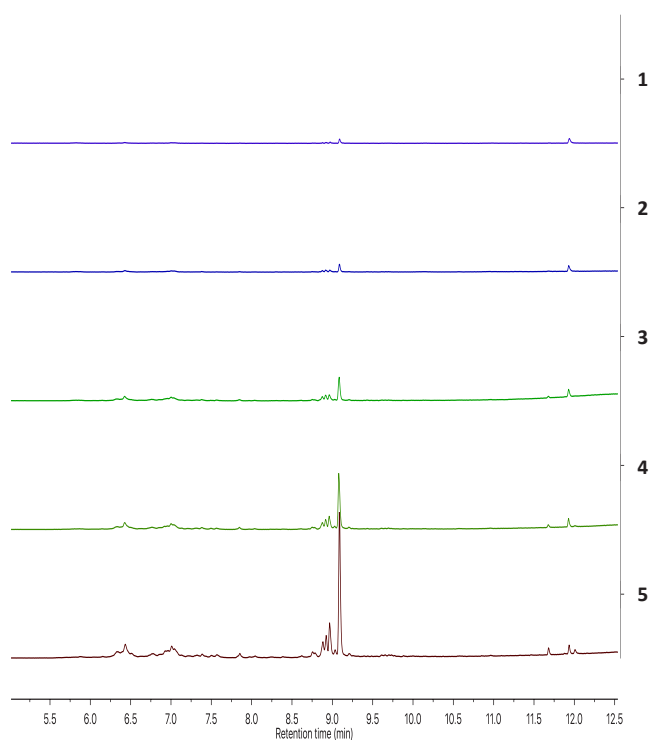




## 4.7 GC-EI-MS ANALYSIS OF S-PRENYL-L-CYSTEINE METHYL ESTER

Due to their hydrophobic nature and their low boiling point many isoprenoids from C10 to C40 are commonly analyzed by GC-EI-MS. The latter has been used for a long time to analyze prenyl groups from prenylated proteins released after iodomethane or Raney Ni cleavages (Epstein et al., 1991; Sorek et al., 2013). As explained (**section 2.5.1**), these procedures are dangerous, responsible for several artifacts and do not allow the distinction between geranylgeranyl or phytol after hydrogenation over platinum. For all these reasons, they were therefore not considered to study the protein prenylated *in vivo*.

However, we were interested in analyzing by GC-EI-MS the S-prenyl-L-cysteine methyl ester (S-Pre-L-cys OMe) released after tryptic digestion without any derivatization. The S-far-L-cys OMe is highly hydrophobic and only contain a free amine from the cysteine (pKa 10.25). Consistent is the fact that neutral S-far-L-cys OMe can theoretically be obtained at pH12 and volatile enough for GC-MS analysis. Accordingly, it might be possible to perform a liquid/liquid extraction with organic solvent to enrich specifically organic fraction in S-Pre-L-cys OMe, while most peptides would not be able to diffuse as well. This method free of derivatization may also improve the signal of S-Pre-L-cys OMe as compared to AA or small peptides which could be also theoretically detected if derivatized (Cunha et al., 2011; Pérez-Palacios et al., 2015). The S-far-L-cys OMe being commercially available, the molecule and Fol diluted in EtOH have been analyzed using GC-EI-MS (**Figure 78**). The Fol was detected at  $R_t = 8.82$  min and identified by its EI-MS fragments, in which the most abundant ion was  $m/z = 69$  corresponding to the  $C_5H_9$  fundamental unit of isoprenoids. In contrast, S-Far-L-cys OMe resulting in a main peak at  $R_t = 9.13$  min with a fragmentation pattern sharing  $m/z = 69.1$  (100) as most abundant ions and differing from the ions  $m/z = 136.2$  (19.33) ;  $155.1$  (13.67) ;  $101.100$  (9.40) ;  $169.1$  (3.96) ;  $195.1$  (2.91) ;  $205.2$  (1.29) ;  $238.2$  (0.55). Using the structure of S-Far-L-cys OMe, a simulation of possible molecular formulae corresponding to these  $m/z$  was performed using Fragment Formula Calculator (FFC) software (Wegner et al., 2014). These fragments could either correspond to the amine or reveal the presence of Sulfur inducing Sulfur-dependent fragmentation (**Figure 79**). According to literature  $\beta$ -cleavage and heterolytic cleavage produce intermediates reacting by H-transfer, 2H-transfer or 1,2 hydride shift (Patai, 1980; Zappey, 1991). Also,  $\alpha$ -cleavage may occur in thioether radical cations as shown by experiments with ethyl propyl thioether (Patai, 1980; Zappey, 1991).

**A****B****C****Figure 78 Analysis of S-Far-L-cys by GC-EI-MS.**

(A) GC-EI-MS superimposed chromatograms and Rt obtained after injection of 1  $\mu$ g Farnesol (blue) and S-Far-L-cys OMe in  $\text{CHCl}_3$ . (B) Comparison of  $m/z$  from fragments of S-Far-L-cys OMe at 9.13 min (red) and farnesol at 8.82 min (blue) for a R Match > 950 (NIST, Gaithersburg, Maryland). Simulation of possible molecular formulae for fragments detected by comparison of the  $m/z$  from characteristic fragments with the developed formula of S-Far-L-cys OMe using FFC software (Wegner et al., 2014) (green). (C) Calibration curve was performed by injection in GC-EI-MS of 1  $\mu$ l S-Far-L-cys OMe solutions at 0.05 (1), 0.1 (2), 0.25 (3), 0.5 (4), 1 mg/ml (5) in

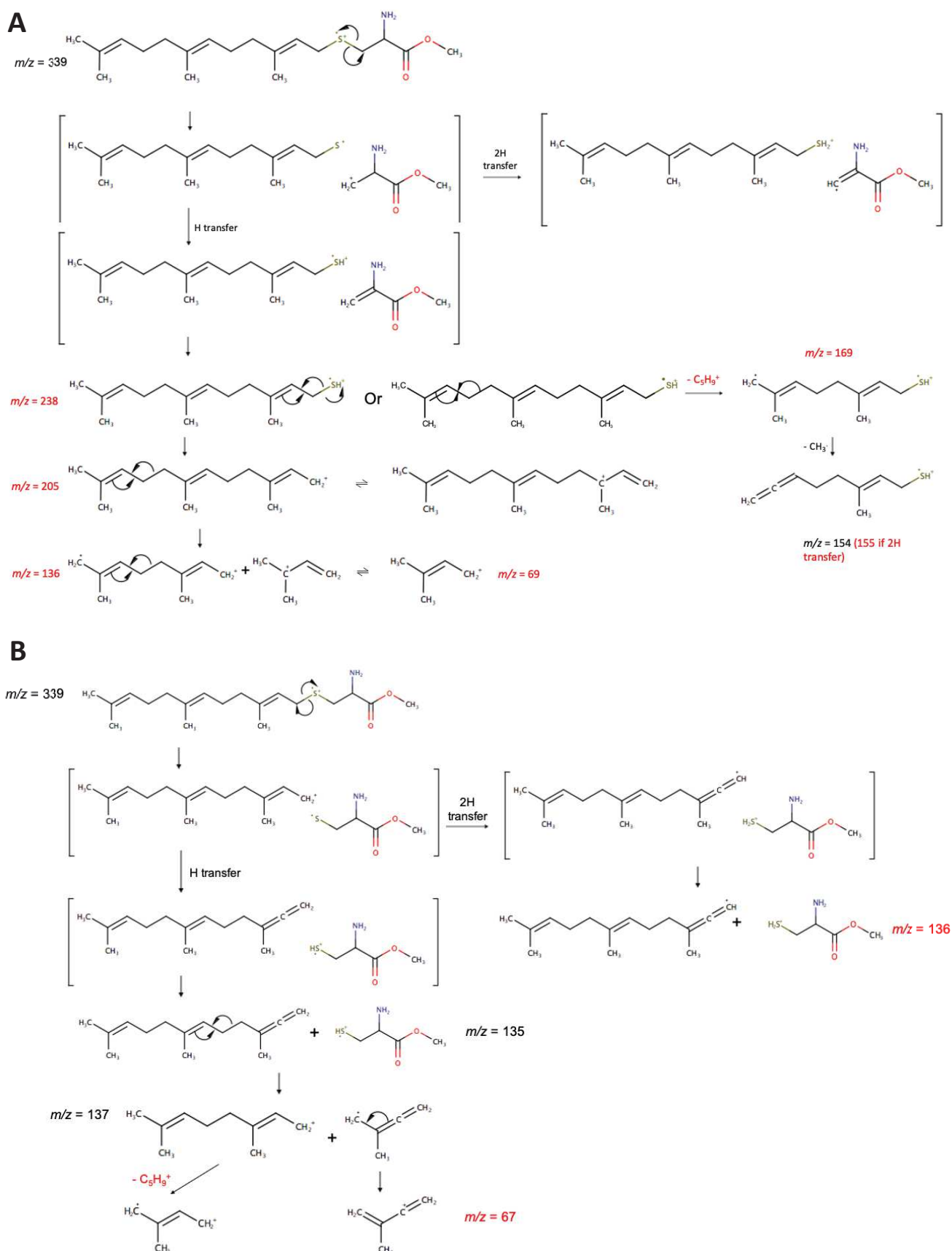


**Figure 79 Hypothetical fragmentation mechanisms of S-Far-L-cys OME.**

Fragmentation mechanisms were suggested according to the molecular formulae obtained by simulation with FFC software (Wegner et al., 2014) and the mechanisms described in the literature for prenyl alcohols and ethyl propyl thioether. Ion with  $m/z$  mostly detected in S-far-L-cys OME analysis (red) or not (black) following fragmentation starting from (A) heterolytic cleavage of C-S on the cysteine side or (B) from the farnesyl side.



Except for the  $m/z$  69 ion, supporting the presence of an isoprenic unit, it seems that the  $m/z$  = 238, 205 and 169 ions are produced after heterolytic cleavage of the C-S bond on the cysteine side followed by H-transfer to the farnesylthiyl radical, whereas the  $m/z$  = 155 ion might be produced by 2H transfer (**Figure 79**). Also, another part of the  $m/z$  = 136 and 67 ions detected may come from the heterolytic cleavage of the C-S bond on the farnesyl side, producing therefore these ions from Cys and/or Fol. The mechanisms of the  $m/z$  ions 195, 143 and 101 have not been elucidated, but as the molecular formulae obtained by simulation suggest, they are probably derived from  $\alpha$ -cleavage at the C=O or C-S bonds within the Cys moiety.

According to these results, S-Far-L-cys OMe in EtOH and CHCl<sub>3</sub> could potentially be detected by GC-EI-MS without derivatization. Still, it could be an impurity or a degradation product as high temperatures produced in the GC injector and oven can damage molecules (Rood, 1999; Rood, 1999). Therefore, we had no certitude that the detected molecule was the S-Far-L-cys OMe even if it was related to. Nevertheless, assays were performed by immunoprecipitating GFP-CVIM or GFP-SVIL from tobacco leaves using GFP-Trap\_MA and two batch of GFP-Trap v1. After on-beads tryptic digestion, the aqueous phase was extracted with CHCl<sub>3</sub> and then concentrated for analysis by GC-EI-MS. Prior to CHCl<sub>3</sub> extraction, the aqueous phase has been adjusted to pH 12 to form the neutral S-Far-L-cys OMe. As a result, Neither Fol nor S-far-L-cys OMe was detected in the GFP-CVIM leaf IP samples (**Figure 80**). However, other molecules were detected in IP samples with the GFP-Trap\_MA and compared with the NIST database. Among annotations, lipids like palmitic acid, stearic acid or contaminants such as phthalates have been selected for a R match > 950 (**Table 7**). Nonetheless, this method did not seem to work out as no prenyl was seen and molecules detected previously were not observed anymore. Also, it was noticed that many impurities were detected in GC-MS with our GFP-Trap v1, supporting contamination from the GFP-Trap synthesized (**Figure 80**).

Finally, to overcome doubt about compatibility of S-Far-L-cys with the GC system, a derivatization was performed with similar samples and analyzed by P. Adam and P. Schaeffer (Institut de Chimie, Biogéochimie moléculaire, Strasbourg, France). The results were also negative, confirming the absence of S-far-L-cys OMe. Considering contaminations and negative results, our analysis strategy undergone to targeted metabolomic analysis using HPLC-MS/MS with tetrapeptides and S-Far-L-cys OMe references as well as IP sample from plant material.

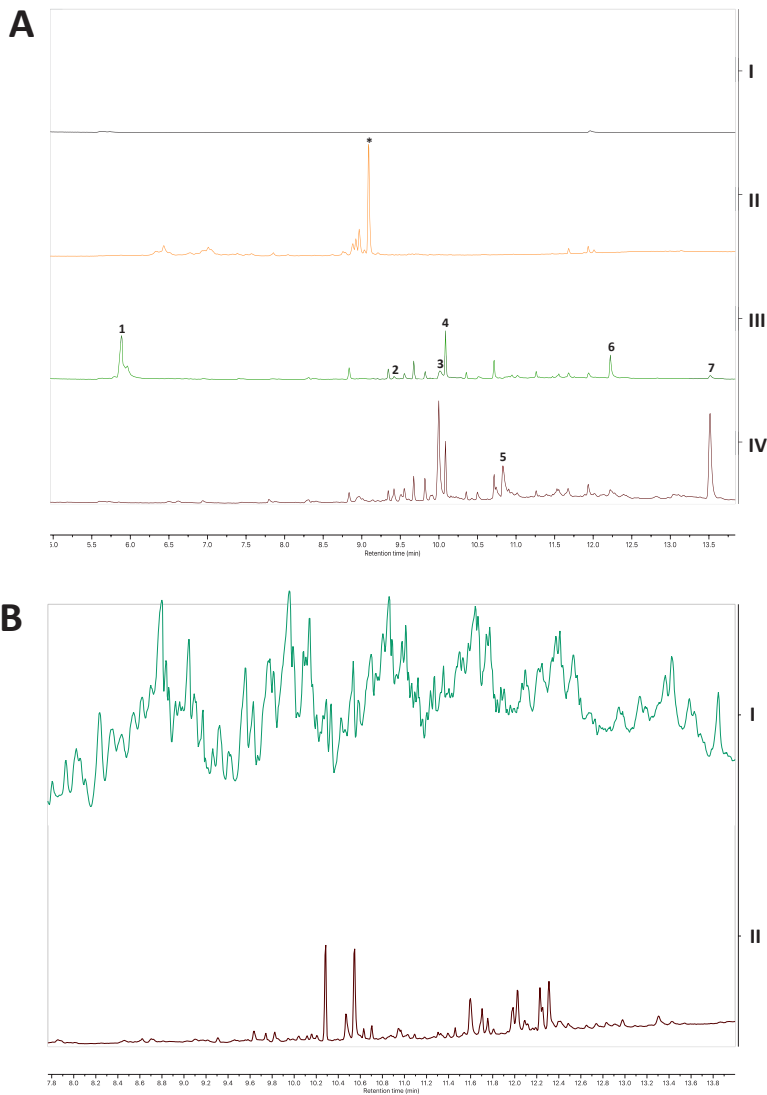


**Figure 80 GC-EI-MS analysis of protein samples processed by on-beads tryptic digestion method.**

(A) GC-EI-MS of stacked chromatograms obtained with (I) CHCl<sub>3</sub> control, (\*,II) 1 μg S-Far-L-cys OMe, (III) His-GFP-CVIM reference and (IV) GFP-CVIM from tobacco leaves IP with GFP-Trap\_MA and processed using on-beads method with trypsin digestion.

Peaks were annotated using NIST database (R-Match > 900) for (1) dithioethanol, (2) hydroxyfarnesol, (3), palmitic acid, (4) undefined, (5) Stearic acid, (6) phtalic acid, (7) Squalene.

(B) Comparison of GC-EI-MS chromatograms of GFP-CVIL CHCl<sub>3</sub> obtained by IP and on-beads tryptic digestion of tobacco leaves protein extract with GFP-Trap v1 prepared in (I) water /vacuum pump oil using plastic tubes for sample preparation and (II) water/toluene using glass vessel for sample preparation.

**Table 7 GC-EI-MS result for compounds varying between GFP-CVIM digested sample and controls.**

Retention times (Rt) and *m/z* of fragments from compounds observed by comparative study between CHCl<sub>3</sub> samples obtained after on-beads digestion of His-GFP-CVIM reference, and GFP-CVIM tobacco leaf samples. Molecules were annotated by comparing GC-EI-MS spectra to NIST database, only annotation with R-match > 900 were considered.

N°	Rt (min)	<i>m/z</i> Fragments	NIST ID
1	6.887	92.1 (100.00) 154.1 (65.49) 79.1 (56.90) 64.1 (43.77) 61.1 (13.95) 110.1 (12.74) 107.1 (10.38) 173.1 (0.09)	Dithioethanol
2	9.417	58.1 (100.00) ; 71.2 (67.41) 83.2 (63.55) ; 95.2 (39.92) ; 109.1 (35.41) ; 123.1 (32.40) ; 250.3 (10.45) 193.1 (9.20) 165.3 (8.79) ; 281.2 (3.28)	Hydroxyfarnesol
3	10.01	149.1 (100.00) ; 73.1 (21.56) ; 57.2 (21.07) ; 129.2 (13.63) ; 83.1 (13.05) ; 213.2 (6.73) ; 256.3 (5.33) ; 223.1 (4.91) ; 278.2 (0.66)	Palmitic acid
4	10.086	73.2 (100.00) ; 147.1 (60.15) ; 281.1 (57.32) ; 221.1 (43.88) ; 355.1 (27.97) ; 429.1 (21.72) ; 207.1 (17.63) ; 341.0 (16.99) ; 503.1 (14.34)	
5	10.83	73.1 (100.00) ; 60.1 (71.41) ; 57.2 (68.15) ; 55.2 (66.81) ; 129.2 (53.98) 69.2 (45.77) ; 83.2 (40.03) ; 284.3 (33.61) ; 185.2 (28.13) ; 241.3 (26.38)	Stearic acid
6	12.22	149.1 (100.00) ; 167.1 (29.37) ; 57.2 (14.73) ; 71.2 (11.83) ; 150.1 (11.64) ; 70.2 (8.35) ; 279.2 (8.03) ; 55.2 (5.77) ; 113.2 (5.67) ; 104.1 (5.00)	Phtalic acid
7	13.517	69.2 (100.00) ; 81.2 (58.87) ; 95.2 (17.63) ; 137.2 (14.84) ; 136.20(14.41) ; 121.2 13.76) ; 123.2 (10.92) ; 175.2 (3.04) ; 341.3 (2.48) ; 203.2 (2.40)	Squalene

## 4.8 TARGETED METABOLOMICS STUDY OF PRENYLATED PROTEINS USING HPLC-TQ-MS/MS

The mass spectra and characteristic fragments of CVIM, CVIL, SVIL tetrapeptides and S-Far-L-cys OMe were determined by infusion and UPLC-TQ-MS/MS by J. Zumsteg (IBMP, Strasbourg). The references were well separated and the corresponding  $[M+H]^+$  ions detected with  $z=1$  (.

**Table 8, Figure 81**). Preliminary results obtained at the end of our proteomic analysis of prenylated proteins were confirmed. Accordingly, the metabolomic analysis was pursued on the different GFP-sensors being purified by IP with GFP-Trap v1 and 5 g starting plant material (**Table 9**). The on-beads tryptic digestion method was used to promote the detection of tetrapeptides or S-prenyl-L-cys MeO from the C-ter end rather than GFP peptides. Only SVIL have been significantly detected at intensities  $>10^6$  in the corresponding purified GFP-SVIL from tobacco leaves, by the presence of the ion  $[M+H]^+ = 431.2$  with MS/MS transitions 245.1 (quantifier) and 300.2, 113.2 (qualifiers) (**Figure 82**). Other ions with similar fragmentation have been detected in the IP samples GFP-CVI(L/M), but also found in the negative control. They were therefore considered as background signals. Also, these results suggest that trypsin would ensure cleavage in front of Ser as SVIL has been identified. It appeared that trypsin may have troubles to cut in front of Cys according to the absence of CVI(L/M) peptide in plant samples and even in the reference His-GFP-CVIM. Furthermore, this hypothesis is reinforced by the absence of S-Far-L-cys OMe in plant IP samples, while being well detected in the reference (**Figure 82**). Nevertheless, it cannot be excluded that something bound the end of a CaaX but not SaaX protein, preventing therefore the cleavage by trypsin.

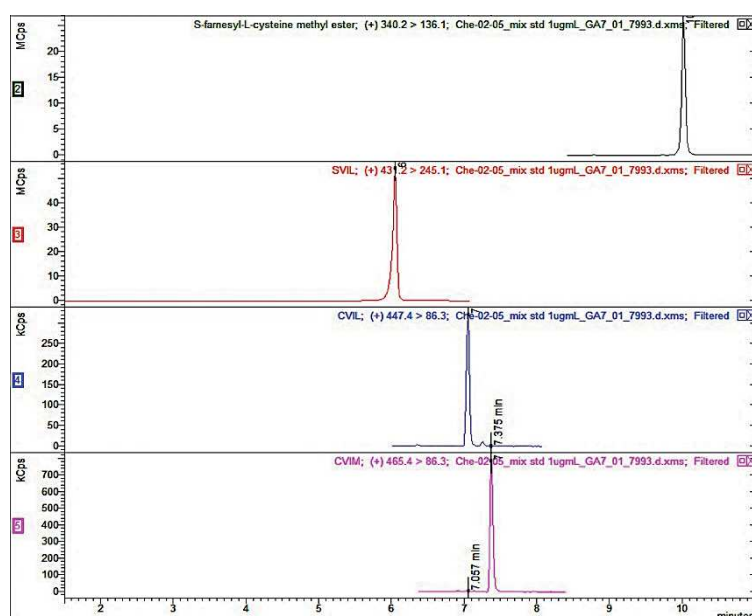
Our targeted metabolomics study proved that the on-beads tryptic digestion method releases the SVIL peptide in the presence of Ser. This confirmed that the protocol allows the isolation of an intact GFP-SVIL, but the absence of GFP-CaaX traces remains mysterious. If the digestion is inefficient close to a Cys, peptides with up to five additional AA might be obtained. Nevertheless, it was not possible to reject the hypothesis that the quantity of CVI(L/M) obtained from GFP-CaaX IP was too low, especially since these tetrapeptides showed problems to be ionized, can dimerize or may be retained on the column. In addition, only S-Far-L-cys OMe was sought, but it cannot be excluded that another prenyl group is used to modify this protein under those conditions. Without other S-prenyl-L-cys OMe references it was not possible to determine the origin of the missing signal for CVI(L/M) and S-Far-L-Cys OMe in plant samples.



**Table 8** Analysis of the tetrapeptides SVIL, CVIL, CVIM and S-Far-L-cys OMe by HPLC-TQ-MS/MS.

as indicated retention time (Rt), Masse (M) and  $m/z$  of parent ions and their characteristic transitions (>) after fragmentation.

Name	Molecular formula	M ( $m/z$ detected)	Rt (min)	Fragments (collision energy)
SVIL	C <sub>20</sub> H <sub>38</sub> N <sub>4</sub> O <sub>6</sub>	430.55 ([M+H] <sup>+</sup> = 431.2)	6.05	431.2 > 245.1 (12 eV) 431.2 > 306.2 (11 eV) 431.2 > 113.2 (36 eV)
CVIL	C <sub>20</sub> H <sub>38</sub> N <sub>4</sub> O <sub>5</sub> S	446.61 ([M+H] <sup>+</sup> = 447.4)	7.03	407.4 > 86.3 (22 eV) 407.4 > 245.2 (12 eV) 407.4 > 316.2 (9 eV)
CVIM	C <sub>19</sub> H <sub>36</sub> N <sub>4</sub> O <sub>5</sub> S <sub>2</sub>	464.64 ([M+H] <sup>+</sup> = 465.4)	7.38	465.4 > 86.3 (22 eV) 465.4 > 263.1 (12 eV) 465.4 > 316.2 (9 eV)
S-Far-L-cys OMe	C <sub>19</sub> H <sub>33</sub> N <sub>2</sub> O <sub>2</sub> S	339.54 ([M+H] <sup>+</sup> = 340.2)	10.00	340.2 > 136.1 (X eV) 340.2 > 81.2 (20 eV) 340.2 > 121.2 (14 eV)

**Figure 81** HPLC-TQ-MS/MS stacked chromatograms from the MRM analysis of tetrapeptides.

100 ng SVIL (red), CVIL (blue), CVIM (pink) and S-Far-L-cys OMe (green) references solubilized in MeOH.

**Table 9** Conditions used to prepare samples for metabolomic analysis by UPLC-TQ-MS/MS of immunoprecipitated GFP-sensors.

Reference (ref) and plant material (leaf). In white, results obtained for tetrapeptides detected and S-Far-L-cys OMe according to reference values.

Sample	Plant material (g)	Sample volume (μl)	GFP-Trap	Digestion type	CaaX/sample	Farnesyl-C-OMe
GFP-CVIM and GFP-SVIL from leaf	5	100	GFP-Trap_v1	On-beads	SVIL /leaf SVIL	<b>X</b>
Previous sample concentrated 2x + GFP-CVIL leaf and BY-2	5	50	GFP-Trap_v1	On-beads	SVIL /leaf SVIL	
GFP-CVIM and GFP-SVIL from leaf + GFP-CVIM ref	5	50	GFP-Trap_v1	On-beads	SVIL /leaf SVIL	
GFP-SVIL from leaf + GFP-CVIL from BY-2 induced ± FOS ± spiking of S-Far or GFP-CVIM ref	5	80	GFP-Trap_v1	On-beads ± DTT	SVIL /leaf SVIL	

The dimerization or molecules degradation was evaluated using a similar workflow with BY-2 or tobacco leaves containing supposed prenylated proteins or unprenylated form. Accordingly, DTT was added to avoid disulfide bridge formation or references were spiked before initiate the on-beads tryptic digestion. Although the TIC signal was low, SVIL was again detected in the IP samples of GFP-SVIL from tobacco leaves (**Figure 83**), while not the CVIL in BY-2 cells inhibited by FOS. Although spiked CVIM and S-Far-L-cys OMe were detected, these molecules were not detected in samples containing DTT, suggesting that dimerization or oxidation is not responsible for the absence of CaaX tetrapeptide signal. Therefore, the absence of-detection of targeted molecules is not due to adsorption on a surface but may results from their absence in sample analyzed. As proposed earlier, the presence of a Cys next to the trypsin cleavage site has been reported to adversely affect digestion. The molecules to be detected would rather correspond to tetrapeptides, S-Far-L-cys OMe, S-geranylgeranyl-L-cysteine methyl ester (S-GG-L-cys OMe) with four or five additional AA. On the top of that, other prenyls like geranylarnesyl, solanesyl and modifications such as palmitoylation may occur at the C-ter end of prenylated proteins. Nonetheless, the targeted metabolomics was restricted to our references as its resolution is not sufficient for *de novo* identification.

By this study we were able to demonstrate that despite high sensitivity, targeted metabolomic analysis is a limited technique as extremely dependent on reference molecules. In our case, it is difficult to obtain all putative molecules including the unexpected. As a result, we were able to demonstrate that the on-beads digestion protocol with trypsin released SVIL tetrapeptide, being identified by its  $R_t$  and daughter ions. However, none of the other expected metabolites could be detected suggesting that tryptic digestion may release other types of molecules or that the GFP-sensor undergoes other modifications we did not take into account. In the absence of references and the lack of knowledge on the mechanisms of protein prenylation in plants, this protocol was considered as not suitable for the analysis of GFP-CaaX proteins. With this respect, a comparative study between samples containing prenylated or unprenylated protein using non-targeted metabolomics appeared to be more appropriated. We followed up our study by this kind of approach in order to extend the analysis to putative compounds for which we do not have references. However, this method is very resolute, but much less sensitive than targeted metabolomics, therefore we have upgraded our GFP-Trap in order to obtain an equivalent result to that of the commercial GFP-Trap\_MA.

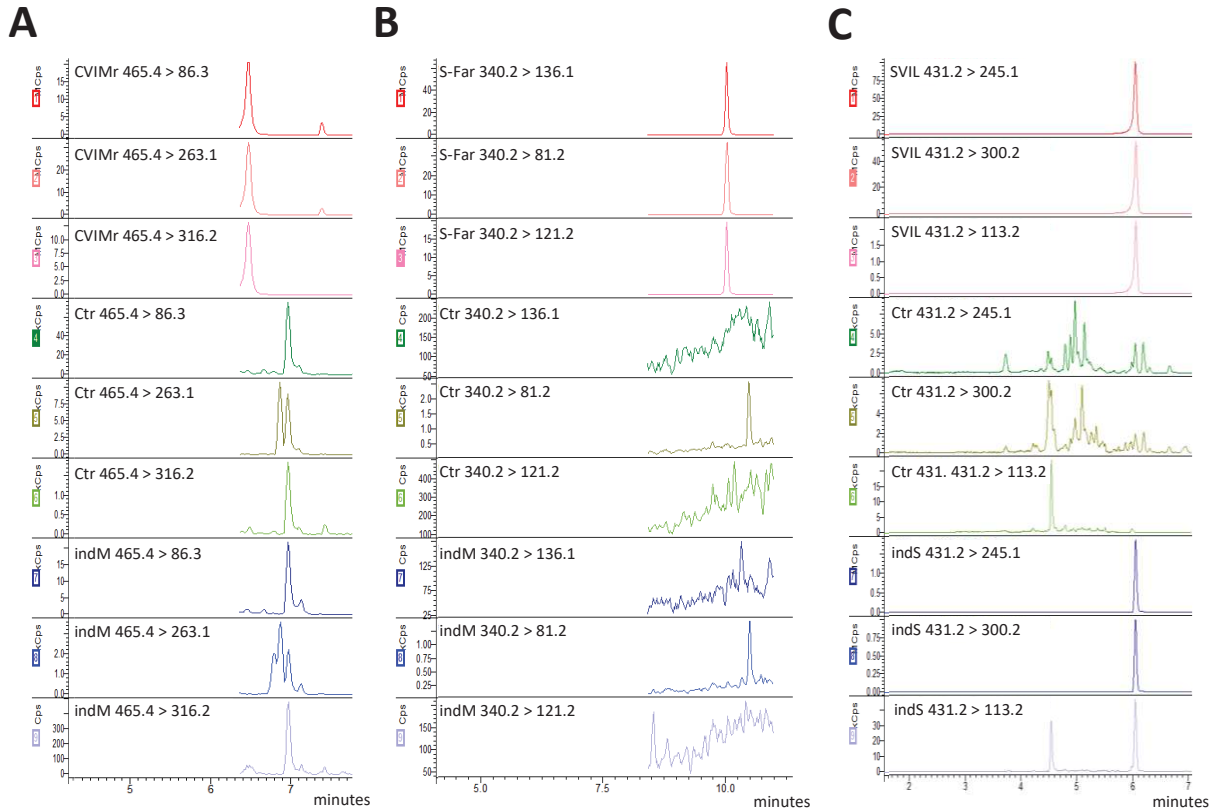


**Figure 82 Comparative study of S-Far-L-cys OMe and CVIM tetrapeptides by using targeted metabolomics.** HPLC-TQ-MS/MS stacked chromatograms from the MRM analysis of peptides samples obtained by immunoprecipitation of (A, B) GFP-CVIM or (C) GFP-SVIL from tobacco leaves using GFP-Trap v1 and on-beads tryptic digestion procedure. Tetrapeptide references (red), negative controls (green) and tobacco leaves expressing GFP-sensor (blue). (A) Chromatograms of CVIM daughter ions 86.3, 263.1 and 316.2 (CVIM), the negative control (Ctr) and tobacco leaves expressing GFP-CVIM (indM). (B) Chromatograms of S-farnesyl-L-cysteine methyl ester (S-Far) daughter ions 136.1, 81.2 and 121.2 ions (S-Far), the Ctr and indM. (C) Chromatograms of SVIL daughter ions 245.1, 300.2 and 113.2 ions (SVIL), the Ctr and tobacco leaves expressing GFP-SVIL (indS).

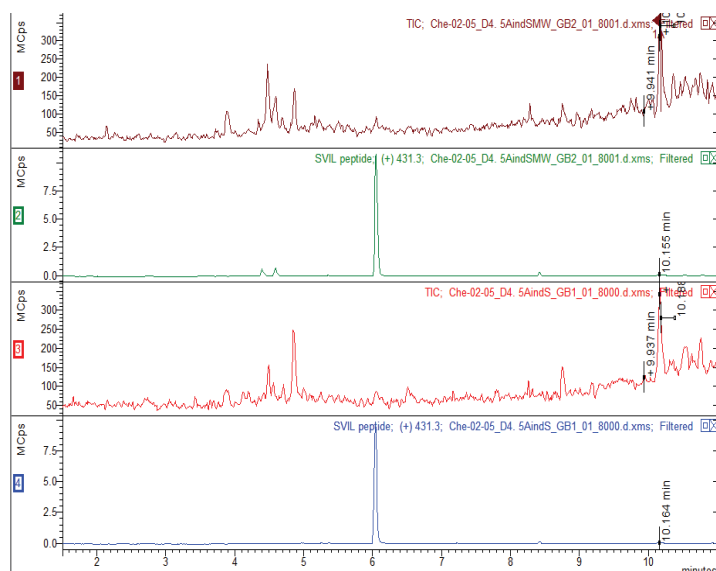


**Figure 83 SVIL tetrapeptides released from GFP-SVIL after on-beads tryptic digestion.**

HPLC-TQ-MS/MS stacked chromatograms from the MRM analysis of peptides samples obtained by IP of GFP-SVIL from tobacco leaves using GFP-Trap v1 and on-beads tryptic digestion procedure. TIC chromatogram (red) and the SVIL ion trace (blue) for each replicate.

## 4.9 OPTIMIZATION OF A GFP-TRAP V2 FOR NON-TARGETED METABOLOMICS

The GFP-trap v1 was a great aid to clear and explore approaches for protein prenylation analysis at low-cost. However, weaknesses in its selectivity and capacity were noticed and pointed out as opposed to the commercial GFP-Trap<sub>MA</sub> (section 4.4.3). Up to now, these flaws have not been critical as no GFP-Trap at all allowed to characterize our prenylated GFP-sensor. Nevertheless, the former can be critical in the non-targeted metabolomic analysis, in which all ionized molecules are detected, improving the risk of missing low represented molecules as compared to more abundant molecules. Accordingly, we have developed a new protocol by modulating some key factors mentioned in section 4.3.

### 4.9.1 To Remove Lipids Contamination and Reduce Loss of Material

Since, oil phase was responsible for high lipids contamination detected in our GC-MS analysis (Figure 80), it was replaced by toluene. As no report about synthesis of MAPs with Toluene/H<sub>2</sub>O emulsion was reported, the HLB value was fixed to 5 as recommended and NaCl has been removed (Tadros, 2013). Therefore, proportion of Span 80 (HLB = 4.3) and Tween 80 (HLB = 15) already used for the GFP-Trap v1 was recalculated following reported formulae (Kruglyakov, 1976). Accordingly, the optimum ratio was defined as 14/1 (Span 80: Tween 80, w/w). However, preliminary assays in 1.5 ml Eppendorf tubes were carried out comparing variation in emulsifiers ratios of the GFP-Trap v1 protocol and the new one. With this respect, the ratios

2:1, 1:2, 14:1 or 1:14 of blended emulsifier (Span 80:Tween 80, w/w), at 3 % or 8.5 % (v/v) were tested. As far as magnetic stirring promotes formation of undesired aggregates (**section 4.4.1**), it was replaced by rotary shaking. Observation of particles using DIC microscopy revealed that the optimal condition is 8.5% emulsifiers in a 2:1 or 14:1 ratio (Span 80:Tween 80, w/w) (**Figure 84**), resulting in smooth MAPs with mean size  $21 \pm 11.3$  and  $15.5 \pm 8.6 \mu\text{m}$ , respectively (**Figure 85**). All other conditions lead to bigger, unshaped particles or emulsion breakdown. Consequently, the particles produced by toluene/H<sub>2</sub>O emulsion containing 8.5 % of Span 80/Tween 80 (w/w) in a 14:1 ratio have been selected for a larger scale production. Furthermore, the magnetization of MAPs was not sufficient as important loss of particles was observed during the preparation but also during the IP (**section 4.4.1**).

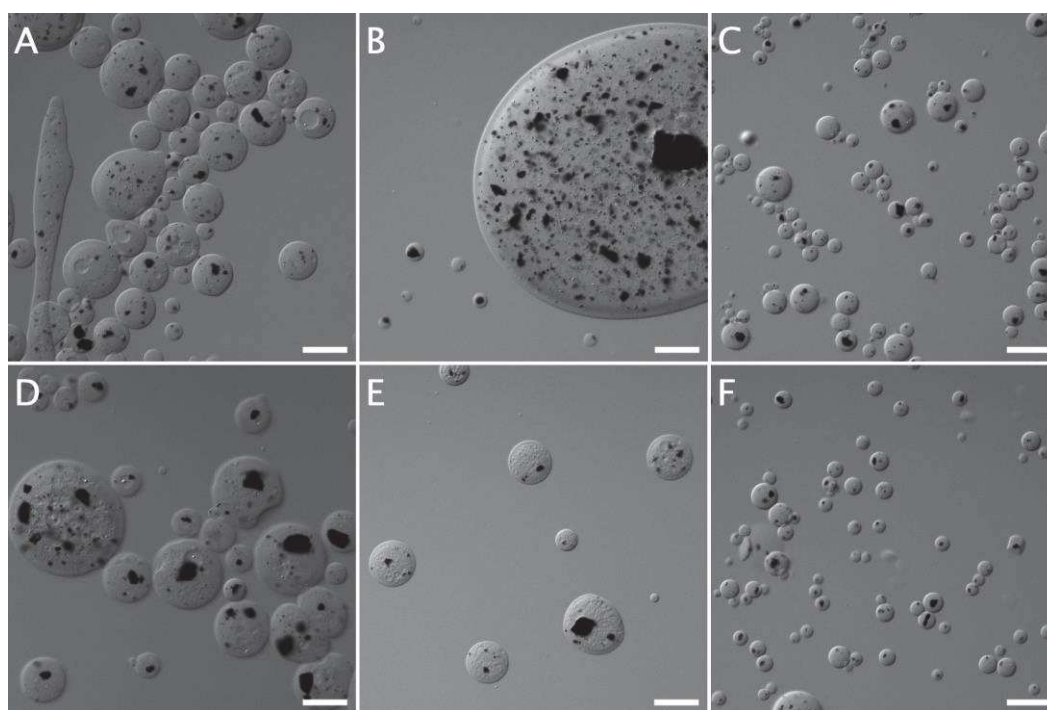


**Figure 84 Comparison of surfactant ratio for MAPs synthesis using Toluene/H<sub>2</sub>O emulsion.**

DIC microscopy observation of MAPs synthesized with water/toluene emulsion at different concentration (%) and ratio of Span 80:tween 80 (w/w). (A) 3% 2 :1, (B) 3% 14 :1, (C) 8.5% 2 :1, (D) 3% 1 :2, (E) 3% 1 :14, (F) 8.5% 14 :1. Scale bar = 50  $\mu\text{m}$

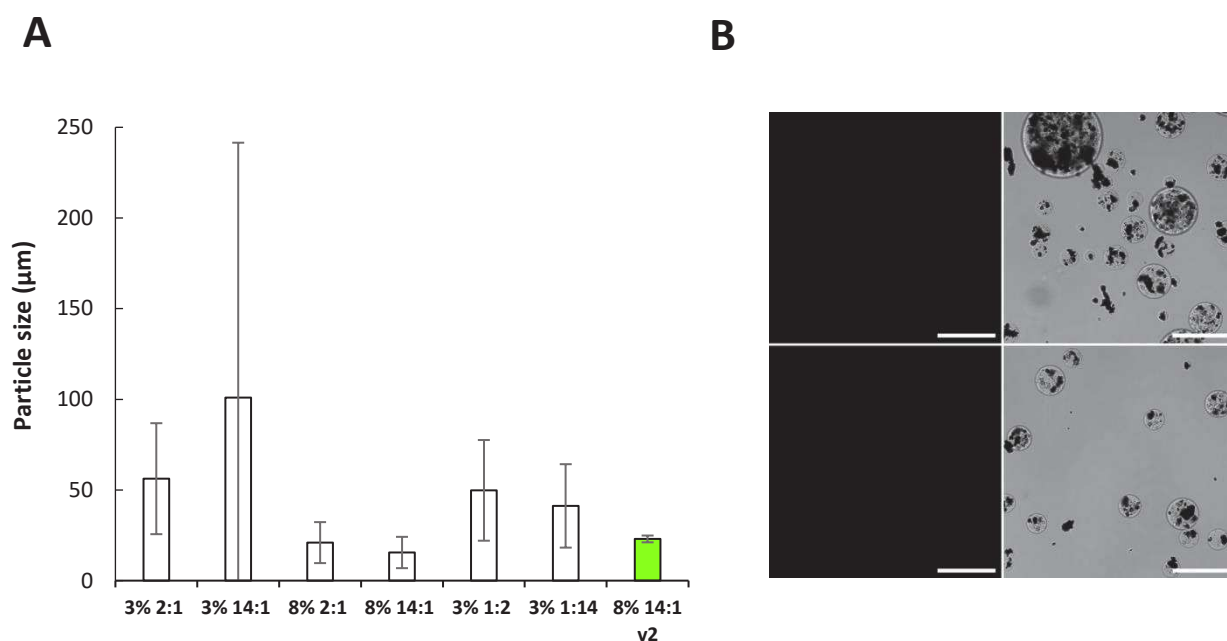


**Figure 85 Size of MAPs produced by Toluene/H<sub>2</sub>O emulsion is dependent of surfactant ratio.**

(A) Comparison of average particle size from confocal microscope observation of MAPs synthesized by using water/toluene emulsion at 3 and 8.5 % of blend emulsifiers consisting in Span 80:tween 80 (*w/w*) at ratio 2:1, 14:1, 1:2 and 1:14. The condition 8.5% 1:2 and 1:14 showed presence of aggregates > 1 mm and could not be analyzed by confocale microscopy. The 8.5 % 14:1 v2 (Green) corresponds to 8.5 % 14:1 with a ratio agarose/magnetite 1:2 (*w/w*) rather than 4:1. (B) Observation by confocal microscopy of MAPs 8.5 % 14:1 v2. Fluorescence channel GFP (left) merged with DIC view (right). Scale bar = 50 µm



It was proposed to decrease the amount of matrix/particle as suspected to be involved in the adsorption of unspecific proteins. Therefore, this ratio has been increased to 2:1 to improve the magnetization and reduce loss of MAPs at a larger scale. In this regard, the equipment was adapted to prepare the emulsion at a middle scale, using a round flask as a container and anchor-type dispenser to prepare the emulsion. In our conditions, starting from 0.66 g Fe<sub>3</sub>O<sub>4</sub> and 0.33 g agarose, we obtained about 10 g of wet MAPs < 73 μm (~ 0.75 mg of dried MAPs) with a magnetization time of less than 1 min. However, despite 75 % yield (x4 up), it was noticed that emulsion was less stable implying to keep the disperser running during the cooling process on ice. Despite this problem, the observation of MAPs < 73 μm by microscopy confirmed that new MAPs are spherical and contain more magnetite/particles (**Figure 85**). Thus, this new batch of MAPs was used to optimize cross-linking/functionalization steps.

#### **4.9.2 Improve Selectivity and Capacity of the GFP-Trap**

We saw numbers of unspecific interactions using our matrix (**section 4.4.3,4.6**). An easy solution proposed to replace the crosslinker and/or the linker for protein attachment was the DVS (**section 4.3.4**). For instance, DVS offers other physicochemical properties and can be employed as a cross-linker and functionalization agent. Thus, trials using different combinations between cross-linking with epichlorohydrin (E) or DVS/Dextran T500 (D) and functionalization in glyoxyl-agarose (G) or DVS-agarose have been performed to obtain DD, ED, EG, DG batches (**Table 10**). Since, we confirmed the attachment of Nb-tRFP@GFP onto our GFP-Trap v1, the protein RFP fused to the nanobodies in Nb-tRFP@GFP becomes useless and was suspected to promote unspecific adsorption of other proteins too. Consequently, new bivalent nanobodies (NbD@GFP) have been produced by cloning in frame the sequence of *NbCh@GFP* (Rothbauer et al., 2006) with the one coding for *NbSF@GFP* (Twair et al., 2014) (**Figure 87**). The purified NbD@GFP, provided by Vianney Poignavent, were immobilized on MAPs activated with glyoxyl agarose or DVS (Hjertén et al., 1987; López-Gallego et al., 2013; Santos et al., 2015). Until now, MAPs were saturated in Nb@GFP indeed, this time we compared two different amounts of NbD@GFP 0.23 mg/mg of dried MAPs (Full) and 0.12 mg/mg (1/2) to evaluate their influence on the selectivity and capacity of GFP-Trap to bind GFP-sensor. The attachment of the new NbD@GFP was confirmed by IP of 15 ng purified His-GFP-CVIM protein and observation by confocal microscopy (**section Figure 86**). As a result, no more RFP was observed and the GFP was well purified locating only at the surface of GFP-Trap.



**Table 10 Cross-linking and functionalization for the GFP-Trap optimization.**

Highlighted in green, the different combinations of cross-linking with divinylsulfone (DVS) or epichlorohydrin and functionalization into DVS-agarose or glyoxyl-agarose performed on MAPs synthesized by the W/O suspension method with a water/toluene blend.

Name	Cross-linking DVS	Cross-linking Epichlorhydrin	Functionalization DVS-agarose	Functionalization Glyoxyl-agarose
DD				
DG				
ED				
EG				

MQVQLQESGGALVQPGGSLRLSCAASGFPVNRYSMRWYRQAPGKEREWVAGMSSAGDRSSYEDSVKQ  
 RFTISRDDARNTVYLQMNSLKPEDTAVYYCNVNVGFEYWGQGTQVTVSSGGGGSGGGGSGGGSGQVQL  
 QESGGGSVQAGGSLKLSCAASGGAYRNACMGWFRQAPGKEREGVAIINSVDTTYADPVKGRFTISRDNK  
 KSTVYLLMNSLKPEDTAIYYCAQVARVVCVCGDKLGASGNYWGQGTQVTVSSHHHHHHWSHPQFEK

**NbCh@GFP** (12.8 kDa)    **NbSF@GFP** (13.9 kDa)    **Total protein = 29.8 kDa**

**Figure 87 Peptidic sequence of the bivalent nanobodies (NbD@GFP).**

Sequence elements include the NbCh@GFP (blue), the NbSF@GFP (green). Additional elements were added to the sequence such as a linker connecting the nanobodies and a polyhistidine-tag located at the C-terminus end of the protein, for easy purification (black).

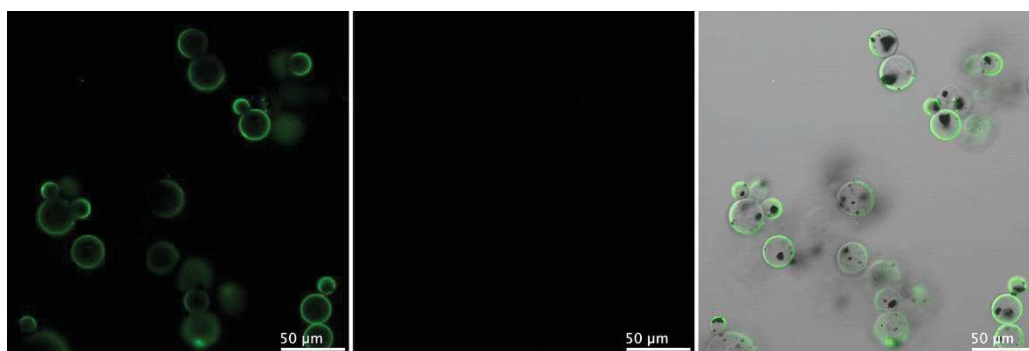


**Figure 86 New GFP-Trap without RFP signal as compared to the GFP-Trap v1.**

Observation by confocal microscopy of GFP-CVIM immunoprecipitated onto GFP-Trap EG. Fluorescence in GFP channel (left), RFP channel (middle) and both channel merged with DIC view (right). Scale bar = 50 µm

### 4.9.3 Evaluation of the New Optimized GFP-Trap Systems

As previously (section 4.4.3), the newly synthesized GFP-Trap DD, DG, ED, EG were compared by IP of 750 mg BY-2 cells expressing GFP-CVIL or 750 mg tobacco leaves expressing GFP-SVIL with proteases inhibitors. The analysis of immunoprecipitated proteins by SDS-PAGE and Western blot confirmed that each batch was able to immunoprecipitated the GFP-(C/S)VIL with a major band at ~ 35 kDa that can be visualized (Figure 89). Among the tested combinations, the GFP-Trap DG led to the best results, combining high selectivity and good capacity to bind GFP-sensor. As a matter of fact, except the GFP-sensor, proteins lower than 40 kDa were not observed in DG as compared to the other batches, supporting that cross-linking with DVS/Dextran T500 fixed a pore exclusion size about 40 kDa as reported (Hjertén et al., 1987). Also, it appeared that unspecific proteins binding is reduced by using half concentration of NbD@GFP, confirming that saturation of the support affects negatively the selectivity. Therefore, we select the GFP-Trap DG ½ batch (= GFP-Trap v2) to compare its efficiency with the commercial version GFP-Trap\_MA (Chromotek, Planegg Germany).

In this prospect, IPs were performed with 5 µl of GFP-Trap\_MA, 6 % GFP-Trap EG ½ (equivalent of the GFP-Trap v1 with NdD@GFP) or 2.5 % GFP-Trap v2 following the same procedure with GFP-CVIL from BY-2 cells and GFP-CVIM from tobacco leaves. The immunoprecipitated proteins were analyzed by SDS-PAGE followed by gel staining or Western blot (Figure 88). Consistent is the fact that the amount and purity of purified GFP-sensor protein was significantly increased and is now equivalent to the commercial GFP-Trap Magnetic Agarose (GFP-Trap\_MA) used in our first assay (section 4.4.3). However, the quantity of beads in our GFP-Trap v2 could be slightly larger. To definitely conclude on both capacity and selectivity, it would be necessary to make a careful calibration to level the quantity of microparticles to that of the commercially available GFP-Trap\_MA. Although DVS and Dextran T500 add some fees to the production of the GFP-Trap v2, the cost remains similar since yield was improved and the amount of nanobodies used, lower.

Altogether, our optimization in few steps lead to a GFP-Trap v2 being now at least equivalent to the commercially available GFP-Trap\_MA, for both selectivity and capacity to bind GFP-sensor proteins. Thus, we used the GFP-Trap v2 to purify GFP-sensor proteins for non-targeted metabolomic analysis.

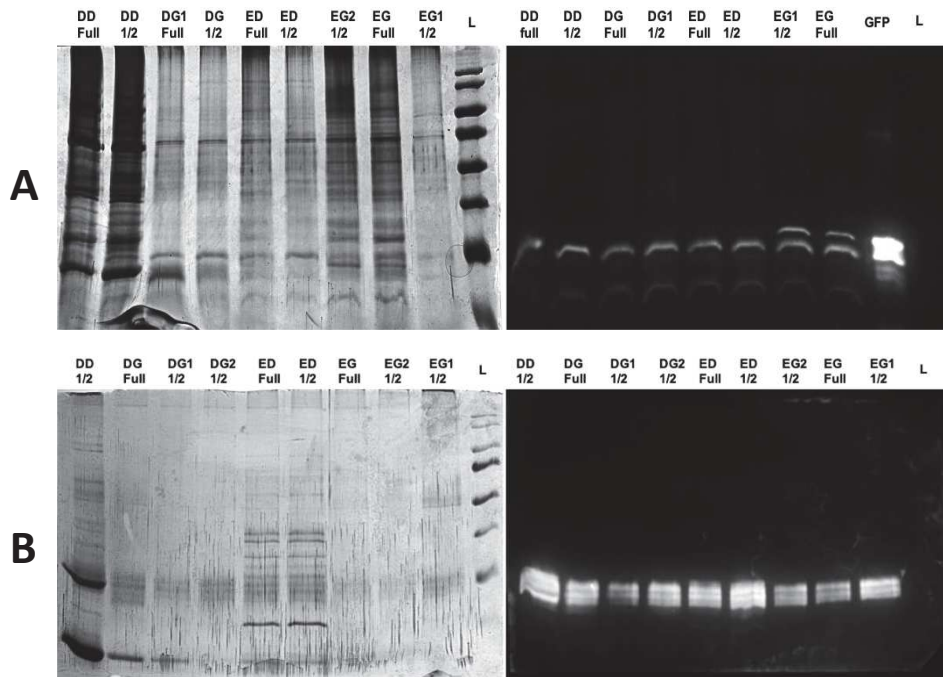


**Figure 89 Comparison of efficacy for GFP-Trap v2 prototypes to bind GFP-sensors.**

Silver nitrate-stained SDS-PAGE and Western blot analysis using rabbit IgG @GFP-CaaX of proteic fractions obtained by immunoprecipitation of (A) prenylated GFP-CVIL from BY-2 cells and (B) unprenylable GFP-SVIL from tobacco leaves. IP was carried out with 5  $\mu$ l of 2.5 % GFP-Trap DD, ED, DG, EG consisting in combination of cross-linking and functionalization presented in the table 10. The GFP-Trap v2 proptotypes were saturated in NbD@GFP (Full) or with the half concentration (1/2). Two different batches were synthesized for the EG (EG1 and EG2) and DG (DG1 and DG2) prototypes. The batch 1 was prepared wiith a ratio 1:4 ( $Fe_3O_4$ :agarose, w/w) and the batch 2 with a ratio 2:1 as the other prototypes. Ladder (L). To note, His-GFP-CVIL reference (GFP-CVIL) was filed onto western blot (A) in order to compare molecular weight between prenylated GFP from plant and not prenylated His-GFP-CVIL from bacteria.

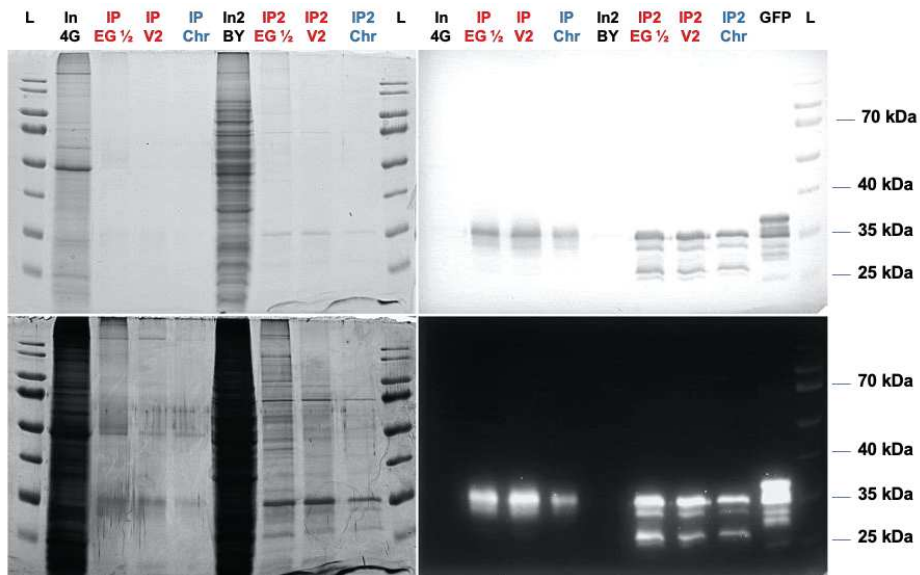


**Figure 88 The final GFP-Trap v2 is equivalent to the commercially available GFP-Trap\_MA (Chromotek).**

Immunoprecipitation of proteins from 750 mg of tobacco leaves containing prenylated GFP-CVIM (IP) and 750 mg BY-2 cells containing prenylated GFP-CVIL (IP2) was performed by using our homemade (Red) 6% GFP-Trap EG 1/2 (EG 1/2), 2.5 % GFP-Trap v2 (V2) and the Chromotek GFP-Trap\_MA (Blue Chr). Immunoprecipitated proteins were then analyzed by SDS-PAGE or Western blot immunostained with IgG @GFP-CaaX. Coomassie blue-stained gel (up left), silver nitrate-stained gel (down left), Western blot stained with NBT/BCIP (up right) or with chemoluminescence (down right).

## 4.10 COMPARATIVE NON-TARGETED METABOLOMICS USING UPLC-QTOF-MS/MS

It should be mentioned here that large amount of information has been obtained from the previous analyses. As mentioned in the introduction, the prenylation process is in fact made up of different steps leading to functional prenylated proteins (**section 2.3.1**). RAS plasma membrane localization requires an additional palmitoylation, while prenylation alone targets RAS to the ER membrane. Furthermore, our model of study about dynamic flexibility of PPTs activities suggests that alternative substrates such as phytol may be involved in protein prenylation in plants (Huchelmann, 2013). Besides, it was shown that carboxymethylation contribute to membrane targeting (Rodríguez-Concepción et al., 2000; Bracha-Drori et al., 2004; Yang et al., 2011). Considering all these possibilities and number of AA depending on the trypsin cleavage site, we set up a comparative non-targeted analysis with GFP-CaaX protein references and samples prepared as in the targeted metabolomics analysis but analyzed by using high-resolution mass spectrometry (HR-MS) with HPLC-QTOF-MS/MS.

The HR-MS provides a much better resolution on  $m/z$  value ( $\geq 5$  digits) detected than TQ-MS/MS analysis indeed. It becomes possible to associate molecular formulae of putative compounds registered in a database to  $m/z$  detected in non-targeted metabolomics study (Schymanski et al., 2015). In addition, the fragmentation pattern obtained by HR-MS allows clustering of metabolites into family of compounds according to parent and daughter  $m/z$  (Li et al., 2020). This type of approach enables the identification of hypothetical metabolites on differences detected by using comparative analysis between the samples with prenylated GFP-sensor and unprenylated negative controls. For instance, this approach was used to identify variation of azelaic acid and other putative metabolites associated to BW312 *Hordeum vulgare* semi-dwarf mutants compared to wild type plants (Villette et al., 2018). Thus, a database of molecular formulae from 346 potential compounds was generated, considering three cleavage sites before the CaaX Box, miss-cleavage of trypsin, classical and alternative prenyl substrates, variations between proteolysis and carboxymethylation, palmitoylation with or without prenylation and homodimers of tetrapeptides or associated to GSH or CoA by disulfide bridge (**Annexe 1**). The non-targeted metabolomics was initiated with the HR-MS analysis of available tetrapeptides and S-Far-L-cys OMe references. Then samples of GFP-CVIL protein were immunoprecipitated with GFP-Trap v1 and v2 from 5 g of BY-2 cells inhibited or not with 100

$\mu\text{M}$  FOS and  $10 \mu\text{M}$  MV. Several molecules have been detected and associated with hypothetical metabolites registered in our database (**Table 11**). Nevertheless, the signal detected in our samples was relatively low with isotopic profile consistency often over the limit of validation ( $m\text{Sigma} > 30$ ). Moreover, the retention times were generally not consistent with the polarity of corresponding metabolites as compared to analyzed references. For instance, the pentapeptide KCVIL more hydrophilic than CVIL was associated to a molecule with  $R_t = 10.96$  min, while CVIL reference is detected at 7.28 min. In fact, the variability between samples indicated that for the exception of one annotation, all detected molecules correspond to other compounds or to the background. Only, the annotation S-GG-L-cys ( $\text{C}_{23}\text{H}_{39}\text{NO}_2\text{S}$ ) was consistent with the  $m/z$  detected at  $R_t = 10.94$  min as compared to both  $R_t$  (9.85 min) and hydrophobicity of the S-Far-L-cys OMe reference. Interestingly, the S-GG-L-cys was absent from the negative control but detected in two IP samples from induced BY-2 as compared to unprenylated BY-2 cells, in which at least three times less signal was observed in only one replicate. These results are in adequation with the expected geranylgeranylation of GFP-CVIL protein in BY-2 cells, but without carboxymethylation. However, the latter were not reproducible as observed after reinjection of more concentrated samples and replicate of the whole experiment using the GFP-Trap v2, which is more effective than the GFP-Trap v1.

Despite the consideration of 346 metabolites resulting from hypothetical modifications of the GFP-CaaX C-ter end *in vivo* or after IP and tryptic digestion, results were obtained using non-targeted metabolomics was not reproducible. Still, the expected metabolites may have been hidden by other more abundant compounds, especially since HR-MS is less sensitive than UPLC-TQ-MS/MS used in our targeted metabolomics analysis. Finally, some possibilities of modification or degradation may have not been considered in our database.

Therefore, we synthesized S-GG-L-cys OMe and S-phytyl-L-cysteine methyl ester (S-Phy-L-cys OMe) references to clear up some of our last hypotheses

**Table 11 Overview of the non-targeted metabolomic analysis.**

(I) Conditions used to prepare sample for UPLC-QTOF-MS/MS non-targeted metabolomic analysis of immunoprecipitated GFP-sensors reference and plant material. (II) HR-MS results of non-targeted metabolomics study of GFP-CVIL immunoprecipitated from induced BY-2 cells (GFP-CVIL prenylated) and BY-2 cells inhibited with 100  $\mu$ M fosmidomycin 10  $\mu$ M mevinolin (GFP-CVIM not prenylated) as compared to negative control (control -). Digestion was performed following on-beads tryptic digestion method and annotation of metabolites detected at Rt < 2 min were automatically considered as background or calibrant. In red, metabolites for which area was significant (> 10 000).

Sample	Plant material (g)	Sample volume ( $\mu$ l)	GFP-Trap	Digestion type
GFP-CVIL BY-2 GFP-CVIL BY-2 + 100FOS10MV	5	100	GFP-Trap v1	On-beads
GFP-CVIL BY-2 GFP-CVIL BY-2 + 100FOS10MV	5	100	GFP-Trap v1 GFP-Trap v2	On-beads

RT [min]	m/z meas.	M meas.	$\Delta$ m/z [ppm]	mSigma	Ions	Name	Molecular Formula	Control -	GFP-CVIL prenylated	GFP-CVIL not prenylated
8.70	571.32839	570.32111	2.028	$\infty$	[M+H] <sup>+</sup>	GQKS-geranyl-L-Cysteine methyl ester (-CH3)	C26H46N6O6S	1580	33379	9198
8.41	446.25546	890.49636	-0.644	11.2	[M+H+H] <sup>2+</sup>	CVIL Homodimer	C40H74N8O10S2			1956
7.62	593.31352	592.30624	-2.412	$\infty$	[M+H] <sup>+</sup>	KCVIM	C25H48N6O6S2		23370	7807
7.30	431.28632	430.27904	-0.211	$\infty$	[M+H] <sup>+</sup>	SVIL	C20H38N4O6	8912	3433	7919
6.44	593.31286	592.30558	0.800	25.1	[M+H] <sup>+</sup>	KCVIM	C25H48N6O6S2		27222	9415
5.67	258.15166	257.14438	-2.207	$\infty$	[M+H] <sup>+</sup>	S-Geranyl-L-cys methyl ester (-CH3)	C13H23NO2S	2750		
5.30	326.21506	325.20779	0.719	$\infty$	[M+H] <sup>+</sup>	S-Farnesyl-L-cys methyl ester (-CH3)	C18H31NO2S	2794	5417	
14.47	685.49147	684.48420	-2.569	$\infty$	[M+H] <sup>+</sup>	S-palmitoyl-L-cysteine methyl ester (non proteolysed VIL)	C36H68N4O6S			724
11.93	669.40918	668.40190	2.070	$\infty$	[M+H] <sup>+</sup>	S-Farnesyl-L-cys methyl ester (non proteolysed VIM)	C34H60N4O5S2			3756
11.82	673.43236	672.42508	0.988	$\infty$	[M+H] <sup>+</sup>	GQKS-palmitoyl-L-cysteine methyl ester (-CH3)	C32H60N6O7S	7764	12350	6658
11.05	544.41724	543.40997	-1.291	23.6	[M+H] <sup>+</sup>	S-presqualene-L-cysteine methyl ester	C34H57NO2S			9734
11.01	797.50256	796.49528	-0.248	$\infty$	[M+H] <sup>+</sup>	KS-farnesyl-L-Cysteine methyl ester (Non proteolysed VIM)	C40H72N6O6S2			557
11.00	669.40896	668.40168	2.379	21.5	[M+H] <sup>+</sup>	S-Farnesyl-L-cys methyl ester (non proteolysed VIM)	C34H60N4O5S2			13251
10.96	575.35848	574.35120	-0.091	$\infty$	[M+H] <sup>+</sup>	KCVIL	C26H50N6O6S		1890	
10.94	394.27664	393.26937	-1.987	$\infty$	[M+H] <sup>+</sup>	S-Geranylgeranyl-L-cys	C23H39NO2S		31957	48117
10.82	653.40548	652.39820	-0.009	$\infty$	[M+H] <sup>+</sup>	GQKS-farnesyl-L-Cysteine methyl ester	C32H56N6O6S			13653
									10204	3663
										5233



## 4.11 SYNTHESIS OF S-PRENYL-L-CYSTEINE METHYL ESTER

S-GG-L-cys OMe and S-Phy-L-cys OMe are not commercially available. Relatively simple synthesis protocols have been described to produce S-Far-L-cys OMe from cysteine-OMe and a farnesyl halide. First, the prenyl alcohol (PreOH) is used to synthesize prenyl halide, which is then allowed to react with cysteine OMe (**Figure 90**). Halogenation of prenyl alcohol protocols have been reported, yielding prenyl halides > 90% using bromination or chlorination (Aguilar et al., 2014; Tang et al., 2018). The reaction between prenyl halide and the cysteine OMe can be achieved efficiently either by using DIEAE in DMF or  $Zn(OAc)_2$  as reported for the synthesis of S-Far-L-cys-OMe with yields of 43 % and 100 %, respectively (Kale et al., 2003; Liu et al., 2004). Although the reaction with the DIEAE results in a lower yield, the protocol is simpler and does not require to maintain the temperature at 0°C over the reaction time. Also, cysteine-OMe and the GGol, Fol as well as phytol are available at affordable prices and small amount are needed to analyze molecules by HPLC-MS/MS. Thus, the synthesis of the S-Far-L-cys-OMe, S-GG-L-cys-OMe and S-Phy-L-cys-OMe references was carried out using  $PBr_3$  to produce Far-Br, GG-Br and Phytol-Br (Aguilar et al., 2014), and DIEAE in DMF for the prenylation of the cysteine OMe (Kale et al., 2003). The synthesis of S-Far-L-cys-OMe, S-GG-L-cys-OMe and S-Phy-L-cys-OMe has been successfully achieved as shown by the  $H^1$  NMR spectra obtained after purification of compounds on a silica gel column (**Figure 91**). Using this protocol > 500 mg for each of the references have been obtained. These results confirmed that this protocol is suitable for the synthesis of all S-prenyl-L-cys-OMe. However, it has been found that S-prenyl-L-cys-OMe are unstable and degraded if they are not stored in the presence of argon and at least at -20°C (**Figure 90**). This degradation may result from a reduction of double bonds carried by the prenyl chain or from the loss of the methyl on the cysteine carboxy group.

In this context, the newly synthesized references degraded or not were used in non-targeted metabolomics analysis.



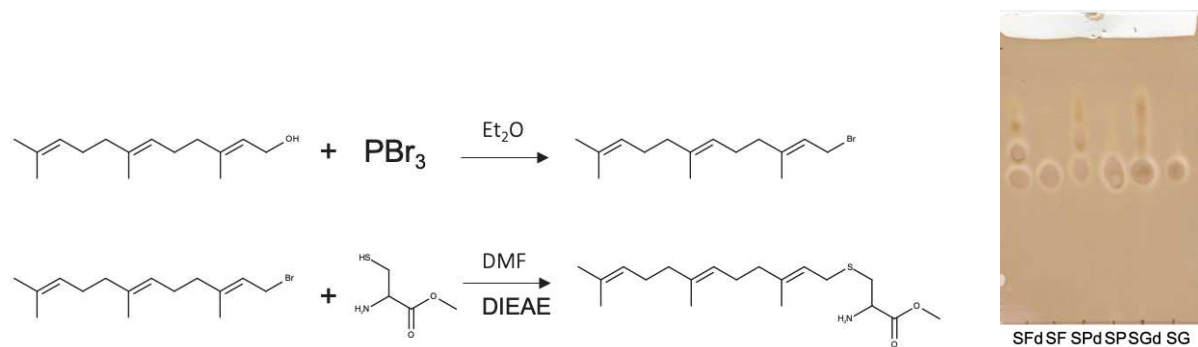


**Figure 90 Scheme of S-farnesyl L-cysteine methyl ester (S-Far-L-cys OMe) synthesis and TLC of degraded/pure products.**

(A) First, farnesol is bromated with  $\text{PBr}_3$  in  $\text{Et}_2\text{O}$ . Then S-Far-L-cys OMe (SF) was obtained from the reaction between farnesyl bromide and L-cysteine-O-methyl ester. This synthesis was extended to S-GG-L-cys OMe (SG) and S-Phy-L-cys OMe (SP). (B) All fresh products SF, SG, SP or stored two months at  $4^\circ\text{C}$  under argon (followed by d) were spotted on TLC, which was run into  $\text{EtOAc}:\text{MeOH}$  1:1, v/v and revealed using  $\text{KMnO}_4$  reagent.

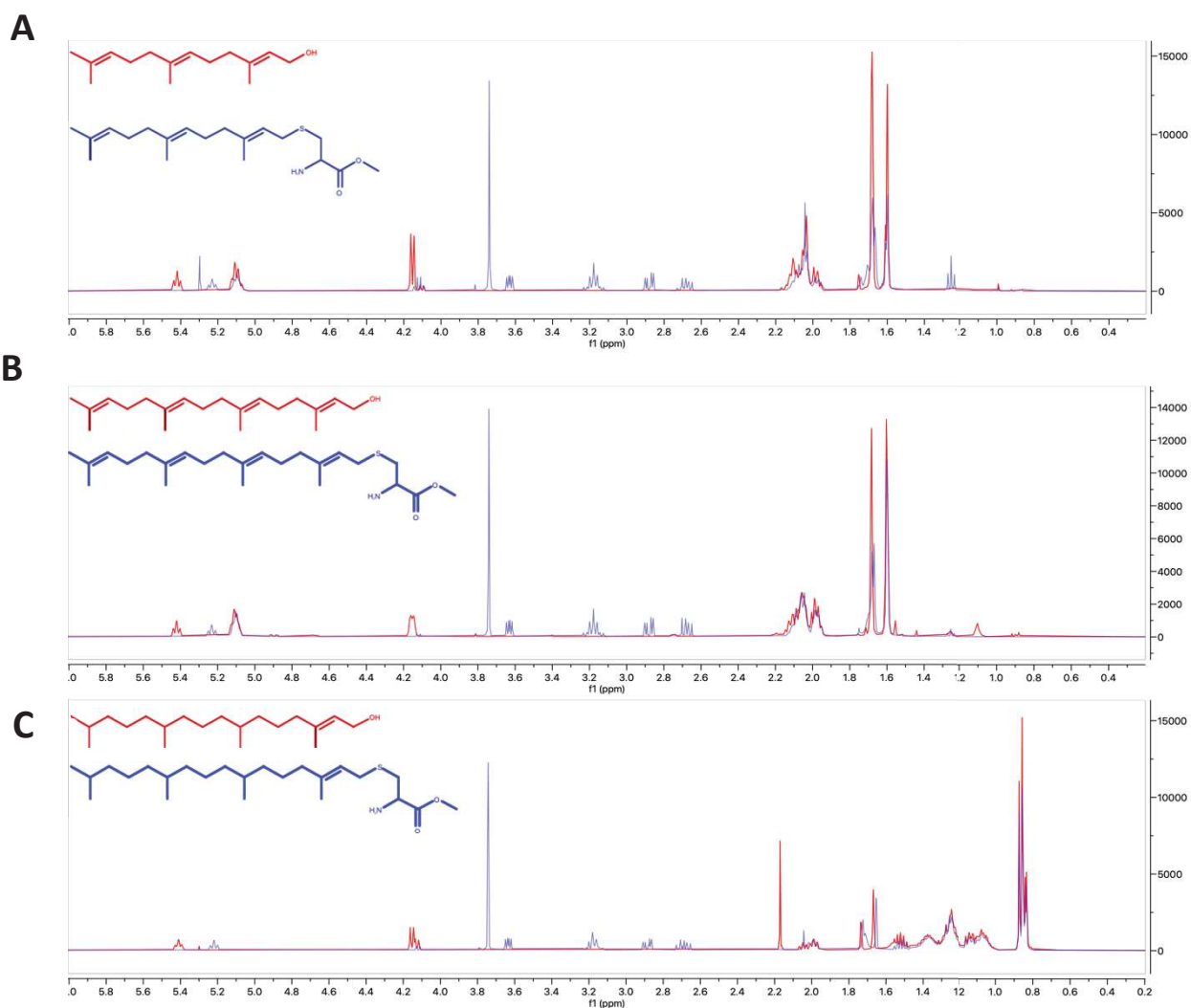


**Figure 91 S-Prenyl-L-cysteine were successfully synthesized.**

Superimposed  $^1\text{H}$  NMR spectra of prenyl alcohol (red) and S-Pre-L-cys OMe (blue) in  $\text{CDCl}_3$ . (A) Farnesol/S-Farnesyl-L-cys OMe, (B) Geranylgeraniol/S-Geranylgeranyl-L-cys-Ome, (C) Phytol/S-Phy-L-cys OMe

## 4.12 IDENTIFICATION OF S-FARNESYL-L- CYSTEINE IN GFP-CVIM PURIFIED FROM TOBACCO LEAVES

A final trial was performed by immunoprecipitating the GFP-SVIL and -CVIM proteins from tobacco leaves as previously. The new purified protein samples and the standards S-Far-L-cys OMe, S-GG-L-cys OMe and S-Phy-L-cys OMe undegraded and degraded were analyzed using non-targeted metabolomic analysis procedure. Although no tetrapeptides were identified, the S-far-L-cysteine (S-Far-L-cys) with  $[M+H]^+ = 326.214337$  was detected at  $R_t = 10.07$  min only in samples containing the GFP-CVIM prenylated *in planta* and S-Far-L-cys OMe samples (**Table 12**). Interestingly, this molecule is increased in the degraded S-far-L-cys OMe sample, suggesting that degradation of S-far-L-cys OMe occur at the methyl ester group yielding S-Far-L-cys. Surprisingly, as on the TLC, it appears that S-far-L-cys is more hydrophobic than S-Far-L-cys OMe, which does not make sense, except if cyclisation occurred. The degradation product will be analyzed by NMR to confirm the structure of supposed S-far-L-cys.

## 4.13 CONCLUSION

In conclusion, during this extensive development phase, we have developed a sustainable approach to purify the GFP-sensor proteins expressed and prenylated in plants. In addition, a targeted digestion method has been developed to optimize the analysis of the non-structured C-ter end including the basic domain and prenylated cysteine. Also, we have shown that S-Pre-L-cys OMe and tetrapeptides CaaX are detected mainly with  $m/z = 1$  after separation and analysis by HPLC-MS/MS. The non-targeted metabolomic analysis confirmed the farnesylation of GFP-CVIM protein in *N. tabaccum* under standard conditions. However, our results indicate that the S-prenyl-L-cysteine methyl ester are not stable and degrades at the carboxymethyl function. It was therefore not possible to confirm the carboxymethylation state of the terminal cysteine from the prenylated GFP-CVIM. Finally, although proteomics did not enable the identification of prenyls on the GFP-sensors under our condition, some proteins relevant with isoprenoids metabolism and photosynthesis were annotated recurrently and explicitly in the samples in which the sensors are prenylated. Despite the lack of function of our GFP-sensor protein, these results suggest that interaction with other proteins related to photosynthesis or biosynthesis of isoprenoids occur.

**Table 12 Identification of S-farnesyl-L-cysteine in GFP-CVIM prenylated in plants.**

HR-MS results of non-targeted metabolomics study of tetrapeptides and S-prenyl-L-cysteine methyl ester references (Blue) or GFP-sensor (green) immunoprecipitated from induced *N. tabacum* leaves (GFP-CVIM prenylated) as compared to negative control (Control do not express GFP-CVIM and GFP-SVIL unprenylable). Digestion was performed following on-beads tryptic digestion method and annotation of metabolites detected at Rt < 2 min were automatically considered as background. In red, metabolites for which area was significant (> 10 000). Solution of 0.2 mg/ml of references: CVIM and SVIL tetrapeptides, S-farnesyl-L-cysteine methyl ester degraded (S-Fard) or not (S-Far), S-geranylgeranyl methyl ester degraded (S-GGd) or not (S-GG) and S-phytyl-L-cysteine methyl ester degraded (S-Phyd) or not (S-Phy).

RT [min]	m/z meas.	$\Delta m/z$ [ppm]	mSigma	Name	Molecular Formula	CVIM	SVIL	S-Fard	S-Far	S-GGd	S-GG	S-Phyd	S-Phy	Control	GFP-CVIM prenylated			GFP-SVIL unprenylable			
10.07	326.214337	-1.501	10.4	S-Far-L-cys	C18H31NO2S			7193872	294204	8682		11050	3312			27004	35784	31726			
9.04	340.229996	-1.413	$\infty$	S-Far-L-cys OMe	C19H33NO2S			6478004	7498692							6220			4974	5282	5210
10.40	476.355020	-1.381	8.2	S-GG-L-cysteine OMe	C29H49NO2S			3068	8010	588752	1183330			3522	2534	5120	532	4776	1914		
10.70	394.277109	-2.745	5.7	S-GG-L-cys	C23H39NO2S			670		1409508	666076	20674	6718			3078					
10.59	408.292464	-1.501	6.1	S-GG-L-cys OMe	C24H41NO2S					2001144	3216484	93936	27868								
11.11	400.323416	-2.402	26.2	S-Phy-L-cys	C23H45NO2S							7554768	1056440	4878		7440			4356		
10.31	414.341760	4.18	$\infty$	S-Phy-L-cys OMe	C24H47NO2S							7673854	7673854								
6.37	465.219315	-1.449	21.1	CVIM peptide	C19H36N4O5S2	4487756	9122	3760	4540			3928			2290		2202			1246	
6.78	465.219284	-1.515	22.3	CVIM peptide	C19H36N4O5S2	70024		21522	12156	7614	9632	8696	6592				788				
7.15	465.21923	-0.364	20.9	CVIM peptide	C19H36N4O5S2	7673854	121578	42230	33370	25240	26912	18302	14790	3668	1566					662	
6.71	431.287989	3.65	$\infty$	SVIL peptide	C20H38N4O6		7673854						1958					3490			
8.25	464.211728	-0.939	25.9	Homodimer CVIM	C38H70N8O10S4	3664644	59636	19866	3470	2558	3988				2300				482		
8.27	927.416511	-0.583	23.1	Homodimer CVIM	C38H70N8O10S4	3881960	130748			3926			1962								
8.46	464.211044	-0.952	19.8	Homodimer CVIM	C38H70N8O10S4	3428396	67450		9090			2726	1142			1276					

# 5 SCREENING FOR PROTEIN PRENYLATION INHIBITORS AND APPLICATIONS



## 5.1 INTRODUCTION

Since the 1990s, protein prenylation was considered as a promising target for the treatment of human pathologies such as progeria and cancer (**section 2.6**). This study aims to purpose new compounds acting on unconventional targets. That is why, we screened 20 pure compounds and 13 extracts using the BY-2 GFP-CVIL cells model. Our collaboration with C. Vonthron-Sénécheau (LIT, Strasbourg), working on natural antiprotozoal molecules, allowed to screen extracts from red alga and anthranoids being active against *P. falciparum*. In addition, L. Desaubry (ex-LIT researcher), working in cardio-oncology and medicinal chemistry, enabled us to test a series of prohibitin (PHB) ligands being effective on mammalian cancer cell lines.

From another point of view, studies in *Catharanthus roseus* and *N. tabacum* have shown that inhibition of protein prenylation influences the biosynthesis of specialized metabolites. For instance, the monoindole terpene alkaloids (MIAs) such as vinblastine, vincristine are blockbuster anticancer compounds found in *C. roseus* and other Apocynaceae species. These molecules derived from the condensation of tryptophane and secologanin (sesquiterpene) moieties. Interestingly, under inhibition with PFT inhibitors such as Manumycin A, Chaetomelic acid A or gene silencing of CrPFT and CrPGGT-I by RNAi, the biosynthesis of MIAs in *C. roseus* is depleted (Courdavault et al., 2005; Courdavault et al., 2009; Kumar et al., 2020). Also, Experiments with *S*-carvone and GGTi-2133 evidenced that protein prenylation inhibition shutdown the production of capsidiol in tobacco leaf discs (Huchelmann et al., 2014). Both specialized metabolites are regulated by MeJA-signaling being dependent of prenylated proteins signal transduction, especially under stress conditions. Although capsidiol has not such interest for human application, MIAs as anticancers are highly valuable, and production of these molecules remains extremely dependent of plant sourcing (Martino et al., 2018). Less but not negligible interest exist in several other MIAs such as ibogaine, yohimbine being also used for the treatment of addictions and erectile dysfunction respectively (Tam et al., 2001; Belgers et al., 2016; Kregel et al., 2019). Furthermore, some prenylated proteins were characterized in hormone biosynthesis or signaling being involved in response to stress, but also development such as CYP85A2 (**2.3.3**). Considering, that many other terpenes are valuable not only in pharmaceuticals, but also in agronomy or cosmetics, is pharmaceuticals the only application of protein prenylation inhibitors?

Accordingly, this chapter also discuss about putative applications for protein prenylation inhibitors in the production of valuable plant specialized metabolites such as carotenoids. Actually, carotenoids due to their antioxidant properties are widely used in agroindustry for food conservation and quality (Novoveská et al., 2019; Nabi et al., 2020). Nonetheless their production remains extremely limited and expensive. Recently increased in demands of more active keto-carotenoids such as astaxanthin or canthaxanthin for pet food production pushed investigation of new sourcing alternatives. In 2018, astaxanthin market represented 600 million USD and is expected to reach over 800 million by 2026. In this context, we evaluated the inhibition of protein prenylation in the production of carotenoids in tobacco plant.

## 5.2 SCREENING FOR PROTEIN PRENYLATION INHIBITORS

### 5.2.1 Rhodophytes Extracts and Subfractions

In *P. falciparum* the apicoplast involved in the biosynthesis of isoprenoids through MEP pathway was inherited from a red alga (section 2.2.3.2). This basis tethered our guideline proposing that molecules acting in red alga isoprenoids metabolism could interfere with that of *P. falciparum*, especially for protein prenylation which diverged over time (section 2.7.2). Hence, we performed a screening of red algae extracts and subfraction to evaluate their ability to inhibit protein prenylation in our BY-2 model. A total of 13 extracts/fractions were screened using the BY-2 model expressing the GFP-CVIL protein (Table 13). Fractions from EtOAc extracts of *Mastocarpus stellatus* (Ms-F2 and F3), *Placanium cartilagineum* (Pc F1) and *Dilsea carnosa* (Dc F2) showed the best inhibition results at 40 µg/mL with membrane/nucleus phenotypes in ~20% of the observed cells (Figure 92). To some extent, metabolites contained in those extracts appear as being endowed with the faculty to interfere with protein prenylation, statistical analysis (n=3) revealed no significant difference. Surprisingly, the fraction Pc F3 exhibit protein prenylation inhibition, while this fraction was inactive at 100 µg/ml in the pLDH assay. Moreover, the latter exhibited a higher inhibition of protein prenylation than Pc F2, whereas the reverse was observed in pLDH inhibition assay. Similarly, Ct F2 being very active in the pLDH assay was inactive in the inhibition of protein prenylation assay. A much higher inhibition was expected according to our hypothesis of Plasmodium/Alga relationship and the results of these fractions on pLDH inhibition test. In this context, it is therefore questionable if the activity observed on pLDH assay and protein prenylation inhibition assays result from the same molecule(s). Nevertheless, the high variability and rather low inhibition rates are supported by a low solubility of some extracts in DMSO stock solutions and in the culture medium. In addition, DMSO is known to promote the oxidation of some molecules as exemplified with vismiones but other too (Engeloch et al., 2008), and could have by the way contribute to a partial loss of extracts activity (Epstein and Sweat, 1967; Galle, 2015). Consistent is fact that even if most of these extracts exhibit high activity on the pLDH assay at 100 µg/ml (> 85 %), inhibition drops down at 10 µg/ml, and our trials were fixed at 40 µg/ml. Unfortunately, it was not possible to rise higher concentration because of the low extract's solubility. Furthermore, no fluorescence was observed in BY-2 cells treated with fraction 4 of *Dilsea carnosa* (Dc F4) and the EtOAc extract of *Callithamnion tetricum* (Ct EtOAc).



The morphology of Dc F4 or Ct EtOAc-treated BY-2 cells indicated a death of all cells, suggesting that these extracts contain cytotoxic molecules for BY-2 cells. Further experiments with lower concentrations need to be investigated. With this respect, how to decipher whether inhibition of *P. falciparum* with red alga extracts depends on protein prenylation? A perspective would still be to isolate the active compounds from these extracts by using bioguided fractionation or the method of pharmacophoric deconvolution developed during the *PhD* work of L. Margueritte at the LIT (Margueritte et al., 2019).

Accordingly, the latter was used by L. Margueritte to identify molecules responsible for *P. falciparum* inhibition in the fraction Dc F2 from *Dilsea carnosa* (Margueritte, 2018). Dc F2 is one of the most active fraction against *P. falciparum* at the pLDH test, and it also exhibits a moderate protein prenylation inhibition in our model (**Figure 92**). A pharmacophoric fingerprinting was established by comparing the NMR spectra of inactive and active fractions after bioguided fractionation of Dc F2 (Margueritte, 2018). Accordingly, different pharmacophoric fingerprints were obtained, proposing that the activity would be carried by several molecules, but the molecule(s) being involved in the activity of Dc F2 remain unidentified. As a result, some signals revealed the presence of sterols with unsaturated side chains or compounds similar to eleganolone, a diterpene isolated from *Bifurcaria bifurcata* and already described for its antiprotozoan properties on *P. falciparum* and *Trypanosoma brucei* (Galle, 2015; Margueritte, 2018). Based on its structural similarities with GGPP, this compound, could potentially interfere with PGGT activity. Consequently, trials of purification and analysis using HPLC-UV/MS-SPE-NMR were carried out, but they all failed as  $R_t$  of targeted compounds were shifted in between successive run. The capture on SPE by the HPLC-UV/MS-SPE-NMR is highly dependent of compounds  $R_t$  indeed, too much variability in this parameter irretrievably leads to inefficient trapping and bad NMR signal. As a matter of fact, the solubility or degradation of compounds was also suggested as the main cause for variability in L. Margueritte PhD study (Margueritte, 2018).

All in all, our screening of rhodophyte extracts and subfraction have shown positive but not significant results for *M. stellatus*, *P. cartilagineum* and *D. carnosa* extracts, hence problems of solubility and/or degradation call for purification before next investigations. Although, the solubility is quite problematic, it supports that the fraction is lipid-rich, which could inhibit protein prenylation in BY-2 cells and *P. falciparum* as well.

**Table 13 Inhibition of protein prenylation by rhodophyte EtOAc extracts and subfractions.**

The inhibition of *P. falciparum* NF54 strain by of 100 or 10 µg/ml EtOAc extracts and subfractions (F1 to F4) from different species of Alga was tested using pLDH inhibition assay (Margueritte et al., 2019). The most active and two inactive fractions were selected to test protein prenylation inhibition. The latter was evaluated at 40 µg/ml on BY-2 cells expressing, a sensor of geranylgeranylation GFP-CVIL.

Genus	Species	Extract type	pLDH Inhibition %	
			100 µg/ml	10 µg/ml
<i>Dilsea</i>	<i>carnosa</i>	EtOAc	98	23
		F2	98	9
		F3	82	6
		F4	82	1
<i>Mastocarpus</i>	<i>stellatus</i>	EtOAc	84	3
		F2	96	4
		F3	96	12
<i>Callithamnion</i>	<i>tetricum</i>	EtOAc	81	15
		F2	98	24
		F3	98	17
<i>Gracilaria</i>	<i>gracilis</i>	EtOAc	88	5
<i>Plocamium</i>	<i>cartilagineum</i>	F1	98	3
		F2	10	1
		F3	5	1

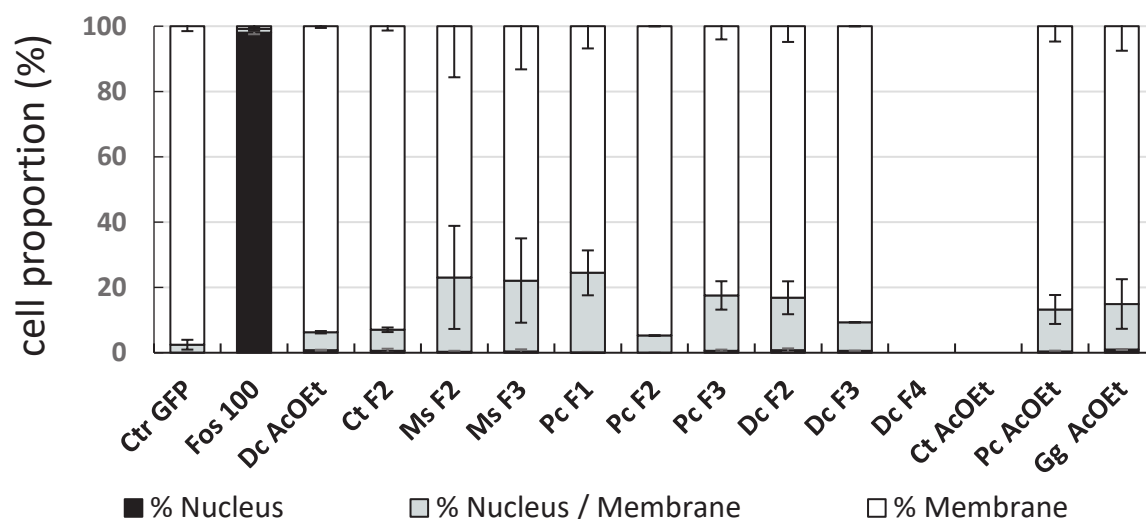


**Figure 92 Antiplasmodial rhodophyte *M. stellatus*, *P. cartilagineum* and *D. carnosa* extracts-induced inhibition of protein prenylation.**

Tobacco GFP-CVIL cells were treated for 3 hours with 40 µg/ml of EtOAc and subfractions (F1-F4) extracts isolated from *Dilsea carnosa* (Dc), *Mastocarpus stellatus* (Ms), *Callithamnion tetricum* (Ct), *Gracilaria gracilis* (Gg), *Plocamium cartilagineum* (Pc) (Table 15). A nuclear distribution of the fluorescent protein determined by confocal microscopy is indicative for protein prenylation. The distribution was compared to references including untreated cells (Ctr) and treated with 100 µM fosmidomycin (FOS 100). Results of inhibition were not significant after statistical analysis using Levene with Kruskal-Wallis tests followed by a Dunnett's post-hoc test (n=3)



## 5.2.2 Synthetic Compounds Interacting with Prohibitins

Most of RAS proteins are prenylated and a deregulation of their activity is associated with various forms of cancer. Interestingly, several inhibitors of prohibitins (PHB) exhibit good activities against neuroblastoma, breast cancer, lung but can also stimulate osteoclastogenesis (Rajalingam et al., 2005; Moncunill-Massaguer et al., 2015; Hati et al., 2016; MacArthur et al., 2019). PHB are involved in various signaling cascades, including the Ras/mitogen-activated protein kinase/ extracellular signal-regulated kinase (Ras/MAPK/ERK) pathway, requiring prenylated RAS proteins (Mishra et al., 2010; Chowdhury et al., 2014). In plants PHB were found to contribute to mitochondrial biogenesis but also stress response and a decrease in prohibitin by silencing induce senescence and alter plant development in *Petunia x hybrida* (Chen et al., 2005; Ahn et al., 2006; Wang et al., 2010). In this context, we wanted to evaluate whether PHB can contribute to the regulation of protein prenylation. Therefore, a selection of 10 synthetic molecules whose activities have been evaluated on different cancers or transformed cell lines were provided by Dr. Laurent Desaubry (ex-LIT researcher) (**Figure 93**). Most of them are reported to be cytotoxic and to interact with PHB proteins (**Table 14**).

### 5.2.2.1 Inhibition of protein prenylation

Accordingly, chemical complementation assays were performed to refine which biosynthesis step might be affected. To do so, different biosynthesis intermediates were applied to evaluate their capacity to prevent the inhibition induced in the presence of fosmidomycin (FOS-100  $\mu$ M) and mevinolin (MV -10  $\mu$ M). The molecules were tested at different concentrations to evaluate their ability to inhibit the prenylation of the GFP-CVIL sensor. Among all tested compounds, IN2 interfered with protein prenylation (**Figure 94**). This inhibitor is quite efficient, as a delocalization of the GFP-CVIL sensor into the nucleus was observed at 1  $\mu$ M for ~60% of treated BY-2 cells when compared to control cells. In addition, at 10  $\mu$ M, a complete inhibition of protein prenylation is observed, similar to a total shutdown of isoprenoid biosynthesis (FOS 100  $\mu$ M + MV 10  $\mu$ M) in BY-2 cells. Same results were obtained in tobacco leaves expressing the GFP-CVIL protein (**Figure 94**).

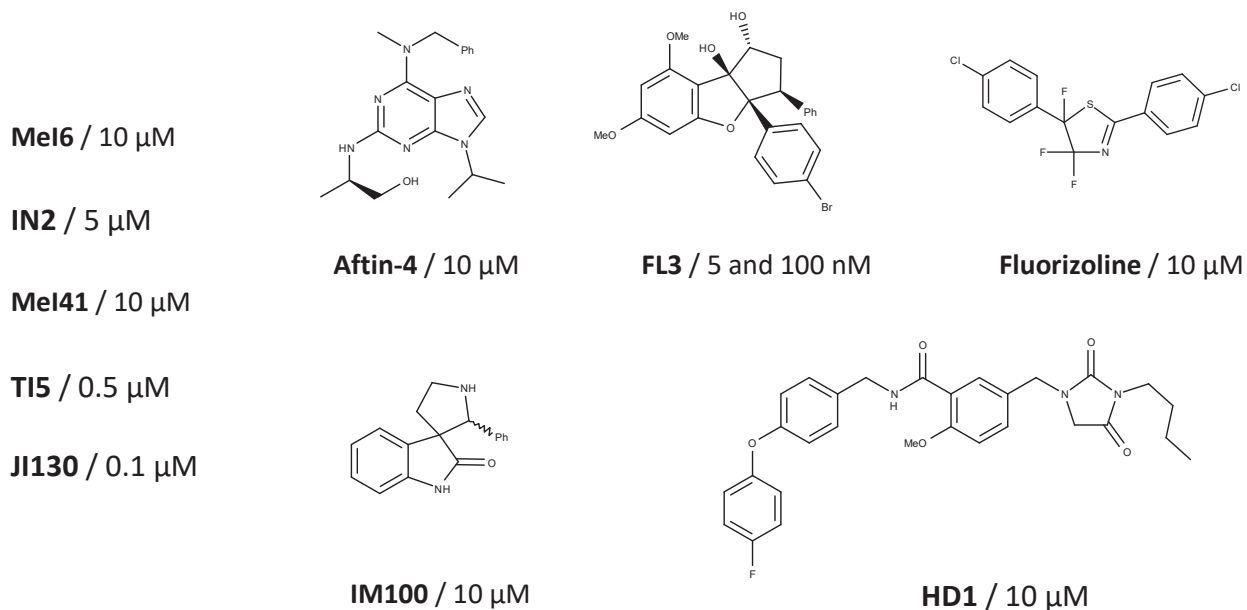


**Figure 93 Prohibitin ligands evaluated in protein prenylation inhibition assay.**

Structures and concentrations of some prohibitin ligands used in the protein prenylation inhibition assay with our BY-2 model expressing GFP-CVIL protein. The structures of MeI6, IN2, MeI45, TI5, JI130 are not shown because under confidential agreement

**Table 14 Prohibitin ligands as anticancer agents.**

Examples of biological activities for some of the synthetic molecules described as prohibitin (PHB) ligands and used in our screening of protein prenylation inhibitors.

Name	Activities reported	References
<b>Aftin-4</b>	Promotes A $\beta$ 42 production in neurons. interact with three proteins related to neural degeneration: PHB1. voltage-dependent anion channel 1 (VDAC1) and mitofilin	Bettayeb et al., 2012;
<b>FL3</b>	Cytotoxic on cancer cells. blocks the interaction of PHBs with C-RAF and KRAS	Polier et al., 2012; Yurugi et al., 2017
<b>Fluorizoline</b>	Cytotoxic on cancer cells. disrupt the interaction of C-RAF and active RAS in cells	Polier et al., 2012; Moncunill-Massaguer et al., 2015; Yurugi et al., 2017
<b>IM100</b>	Cytotoxic on cancer cells. bind to HDAC2 and PHB2	Hati et al., 2016
<b>HD1</b>	Bind AMPK to relieve the inhibition induced by PHB2	WO/2012/026495
<b>Sulfoamidin 1m</b>	Binds PHB1 and inhibits osteoclastogenesis	Lee et al., 2010; Chang et al., 2011

Interestingly, this effect is observed only in the line expressing a GFP-CVIL protein suggesting a specific effect on protein geranylgeranylation. At this stage, it can be hypothesized that a MEP pathway enzyme, the biosynthesis of GGPP or PGGT activity is targeted because our system does not allow the discrimination.

#### 5.2.2.2 Does IN2 inhibit known targets?

We chose to work with a reference concentration of 5  $\mu$ M IN2 allowing a nearly total inhibition of protein geranylgeranylation in tobacco BY-2 cells (**Figure 94**). The inhibition was reversed by the addition of 20  $\mu$ M GGol, indicating that IN2 might not alter PGGT-I activity directly (**Figure 95**). Interestingly, 1 mM of 1-deoxy-*D*-xylulose (DX), an early precursor in the biosynthesis of GGPP by the MEP pathway, was also able to relieve partially the inhibition. At the opposite, up to 2 mM MVA was not able to rescue protein prenylation. One option would be that IN2 acts as a competitor inhibitor of DXS. However, these results suggest that IN2 would neither act on PGGT-I nor on an enzyme involved in the biosynthesis of GGPP. We then checked if any of the enzymes in the MEP pathway could be affected. In fact, inhibition of the MEP pathway by FOS or oxoclozoxone is well known to induce bleaching phenotype in plants, for which chlorophyll biosynthesis requires MEP precursor (Kamuro et al., 1986). Accordingly, one-week-old *A. thaliana* plantlets were grown on medium containing 1 or 10  $\mu$ M IN2. After three weeks, even if roots appeared to be a little bit shorter to that of the DMSO control, no bleaching was observed, suggesting that IN2 does not inhibit an enzyme from the MEP pathway (**Figure 96**). This was confirmed testing IN2 on *E. coli* *dxs::KAN* DY329 conditional mutant strain. Actually, this *dxs* mutant is auxotroph for DX and does not grow in the presence of MEP pathway enzyme inhibitor. Nonetheless, inhibition test with 1 and 10  $\mu$ M IN2 did not affect at all the growth of *dxs::KAN* DY329 strain supplemented with DX (**Figure 96**). Although a problem in the penetration of IN2 in *E. coli* could be responsible of the negative result, this hypothesis was impaired as IN2 was efficient in *A. thaliana*. Altogether, these results support that inhibition of protein geranylgeranylation by IN2 result from another mechanism than MEP biosynthesis enzyme or PPTs inhibition. Consequently, we explored other hypothesis by comparing the effect of IN2 to those of S-carvone, which affect plant signalization.

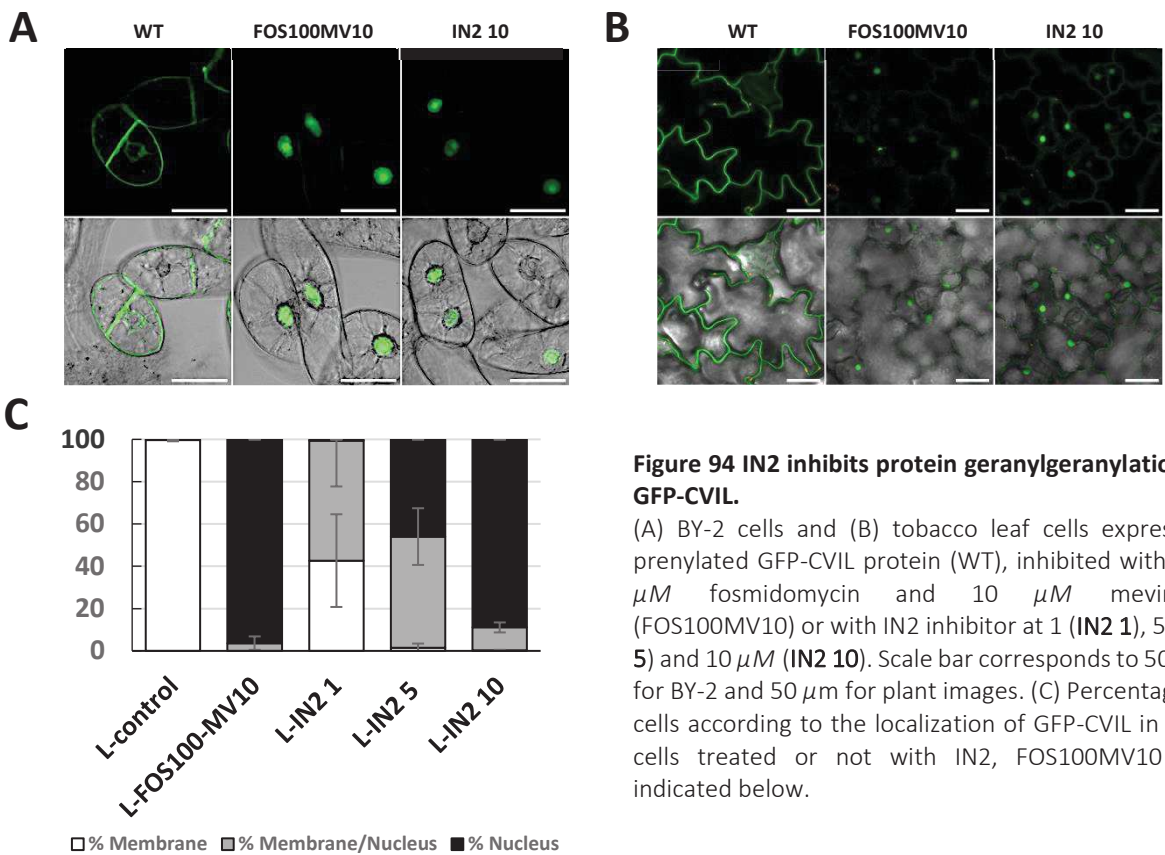


**Figure 94 IN2 inhibits protein geranylgeranylation of GFP-CVIL.**

(A) BY-2 cells and (B) tobacco leaf cells expressing prenylated GFP-CVIL protein (WT), inhibited with 100  $\mu$ M fosmidomycin and 10  $\mu$ M mevinolin (FOS100MV10) or with IN2 inhibitor at 1 (IN2 1), 5 (IN2 5) and 10  $\mu$ M (IN2 10). Scale bar corresponds to 50  $\mu$ m for BY-2 and 50  $\mu$ m for plant images. (C) Percentage of cells according to the localization of GFP-CVIL in BY-2 cells treated or not with IN2, FOS100MV10 are indicated below.

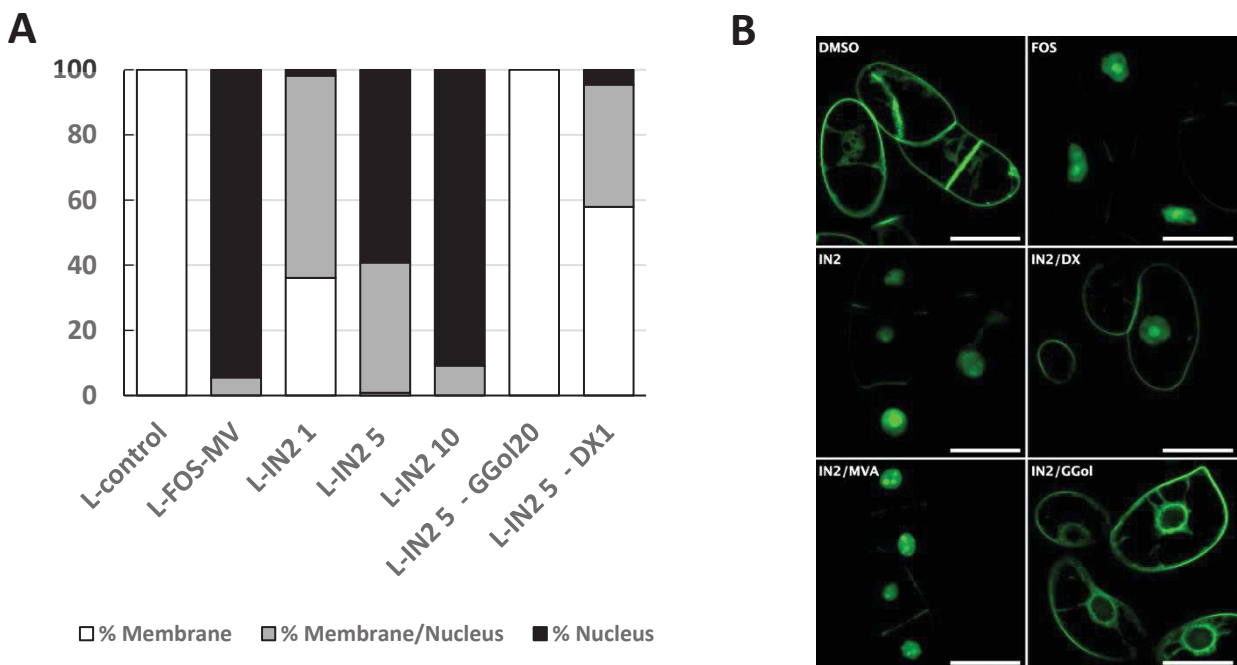


**Figure 95 IN2 does not target the PGGT-I.**

(A) percentage of cells according to the localization of GFP-CVIL in BY-2 cells inhibited or not with 100  $\mu$ M fosmidomycin and 10  $\mu$ M mevinolin (FOS100MV10), IN2 inhibitor at 1 (IN2 1), 5 (IN2 5) and 10  $\mu$ M (IN2 10) alone or 5  $\mu$ M IN2 complemented with 20  $\mu$ M geranylgeraniol (IN2 5-GGol20) or 1 mM DX (IN2 5-DX1). (B) Confocal microscopy observation of BY-2 cells treated with IN2 10  $\mu$ M and complemented by 1 mM DX, 2 mM MVA or 20  $\mu$ M GGol,

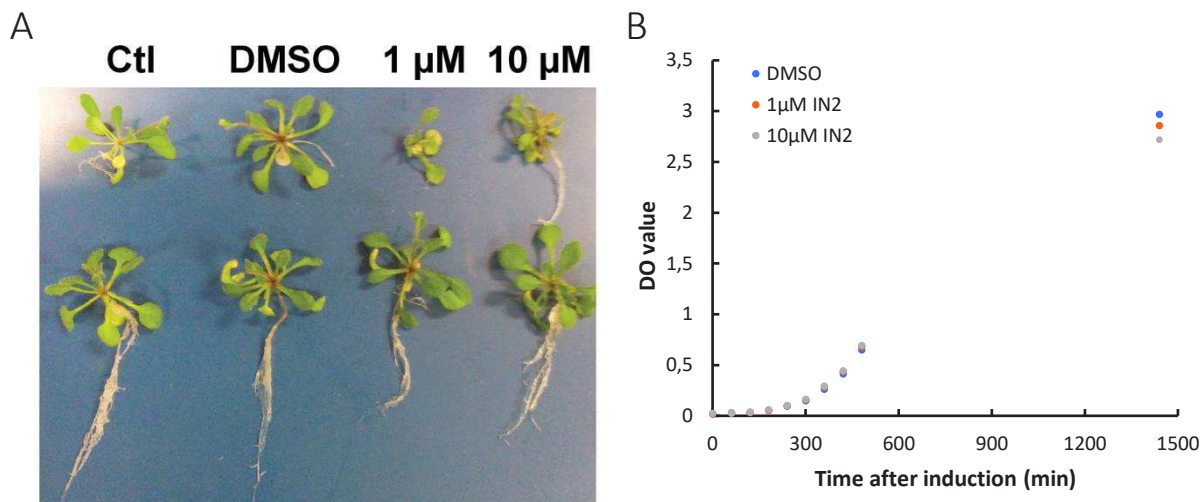


**Figure 96 IN2 does not target MEP pathway enzymes.**

(A) One-week-old *A. thaliana* plantlets were transferred on agar solid medium supplemented with DMSO (Ctl) or 1 and 10  $\mu$ M IN2 for three weeks. The absence of bleaching support that MEP pathway is not affected. (B) Growth of *E. coli dxs::KAN DY 329* strain grew for 24h in liquid medium supplemented with 1-deoxy-*D*-xylulose (DX) with DMSO as negative control and 1 or 10  $\mu$ M IN2. The optical density was measured each hour during 8h and at 24h (experiments were done by Marianne Dubois – Master student).

### 5.2.2.3 IN2 inhibit protein prenylation through atypical target

It has been shown that the elicitation of tobacco leaves with cellulase induces an increase in the activity of HMGR for the production of capsidiol from FPP (Dorey et al., 1997). Previous research has reported that at 2 mM, *S*-carvone deplete capsidiol production via inhibition of prenylation of proteins potentially involved in the signal integration (Huchelmann et al., 2014). We wanted to investigate whether IN2 mimics *S*-carvone in a tobacco leaf-disk assay by measuring capsidiol production excreted from the culture medium. To this end, we analyzed hexane extracts of treated sample culture medium by GC-MS (Figure 97). As a matter of fact, no difference in the capsidiol content of culture media was observed between the control and IN2 treatment as compared to *S*-carvone. But, two other unidentified metabolites associated to IN2 treatment appeared at  $R_t = 6.82$  min and  $R_t = 23.3$  min indeed. Taking together, our results support that IN2 inhibit protein prenylation in a different manner than FOS or *S*-carvone. Another hypothesis would be that IN2 negatively control an enzyme of the MEP pathway. In this case, GGPP produced via the MEP pathway could not anymore be synthesized and the PGGT-I would not be able to catalyze the reaction because of the absence of one of its substrates. Hence, alternative approaches have to be considered.



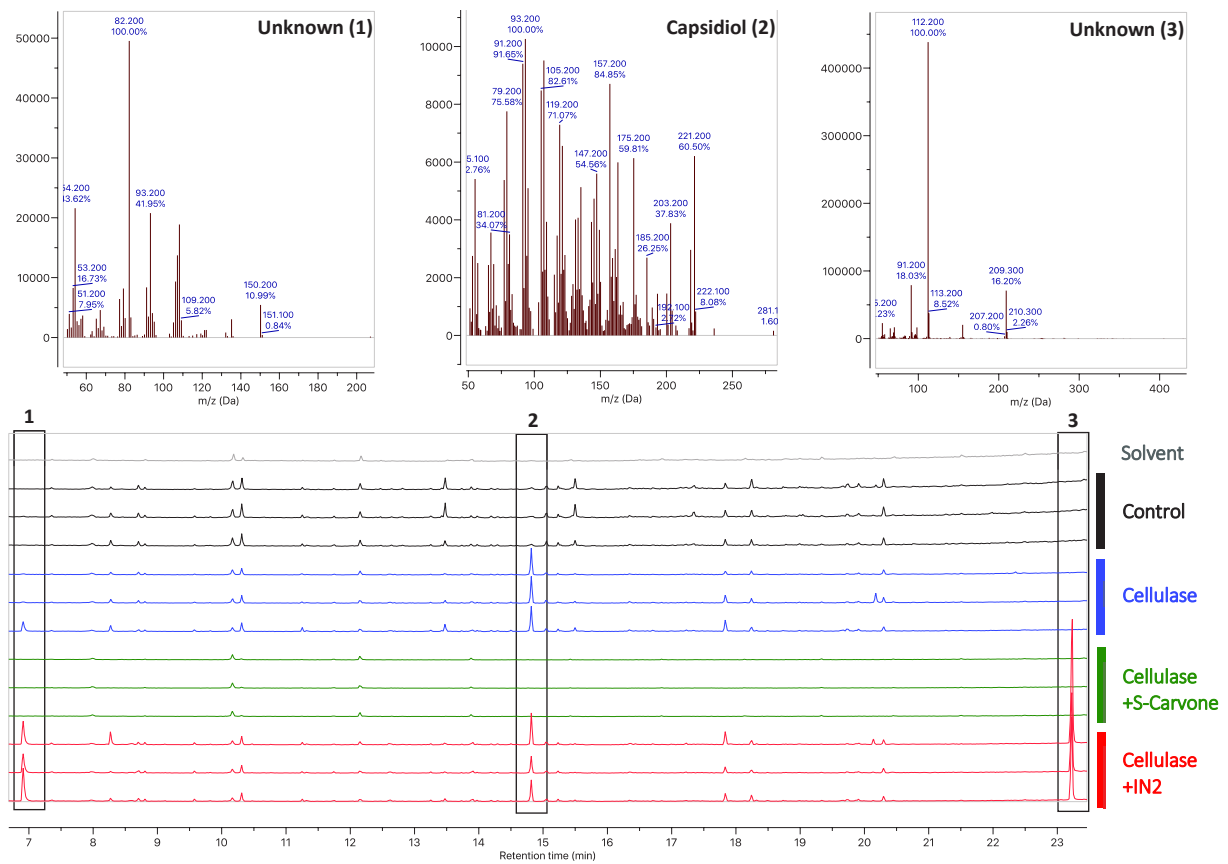


**Figure 97 Capsidiol production is not depleted by IN2.**

Stacked GC-EI-MS chromatograms of hexane extracts from the culture media of tobacco leaf-discs floated 18h on 50  $\mu\text{M}$   $\text{KH}_2\text{PO}_4$  (**Black**), elicited with 0.5 % cellulase alone (**Blue**) or supplemented with 2 mM S-carvone (**Green**) or 10  $\mu\text{M}$  IN2 (**Red**). The molecules highly influenced by treatments were numerated from 1 to 3 and their MS spectra represented above.

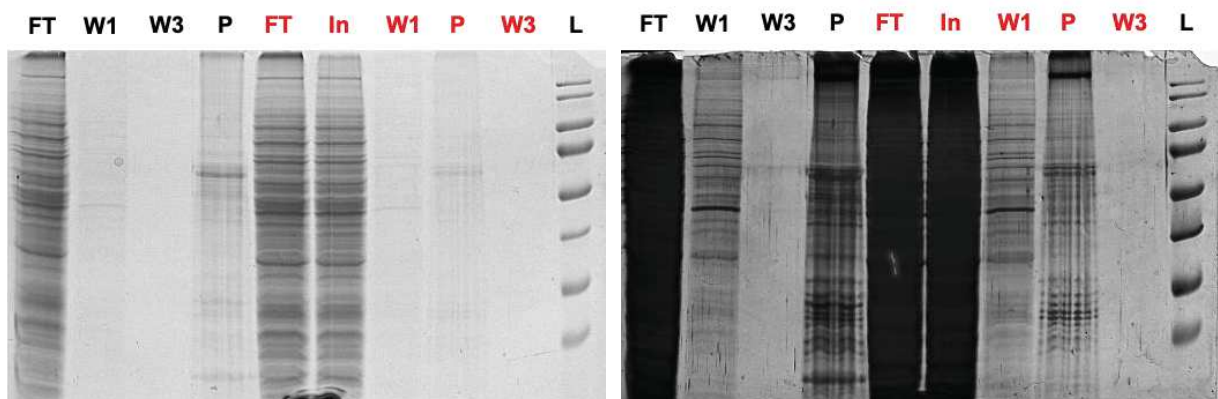


**Figure 98 Low selectivity of IN2-agarose affinity purification support for elucidation of target proteins.**

SDS-PAGE gel of 20  $\mu\text{l}$  protein purified by affinity purification with sepharose (**black**) and sepharose-IN2 matrices (**Red**). Images after staining with blue coomassie (**left**) and silver nitrate (**right**) reagents. Total protein extract (**In**), Flow through (**FT**), wash with TE buffer (**W1**), wash with IPB (**W3**), ladder (**L**)

#### 5.2.2.4 Identification of IN2 Targets by Affinity Purification and Proteomics

A widely used technique to identify inhibitor targets is the purification by affinity prior to proteomics analysis. Accordingly, an agarose matrix coated with IN2 has been provided by L. Desaubry and his PhD student Tabti Redouane (LIT, Strasbourg) in order to purify and identify prospective targets of IN2. We performed a preliminary experiment with BY-2 protein extracts. Those extracts were incubated with the IN2-matrix and its capacity to bind specific proteins was compared to non-grafted agarose support. Nevertheless, no significant enrichment could be observed on the stained SDS-PAGE in the presence of IN2 tracks (**Figure 98**). In this regard, it can be concluded that the IN2-coated matrix used for the affinity purification was not selective enough as compared to the control matrix. Thus, it does not allow sufficient enrichment to perform proteomics analysis and the experiment was not followed-up. The type of matrix used to link IN2 could explain this lack of selectivity, agarose beads being described as more or less selective depending on their porosity and the type of cross-linking employed (Zhao et al., 2009).

Moreover, the type of linker used to attach IN2 to the matrix may significantly influence the selectivity of the support as observed for the synthesis of our GFP-Trap. Finally, it would be necessary to perform cell fractionation to target proteins from specific cell compartments and also to reduce the number of proteins present in the extracts prior to affinity purification. Additional trials should be performed on protein extracts from cell fractions, by trying other purification conditions and using the MAPs synthesized for our GFP-Trap to link IN2 rather than nanobodies.



### 5.2.3 Vismiones: Antimalarial Prenylated Anthranoids

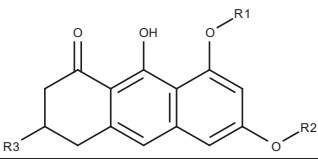
Anthranoids are tricyclic phenolic compounds produced in various plant such as Rhamnaceae, Polygonaceae, Hypericaceae family and also fungi belonging *Cortinarius*, *Dermocybe* genera (Westendorf, 1993; Gill, 2001). Among the anthranoids, vismiones represent a family of compounds characterized by a prenyl moiety, which derives from the metabolism of isoprenoids. These molecules have been characterized for their antibacterial, antiviral, antifungal and antimalarial properties (Botta et al., 1986; Galle, 2015; Sass et al., 2019). For this reason, a series of synthetic vismiones and analogues have been tested on *P. falciparum* and *Leishmania donovani* by the C. Vonthon-Sénécheau team (LIT) (Galle, 2015; Wasser, 2018). Their work confirmed the antimalarial and antileishmanial activities of these compounds. However, the biological targets involved in the observed antiprotozoal activity were not characterized. One hypothesis put forward was that vismiones could interfere *via* their prenyl moiety within the metabolism of isoprenoids. That is why a previous screen was performed with the acetyl vismiones D (AVD) on the model of BY-2 cells expressing GFP-CVIL. As a result, a particular phenotype of fluorescence in punctated structures and cytosol has been noticed (Hartmann et al., 2015).

In order to confirm these first results and to study the structure-activity relationship on protein prenylation inhibition, further experiments were performed with a series containing AVD, vismione D (VD), VH and 9 synthetic dihydroanthracenone analogs (**Table 15**).

A preliminary test showed that the synthetic compounds at the concentration tested had no effect on GFP-CVIL prenylation, but the phenotype associated to AVD treatment in previous study was also observed with VD and particularly with VH (**Figure 99**). Because anthranoids are autofluorescent compounds, the signal we observed could be associated to vismiones used to treat cells rather than that of expressed GFP-CVIL emission. Thus, control experiments using BY-2 cells treated by VH, VD or AVD without induction of the GFP-CVIL protein were performed and confirmed our hypothesis (**Figure 99**). Unfortunately, the fluorescence induced by vismiones treatment was found in both GFP and RFP channels being therefore undistinguishable under our setup. With this respect, how could we conclude on the effect of vismiones on protein prenylation? Is there any solution to unambiguously discriminate GFP and RFP fluorescent markers from the vismiones?

**Table 15 Structure and antiprotozoal activity of vismiones and synthetic anthranoids used in the GFP-CVIL prenylation inhibition assay.**

Synthetic and natural anthranoids IC<sub>50</sub> were determined on axenic amastigot cultures of *L. donovani* by estimation of cell viability using resazurin test (n = 1 synthetic, n = 2 natural compounds) (Galle, 2015; Wasser, 2018). Vismiones IC<sub>50</sub> was also evaluated on intraerythrocytic chloroquine-resistant *P. falciparum* K1 or sensible 3D7 strain by incorporation of tritied hypoxanthine (n=2) or pLDH assay respectively (Galle, 2015). Cytotoxicity tests were performed on rat skeletal muscle cells L6 and used to determine selectivity index (SI). References: anti-*Leishmania* activity, miltefosine IC<sub>50</sub> = 232 nM. Antimalarial activity, chloroquine IC<sub>50</sub> = 0.15 μM; cytotoxicity: podophyllotoxine IC<sub>50</sub>(L6) = 15.7 nM for *L. donovani* and 19 nM for *P. falciparum* assays.

							
Synthetic	R1	R2	R3	<i>L. donovani</i> IC <sub>50</sub> (μM)	IS <i>L. donovani</i> / L6	<i>P. falciparum</i> K1 and 3D7 strain* IC <sub>50</sub> (μM)	IS <i>P. falciparum</i> K1 / L6
NW 211 01	H	H	OH	11.58	16.965		
NW 184 01	H	Dimethylallyl	OH	0.01	401.445		
NW 0182 01	H	Me	OH	1.01	19.874		
NW 0129 01	H	Me	(CH <sub>3</sub> ) <sub>2</sub>	0.51	13.492		
NW 0186 01	H	PEG3	OH	2.8	43.398		
NW 0124 01	H	Dimethylallyl	(CH <sub>3</sub> ) <sub>2</sub>	0.34	13.954		
NW 0188 01	H	Geranyl	OH	0.072	38.252		
<b>Vismiones (Natural)</b>							
VH	H	Dimethylallyl	O(Ac)Me	0.06	15	1.78 / 18.4*	0.48
VD	H	Geranyl	(OH)Me	0.084	10	1.03	0.83
AVD	H	Geranyl	O(Ac)Me	0.09	6	0.72 / 3.2*	1.26

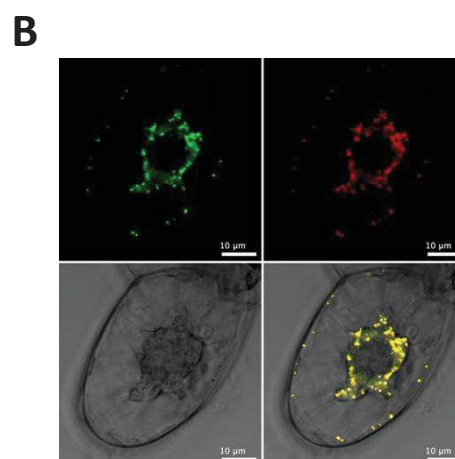
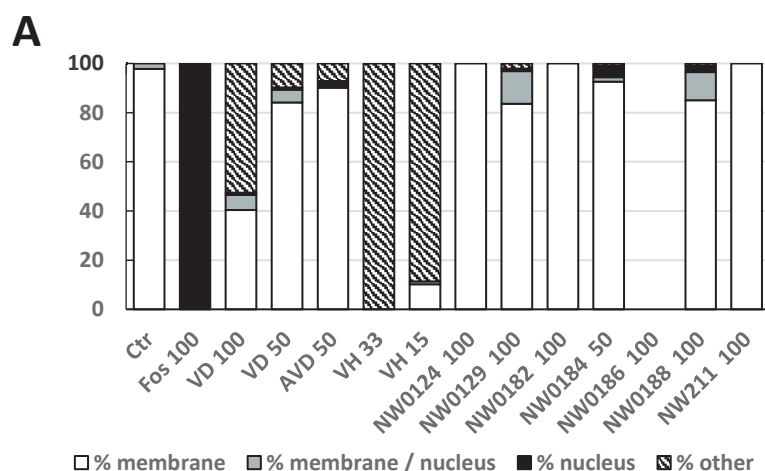


**Figure 99 Phenotypes observed in vismiones treated BY-2 cells expressing GFP-CVIL.**

(A) percentage of cells according to the localization of GFP-CVIL in BY-2 cells treated or not with natural and synthetic anthranoids at concentration ranging from 15 to 100 μM. Other phenotype corresponds to a GFP fluorescence localized in punctated structure or cytoplasm of cells. (B) Fluorescence signal observed by confocal microscopy in BY-2 cells treated with 33 μM VH. GFP fluorescence channel 500 to 550 nm (up left), RFP fluorescence channel 600 to 700 nm (up right), DIC view (down right), merged channel (down right)

Accordingly, a spectral imaging (SI) method was adapted and used to characterize the fluorescence of vismiones in BY-2 cells while unmixing it from the fluorescence of other markers such as GFP (**Figure 100**). This discrimination method was developed in the **section 6**, it confirmed that the autofluorescence of vismiones and related metabolites is responsible for the phenotype observed and has nothing to do with an interference with protein prenylation (**Figure 100**).

Unexpectedly this analysis also revealed that among cells treated with VH, many exhibited VH-fluorescence were devoid of a GFP signal when induced with DEX (**Figure 101**). This observation suggests that VH may interfere with the transcriptional DEX induction system or alternatively with protein translation blocking the production of GFP. Thus, these hypotheses were evaluated using Rt-qPCR of GFP-CVIL RNA and a western blot of the GFP-CVIL protein (**Figure 102**). As a result, the Rt-qPCR of GFP-CVIL RNA from BY-2 cells treated with 15  $\mu$ M VH, AVD, NW0184 did not show any significant influence of anthranoids on GFP-CVIL transcripts (**Figure 102**). At the opposite, the western blot of immunoprecipitated GFP-CVIL from BY-2 cells treated with 5, 10 and 25  $\mu$ M VH evidenced the absence of GFP-CVIL in protein extracts at all VH concentration but not in FOS-treated cells (**Figure 102**). In this respect, our result suggests that vismiones does not affect the transcription but more likely impact the translation or at least a post-transcriptional stage. Still, these experiments have been done a single time and have to be reproduced.

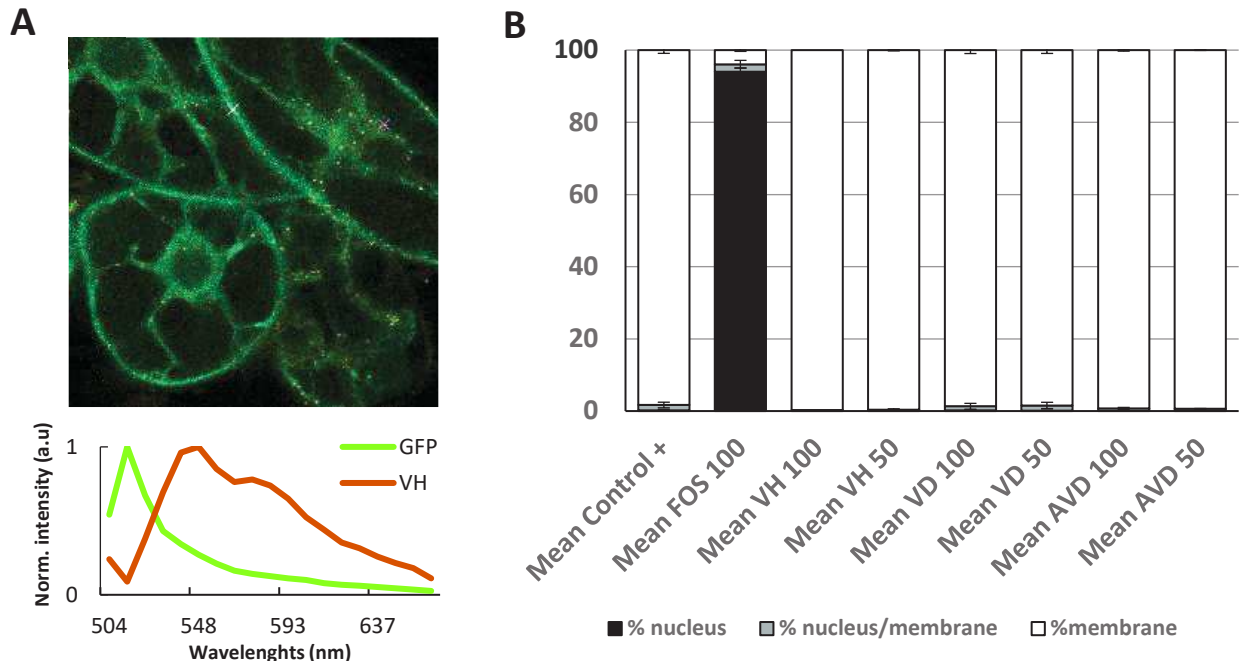


**Figure 100 Vismiones does not inhibit the prenylation of GFP-CVIL in BY-2 cells.**

(A) BY-2 VH-treated cells expressing GFP-CVIL observed by spectral imaging method at  $\lambda_{488}$  settings (up), spectra collected in the membrane (green) and in punctated structure (orange). (B) Percentage of cells according to GFP-CVIL signal in BY-2 cells treated or not with vismione H (VH), vismione D (VD) and acétylvismione D (AVD) at 50 and 100  $\mu\text{M}$  prior to observation by confocal microscopy.

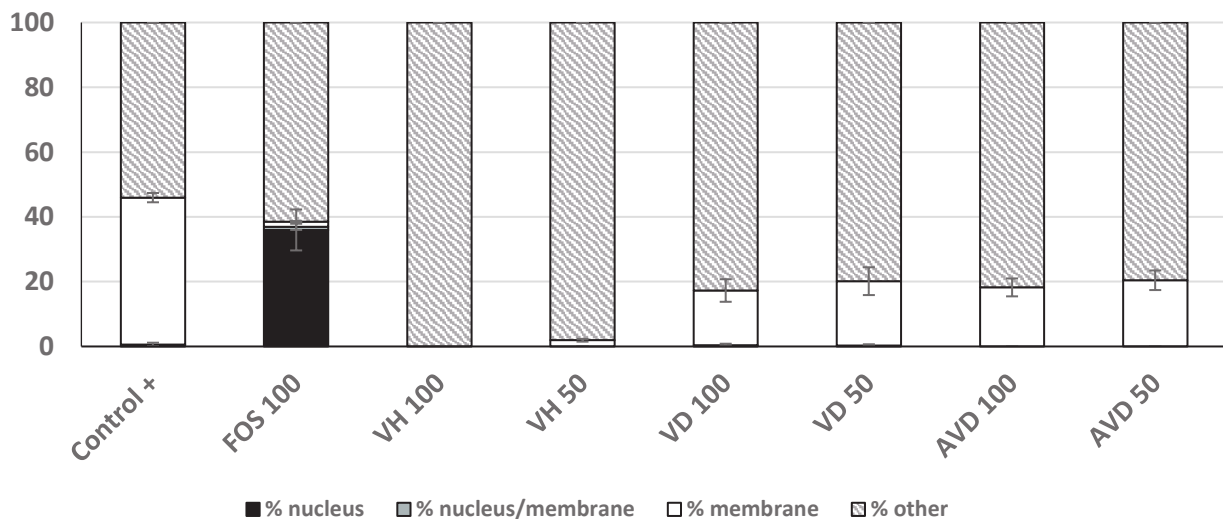


**Figure 101 Vismiones decrease GFP-labelled cells.**

Percentage of cells with GFP-CVIL signal according to its localization in the nucleus (black), in the nucleus and the membrane (grey), in the membrane (white) and non GFP fluorescence signal (hatched) in BY-2 cells treated or not with vismiones at 50 and 100  $\mu\text{M}$  and observed by spectral imaging

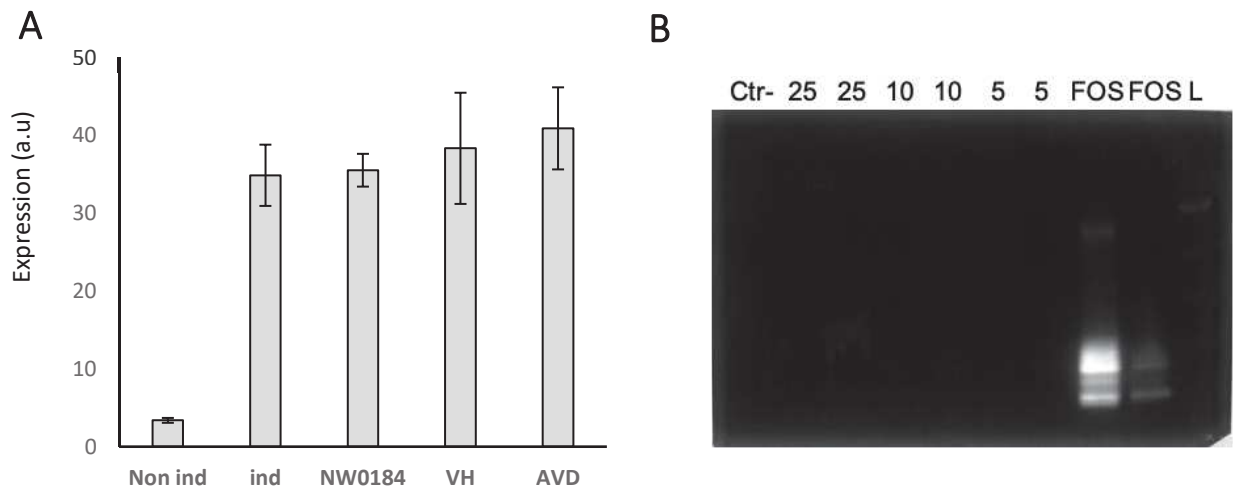


**Figure 102 Vismiones does affect the translation of GFP-CVIL but not transcription.**

(A) Expression level of GFP-CVIL measured by Rt-qPCR analysis of BY-2 cells treated without induction of GFP-CVIL (Ctr-), induced 18h with 30  $\mu$ M dexamethasone (ind) or treated with 15  $\mu$ M NW0184, vismione H (VH) or acetylvismione D (AVD) 3h before induction. (B) Western blot analysis of GFP-CVIL immunoprecipitated with GFP-Trap v2 from BY-2 cells treated with 5, 10 and 25  $\mu$ M of VH or 100  $\mu$ M fosmidomycin (FOS) prior to induction of the GFP-CVIL. The latter was immunostained by IgG @GFP-CaaX and revealed using LumiPhos (Pierce™).





## 5.3 APPLICATION OF PROTEIN PRENYLATION INHIBITION IN METABOLITE ENGINEERING

### 5.3.1 Elicitation and Inhibition of Protein Prenylation

In plants, the inhibition of protein prenylation down-regulates the biosynthesis of some specialized metabolites such as MIAs in *Catharanthus roseus* or capsidiol in *N. tabacum* (Courdavault et al., 2009; Huchelmann et al., 2014; Kumar et al., 2020). Moreover, cellulase induces HMGR activity in elicited tobacco leaves improving MVA biosynthesis needed for the capsidiol production (Huchelmann et al., 2014). But, in the presence of *S*-carvone, an inhibitor of protein prenylation, capsidiol is not further produced, while HMGR is still very active (Huchelmann et al., 2014). Thus, we were interested in investigating how the tobacco leaf uses this MVA pool produced in elicited conditions and whether this type of strategy can be used to control fluxes of isoprenoid precursor for the biosynthesis of other metabolites.

Preliminary experiments performed in the team revealed some differences in carotenoid profiles observed in unsaponifiable fractions isolated from young leaves SH6 *N. tabacum* lines treated with 0.5% cellulase, 2 mM *S*-carvone and 1mM MVA (**Figure 103**). Moreover, feeding experiments with [<sup>14</sup>C]MVA have shown that after separation of unsaponifiable on TLC, under those conditions, accumulation of radioactivity was detected in a product whose R<sub>f</sub> = 0.9 comigrating with yellow-orange carotenoids on TLC under white light (**Figure 103**). This experiment was reproduced by A. Lipko and a purification of the retardation factor R<sub>f</sub> = 0.9 spot by semi-preparative TLC followed by HPLC-UV-MS analysis showed that molecules were copurified under these conditions including carotenoids detected at 470 nm (**Figure 104**). Among the carotenoids, the main compound detected at 470 nm has a *m/z* = 567 being close to that of carotenoids containing endoperoxide group, such as the β-carotene-5.8 endoperoxide with a *m/z* = 569 (**Figure 104**). These carotenoids are synthesized in plants in response to light stress (Fiedor et al., 2005; Ramel et al., 2012).

We aimed to pursue these studies in order to identify the carotenoid structure by NMR. However, a relocation of the laboratory has been carried out inducing changes in the growth chamber and notably the type of light used. Of note, it has been shown that light plays a key role in the regulation of isoprenoid pathways as well as in the protein prenylation.

Actually, the *A. thaliana era1* mutant, lacking of PFT activity, exhibit a stronger phenotype if grown under red light as compared to blue light (Rodríguez-Concepción et al., 2004; Jalakas et al., 2017; Chenge-Espinosa et al., 2018).

Furthermore, MVA was reported to influence the carotenoids biosynthesis, but its role within this process remains unclear. On one hand, it could be converted into IPP and undergoes chloroplasts for carotenoids biosynthesis, on the other hand it could act as a regulator of MEP pathway. Since tobacco lines expressing GFP-sensor have been engineered and are now part of our toolbox to study MEP/MVA crosstalk for protein prenylation, further studies may be performed with these lines too. In this context, we had to be sure that GFP-sensor T-DNA insert does not influence the plant response to treatment as compared to SH6 WT. Finally, the enantiomers of terpenes can have different biological activities such as carvone and other monoterpenes with their odor or spasmolytic activity in animals. Similarly, it has been shown that strigolactone synthetic enantiomers interact with distinct plant receptors indeed (Friedman and Miller, 1971; Sousa et al., 2008; Scaffidi et al., 2014).

For these reasons, the experiments were pursued and completed by considering other factors such as light, the plant genotype or the *R*-carvone enantiomer. We investigated a total of 60 conditions to evaluate how both enantiomers and light affect the biosynthesis of carotenoids and other metabolites, in four SH6 tobacco plant lines elicited with cellulase and fed or not with additional MVA.

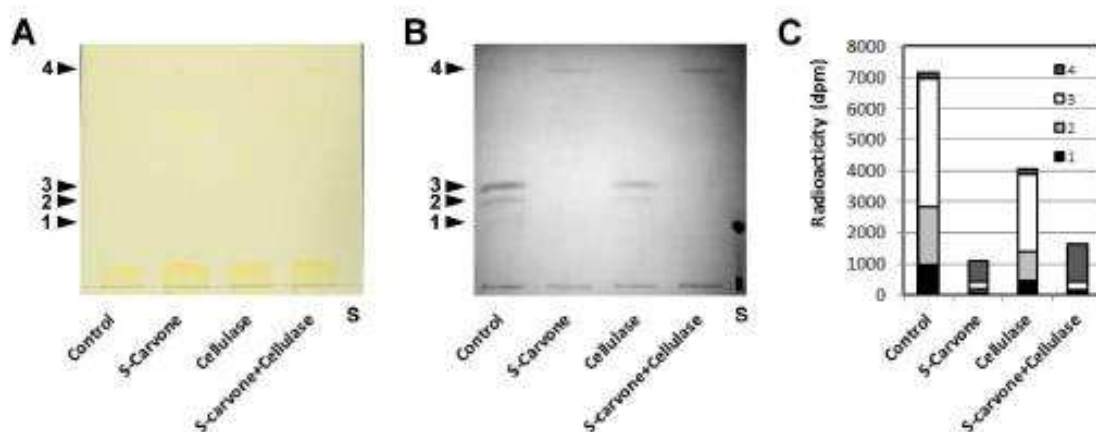


**Figure 103 De novo synthesis of MVA-derived lipids in *S*-carvone treated leaf discs.**

Leaf-discs were incubated with [ $^{14}$ C]MVA (1  $\mu$ Ci) for 6h and floating either on H<sub>2</sub>O alone (Control) or supplemented with 0.5 % cellulase and/or 2 mM *S*-carvone. After lipid extraction, saponified products were separated on a TLC plate and radioactivity in the four major bands (1-4) were measured by scintillation counting. S corresponds to a radioactive phytosterol standard. These incorporation rates indicate de novo synthesis of MVA-derived isoprenoid metabolites under the various conditions. (A) Photography of carotenoids (yellow) on the TLC plate after 2 runs in CH<sub>2</sub>Cl<sub>2</sub>. (B) Autoradiography of the TLC plate illustrated in A. Quantification in dpm of the radioactivity found in each band as indicated in A and B (band 1: black, band 2: light grey, band 3: white and band 4: dark grey).

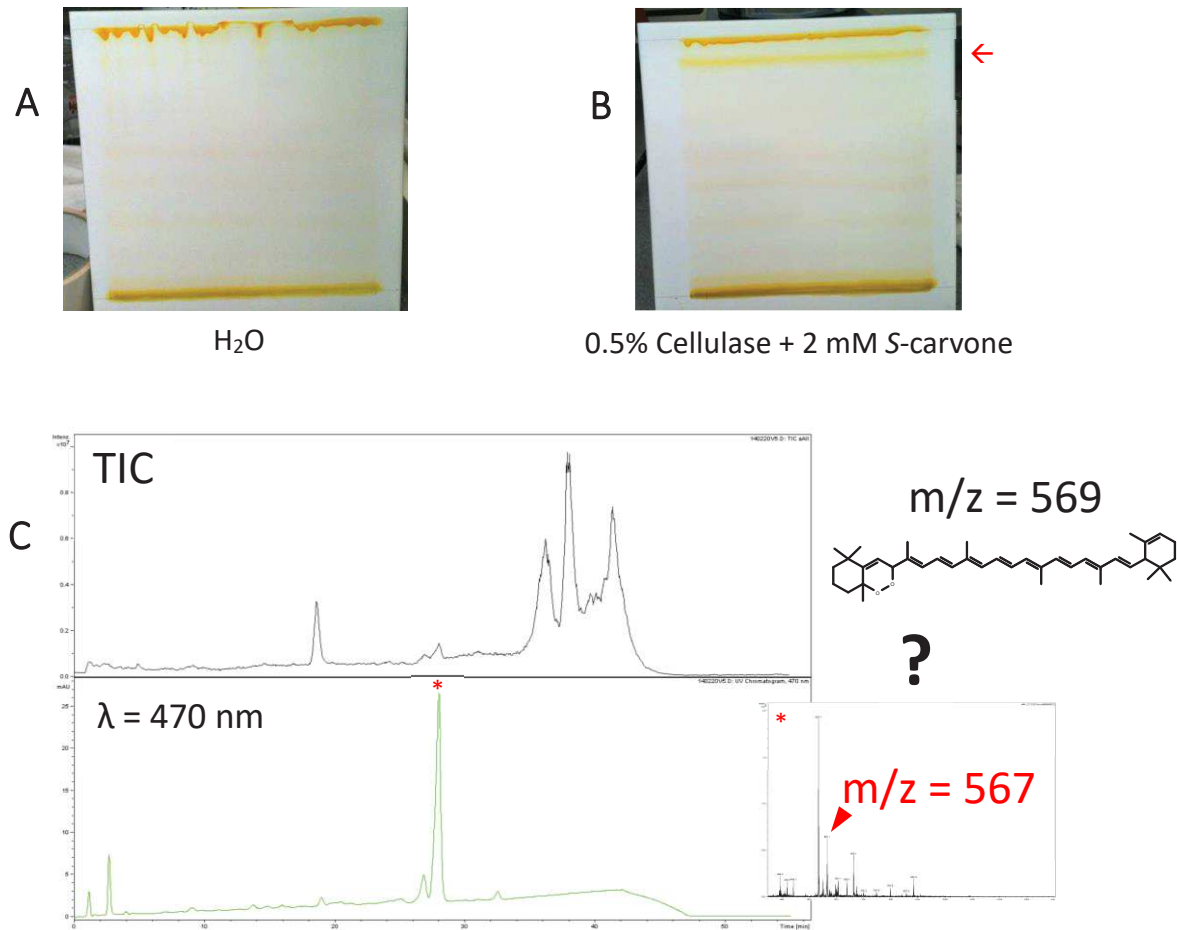


**Figure 104** *De novo* synthesis of a putative carotenoid containing endoperoxide in S-carvone treated leaf discs. Leaf-discs from young leaves were incubated with floating either on (A) H<sub>2</sub>O alone or (B) supplemented with 0.5 % cellulase and 2 mM S-carvone. The bands at R<sub>f</sub> = 0.9 (←) was scrapped and analyzed by HPLC-UV-MS with UV (C). The TIC (up) was compared to UV chromatogram at excitation wavelength λ = 470 nm (down) and MS spectrum of the main peak detected at 470 nm (\*). A m/z = 567 was detected and associated to a putative carotenoid containing endoperoxide such as β-carotene-5,8-endoperoxide with a m/z = 569. These compounds are reported to be produced after photosensitized oxidation of β-carotene solutions by O<sub>2</sub> (Montenegro et al., 2002) or found in plant leaves in response to light stress (Ramel et al., 2012a, 2013b)

### 5.3.2 Analysis of Metabolites from Tobacco Leaves

To increase resolution of TLC, a HPTLC analysis of unsaponifiable fractions isolated from the tobacco leaf discs was applied. HPTLC plates were visualized at 254 nm, 365 nm and after treatment with vanillin sulfuric acid reagent. Actually, several aromatic compounds such as alkaloids or simple phenol absorb at 254 nm, while polyphenols such as coumarins, flavones, anthocyanins usually fluoresce under excitation at 365 nm. In contrast, vanillin sulfuric acid reagent is a common revelator allowing detection and discrimination of non-fluorescent terpenes (Wagner et al., 1984). As a result, this combination enables the analysis of compounds among alkaloids, polyphenols and terpenes family. All tobacco lines tested behaves identical for the production of metabolites. However, light quality and metabolite treatments revealed some striking differences in the profiles (**Figure 105, Table 16**).

Carotenoids emerging as yellow orange bands under white light with retardation factor ( $R_f$ ) > 0.4 vary only slightly depending on the type of light used to grow plants (**Figure 105**). Interestingly, two intense yellow orange spots with  $R_f = 0.04$  and  $0.06$  are present only if the tobacco grew under blue light conditions. These molecules probably correspond to more polar carotenoids and have not been observed in the preliminary studies with plants grown under red light. Other light-dependent variations were observed for molecules detected at 365 nm or after use of vanillin sulfuric acid reagent. For example, the intensity of a purple spot visible only after vanillin sulfuric acid development with a  $R_f = 0.52$  is decreased in blue light and becomes barely visible in the greenhouse condition. It is interesting to note that the profiles observed in the greenhouse conditions are slightly different from those obtained in the blue and red light. Thus, the effect produced by sunlight on the plant would not be simply the addition of the blue-light and red-light alone effects, but another effect inducing a different behavior of the plant. This could be explained by the presence of UV-B in the sunlight, which was reported as an inducer of specialized metabolites biosynthesis against plant growth. Accordingly, these metabolites reduced in the greenhouse conditions and revealed by the vanillin sulfuric acid may corresponds to primary metabolites (Mewis et al., 2012).

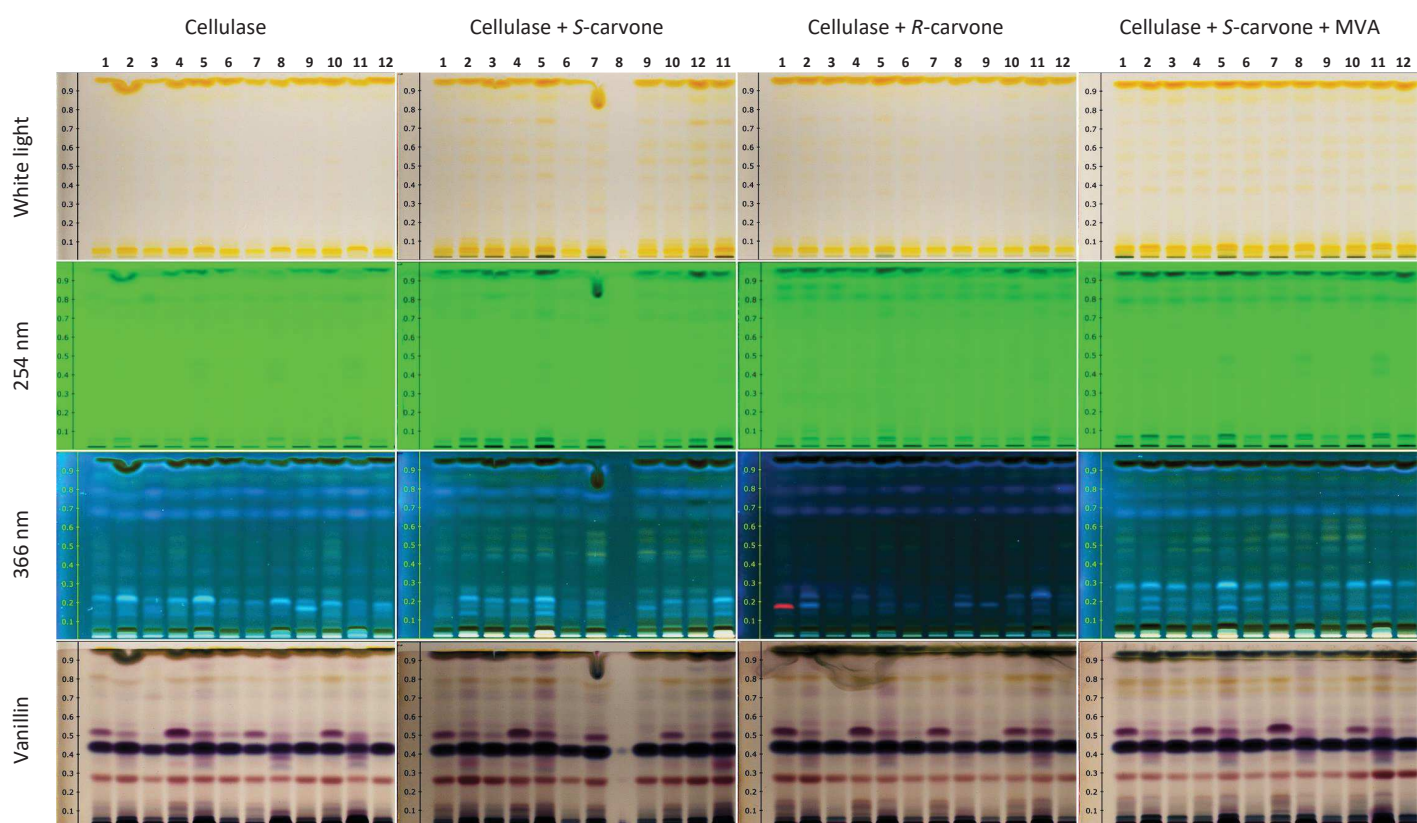


**Figure 105 Influence of light and inhibitor of protein prenylation on tobacco leaf metabolite profiles.**

HPTLC plates of the unsaponifiable fractions obtained from leaf discs punched in plants cultivated under red light (1, 4, 7, 10), blue light (2, 5, 8, 11) and in the greenhouse (3, 4, 9, 12) prior to treatments with cellulase alone (1<sup>st</sup> column) or supplemented with S-carvone (2<sup>nd</sup> column), R-carvone (3<sup>rd</sup> column) or both S-carvone and MVA (4<sup>th</sup> column). The TLC plates were chromatographed two times in CH<sub>2</sub>Cl<sub>2</sub> before their visualization under white light (1<sup>st</sup> row), at 254 nm (2<sup>nd</sup> row), 365 nm (3<sup>rd</sup> row) and after revelation using vanillin sulfuric reagent (4<sup>th</sup> row)

Regarding the impact of the treatments used on the metabolite's profiles, we found that cellulase alone has few effects on the content of carotenoids and other molecules observed on HPTLC plates. Nevertheless, cellulase combined to *S*-carvone or *R*-carvone treatment highly increases the content of all carotenoids, and even more with the addition of MVA to *S*-carvone (**Figure 105**). Moreover, two carotenoids at  $R_f = 0.27$  and  $0.37$  differ between *S*-carvone and *R*-carvone treatments alone. Surprisingly, feeding with MVA of *S*-carvone treated leaf discs induced changes of the carotenoid with a  $R_f = 0.27$  into the carotenoid with a  $R_f = 0.37$ , resulting in a carotenoid profile similar to the fractions from *R*-carvone treated leaf discs. The biosynthesis of carotenoids from the MVA pathway has been described for Gram-positive bacteria. But, the latter is not compartmentalized as in plants, in which the phytoene is produced from the plastidial MEP pathway derived GGPP pool (Ruiz-Sola and Rodríguez-Concepción, 2012; Hagi et al., 2015). Our results showed that the MVA can contribute to the biosynthesis of carotenoids or at least their regulation in plant elicited by cellulase and inhibited by *S*-carvone. These results are consistent with previous reports, in which light influenced carotenoids biosynthesis and MVA was able to restore the lack of MEP precursors for chloroplast and etioplast development (Nagata et al., 2002; Rodríguez-Concepción et al., 2004; Lichtenthaler, 2007). Nonetheless, control condition with MVA alone has to be performed to make such relation between MVA reversion of *S*-carvone-inhibited protein prenylation and carotenoids produced.

**Table 16 Overview of metabolites from tobacco leaves influenced by light and/or protein prenylation inhibition.** Retardation factor ( $R_f$ ) of some spots after HPTLC of unsaponifiable fraction from tobacco leaf resolved in two times in  $\text{CH}_2\text{Cl}_2$ . The colors correspond to the detection mode used, white light (**yellow**), 365 nm (**blue**), acidic vanillin sulphuric acid (**pink**). Spots which vary depending on the treatments have been highlighted in bold.

	Ctr	Cellulase	Cellulase + S-Carv	Cellulase + R-Carv	Cellulase + S-Carv + MVA
Blue light	0.04 <sup>++</sup> ; 0.06 <sup>++</sup>	0.04 <sup>++</sup> ; 0.06 <sup>++</sup> ; <b>0.9<sup>±</sup></b>	0.04 <sup>++</sup> ; 0.06 <sup>++</sup> ; <b>0.27<sup>+</sup></b> ; <b>0.9<sup>++</sup></b>	0.04 <sup>++</sup> ; 0.06 <sup>++</sup> ; <b>0.37<sup>+</sup></b> ; <b>0.9<sup>±</sup></b>	0.04 <sup>++</sup> ; 0.05 <sup>++</sup> ; <b>0.37<sup>+</sup></b> ; <b>0.86<sup>++</sup></b>
	0.13 <sup>++</sup> ; 0.22 <sup>++</sup>	0.13 <sup>++</sup> ; 0.22 <sup>++</sup>	0.13 <sup>++</sup> ; 0.22 <sup>++</sup> ; <b>0.28<sup>+</sup></b>	0.13 <sup>++</sup> ; 0.22 <sup>++</sup>	0.13 <sup>++</sup> ; 0.22 <sup>++</sup> ; <b>0.28<sup>+</sup></b>
	0.52 <sup>+</sup> ; 0.33 <sup>+</sup>	0.52 <sup>+</sup> ; <b>0.37<sup>++</sup></b> ; 0.33 <sup>+</sup>	0.52 <sup>+</sup> ; 0.33 <sup>+</sup>	0.52 <sup>+</sup> ; 0.33 <sup>+</sup>	0.52 <sup>+</sup> ; <b>0.79<sup>+</sup></b> ; 0.33 <sup>+</sup>
Red light	0.05 <sup>++</sup>	0.05 <sup>++</sup> ; <b>0.9<sup>±</sup></b>	<b>0.27<sup>+</sup></b> ; 0.05 <sup>++</sup> ; <b>0.9<sup>++</sup></b>	<b>0.37<sup>+</sup></b> ; 0.05 <sup>++</sup> ; <b>0.9<sup>±</sup></b>	<b>0.37<sup>+</sup></b> ; 0.05 <sup>++</sup> ; <b>0.9<sup>++</sup></b>
	0.13 <sup>+</sup>	0.13 <sup>+</sup>	0.13 <sup>+</sup>	0.13 <sup>±</sup>	<b>0.28<sup>+</sup></b> ; 0.13 <sup>+</sup>
	0.52 <sup>++</sup> ; 0.04 <sup>±</sup>	0.52 <sup>++</sup> ; 0.04 <sup>+</sup>	0.52 <sup>++</sup> ; 0.04 <sup>++</sup>	0.52 <sup>++</sup> ; 0.04 <sup>++</sup>	0.52 <sup>++</sup> ; 0.04 <sup>+</sup> ; <b>0.79<sup>+</sup></b>
Greenhouse	0.05 <sup>++</sup>	0.05 <sup>++</sup> ; <b>0.9<sup>±</sup></b>	<b>0.27<sup>+</sup></b> ; 0.05 <sup>++</sup> ; <b>0.9<sup>++</sup></b>	<b>0.37<sup>+</sup></b> ; 0.05 <sup>++</sup> ; <b>0.9<sup>±</sup></b>	<b>0.37<sup>+</sup></b> ; 0.05 <sup>++</sup> ; <b>0.9<sup>++</sup></b>
					<b>0.28<sup>+</sup></b>
	0.52 <sup>±</sup> ; 0.04 <sup>±</sup>	0.52 <sup>±</sup> ; 0.04 <sup>±</sup>	0.52 <sup>±</sup> ; 0.04 <sup>±</sup>	0.52 <sup>±</sup> ; 0.04 <sup>±</sup>	0.52 <sup>±</sup> ; 0.04 <sup>±</sup> ; <b>0.79<sup>+</sup></b>

<sup>±</sup> barely visible; <sup>+</sup> low intensity; <sup>++</sup> high intensity

Furthermore, aromatic compounds follow the same trend than carotenoids such as a metabolite with  $R_f = 0.88$  observed at 254 nm or with  $R_f = 0.29$  at 365 nm (**Figure 105, Table 16**). The differences between profile observed in extracts from leaf discs treated with *S*-carvone and *R*-carvone support the hypothesis of a plant response adapted to the stereochemistry of carvones as reported for strigolactone, which by the way is a  $\beta$ -carotene catabolite (Scaffidi et al., 2014). With this respect, it would be interesting to compare MVA with *R*-carvone to MVA and *S*-carvone treatments. If differences occur this approach would be suitable for specific production of carotenoids using stereoselectivity of protein prenylation inhibitors.

Next, in order to control whether the protein prenylation or stereospecific response from plant to each enantiomer are responsible of the profile observed, we also analyzed by GC-EI-MS the capsidiol and other metabolites from the culture medium of treated leaf discs.



### 5.3.3 Analysis of Metabolites from the Culture Medium

Hexane extracts were isolated from the 60-culture media and were analyzed by GC-EI-MS. The GC-EI-MS chromatograms of the hexane extracts showed little differences between genotypes or light as compared to the treatments used (**Figure 106-Figure 109**,

**Table 17**). Capsidiol was identified according to its MS spectrum and despite detection of traces in some samples of *S*- and *R*-carvone conditions, it was significantly detected at 14.65 min only in extracts from the culture media of leaves treated with cellulase and confirm that like the *S*-carvone, the *R*-carvone inhibits the protein prenylation (**Figure 109**). Interestingly, MVA did not restore *S*-carvone-inhibited capsidiol production, whereas MVA does restore protein prenylation in our BY-2 GFP-CVIL model. These results confirmed that the *S*-carvone doesn't inhibit protein prenylation like FOS as reported (Huchelmann et al., 2014), but also suggest that the inhibition of capsidiol production by *S*-carvone is not directly dependent of protein. Furthermore, by observing the differences between the type of light used for plant growth, only blue light seems to increase the content of metabolites found in the culture medium extracts (**Figure 106**). Therefore, some molecules detected between 16 and 16.5 min are present only with blue light and the concentration of the molecule 12 with  $R_t = 17.64$  min is significantly increased as compared to the red light (**Figure 107**, **Figure 108**). The blue light has been reported to inhibit the plant growth to promote the production of specialized metabolites as illustrated by the increase of artemisinin production in *Artemisia annua* overexpressing CRY1 Arabidopsis blue light receptor (Hong et al., 2009).

However, as capsidiol, the highest differences were observed when elicitation and treatment with carvones and/or MVA were performed. For example, nicotine was identified at 8 min as compared to its reference and was significantly increased with cellulase combined or not to *S*-carvone and MVA. In contrast, the former was almost absent from the other conditions. Surprisingly, these results prove that the presence of nicotine in the medium is not due to the release of intracellular content following the cellulase treatment, but that both *S*-carvone and *R*-carvone would inhibit the biosynthesis or the excretion of nicotine induced by the presence of cellulase. In addition, the phenomenon seems to be slightly regulated by the light as shown by a significant decrease of nicotine in greenhouse plant treated with *S*-carvone and MVA or *vice-versa* for the cellulase alone.

**Table 17 Compounds detected in GC-EI-MS and influenced by treatments tested.**

Main molecules influenced by one or more conditions and detected in the GC-EI-MS analysis of hexane extracts from tobacco leaf disc culture media of which 60 conditions were evaluated

Name	Rt (min)	<i>m/z</i> (relative intensity)
1. Capsidiol	14.55	93.100 (100.00), 107.100 (91.07), 157.100 (81.28), 121.100 (64.70), 79.100 (61.09), 175.100 (60.56), 221.200 (56.25)
2. Nicotine	8.00	84.100 (100.00), 133.100 (39.87), 161.100 (21.14), 162.100 (19.40), 119.100 (9.34), 92.100 (6.12), 118.100 (6.08)
3	8.35	98.100 (100.00), 70.100 (35.67), 69.100 (33.20), 99.100 (5.25), 53.100 (4.68), 55.100 (4.33), 67.100 (4.28)
4	8.43	82.100 (100.00), 69.100 (27.43), 54.100 (26.65), 166.100 (14.10), 123.100 (12.66), 138.100 (11.92), 97.100 (9.71)
5	8.81	109.100 (100.00), 82.100 (50.84), 91.100 (48.87), 79.100 (43.80), 97.100 (34.82), 123.100 (25.25), 148.100 (10.00)
6	8.86	109.100 (100.00), 91.100 (41.54), 82.100 (37.49), 79.100 (35.85), 54.100 (25.68), 133.100 (10.82), 151.100 (7.16)
7	10.12	124.100 (100.00), 69.100 (92.60), 98.100 (89.62), 125.100 (58.78), 55.100 (27.15), 149.100 (9.50), 191.200 (4.09)
8	10.21	82.100 (100.00), 106.100 (84.74), 148.100 (62.11), 91.100 (54.98), 54.100 (49.54), 79.100 (32.43), 166.100 (3.87)
9	10.52	98.100 (100.00), 111.100 (82.25), 55.100 (54.83), 166.100 (52.65), 82.100 (38.58), 151.100 (37.93), 127.100 (31.57)
10	10.80	71.100 (100.00), 85.100 (99.26), 55.100 (84.34), 97.100 (77.11), 109.100 (44.12), 125.100 (31.91), 137.000 (17.44)
11	11.01	55.100 (100.00), 83.200 (96.22), 97.100 (89.33), 69.100 (83.89), 111.100 (45.77), 125.200 (15.55), 196.200 (3.28)
12	17.64	81.100 (100.00), 95.100 (65.77), 121.100 (58.62), 55.200 (50.58), 69.200 (48.30), 245.200 (19.30), 227.200 (11.74)
13	19.73	98.100 (100.00), 239.300 (62.92), 57.200 (60.16), 74.100 (57.64), 134.100 (48.58), 257.300 (22.87), 299.300 (9.82)
14	20.51	117.100 (100.00), 98.100 (57.64), 239.300 (52.48), 57.100 (52.45), 158.100 (38.67), 207.100 (22.78), 281.000 (12.76), 341.100 (5.59)
15	20.81	149.100 (100.00), 57.100 (42.13), 71.100 (20.24), 293.200 (17.83), 111.200 (7.03), 83.100 (5.52), 167.100 (5.45)
16	21.14	57.200 (100.00), 71.100 (77.30), 85.200 (55.32), 117.100 (28.73), 207.100 (20.27), 281.100 (11.63), 341.200 (9.54)
17	21.25	98.100 (100.00), 57.200 (63.13), 74.100 (57.13), 134.100 (50.12), 267.300 (39.02), 285.300 (16.86), 207.000 (16.73)

The cellulase also induced the biosynthesis or the excretion of the molecule 16 but in general, the presence of either carvones in the medium induced more changes than the elicitation alone (**Figure 109**). Thus, the content of molecules 3 to 10 detected between 8.3 and 11 min was significantly increased when leaves were treated with either or both *S*-carvone and MVA in contrast to *R*-carvone. Conversely, the molecule 13, 14 and 17 were significantly increased with *R*-carvone, unlike *S*-carvone and MVA treatment, which seem to inhibit their production or excretion in the culture medium. These results are consistent with hypotheses evidenced by the HPTLC analysis of *S*- and *R*-carvone treated leaf extracts and confirmed a stereospecific response of tobacco to carvone enantiomers (**Figure 105**). Unfortunately, in the absence of standard we could not identify varying metabolites.

The role of monoterpenes has been so far attributed to plant defense against herbivores, bacteria, fungi or insect attraction and repulsion (**section 0**). Consistent is the fact that variation of monoterpene content in several plants such as in *Salvia officinalis*, *Mentha x piperita* or *Pinus sp.* occurred during hydric, light and heat stress (Selmar and Kleinwächter, 2013). Nonetheless, is plant defense the only raison d'être of monoterpenes? Why do monoterpenes such as carvone,  $\alpha$ -pinene, limonene would be increased under abiotic stress? For that reason, it can be speculated that another role of monoterpenes might be the regulation of cell mechanism for development, differentiation and plant adaptation as well. Altogether, these results proved that plant metabolites content and notably carotenoids can be monitored by using protein prenylation inhibitors. With this respect, this study offers new perspectives in term of valuable metabolites production and shaded plant physiology aspects for further investigations. In our case, it would be necessary to repeat these experiments to strengthen our statistical tests by using ANOVA rather than a Kruskal-Wallis test to confirm all the observed differences. Also, purification and analysis by HPLC-UV-MS and NMR is now required to identify the carotenoids and other metabolites described in our study in order to better understand the metabolic origin of the observed changes. Although we observed changes with MVA, it remains unclear if MVA is used as precursor for the biosynthesis of carotenoids or if it acts as a regulator of the MEP pathway *via* prenylated proteins.

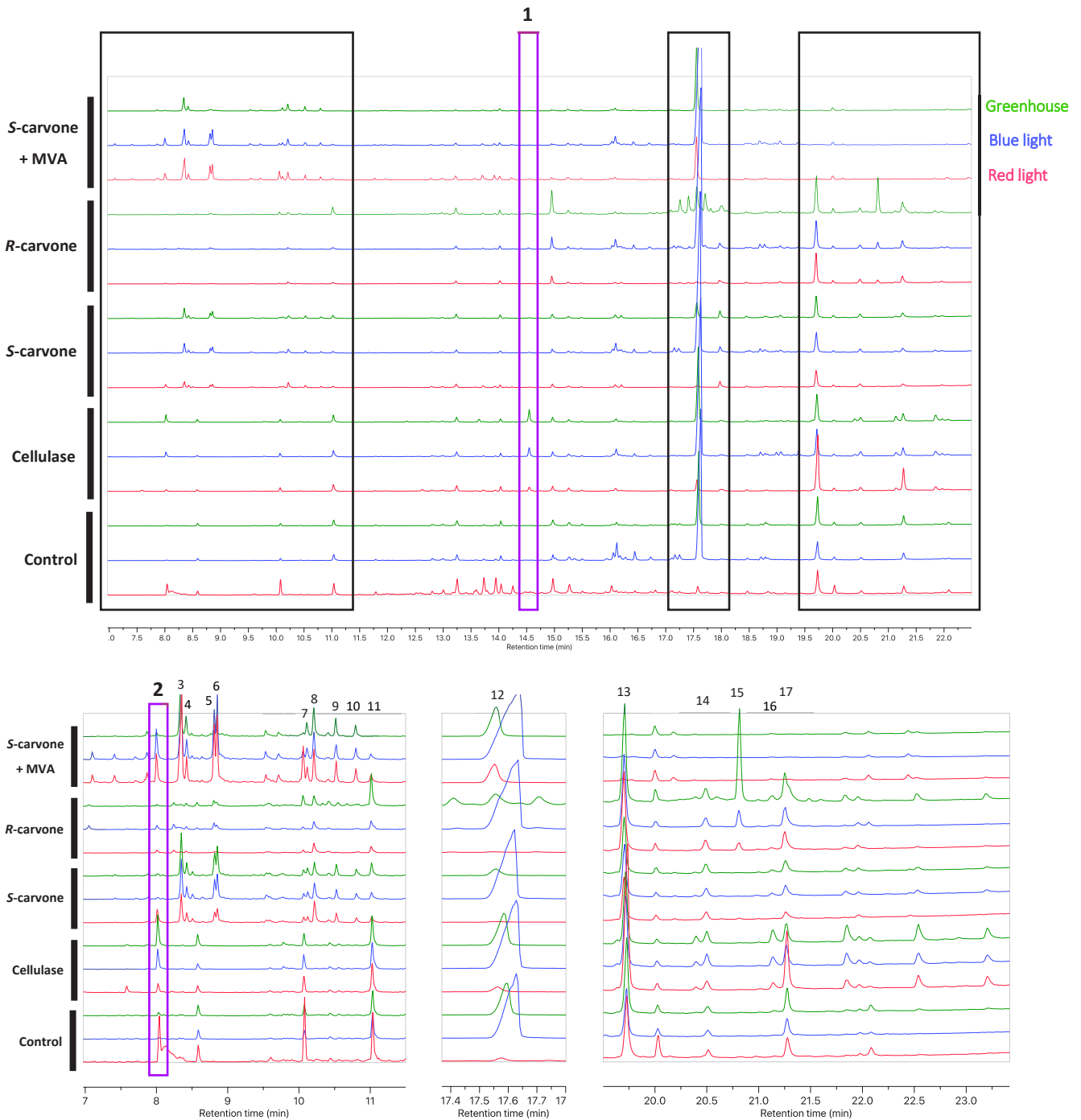


**Figure 106 Protein prenylation inhibition and MVA complementation induce changes in metabolites from tobacco leaves culture media.**

Stacked GC-EI-MS chromatograms of hexane extracts from the culture media of tobacco leaf discs punched on plants cultivated under red light (red), blue light (blue), greenhouse (green). Leaf discs were floated on 50  $\mu$ M  $\text{KH}_2\text{PO}_4$ , elicited with 0.5 % cellulase alone or supplemented with 2 mM *S*-carvone, *R*-carvone or both 2 mM *S*-carvone and 1 mM MVA. Global view (up) and zoom on area in which the molecules 1 to 17 were highly influenced by treatments (down).

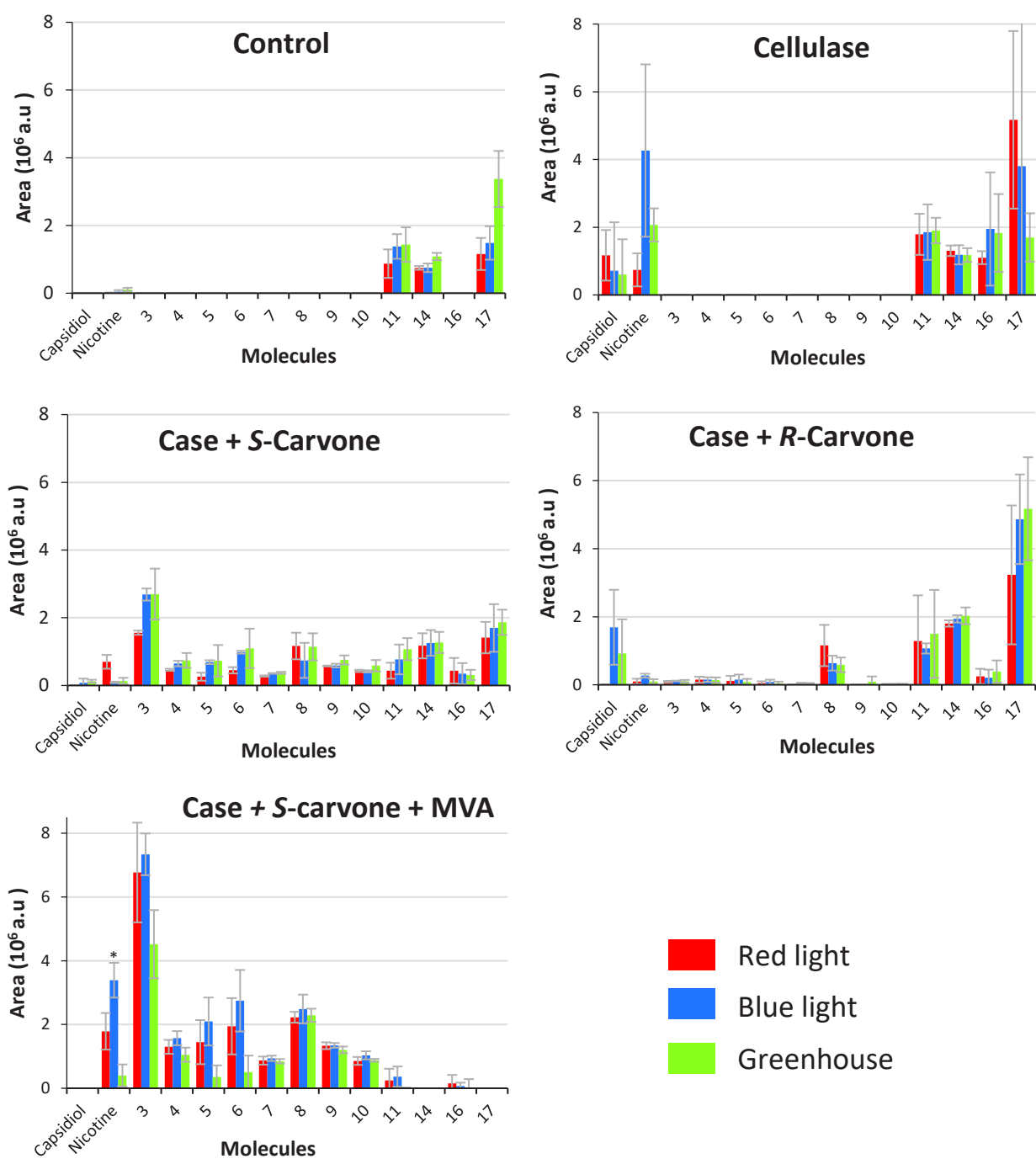


**Figure 107 Light does not affect most metabolites found in culture medium after treatments.**

Relative quantification of area under peaks of low abundant molecules (Area <  $10 \cdot 10^6$  in at least one condition) 1 to 11, 14, 16 and 17 detected by GC-EI-MS analysis of culture media from tobacco leaf discs punched on plants cultivated under red light (red), blue light (blue), greenhouse (green). Leaf discs were floated on  $50 \mu\text{M}$   $\text{KH}_2\text{PO}_4$ , elicited with 0.5 % cellulase alone or supplemented with 2 mM *S*-carvone, *R*-carvone or both 2 mM *S*-carvone and 1 mM MVA. \* p-value < 0.05 at the Kruskal-Wallis test followed by Dunnett post-hoc test (n=3)

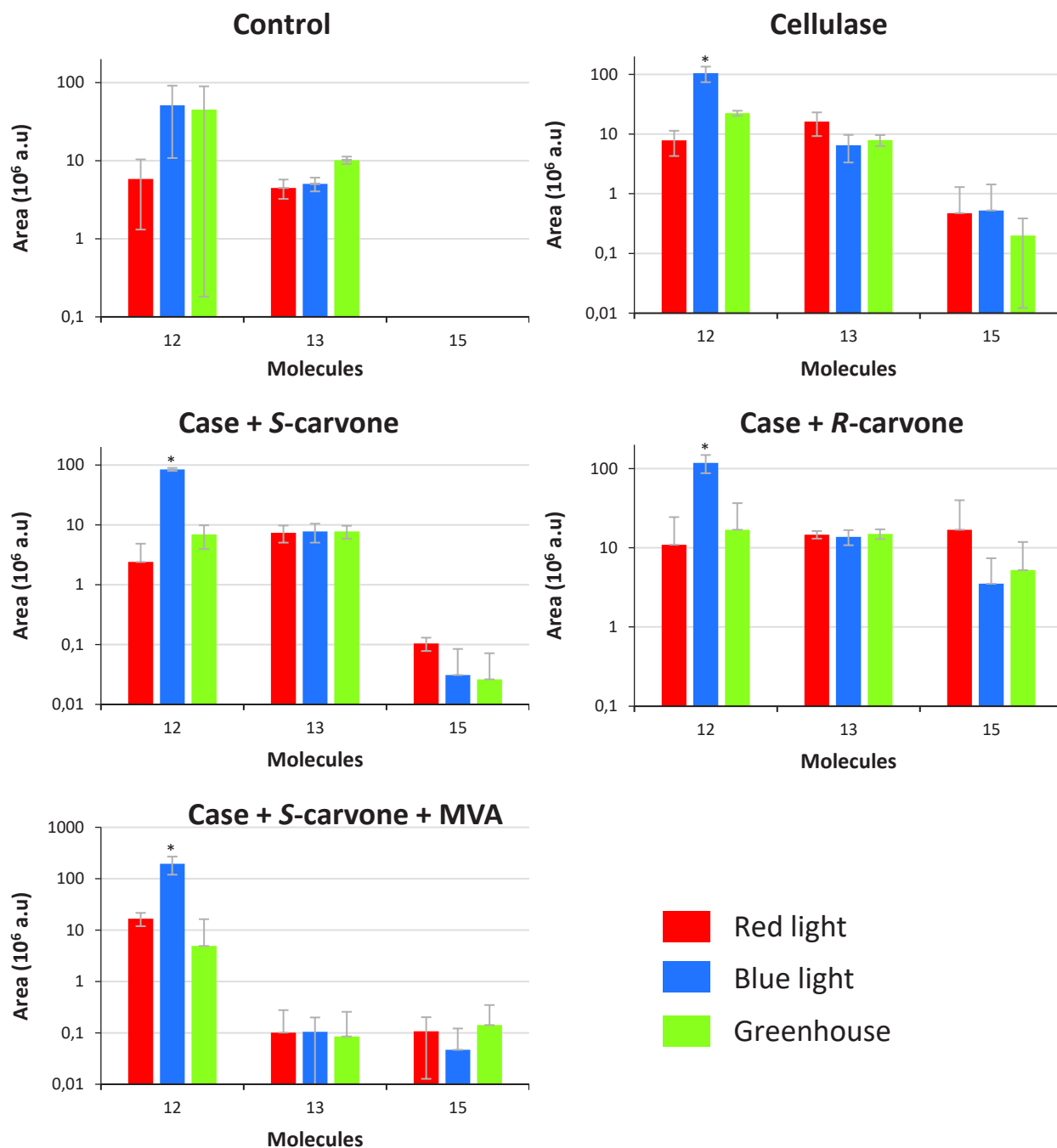


**Figure 108 Blue light influence abundant metabolite 12 culture medium content.**

Relative quantification of area under peaks of abundant molecules (Area > 10.10<sup>6</sup> in at least one condition) 12, 13 and 15 detected by GC-EI-MS analysis of culture media from tobacco leaf discs punched on plants cultivated under red light (red), blue light (blue), greenhouse (green). Leaf discs were floated on 50 μM KH<sub>2</sub>PO<sub>4</sub>, elicited with 0.5 % cellulase alone or supplemented with 2 mM S-carvone, R-carvone or both 2 mM S-carvone and 1 mM MVA. \* p-value < 0.05 at the Kruskal-Wallis test followed by Dunnett post-hoc test (n=3)

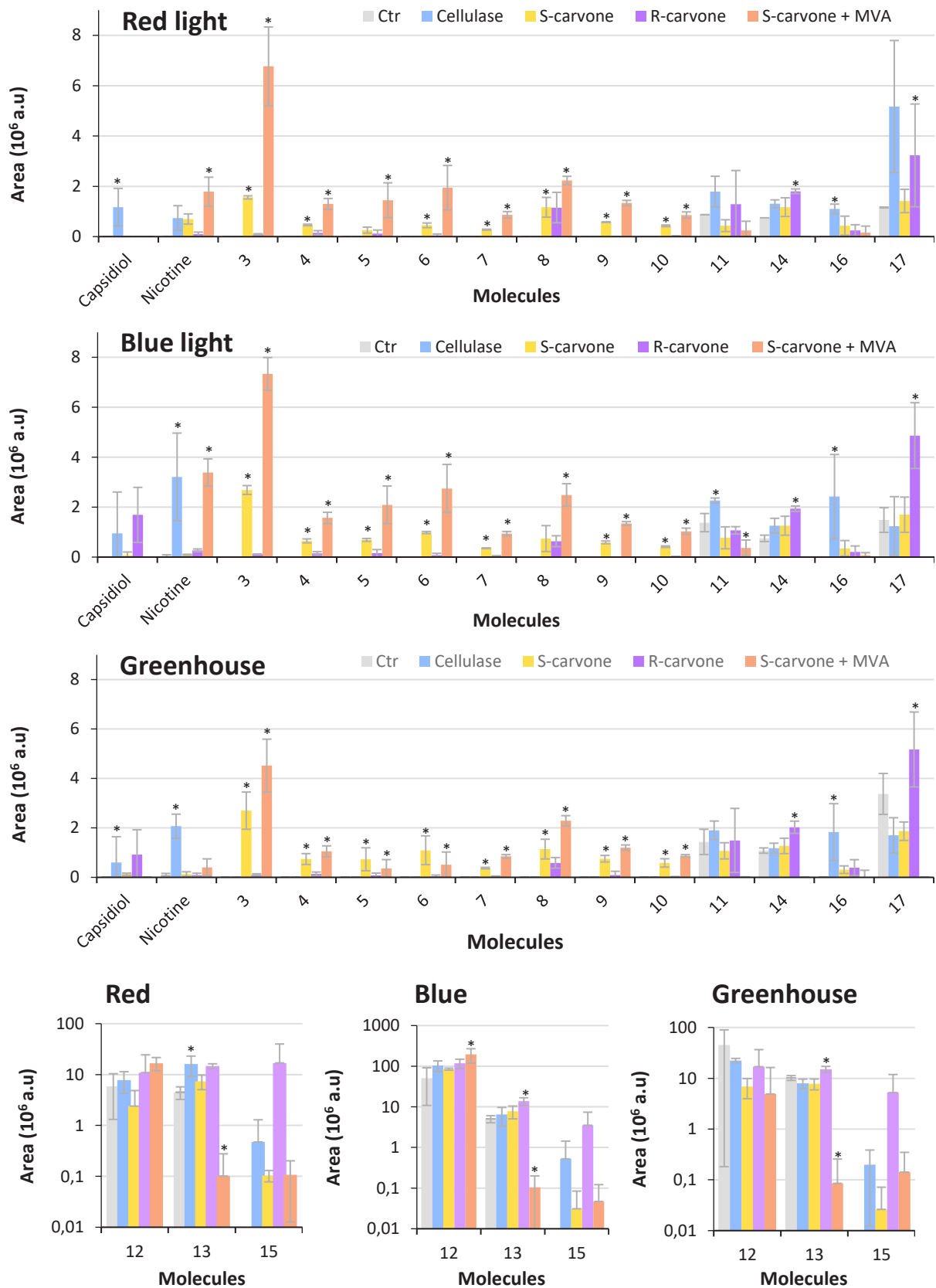


**Figure 109 Protein prenylation inhibitors and MVA influence metabolites found in the culture medium.**

Relative quantification of area under peaks of molecules 1 to 17 detected by GC-EI-MS analysis of culture media from tobacco leaf discs punched on plants cultivated under red light, blue light, greenhouse. Leaf discs were floated on 50  $\mu\text{M}$   $\text{KH}_2\text{PO}_4$  (grey), elicited with 0.5 % cellulase alone (blue) or supplemented with 2 mM S-carvone (yellow), R-carvone (purple) or both 2 mM S-carvone and 1 mM MVA (orange). \* p-value < 0.05 at the Kruskal-Wallis test followed by Dunnett post-hoc test (n=3)

## 5.4 CONCLUSION

In this study we identified the synthetic compound IN2 as a novel inhibitor of protein prenylation whose mechanism of action differs from conventional inhibitors of the MEP pathway or protein prenyltransferases. Although the target and mechanism of action involved in its activity have not been yet characterized, the results obtained in our BY-2 cell model demonstrated that its efficiency is at least 10-fold higher than that of our reference compound fosmidomycin.

In addition, unlike tested vismiones and synthetic dihydroanthracenones (DHA), the trials with red algae extracts effective against *P. falciparum* have shown that they also likely contain molecules able to inhibit protein prenylation. Thus, these results propose that the inheritance of the MEP pathway from a Rhodophyte in Apicomplexa can be used to identify new inhibitors of protein prenylation with antimalarial activity. Nevertheless, the activity obtained was low and experiments do not allow to conclude on the common nature of the molecules involved in the activity on pLDH of *P. falciparum* and the inhibition of protein prenylation.

Furthermore, we demonstrated that the carotenoids and other metabolites content in tobacco leaves can be modified by using *S*-carvone identified as a protein prenylation inhibitor in tobacco (Huchelmann et al., 2014). Remarkably, these experiments also provide some evidence that the MVA plays a key role in the regulation or biosynthesis of carotenoids, although MEP pathway is reported for a long time to supply carotenoids in plants (Steele and Gurin, 1960; Disch et al., 1998; Lichtenthaler, 2007; Vranová et al., 2013)). For the first time we reported effects of isoprenoids on azine type alkaloids, as shown by the influence on nicotine production or excretion from tobacco leaves elicited with cellulase and treated with *S*-carvone and MVA. Finally, the comparison of *S*-carvone and *R*-carvone effects on elicited tobacco plant showed that plants as animals respond specifically to the stereochemistry of monoterpenes. All in all, these results support that the research on protein prenylation inhibitors provides therapeutic compounds as well as powerful tools to understand the metabolism and its regulation in plant for application such as metabolic engineering of valuable compounds.

Although anthranoids had no effect on the inhibition of protein prenylation, we were able to demonstrate that these compounds are actually autofluorescent and are responsible of the peculiar phenotype reported in the literature (Hartmann et al., 2015)





# 6 OBSERVATION AND ANALYSIS OF ANTHRANOIDS IN LIVING CELLS USING SPECTRAL IMAGING COUPLED TO MASS- SPECTROMETRY



## 6.1 INTRODUCTION

In our screening of protein prenylation inhibitors, a particular phenotype of fluorescence was observed in BY-2 cells treated with the vismiones and appears to be independent of our fluorescent GFP and RFP markers (**section 0**). Since autofluorescence of some anthranoids was reported in the literature (Fujii et al., 1997; Galle, 2015; Verebova et al., 2016; Duval and Duplais, 2017), we proposed that the observed fluorescence in treated BY-2 cells corresponds to autofluorescence of vismiones. Previous work has shown that the degradation of vismiones into anthrone, anthraquinones and bianthrone occurs under oxidative conditions like in DMSO (Galle, 2015). Interestingly, AVD and anthraquinones such as emodin or quinizarin have been described for their fluorescence properties, but vismiones fluorescence was never characterized *in cellula* (Sedaira et al., 1998; da Cunha et al., 2014; Galle, 2015). Besides, the excitation of AVD is theoretically not possible at 488 nm (Galle, 2015). As a matter of fact, our confocal microscope observations were carried out with excitation at 488 nm raising the question: where does the fluorescence observed *in vivo* come from? Is it the vismione, a degradation product or metabolites induced in BY-2 cells? Also, AVD and VH are reported to be effective against *P. falciparum* and *L. donovani*, but the targets and mechanism of action remain unknown. In this context, could we use autofluorescence of vismiones to understand their antiprotozoal activity? On the top of that, considering that some aspects of vismiones biosynthesis in plants remains unknown and anthranoids are valuable compounds (François et al., 1999; Gill, 2001; Han et al., 2001; Galle, 2015), is it possible to trace these compounds in their host plant? These aspects definitely deserve to pay attention to results obtained in our BY-2 cells model. Accordingly, we are interested in localizing and understanding whether the fluorescence observed in BY-2 cells was related to vismiones or to the anthraquinones resulting from their metabolization *in cellula*. Nevertheless, the classical detection method of confocal microscopy did not allow to discriminate fluorescence signals in vismiones-treated cells expressing GFP or RFP markers (**section 0, Figure 99**). At present, microscopy technologies such as spectral imaging (SI) enable the observation and discrimination of naturally occurring fluorescent compounds in plants by comparing fluorescence spectra observed *in cellula* with that of references (Conéjéro et al., 2014). SI analysis was therefore adapted to the observation of anthranoids in BY-2 cells treated first with VH, then with other vismiones and synthetic DHA (Wasser, 2018).



## 6.2 EVALUATION OF ANTHRANOID CYTOTOXICITY USING SPECTRAL IMAGING

We proposed to use SImaging to observe vismiones, therefore a proof of concept was designed. With this regard, VH, related anthraquinones and other natural phenolic compounds described for their biological activities and/or their fluorescence (**Table 18**) were utilized. However, no experiments using SImaging had been carried out in the institute, and several compounds were described for some toxicity. Thus, we performed viability assays not only to evaluate the cytotoxicity of the selected compounds, but also to test if SImaging is suitable to discriminate markers from the vismione induced signal in BY-2 cells. To this end, A double staining method with propidium iodide (PI) and fluorescein diacetate (FDA) was used to evaluate cell viability (Hemmerlin and Bach, 2000). Accordingly, PI penetrates in dead cells, staining their nuclei and emitting thus red fluorescence ( $\lambda_{Em}$  636 nm), and FDA being only deacetylated by living cells labels the cytoplasm and nucleus with a blue-green fluorescence ( $\lambda_{Ex}$  494,  $\lambda_{Em}$  521 nm). First, BY-2 cells were treated for 24 h with 25, 50 and 100  $\mu$ M of the candidate anthranoids: either VH, quinizarin (Qui), emodin (Emo), the naphtoquinones lapachol (Lap), plumbagin and quinoclamine or other compounds such as fraxetin (Fra), benz[g]iquinoline and dicoumarol. Then treated BY-2 cells were labelled with PI/FDA before being observed by SImaging. Observations were performed with  $\lambda_{Ex}$  488 nm as excitation wavelength and collecting fluorescence between 498 and 664 nm incremented in 18 channels of 9 nm ( $\lambda_{488}$ ).

Consistent is the fact that cytotoxicity after 24h did not exceed 10% for a majority of compounds at concentrations ranging from 25 to 100  $\mu$ M as compared to the negative (1 %) and the farnesol positive controls (100%, 75  $\mu$ M) (**Figure 110**). In contrast, the cytotoxicity of dicoumarol (22% PI, 50  $\mu$ M), plumbagin (50%, 50  $\mu$ M), Lap (17% PI, 50  $\mu$ M) and especially benz(g)isoquinoline (100%, 25  $\mu$ M) was considered as too high for our proof of concept. Although Lap cytotoxicity was >10%, it did not exhibit a particular fluorescence, it was therefore conserved as negative control because structurally similar to anthranoids (**Figure 111**). Besides, benz(g)quinoline phenotype was considered as dead cell phenotype clearly identifiable by the separation of BY-2 cell wall and cell membrane (**Figure 111**).

**Table 18 compounds used for SImaging proof of concept of vismiones and related compounds metabolization.**

Structure and biological activities of compounds selected for fluorescence observation by SImaging and viability assay

Name	Structure	Biological activity
Vismione H (VH)		Antiprotozoan ( <i>P. falciparum</i> , <i>Leishmania sp.</i> ), treatment of skin disease (Botta et al., 1986; François et al., 1999; Galle, 2015)
Madagascine		Vasodilator (Chen et al., 2016)
Emodin (Emo)		Laxative, anti-metastasis, anti-inflammatory, antiviral, antibacterial, anti-allergic, neuroprotective, immunosuppressive, anti-osteoporotic, antidiabetic, hepatoprotective activities (Srinivas et al., 2007; Dong et al., 2016)
Quinizarin (Qui)		Stimulate cell growth of fibroblast L929 line (Zengin et al., 2016), insecticide (Drummond et al., 2014), anti-metastasis (Rossi et al., 2010)
Dicoumarol		Anticoagulant (Sun et al., 2020),
Benz[g]isoquinoline		
Fraxetin (Fra)		Antibacterial (Wang et al., 2014a), analgesic (Okuyama et al., 1996), Iron uptake in plant (Tsai et al., 2018), neuroprotective (Molina-Jiménez et al., 2004), anticancer (Ren et al., 2020)
Quinoclamín		Anticancer (Cheng et al., 2009), herbicide (Altland et al., 2007)
Lapachol (Lap)		Anticancer, antibacterial, antifungal, antiviral, antiprotozoal, insecticidal, antiinflammatory, and antipyretic (Epifano et al., 2014; Hussain and Green, 2017)
Plumbagin		Anticancer, antiinflammatory, antibacterial, antifungal (Padhye et al., 2012; Liu et al., 2017)

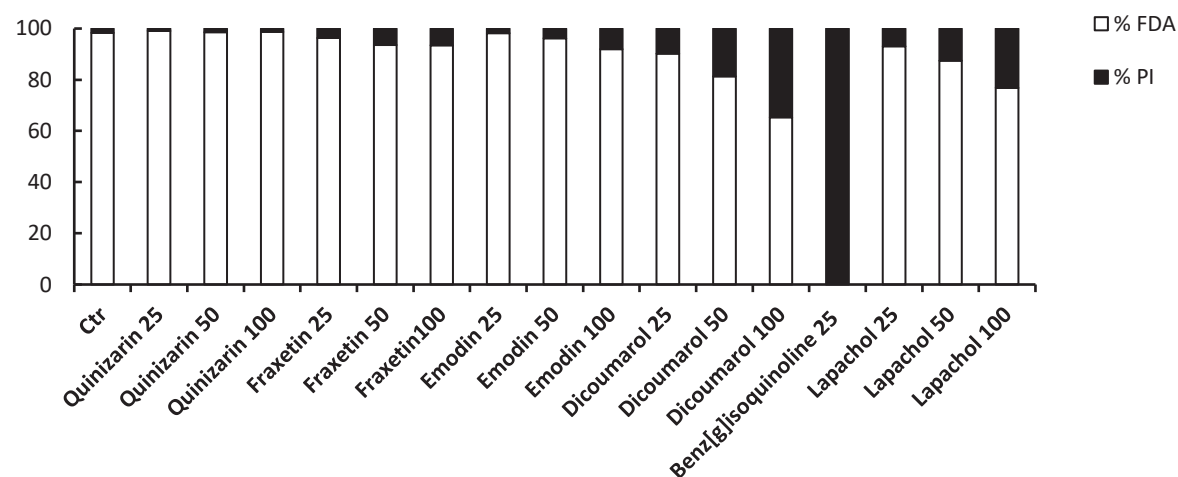


**Figure 110 Anthranoids exhibit low cytotoxicity in BY-2 cells after 24h of treatment.**

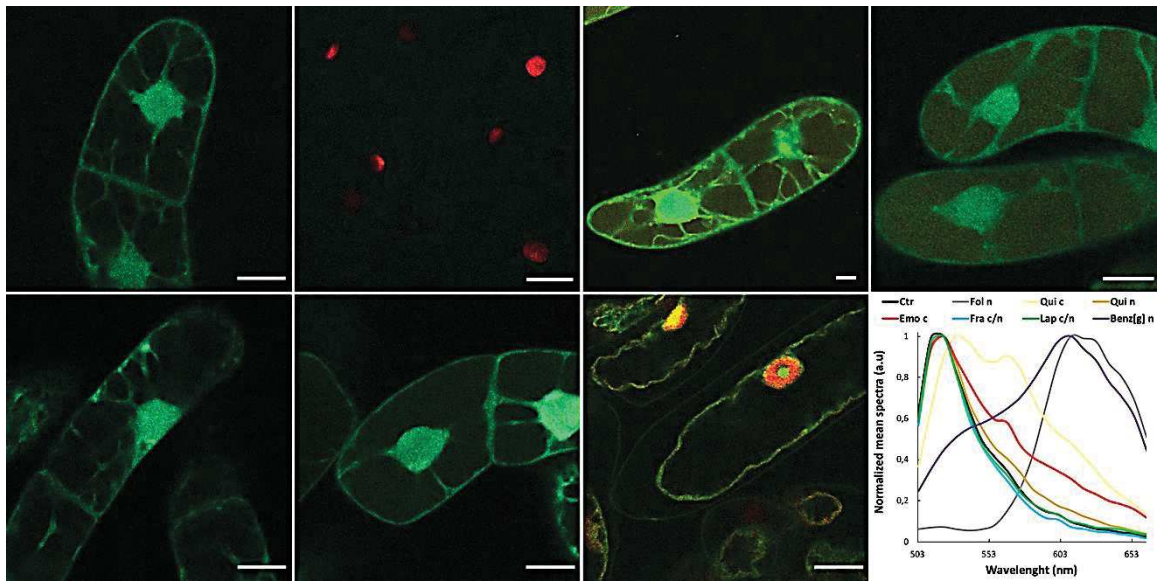
Evaluation of viability using FDA/PI assay and SImaging observation of BY-2 cells treated 24 h with 25, 50 and 100  $\mu$ M of Quinizarin, Fraxetin, Emodin, Dicoumarol, benz[g]isoquinoline and lapachol. The percentage of cells labeled by PI (% PI) was considered as dead and the cells labelled by FDA (% FDA) were still alive after 24 h.

At  $\lambda_{488}$ , unlike Lap, all anthranoids exhibit a clear fluorescence contrasting with that of the PI in the nucleus or FDA alone in the cytoplasm (**Figure 111**). For instance, living Qui-treated cells labelled with FDA/PI exhibit a fluorescence in the nucleus with spectrum and  $\lambda_{Em} = 521$  nm, corresponding to the FDA. Oppositely, in the cytoplasm, the fluorescence  $\lambda_{Em}$  was shifted from 521 to 530 nm and a shoulder appeared at 565 nm. These results confirmed that Qui-treated cells are alive and suggest a co-labelling between Qui and FDA in the cytoplasm, hence hybrid spectra were recorded. This was also observed at a lower scale in Emo-treated cells, indicating that concentration and/or quantum yield of Emo must be lower than Qui. Surprisingly, time-lapse experiments with FDA-labelled cells treated by VH confirmed this co-labelling. With this respect, the FDA fluorescence in the cytoplasm was replaced by the VH one after fading of the former, and punctated structures were labeled too (**Figure 111**). Interestingly, the fluorescence that has been described for AVD and anthrone/anthranol forms suggests that they cannot be excited at  $\lambda_{Ex} 488$  nm (Cameron et al., 1976; Fujii et al., 1997; Galle, 2015), but more about  $\lambda_{Ex} 400$  nm with  $\lambda_{Em} 540$  nm. In contrast, anthraquinones, fluoresce under  $\lambda_{488}$  conditions with emissions from 550 to 590 nm as suggested by our results and data in the literature (Fujii et al., 1997; Verebova et al., 2016; Duval and Duplais, 2017). Accordingly, fluorescence observed at  $\lambda_{488}$  in our preliminary assay and these one might correspond to anthraquinones forms rather than vismione. Finally, Fra-treated cells showed no fluorescence at  $\lambda_{488}$ , which is consistent with the literature, as coumarins emit fluorescence *in vivo* with lambda  $\lambda_{Ex} 320-380$  nm and  $\lambda_{Em} 400-460$  nm (Duval and Duplais, 2017; Tsai et al., 2018).

Altogether, our results indicate that the SImaging is a suitable tool to identify and discriminate fluorescence *in cellula*. We demonstrated that Fra, Lap and anthranoids tested exhibit relatively low cytotoxicity at 24h in BY-2 cells. In comparison to our first hypothesis (**section 0**), it seems that fluorescence observed at  $\lambda_{488}$  in VH-treated cells rather corresponds to VH related-anthraquinones. Since vismione anthrone/anthranol forms and coumarins are described to emit fluorescence under excitation at  $\sim 400$  nm (Fujii et al., 1997; Galle, 2015; Duval and Duplais, 2017), SImaging should be adapted to observe these molecules too.



A



B

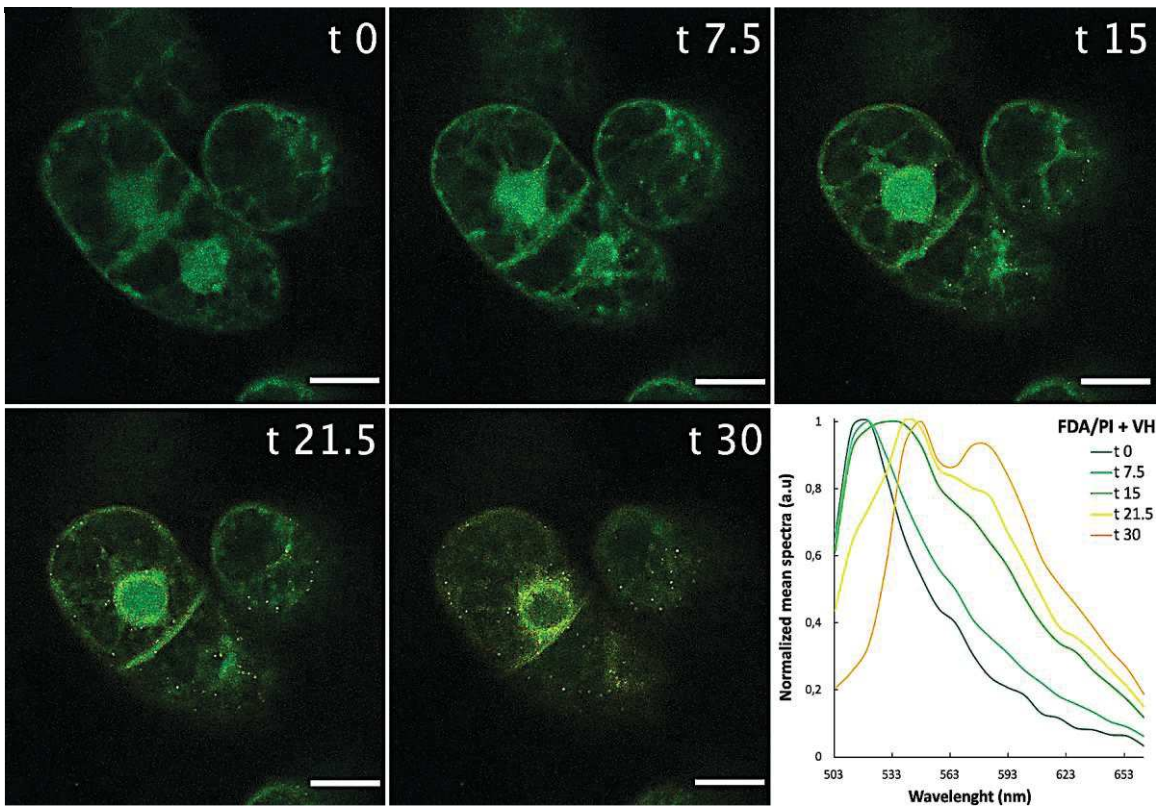


**Figure 111 Spectral imaging allows observation of cell viability markers and anthranoids.**

(A) Lambda view of Slmaging observations at  $\lambda_{488}$  of BY-2 cells negative control (Ctr) or treated 18h with 75  $\mu\text{M}$  of farnesol (Fol), 50  $\mu\text{M}$  of quinizarin (Qui), emodin (Emo), fraxetin (Fra), lapachol (Lap) or benz(g)isoquinoline (benz(g)), then stained with FDA/PI 7.5 and 75 mM respectively, scale bar = 20  $\mu\text{m}$ . Plotted on the graph, the fluorescence normalized mean spectra picked in 10 different points of the BY-2 cytoplasm (c), nucleus (n) or both (c/n). (B) BY-2 cells treated 18h with 50  $\mu\text{M}$  of VH, then stained with FDA/PI prior to time-lapse observation at 0, 7.5, 15, 21.5 and 30 min using Slmaging at  $\lambda_{488}$  settings. Plotted on the graph, the fluorescence normalized mean spectra picked in 10 different points of the BY-2 cytoplasm at the same time points.

Therefore, we explored these hypotheses throughout a proof of concept study on the “Spectral imaging associated to mass spectrometry, a novel approach to identify the naturally occurring fluorescent vismione and related anthranoids in living cells”. In this study, the compounds with a %PI > to 10% after 24 h were excluded, except the prenylated naphthoquinone lapachol (17% at 50  $\mu$ M) which did not show any particular fluorescence and was conserved as a negative control.

This proof of concept is the matter of a manuscript, the results are therefore organized as such for publication but adapted to the thesis.

## 6.3 VISUALIZATION OF ANTHRANOIDS IN LIVING CELLS USING SPECTRAL IMAGING

**Title:** Spectral imaging associated to mass spectrometry, a novel approach to identifying the naturally occurring fluorescent vismione and related anthranoids in living cells

**Auteur:** Q. Chevalier, J-B Gallé, N. Wasser, V. Mazan, M. Elhabiri, C. Villette, J. Mutterer, M.M. Elustondo, H. Schaller, A. Hemmerlin, C. Vonthron-Sénécheau

### 6.3.1 Abstract

Vismione H (VH) is a fluorescent prenylated anthranoid produced in plants (Hypericaceae family), with antiprotozoal activities that fight malaria and leishmaniasis. Little is known of its biosynthesis and metabolism or of its mode of action against the parasites. When VH is isolated from *Psorospermum glaberrimum*, it can promptly be converted into madagascine anthrone, anthraquinone or bianthrone. The later can be differentiated according to their fluorescent properties. To locate the fluorescence of VH in living plant cells without mistaking it with that of corresponding metabolites, an original strategy combining spectral imaging (SI) confocal microscopy and non-targeted metabolomics using mass spectrometry was developed. Madagascine, emodin, quinizarin as well as lapachol and fraxetin were studied. The technique readily allowed a spatio-temporal identification, characterization and discrimination of spectral fingerprints from anthranoid-derived metabolites. Furthermore, our study validates the capability of plant cells to metabolize anthranoids such as VH into Mad anthrone and anthraquinones as well as into unexpected metabolites, drawing up new hypotheses of anthranoids metabolic pathways in plants.

### 6.3.2 Introduction

The plant kingdom is a source of ~200.000 identified specialized metabolites. Among these, ~10.000 phenolic compounds (or polyphenols) are used as industrial ingredients in the pharmaceutical, cosmetics and agri-food industries on account of their diverse bioactive properties (Pichersky and Lewinsohn, 2011; Tissier et al., 2014). Still, the biosynthesis and action mechanisms of many polyphenols and especially anthranoids remain unclear (**Figure 112**). Traditionally anthraquinones like emodin (Emo) have been used as pigments and essential constituents of many purgative plants.

Today, more than a dozen different therapeutical activities could be attributed to Emo, ranging from laxative to antineoplastic properties (Srinivas et al., 2007; Dong et al., 2016). Even though the Emo's action mechanisms are not fully understood, the laxative properties of anthraquinones have been well described and require the presence of hydroxyl groups in position 1 and 8 (**Figure 112**). Furthermore, some prenylated anthranoids such as vismiones have shown promising antimalarial activity, but their molecular targets are still unknown and their biosynthesis from atrochryson remains hypothetical (François et al., 1999; Galle, 2015).

Biosynthesis of anthranoids occurs through two distinct pathways in plants (**Figure 112**): the polyketide pathway occurs in Rhamnaceae, Fabaceae, Aloeaceae, Polygonaceae and the shikimate/*o*-succinylbenzoic pathway is found in Rubiaceae (Han et al., 2001). Very little is known about the enzymology of these biosynthetic pathways in plants, especially in the polyketide pathway in which only the first step ensured by a polyketide synthase has been described (Han et al., 2001). The latter results in the formation of an octaketide from the addition of seven malonyl-CoA onto Acetyl-CoA. With the fruit bodies from blood-red toadstool *Cortinarius sanguineus* (Syn. *Dermocybe sanguinea*), feeding experiments with [<sup>14</sup>C]endocrocin, a carboxylic acid progenitor of "neutral" anthraquinones were performed (Gill, 2001). The results suggest that 8-hydroxymethylation and 4-hydroxylation can occur to yield dermolutein and dermorubin but not "neutral" anthraquinones such as Emo and dermoglaucine which require a decarboxylation at the C2 position (Gill, 2001). In addition, incorporation of [2,4-<sup>3</sup>H<sub>2</sub>]emodin 6-O-β-D-glucopyranoside in fruit bodies of *Cortinarius semisanguineus*. showed that Emo can be 6-hydroxymethylated and also 5- or 7-hydroxylated as radiolabeling was found in dermoglaucin and dermocycin (Gill, 2001). Moreover, similar experiments suggested that dihydroanthracenones such as torosachryson and atrochryson are pivotal intermediates in the biosynthesis of the anthraquinones afore mentioned, due to their structure they also emit bright fluorescence in water. Another study proposed a biosynthetic pathway for monodictyphenone and emodin derivatives in keeping with genome mining and characterization of biosynthetic intermediates in *Aspergillus niger* deletion strains (Chiang et al., 2010). However, these experiments indicate that O-methylation, oxidation, hydroxylation, dimerization, glycosylation can be achieved by enzymes, whereas other can result from chemical reaction such as tautomerization, photoisomerization and photochemical hydroxylation (Fain et al., 2006; Furumoto and Jindai, 2008; Elkazaz and Jones, 2010).

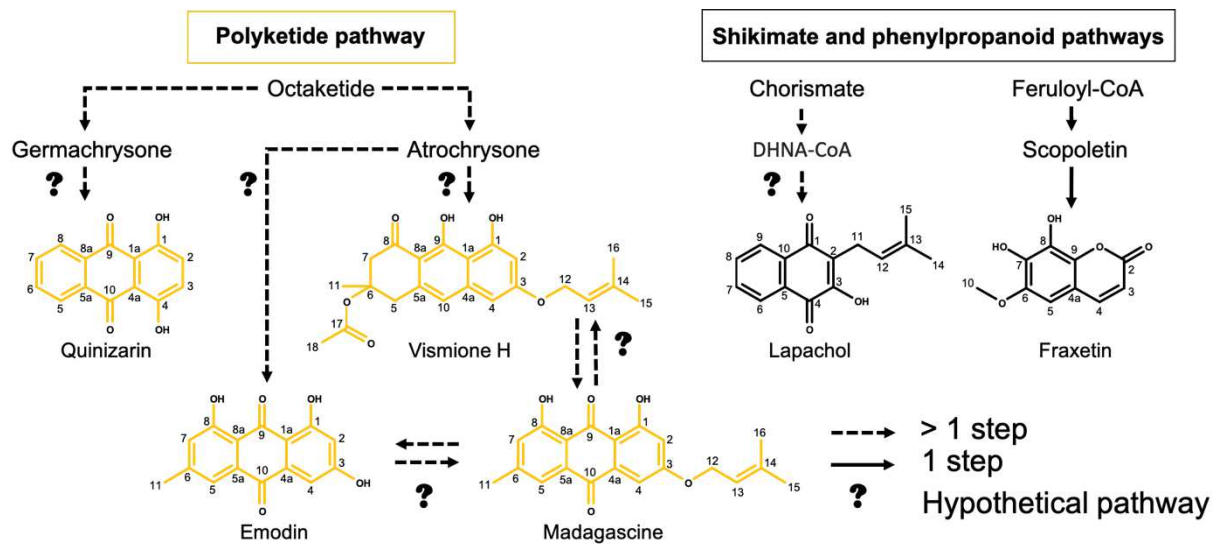


**Figure 112. State of the art on the biosynthesis and structures of anthranoids (orange) and other phenolic compounds (black) studied.**

Although, many intermediates of these molecules are characterized and not represented herein, the question marks call out to the lack of knowledge of many steps in the polyketide biosynthesis pathway. Therefore, enzymatic mechanisms as well as chemical reactions may be suspected in these steps

Thus, under oxidative conditions like in DMSO, the VH isolated from *Psorospermum glaberimum* is subjected to a rapid degradation resulting in the anthrone form, which is then oxidized into its anthraquinone form madagascine (Mad) or alternatively dimerized into bianthrone (Galle, 2015). Forasmuch as anthranoids fluorescence was partly described, could these properties be used to compare if similar events occur in living plant cells?

Within the entire UV-Vis spectrum, more than 300 naturally occurring fluorescent compounds have been reported with quantum yields ranging from 0.01% to 100% *in vitro* (Duval and Duplais, 2017). Interestingly, anthranoids are fluorescent and in spite of their structural similarities, their fluorescence properties differ from each other, allowing their differentiation by fluorescence analysis. Thus, the acetyl-vismione D solubilized in MeOH emits green fluorescence ( $\lambda_{Em} = 534$  nm) with a low quantum yield of about 2% (Galle, 2015), whereas anthrones/anthranols emit a blue light ( $\lambda_{Em} = 458$  nm) in alcohol and a strong yellow-green fluorescence in water ( $\lambda_{Em} = 539$  nm) (Fujii et al., 1997). For their part, anthraquinones such as Qui and hypericin exhibit good fluorescence properties in the orange to far red window (570-675 nm) with quantum yield up to 30 % (Fujii et al., 1997; Verebova et al., 2016; Duval and Duplais, 2017). Despite this knowledge and the interest in anthranoids, vismiones have never been observed *in vivo* and the particular fluorescence of anthranoids has never been used to understand in depth their behavior within cells.

Consistent is the fact that little information on the biosynthesis of anthranoids in plant has been reported and differences between the anthranoids biological activities are observed. Accordingly, we were interested in tracking vismiones and related anthranoids *in cellula* using their particular fluorescence to identify each of vismiones and putative anthrones or anthraquinones at the subcellular level. Fluorescence microscopy has been used as a fundamental tool to monitor reported fluorescent probes *in cellula* for biomedical research or to understand metabolic pathway. Although, the spectral properties of several anthranoids in solution have been described, the physiological conditions are never ideally simulated *in vitro*. As a matter of fact, metabolism, catabolism and storage of metabolites can take place in more than three different cell compartments and tissues (Han et al., 2001). Also, it has been shown that the number and position of substituents, especially hydroxyls on anthranoids, largely influence their physico-chemical (*i.e.*, protonation properties) and fluorescence properties. Therefore, if biochemical and physicochemical parameters are not considered and well

evaluated, the fluorescence properties of anthranoids and other phenolic compounds in solution may be misleading to outline their behavior in a cellular context.

SI-maging is a suitable tool to accurately observe and identify *in plantae* several auto-fluorescent phenolic compounds such as simple phenols, vanillin and mangiferin (Conéjéro et al., 2014; Talamond et al., 2015). In fact, this method enables fluorescence signal detection of the sample in multiple independent channels with a resolution < 10 nm. Hence, SI-maging offers a considerable advantage to discriminate related fluorescence signals compared to the classical approach employed in fluorescence microscopy. In this respect, we used the SI-maging method to analyze and compare the fluorescence of VH, related anthranoids (Mad, Emo, Qui) and a prenylated naphthoquinone (Lap) in treated tobacco BY-2 cells. The latter was chosen as a plant model because cheap, safe, easy to handle and free of autofluorescent compounds under standard condition (Nagata et al., 1992). Besides, fraxetin (Fra) was used as a positive control, since its fluorescence and biosynthesis are reported in BY-2 cells (Tsai et al., 2018). The comparison of reference spectra to those recorded by SI-maging observation allowed the identification of the signal from natural products observed in different cell compartments at a single time point. To characterize the molecules on the basis of their fluorescence observed by SI-maging, we compared our SI-maging results to those from a spectrofluorometric analysis of references in model solution. From another point of view, we carried out a metabolomic analysis of BY-2 treated cell extracts to provide unambiguous annotation of fluorescent metabolites.

### **6.3.3 Materials and Methods for publication**

#### **6.3.3.1 Chemicals**

Fraxetin (7,8-dihydroxy-6-methoxy-coumarin), quinizarin (1,4-dihydroxy-anthraquinone), emodin (1,3,8-trihydroxy-6-methyl-9,10-anthracenedione), lapachol (2-hydroxy-3-(3-methyl-2-butenyl)-1,4-naphthoquinone) were purchased from Sigma-Aldrich. Vismione H and madagascine were obtained from PGE2 fraction of *P. glaberimum* as previously described (Galle, 2015). Other chemicals were from usual commercial sources with the highest purity available.

### 6.3.3.2 Protonation properties (supplementary data)

The UV-visible absorption spectrophotometric titrations *versus* pH of Fra, Lap, VH, Mad and Emo were performed using an automatic titrator system 794 Basic Titrino (METROHM) with a combined glass electrode (METROHM 6.0234.500, Long Life) filled with 0.1 M NaCl in water/ethanol 50/50 v/v and connected to a microcomputer (TIAMO light 1.2 program). The combined glass electrode was first calibrated as a hydrogen concentration probe by titrating known amounts of hydrochloric acid ( $\sim 1.72$  or  $\sim 4.6 \times 10^{-1}$  M from HCl, SIGMA-ALDRICH, puriss pa, >37 %) with CO<sub>2</sub>-free sodium hydroxide solution ( $\sim 0.98$  M or  $\sim 1.23 \times 10^{-1}$  M from NaOH, BDH, AnalaR, 98%). The HCl and NaOH solutions were freshly prepared and titrated with sodium tetraborate decahydrate (B<sub>4</sub>Na<sub>2</sub>O<sub>7</sub>·10H<sub>2</sub>O, FLUKA, puriss, p.a., > 99.5%) and potassium hydrogen phthalate (C<sub>8</sub>H<sub>5</sub>KO<sub>3</sub>, FLUKA, puriss, p.a., > 99.5%), respectively, with methyl orange (RAL) and phenolphthalein (PROLABO, purum) used as colorimetric indicators. The GLEE program (Gans, 2000), was applied for the glass electrode calibration (standard electrode potential  $E_0$ /mV and slope of the electrode/mV pH<sup>-1</sup>) and to check carbonate levels of the NaOH solutions used (< 5 %). The autoprotolysis constant of water in water/ethanol 50/50 v/v medium was fixed at 15.75 (Fonrodona et al., 1996).

An aliquot of 40 mL of solutions containing 136 μM Lap, 63.2 μM VH, 43.8 μM Emo, 35 μM Mad or 70.9 μM Fra was introduced in a jacketed cell (METROHM) maintained at 25.0(2) °C (LAUDA E200 thermostat). The initial pH was adjusted to  $\sim 2.9$ -3.3 with HCl (SIGMA-ALDRICH, puriss pa, >37%) and the titration was then carried out by automatic addition (automatic titrator system 794 Basic Titrino) of known volumes of NaOH solutions (BDH, AnalaR). After each addition (*i.e.* DET method - Dynamic Potential Titration - with a measuring point density of 3), an absorption spectrum was repeatedly recorded using a Varian CARY 50 spectrophotometer fitted with Hellma optical fibres (HELLMA, 041.002-UV) and an immersion probe made of quartz suprasil (HELLMA, 661.500-QX) and interfaced (CETRIB) with the potentiometric unit. The spectrophotometric data were then analysed with SPECFIT program (Hippler, 1993), which adjusts the absorptivities, and the stability constants of the species formed at equilibrium. SPECFIT uses factor analysis to reduce the absorbance matrix and to extract the eigenvalues prior to the multiwavelength fit of the reduced data set according to the Marquardt algorithm (Marquardt, 1963; Maeder and Zuberbuehler, 1990).



### 6.3.3.3 Spectrofluorimetric analysis

Different solutions of the pure compounds at 0.01 mg/ml were prepared from stock solutions prepared in EtOH at 1 mg/ml and then diluted either in EtOH/H<sub>2</sub>O 1:1 v/v, 0.1 M NaCl adjusted with HCl 10<sup>-2</sup> M (pH 2), Na<sub>2</sub>B<sub>4</sub>O<sub>7</sub> 0.1 M (pH 10), NaOH 10<sup>-2</sup> M (pH 12) or in EtOAc. The absorbance spectra of (de)protonated species in solution were checked by UV-Vis absorption spectrophotometry from 260 – 800 nm using a Cary 5000 UV-Vis-NIR spectrophotometer (Agilent, Santa Clara USA) prior to any fluorescence analysis. Fluorescence spectra of solutions diluted 10-fold were recorded with 3.5 ml Suprasil® quartz optical cells of 10 mm pathlength using a LS-55 spectrofluorimeter monitored with UV Winlab 5.1 software (Perkin Elmer, Waltham USA). For each compound, a fluorescence spectrum was recorded by exciting at the maximum absorption wavelength, and instrumental parameters were adjusted to a scanning speed of 400 nm/min, slit widths of 10 and 15 nm for EtOAc and ethanolic solutions, respectively. The fluorescence spectra of each compound were established by successive measure of the excitation ( $\lambda_{\text{Ex}}$ ) and emission ( $\lambda_{\text{Em}}$ ) maxima. A FluoroMax-4 spectrofluorimeter (HORIBA) was used to accurately determine the quantum yields of anthranoids at 0.001 mg/ml (0.0015 mg/ml for emodin) in solutions at pH 2 and at pH 10 only for VH and Fra. The quantum yields of the fluorescent species ( $\Phi_F$ ) were calculated by using the equation below with either rhodamine 6G (R6G) or cresyl violet used as references.

$$\Phi_F = \Phi_R \frac{\int I_F A_R n_F^2}{\int I_R A_S n_R^2}$$

$\Phi_R$  corresponds to the quantum yield of reference. The indices F and R denote sample and reference, respectively. The integrals over I represent areas of the corrected emission spectra, A is the optical density at the excitation wavelength and  $n_R$  and  $n_S$  correspond to the refractive index of the reference and the sample solutions, respectively.

### 6.3.3.4 Ca<sup>2+</sup> and Mg<sup>2+</sup> chelating assay

Fresh stock solutions of VH and Fra at 1 mg/ml in EtOH were further diluted at 0.01 mg/ml in EtOH/H<sub>2</sub>O 1:1 v/v and in 0.1 M NaCl. UV-Vis spectrophotometric titrations of the solutions were then carried out by adding increasing amounts of CaCl<sub>2</sub> or MgCl<sub>2</sub> and monitored using a Cary 5000 UV-Vis-NIR (Agilent, Santa Clara USA). 25  $\mu$ l of 0.1 M CaCl<sub>2</sub> or MgCl<sub>2</sub> prepared in water were successively added to 250  $\mu$ l of the ligand solution in a 3.5 ml Suprasil® quartz optical cells.

The  $\text{Ca}^{2+}$  and  $\text{Mg}^{2+}$  chelating properties of VH and Fra were also investigated by fluorescence emission, adding 150 and 300  $\mu\text{l}$  of 0.1 M  $\text{CaCl}_2$  or 0.1 M  $\text{MgCl}_2$  solution to VH and Fra solutions, respectively. The quantum yields of the  $\text{Ca}^{2+}$  and  $\text{Mg}^{2+}$  chelates with VH and Fra were measured as described in the *spectrofluorimetric analysis* section.

#### **6.3.3.5 Plant material and treatment**

The *Nicotiana tabacum* cv. Bright Yellow 2 (tobacco BY-2) cell suspension was made available by Toshiyuki Nagata (Tokyo University, Japan) and cultivated at 26 °C, on a rotary shaker set at 140 rpm and in the dark, in modified Murashige and Skoog (MS) medium as described (Hemmerlin and Bach, 2000). For treatments, 7-d-old cells were diluted five-fold into fresh MS medium and 3 ml were distributed in 6-well culture plates (*Sarstedt*, Nümbrecht, Germany) containing 25 or 50  $\mu\text{M}$  of either phenolic compounds. *Slmaging* acquisitions were carried out either after 5 minutes (5 min) incubation or after 18 hours (18 h). Viability of tobacco BY-2 cells incubated 18 h with phenolic compounds was evaluated by a dual staining fluorescent technique using fluorescein diacetate (FDA) and propidium iodide (PI) as previously described (19). Markers were added at a final concentration of 0.01  $\mu\text{M}$  prior observation by *Slmaging* using  $\lambda_{\text{Ex}}$  488 nm and emission wavelength ranging from 498 – 664 nm (**section 0**)

#### **6.3.3.6 Spectral imaging (*Slmaging*) microscopy**

Treated cells or pure compounds at 1 mM in the solutions at pH 2, pH 10 and pH 12 were observed using a LSM780 confocal laser microscope (Carl Zeiss, Jena Germany) equipped with an inverted Zeiss AxioObserver Z1, a Plan-Apochromat 20x/0.8 M27 objective, a numerical zoom adjusted at 2.8 and a laser power of 5 %. Images and emission spectra were acquired using the excitation wavelengths at 405 ( $\lambda_{405}$ ) and 488 nm ( $\lambda_{488}$ ) with the emission wavelengths distributed in 9 nm increments ranging from 415 to 664 nm and from 498 to 664, respectively. The spectral analysis was done after the extraction of spectra by manual component extraction of 1  $\mu\text{m}$  circles spotted in fluorescent areas.

#### **6.3.3.7 Spectral data analysis**

The dataset consisted of 10 spectra/cell collected from five cells in three independent biological replicates for each treatment, after 5 min and 18 h. Intensities per channels of each spectrum were averaged per cell and normalized to 1 before statistical analysis with R software V4.0.0 (GNU GPLv2, R Core Team) and RStudio V 1.2.5001 (AGPLv3, RStudio) using the ChemoSpec package V5.2.12. A distant matrix was established for each dataset applying the Pearson's

correlation coefficient, and a robust principal component analysis (PCA) was performed. The same procedure was used with solutions of pure compounds to analyze 10 spectra/acquisition in triplicate.

#### **6.3.3.8 LC-MS/MS analysis**

25 mg of freeze-dried BY-2 cells treated 15 min and 18 h with 50  $\mu$ M of each compound were extracted three times in 300  $\mu$ l MeOH, sonicated during 20 min at 80 kHz (Fisherbrand™ S-series), and the total extract was filtered prior to analysis. Standard solution at 0.002 mg/ml in EtOH and MeOH extracts from three independent biological replicates were analyzed by non-targeted metabolomics approach performed on the UltiMate 3000 UHPLC system (ThermoFisher, Waltham Massachusetts) coupled to the ImpactII (Bruker, Billerica Massachusetts) high resolution Quadrupole Time-of-Flight (QTOF) as previously described (Villette et al., 2018). In addition, a library of putative metabolites was generated after *in silico* enzymatic digestion of phenolic compounds simulated by MetaboScape v4.0 (Bruker). A statistical analysis was performed by comparing the area obtained under the chromatogram curve of the different metabolites analyzed in triplicates. The homogeneity of the variance was checked with a Levene prior to a Kruskal-Wallis test, followed by multi comparison procedure using post-hoc Dunnett's test.

### **6.3.4 Results and Discussion**

#### **6.3.4.1 pH influences the spectral properties of compounds in solution**

The fluorescence of anthranoids as well as that of coumarin is dependent on the ionic strength as well as the medium acidity. As a matter of fact, pH and salt composition in plant cell compartments are subject to fluctuations depending on the genotype, cell type, developmental stage and environment (Binzel et al., 1988; Carden et al., 2003). Since the intracellular pH in plant cells ranges from 5 in the primary vacuole, up to 8 in the mitochondrial matrix and peroxisomes (Martinière et al., 2013; Shen et al., 2013), a detailed physico-chemical investigations of our compounds has to be performed beforehand. In this context,  $pK_a$  values and absorption spectrophotometric properties were determined to evaluate in depth the fluorescence properties of the pure species from each compound in solution (**Table S 1**).

**Table S 1** pK<sub>a</sub> values of pure compounds measured in solution.<sup>a</sup>

	pK <sub>a1</sub>	pK <sub>a2</sub>	pK <sub>a3</sub>
Vismione H (VH)	7.2 ± 0.2	13.2 ± 0.2	na
Emodin (Emo)	7.10 ± 0.06	12.70 ± 0.06	> 13
Madagascine (Mad)	11.1 ± 0.1	> 13	na
Quinizarin (Qui) <sup>b</sup>	8.50 ± 0.03	10.65 ± 0.05	na
Fraxetin (Fra)	8.5 ± 0.5	> 9.75	na
Lapachol (Lap)	6.7 ± 0.1	na	na

<sup>a</sup> From UV-Vis absorption spectrophotometric titrations *versus* pH in EtOH/water 1:1 v/v with 0.1 M of NaCl; T = 25°C.

<sup>b</sup> From reference (Sedaira et al., 1998). na = not applicable. Error given as  $\sigma$  with  $\sigma$  = standard deviation.

Therefore, prior to the SImaging analysis, the determination of the pK<sub>a</sub> values and absorption spectrophotometric properties was needed to evaluate in depth the fluorescence properties of the pure species from each compound in solution. To find a compromise between the solubility of anthranoids and a high ionic strength as inside the cells, the pK<sub>a</sub> values of the selected compounds were measured in EtOH/water 1:1 supplemented with 0.1 M NaCl. Lap displays only one ionisable site while VH, Fra and Mad possess two protonation sites. Only Emo is characterized by three phenolic units. Under our experimental conditions, all pK<sub>a1</sub> could be characterized and were calculated to be below 9 except for Mad for which pK<sub>a1</sub> was measured to be 11.1 ± 0.1 (*i.e.*,  $\beta$ -hydroxy-ketone unit stabilized by hydrogen bond). The pK<sub>a</sub> value determined for Lap (pK<sub>a</sub> = 6.7 ± 0.1) was found to be in excellent agreement with data reported elsewhere (pK<sub>a</sub> = 6.31 ± 0.03) under the same experimental conditions (Ossowski et al., 2008). As stated above, Emo and VH both display a second ionisable site for which the corresponding pK<sub>a2</sub> values were measured to be 12.7 ± 0.2 and 13.2 ± 0.2, respectively (**Table S 1**). For Emo, the second protonation site could be assigned to the 8-hydroxy group, while the first one was easily assigned to the 3-hydroxy unit. These data are in agreement with pK<sub>a</sub> values (pK<sub>a1</sub> = 8.0 ± 0.1 and pK<sub>a2</sub> = 10.9 ± 0.2.) reported for Emo in MeOH/water 3:1 (da Cunha et al., 2014). The second pK<sub>a</sub> value of Fra could not be determined under our experimental conditions. Consistent is the fact that Fra was most likely degraded with a putative lactone breakage at pH > 9-10. For Emo and Mad, the other pK<sub>a</sub> values were estimated to be above 13 and could not be determined under our experimental conditions. Finally, the pK<sub>a</sub> values of Qui have been reported to be 8.5 and 10.65 in EtOH/water 1:1 (Sedaira et al., 1998) and were not re-determined in this study.

It is noteworthy that all investigated compounds showed at least two main absorption bands, one with high absorptivity at wavelengths < 300-320 nm and another less intense one lying at much lower energies (from 350-600 nm, **Figure S1**). Whatever the system examined, a significant bathochromic shift of the absorption lying at lower energies was observed upon increasing pH. Only VH stands in interesting contrast with a hypochromic shift of the main absorption band and the appearance of a weak absorption band centered at about 500 nm under basic conditions. These results clearly showcase the impact of the medium acidity and the corresponding hydroxyl deprotonations on the investigated polyphenols absorption spectral characteristics (Friedman and Jürgens, 2000; Giusti and Wrolstad, 2001).

Accordingly, the second absorption band from 350-600 nm was considered as more relevant for evaluating the changes of fluorescence between the protonated species. Also, the former is suitable for observation with our SImaging settings and those of most confocal microscopes. Among the six compounds studied, with the exception of Lap, all emitted fluorescence light when excited between 350-520 nm (**Figure 113**). In organic solvent such as EtOAc, VH did not exhibit fluorescence emission as compared to anthraquinones, whereas Fra could only be excited  $\lambda < 330$  nm (**Figure S2**). However, in saline ethanolic solution at pH 2 (*i.e.*, fully protonated and neutral species whatever the system considered), VH and anthraquinones were found to be fluorescent and their absolute quantum yields  $\Phi_F$  range from 0.4 to 15% (**Table 19, Figure 113**). Surprisingly, Mad only differs from the Emo at the 3-OH position (prenylated 3-OH group for Mad), albeit its absolute quantum yield  $\Phi_F = 4.85\%$  was found to be 10 times higher than that of Emo  $\Phi = 0.4\%$ . The 1,4-dihydroxyanthraquinone Qui was found to be the most fluorescent system with  $\Phi_F = 15\%$ . These results indicate that the number and position of hydroxyl groups as well as substitution (*e.g.*, prenyl group on position 3 for Mad) of anthraquinones contribute to the brightness of their fluorescence emission. In addition, anthraquinones show a drastic loss of their fluorescence emission intensity when the pH value is higher than  $pK_{a1}$  (*i.e.*, monodeprotonated species), and vice versa for Fra or VH (catechol for Fra or naphthalene-1,8-diol for VH, (**Figure S2**)).

Interestingly, the  $\lambda_{Em}$  measured for VH bathochromically shifted from 484 to 532 nm at pH 10, and the corresponding absolute quantum yield  $\Phi = 31\%$  was found to be 9 times higher than that measured at pH 2 (**Table 19**). Nonetheless, subsequent pH increase up to 12 and higher lead to a progressive loss of fluorescence, the full deprotonation of vismione likely promoting its degradation into anthraquinone or bianthrone as observed in DMSO (Hlasiwetz and Grabowski, 1867; Cameron et al., 1976; Galle, 2015). The high fluorescence of VH observed in solution at pH 10 containing  $\text{Na}_2\text{B}_4\text{O}_7$  and associated to the  $\text{LH}^-$  species is probably related to the anthranol form of VH rather than the anthrone which is typically not fluorescent (Fujii et al., 1997). The observation of anthranol form can be explained by both deacetylation of VH in mild alkaline condition and the presence of  $\text{Na}_2\text{B}_4\text{O}_7$  which promote the anthranol tautomer emitting strong yellow-green fluorescence as in the Schouteten reaction (Jarvis et al., 1967; Castro et al., 2017).

These results indicate that for intracellular pH ranging from 4 to 7.8, with the exception of Lap and Fra, all compounds emit fluorescence if excited at  $\lambda_{Ex}$  ranging from 392 to 480 nm. To test this hypothesis, we then compared the reference emission spectra established by our spectrofluorimetric analysis for these compounds to the corresponding spectra measured by Smaging in solution and in living treated BY-2 cells.

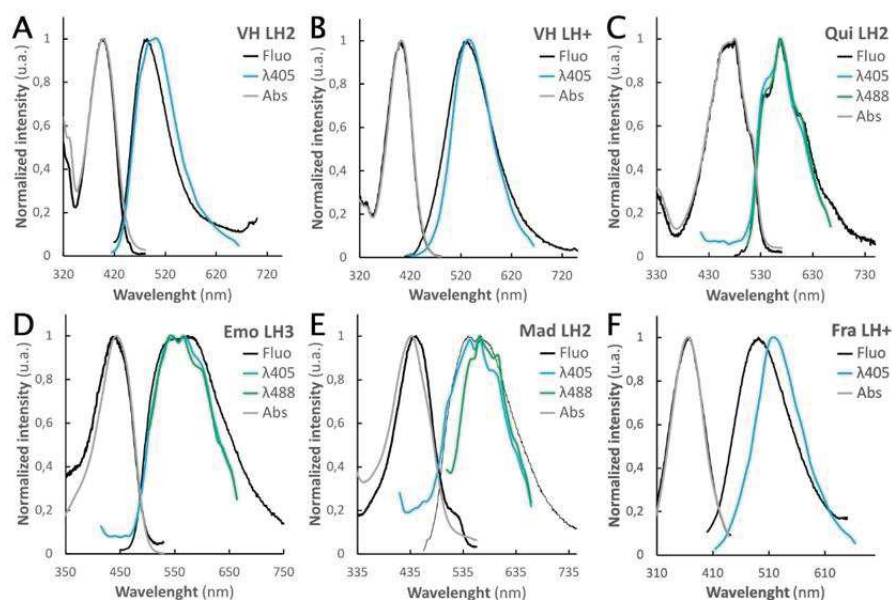


**Figure 113.** Normalized excitation/emission and absorption spectra.

Vismione H VH (A, neutral LH2 species and B, monodeprotonated LH<sup>-</sup> species), quinizarin Qui (C, neutral LH2 species), emodin Emo (D, neutral LH3 species), madagascine Mad (E, neutral LH2 species), fraxetin Fra (F, monodeprotonated LH<sup>-</sup> species) in ethanolic solutions. Excitation and emission spectra obtained from the spectrofluorimetric analysis (black), absorption spectra obtained from the UV-Vis analysis (grey) and spectral imaging at  $\lambda_{405}$  (blue) and/or  $\lambda_{488}$  (green) excitation.

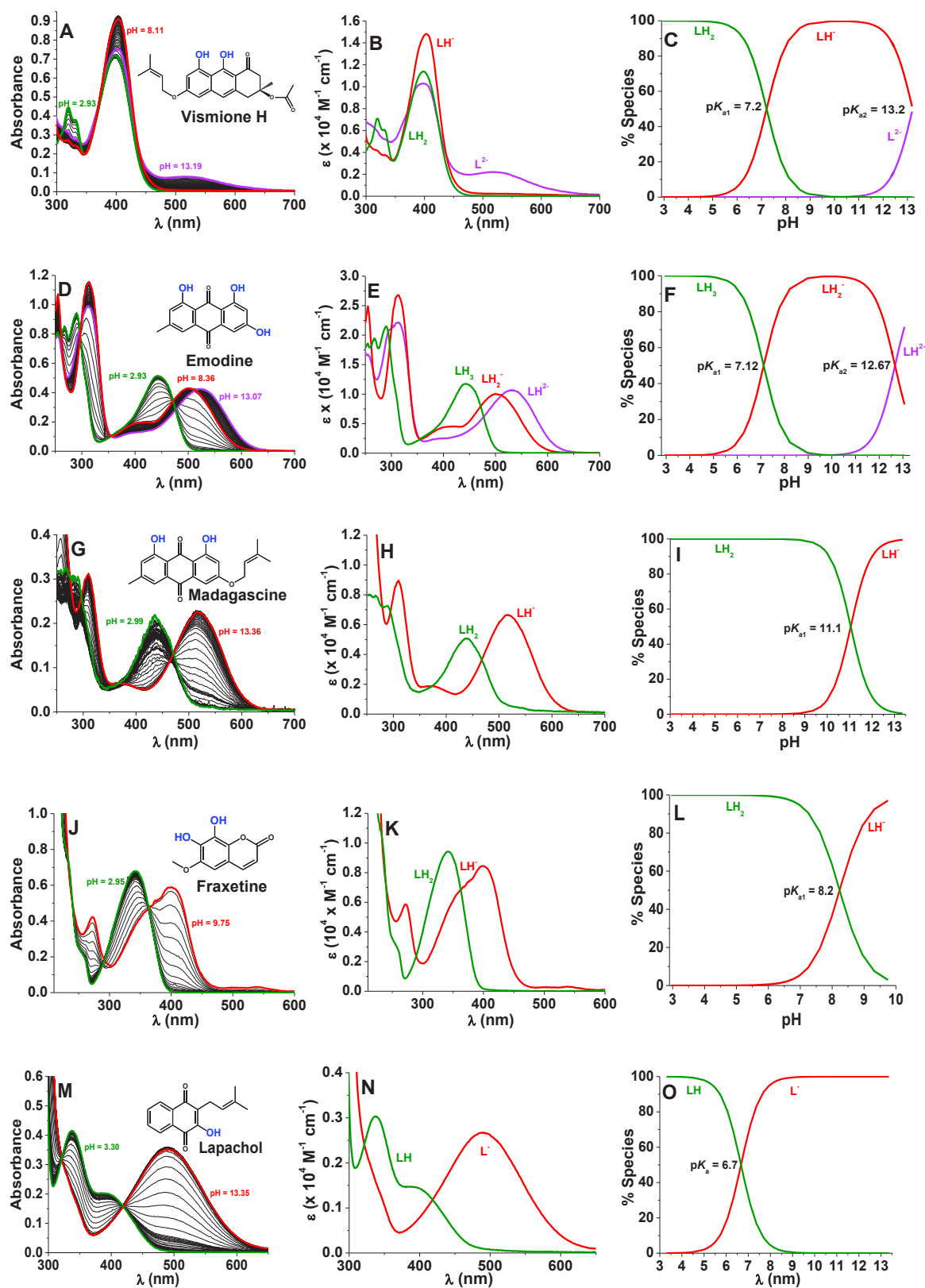


**Figure S1.** UV-Vis. absorption spectrophotometric titrations versus pH of most of the compounds considered in this work (Left). Electronic absorption spectra of their protonated species and (right) distribution diagrams as a function of pH of their protonated species. Vismione H (Figures A, B, C); Emodin Emo (Figures D,E,F), Madagascine Mad (Figures G,H,I), Fraxetin Fra (Figures J, K, L) and Lapachol Lap (Figures M, N, O). Solvent: EtOH/water 1:1 v/v; I = 0.1 M (NaCl); T = 25°C.

Table 19 Main photophysical characteristics evaluated for the pure compounds investigated in this work.

	[C] ( $\mu\text{M}$ )	$\lambda_{\text{abs}} = \lambda_{\text{ex}}$ (nm)	$\epsilon$ ( $\times 10^4 \text{ M}^{-1} \text{ cm}^{-1}$ )	$\lambda_{\text{Em}}$ (nm)	$\Phi_{\text{F}}$ (%)	Brightness	Imaging $\lambda_{\text{Em}}$ (nm)
Vismione H VH (LH <sub>2</sub> ) <sup>a</sup>	2.6	398	7.27	484	3.7	268.990	503
Vismione H VH(LH <sup>+</sup> ) <sup>b</sup>	2.6	403	14.0	532	31.0	4.340.000	539
Ca-Vismione H (LCa) <sup>c</sup>	2.6	404	13.0	548	21.4	2.782.000	-
Emodin Emo (LH <sub>3</sub> ) <sup>a</sup>	5.55	443	31.3	575	0.41	128.330	565
Madagascine Mad (LH <sub>2</sub> ) <sup>a</sup>	2.96	444	6.45	544	4.85	312.825	565
Quinizarin Qui (LH <sub>2</sub> ) <sup>a</sup>	4.16	480	3.78	569	15.13	571.914	565
Fraxetin Fra (LH <sup>+</sup> ) <sup>b</sup>	4.8	366	10.5	492	1.15	120.750	521
Ca-Fraxetin (LCa) <sup>c</sup>	4.8	391	8.71	462	-	-	521

<sup>a</sup> In EtOH/H<sub>2</sub>O 1:1 v/v, 0.1 M NaCl adjusted with 0.01 M HCl at pH 2

<sup>b</sup> In EtOH/H<sub>2</sub>O 1:1 v/v, 0.1 M NaCl adjusted with 0.01 M Na<sub>2</sub>B<sub>4</sub>O<sub>7</sub> at pH 10

<sup>c</sup> EtOH/H<sub>2</sub>O 1:1 v/v, 0.1 M NaCl supplemented with 0.01 M CaCl<sub>2</sub>

The errors on  $\epsilon$  and  $\Phi_{\text{F}}$  are estimated to 10%, the errors on  $\lambda$  are estimated to  $\pm 1$  nm

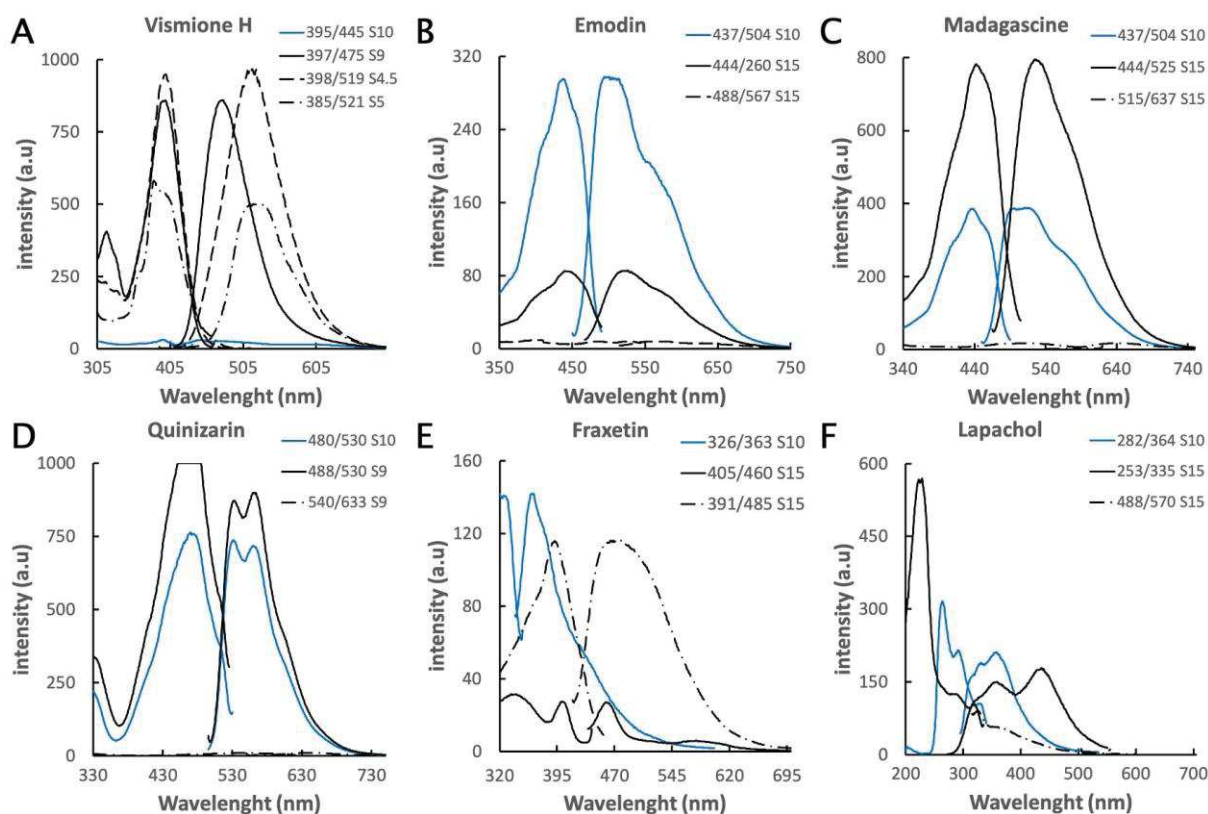


Figure S2. Fluorescence emission/excitation spectra from species studied.

Vismione H VH 2.6  $\mu\text{M}$  (A); emodin Emo 5.5  $\mu\text{M}$  (B); madagascine Mad 3  $\mu\text{M}$  (C); quinizarin Qui 4.2  $\mu\text{M}$  (D); fraxetin Fra 4.8  $\mu\text{M}$  (E); lapachol Lap 4.12  $\mu\text{M}$  (F) in different solvents, EtOAc (blue) and ethanolic solution (black), at pH 2 (solid line), pH 10 (dashed line) and pH 12 (dashed dotted line). S value corresponds to excitation/emission bandwidths of the spectrofluorimeter.



#### 6.3.4.2 Changes of fluorescence in cellula characterized by spectral imaging

Slmaging method was used to discriminate mixed fluorescent signals from the studied compounds in solution and in treated BY-2 cells with a special focus on vismione (blue to green-yellowish emission) and related anthraquinones (yellow to red emission). With respect to the photophysical data, two different settings have been selected for the excitation and the detection of fluorescence using Slmaging:  $\lambda_{\text{Ex}} = 405 \text{ nm}$  ( $\lambda_{405}$ ) with emission spectra range from 415 to 664 nm, and  $\lambda_{\text{Ex}} = 488 \text{ nm}$  ( $\lambda_{488}$ ) with emission spectra range from 495 to 664 nm. Interestingly, the emission spectra of the pure compounds in solution obtained by Slmaging analysis at  $\lambda_{405}$  and  $\lambda_{488}$  were found to be consistent with the results derived from the spectrofluorimetric approach (**Figure 113**). Nevertheless, small variations in the  $\lambda_{\text{Em}}$  were observed such as a decrease of the shoulder intensity of Emo LH<sub>3</sub> at 575 nm or a shift from 484 to 503 nm and from 492 to 521 for the maximum of emission for VH LH<sub>2</sub> and Fra LH<sup>-</sup>. It can be proposed that these discrepancies could be related to the detection method which is less resolutive in Slmaging (9 nm) as compared to classical spectrofluorimetry (1 nm). In addition, the hydrophobicity of Mad (3-O-prenylated emodin derivative) was highlighted by the observation of aggregates at 1 mM Mad in hydroalcoholic solution at pH 2. Although the  $\Phi_{\text{F}}$  of Mad is higher than that of Emo, the lower solubility of Mad as compared to Emo may result in a lower fluorescence signal from molecules detected in solution, decreasing the quality of spectra recorded at  $\lambda_{488}$  and  $\lambda_{405}$  for Mad in solution. It is important to notice that this problem of solubility was also observed when the anthranoids were diluted at 50 and 25  $\mu\text{M}$  in the cell culture medium leading to the formation of aggregates still present after 18 h.

Very low fluorescence intensities were detected in the Ctr and Lap-treated cells defining the autofluorescence threshold in tobacco BY-2 cells. For all other compounds, an emergence of fluorescence was promptly observed in treated BY-2 cells (5 min) being stable after 18 h treatments with 25  $\mu\text{M}$  (**Figure 114**, **Figure S3**) and 50  $\mu\text{M}$  (**Figure S3**, **Figure S4**). Overall, excitation at  $\lambda_{405}$  resulted in a stronger fluorescence signal than at  $\lambda_{488}$ , but the opposite was observed with madagascine- (Mad) and quinizarin-treated cells (Qui). As our spectral data analysis points out, only Fra-treated cells did not exhibit any fluorescence signal at  $\lambda_{488}$ , and apart from VH, the spectra observed after 5 min of treatment display the same  $\lambda_{\text{Em}}$  and shape at both wavelength settings (**Figure 114**, **Figure S4**).

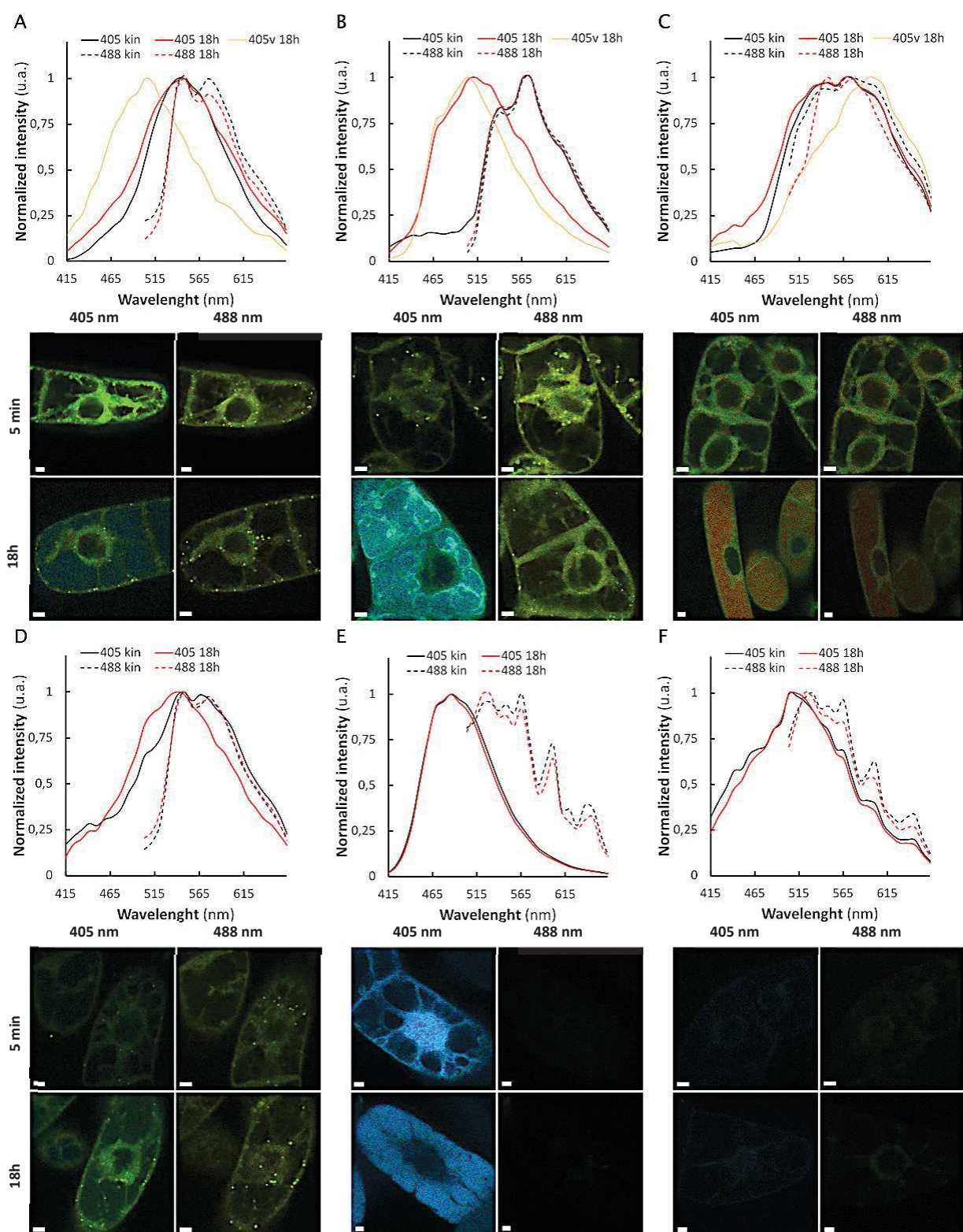


**Figure 114.** Normalized mean spectra and images from Slmaging analysis of cells treated with 25  $\mu\text{M}$ .

At  $\lambda_{405}$  (solid line) and  $\lambda_{488}$  (dashed line) of BY-2 cells treated 5 min (kin) and 18 h with 25  $\mu\text{M}$  of vismione H (A), quinizarin (B), emodin (C), madagascine (D), fraxetin (E) and the negative control (F). Spectra observed after 5 minutes (black), after 18h (red) and in the vacuole after 18h (red light). Spectra observed in primary vacuole at  $\lambda_{405}$  after 18 h are specified with a "v" after the labels.



Actually, the PCA of the normalized mean spectra support that the spectrum observed at  $\lambda_{488}$  share similarities with Qui and especially Mad, but not with spectra derived from Emo-treated cells (**Figure 115**). Besides, the maxima of emission observed at  $\lambda_{488}$  mostly in vesicular bodies from both VH and Mad-treated cells were centered at 539 nm and 575 nm, respectively. Even though intensities were similar, the maximum of emission in Qui-treated cells is centered at 575 nm. These results strongly suggest that within the first minutes VH- and Mad-cell treatment resulted in similar molecules differing from those produced by either Emo- and Qui-cell treatments. Interestingly, fluorescence emission detected after 5 min is usually observed first in the cytoplasm and/or the membrane, and then in additional structures such as the nuclear membrane, ER and in vesicular bodies with anthranoids treatments. Only for Fra-treated cells excited at  $\lambda_{405}$  fluorescence emission is observed in the nucleus. Thus, molecules might enter within the BY-2 cells by simple diffusion and undergo in different cell compartments following their polarities. In addition, the difference of shape and intensity between spectra collected in VH-treated cells suggest that at  $\lambda_{405}$  the VH LH<sup>-</sup> is detected in the cytosol or ER and at  $\lambda_{488}$  mainly anthraquinones in vesicular bodies.

After 18h, slight variations in fluorescence intensities using excitation at  $\lambda_{488}$  and  $\lambda_{405}$  were observed. In particular for anthranoids, it was found that the localization and emission spectra of these compounds did not change significantly over time and corresponded well with each other. Nevertheless, at  $\lambda_{405}$ , the shape of the emission spectrum of Mad-treated cells was found to be closely related to that of VH.

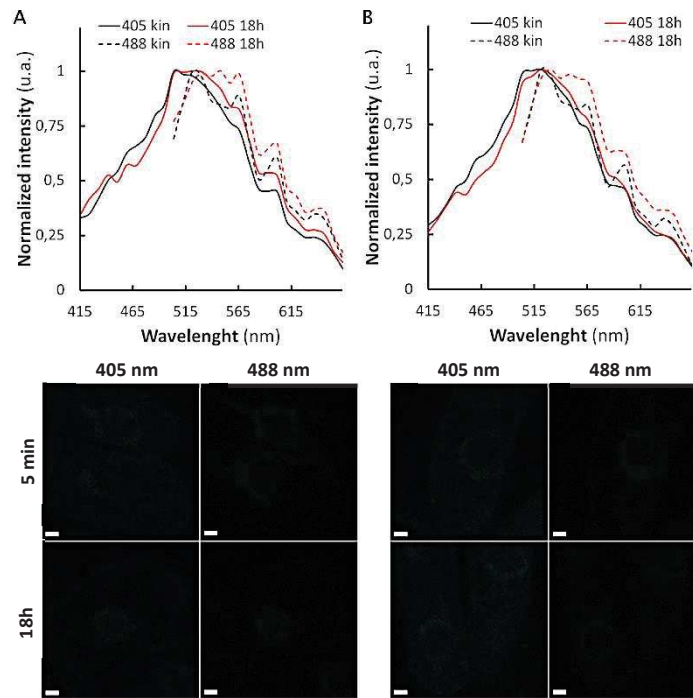


**Figure S3.** Normalized mean spectra and images from Slmaging analysis of Lapachol treated cells. At  $\lambda 405$  (solid line) and  $\lambda 488$  (dashed line) of BY-2 cells treated 5 min (kin) and 18 h with 25  $\mu\text{M}$  (A) and 50  $\mu\text{M}$  (B) of lapachol (Lap).

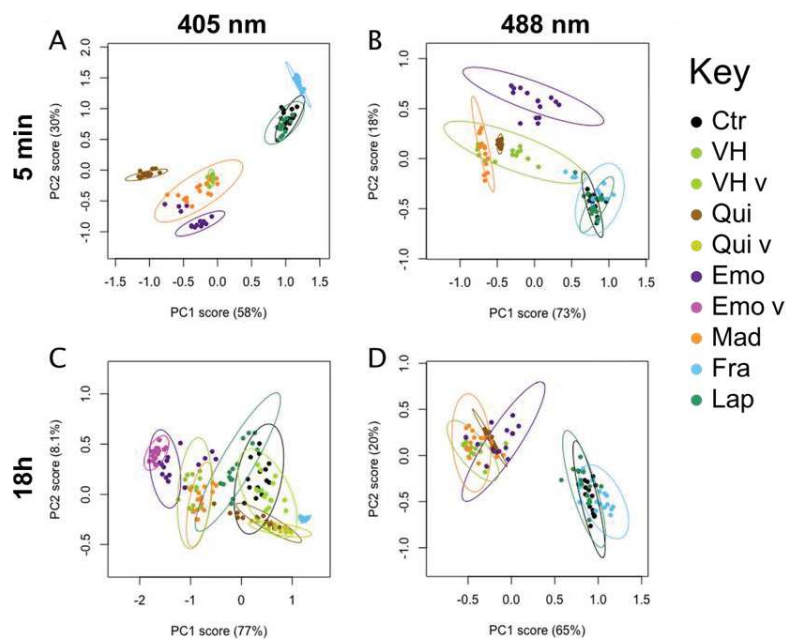


**Figure 115.** PCA of the normalized mean spectra obtained by Slmaging analysis of BY-2 cells.

Treated cells or not (Ctr) with 25  $\mu\text{M}$  of vismione H (VH), quinizarin (Qui), emodin (Emo), madagascine (Mad), fraxetin (Fra) and lapachol (Lap) after 5 min (A, B) and 18 h (C, D). Spectra observed at  $\lambda 405$  nm (A, C) and at  $\lambda 488$  nm (B, D) in control and treated cells. Spectra observed in the primary vacuole at  $\lambda 405$  after 18 h are specified with a “v” after the labels. 10 spectra/cell were averaged and normalized in five cells for three independent biological replicates

Other treatments have been associated either to the appearance of a new fluorescence emission signal in the primary vacuole or to the translocation of an identical fluorescence signal from the nucleus to the primary vacuole as seen for Fra treated cells (**Figure 114, Figure S4**). These results were further validated by a PCA of the normalized mean spectra (**Figure 115, Figure S5-7**), giving rise to clustering of fluorescence spectra according to structural similarities between the tested molecules on BY-2 cells. For instance, exciting at  $\lambda_{488}$ , the normalized mean spectra of anthranoids treated cells are clustered together, indicating that anthraquinones were observed unlike with the Ctr, Lap and Fra being not fluorescent under these settings. In addition, normalized mean spectra collected at  $\lambda_{405}$  and  $\lambda_{488}$  within the cytoplasm, ER and vesicular bodies in VH and Mad-treated cells were found to be similar and even closer after 18 h than after 5 min. Therefore, they were clustered together in the PCA. Conversely, the Emo normalized mean spectra are significantly different at  $\lambda_{405}$  and slightly less different at  $\lambda_{488}$ . These results are thus consistent with the degradation of VH in Mad as observed in DMSO and indicate that VH is transformed *in vivo* into anthraquinones with a structure closer to that of Mad than to that of Emo. Furthermore, the PCA of normalized mean spectra at  $\lambda_{405}$  clearly confirmed the apparition of new fluorescence observed at 18 h in the primary vacuoles of VH-, Emo- and Qui-treated cells, while not under  $\lambda_{488}$  settings. The fluorescence detected in the vacuole is similar to that detected in the cytoplasm for Emo unlike VH, for which the fluorescence observed in primary vacuole is significantly different from that in the cytoplasm, ER and vesicular bodies.

As a partial conclusion, SImaging analysis allowed us to accurately track the fluorescence of VH, related anthranoids and the coumarin positive control (*i.e.*, fraxetine Fra) compared to Lap which exhibit no particular fluorescence in living cells. Moreover, the new fluorescence spectra observed after 5 min and 18 h evidenced the formation of related metabolites such as Mad in VH-treated BY-2 cells. Surprisingly, the fluorescence emission spectra of Fra and VH detected in the treated BY-2 cells seem to correspond to deprotonated species although these compounds were localized in the cell compartment whose acidity is well below  $pK_{a1}$  values (*i.e.*,  $pK_{a1} = 8.5$  for Fra and  $pK_{a1} = 7.2$  for VH). Since anthraquinones and Fra have been described as chelating agents for cations such as  $Mg^{2+}$  or  $Fe^{2+}$  (Sedaira et al., 1998; Tsai et al., 2018), we have investigated the influence of metal chelation on the fluorescence emission of VH. Complexation of divalent metal cations such as  $Ca^{2+}$  and  $Mg^{2+}$  was thus examined with VH.

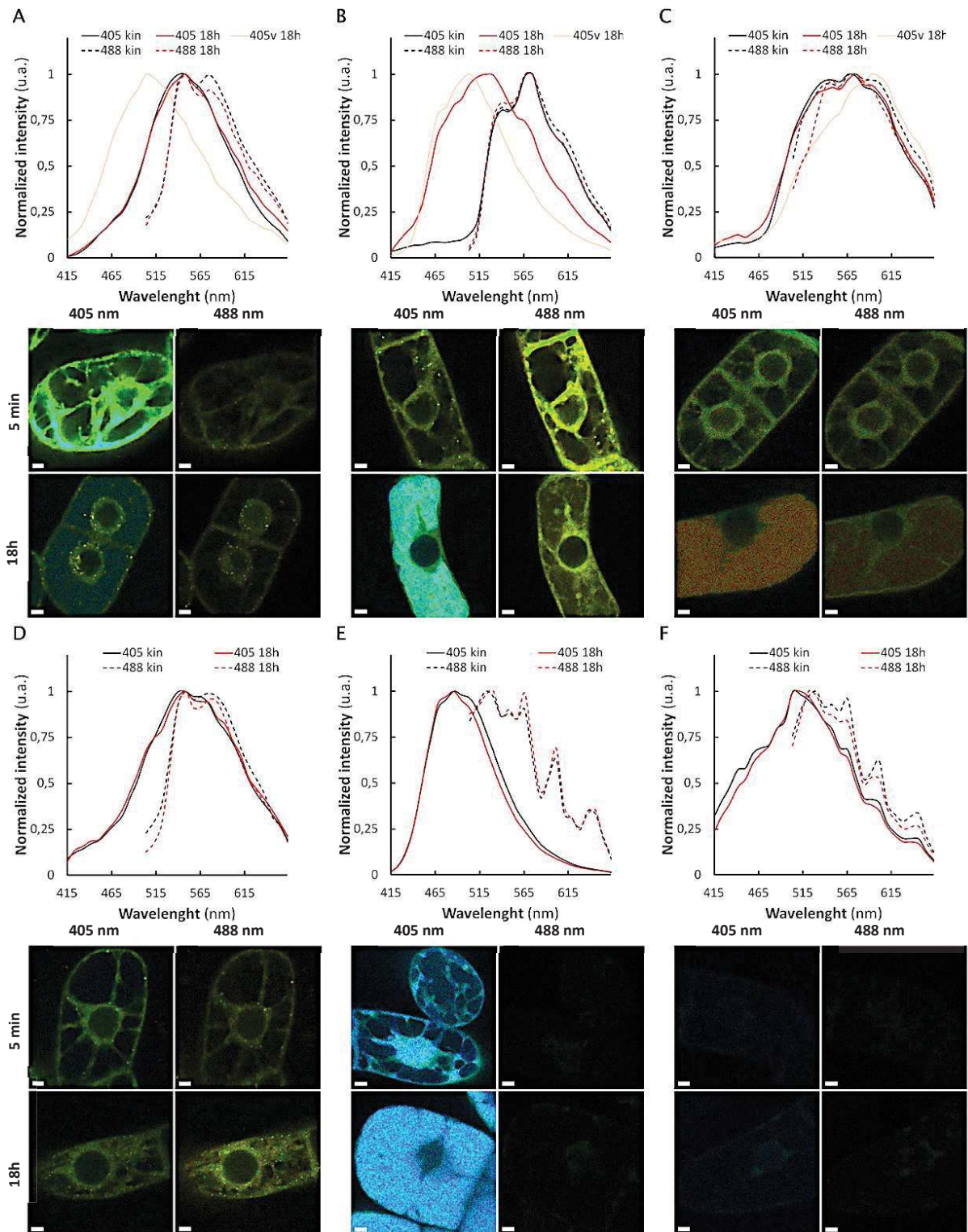


**Figure S4. Normalized mean spectra and images from Slmaging analysis of cells treated with 50  $\mu$ M.**

At  $\lambda_{405}$  (solid line) and  $\lambda_{488}$  (dashed line) of BY-2 cells treated 5 min (kin) and 18 h with 50  $\mu$ M of vismione H VH (A), quinizarin Qui (B), emodin Emo (C), madagascine Mad (D), fraxetin Fra (E) and the negative control (F). Spectra observed after 5 min (black), after 18 h (red) and in the vacuole after 18 h (red light).

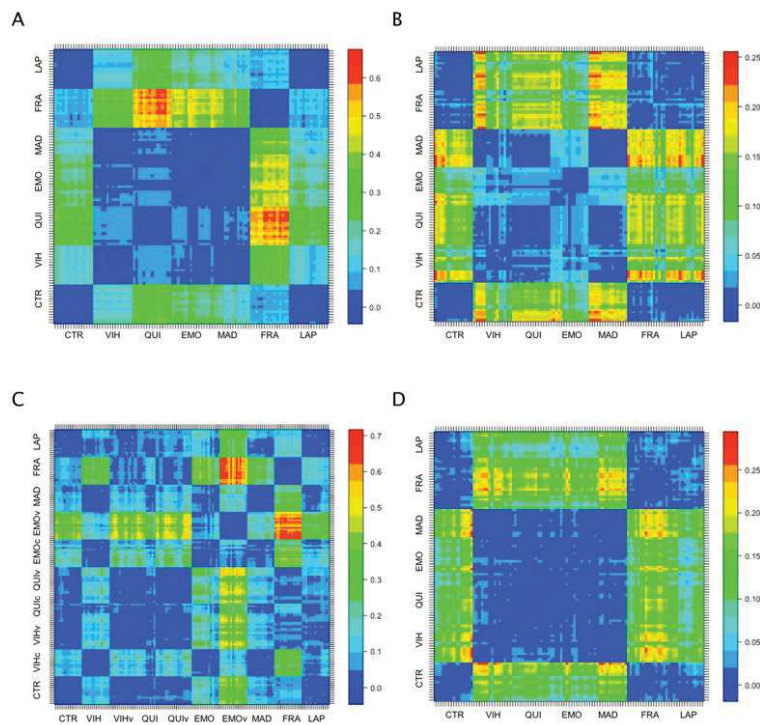
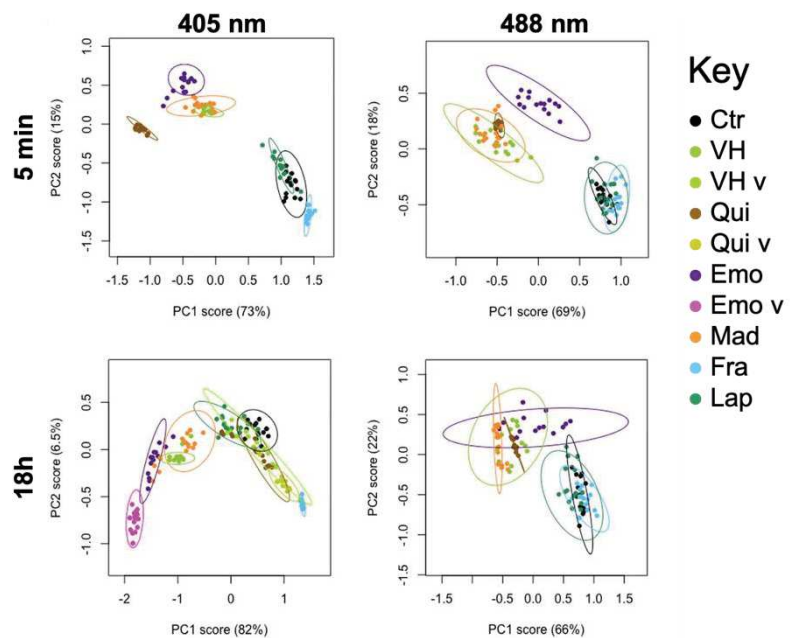


**Figure S5.** Distant matrix of normalized mean spectra obtained by SImaging analysis of cells treated or not with 25  $\mu\text{M}$  of phenolic compounds.

After 5 minutes (A, B) and 18 h (C,D). Spectra observed at  $\lambda 405$  nm (A, C) and  $\lambda 488$  nm (B,D) in control cells (CTR) and treated cells: vismione H (VH), quinizarin (Qui), Emodin (Emo), madagascine (Mad), fraxetin (Fra) and lapachol (Lap). Spectra observed at  $\lambda 405$  in primary vacuoles after 18h are specified with a "v" after the labels. 10 spectra/cell were averaged and normalized in five cells for three independent biological replicates

**Figure S6.** PCA of normalized mean spectra obtained by SImaging analysis of BY-2 cells treated or not with 50  $\mu\text{M}$  of phenolic compounds.

After 5 minutes (A, B) and 18h (C,D). Spectra observed at  $\lambda 405$  nm (A, C) and  $\lambda 488$  nm (B,D) in control cells and treated cells. Spectra observed at  $\lambda 405$  in primary vacuoles after 18 h are specified with a "v" after the labels. 10 spectra/cell were averaged and normalized in five cells for three independent biological replicates





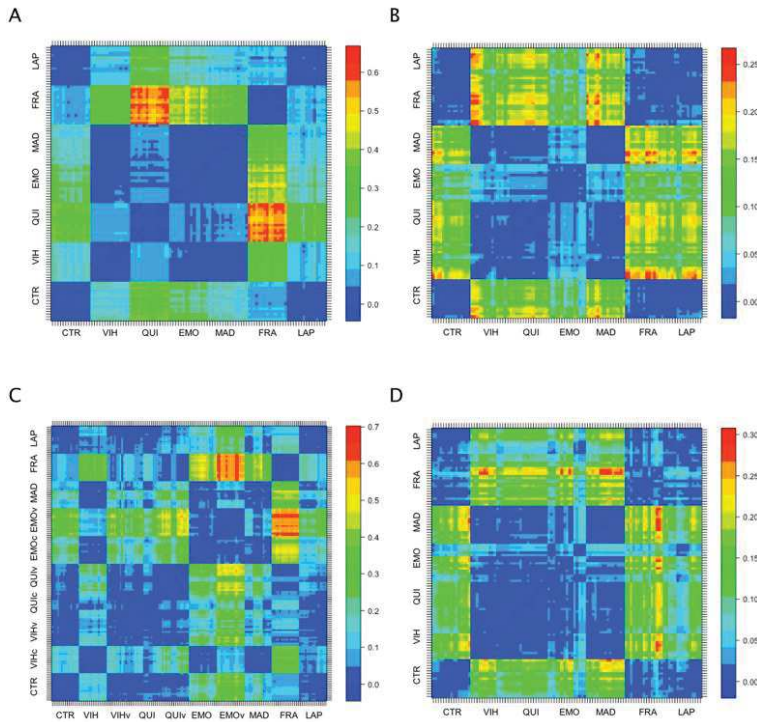


**Figure S7** Distant matrix of normalized mean spectra obtained by Slmaging analysis of cells treated or not with 50  $\mu$ M of phenolic compounds.

After 5 minutes (A, B) and 18 h (C,D). Spectra observed at  $\lambda$ 405 nm (A, C) and  $\lambda$ 488 nm (B,D) in control cells (CTR) and treated cells: vismione H (VH), quinizarin (Qui), Emodin (Emo), madagascine (Mad), fraxetin (Fra) and lapachol (Lap). Spectra observed at  $\lambda$ 405 in the primary vacuoles after 18 h are specified with a "v" after the labels 10 spectra/cell were averaged and normalized in five cells for three independent biological replicates

#### 6.3.4.3 Metal chelation influence VH fluorescence properties

Calcium and magnesium have been selected for complexation studies not only because of their abundance in plant cells, but also for their key role in cell structure as well as in cell physiology within the signaling or water splitting complex of chlorophyll in plants and cyanobacteria (Hepler, 2005; Waters, 2011). In addition, electronegativity of  $\text{Mg}^{2+}$  is higher than  $\text{Ca}^{2+}$  and *vice versa* for the atomic radius. Thus, we evaluated the absorption and fluorescence properties of 2.6  $\mu\text{M}$  VH and 11.5  $\mu\text{M}$  Fra in EtOH/water 1:1 v/v containing 0.1 M of NaCl in the presence of  $\text{Mg}^{2+}$  or  $\text{Ca}^{2+}$ . Under our experimental conditions, VH chelates both  $\text{Mg}^{2+}$  and  $\text{Ca}^{2+}$  with a comparable affinity (**Figure 116**). From the UV-Vis. absorption titrations,  $\log K_{\text{VHM}}$  values of  $2.31 \pm 0.07$  and  $2.24 \pm 0.06$  were calculated and indicated that substantial amounts of VH-Ca or VH-Mg can be formed within the cells. In both cases, about 70% of complexation of VH (26  $\mu\text{M}$ ) was achieved with 6 mM of  $\text{CaCl}_2$  or  $\text{MgCl}_2$ . Although VH displays similar binding strength with these metal ions, the absorption data suggested different binding modes. Marked spectral variation were observed in the case of  $\text{Ca}^{2+}$  compared to  $\text{Mg}^{2+}$  most likely due to different coordination preferences. As reported, in proteins, carboxylates preferentially act as bidentate binders with  $\text{Ca}^{2+}$  and as monodentate ligands with  $\text{Mg}^{2+}$  (Dudev and Lim, 2004). This property could explain our absorption data with VH acting as bidentate ligand with  $\text{Ca}^{2+}$  ( $\beta$ -hydroxy-ketone binding unit leading, **Figure S8**), while preferentially coordinating  $\text{Mg}^{2+}$  with monodentate binding unit mode (phenolate unit, **Figure S9**). Fluorescence analysis of VH-Ca and VH-Mg complexes in solution confirmed the influence of chelation on the fluorescence properties of the compound. The maximum of emission  $\lambda_{\text{Em}}$  for VH-Ca and VH-Mg ( $549 \pm 1$  nm) complexes was found to be higher than that of the VH  $\text{LH}^+$  species ( $532 \pm 1$  nm) (**Table 19**). Nonetheless, the  $\Phi_{\text{F}}$  of VH-Ca (19.8%) and VH-Mg (18.6%) complexes were substantially lower than that of VH  $\text{LH}^+$  (31%) species, but still much higher than the neutral species (3.7% for VH  $\text{LH}_2$ ).

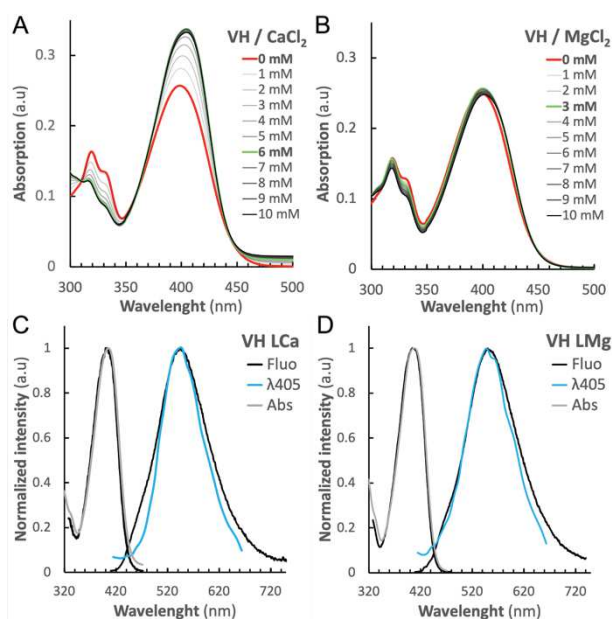


**Figure 116.** Vismione H vh photophysical properties are influenced by metal cations complexation.

(A-B) absorption spectra of metal complexes formed by vh with different amount of (A) ca(ii) and (B) mg(ii) spectra with no complex formed (bold red) and with the highest changes in the absorption spectrum (bold green). normalized fluorescence (black), absorption (grey) and simaging spectra of (C) vh-ca and (D) vh-mg complexes at  $\lambda_{405}$  settings

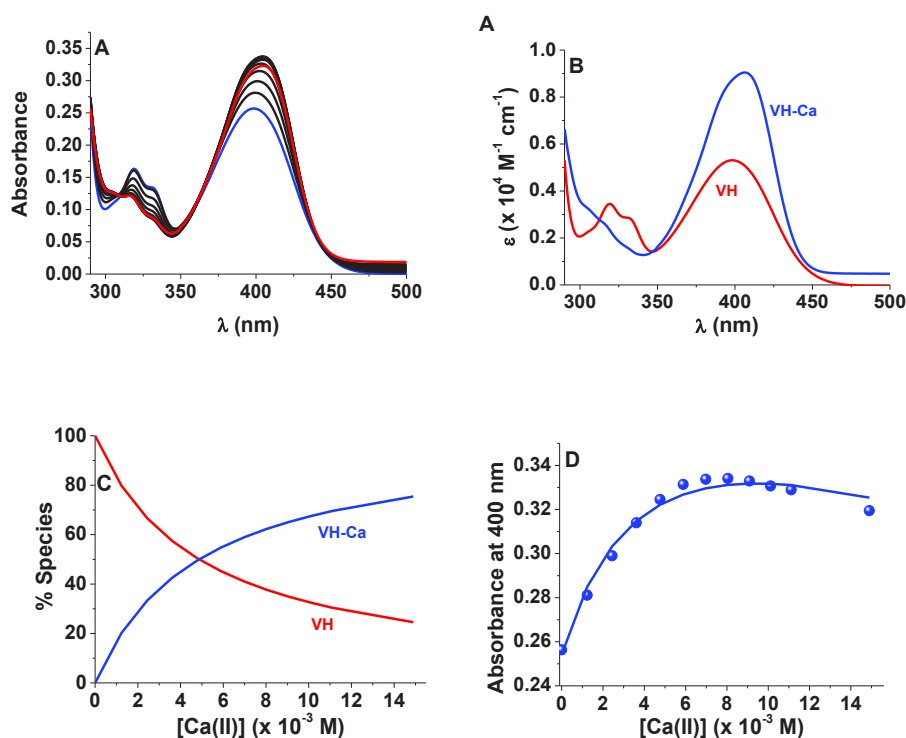


**Figure S8 UV-Vis.** absorption titration of vismione H by Ca(II).

(A) Absorption spectral variation of VH as a function of  $[Ca(II)]$ . (B) Electronic absorption spectra of VH and its Ca(II) complex. (C) Species distribution diagrams as a function of  $[Ca(II)]$ . (D) Absorbance at 400 nm versus  $[Ca(II)]$  compared to the calculated data (solid line). Solvent: EtOH/water 1:1 v/v,  $I = 0.1 M NaCl$ ;  $T = 25^\circ C$ ;  $[VH] = 26 \mu M$ .

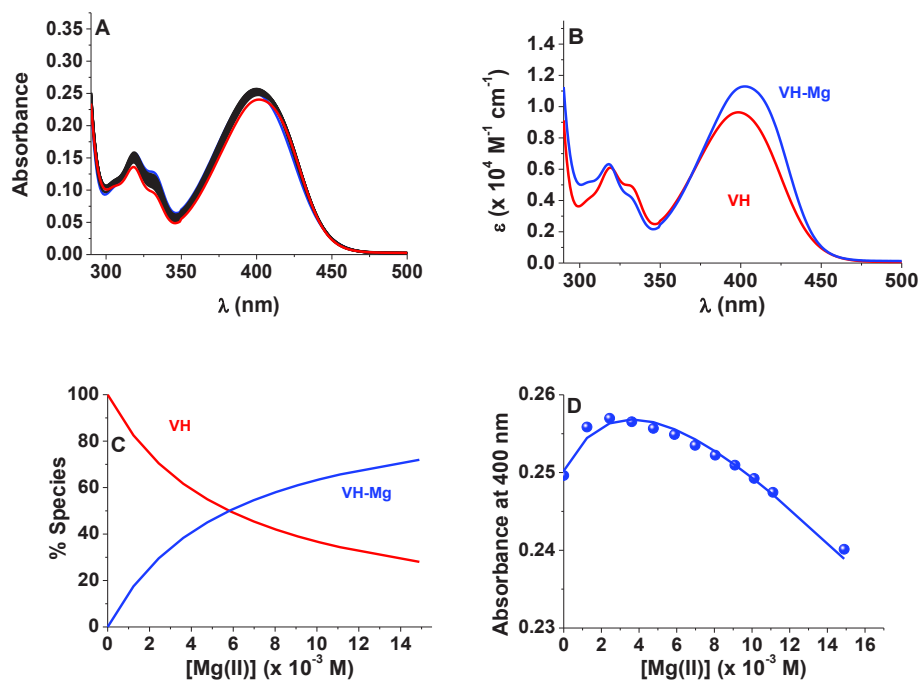


**Figure S9** UV-Vis. absorption titration of vismione H by Mg(II).

(A) Absorption spectral variation of VH as a function of [Mg(II)]. (B) Electronic absorption spectra of VH and its Mg(II) complex. (C) Species distribution diagrams as a function of [Mg(II)]. (D) Absorbance at 400 nm versus [Mg(II)] compared to the calculated data (solid line). Solvent: EtOH/water 1:1 v/v, I = 0.1 M NaCl; T = 25°C; [VH] = 26 μM.

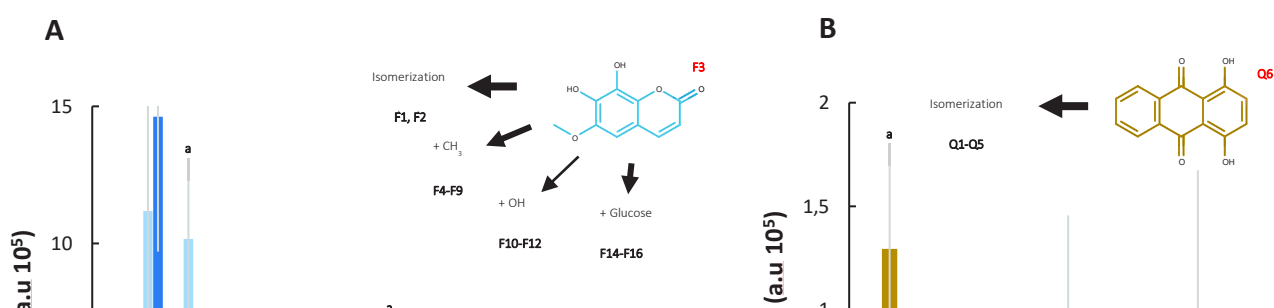


#### 6.3.4.4 Metabolization of VH into anthrone, anthraquinones and more polar compounds

An increase in the polarity of metabolites is typically observed and results from the glycosylation or oxidation by cytochrome P450 for the storage and sequestration of phenolic compounds into the primary vacuole, as described with Fra (Lefèvre et al., 2018; Stringlis et al., 2019). To identify putative related metabolites involved in the fluorescence spectra characterized by SImaging, a non-targeted metabolomics analysis was carried out using ESI/UPLC-QTOF-MS<sup>2</sup> and MeOH extracts isolated from treated and non-treated BY-2 cells. The comparison of the results with a database including the references and their related metabolites obtained by *in silico* enzymatic digestion revealed variations in the concentration of 54 molecules specific to treatments, with *m/z* attributed to references or putative catabolites (Figure 117, Table S3-4).

Apart from Lap (Figure S3, Figure S10, Table S2), all references were detected as expected in corresponding MeOH extracts of BY-2 cells treated 15 min and 18 h. In addition, the total contents of metabolites detected in Emo and Qui-treated cells were doubled after 18 h, vice-versa for Mad or VH treated cells and remains constant for Fra-treated cells (Figure 117). Although, related metabolites seem to be accumulated in Emo, Qui and Fra-treated cells, the proportion of references was 26, 3.5 and 16 times lower after 18 h, confirming their subsequent metabolization. In contrast, the Mad and VH proportion in treated cells remains 39 % and 22 % respectively, supporting either that VH and Mad are transformed into non-annotated metabolites and/or non-prenylated anthranoids are easier to be catabolized by BY-2 cells.

The results of Fra MeOH extracts (Figure 117) were consistent with those described for BY-2 cells treated 60 min with 20  $\mu$ M of Fra (Lefèvre et al., 2018). Nevertheless, no di-oxygenated coumarin was detected (Figure 117, Table S3). Our coumarin mixture consisted in 99.4 % of 12 tri-oxygenated forms distributed in Fra and its isomers (F1-F3), six methylated (F4-F9) and three glycosylated forms (F14-F16). The remaining 0.6% corresponds to tetra-oxygenated coumarins including sideretin and two isomers (F10-F12) plus another methoxylated form (F13). Our results suggest that at 15 min, Fra (33.7 %) was quickly isomerized in F2 (37 %) which is more polar, then both were methylated or glycosylated, resulting in F8 (16.3 %) and F9 (1%) or F15 (7 %) and F16 (2.3 %), respectively, the other forms representing only 2.7 % of the mixture.



After 18 h, with the exception of F2, F15 and F16, the trend was completely reversed and the quantity of Fra (2 %), F8 (2.5 %) and F9 (0.4 %) were 16, 6 and 2-fold lower respectively, unlike the other forms which were 4 to 327-fold higher. Interestingly, the F1 isomer appeared to be significantly increased from 1% to 7 % between 15 min and 18 h as well as other methylated (F4, F5), hydroxylated (F10) and glycosylated (F14) forms, which were 6 to 33-fold higher and might be related to F1.

Thus, the accumulation of Fra derivatives seems to be highly regulated as suggested by the constant level of F2 and glycosylated forms F15 and F16 after 18 h, indicating a putative concentration limit of these forms which could explain the distribution into other more polar forms such as F1 and F14. Surprisingly, we never observed more than 12 % of glycosylated derivatives of Fra unlike the 63 % described in 7 days-old BY-2 cells treated with 20  $\mu$ M of Fra (Lefèvre et al., 2018), proposing that Fra isomerization into F2 (50 %) remains the privileged mechanism for long-term storage in the primary vacuole compared to glycosylation. As a result, BY-2 cells metabolized Fra into a mixture of more polar metabolites as indicated by the decrease in  $R_t$  in order to transport and store them from the cytosol and nucleus to the primary vacuole as observed by Slmaging. The fluorescence observed by Slmaging at  $\lambda_{405}$  in 5 min and 18 h Fra-treated cells would thus correspond to F2 and related metabolites instead of Fra  $LH^-$ , which has a low  $\Phi_F$  and  $\lambda_{Em}$  of 521 nm in Slmaging. Nevertheless, it cannot be excluded that the spectrum obtained especially at 5 min results from the mixture of Fra and related metabolites and/or their corresponding metal complex with a divalent cation. Interestingly, the regulation of Fra metabolization by BY-2 cells in each form might be tightly adjusted to the environment. Actually, a balance between the solubility of metabolites, the regulation of enzymes involved in feedback loops and cytotoxicity could explain this variation. In this respect, metabolites with an intermediate polarity would be preferred for each cluster as well as the increase of methylated forms after 18 h as reported with 1-hydroxycantinin-6-one in *Alianthus altissima* (Osoba and Roberts, 1994). Furthermore, similarities with Fra metabolization were observed in the response of BY-2 cells to anthranoids, as indicated by the comparison of  $R_t$ ,  $m/z$ , fragments and the proportion of related anthranoids and references detected in MeOH extracts at 15 min and 18 h. Interestingly, only Qui (Q6) and five isomers (Q1-Q5) were specifically identified in Qui-treated cells in contrast to Emo, Mad and VH treatments which shared few common metabolites at 15 min and 18 h (**Figure 117, Table S 4**).

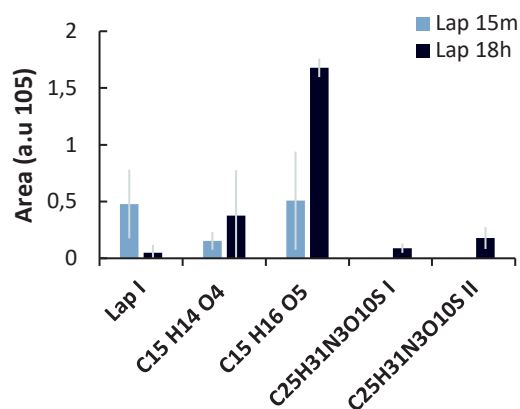


**Figure S10** Non targeted metabolomic analysis using ESI/UPLC-QTOF- MS2 analysis of MeOH extracts from BY-2 cells treated 15 min and 18 h with 50  $\mu$ M lapachol Lap.

**Table S2.** Metabolites identified in metabolomic analysis of MeOH extracts from BY-2 cells treated with 50  $\mu$ M Lap. Exact mass-to-charge ratio ( $m/z$ ), detected ion, retention time ( $R_t$ ),  $m/z$  ratio of parent,  $\Delta m/z$  (ppm), variation of isotopic ratio (mSigma) and fragment ions were obtained from the UPLC/ESI-QTOF-MS<sup>2</sup> (QTOF) chromatograms in positive ionization mode.

#	measured $m/z$	Detected Ion	Rt (min)	$\Delta m/z$ [ppm]	mSigma	Molecular Formula	Annotation	fragments $m/z$ (Relative intensity %)
L1	243,1017	[M+H] <sup>+</sup> [M+Na] <sup>+</sup>	8.98	0.42	13.7	C <sub>15</sub> H <sub>14</sub> O <sub>3</sub>	Lap isomer I	205.048 (18), 187.038 (100), 159.043 (80), 131.049 (4.7), 105.033 (3.1), 61.039 (1.8), 43.017 (6)
L2	259,0967	[M+H] <sup>+</sup> [M-H <sub>2</sub> O+H] <sup>+</sup> , [M+Na] <sup>+</sup>	7.51	0.82	7.6	C <sub>15</sub> H <sub>14</sub> O <sub>4</sub>	OH-Lap	223.076 (4.4), 195.080 (1.6), 159.044 (2.2), 71.049 (2.6), 61.039 (100), 43.053 (12)
L3	277,1073	[M+H] <sup>+</sup> [M+Na] <sup>+</sup> , [M-H <sub>2</sub> O+H] <sup>+</sup>	8.00	0.667	2.6	C <sub>15</sub> H <sub>16</sub> O <sub>5</sub>	2xOH-Lap	241.085 (24), 219.056 (100), 195.080 (25), 175.038 (47), 69.069 (73)
L4	566,1806	[M+H] <sup>+</sup>	5.58	-0.315	10.2	C <sub>25</sub> H <sub>31</sub> N <sub>3</sub> O <sub>10</sub> S	GSH-Lap I*	
L5	566,1804	[M+H] <sup>+</sup>	7.62	0.24	12.0		GSH-Lap II*	

**Table S3.** Metabolites identified in metabolomic analysis of MeOH extracts from BY-2 cells treated with 50  $\mu$ M Fra. Exact mass-to-charge ratio ( $m/z$ ), detected ion, retention time ( $R_t$ ),  $m/z$  ratio of parent,  $\Delta m/z$  (ppm), variation of isotopic ratio (mSigma) and fragment ions were obtained from the UPLC/ESI-QTOF-MS<sup>2</sup> (QTOF) chromatograms in positive ionization mode. <sup>a, b, c</sup> fragments of isomer 1, 2, 3 respectively. \* No fragmentation spectrum available.

#	measured $m/z$	Detected Ion	Rt (min)	$\Delta m/z$ [ppm]	mSigma	Molecular Formula	Annotation	fragments $m/z$ (Relative intensity %)			
								$m/z$	a	b	c
F1	209.0445	[M+H] <sup>+</sup>	4.88	0.184	4.8	C <sub>10</sub> H <sub>8</sub> O <sub>5</sub>	Fra Isomer I <sup>a</sup>	194.021	48	56	51
F2	209.0444	[M+H] <sup>+</sup>	5.54	-0.085	3.2		Fra isomer II <sup>b</sup>	166.026	18	23	22
F3	209.0444	[M+H] <sup>+</sup> [M+Na] <sup>+</sup> , [M+NH <sub>4</sub> ] <sup>+</sup>	6.00	0.19	4.7		Fraxetin <sup>c</sup>	153.054	14	17	17
								149.023	29	35	33
								135.044	8	12	11
F4	223.0603	[M+H] <sup>+</sup>	5.51	0.99	10.5	C <sub>11</sub> H <sub>10</sub> O <sub>5</sub>	Me-Fra isomer I <sup>a</sup>	208.036	-	51	35
F5	223.06	[M+H] <sup>+</sup>	5.81	-0.42	2.9		Me-Fra isomer II <sup>b</sup>	190.026	49	68	51
F6	223.0601	[M+H] <sup>+</sup>	5.86	-0.26	7.7		Me-Fra isomer III*	179.034	13	19	15
F7	223.0603	[M+H] <sup>+</sup>	6.08	0.835	2.3		Me-Fra isomer IV*	162.031	48	49	47
F8	223.0602	[M+H] <sup>+</sup> [M+Na] <sup>+</sup>	6.47	0.268	5.0		Me- Fra isomer V <sup>c</sup>	149.023	7	3	-
F9	223.06	[M+H] <sup>+</sup>	6.70	-0.56	16.5		Me- Fra isomer VI*	107.049	10	3.7	11
								78.046	-	3.5	3.1
F10	225.0394	[M+H] <sup>+</sup>	4.69	0.18	4.2	C <sub>10</sub> H <sub>8</sub> O <sub>6</sub>	OH- Fra isomer I <sup>a</sup>	210.016	100	100	100
F11	225.0395	[M+H] <sup>+</sup>	4.95	0.473	1.5		OH- Fra isomer II <sup>b</sup>	182.021	4.7	-	6.1
F12	225.0394	[M+H] <sup>+</sup>	5.61	0.18	11.8		OH- Fra isomer III <sup>c</sup>	165.018	7.0	7.0	4.7
								154.026	10	10	10
F13	239.0551	[M+H] <sup>+</sup>	5.54	0.56	3.1	C <sub>11</sub> H <sub>10</sub> O <sub>6</sub>	MeOH- Fra*				
F14	371.0976	[M+H] <sup>+</sup>	4.88	0.794	6.8	C <sub>16</sub> H <sub>18</sub> O <sub>10</sub>	Glu- Fra isomer I*	209.044	100	100	
F15	371.0975	[M+H] <sup>+</sup>	5.48	0.592	0.2		Glu- Fra isomer II <sup>a</sup>	194.021	4.2	4.4	
F16	371.0977	[M+NH <sub>4</sub> ] <sup>+</sup> , [M+Na] <sup>+</sup>	5.53	0.831	6.1		Glu- Fra isomer III <sup>b</sup>	145.085	-	4	
								71.049	-		



Synthetic origin of Qui with a 4-OH group may explain this difference and the absence of methylated, hydroxylated or glycosylated forms. It also means that Q1-Q5 might differ from Qui in the 1-OH function, and therefore that the putative isomerase involved are less selective than those responsible of other modifications. Another possibility is a chemical isomerization or tautomerization of anthranoids *via* a non-dependent enzymatic pathway, which may be promoted by redox reactions (Fain et al., 2006). The fluorescence observed by SIMaging at  $\lambda_{488}$  in the cytoplasm and vesicular bodies in Qui-treated cells is consistent with its detection in MeOH extracts at 5 min and 18 h. In the absence of Q1-Q5 references we were not able to confirm whether isomers contributed to the fluorescence observed and especially that observed at  $\lambda_{405}$ . It can be speculated that Q1-Q5 are also fluorescent and distributed in different cell compartments according to their polarity. Thus, Q4-Q6 would stain vesicular bodies and cytoplasm observed immediately at  $\lambda_{488}$ . While Q1-Q3, whose concentrations are significantly increased after 18 h, would be located in the primary vacuole and observable only at  $\lambda_{405}$ . Obviously, another non-associated metabolite could also be responsible of the observed fluorescence.

In the other anthranoids-treated cells, eight isomers of Emo (A1-A7, A9) have been detected. In addition, five methylated (A10-A14), two hydroxylated (A15, A16), two methoxylated (A17, A18) and four glycosylated (A24-A27) forms were also significantly detected only in Emo-treated cells (**Figure 117, Table S 5**). Surprisingly, Emo (A8) and A1-A6 isomers were almost exclusive to Emo-treated cells and after 18 h A1-A5 increased from 14 to 59 % of the overall content, whereas the A7 and A9 isomers were specific to Mad and VH-treated cells, respectively. These results support those obtained previously by SIMaging for Emo-treated cells 5 min and 18 h. The fluorescence observed at  $\lambda_{405}$  and  $\lambda_{488}$  was mainly seen in the cytoplasm and some vesicular bodies, it likely corresponds to Emo and A6 isomer as well. However, as for Qui, the A1-A6 isomers and other related metabolites likely contribute to the observed fluorescence.

For instance, the fluorescence in the primary vacuole observed at  $\lambda_{405}$  after 18 h might be associated to a mixture of hydrophilic isomers (A1-A4), glycosylated (A24, A25) or hydroxylated (A15, A16) forms which were significantly increased after 18 h compared to 15 min. In addition, VH (A23) as well as madagascine anthrone and two isomers (A19-A21) were detected only in VH-treated cells, while Mad (A22) was common to VH and Mad-treated cells.

**Table S 4.** Metabolites identified in metabolomic analysis of MeOH extracts from BY-2 cells treated with 50  $\mu\text{M}$  Qui. Exact mass-to-charge ratio ( $m/z$ ), detected ion, retention time (Rt),  $m/z$  ratio of parent,  $\Delta m/z$  (ppm), variation of isotopic ratio (mSigma) and fragment ions were obtained from the UPLC/ESI-QTOF-MS2 (QTOF) chromatograms in positive ionization mode.

#	measured $m/z$	Detected Ion	Rt (min)	$\Delta m/z$ [ppm]	mSigma	Molecular Formula	Annotation	fragments $m/z$ (Relative intensity %)					
								$m/z$	a	b	c	d	e
Q1	241.0495	[M+H] <sup>+</sup>	5.86	0.158	1.9	C <sub>14</sub> H <sub>8</sub> O <sub>4</sub>	Qui isomer I <sup>a</sup>	241.049	100	100	100	100	100
Q2	241.0498	[M+H] <sup>+</sup>	6.36	1.25	5.7		Qui isomer II <sup>*</sup>	213.054	20	16	20	18	21
Q3	241.0496	[M+H] <sup>+</sup>	7.74	0.6	8.9		Qui isomer III <sup>b</sup>	185.059	27	26	24	26	28
Q4	241.0492	[M+H] <sup>+</sup>	8.3	-1.44	2.0		Qui isomer IV <sup>c</sup>	157.064	21	18	18	18	20
Q5	241.0495	[M+H] <sup>+</sup>	8.59	0.29	3.6		Qui isomer V <sup>d</sup>	129.069	7.7	5.5	6.4	-	6.8
Q6	241.0496	[M+H] <sup>+</sup>	10.49	0.021	4.3		Quinizarin <sup>e</sup>	59.049	-	-	-	-	-

**Table S 5.** Metabolites identified in non-targeted metabolomic analysis of MeOH extracts from BY-2 cells treated with 50  $\mu\text{M}$  Emo, Mad and VH.

Exact mass-to-charge ratio ( $m/z$ ), detected ion, retention time (Rt),  $m/z$  ratio of parent,  $\Delta m/z$  (ppm), variation of isotopic ratio (mSigma) and fragment ions were obtained from the UPLC/ESI-QTOF-MS2 (QTOF) chromatograms in positive ionization mode.

#	measure d $m/z$	Detecte d ion	Rt (min)	$\Delta m/z$ [ppm]	mSigma	Molecular Formula	Annotation	fragments $m/z$ (Relative intensity %)							
								$m/z$	a	b	c	d	e	f	g
A1	271.0600	[M+H] <sup>+</sup>	5.8	0.06	2.7	C <sub>15</sub> H <sub>10</sub> O <sub>5</sub>	Emo isomer I <sup>*</sup>	253.049	-	-	-	-	1.4	1.5	1.5
A2	271.0602	[M+H] <sup>+</sup>	6.17	0.387	2.6		Emo isomer II <sup>a</sup>	229.049	42	43	41	40	19	-	-
A3	271.0601	[M+H] <sup>+</sup>	7.54	0.03	9.0		Emo isomer III <sup>b</sup>	201.054	23	23	24	23	-	-	-
A4	271.0602	[M+H] <sup>+</sup>	7.71	0.636	4.8		Emo isomer IV <sup>c</sup>	197.059	-	-	-	-	14	17	17
A5	271.0601	[M+H] <sup>+</sup>	8.49	0.324	1.1		Emo isomer V <sup>d</sup>	173.059	12	12	13	12	4.4	-	-
A6	271.0601	[M+H] <sup>+</sup>	9.06	0.56	0.8		Emo isomer VI <sup>e</sup>	169.064	-	-	-	-	-	4.8	4.2
A7	271.0603	[M+H] <sup>+</sup>	9.99	1.265	15.4		Emo isomer VII <sup>*</sup>	145.064	3.8	3.6	4.3	-	-	-	-
A8	271.0601	[M+H] <sup>+</sup>	10.38	0.396	9.1		Emodin <sup>f</sup>	115.054	-	1.6	1	1.4	1	1.5	-
A9	271.0602	[M+H] <sup>+</sup>	11.73	0.747	3.0		Emo isomer VIII <sup>g</sup>	95.013	1.7	1.3	1.4	1.3	-	-	-
A10	285.0757	[M+H] <sup>+</sup>	7.64	-0.02	9.6	C <sub>16</sub> H <sub>12</sub> O <sub>5</sub>	Me-Emo I <sup>a</sup>	252.042	-	2.6	3.4	-	-	-	
A11	285.0758	[M+H] <sup>+</sup>	8.42	0.21	9.8		Me-Emo II <sup>b</sup>	242.056	6.5	-	10	-	-	-	
A12	285.076	[M+H] <sup>+</sup>	8.94	1.01	8.7		Me-Emo III <sup>*</sup>	211.075	6.1	9.9	-	-	-	-	
A13	285.076	[M+H] <sup>+</sup>	9.55	1.025	2.0		Me-Emo IV <sup>*</sup>	196.052	-	1.9	1.9	-	-	-	
A14	285.0758	[M+H] <sup>+</sup>	11.01	0.02	3.8		Me-Emo V <sup>c</sup>	168.056	-	-	-	-	-	-	
A15	287.0552	[M+H] <sup>+</sup>	7.4	0.413	2.1	C <sub>15</sub> H <sub>10</sub> O <sub>6</sub>	OH-Emo I	269.044 (9.2), 241.049 (27), 213.054 (10), 199.038 (4.9), 185.059 (3.2), 157.064 (2.8)							
A16	287.0551	[M+H] <sup>+</sup>	7.88	0.226	3.5		OH-Emo II <sup>*</sup>								
A17	301.0709	[M+H] <sup>+</sup>	7.17	0.82	12.2	C <sub>16</sub> H <sub>12</sub> O <sub>6</sub>	MeOH-Emo I <sup>a</sup>	255.065	11.5	10.5	-	-	-	-	
A18	301.0709	[M+H] <sup>+</sup>	9.63	0.7	3.6		MeOH-Emo II <sup>b</sup>	227.069	-	-	-	-	-	-	
A19	325.1439	[M+H] <sup>+</sup>	8.85	1.32	27.5	C <sub>20</sub> H <sub>20</sub> O <sub>4</sub>	Mad anthrone I <sup>*</sup>	257.080	100	100	-	-	-	-	
A20	325.1435	[M+H] <sup>+</sup>	10.62	0.571	4.8		Mad anthrone II <sup>a</sup>	239.070	19.8	-	-	-	-	-	
A21	325.1435	[M+H] <sup>+</sup> , [M+Na] <sup>+</sup>	11.46	0.2275	10.8		Mad anthrone III <sup>b</sup>	211.075	11.2	-	-	-	-	-	
A22	339.1226	[M+H] <sup>+</sup> , [M+Na] <sup>+</sup>	11.73	0.92	4.3	C <sub>20</sub> H <sub>18</sub> O <sub>5</sub>	Madagascine	283.060 (8.5), 271.060 (100), 197.059 (3.1), 69.069 (9.1)							
A23	385.1645	[M+H] <sup>+</sup> , [M+Na] <sup>+</sup>	10.63	0.512	4.9	C <sub>22</sub> H <sub>24</sub> O <sub>6</sub>	Vismione H	Only [M+Na] <sup>+</sup> 347.125 (14), 287.091 (100), 269.080 (26), 245.080 (39), 60.081 (6)							
A24	433.1131	[M+H] <sup>+</sup>	6.17	0.3	22.4	C <sub>21</sub> H <sub>20</sub> O <sub>10</sub>	Glu-Emo I <sup>a</sup>	271.060	100	100	100	-	-	-	
A25	433.113	[M+H] <sup>+</sup>	7.54	-0.15	17.4		Glu-Emo II <sup>*</sup>	229.049	4.8	4.3	4.5	-	-	-	
A26	433.113	[M+H] <sup>+</sup>	8.44	0.505	6.6		Glu-Emo III <sup>b</sup>	85.028	15	11	12	-	-	-	
A27	433.1132	[M+H] <sup>+</sup> , [M+Na] <sup>+</sup>	9.03	0.888	5.6		Glu-Emo IV <sup>c</sup>	69.033	3.9	2.3	3.4	-	-	-	

These results confirmed that VH is also converted into madagascine anthrone and Mad *in vivo*, but the anthrone A20 (42 %) remains the main metabolite detected unlike in DMSO for which Mad and bianthrone prevail after 8 h (Galle, 2015).

Interestingly, these observations confirm that the bright fluorescence observed at  $\lambda_{405}$  mainly in the cytoplasm and ER, which was associated to VH LH<sup>-</sup> and/or Ca<sup>2+</sup> complex, corresponds to a mixture of anthranol forms of Mad and VH anthrones, as previously hypothesized. It is possible that intracellular O<sub>2</sub> and redox levels, or chelation of divalent cations such as Ca<sup>2+</sup> stabilize these forms *in cellula* as boron in sodium tetraborate buffer (Hlasiwetz and Grabowski, 1867; Cameron et al., 1976; Fujii et al., 1997). Unfortunately, the metabolite responsible for the fluorescence observed at  $\lambda_{405}$  in the primary vacuole of VH-treated cells after 18 h could not be characterized and most likely corresponds to a non-annotated metabolite. Furthermore, it is relevant that the fluorescence observed at  $\lambda_{488}$  by SIMaging in the cytoplasm and vesicular bodies of Mad and VH-treated cells was clustered together in the PCA, considering that the anthraquinones detected at 5 min and 18 h were the same. Although after 18 h the amount of VH, Mad and A20 remained insignificantly altered in VH-treated cells, the madagascine anthrone isomers A19, A21 were not detected anymore, and Mad in Mad-treated cells was considerably decreased after 18 h. Unexpectedly, Mad which is the less polar molecule (R<sub>t</sub> = 11.73 min) was metabolized into A9 isomer rather than Emo (A8), suggesting that Mad is isomerized prior to deprenylation in BY-2 cells.

Taken together, these results point out that 3-OH on anthranoids is a key position which contributes to at least two independent anthranoids metabolization pathways in BY-2 cells. Thus, a free 3-OH allows anthranoids metabolization into very polar Emo isomers (A1-A6) as well as hydroxylated, methylated or glycosylated forms. Whereas if the same 3-position is substituted with a prenyl group as in VH or Mad, the metabolization is altered producing mostly hydrophobic Emo isomers (A7-A9). This situation can result from a different subcellular localization of isomerases involved in the production of A1-A6 from those producing A7-A9. Considering this hypothesis, the more polar Emo would be immediately accessible for specific isomerases located in hydrophilic compartments such as the cytosol or primary vacuole. While the less polar Mad and VH would be located initially in hydrophobic compartments such as membranes or lipid droplets prior to the prenyl cleavage triggering transformation by other isomerases. Another hypothesis would be an inhibition of chemical

isomerization/tautomerization either by the hydrophobic environment itself or by the 3-O-prenyl, thus preventing electron transfer from the aromatic ring to 3-OH and therefore promoting the formation of A7-A9 isomers rather than Emo and A1-A6 isomers.

As isomers were detected in all treatments with anthranoids and Mad as well as anthrones were also quickly detected in the analysis of VH reference in solution, the chemical isomerization/tautomerization and VH deacetylation seem to be the most relevant hypothesis. Chemical reaction, which is closely dependent on the cellular environment (pH, ions, redox status) could also explain the high variability observed for anthranoids-related metabolites. Nevertheless, in the absence of transcriptomics or proteomics data, our study did not enable us to conclude on the precise mechanism involved in the isomer's formation. However, deprenylation in Mad and VH-treated cells or hydroxylation, methylation and glycosylation steps specific to Fra and Emo treatments, must be dependent on an enzymatic pathway as already described for Fra (Tsai et al., 2018). Finally, it is important to notice that even after 18 h, the few metabolites annotated in MeOH extracts from Qui-, Mad- or VH-treated cells and their low accumulation area compared to Fra indicate that other metabolization pathways exist. However, these metabolites were not annotated. In spite of the variability and the lack of references to confirm the identification of the putative metabolites, the non-targeted metabolomic analysis clearly supported our Slmaging data as well as our hypothesis of anthranoids metabolization in BY-2 cells.

For the first time, we characterized the fluorescence *in cellula* of VH as well as its degradation products known as madagascine anthrone and Mad. This proof of concept demonstrates that Slmaging is particularly sensitive and suitable for the observation of anthranoids *in vivo*. More precisely, Slmaging allowed localizing and discriminating over time and in living cells the fluorescence of each of the studied fluorescent compounds and their related fluorescent metabolites. The fruitful combination of Slmaging with the non-targeted metabolomic analysis by ESI-UPLC-QTOF-MS<sup>2</sup> was particularly effective in identifying key metabolites, thus highlighting the pivotal role of 3-OH position in distinct metabolization pathways for Emo and prenylated anthranoids such as VH and Mad. Surprisingly, the studied anthranoids have never been identified in *N. tabacum*, but our data unambiguously demonstrate that BY-2 cells are competent to absorb and metabolize all of the tested compounds. As observed by Slmaging,

different cell compartments contribute to the metabolization process especially for VH and related anthranoids, involving at least four cell compartments (primary vacuole, cytoplasm, ER and vesicular bodies). According to our results, metabolic pathways in BY-2 cells have been hypothesized, supporting that some steps are catalyzed by enzymes while other are most likely the result of chemical reactions inherent to anthranoids structure and to the intracellular environment. Although our results indicate that the isomerization/tautomerization of anthranoids is chemically triggered, the remarkable distribution of these isomers according to their polarity and in relation to each treatment is consistent with a well-orchestrated set of isomerases. Transcriptomics or proteomics approaches on cell fractions containing the isolated organelles depending on the fluorescence would be helpful to clarify these aspects. Unexpectedly, our results obtained with Fra markedly differ from those previously described for BY-2, suggesting that glycosylation is not the main storage mechanism for Fra in *N. tabacum*. Alternatively, it appears that isomerization, methylation or hydroxylation most likely prevail for efficient storage of related metabolites in the primary vacuole. Lower energetic costs or mobilization of sugars by young BY-2 cells for their growth may explain this difference. No other di-hydroxylated forms were detected unlike those which have been reported. Finally, our SImaging approach demonstrates that Fra and/or other tri- or tetra-hydroxylated forms can brightly emit fluorescence *in vivo* especially if they are deprotonated or complexed to metal ions.

### **6.3.5 Conclusion**

This paper describes the implementation of SImaging as a powerful tool to study fluorescence as well as metabolization processes of anthranoids and other naturally occurring molecules in living cells. Our approach, which combines SImaging analysis and non-targeted metabolomics, readily allows identifying and characterizing the spectral fingerprints from references and related metabolites. In addition, due to its low cost, low autofluorescence and heterogeneous metabolism, the BY-2 cell model is of particular interest for this proof of concept and could undoubtedly contribute to further research. Still, as long as anthranoids and other naturally occurring fluorescent compounds are valuable, it would be interesting to extend this study carried out on the BY-2 model to other plants to investigate the biosynthesis pathways and the influence of some factors on the metabolism of naturally occurring compounds. From another

point of view, the developed approach offers interesting perspectives in the medical field, as VH and similar compounds have been described for their antimalarial properties and the biological targets and action mechanisms remain unknown.

A link between the plant and *P. falciparum* was however established since the apicoplast has been reported to be inherited from a red alga. In the end, it would be interesting to compare the results obtained with BY-2 cells to those of red blood cells infected by *P. falciparum* treated with VH and analogues, therefore opening an avenue to fluorescence localization/structure/activity relationships studies.

### **6.3.6 Acknowledgments**

This work was partly supported by the CNRS (LIMA, UMR 7042, Strasbourg) and the University of Strasbourg. We thank Dr. Gilles Ulrich (ICPEES, UMR 7515, Strasbourg) for providing the spectrofluorometer for establish reference spectra and quantum yields. A wholehearted thanks to Pr. Thomas J. Bach (IBMP, UPR 2357, Strasbourg) for allowing access to its phenolic compounds collection. We are also grateful to Dr. Stephanie Riché and Sridevi Ramanoudjame (LIT, UMR 7200, Strasbourg) for excellent technical assistance to purify vismione H.



## 6.4 IDENTIFICATION OF ANTHRANOID SUBCELLULAR LOCALIZATION

In our proof of concept, it was found that a number of structures are labelled by the anthranoids used and/or their related metabolites. In fact, more than three compartments are labelled by VH including cytoplasm, vacuole and other more hypothetical such as ER, Golgi or somehow vesicular bodies. Viability tests with the FDA/PI have shown that the cytoplasm is labeled by VH and anthraquinones while the nucleus was never found labeled (**Figure 111**). Besides, some metabolites were detected at  $\lambda_{405}$  in the primary vacuole of BY-2 cells treated during 18h with anthranoids, particularly with those which are not prenylated (**section 6.3**). The primary vacuole, which was labeled by Fra, Emo, Qui and VH related metabolites after 18h was easily recognized in plant cells as it takes over 90% of the cell volume indeed. Although the VH/anthrone marker labels reticulated structures typical of ER in plants, we wanted to confirm this hypothesis by doing colocalization experiments with an ER marker. In addition, different vesicular bodies were distinctively labelled between VH/anthrone and anthraquinone forms. In plant cells, many organelles present vesicular bodies such as Golgi apparatus, mitochondria, chloroplasts, peroxisomes as well as endosomes, lysosomes, lipid droplets and other vesicles. Even though the size and dynamic suggest that a part of vesicular bodies observed corresponds to Golgi apparatus, we performed a series of colocalization experiments with biological marker and chemical probes as well. Accordingly, investigations were pursued in reference cell lines expressing ER and Golgi apparatus localized GFP, treating them with VH, vismione D (VD) or AVD.

### 6.4.1 ER Localization of Anthranoids

Since VH/anthrone fluorescence labeled a reticulated structure in BY-2 cell, we proposed that it corresponds to ER. To test this hypothesis, BY-2 cells expressing constitutively a sGFP protein with a HDEL peptide signal (GFP-HDEL) targeting the ER were treated with 50  $\mu$ M VH, VD or Qui. Therefore, the BY-2 cells were observed using SIMaging at  $\lambda_{405}$  and  $\lambda_{488}$  settings as previously described (**section 6.3**), and then compared to spectra of the pure reference and BY-2 expressing GFP-HDEL without treatment.



Although a slight shift in the  $\lambda_{Em}$  of sGFP from 502 nm to 512 nm was observed at  $\lambda_{488}$ , results from the control cells are congruent with the localization and fluorescence spectrum expected ( $\lambda_{Ex}$  483 nm,  $\lambda_{Em}$  502 nm). Accordingly, the GFP fluorescence spectrum obtained in the ER exhibit strong intensity at  $\lambda_{488}$  and almost nothing at  $\lambda_{405}$  nm (**Figure 118**). Conversely, the fluorescence of VH-treated cells results both in a similar GFP-signal intensity at  $\lambda_{405}$  and  $\lambda_{488}$  in the ER. This result suggests that VH and GFP-CVIL colocalize and Förster resonance energy transfer (FRET) may occur, otherwise fluorescence of VH would be observed at  $\lambda_{405}$ . Actually, this phenomenon takes place between two fluorophores only if they are close (1-10 nm) and the emission spectrum of the one superimposes with excitation spectrum from the other. In our context, it can be speculated that VH LH2 species ( $\lambda_{Ex}$  403 nm,  $\lambda_{Em}$  482 nm) could excite the GFP-HDEL ( $\lambda_{Ex}$  483 nm,  $\lambda_{Em}$  512 nm) if they colocalize indeed. Moreover, at  $\lambda_{488}$  some vesicular bodies moving along the ER were observed with fluorescence spectrum similar to that of Mad. Furthermore, at  $\lambda_{405}$  the VD-treated cells exhibited a fluorescence in the vacuole and a strong fluorescence in the ER. The spectrum from the ER fluorescence also suggests colocalization of sGFP and VD as indicated by the  $\lambda_{Em}$  503 nm like that of sGFP and a shoulder at 530 nm, which is close to that of VD alone indeed. Nonetheless, the VD/anthrone signal was not totally quenched by the FRET with GFP-HDEL as compared to VH. For this reason, we supposed that FRET efficiency with VD is lower than that of VH. It could be explained by a longer distance between VD and GFP-HDEL or a lower compatibility of VD emission and GFP-HDEL excitation spectra. However, other experiments such as FLIM have to be conducted to characterize FRET efficiency with VH and VD. In contrast, at  $\lambda_{488}$ , less vesicular bodies were observed with VD treated cells as compared to VH, suggesting that VD being characterized by a 6-MeOH and 3-O-Geranyl groups is less degraded into Mad-like anthraquinone as compared to VH, which is substituted by a 6-AcOMe and/or 3-O-DMA group.

In our proof of concept, we proved that vismiones can be degraded into anthraquinones *in vivo*, but their fluorescence remains relatively weak as compared to GFP-HDEL or the anthrone/anthranol vismione. In order to verify the localization of anthraquinones too, additional experiments were performed with the same cell line treated by 50  $\mu$ M Qui being the most fluorescent anthraquinones. A low difference in spectra collected at  $\lambda_{405}$  and  $\lambda_{488}$  was observed in the ER of Qui-treated cells, indicating that there is at least co-labelling.

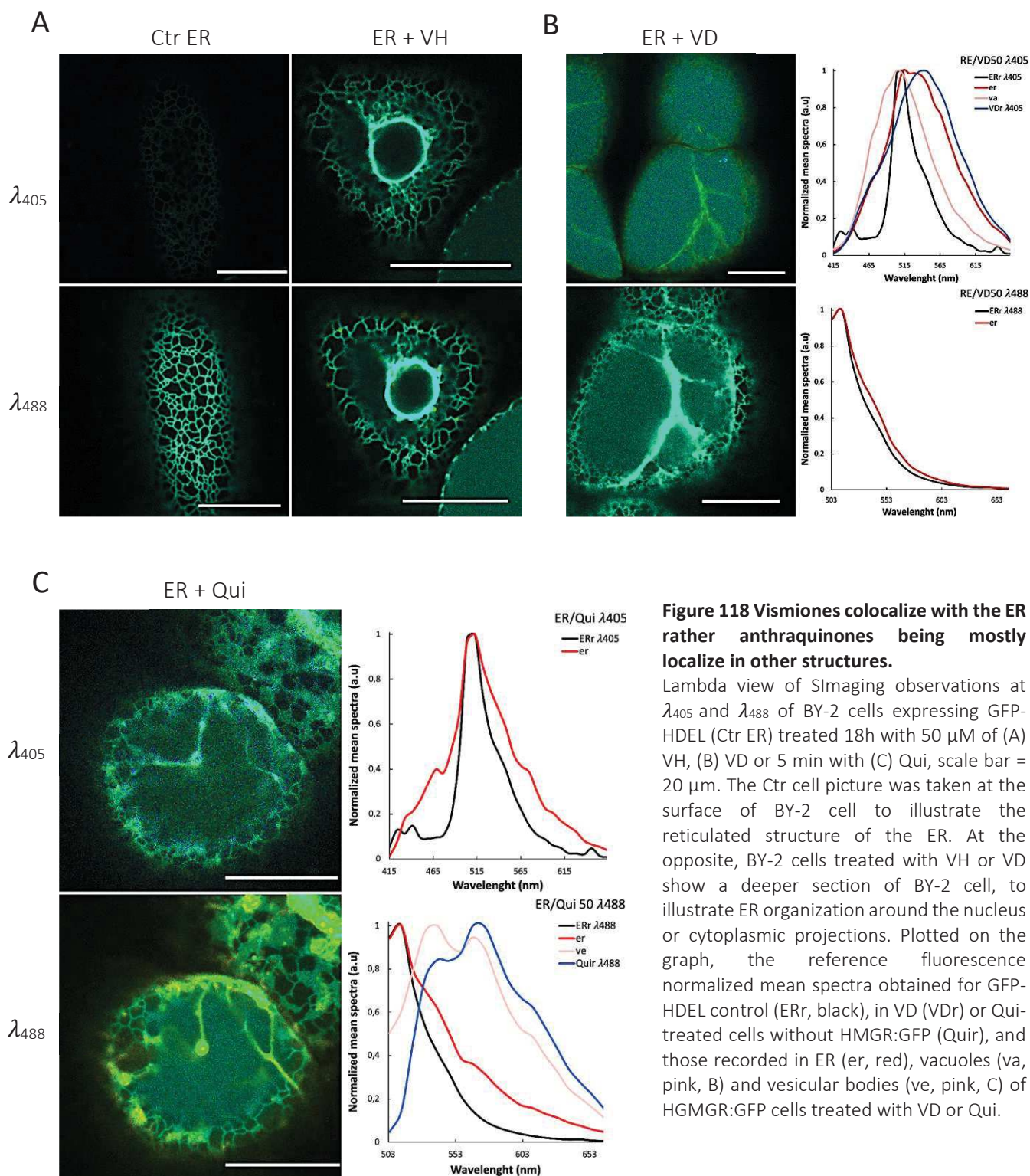


**Figure 118 Vismiones colocalize with the ER rather anthraquinones being mostly localize in other structures.**

Lambda view of SImaging observations at  $\lambda_{405}$  and  $\lambda_{488}$  of BY-2 cells expressing GFP-HDEL (Ctr ER) treated 18h with 50  $\mu$ M of (A) VH, (B) VD or 5 min with (C) Qui, scale bar = 20  $\mu$ m. The Ctr cell picture was taken at the surface of BY-2 cell to illustrate the reticulated structure of the ER. At the opposite, BY-2 cells treated with VH or VD show a deeper section of BY-2 cell, to illustrate ER organization around the nucleus or cytoplasmic projections. Plotted on the graph, the reference fluorescence normalized mean spectra obtained for GFP-HDEL control (ERr, black), in VD (VDr) or Qui-treated cells without HMGR:GFP (Qui), and those recorded in ER (er, red), vacuoles (va, pink, B) and vesicular bodies (ve, pink, C) of HGMGR:GFP cells treated with VD or Qui.



Nevertheless, the fluorescence at  $\lambda_{488}$  being more suitable for the observation of Qui, clearly demonstrates that Qui and related metabolites mostly localized in the cytoplasm and vesicular bodies of varying size (**Figure 118**). Interestingly, the spectra obtained in these vesicular bodies was correlated with that of Qui, but it seemed to be shifted to that of GFP. Actually, there must be a co-labelling between the ER and these vesicular bodies, hence hybrid fluorescence spectrum observed. Taken together our results suggest that anthraquinones tightly localized to the ER, and a large amount are distributed in vesicular bodies, which can be assimilated to Golgi apparatus. With this respect, it is important to notice that the Golgi apparatus arises from the ER, which appeared to be labelled by VH, VD and AVD as well. Therefore, similar experiments were performed with BY-2 cells expressing a Golgi marker (**Figure 119**).

#### **6.4.2 Golgi Localization of Anthranoids**

The Golgi apparatus is an organelle involved mainly in the maturation and distribution of a large number of proteins and metabolites in cells (Hawes, 2004). The former being a part of the endomembrane system is made up of a collection of fused, flattened membrane-enclosed discs known as cisternae budding off the ER (Hawes and Satiat-Jeunemaitre, 2005). Golgi apparatus is broken down into *cis*-, medial and *trans*-Golgi forming two mains network piloting retrograde and anterograde transport in eukaryotic cells: the *cis*-Golgi network (CGN) and the *trans*-Golgi network (TGN) (Hawes, 2004; Schoberer and Strasser, 2011; Rosquete et al., 2018). The CGN is responsible for exchange of proteins and metabolites with the ER, while the TGN cover the transit of exocytosis, secretory and endocytosis vesicles with the plasma membrane. Besides, the medial Golgi contribute to the maturation of proteins by glycosylation and ensure a part of polyose biosynthesis such as xyloglucans or galacturonans.

All our results converge to the same point, suggesting that tested anthranoids label Golgi apparatus. With respect to Golgi apparatus complexity, the limited choice of marker we have only allows partial identification of Golgi compartments. Therefore, BY-2 cells expressing constitutively the eGFP-fused to alpha-mannosidase II ( $\alpha$ M-II-GFP), which localize in the medial-Golgi compartment, were treated with 50  $\mu$ M of VH or VD (Nebenführ et al., 1999).

The treated BY-2 cells were observed using SImaging at  $\lambda_{405}$  and  $\lambda_{488}$  settings and compared to the eGFP and VH reference spectra (**Figure 120**). The  $\lambda_{Em}$  recorded for eGFP in SImaging was 530 nm as compared to the spectrum recorded in solution ( $\lambda_{Ex}$  488 nm,  $\lambda_{Em}$  510 nm). Besides, the control cells fluorescence and its localization were consistent with those expected, as shown by the Golgi vesicles with intense GFP fluorescence at  $\lambda_{488}$  and weaker at  $\lambda_{405}$ . The difference in the  $\lambda_{Em}$  may be explain by the resolution of SImaging as well as incidence of intracellular environment on the GFP-fluorescence properties.

In contrast to ER result, the VH-treated cells exhibit same  $\alpha$ M-II-GFP signal than the control at both  $\lambda_{488}$  and  $\lambda_{405}$ , suggesting that FRET also occur or  $\alpha$ M-II-GFP signal hid the VH and related anthraquinones. Thus, how to observe VH if the signal is hidden by  $\alpha$ M-II-GFP fluorescence? Consistent is the fact that dual excitation was reported as a solution to reduce artefact or improve discrimination between fluorophores using SImaging (Berg, 2004). With this respect, other observations were carried out using dual excitation at  $\lambda_{Ex}$  405 nm and  $\lambda_{Ex}$  488 nm with a micro beam splitter (MBS) 488 nm to avoid Rayleigh signal. Actually, without MBS 488 nm, acquisition of fluorescence would be saturated by the laser exciting at 488 nm indeed. In our experiment, two laser power settings were defined in order to give more power to  $\alpha$ M-II-GFP with  $\lambda_{Ex}$  488 or anthranoids fluorescence with  $\lambda_{Ex}$  405 nm. First excitation power was set at 1%  $\lambda_{Ex}$  405 and 3%  $\lambda_{Ex}$  488 ( $\lambda_{405/488}$ ).

These settings allowed an observation in VH-treated cells expressing  $\alpha$ M-II-GFP of vesicles labeled mostly with  $\alpha$ M-II-GFP and others with mostly Mad-like fluorescence signal (**Figure 119**). The spectra recorded in each of labeled vesicles exhibit a shoulder as compared to reference spectra (). Accordingly, VH and  $\alpha$ M-II-GFP fluorescence merged in medial Golgi vesicles but FRET does not occur otherwise no VH fluorescence could be observed. Dual excitation appeared to be really useful to finely characterize merged fluorescence in living cells, but both anthrone and anthraquinones fluoresce under these conditions. Therefore, which one labelled medial Golgi vesicles and/or other vesicular bodies? Forasmuch as a lower number of vesicles labeled by Mad-like fluorescence was detected in VD-treated cells as compared to VH, we performed other experiments with VD in order to promote the fluorescence of anthrones rather than that of anthraquinones. Consistent is the fact that almost no vesicular bodies associated to  $\alpha$ M-II-GFP fluorescence were observed in VD-treated cells under  $\lambda_{405/488}$ .

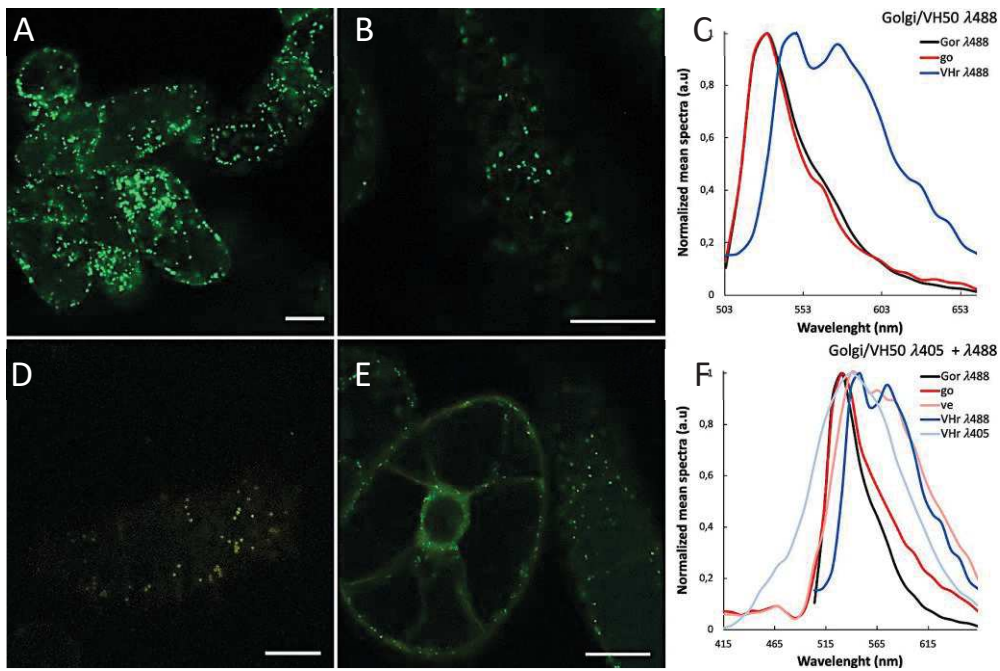


**Figure 119** VH does label medial Golgi and other vesicles.

Lambda view of Sl imaging observations at  $\lambda_{488}$  of (A)  $\alpha$ M-II-GFP BY-2 control cells and those treated 18h with (B) 50  $\mu$ M of VH, scale bar = 20  $\mu$ m. (C) The normalized mean spectra were recorded into the Golgi vesicles of control cells (A, Gor), VH-treated  $\alpha$ M-II-GFP cells (B, go) and VH-treated cells without  $\alpha$ M-II-GFP (D, VHr). (E) Observation at  $\lambda_{405/488}$  of BY-2  $\alpha$ M-II-GFP treated with 50  $\mu$ M of VH associated to (F) the normalized mean spectra found in Golgi vesicles (go) and other vesicular bodies (ve) as compared to references Gor and VHr detected in Golgi vesicles (go) and other vesicular bodies (ve) as compared to references Gos and Vhr (F).

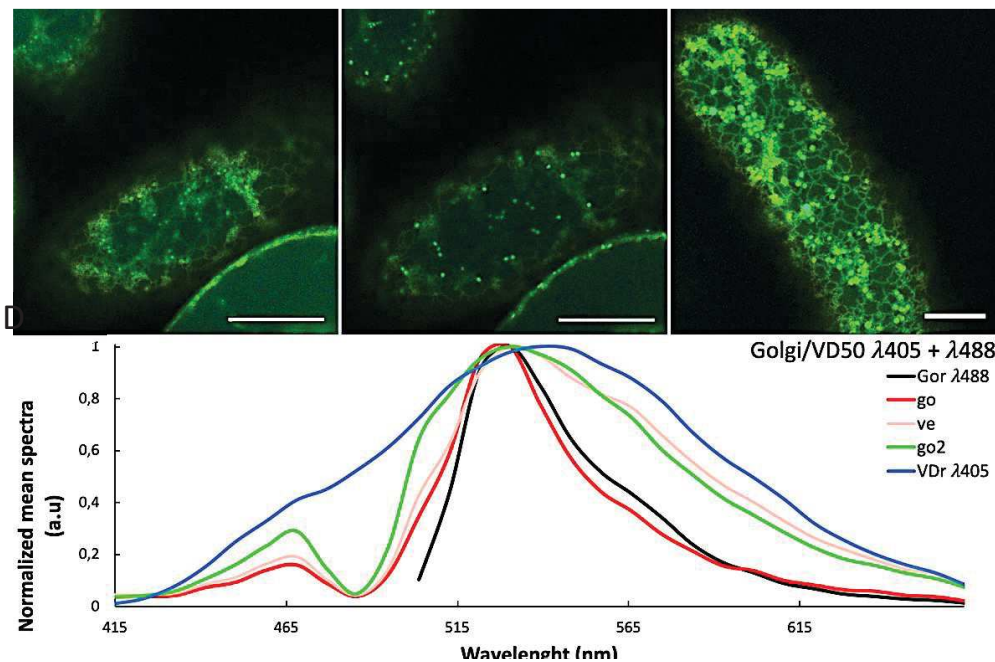


**Figure 120** VD/anthrone label medial Golgi vesicles.

Lambda view of Sl imaging observations at (A)  $\lambda_{405/488}$  and (B, C)  $\lambda_{405L/488}$  of  $\alpha$ M-II-GFP BY-2 cells treated 18h with 50  $\mu$ M VD, scale bar = 20  $\mu$ m. (D) The spectra recorded at  $\lambda_{405/488}$  settings into vesicular bodies associated to Golgi apparatus (go2) and those obtained by using  $\lambda_{405L/488}$  settings in the same structure with a high signal of  $\alpha$ M-II-GFP at  $\lambda_{405L/488}$  (go) or those with a higher anthrone signal (ve) as compared to the  $\alpha$ M-II-GFP control cells (Gor) and VD-treated cells without  $\alpha$ M-II-GFP (VDr).

Moreover, the presence of other vesicles with a fluorescence spectrum closer to that of  $\alpha$ M-II-GFP were also observed. Nevertheless, it was difficult to make the difference between spectra of anthrone and GFP under these conditions. In order to reduce the excitation of anthrone and improve the GFP fluorescence, the laser power was adjusted to 0.5%  $\lambda_{\text{Ex}} 405$  and 3%  $\lambda_{\text{Ex}} 488$  ( $\lambda_{405L/488}$ ). These conditions clearly improved the signal of  $\alpha$ M-II-GFP in the vesicles previously associated to VD/anthrone (**Figure 120**). As a matter of fact, we can conclude that vismiones and anthrone/anthranol forms localized in Golgi vesicles. Considering that *cis*- or *trans*-Golgi vesicles are not labelled by  $\alpha$ M-II-GFP being mostly in the medial-Golgi, we could not conclude if vismione/anthrone is specific of medial-Golgi or if they label other Golgi compartments. Still, it can be speculated that *cis*- and *trans*-Golgi may be a part of vesicles observed without GFP-HDEL fluorescence (**Figure 120**).

In the end, our study of the vismiones and related metabolites subcellular localization with marker proteins has validated the presence and differential distribution of vismione/anthrone and anthraquinone forms within the ER and Golgi apparatus. However, we were able to show that other vesicular bodies are specifically labeled by Mad related anthraquinones. Forasmuch as Mad and its related metabolites are very hydrophobic (**section 6.3**), it is possible that these vesicular bodies correspond to lipid droplets. Therefore, this hypothesis was explored by using Nile Red probe, reported as an efficiently probe for lipid droplets (Greenspan et al., 1985).

### 6.4.3 Lipid Droplets Localization of Anthranoids

Lipid droplets are organelles originate from the ER as well, they play a key role not only in the storage of many lipids for cell development and signaling in plants, but also for the sequestration toxic compounds to prevent lipotoxicity or oxidative stress (Olzmann and Carvalho, 2019). As long as Mad and its related metabolites are highly hydrophobic and their spectral fingerprint were observed in unidentified vesicular bodies, we privileged the lipid droplets hypothesis. The latter are traditionally observed using Nile red (NR), which exhibit strong fluorochromic properties, depending on the hydrophobicity and concentration of lipoproteins. In hydrophobic environments, NR can be visualized following an excitation at 487-489 nm range and observation of fluorescence at 530-550 nm. A bathochromic shift of the NR  $\lambda_{Ex}$  to 514-550 nm and emission fluorescence  $> 590$  nm is observed in more hydrophilic environment, labeling an extensive network of internal membrane *in cellula* (Greenspan et al., 1985). Besides, hydrophilic environment and high concentration of lipoproteins reduce the fluorescence intensity of NR, making lipid droplets as clear yellow spotlight unlike other cell compartments.

Therefore, BY-2 cells treated or not with 50  $\mu$ M of VH were stained with NR in order to evaluate the presence of Mad-like anthraquinones in lipid droplets. The BY-2 cells were observed using SImaging at  $\lambda_{488}$  setting and also  $\lambda_{Ex}$  514 with emission of fluorescence from 519 to 693 nm ( $\lambda_{514}$ ). A strong yellow-gold fluorescence of NR ( $\lambda_{Em}$  603 nm) was observed in lipid droplets of BY-2 control cells at both  $\lambda_{488}$  and  $\lambda_{514}$  settings (**Figure 121**). Overall, VH-treated cells exhibited more intense fluorescence than control cells at both SImaging settings. Hence, presence of VH and related metabolites in the same compartments may have increase hydrophobicity or FRET happened. Like in control cells, a yellow-gold fluorescence is observed in the lipid droplets but also in several membranes including the plasma membrane, Golgi vesicles membranes and the tonoplast. In these cell compartments and especially in lipid droplets, the fluorescence spectrum at  $\lambda_{488}$  consisted in VH/NR hybrid spectrum as compared to references, confirming a co-labelling of NR and Mad-like anthraquinones (**Figure 121**). Moreover, at  $\lambda_{514}$ , the red fluorescence of NR in the cytoplasm or ER was higher to that of the control, supporting an increase in the polarity of these compartments. It can be speculated that the pH is decreased, or polar metabolites content increased by VH treatments.



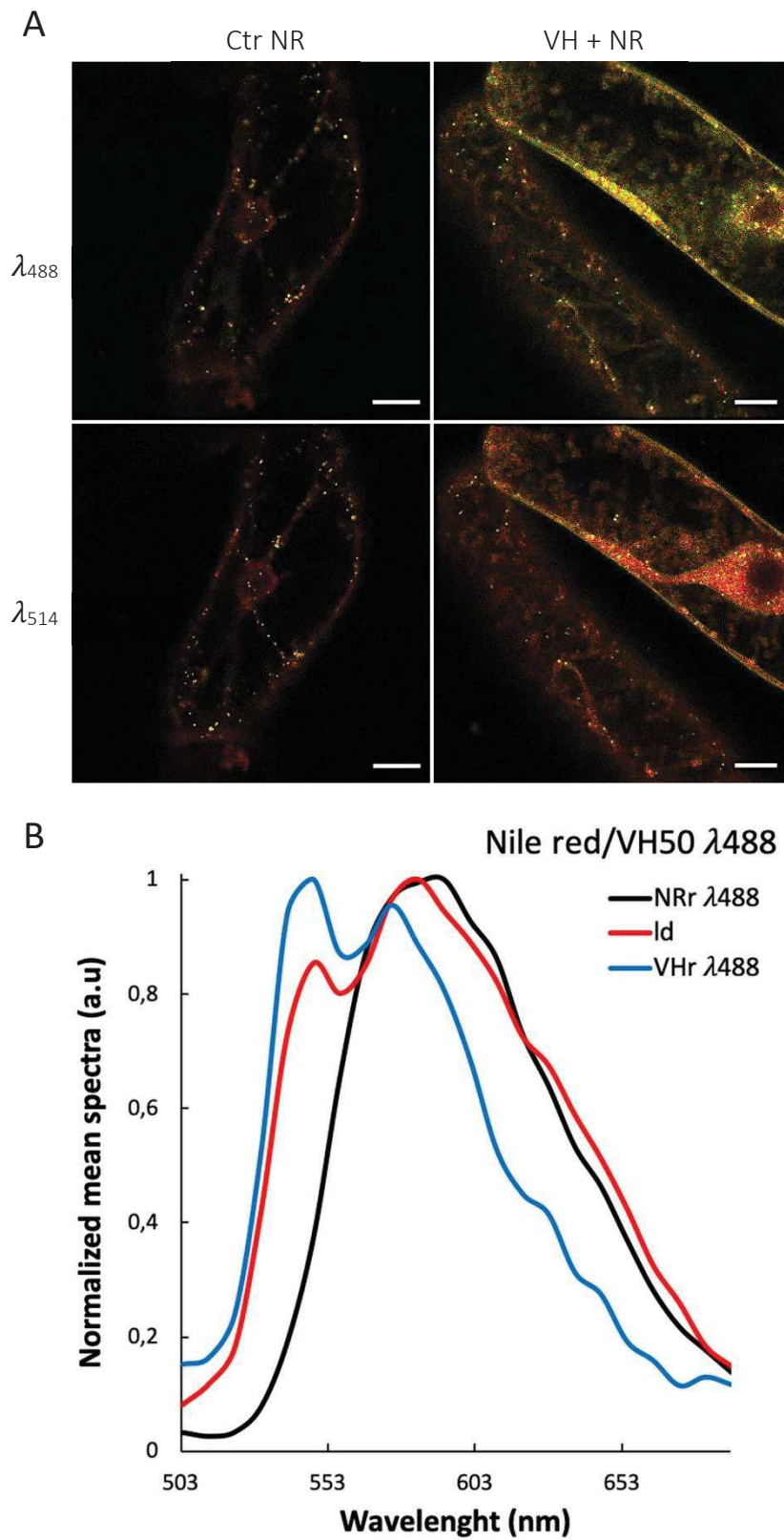


**Figure 121** Madagascine-like anthraquinones label lipid droplets.

(A) Lambda view of SImaging observations at  $\lambda_{488}$  or  $\lambda_{514}$  of  $\alpha$ M-II-GFP BY-2 cells treated 18h with 50  $\mu$ M VH, scale bar = 20  $\mu$ m. (B) The normalized mean spectra recorded at  $\lambda_{488}$  settings into lipid droplets of control BY-2 cells (NRR) and treated with 50  $\mu$ M VH (Id) as compared to the VH-treated cells without NR (VHR).

To conclude, in BY-2 cells, vismiones and related metabolites evolved in at least six different compartments in 18h time-lapse (**Table 20**) Thus, vismione and anthrone forms are particularly localized in the ER and Golgi apparatus while their related metabolites are distributed in the lipid droplets if they are highly hydrophobic or in vacuole if hydrophilic.

As a matter of fact, our results obtained on BY-2 cells fit with the hypothesis of vismiones degradation into anthrone and anthraquinone *in vivo*. Still, it appeared that VH not only result in Mad anthrone and Mad like in DMSO (Galle, 2015), but also in several isomers indicating specific metabolization in BY-2 cells. Although, Mad anthrone form are degraded quickly into anthraquinone in DMSO, it persists over 18h in BY-2 cells, suggesting somehow anthrone stabilization *in cellula*. It is still unclear whether the fluorescence observed in the vacuole of VH-treated cells corresponds to the non-prenylated anthrone/anthranol forms or another metabolite. Nonetheless, we clearly demonstrate that 3-O-Prenyl and a 6-AcOMe or 6-MeOH strongly decrease the metabolization and transport of anthranoids into the vacuole. In this context, functions in C-3 and C-6 position play a primordial role in the metabolism pathways of anthranoids in BY-2 cells. Accordingly, vismiones/anthrone might be the active forms and their stability would drive activity against *P. falciparum* and *L. donovani in vivo*, as suspected previously (Galle, 2015; Wasser, 2018). To some extent, it can be speculated that vismiones/anthrones and prenylated related anthranoids are the most active because the parasite like BY-2 cells could not be able to ensure their efficient metabolization and sequestration into primary vacuole.

For the first time we reported a detailed picture of vismiones and related metabolites *in cellula*. Consistent is the fact that most active vismione/anthrone against *P. falciparum* exhibit a particular subcellular distribution in BY-2 cells as compared to anthraquinones counterpart. At present, we can hypothesis that targets of vismiones and related metabolites could be localized in ER, Golgi apparatus. Since a series of dihydroanthracenones (DHA) analogs of vismiones has been synthesized by N. Wasser (Wasser, 2018), and were tested on *L. donovani*, investigations were extended to a fluorescence localization-structure-activity relationship study using these analogs.

**Table 20** Overview of vismiones and related anthranoids subcellular distribution in living BY-2 cells.

Are indicated, the localization and the relative level of fluorescence observed by SIMaging in each cell compartment. Darker is the green color, higher was the intensity/occurrence of fluorescence observed. A black box highlights the absence of fluorescence. Since the fluorescent molecules in the vacuole of vismiones treated cells couldn't be definitely confirmed, this condition was question marked.

	Plasma membrane	Cytoplasm	Vacuole	ER	Golgi body	Lipid droplets	Nucleus
Vismione/anthrone	Light Green	Dark Green	Light Green with ?	Dark Green	Dark Green	Light Green	Black
Mad-like anthraquinone	Light Green	Light Green	Black	Light Green	Light Green	Dark Green	Black
Anthraquinone	Light Green	Dark Green	Dark Green	Light Green	Light Green	Light Green	Black

## 6.5 COMPARISON OF THE VISMIONES AND SYNTHETIC DIHYDROANTHRACENONES FLUORESCENCE

### 6.5.1 To Study Relationship Between Localization-Structure-Activity of Anthranoids using Slmaging

A structure-activity relationship study conducted with vismiones and the series of synthetic DHA tested on *L. donovani* (Table 15), proved that the protection of 3-OH position by a methyl or a prenyl (DMA or geranyl) as well as a 6-OH rather than AcOMe increase the stability of the DHA in solution (Wasser, 2018). However, the relationship between activity and compounds localization was not evidenced in an *in vivo* study. We demonstrated that VH is metabolized in BY-2 cells into anthranol/anthrone ( $\Phi_F$  31%,  $\lambda_{Ex}$  403 nm,  $\lambda_{Em}$  532/539 nm) and anthraquinones such as Mad ( $\Phi_F$  5 %,  $\lambda_{Ex}$  437 nm,  $\lambda_{Em}$  544/575 nm), whose fluorescence and localization were detailed by Slmaging (section 6.3). We reported that the vismiones anthranol/anthrone forms mostly labelled the ER, Golgi apparatus and the cytoplasm while the related anthraquinone forms preferentially labelled lipid droplets. Moreover, a low fluorescence at 503 nm was observed in the primary vacuole only after 18h but could not be definitely associated to a metabolite. In fact, it could be either the neutral forms of VH and anthranol/anthrone at acidic pH ( $\lambda_{Em}$  484 nm and 503 in Slmaging) or another non-annotated metabolite. Metabolization and transport of secondary metabolites into the primary vacuole is a recurrent phenomenon in plants indeed, but it occurs in *P. falciparum* and *L. donovani* too. The former enables to limit adverse interactions of toxic molecules with cellular machinery like the heme in *P. falciparum* (Ref), or to store molecules for further uses such as fraxetin in the iron uptake (Ref). Our screening of protein prenylation inhibitors results indicated that BY-2 cells treated with synthetic DHA showed normal phenotype of GFP-sensor as compared to vismiones, in which signal in the RFP-channel was detected (Table 15, Figure 99). The particular “dots” phenotype observed at  $\lambda_{Ex}$  488 nm in classical confocal microscopy only in VH, AVD, VD treatments corresponded to lipid droplets labeled by vismione related anthraquinones. In this context, are the synthetic DHA not metabolized in BY-2 cells? where do they localize *in cellula*?

In order to definitively confirm this hypothesis and evaluate the impact of different functions on DHA metabolization, we performed Slmaging fluorescence analysis of BY-2 cells treated 5 min and 18h with vismiones and synthetic DHA.

## 6.5.2 Prenylated DHA are Not Metabolized and Transported into the Vacuole of Living Cells

We want to answer the question of whether a protection of the 6-OH function with a prenyl group enhances the stability of DHA. Moreover, no anthraquinone fluorescence was detected with DHA treatments, suggesting that AcOMe at the C-3 position of vismiones also promotes their oxidation *in vivo*. Accordingly, the most active compounds should not be observed in lipid droplets at  $\lambda_{488}$  or in the primary vacuole at  $\lambda_{405}$ .

For this reason, the synthetic DHA NW211, NW0129, NW0184 and NW0188 (**Table 15, Figure 122**), were compared to VH, VD and AVD by Slmaging analysis of BY-2 cells treated for 5 min and 18 h with 50  $\mu$ M of each DHA. As a result, the BY-2 cells treated with synthetic DHA observed at  $\lambda_{488}$  did not emit fluorescence neither at 5 min nor at 18h, unlike the vismiones-treated cells. Consequently, the absence of methyl at C-3 of the DHA prevents their degradation into anthraquinones in BY-2 cells (**Figure 122**). However, at  $\lambda_{405}$ , all DHA emitted intense fluorescence corresponding to that described for the VH anthranol/anthrone forms in the cytoplasm, the ER and Golgi vesicles at 5 min. After 18 h, AVD and VD-treated cells showed similar spectral fingerprints and localization to those described for VH. Conversely, no changes in the prenylated DHA fluorescence could be evidenced when compared to NW211 and NW0129-treated cells, where a new fluorescence was exclusively found in the primary vacuole. These experiments confirmed that 6-OH and 3-O-Prenyl highly improve the stability of DHA *in vivo*, avoiding their metabolization into anthraquinones or related metabolites and transport inside the primary vacuole of BY-2 cells. The non-targeted metabolomics of MeOH extract from BY-2 cells treated with 50  $\mu$ M NW0184 5 min and 18h supported Slmaging results, as no anthraquinone was detected. Surprisingly, only corresponding to oxidized or reduced methylated NW0184 or glycosylated NW0184 were annotated (**Table 21**). Although NW0184 content was decreased after 18h of treatment, it seems that NW0184 is metabolized by BY-2 cells into molecules that cannot be transported in the primary vacuole or do not emit fluorescence. To note, we found NW0184 in

To conclude, the fluorescence localization-structure-activity relationship study using a SImaging approach coupled to non-targeted metabolomic analyses, confirmed the key role of positions C-3 and C-6 in the stability and localization of vismiones and DHA *in vivo*. Similarities between plant and protozoa could exist as suggested by the correlation between strong antiprotozoal activity of NW0184 and its stability *in vivo*. Nevertheless, it was not possible to definitely conclude on the relation between localization and activity with our BY-2 model. Further study might be carried out using this approach on cells infected by *L. donovani* or *P. falciparum*, which are more appropriate to investigate metabolism processes and biological targets. However, since *P. falciparum* possesses a parasitophoric vacuole, and *L. donovani* literally swim in a host cells endosome, it is quite plausible to observe similar results with these parasites. From another point of view, BY-2 is an interesting model for preliminary studies of protozoa mechanisms, because cheap, easy to handle and free of autofluorescent compounds under standard condition.

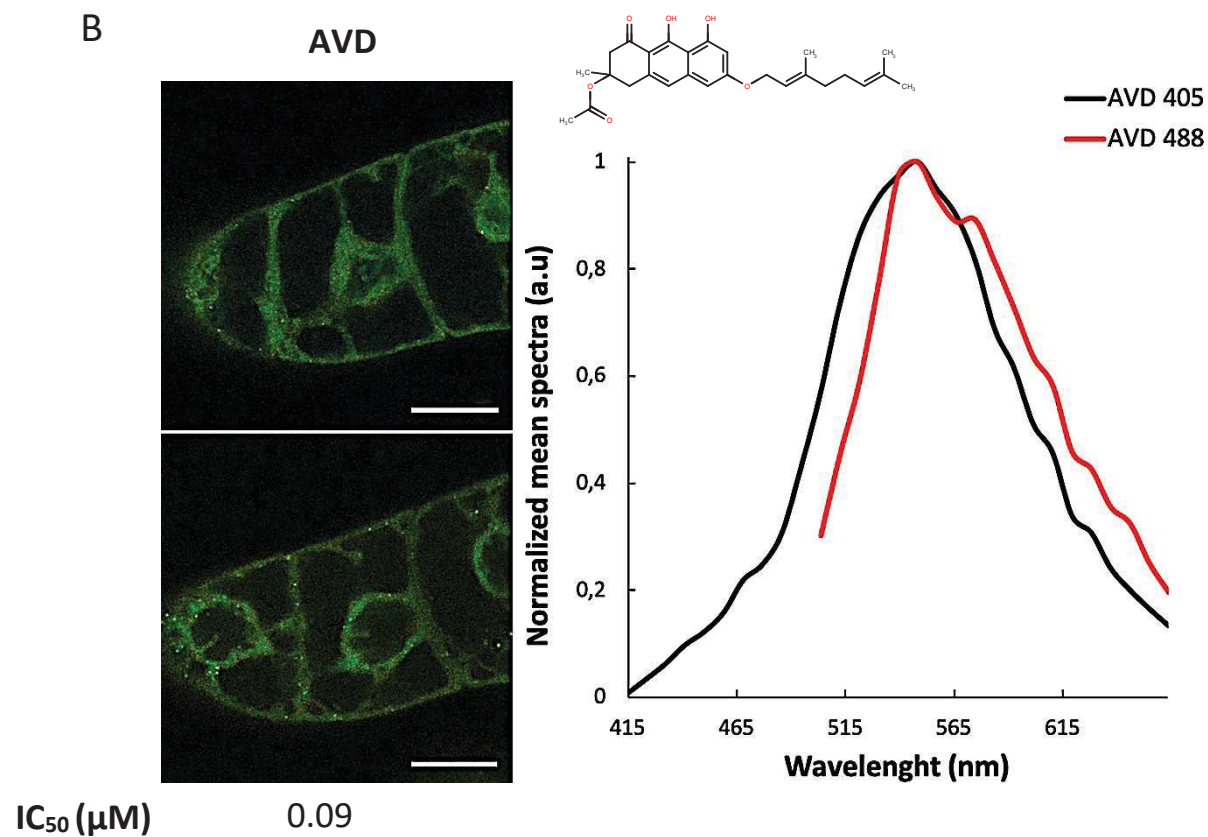
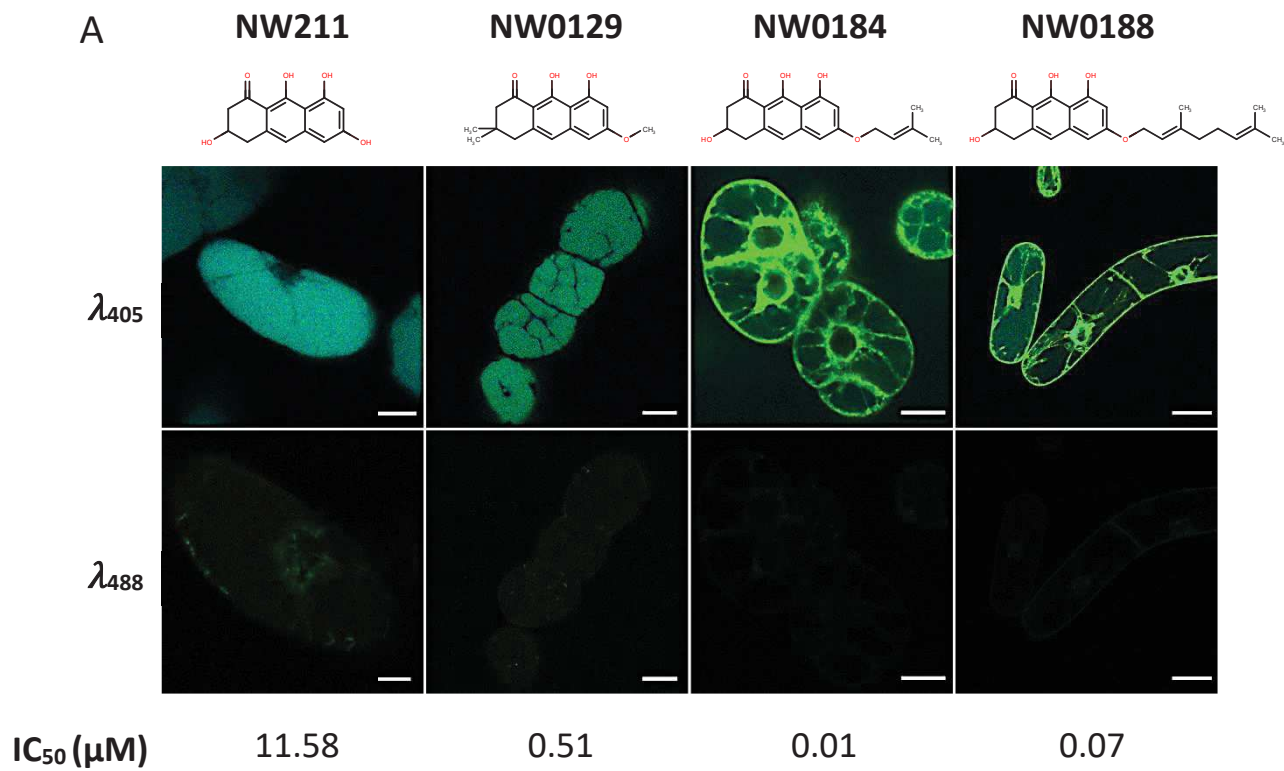


**Figure 122** Prenylated DHA are not metabolized and transported into the primary vacuole.

IC<sub>50</sub> of synthetic DHA on *L. donovani* amastigote (Wasser, 2018) and lambda view of Simaging observations at  $\lambda_{405}$  and  $\lambda_{488}$  of BY-2 cells treated 18h with 50 μM of NW211, NW0129, NW0184 and NW0188 (A) or AVD with spectra recorded at  $\lambda_{405}$  and  $\lambda_{488}$  settings into lipid droplets(B), scale bar = 20 μm.

## 6.6 CONCLUSION

This study on the fluorescence properties of vismiones and related anthranoids in BY-2 is somewhat different from protein prenylation, however it was essential to define unequivocally the effect of vismiones on protein prenylation. Exceptionally, our study showcases a prominent interest of Smaging associated with non-targeted metabolomics to carefully characterize the fluorescence of natural compounds *in vivo* as well as their metabolization processes. Here we established for the first time the fluorescence properties and a differential distribution between vismiones/anthrones and related anthraquinones within cell compartments of tobacco BY-2 cells. Unexpectedly, these compounds are not reported in tobacco, while our results suggest that BY-2 cells are capable of specific metabolization. Besides, our study of relationship between localization-structure-activity with vismiones and synthetic DHA are consistent with their stability reported *in vitro*. In this respect, we have pinpointed that NW0184 (3-Oprenyl and 6-OH groups) is not metabolized and sequestered into the vacuole and lipid droplets of BY-2 cells unless natural anthranoids. In this regard, as VH and NW0184 are effective against *P. falciparum* and *L. donovani*, it might be thus successful to extend this whole strategy to these parasites too. Here we propose Smaging as a booster for identification of biological targets and studies of fluorescent compounds metabolization process *in vivo*.

**Table 21 NW0184 is not metabolized in anthraquinone in BY-2 cells.**

Metabolites identified in non-targeted metabolomic analysis of NW0184 reference (NW0184) and MeOH extracts from BY-2 cells treated with 50  $\mu$ M NW0184 (n=1) for 15 min and 18h. Exact mass-to-charge ratio (m/z), detected ion, retention time ( $R_t$ ), m/z ratio of parent,  $\Delta m/z$  (ppm), variation of isotopic ratio (mSigma) and fragment ions were obtained from the HPLC/ESI-QTOF-MS/MS chromatograms in positive ionization mode. Are represented the putative oxidized (NW0184 MeOX) and reduced methylated NW0184 (NW0184 Me) as well as glycosylated form (NW0184 Glc). Isomer are numbered by I and II.

m/z meas	RT [min]	$\Delta m/z$ [ppm]	mSigma	Molecular Formula	Ions	Name	NW0184	NW0184 15 min	NW0184 18h
329,1384	9.20	0,395	22.9	C19H20O5	[M+H] <sup>+</sup>	NW 0184 I	10284		
329,1383	10.11	0,46	4.9	C19H20O5	[M+H] <sup>+</sup>	NW 0184	833764		
341.1389	8.15	2.271	6.8	C20H20O5	[M+H] <sup>+</sup>	NW0184 MeOx I		128234	11184
341.1386	10.29	-0.479	27.8	C20H20O5	[M+H] <sup>+</sup>	NW0184 MeOx II		36806	19324
343.1544	9.93	1.410	8.0	C20H22O5	[M+H] <sup>+</sup>	NW0184 Me		8452	37500
491.1913	8.58	0.406	12.8	C25H30O10	[M+H] <sup>+</sup>	NW0184 Glc		33756	35876





## 7 DISCUSSION



After three years investigating the protein prenylation's far side, I come away from this expedition full of new features undoubtedly outlining the complexity of the living world we are dealing with after more than three thousand million years. Relatively speaking, these data are only a few grains of dust in an infinite universe, however, they depict of what an organism is in a kind of philosophical sense: a flexible form of matter that actively adapts to its environment using energy from disorder, to oppositely self-organize in order to maintain somehow an equilibrium. In this context, it is important to notice that equilibria are not static, but dynamic, and are influenced by the environment and organisms themselves. Protein prenylation is no exception to the rule, and mechanisms have been selected during the evolution to allow some flexibility and maintain equilibrium (homeostasis) of eukaryotic cells. The introduction brings together elements demonstrating that the dynamic flexibility of isoprenoid metabolism and PPTs activities is at the core of the resistance to inhibitors of protein prenylation developed by cancer cells and *P. falciparum* (**section 2.2.30**). However, should we consider that the homeostasis in a cancer cell or PPTs plant mutants is similar to their “healthy” counterparts? From my point of view, I would definitely say no and these examples pinpoint the lack of knowledge on the cellular mechanisms that trigger the flexibility of PPTs activities which maintains the homeostasis in these cells. This raises the question of what rules do these cells adhere to ensure protein prenylation? Accordingly, my thesis aimed to light on cellular mechanisms making the dynamic flexibility of PPTs activities possible by using plant models sketching the protein prenylation in Humans and *P.falciparum*. In this context, I pursued firsts investigations made by the team using the plant model expressing GFP-CaaX protein prenylation sensors of type-I protein farnesylation and geranylgeranylation.

Accordingly, we evidenced that MeJA and ethylene act alone or in synergy, pushing the PFT to prenylate the GFP-CVIL being normally substrates of PGGT-I in our plant model. At the opposite, cytokinin being reported to antagonize the stress response has decreased the effect of MeJA, confirming the role of hormones in the flexibility of PPTs activities *in vivo*. Stress hormones show up to stimulate the expression of HMGR (Courdavault et al., 2009)). Accordingly, 1 mM MVA rescued protein prenylation suggesting a potential role of this metabolite in this process. In this regard we were not able to decipher whether a threshold value of MVA level was integrated to switch on the adaptation mechanisms responsible for prenylation of GFP-CVIL by the PFT.

Nonetheless, it was astonishing that MeJA-induced flexibility of PFTs is active only in the presence of both FOS and MV inhibitors, suggesting that an increase in MVA alone is not sufficient to switch on the flexibility of PFTs *in vivo*. Other factors such as recruitment of chaperones or changes in 3D conformation induced by interacting proteins might be somehow involved in the PFT activity changes. Furthermore, since JA is ranging from 0.035 to 5  $\mu\text{mol/g}$  in tomato (Zadra et al., 2006) and MVA in yeast is about 70  $\text{nmol/g}$  of dry weight (Castaño-Cerezo et al., 2019), the hormones and MVA concentration could be in excess ( $> \mu\text{M}$ ) as compared to concentration reported in physiological conditions ( $< 1 \mu\text{M}$ ). However, it should be considered that we do not know how much substrate get absorbed by our plant material in our condition, also we have never been able to quantify accurately these metabolites in specific cell compartments. It is thus conceivable that locally, the cell would be able to provide concentrations in a micromolar range, by releasing vesicular content or by activating transporters in peroxisome or ER membranes, ensuring thus localized efflux of MVA or IPP to sustain protein prenylation up. Thus, these aspects remain unclear, and our results with the GFP-CVIL and GFP-CVIM sensors expressed in the *era1-9* mutant lacking PFT activity did not make the interpretation easier. Actually, although in *ggb2* the GFP-CVIM is not affected and *vice versa* for the GFP-CVIL in *era 1.9*, both GFP-CVI (M/L) localizations are impacted suggesting that protein geranylgeranylation is somehow dependent of PFT activity, at least for our GFP-sensors. Accordingly, we suggested either that some unidentified farnesylated proteins are needed for efficient geranylgeranylation of GFP-CVIL, or that of the PGGT-I in this condition privileged as it can be the prenylation of more essential farnesylated proteins.

Consistent with the latter is the fact that GGol was able to rescue GFP-CVIM prenylation and not GFP-CVIL in *era1-9*, whereas complementation with Fol failed to restore GFP-CVIM in this mutant. Therefore, in *era1-9*, the PGGT-I activity is flexible and might be overbooked by the prenylation of other proteins theoretically farnesylated that are critical in the basal metabolism (**section 0**), rather than geranylgeranylated proteins, being related to defense and adaptation processes. These results are relevant in comparison with the PGGT-I CaaX substrate selectivity described *in vitro* and the stronger phenotype characterized in *era1* as compared to *ggb2* (**section 2.4.2**). At first sight, it appears that both PFT and PGGT-I are flexible *in vivo*, but PGGT-II and PGGT-III have been reported and other mechanisms for membrane targeting do exist (**section 2.3**).

Although the GFP-sensor was engineered to be specific of prenylation type-1, it could be theorized that those proteins are also flexible and able to ensure protein prenylation under stress conditions. Thus, it cannot be excluded that another PGGT or other lipidation balanced the lack of PFT activity in *era1-9*. In this respect, a low but still detectable GFP signal was observed in the membrane of both *era1-9::GFP-CVI(L/M)* and the mutant *plp* does survive without PFT and PGGT-I (**section 2.4.2**). Altogether, these elements raised the question of how far protein prenylation can be flexible *in vivo*?

As a matter of fact, many different prenyl diphosphates are biosynthesized in plants and addressed to different cell compartments for exert their functions (**section 0**). We were always wondering how PPTs compete with other giants such as squalene synthase or phytoene synthase to hook up their prenyl substrates. For this reason, it has been proposed that other prenyls could be (re)used by plant cells to ensure protein prenylation under critical inhibition of MVA or/and MEP pathways (Huchelmann et al., 2014). In this context, chlorophylls provides large phytyl feedstock of diphosphate which is usually mobilized for tocopherol production (Gutbrod et al., 2019). It was hypothesized that phytyl diphosphate could also be recycled for protein prenylation as size of phytyl is similar to that of GGPP. This hypothesis was confirmed by A. Huchelmann (Huchelmann, 2013), who showed that 50  $\mu$ M phytol partially rescued the prenylation of GFP-CVIL expressed in *ggb2* and in tobacco leaf discs treated with FOS and MV. Thus, the model of fluorescence tracking with GFP-sensor provides a snapshot of the protein prenylation state in cells and showcases the influence of treatments on this state in a "physiological condition". Nonetheless, it does not provide any evidence of what happened at a molecular level within plant cells. In this respect, how are the GFP-sensors prenylated into plant cells under the conditions tested? What kind of prenyl could be transferred? Are other modifications being capable to rescue membrane targeting of prenylated proteins? As introduced, most protocols described were unappropriated to characterize prenyls transferred onto prenylated proteins *in vivo* and particularly *in planta* (**0**).

After three years of development (**section 4**), we address a new pipeline for the unambiguous analysis of prenylated protein modified *in vivo* by non-targeted metabolomics (**section 4.10, 4.12**) and putative interacting proteins by proteomics (**section 4.6.2**). The purification of all GFP-sensors was successfully carried out by immunoprecipitation with commercial and homemade GFP-Traps (**section 4.9.3**). This technic readily allows a significant enrichment of tagged GFP-CaaX proteins in a minimum of two hours. Unexpectedly, we observed that

immunoprecipitated GFP-sensors are degraded at the C-ter end by proteases in BY-2 cell extracts while not in tobacco leaves. However, we were not able to determine if these proteases are not expressed in tobacco leaves or if the GFP-sensors were modified or were interacting with protein(s) protecting them from the degradation by proteases. Also, the cOmplete® cocktail inhibitor reduced this phenomenon but still exhibit limited efficiency (**section 4.4.4**). Other trials should be performed with E-64, PMSF inhibitor of cysteine protease or pepstatin inhibiting aspartic proteases respectively (Mandal et al., 2014; Mandal et al., 2016). Taking advantage of these results, we took advantage of these properties to develop efficient and specific on-beads tryptic digestion of our GFP-sensors. I definitely recommend this approach to study post-translational modification of unstructured domain found in proteins including C-ter of various prenylated proteins.

By the way, I also demonstrated that GFP-Trap production can be achieved at low cost by using customizable and relatively simple procedure (**section 4.34.9**). To note, 1 kg of spinach and 3 L of mammalian cultured cells were usually employed in the 1990s (Shipton, Parmryd, Farnsworth). With our GFP-Trap v2, a minimum of 5 g of plant material affords sufficient amount of purified prenylated GFP-CaaX for the analysis by non-targeted metabolomics while 750 mg gave good results in proteomics (**section 4.12**). This system is also suitable for immobilization of other proteins such as PPTs or even substrates like our inhibitor IN2. Although proteomic analysis of peptides with  $m/z > 1$  allowed detection of the GFP-sensor protein and putative protein partner peptides, no information about the protein C-ter end could be afforded neither after tryptic nor AspN digestions. In fact, it appears that CVIL, CVIM, SVIL tetrapeptides and prenylated C-ter end are highly hydrophobic and mostly ionize with one charge (**section 4.6.24.8**). At the opposite, non-targeted metabolomics approach allowed the accurate detection and identification of prenylated cysteine, being released after on-beads tryptic digestion of GFP-CVIM purified from tobacco leaves. What a surprise we had when we discovered that the metabolite released and detected correspond to S-Far-L-cys rather than S-Far-L-cys OMe (**section 4.12**).

Nonetheless, since the synthesized reference have shown prominent degradation under standard conditions, it was not possible to conclude whether S-Far-L-cys results from a spontaneous degradation during sample preparation of plant material or if the protein is not carboxymethylated *in vivo* indeed. Actually, it is stated that the carboxymethylation catalyzed by ICME is the last and the only reversible step after prenyl transfers and proteolysis of a

prenylated protein (Michaelson et al., 2005; Bracha-Drori et al., 2008; Yalovsky, 2011; Hildebrandt et al., 2016). Accordingly, this modification appears to be an additional lever to regulate the membrane targeting of prenylated proteins. In this context, we have now to confirm that the S-far-L-cys is not an artifact, but one of the best molecular shots we ever saw of a farnesylated GFP-CVIM C-ter residue modified *in vivo*, by tobacco leaf cells under physiological condition. Further analysis of S-Far-L-cys in NMR will be carried out as unexpectedly, the product seems to be more hydrophobic than S-far-L-cys OMe, suggesting a possible cyclization. This experiment could allow the establishment of the degradation mechanism in order to avoid this phenomenon if it occurs in our protein samples too.

Remain the question of why most articles, on animal models, have identified and reported prenylated peptides with carboxymethyl in the  $m/z$  detected? One reason may be explained by artifacts due to experimental conditions (**section 0**), but we also noticed that the signal detected remains relatively low (area <  $10^5$ ) even by purifying GFP-sensor from 5 g of plant material (~1.7  $\mu\text{g}$  of purified GFP-CVIM). As a matter of fact, several other metabolites were non-specifically annotated in our non-targeted metabolomic analysis using 346 compounds customized library, and even more protein was annotated/predicted by MASCOT in the proteomics analysis (100 to > 700 annotations). With this respect confusion remains possible with low signals especially when hundreds of molecules are simultaneously analyzed. In our case the analysis of S-Pre-L-cys OMe references degraded or not it was critical to identify unambiguously the S-far-L-cys. Another proposition support that our GFP-CVIM is effectively not carboxymethylated either because of the absence of ICME recognition elements or because the basic domain allows interaction with other proteins that regulate GFP-CVIM carboxymethylation. With this regard, our proteomic analysis of GFP-CVIM support the second hypothesis. Even though robust statistical analysis was not performed as various experimental conditions were tested, we were surprised to detect some proteins specifically annotated in samples with prenylated GFP-sensor. Remarkably these proteins are related to isoprenoids metabolism, photosynthesis machinery, vesicular transport and hormone signaling (**section 4.6.2**, ).

With this respect, several prenylated proteins are associated to these functions and protein prenylation is regulated by stress hormones, light and isoprenoid pool (**section 2.3.3**). Also,



some aspects on the substrate supplying remain unclear as PPTs are described as cytosolic and the GGPP derived from the MEP pathway in chloroplasts. Thus, how do GGPP comes to the PPTs? Astonishingly, a single time we captured the two farnesyl transferase subunits with 10 other proteins (**section 4.6.2, Table 6**), but these results were not reproduced and remain a mystery. Still, it can be speculated that these proteins take place in a whole complex to regulate the PFT activity according to light, hormones and/or substrate supplying via vesicular transport.

Altogether, these results support the fact that the absence of GFP-sensor interaction is not trivial. Although the GFP-sensors are devoid of calmodulin catalytic activity, the basic domain and prenylation may be sufficient for specific interaction with plasma membrane lipids, but also interaction with other proteins. Further studies have to be pursued using both proteomics and non-targeted metabolomics on other prenylated proteins involving a biological function and not only the sensor. Very recently, another protocol of purification by thiopropyl-based capture was published and seems to be adapted for the unambiguous analysis of prenylated proteins and interactants too (Wilkins et al., 2020). In this approach prenylated proteins were purified by thiopropyl based capture and analyzed using proteomics approach. The authors have identified 23 prenylated proteins including only three carboxymethylated form, which is steady with the absence of a methyl on S-far-L-cys found in our study. Although this strategy seems to be very efficient to analyze “prenylomes”, several steps are required increasing time of the experiment (~40h) and therefore the risk of spontaneous degradation of prenylated cysteine at the carboxymethylated group. Also, this approach only allows molecular characterization and not cellular localization by fluorescence. A comparative analysis should be performed with GFP-sensor purified by IP and thiopropyl-based capture as a control for validation. As a conclusion, in 2020 two methods for unambiguous analysis of prenylated proteins are suitable. At first glance, our method allows a functional and molecular characterization of a tagged prenylated protein and thiopropyl-based capture enable the study of prenylome. Today, we should be able to decipher the protein prenylation machinery of eukaryotes *in vivo* and supply a better scheme of resistance to protein prenylation inhibitors in cancer and malaria.

In this prospect, our screening of protein prenylation inhibitors on BY-2 cells expressing GFP-CVIL already proposed new candidates.

With this respect, some candidates might be found in rhodophytes as extracts from *M. stellatus*, *P. cartilagineum*, *D. carnosus* and exert inhibition of protein prenylation as well as antimalarial activity (**section 5.2.1**). Nonetheless, the inhibition remained relatively low as critical problems such as low solubility of extracts and a dilution of active compounds by inactive compounds in the extracts. Even though the hypothesis of using relation between rhodophytes and *P. falciparum* seems to be relevant, further studies must definitely be carried out with pure compounds. Our results also support that the relation between antimalarial activity and protein prenylation inhibition is not trivial as some extracts were effective against *P. falciparum* but not on the inhibition of protein prenylation and *vice versa* (**section 2.2.3.2**). Luckily, within the 10 ligands of prohibitins tested, we identified IN2 as a very potent inhibitor of protein prenylation capable to fully inhibit the GFP-CVIL prenylation in BY-2 cells, in plant and even in the presence of 1 mM MVA. To note, the latter impairs normally the inhibition of protein prenylation by inducing flexibility of the PFT under the presence of FOS with MV or in the mutant *ggb2*. A trial was performed to compare inhibition properties of IN2 to those of *S*-carvone described as an atypical inhibitor of protein prenylation affecting capsidiol production (Huchelmann et al., 2014). Nonetheless, the capsidiol production was not impacted by IN2 at all (**Figure 97**). Altogether, our results comfort that IN2 impact protein prenylation through an atypical target, nonetheless we were not able to determine it at all (**section 0**). In this context we tried affinity purification with an IN2-agarose resin, but this trial failed resulting in an inefficient capture of IN2 targets. Further assay may be attempted after cell fractionation or with tobacco leaves to decrease the risk of protein degradation by BY-2 cells proteases as characterized with our GFP-sensor.

Moreover, we capitalized the effort invested in establishing the relation between MVA stimulation *via* cellulase elicitation, the protein prenylation inhibition by the *S*-carvone and the influence on capsidiol biosynthesis. Since MVA was found to provide carotenoids biosynthesis (Camara et al., 1992; Schwender et al., 1996; Vranová et al., 2013; Stanley and Yuan, 2019), I pursued preliminary studies on the suitability of such treatments to drive the production of carotenoids being highly valuable. This innovative approach was fruitful as we not only confirmed that the *S*-carvone highly improves the carotenoids content of elicited tobacco leaves, but we also address new features.

In this respect, we proved that *R*-carvone enantiomers induce the biosynthesis of at least one other carotenoid than *S*-carvone. Surprisingly, the addition of MVA to *S*-carvone restored a similar carotenoids profile to the *R*-carvone. Thus, these results propose new perspectives in enantioselective biosynthesis of carotenoids through the influence of monoterpenes enantiomers. Also, we showed that light quality influences carotenoids profiles, but independently of protein prenylation inhibitors or MVA treatments. The production of carotenoids was maximum with blue light as compared to the red light and greenhouse conditions. These results are congruent with what was reported for artemisinin in *A. annua* but also the fact that blue light influences positively the protein prenylation in *era1* as compared to red light (Hong et al., 2009; Jalakas et al., 2017). Not surprisingly several differences were observed in the metabolites extracted from the culture media of elicited tobacco leaves and mostly found between chemical treatments (**section 0**). As for carotenoids, the blue light resulted in the highest number of metabolites detected. What a surprising news was that metabolites detected between the culture medium of *S*-carvone and *R*-carvone treatments were almost totally different (**section 5.3.25.3.3**). However, only nicotine and capsidiol were identified letting mystery to all other metabolites. Astonishingly, the nicotine was found only in cellulase alone or combined to *S*-carvone with MVA, suggesting a relation between prenylated proteins and nicotine biosynthesis or excretion. Although MVA restore protein prenylation under inhibition with *S*-carvone, we were not able to define whether the biosynthesis or the excretion of nicotine and capsidiol are affected. As reported, the *S*-carvone inhibits protein prenylation but also the *epi*-aristolochene synthase expression (Huchelmann et al., 2014). In this context, our results are consistent with the fact that capsidiol may not that be appropriated to report on protein prenylation state, otherwise the MVA should have restored capsidiol in the culture medium as it restores the localization of the GFP-CVIL sensor (**Figure 106**). Accordingly, the absence of capsidiol under cellulase with the *S*-carvone must depend on the inhibition of *epi*-aristolochene synthase transcription rather than inhibition of protein prenylation. In contrast, the nicotine found in the medium appeared to obey to the same rule than prenylated proteins. Further experiments of nicotine GC-MS analysis in the culture media and in tobacco leaf discs may light on implication of prenylated proteins in the biosynthesis or the transport of nicotine in tobacco.

Therefore, we definitely proved that inhibitor of protein prenylation can be used to drive the production of valuable metabolites including carotenoids but also specialized metabolites such as nicotine. Still, is that volatile monoterpenoids only biosynthesized for plant defense or interaction with pollinators? For instance, it was reported that plants such as *Rosmarinus officinalis*, *Pinus* sp. *Quercus* sp. exert emission of monoterpenes like  $\alpha$ -pinene or  $\beta$ -myrcene in response to water loss, reduced O<sub>2</sub> environment or heat stress (Loreto et al., 1998; Ormeño et al., 2007). Originally, it was shown that oxidated monoterpenes evaluated as herbicides such as (+)-citronellal had a strong antimicrotubule efficacy, while (-)-menthone (+)-carvone were moderately effective (Chaimovitsh et al., 2017). Interestingly, the authors also noticed enantioselective effect as (-)-carvone did not exhibit antimicrotubule efficacy. In regard to our carotenoid's experiments, geraniol, citral and their two geometric isomer (geranial and neral) induce senescence in tomato (Ghosh et al., 2013). Geraniol was found to be phytotoxic as farnesol (Hemmerlin and Bach, 2000), and it was evidenced that geraniol acts in ethylene dependent and independent ways. This hypothesis of regulation role from monoterpenes might be investigated as influence on carotenoids are now reported too.

For the best of our knowledge vismiones and synthetic DHA did not inhibit protein prenylation at all, but they shed the light on a remarkable fluorescence. Although my PhD was about protein prenylation, I decided to explore these properties and take advantage of them by using Slmaging. This approach was complemented with a descent spectrofluorimetric study and a non-targeted metabolomics to characterize fluorescence spectra of VH, madagascine, emodin, quinizarin, fraxetin and to understand how these compounds are metabolized *in vivo*. Why have I pushed on this project? First, the fluorescence of AVD was reported, but on the basis of spectrofluorimetric analysis it was assumed that these compounds due to their low quantum yield were not bright enough for observation *in vivo*. As matter of fact, the fluorescence of vismiones literally blew out the GFP-sensor fluorescence in treated BY-2 cells, while excitation at 488 nm does normally not allow observation of vismione (**section 6.3**). Consequently, I was not able anymore to distinguish the GFP or RFP fluorescent marker than that of vismiones. The Slmaging remarkably solved this problem and allowed to explain the fluorescence observed and also the atypical phenotype reported previously in the protein prenylation inhibition assay (Hartmann et al., 2015). To note, we were not able to distinguish the fluorescence of vismiones

and anthrones/anthranols forms as both appeared spontaneously according to our non-targeted metabolomic analysis, and result in similar fluorescence spectra.

Secondly, vismiones and DHA stability have shown interesting antiprotozoan properties, but the action mechanism(s) remains unknown. However, it was proved that the stability *in vitro* and the antileishmanial properties of 3-O-prenyl and 6-OH synthetic DHA were increased as compared to vismiones or unprenylated DHA. I used the method developed to demonstrate that the more stable compounds are also the less metabolized and transported into primary vacuole and lipid droplets. The cell organelles labeled are connoted as sequestration compartments in plants (**section 6.3**). I was astonished by this fact, because our results obtained in BY-2 cells not only pinpoint for the first time the localization/metabolization of vismiones and DHA *in vivo*, but do also support that NW0184 (3-O-prenyl and 6-OH) might be the most active against *L. donovani* because not well metabolized and transported into the parasitophoric vesicles. Accordingly, further studies have to be carried out on cells infected by *L. donovani* and even *P. falciparum* to confirm our hypothesis but also to identify the targets of these compounds, as they localize into the ER, Golgi and the cytosol (**section 6.4**)

Nonetheless, since vismiones result in a cocktail of anthrones and anthraquinones and they are very sensitive to pH, multivalent cations and redox level, it can be speculated that the effect of these compounds simply results from an oxidative stress and not a specific interaction with a receptor or another enzyme. This hypothesis has to be tested in order to determine the accurate action mechanism(s), but today, the approach developed can be used and combines to proteomics, transcriptomics analysis to understand these aspects.

SI-maging definitely offer promising perspectives in the design of new ratiometric probes to accurately observe fluorescence localization and quantify changes in calcium, pH, lipids, etc in cellular compartments, in real time. In this context, vismiones do represent one of the most beautiful examples of fluorescence I have ever seen, and combines to SI-maging it clearly opens the door to the concept of multiple-labeling with a single molecule. As a wink, I personally defined it as a pro-probe.

In the end, I consider this thesis as successful as we brought new relevant elements, stress was defined as a physiological condition inducing flexibility of PPTs, in the Arabidopsis *era1* mutant the flexibility of PPTs was specified and a new method for unambiguous identification of prenylated proteins was set up and optimized for sustainable and investigation in PPTs-induced

flexibility. Besides, we identified a potent inhibitor of protein geranylgeranylation being at least 10 times more efficient than the fosmidomycin reference and acting via atypical and unknown action mechanism. On the top of that, we evidenced for the first time the fluorescence of vismiones in plant organism and developed a new method to study metabolization processes and transport of naturally occurring fluorescent compounds.

I think that one of the biggest challenges for the future is the development of efficient methods for *in vivo* study. Until now many preliminary and preclinical studies were performed *in vitro* because it is less expensive and easier to monitor but today these approaches face important difficulties concerning drug development and more particularly drug delivery. In fact, many parameters are involved in physiological mechanisms and are influenced by several factors that are not taken into account in classical *in vitro* models.

Today, new techniques and equipment are available and allow the observation and analysis of complex mechanisms in living organisms. The keystone of this thesis was to combine these techniques and develop methods for the observation of protein prenylation but more generally physiological mechanism *in vivo*.

### **7.1.1 Philosophical Note for a New *Philosophiae Doctor***

Still, I remain open-mouthed in front of this fascinating and infinite universe we are living in, being monitored *via* the natural selection of biochemical processes selected over billions of years. Finally, why does life exist? Why does every cell use energy to self-organize and try to maintain order (homeostasis) over generations? Is this simply the response to disorder in order to maintain an equilibrium? My hypothesis suggests that energy cannot be lost, it therefore oscillates within the matter to infinitely organize and disorganize it at every scale without any limits. With this respect, we will always discover problems and solutions, smaller and larger things, living or inert matter over time. However, the frame of reference for time clearly differs between organism and inert matter.

I am not a physicist but metaphorically, to some extent, I consider that relativity also applied to living organisms and in this way the life depicts a sort of singularity in our universe.



# 8 MATERIALS & METHODS





## 8.1 BIOLOGICAL MATERIAL

### 8.1.1 BY-2 cell Suspension

The *Nicotiana tabacum* cv. Bright Yellow 2 (tobacco BY-2) cell suspension made available by Toshiyuki Nagata (Tokyo University, Japan). Cultures were maintained at 26 °C, on a rotary shaker set at 140 rpm and in the dark, in modified Murashige and Skoog (MS) medium as described (Hemmerlin and Bach, 2000). For the treatments, 7-d-old cells were diluted fivefold into fresh MS medium and 3 ml were distributed in 6-well culture plates standard F (*Sarstedt*, Nümbrecht, Germany), then treated or not with drugs and induced or not 3h after the first treatment. Wild-type BY-2 cells (WT) as well as three different cell lines were used: cells transformed with (a) Dex::sGFP-CVIL (Gerber et al., 2009a), (b) cells transformed with a GFP-HDEL fusion construct that remains in the lumen of the endoplasmic reticulum (ER) 35S::ER-sGFP (Gomord et al., 1997), (c) cells transformed with an  $\alpha$ -mannosidase 1–green fluorescent protein fusion construct (Man1-GFP) 35S::Golgi-EGFP that localizes predominantly to the cis-Golgi (Nebenführ et al., 1999).

### 8.1.2 Tobacco Plants

#### 8.1.2.1 GFP-Prenylated protein production

Axenic SH6 WT tobacco (*Nicotiana tabacum*) plants and the Dex::sGFP-CVIL, -CVIM and -SVIL T-DNA insertion lines (Huchelmann, 2013), were grown *in vitro* for one month on MS<sup>1/2</sup> medium with or without 1% sucrose in 100 x 20 mm, PS round Petri dishes (Greener Bio-one, Frickenhausen, Germany), or Corning® Gosselin™ 120 x 120 mm square Petri dishes (Corning Inc., Corning, New-York) the photoperiod was adjusted to 16h/8h (day/night) under OSRAM Biolux L58w/965 neons in a room thermoregulated at 22°C prior to treatment and/or induction.

#### 8.1.2.2 Influence of Protein Prenylation on Metabolites

Axenic SH6 WT tobacco plants and Dex::sGFP-CVIL, -CVIM and -SVIL T-DNA insertion lines were grown *in vitro* as afford mentioned for two weeks prior to the induction of the GFP-CaaX proteins using floating method. The plantlets were then transferred to soil and grew up to about 25 cm (7-8 leaves) in different growing chambers: under OSRAM 18W/77 Fluora neon (red), OSRAM FQ 49W/965 HO neon (blue) and in a greenhouse supplemented with OSRAM Plantastar E40 400 w HPS lamps (sunlight).

### 8.1.3 Arabidopsis Plants

*Arabidopsis thaliana* Col0 wild-type (WT) and the T-DNA insertion mutants of the geranylgeranyl transferase  $\beta$ -subunit *ggb-2* ((Johnson et al., 2005) were transformed with pTA-expressing Dex::sGFP-CVIL and -CVIM and generously offered by D.N. Crowell (Idaho State University, Pocatello, Etats-Unis). The farnesyltransferase  $\beta$ -subunit *era1-9* T-DNA mutant (SALK\_110517) was ordered and sequenced using primers *era1-9* R 5'-CAACAACGGGTCATGCTGCT-3' and *era1* F 5'-ACCTACTGTGGTTTGGCTGC-3'. A F1 line was obtained by crossing *era1-9* with DEX::GFP-CVIL and -CVIL T-DNA insertion lines (Huchelmann, 2013). Plants were germinated on MS<sup>1/2</sup> solid agar medium containing 1% sucrose and 15  $\mu$ M hygromycin. The GFP fluorescence was screened in 3-week-old plants by cutting leaves prior to induction of GFP-sensor using 30  $\mu$ M dexamethasone following floating method (section 8.2.3.2). Then homozygous F2 lines were isolated after inbreeding F1 *era1-9*::GFP-CVIL and -CVIL and selected as for F1 generation. The homozygote character of F2 *era1-9*::sGFP-CVIL and -CVIM lines was confirmed by PCR using forward 5'-ACCTACTGTGGTTTGGCTGC-3' and reverse 5'-CAACAACGGGTCATGCTGCT-3' pair of primers for *era1* character and Lb 1b 5'-TGGCAGGATATATTGTGGTG -3' pair for the wild type. Amplified fragments were separated on 1.5 % agarose gel and analyzed after EtBr staining. New F2 stable lines were cultured as *in vitro* tobacco plant.

### 8.1.4 The *dxs* Deletion Mutant DY329

Inactivation of DXS was realized by disrupting *dxs* with the kanamycin cassette. *Escherichia coli* DY329 strain was engineered as described by Yu et al. and sub-cultured into liquid LB medium supplemented with tetracycline (12.5  $\mu$ g/mL). The primers KANDXS-F (CAGCGTAATAAATAACAATAAGTATTAATAGGCCCTGATGAGTATGGACAGCAAGCGAACCG) and KANDXS-R (CAAGGCCTGGCTGGCATA ATCCCTACTCCACTCCTGCTATGCTTAAGCATATGAATA TCCTCCTTAG) were used for the *in vivo* deletion of *dxs* and the master mix high fidelity PCR with HF buffer was used. This *dxs*::KAN disrupted *E. coli* strain grows exclusively in the presence of 1-deoxy-D-xylulose (DX), which once being phosphorylated into 1deoxy-D-xylulose 5-phosphate will be incorporated into the MEP pathway and used to build up isoprenoids of vital importance. That is why, the recombinant were selected on LB tetracycline (12,5  $\mu$ g/mL) and kanamycin (20  $\mu$ g/mL) plates supplemented with DX and thiamine/pyridoxal. Cultures were

placed at 28°C with 191 RPM overnight. Measures were read at t = 24 h after incubation (BioPhotometer, Eppendorf).

## 8.2 CHEMICALS

### 8.2.1 Screening of Protein Prenylation Inhibitors

#### 8.2.1.1 Natural and synthetic anthranoids:

Natural VH, VD and AVD have been isolated from PGE2 extract of *Psorospermum glaberimum* as previously described by Dr. J.B. Galle (Galle, 2015), and Synthetic DHA has been synthesized by Dr. N. Wasser (Wasser, 2018) during their *PhD* work in Dr. Catherine Vonthron-Sénécheau's lab (CNRS UMR 7200, Illkirch Graffenstaden France) (Galle, 2015; Wasser, 2018)). These molecules were tested against *Plasmodium falciparum* and *Leishmania donovani* as reported (Galle, 2015; Wasser, 2018), and used to evaluate their effects on the inhibition of protein prenylation. Stock solutions of these molecules at 25 mM were prepared shortly before treatments of BY-2 cells at final concentrations tested.

#### 8.2.1.2 Extracts from Red Algae

Extracts and subfractions from five different species of red algae were prepared by Dr. L. Margueritte (PhD 2018) and provided by Dr. Catherine Vonthron-Sénécheau (CNRS UMR 7200, Illkirch Graffenstaden France) (**Figure 92**). These extracts were tested against *Plasmodium falciparum* NF54 as stated (Margueritte, 2018), and used to evaluate their effects on inhibition of protein prenylation. The dried extracts were solubilized in DMSO and added into the culture medium to a final concentration of 40 µg/ml, 3h prior to induction of GFP-CVIL in Dex::sGFP-SVIL BY-2 cells with 15 µM dexamethasone.

#### 8.2.1.3 Synthetic Prohibitins Ligands

Molecules known as prohibitins (PHB) ligands were synthesized and given by Dr. Laurent Desaubry (CNRS UMR 7200, Illkirch-Graffenstaden France). These molecules were solubilized in DMSO at 10 mM and tested as inhibitors of protein prenylation to different concentrations (**Figure 93**)

#### **8.2.1.4 Other compounds used as inhibitor or for complementation assays**

Dexamethasone, *R*-carvone, MVA lactone and Fol mixture of isomers 90% were purchased (*Sigma-Aldrich*, Saint-Louis, Missouri) and GGol mixture of isomer 95 % as well (*Abcam*, Cambridge, United-Kingdom). *S*-carvone was a kind of gift from J. Oosterhaven (*Wageningen*, Netherlands) and MV from Alfred Alberts too (Alberts et al., 1980) *Merck*, Rahway, NJ). Before use, the lactones of MV and MVA were converted to their open acid forms. Fosmidomycin Fos ((Okuhara et al., 1980)) was made available by Robert J. Eilers (*Monsanto*, St. Louis, MO).

### **8.2.2 Inhibition of DY329 Strain**

DY329 pre-cultures (8.1.4) were treated with inhibitors: IN2 at 1  $\mu$ M, 10  $\mu$ M and 50  $\mu$ M and the FOS at 5  $\mu$ M (positive control) in order to measure the effect of IN2 on their DO600. The negative control was obtained with DY329 pre-cultures placed in DMSO, the solvent in which IN2 is diluted.

### **8.2.3 Plant Material Treatments**

#### **8.2.3.1 Prenylation of GFP-CVIL in BY-2 cells**

Inhibition studies were performed using BY-2 Dex::sGFP-CVIL line cells being treated for 3 h with inhibitors, alone or in combination. Then GFP-CVIL protein expression was induced by 15  $\mu$ M (observation of phenotype) or 30  $\mu$ M dexamethasone (production of protein for analysis) for 18 h. For chemical complementation experiments, isoprenols (Farnesol, and geranylgeraniol), MVA, MeJA, Ethephon, IAA, were added together with dexamethasone, but otherwise the same time schedule as described above was followed. Treated cells were then observed by confocal microscopy as reported (Gerber et al., 2009a), and vismione-treated cells were observed by spectral imaging too as described previously (section 6.3.3.6).

#### **8.2.3.2 Prenylation of GFP-CaaX sensors in plant leaves**

Two different methods were employed to induce protein prenylation in tobacco Dex::sGFP-CVIL, -CVIM and -SVIL lines. The first one called “floating” method consisted to cut leaves and incubate them for 6h onto 12-well plates standard F (*Sarstedt*, Nümbrecht, Germany) containing 2 ml/well of MS<sup>1/2</sup> medium with or without inhibitors/substrates prior to induction for 24h in the dark, at 22°C.

The second one called "Inbox" method consisted to water plants with 10 ml of treatment solutions for a 100 x 20 mm round Petri dish (Greener Bio-one, Frickenhausen, Germany) and two times more for a 120 x 120 mm square Petri dish (Corning Inc., Corning, New-York). With this respect, treatment solution, incubation time and temperature were similar, but plant were incubated under light condition (OSRAM Biolux L58w/965 neons) with a photoperiod of 16h/8h (day/night).

### **8.2.3.3 Fluorescence of Vismiones and Synthetic Dihydroanthracenones**

BY-2 Dex::sGFP-CVIL cells were treated 5 min and 18 h with each vismione and some synthetic dihydroanthracenones such as NW0129, NW184, NW0188 or NW211 at 50  $\mu$ M. Then, treated cells were observed by spectral imaging and the results analyzed according to our proof of concept (section 6.3.3.66.3.3.7). The freeze-dried cells treated with NW184 were extracted three times with MeOH and the metabolomic analysis was performed as reported (section 6.3.3.8).

### **8.2.3.4 Effect of Protein prenylation Inhibitors on Metabolites**

Leaf discs of  $\varnothing = 3$  cm were punched between the secondary veins of the tobacco leaves of three different plants for each tobacco line grown as described in the section "Plant material" (8.1.2.2). The leaf discs were floated on  $\text{KH}_2\text{PO}_4$  50  $\mu$ M for 18 h under different conditions. Treatments consisted of stress induction with 0.5% cellulase, supplemented with 2 mM *R*-carvone or *S*-carvone alone or with 1 mM MVA.

## **8.2.4 Synthesis of S-Prenyl-L Cysteine Methyl Ester References**

### **8.2.4.1 Synthesis of farnesyl bromide**

The chemical synthesis of farnesyl bromide was achieved as previously described (Aguilar et al., 2014), conserving equivalent of  $\text{PBr}_3$  and  $\text{Et}_2\text{O}$  for 1.506 g (6.1 mmol) of a farnesol mixture of 90 % isomers (*Sigma-Aldrich*, Saint-Louis, Missouri). The organic phase was decanted, washed with cold 5%  $\text{NaHCO}_3$ , brine, dried over  $\text{MgSO}_4$  and the solvent removed at 40  $^\circ\text{C}/3\text{mmHg}$ , yielding as a pale-yellow liquid (2.073g, 98 %).  $^1\text{H}$  NMR ( $\text{CDCl}_3$ ): d 1.60 (s, 6H), 1.69 (s, 3H), 1.73 (s, 3H), 1.94-2.19 (m,8H), 4.03 (d, J = 8.5 Hz, 2H), 5.1 (m, 2H), 5.53 (t, J = 7.9, 1 H) (Annexe 3).

#### 8.2.4.2 Synthesis of Geranylgeranyl Bromide

Protocol was adapted from the synthesis of farnesyl bromide with 0.5 g (1,72 mmol) of a geranylgeraniol mixture of 95 % isomers (*Abcam*, Cambridge, United-Kingdom). The organic phase was decanted, washed with cold 5% NaHCO<sub>3</sub>, brine, dried over MgSO<sub>4</sub> and the solvent removed at 40 °C/3mmHg, yielding as a yellow liquid (0.597 g, 98 %). <sup>1</sup>H NMR (CDCl<sub>3</sub>): d 1.6 (s, 6H), 1.68 (s, 3H), 1.73 (s, 6H), 1.93-2.17 (m,10H), 4.02 (d, J = 8.4 Hz, 2H), 5.1 (m, 3H), 5.53 (t, J = 7.9, 1 H) (**Annexe 4**).

#### 8.2.4.3 Synthesis of Phytol Bromide

Protocol was adapted from the synthesis of farnesyl bromide with 1.999 g (6.53 mmol) of a phytol mixture of 97 % isomers (*Sigma-Aldrich*, Saint-Louis, Missouri). The organic phase was decanted, washed with cold 5% NaHCO<sub>3</sub>, brine, dried over MgSO<sub>4</sub> and the solvent removed at 40 °C/3mmHg, yielding as a pale-white liquid (2.455 g, 98 %). <sup>1</sup>H NMR (CDCl<sub>3</sub>) : 0.84 (s, 3H), 0.86 (s, 6H), 0.87 (s, 3H), 1-1.45 (m,18H), 1.52 (h,1H), 1.72 (s, 2H), 1.77 (s, 1H), 2.06(dt, XX, 2H) 4.02 (d, J = 8.4 Hz, 2H), 5.53 (t, J = 7.9, 1H) (**Annexe 5**).

#### 8.2.4.4 Synthesis of S-farnesyl-L Cysteine Methyl Ester

To a solution of cysteine methyl ester hydrochloride (905 mg, 5.27 mmol, 1.5 eq) dissolved in 10 ml DMF was added 1 eq of farnesyl bromide (1000 mg, 3.5 mmol). DIEA was then added (1 ml, 5.8 mmol, 1.6 eq) and the mixture was allowed to stir overnight. After diluting the solution with deionized water, it was extracted three times with EtOAc and the combined organic layers were washed once with saturated NaCl and then dried over anhydrous MgSO<sub>4</sub>. After rotary evaporation, the crude product was purified *via* SiO<sub>2</sub> column to afford the desired product in 43% yield. <sup>1</sup>H NMR (CDCl<sub>3</sub>) d 1.6 (s, 3H), 1.67 (s, 6H), 1.71 (s, 3H), 1.93–2.15 (m, 8H), 2.68 (dd, J = 13.5, 7.5, 1H), 2.88 (dd, J = 13.5, 4.6, 1H), 3.1-3.26 (m, 2H), 3.63 (dd, J = 7.7, 4.6, 1H), 3.74 (s, 3H), 5.1 (m, 2H), , 5.23 (t, J = 7.9, 1H) (**Annexe 6**).

#### 8.2.4.5 Synthesis of S-Geranylgeranyl-L Cysteine Methyl Ester

To a solution of cysteine methyl ester hydrochloride (181 mg, 1.05 mmol, 1.5 eq) dissolved in 2 ml DMF was added 1 eq of geranylgeranyl bromide (237 mg, 0.67 mmol). DIEA was then

added (0.2 ml, 1.16 mmol, 1.6 eq) and the mixture was allowed to stir overnight. After diluting the solution with deionized water, it was extracted three times with EtOAc and the combined organic layers were washed once with saturated NaCl and then dried over anhydrous MgSO<sub>4</sub>. After rotary evaporation, the crude product was purified *via* SiO<sub>2</sub> column to afford the desired product in 48 % yield. <sup>1</sup>H NMR (CDCl<sub>3</sub>) δ 1.6 (s, 6H), 1.67 (s, 3H), 1.68 (s, 6H), 1.93–2.15 (m, 12H), 2.69 (dd, J = 13.5, 8, 1H), 2.88 (dd, J = 13.5, 4.6, 1H), 3.1–3.26 (m, 2H), 3.63 (dd, J = 7.7, 4.6, 1H), 3.74 (s, 3H), 5.1 (m, 3H), , 5.23 (t, J = 7.8, 1H) (**Annexe 7**).

#### **8.2.4.6 Synthesis of S-phytyl-L Cysteine Methyl Ester**

To a solution of cysteine methyl ester hydrochloride (905 mg, 5.27 mmol, 1.5 eq) dissolved in 10 ml DMF was added 1 eq of geranylgeranyl bromide (1200 mg, 3.5 mmol). DIEA was then added (1 ml, 5.8 mmol, 1.6 eq) and the mixture was allowed to stir overnight. After diluting the solution with deionized water, it was extracted three times with EtOAc and the combined organic layers were washed once with saturated NaCl and then dried over anhydrous MgSO<sub>4</sub>. After rotary evaporation, the crude product was purified *via* SiO<sub>2</sub> column to afford the desired product in 45 % yield. <sup>1</sup>H NMR (CDCl<sub>3</sub>) δ 0.83 (s, 3H), 0.86 (s, 6H), 0.87 (s, 3H), 1.00–1.43 (m, 18H), 1.52 (h, 1H), 1.65 (s, 2H), 1.72 (s, 1H) 1.91–2.07 (m, 2H), 2.68 (dd, J = 13.6, 7.7, 1H), 2.89 (dd, J = 13.5, 4.6, 1H), 3.1–3.26 (m, 2H), 3.63 (dd, J = 7.7, 4.6, 1H), 3.74 (s, 3H), 5.22 (t, J = 7.8, 1H) (**Annexe 8**).

## **8.3 SYNTHESIS OF A HOMEMADE GFP-TRAP**

### **8.3.1 Synthesis of Magnetic Agarose Particles (MAPs)**

#### **8.3.1.1 Standard procedure**

MAPs were synthesized through water-in-oil suspension thermal regeneration as previously reported, but without carbonate calcium and using Inland 45 (*Inland Vacuum Industries*, New York USA) vacuum pump oil (Gu et al., 2017). The emulsion was performed using magnetic stirring, after cooling, the particles were collected and washed three times each with hexane, EtOH and deionized water. The particles were then mixed with 3% (v/v) epichlorohydrin (*Sigma-Aldrich*, Saint-Louis, Missouri) and 1 M NaOH by 200 rpm agitation at 30°C for 12 h to complete the cross-link reaction.



The cross-linked particles were washed with EtOH and deionized water thoroughly, then filtered through 240, 120 and 73  $\mu\text{m}$  sieves. The < 73  $\mu\text{m}$  batch was conserved and stored in 20% EtOH at 4°C.

### **8.3.1.2 Optimized procedure**

Briefly, 150 ml of toluene HPLC Plus (*Sigma-Aldrich*, Saint-Louis, Missouri) containing 3% or 8.5% emulsifiers, which consisted of Span-80 (*Merck Millipore*, Darmstadt Germany) and Tween-80 (*Sigma-Aldrich*, Saint-Louis, Missouri) in the ratio 14:1, 1:14, 2:1 or 1:2 (w/w), was added into a 250 ml round flask. The organic phase was stirred at 6500 rpm using a T25 Basic ULTRA-THURRAX® disperser (*IKA-Werke*, Staufen im Breisgau, Germany) and heated to 80°C in a water bath. Then 1.0 g of agarose powder D-5 DNA grade (*Euromedex*, Souffelweyersheim, France), 2.0 g of Fe<sub>3</sub>O<sub>4</sub> 20-30 nm 98% (US-research nanomaterial inc, Houston Texas) were added to 25 ml of deionized water and heated to obtain a 4 % (w/v) agarose solution. The agarose solution was then dispersed in the organic phase under continuous stirring at 6500 rpm, 80°C, after 5 minutes temperature was decreased to 70°C for 5 minutes. Then, the speed was increased at 8000 rpm and maintained for 5 minutes more. Thereafter, the reaction system was cooled quickly on an ice-cold water bath while maintaining stirring at 6500 rpm. The particles were collected, washed successively with EtOH and deionized water. The cross-linking of MAPs was performed using either epichlorohydrin as above-mentioned or divinylsulfone (DVS) procedures. The DVS (*Alfa Aesar*, Haverhill, Massachusetts) cross-linking was achieved as reported with 5 g of MAPs and 1g of Dextran 500 (*Amersham Biosciences*, Little Chalfont United-Kingdom) as blocking agent (Hjertén et al., 1987). After cross-linking, the particles were filtered through 240, 120 and 73  $\mu\text{m}$ . The < 73  $\mu\text{m}$  batch was conserved and stored in 20% EtOH at 4°C

### **8.3.2 Functionalization of MAPs in a GFP-Trap**

Before the protein immobilization on the support, the cross-linked MAPs were functionalized by two different procedures according to the literature. The first was the formation of glyceryl agarose using glycidol (*Acros Organics*, Gell, Belgia), which was then oxidized in glyoxyl agarose following a reported protocol (López-Gallego et al., 2013). The other one consisted in the reaction of DVS (*Alfa Aesar*, Haverhill, Massachusetts) with the agarose from MAPs support as described in literature (dos Santos et al., 2015). Nb-tRFP@GFP or NbD@GFP nanobodies in PBS adjusted to pH 10.5 with 1/10 of a 1 M bicarbonate buffer were immobilized on MAPs for 16 h

on a wheel at 7 rpm, 4°C. The MAPs were washed four times with PBS/NaHCO<sub>3</sub> 0.1 M pH10.5 buffer. The grafted glyoxyl agarose was reduced with 1 mg.ml<sup>-1</sup> NaBH<sub>4</sub> (*Sigma-Aldrich*, Saint-Louis, Missouri) for 5 min at RT then 25 min at 4°C, whereas the DVS grafted MAPs were left 2h with 0.1 M PBS/NaHCO<sub>3</sub> pH10.5 and 1 M glycine. Finally, the MAPs were washed three times with PBS pH 7.5 and store at 4°C in deionized water containing 0.05 % NaN<sub>3</sub>.

### 8.3.3 Production of @GFP Nanobodies

#### 8.3.3.1 Nb-tRFP@GFP

The sequences of the Nb-tRFP@GFP consisted of fusion between published GFP enhancer nanobodies ((Rothbauer et al., 2006), Chromotek, Planegg, Germany) and tagRFP ((Merzlyak et al., 2007), Evrogen, Moscow, Russia). Nanobodies sequence was amplified by PCR using primer VP\_SapI-VHH fusion Cter forward (5'-ACTTGgctcttctATGCAGGTGCAGCTGCAGGAGTCTGGrGGA GG-3') and reverse (5'-ATGATgctcttccGGAGGAGACGGTGACCTGGGT-3').

The tagRFP sequence was amplified using primer VP\_TRFP-6his-Cter-sap1 forward (5'-GCTAAGCTCTTCgTCCGGCGGATCCGGCGGCGGAagcgagctgattaaggagaacatg-3') and reverse (5'-GCTAAGCTCTTCgTCAGTGATGGTGGTGGTGGTGGCCGGATCCGCCGCCCTTGTGCCCCAGTTTGCTA GGG-3'), which introduce 3GS3G linker coding sequence at 5' extremity and 6 histidine tag coding sequence at 3'extremity. Both pair of primers carry SapI type II restriction site compatible with subsequent GoldenGate cloning. Amplified DNA fragments were loaded on agarose gel and purified using gel extraction kit (*Macherey-Nagel*, Hoerd, France) according to manufacturer's instructions. Both purified DNA fragments were assembled in one pot reaction using SapI restriction enzyme (10 U), ATP (1 mM), Ligase (5 U), Cutsmart buffer (1x) and 150 ng of the destination vector for cytoplasmic expression (**Annexe 9**). The mix is incubated in PCR machine for 30 min at 37°C followed by 30 min at 18°C, those steps are repeated for 6 cycles. Reaction mix is incubated 1h at 37°C, then 15 min at 50°C and finally enzyme inactivation is performed at 15 min at 80°C. Ligation mix was used to transform *E. coli* Top10 competent cells and plated on LB containing 100 µg.mL<sup>-1</sup> of carbenicillin. LB plate was incubated overnight at 37°C and positive clones were selected by colony PCR and sequencing experiments. The expression was performed in freshly transformed *E. coli* SHuffle T7 Express cells (*New England Biolabs*, Ipswich, Massachussetts) grown in TB medium at 30°C until the culture reach an O.D = 0,8-1 then protein production is induced overnight with 0.1 mM IPTG at 20 °C. Pelleted cells

resuspended in running buffer (50 mM Tris, 300 mM NaCl, 5% glycerol, pH 7,4) were lysed by sonication (100% amplitude for 2 min with 13 mm diameter probe, Vibra-Cell VCX 500 (Sonics & Materials Inc., Newtown, Connecticut). Purification of cytoplasmic extract was carried out using immobilized metal ion chromatography (IMAC) on a 1 ml Ni-NTA column (GE Healthcare Life Science) using 500 mM imidazole in running buffer (50 mM Tris, 300 mM NaCl, 5 % glycerol, pH 8.0) for elution, followed by size exclusion chromatography (SEC) on a Hiload 16/60 Superdex75 prep grade column (GE Healthcare Life Science) in 1x phosphate buffer saline (PBS). The purity of the eluted protein was assessed by Coomassie blue staining of denatured Nbs:tRFP that migrate as a band of 43 kDa in Tris-tricine polyacrylamide gel upon electrophoresis.

#### 8.3.3.2 *NbD@GFP*

Bivalent @GFP nanobodies (Nb) have been designed by fusing two different nanobodies sequences reported in literature, the NbCh@GFP ((Rothbauer et al., 2006), Chromotek, Planegg, Germany) and NbSF@GFP (Twair et al., 2014) to produce bivalent nanobodies. Nb sequence was amplified by PCR using primer NbCh@GFPF (5'-ACTTGgctcttctATGCAGGTGCAGCTGCAGGAGTCTGGrGGAGG-3') and NbCh@GFPR (5'-ACCACGCTCTTCcACCGGATCCGCCTCCGGATCCACCGCCTCCGGATCCACCGCCTCCGGAGGAGACG GTGACCTGGGTCCCCTG-3') for NbCh@GFP or primer NbSF@GFPF (5'-ACTTGgctcttctGGTCAGG TGCAGTTGCAG-3') and NbSF@GFPR (5'-ACCACGCTCTTCCTCACTTTTCGAACTGAGGGTGTGACC AGTGATGGTGTGATGGTGTGATGATACGGTACTTGCCTACC-3') for NbSF@GFP, introducing 3GS3G linker coding sequence and Strep Tag II - 6 histidine tag coding sequence at 3' extremity respectively. Both pairs of primers carry SapI restriction site compatible with subsequent GoldenGate cloning. Amplified DNA fragments were loaded on agarose gel and purified using gel extraction kit (*Macherey-Nagel*, Hoerd, France) according to manufacturer instructions. Both purified DNA fragments were assembled in one pot reaction using SapI restriction enzymes as indicated above, but with the destination vector for periplastic expression (**Annexe 10**). Large-scale production of the bivalent nanobodies constructs was performed by expression in freshly transformed *E. coli* BL21 (DE3) cells grown 4h at 37°C and transferred overnight at 20 °C in auto-inducing ZYP 5052 medium. The nanobodies were extracted from periplasm by

osmotic shock (Habib et al., 2013) and purified at 4 °C by IMAC follow by SEC was carried out as indicated above. Purity of eluted proteins was assessed by Coomassie blue staining of denatured nanobodies that migrate as single bands of 30 kDa in Tris-tricine polyacrylamide gel. Purification yields were estimated from absorbance at 280 nm based on extinction coefficients computed from nanobodies AA composition.

## 8.4 BIOCHEMISTRY AND ANALYTICAL METHODS

### 8.4.1 Immunoprecipitation (IP)

The plant material (750 mg or 5g) was crushed in liquid nitrogen and solubilized in (1.5 mL) IP buffer (IPB) containing  $\text{KH}_2\text{PO}_4$  50 mM, KCl 50 mM, EDTA 1 mM, EGTA 1 mM,  $\text{MgCl}_2$  10 mM, Tergitol NP40 0.5%, Brij-58 0.1% at pH 7.5. Proteins were extracted for 1h at 4°C on a wheel adjusted to 7 rpm. When necessary, protease inhibitor cocktail cOmplete™ (*Roche*, Basel Switzerland) was added (1 tab/ 50 ml). Cellular membranes were pelleted at 16 100 g, at 4°C, and the supernatant was filtered through a 120 µm sieve. In the case of technical replicates, plant material was pooled up to 15 g, therefore extracted with 30 ml of IPB, centrifuged, filtered as previously and then breakdown in 2 ml tubes (*Eppendorf*, Hambourg Germany) or in 15 ml tubes for metabolomics experiments (Corning Inc., Corning, New-York) according to ratio of 0.15 g plant material (0,3 ml supernatant) for 1 µl GFP-Trap.

The IPs were performed by using commercial GFP-Trap M and MA (*Chromotek*, Planegg-Martinsried Germany) and our homemade GFP-Trap v1 (4.4) or GFP-Trap v2 (4.9) systems. Incubation of supernatant was carried out 30 min or 1h at 4°C on a wheel adjusted to 7 rpm. The magnetization of GFP-Trap particles was ensured using a magnetic support prior to remove the supernatant and wash GFP-Trap three times with IPB (1.5 ml) containing 50 µM  $\text{NH}_4\text{HCO}_3$  during 10 min each. Immunoprecipitated proteins were eluted with 25 µl of 1x Laemmli buffer, during 10 min at 80°C and separated by SDS-PAGE, stained and analyzed by Western Blot or digested prior to proteomics or metabolomics. To note immunoprecipitation performed with 50 µl µMACS GFP (*Miltenyi*) following instruction from the kit.

### 8.4.2 IN2-Agarose Affinity Purification

The plant material (750 mg) was crushed in liquid nitrogen and solubilized in (1.5 mL) extraction buffer (TE) consisting in 1% phosphate buffer solution (PBS), 2% sucrose, 1 mM DTT, 1% triton X-100 with 1 tab/50 ml TE of protease inhibitor cocktail cOmplete™ (*Roche*, Basel Switzerland). Proteins were extracted for 1h at 4°C on a wheel adjusted to 7 rpm. Cellular membranes were pelleted at 16 100 g, at 4°C, and the supernatant was filtered through a 120 µm sieve. The IP were performed by using 100 µl of IN2-Agarose resin supplied by L. Desaubry (Ex-LIT researcher). Incubation of the supernatant was carried out with 35 min at 4°C on a wheel

adjusted to 7 rpm. Then, IN2-agarose resin was pelleted by a rapid centrifugation at 16 100 g and the supernatant was discarded. The IN2-Agarose resin was washed three times with 1.5 ml buffer, twice with TE buffer and a last one with IPB buffer, 10 min each. Proteins were eluted with 25 µl of Laemmli buffer (1x), during 10 min at 80°C and separated by SDS-PAGE and stained with Coomassie Blue and silver nitrate.

### **8.4.3 SDS-PAGE**

Separation by SDS-PAGE was performed in gel of 8 x 6,5 cm, 1 mm thickness. 12% acrylamide Gels were prepared by 5 using Mighty Small multiple gel caster SE200 series 8 x 8 cm (*Hoefler Pharmacia Biotech*, San Francisco, California). Separation gel (5 cm) consisted of 9 ml 40% Acrylamide/bis-acrylamide >99% (*Euromedex*, Souffelweyersheim, France), 7.5 ml of 1.5 M Tris UltraPure ESP/EP (*Euromedex*, Souffelweyersheim, France) adjusted to pH 8.8, 13 ml deionized water, 0.3 ml SDS 10% Molecular biology grade (*Euromedex*, Souffelweyersheim, France), 0.15 ml ammonium persulfate (*Merck Millipore*, Darmstadt Germany) and 0.015 ml Temed (*Kodac*, Rochester, New-York). Stacking gel (1.5 cm) was prepared using 2.25 ml 40% Acrylamide/bis-acrylamide, 4.4 ml of 0.5 M Tris pH 6.8, 11 ml deionized water, 0.18 ml SDS 10%, 0.1 ml ammonium persulfate and 0.02 ml Temed. Total volume of samples solubilized in x1 Laemmli buffer were deposited, and electrophoresis was run in Tris/glycine/SDS buffer pH 8.3 following dilution to 1x at 250V, 33 mA/2 gel using Pharmacia Biotech SE250 electrophoresis system (*Hoefler Pharmacia Biotech*, San Francisco, California) monitored by power supply Model 1000/500 (*Bio-Rad*, Hercules, California). After running, gels were stained using Coomassie Blue (InstantBlue™: *Abcam*, Cambridge, United-Kingdom), silver nitrate or analyzed by Western Blot. For resolutive SDS-PAGE analysis, a 12% gel of 20 x 20 cm, 1.5 thickness was prepared using electrophoresis vertical Casting Stand 98-BR (*Bio-Rad*, Hercules, California). Separation was run 3h 15 min at 60 mA using Protein-II xi Cell (*Bio-Rad*, Hercules, California) monitored by power supply Model 1000/500 (*Bio-Rad*, Hercules, California).

### **8.4.4 Silver Nitrate Staining**

Gels labeled or not by InstantBlue™ were decolorized in 100 ml solution 30% EtOH with 10% acetic acid, 45 min under agitation. Then, gels were reduced in 100 ml solution 30% EtOH

containing 2.5 % of 4M sodium acetate solution adjusted at pH 6 in deionized water, 0.1 % sodium thiosulfate for 30 min under agitation and washed three times in deionized water 100 ml, 10 min under agitation. Next, coloration step was carried out using 100 ml of deionized water containing 0.1% AgNO<sub>3</sub> with 37% formaldehyde, 30 min under agitation. Finally, silver nitrate coloration was revealed with 200 ml of 2.5% Na<sub>2</sub>CO<sub>3</sub> with 37% formaldehyde. Reaction was stopped at the desired intensity of coloration using 1% acetic acid solution in deionized water

#### **8.4.5 Western Blot**

0.5 to 1 µg of purified proteins separated by SDS-PAGE were transferred using Trans-Blot® SD (*Bio-Rad*, Hercules, California) semi-dry electrophoretic transfer onto PVDF Immobilon™-P membrane (*Merck Millipore*, Darmstadt Germany) according to Protocol 1.2 reported . Parameters for semi-dry transfer was 20V, 60 mA 10.5 min using cathode buffer containing 25 mM Tris, 40 mM 6-amino-n-caproic acid in 10% MeOH adjusted at pH 9.4. Immunostaining was carried out using rabbit polyclonal antibodies raised against gel-purified recombinant H6-GFP-CVIL protein, and a secondary Goat @rabbit antibody (*ThermoFisher*, Waltham USA) coupled to a phosphatase alkaline. The immunolabeled protein was revealed using LumiPhos 530 (*Lumigen*, Southfield USA) or NBT/BCIP substrates (*Sigma-Aldrich*, Saint-Louis, Missouri).

#### **8.4.6 Digestion of Purified GFP-Sensors**

##### *8.4.6.1 In-gel digestion method*

Immunoprecipitated proteins were separated by SDS-PAGE and labelled by InstantBlue™ or not prior to proteomics analysis.

**IBMC:** Colored protein bands were excised from the SDS-PAGE gel and prepared as previously described (des Georges et al., 2015). Briefly, after bands destaining in 25mM ammonium bicarbonate containing 50% (v/v) acetonitrile, proteins were reduced with 10mM dithiothreitol (DTT) (45 min, 56°C) and further alkylated with 55mM iodoacetamide (in the dark for 1 hour at room temperature) (Simonetti et al., 2016). 40ng of modified sequencing-grade AspN (Promega, Madison, WI) was added on gel pieces for digestion, overnight, at room temperature.

Resulting peptides were extracted from the gel pieces and vacuum-dried in a SpeedVac concentrator.

**LSMBO:** Non colored protein bands were washed, reduced 1h at 60°C by adding dithiothreitol to a final concentration of 10 mM and alkylated 20 min in the dark by adding iodoacetamide to a final concentration of 30 mM. An overnight digestion at 37 °C was performed by adding Asp-N in 25 mM NH<sub>4</sub>HCO<sub>3</sub>. Peptides were extracted (80 % acetonitrile, 0.1% formic acid) and diluted with 0.1% FA prior to mass spectrometry analysis.

Finally, samples were analyzed by NanoLC-Q-Orbitrap-MS/MS (IBMC and LSMBO)

#### ***8.4.6.2 In-solution digestion method***

Proteins eluted in 30 µl of 1x Laemmli buffer, 10 min at 80°C, were then precipitated with five volumes of 0.1 M AcNH<sub>4</sub> in MeOH 24h at -20°C and then pelleted at 16100 g, 4°C. The pellets were then washed three times with AcNH<sub>4</sub> 0.1 M in MeOH 80% and dried to remove residual MeOH. Proteins were resuspended in 50 mM ammonium bicarbonate, before being further reduced (5mM dithiothreitol, 10 min, 95°C) and alkylated (10mM iodoacetamide, 30 min, RT, in the dark). After a quenching step (5 mM dithiothreitol), proteins were digested overnight with 200ng of sequencing-grade porcine trypsin (Promega, Fitchburg, MA, USA) prior to NanoLC-Q-Orbitrap-MS/MS (IBMC).

#### ***8.4.6.3 On-beads digestion method***

Immunoprecipitated proteins on GFP-Trap after washes were resuspended in 100 µl of NH<sub>4</sub>HCO<sub>3</sub> 50 mM containing 100 ng of trypsin gold (*Promega*, Madison, Wisconsin) and digested 20h at 37°C on a rocker mixer. The quantity of trypsin was doubled for protein samples from 5 g of plant material. The supernatant collected after digestion was dried under vacuum and resolubilized in deionized water prior to analysis using NanoLC-Q-Orbitrap-MS/MS (IBMC), UPLC-TQ-MS/MS and UPLC-QTOF-MS/MS analyses (IBMP).

### **8.4.7 Proteomics and Metabolomics**

#### ***8.4.7.1 NanoLC-Q-OrbiTrap-MS/MS analysis for proteomics at the IBMC***

Digested proteins were analyzed on a QExactive + mass spectrometer coupled to an EASY-nanoLC-1000 (Thermo Fisher Scientific) operating in positive mode with a nanoelectrospray



source. Each sample was loaded on a C-18 precolumn (75  $\mu\text{m}$  ID  $\times$  20 mm nanoViper, 3 $\mu\text{m}$  Acclaim PepMap; Thermo-Fisher Scientific) at 800 bars in solvent A.

After desalting and concentration, the pre-column was switched online with the analytical C18 analytical column (75  $\mu\text{m}$  ID  $\times$  25 cm nanoViper, 3 $\mu\text{m}$  Acclaim PepMap; Thermo-Fisher Scientific) equilibrated in solvent A: solvent B (95:5; v/v). Peptides were eluted at a flow rate of 300 nL/min using a gradient from 5% B to 20% B in 120 min, from 20% B to 32% B in 15min, from 32% B to 95% B in 1min and 95% B to 95% B during 24min. The Q-Exactive Plus was operated in data-dependent acquisition mode (DDA) with Xcalibur software (Thermo-Fisher Scientific). Survey MS scans were acquired at a resolution of 70K at 200 m/z (mass range 350-1250), with a maximum injection time at 100ms and an automatic gain control (AGC) set at 3e6. Up to 10 of the most intense multiply charged ions ( $\geq 2$ ) were selected for HCD fragmentation with a normalized collision energy (NCE $\pm 5$ ), at 17.5K resolution, with a maximum injection time at 100ms and AGC set at 1e3. A dynamic exclusion time of 10 s was applied during the peak selection process. Raw files were finally transformed into mgf files using Proteome Discoverer software (v2.0, Thermo-Fisher Scientific).

MS data were searched against the TAIR v10 database with a decoy strategy. We used the Mascot algorithm (version 2.5.1, Matrix Science) to perform the database search with a decoy strategy. Mascot search parameters were as follows: carbamidomethylation of cysteine was set as a fixed modification, whereas N-terminal protein acetylation and oxidation of methionine were set as variable modifications; tryptic specificity with proline restriction and up to three missed cleavages was used. The mass tolerances in MS and MS/MS were set to 10ppm and 0.05Da respectively, and the instrument configuration was specified as "ESI-Trap". The resulting .dat Mascot files were then imported into Proline v1.4 package for further post-processing. (2). Proteins were validated on Mascot pretty rank equal to 1, Mascot score above 25 and 1% FDR on both peptide spectrum matches (PSM score) and protein sets (Protein Set score). The total number of MS/MS fragmentation spectra was used to quantify each protein in each condition performed in three replicates (Bajczyk et al., 2020). Several variable modifications were specifically taken into account: carbamidomethyl (Cys), oxidation (Met), acetyl (protein N-term), Farnesyl-methyl (Cys), Farnesyl (Cys), Geranyl-methyl (Cys), Geranyl-geranyl (Cys) and methyl (Cys).

#### **8.4.7.2 NanoLC-Q-Orbitrap -MS/MS analysis for proteomics at the LSMBO**

NanoLC-MS/MS analyses of the tryptic peptides were performed on a nanoACQUITY Ultra-Performance-LC-system (Waters, Milford, MA) coupled to a Q-Exactive plus Orbitrap mass spectrometer (ThermoFischer Scientific, Bremen, Germany). Samples were loaded on a Symmetry C18 precolumn (20 x 0.18 mm, 5 µm particle size, Waters Corp.). The peptides were separated on an ACQUITY UPLC® BEH130 C18 column (250mm x 75 µm, 1.7 µm particle size, Waters Corp.). The solvent system consisted of 0.1 % FA in deionized water (solvent A) and 0.1 % FA in ACN (solvent B). The samples were loaded into the enrichment column during 5 min at 5 µL/min with 99 % of solvent A and 1 % of solvent B. The elution of the peptides was performed at a flow rate of 450 µL/min with a 1-45 % linear gradient of solvent B in 35 min at 60 °C.

The mass spectrometer source was operated at a spray voltage of 2.1 kV at 250 °C. The system was operated in Data-Dependant-Acquisition (DDA) mode with automatic switching between MS (50 ms/scan on m/z range [300-1800] with R = 70,000) and MS/MS (100ms/scan on m/z range [200-2200] with R = 17,500) modes. The ten most abundant peptides (intensity threshold  $2.10^5$ ), preferably doubly and triply charged ions, were selected on each MS spectrum for further isolation and HCD fragmentation. The dynamic exclusion time was set to 60 sec.

The raw data obtained during nanoLC-MS/MS analyses were converted into “.mgf” files using MSConvert. Semi ASP-N was selected as cleavage enzyme and a maximum of 4 missed cleavage was allowed. For MS/MS parameters, a parent mass tolerance of 10 ppm and a fragment mass tolerance of 0.07 Da were used. Several variable modifications were taken into account: carbamidomethyl (Cys), oxidation (Met), acetyl (protein N-term), Farnesyl-methyl (Cys), Farnesyl (Cys), Geranyl-methyl (Cys), Geranyl-geranyl (Cys) and methyl (Cys).

#### **8.4.7.3 UPLC-TQ-MS/MS Analysis for targeted metabolomics**

CVIM, CVIL, SVIL tetrapeptides (Thermo Fisher Scientific, Waltham Massachusetts) and S-farnesyl-L-cysteine methyl ester (Enzo Life Science Inc., Farmingdale New York) were identified and quantified by UPLC-MS/MS. Quantitative profiles were analyzed using an EVOQ Elite LC-TQ (Bruker, Billerica Massachusetts) equipped with an electrospray ionization source and coupled to a Dionex UltiMate 3000 UHPLC system (Thermo Fisher Scientific, Waltham Massachusetts).

Chromatographic separation was achieved using an Acquity UPLC HSST3 C18 column (100 × 2.1 mm, 1.8 μm; Waters) and pre-column. The mobile phase consisted of (A) water and (B) acetonitrile, both containing 0.1% formic acid. The run started by 2 min of 95 % A, then a linear gradient was applied to reach 100 % B at 12 min, followed by an isocratic run during 2 min. Return to initial conditions was achieved in 1 min and equilibrate for 1 min, with a total run time of 16 min. The column was operated at 35°C with a flow rate of 0.3 ml/min, injecting between 25 or 35 μL samples. Nitrogen was used as the drying and nebulizing gas. The nebulizer gas flow was set to 35 L/h, and the desolvation gas flow to 30 L/h. The interface temperature was set to 350°C and the source temperature to 300°C. The capillary voltage was set to 3.5 kV; the ionization was in positive mode. Low-mass and high-mass resolution was 2 for the first mass analyzer and 2 for the second. Data acquisition was performed with the MS Workstation 8 software and data analysis with the MS Data Review software. The MS/MS MRM transitions are indicated in the **section 4.8 (Table 8)**

#### ***8.4.7.4 UPLC-QTOF-MS/MS Analysis for non-targeted metabolomics***

The peptides obtain after digestion were dried under vacuum and resolubilized in 100 or 50 μl prior to injection between 25 and 15 μl. The procedure used for the analysis of samples was similar to that described for the analysis of phenolic compounds (**section 6.3.3**) with a mass range up to 1500 *m/z*.

#### ***8.4.7.5 GC-EI-MS analysis of S-prenyl-L-cysteine methyl ester***

After on-beads digestion, the supernatant was collected, then GFP-Trap washed twice with 100 μl H<sub>2</sub>O and all fractions were pooled together, the pH was adjusted to 12 with one drop of 1M NaOH. Then hydrophobic peptides/metabolites were extracted three times with 100 μl of CHCl<sub>3</sub> to collect the S-prenyl-L-cysteine methyl ester. Pooled CHCl<sub>3</sub> fractions were concentrated using a vacuum concentrator SPD111V (*Thermo Fisher Scientific*) without heating and then resolubilized to a final volume of 5 μl prior to GC-EI-MS or GC-FID analyses. The GC-EI-MS analysis was performed as reported (Cunha et al., 2011), but without a guard column. Whereas the GC-FID analysis was achieved by P. Adam and P. Schaeffer (Institut de Chimie, Strasbourg).

#### *8.4.7.6 GC-EI-MS analysis of metabolites from the culture medium*

After treatments, the culture medium for each sample was collected and one volume of glacial acetone was added for precipitation during 20 min at RT. The samples were centrifuged at 2500 g, 20 min, 4°C and the supernatant was re-precipitated for 4h at 4°C and then pelleted as afford mentioned. Acetone was evaporated under vacuum and the aqueous residual was extracted twice with EtOAc and then vacuum dried. Dried oil samples were solubilized in hexane prior to GC-EI-MS analysis using an Agilent 6890 gas chromatograph (*Agilent*, Santa Clara USA) equipped with a HP5-MS column (Agilent J & W; 30m long, 0.32mm i.d., 0.25 mm film thickness) coupled to an Agilent 5973N mass spectrometer (Agilent, Santa Clara USA). 2 µl/ sample were injected automatically using an autosampler and injector 7683 series (Agilent, Santa Clara USA) with injector temperature set at 250°C in splitless mode with a ratio of 50. The temperature program starts at 60°C and ends at 300°C at a rate of 10°C per min followed by 5 min fixed at 300°C. Helium was used as the carrier gas with a flow rate of 2 mL/min. The mass spectra were obtained by electronic ionization at 70 eV.

#### *TLC analysis of metabolites from Tobacco leaves*

The treated leaf discs were freeze-dried and extracted three times in 1.5 ml MeOH/CHCl<sub>3</sub> (2:1, v/v) at 25°C, by sonication 30 min at 80 kHz (Fisherbrand™ S-series). The extracts were pooled, vacuum dried and saponified with 2 ml MeOH/KOH 6%, 2h at 75°C. After saponification, deionized water was added and the saponified extracts were re-extracted three times with hexane before being dried under vacuum and stored under argon at -80°C. The samples were resuspended in 50 µl DCM and 15 µl were deposited on a silica gel HPTLC F<sub>254</sub> 20x10 cm plate (*Merck*, Rahway, NJ) using a Linomat 5 system controlled by VisionCATS 2.2.16187.4 software (*CAMAG*, Muttenz Switzerland). The plates were migrated twice in the DCM and observed with the TLC visualizer 2 (*CAMAG*, Muttenz Switzerland) in the visible, at 254 nm, 365 nm and after revelation of the molecules with the vanillin sulfuric acid reagent.

## 8.5 CELL BIOLOGY METHODS

### 8.5.1 Classical Confocal Microscopy

Fluorescent cells were counted at low magnification using a LSM510 confocal laser scanning microscope equipped with x20/0.8 M27 Plan Apochromat Objective and an inverted Zeiss Axio Observer Z1 (*Zeiss*, Oberkochen Germany). At confocal resolution, a minimum of 300 individual cells representative of the various populations were analyzed, and images were acquired using an excitation wavelength 488 nm, collecting fluorescence 500 to 700 nm with a split at 600 nm, short pass filter 555 (Channel GFP 500- 555 nm) and long pass filter 560 (Channel RFP 600-700 nm), a laser power 2-5%, pinhole 20  $\mu\text{m}$  and 42  $\mu\text{m}$ . At high resolution, pictures were taken such that the focal plane included the nucleus and nucleolus. Transmission images were recorded in differential interference contrast mode (DIC). Images acquired under same setup were grouped and used to design figure using Image J 1.53d and FigureJ v1.35 (Wayne Rasband, NIH; <http://rsb.info.nih.gov/ij>). To note MAPs prepared for the GFP-Trap v2 were observed using a Zeiss Imager Z1 inverted fluorescence microscope equipped with a 20x/0.95 KORR Plan Apochromat and an AxioCam MRm (*Zeiss*, Oberkochen Germany). The microscope was piloted using Axiovision40 v4.8.2.0 SP3 software (*Zeiss*, Oberkochen Germany). Transmission images were recorded in differential interference contrast mode (DIC). Images were arranged to design figure as for confocal microscopy

### **8.5.2 Viability of BY-2 treated cells**

Wild type and non-induced BY-2 Dex::CVIL S-GFP cells, prepared as described in the *Plant Material* section, were treated or not treated with VH, NW 184, fraxetine, emodine, quinizarin, lapachol and plumbig at 50 and 100  $\mu\text{M}$  from a freshly prepared 50 mM stock solution in DMSO. The 6 well plates containing the treated BY-2 cells were incubated on a rotary shaker for 18 hours at 140 rpm, 26°C, in the dark. Then fluorescein diacetate (FDA) and propidium iodide (PI) stock solutions at 7.5 mM in acetone were added to a final concentration of 75 and 7.5 nM in 100  $\mu\text{l}$  BY-2 cells spotted onto microscope slide. Then cells were observed by using the spectral imaging method described with the excitation wavelength of 488 nm and the emission wavelengths distributed in 9 nm channels in increments ranging from 498 to 664 nm. Finally, a minimum of 300 cells was counted for each treatment and FDA fluorescence was associated with living cells, while PI fluorescence was associated with dead cells.

### **8.5.3 Localization with Fluorescent Proteins CVIL, ER, Golgi and Nile Red**

The BY-2 35S::ER-sGFP, 35S::Golgi-EGFP or the induced and non-induced Dex::CVIL cell lines grown as described in the *Plant Material* section, were treated with 30  $\mu\text{M}$  VH, 50  $\mu\text{M}$  AVD or VD. The treated BY-2 cells were incubated from 15 min to 18 h on a rotary shaker at 140 rpm, 26°C, in the dark. Then, treated cells were observed using the spectral imaging method as reported and compared to the reference spectra of ER-sGFP, Golgi-EGFP, VH, VD and AVD (**section 6.3.3.6**). The laser power was adjusted between 2 and 13 % depending on the fluorescence intensity. For observation with Nile red, staining was carried out with Nile red (*ThermoFisher*, Waltham USA) stock solution at 94 mM in EtOH diluted to a final concentration of 56  $\mu\text{M}$  in 100  $\mu\text{l}$  of BY-2 cells on a microscope slide 5 min before observation by spectral imaging. In this context, stained cells were observed by using an excitation wavelength of 514 nm and emission wavelengths incremented in 9 nm channels from 535-664 nm.

## 8.5.4 Spectral Imaging Data Analysis

The spectral imaging data were collected with Zen Blue and analyzed using the R software V4.0.0 (GNU GPLv2, R Core Team) with RStudio V 1.2.5001 (AGPLv3, RStudio) and the ChemoSpec package V5.2.12 following the script bellow. The input file consisted in a .csv file with the wavelengths in rows and the average of 10 spectra/cell for 5 cells in three independent replicates for each treatment in columns.

### #Import datamatrix to process spectra

```
matrix2SpectraObject(gr.crit = c("group 1", "group 2", "group 3"),
  gr.cols = c("color 1", "color 2", "color 3"),
  freq.unit = "nm",
  sep = ";",
  int.unit = "intensity",
  descrip = "X",
  in.file = "X",
  out.file = "Y", chk = TRUE)
```

```
Yy <- loadObject("Y")
YyN <- normSpectra(Yy, method = "zero2one", RangeExpress = TRUE)
sumSpectra(YyN)
```

### #Comparison of normalized spectra

```
surveySpectra(YyN, method = c("sem95"),
  by.gr = TRUE)
```

```
sampleDistSpectra(YyN, method = "pearson", plot = TRUE)
```

```
myt <- expression(Title)
plotSpectra(YyN,
  main = myt,
  which = c(1:45),
  yrange = c(0, 1),
  offset = 0,
  amplify = 1,
  showGrid = TRUE,
  lab.pos = 2200,
  leg.loc = "topright")
```

### #PCA Analysis

```
robust <- r_pcaSpectra(YyN, choice = "noscale")
plotScores(YyN, main = myt, robust,
  pcs = c(1,2), ellipse = "rob", tol = "none", leg.loc = list(x = 0.6, y = 1.4))
```

```
class <- c_pcaSpectra(YyN, choice = "noscale")
plotScree(class, main = myt)
```

### 8.5.5 RT-qPCR

100 mg of BY-2 were ground in N<sub>2</sub> before adding 800 µl of tri-reagent (Sigma-Aldrich) and vortexed for 3 min. 200 µl of CHCl<sub>3</sub> were then added before repeating the extraction process for an additional 3 min. Both phases were decanted by centrifugation at 16 100 g, 15 min, 4°C. About 300 µl of the aqueous phase containing RNA was recovered, then precipitated by adding 1 ml of cold isopropanol and stored at -80°C for 20 min. Thereafter, the RNA was pelleted for 15 min at 16 100 g and the supernatant removed. Two washes were performed with 500 µl of glacial EtOH 80% followed by fast centrifugation at 16 100 g, 1 min in between each wash. Finally, pellets were dried to remove traces of EtOH and resolubilized in 40 µl of RNase-free water prior to quantification using Nanodrop (Thermo fisher).

2 µg of RNA were collected to for DNA removal by using DNase I (Thermofisher) following the manufacturer's protocol. After 30 min at 37°C, 100 µl of RNA solution was reprecipitated by adding 250 µl EtOH, and subsequently washed two times as afford mentioned. The reverse transcription (RT) was achieved with an equivalent of 200 ng RNA by using Superscript IV (Thermofisher) and following the manufacturer procedure. RT-qPCR was carried as reported (Hazman et al., 2019), measuring the gene expression of GFP (F 5'- CTGAAGGGCATCGACTTCAA-3', R 5'- CGGCATGATATAGACGTT-3'); L25 (F 5'-CCCCTCACCACAGAGTCT-3', R 5'-AAGGGTGTGTTGTCCTCAAT-3'); Ntubc2 (F 5'- CTGGACAGCAGACTGACA-3', R 5'-, F 5'-CAGGATAATTTGCTGTAACAGATT-3'); EF1-α (F 5'-TGAGCACGCTCTTCTTGCTTCA-3', R 5'-GGTGGTGGCATCCATCTTGTTCA-3').





## 9 REFERENCES



- Agrawal AA, Petschenka G, Bingham RA, Weber MG, Rasmann S** (2012) Toxic cardenolides: chemical ecology and coevolution of specialized plant-herbivore interactions: Tansley review. *New Phytol* **194**: 28–45
- Aguilar BJ, Nkembo AT, Duverna R, Poku RA, Amisah F, Ablordeppey SY, Lamango NS** (2014) Polyisoprenylated methylated protein methyl esterase: A putative biomarker and therapeutic target for pancreatic cancer. *Eur J Med Chem* **81**: 323–333
- Ahn CS, Lee JH, Reum Hwang A, Kim WT, Pai H-S** (2006) Prohibitin is involved in mitochondrial biogenesis in plants. *Plant J* **46**: 658–667
- Aicart-Ramos C, Valero RA, Rodriguez-Crespo I** (2011) Protein palmitoylation and subcellular trafficking. *Biochim Biophys Acta BBA - Biomembr* **1808**: 2981–2994
- Akula MK, Ibrahim MX, Ivarsson EG, Khan OM, Kumar IT, Erlandsson M, Karlsson C, Xu X, Brisslert M, Brakebusch C, et al** (2019) Protein prenylation restrains innate immunity by inhibiting Rac1 effector interactions. *Nat Commun* **10**: 3975
- Al-Babili S, Bouwmeester HJ** (2015) Strigolactones, a novel carotenoid-derived plant hormone. *Annu Rev Plant Biol* **66**: 161–186
- Alberts AW, Chen J, Kuron G, Hunt V, Huff J, Hoffman C, Rothrock J, Lopez M, Joshua H, Harris E, et al** (1980) Mevinolin: a highly potent competitive inhibitor of hydroxymethylglutaryl-coenzyme A reductase and a cholesterol-lowering agent. *Proc Natl Acad Sci* **77**: 3957–3961
- Altland JE, Wehtje G, Gilliam CH, Miller ME** (2007) Liverwort (*Marchantia Polymorpha*) Control with Quinoclamine. *Weed Technol* **21**: 483–488
- Andow D** (1983) The extent of monoculture and its effects on insect pest populations with particular reference to wheat and cotton. *Agric Ecosyst Environ* **9**: 25–35
- Andrabi SBA, Tahara M, Matsubara R, Toyama T, Aonuma H, Sakakibara H, Suematsu M, Tanabe K, Nozaki T, Nagamune K** (2018) Plant hormone cytokinins control cell cycle progression and plastid replication in apicomplexan parasites. *Parasitol Int* **67**: 47–58
- Andres DA, Crick DC, Finlin BS, Waechter CJ** (2002) The Metabolic Labeling and Analysis of Isoprenylated Proteins. *Protein Protoc. Handb. Humana Press, New Jersey*, pp 657–672
- Andrews M, Huizinga DH, Crowell DN** (2010) The CaaX specificities of Arabidopsis protein prenyltransferases explain era1 and ggb phenotypes. *BMC Plant Biol* **10**: 118
- Armstrong CM, Meyers DJ, Imlay LS, Freel Meyers C, Odom AR** (2015) Resistance to the Antimicrobial Agent Fosmidomycin and an FR900098 Prodrug through Mutations in the Deoxyxylulose Phosphate Reductoisomerase Gene (*dxr*). *Antimicrob Agents Chemother* **59**: 5511–5519
- Arnao MB, Hernández-Ruiz J** (2014) Melatonin: plant growth regulator and/or biostimulator during stress? *Trends Plant Sci* **19**: 789–797
- Artz JD, Wernimont AK, Dunford JE, Schapira M, Dong A, Zhao Y, Lew J, Russell RGG, Ebetino FH, Oppermann U, et al** (2011) Molecular Characterization of a Novel Geranylgeranyl Pyrophosphate Synthase from *Plasmodium* Parasites. *J Biol Chem* **286**: 3315–3322
- Ayong L, DaSilva T, Mauser J, Allen CM, Chakrabarti D** (2011) Evidence for prenylation-dependent targeting of a Ykt6 SNARE in *Plasmodium falciparum*. *Mol Biochem Parasitol* **175**: 162–168
- Bader TK, Rappe TM, Veglia G, Distefano MD** (2019) Synthesis and NMR Characterization of the Prenylated Peptide, a-Factor. *Methods Enzymol. Elsevier*, pp 207–238
- Baehr W** (2014) Membrane Protein Transport in Photoreceptors: The Function of PDE. *Invest Ophthalmol Vis Sci* **55**: 8653–8666
- Bajczyk M, Lange H, Bielewicz D, Szewc L, Bhat SS, Dolata J, Kuhn L, Szweykowska-Kulinska Z, Gagliardi D, Jarmolowski A** (2020) SERRATE interacts with the nuclear exosome targeting (NEXT) complex to degrade primary miRNA precursors in Arabidopsis. *Nucleic Acids Res* **48**: 6839–6854
- Bajguz A, Chmur M, Gruszka D** (2020) Comprehensive Overview of the Brassinosteroid Biosynthesis Pathways: Substrates, Products, Inhibitors, and Connections. *Front Plant Sci* **11**: 1034

- Banerjee A, Sharkey TD** (2014) Methylerythritol 4-phosphate (MEP) pathway metabolic regulation. *Nat Prod Rep* **31**: 1043–1055
- Bansal A, Singh M, Rai B** (2016) Human papillomavirus-associated cancers: A growing global problem. *Int J Appl Basic Med Res* **6**: 84
- Belgers M, Leenaars M, Homberg JR, Ritskes-Hoitinga M, Schellekens AFA, Hooijmans CR** (2016) Ibogaine and addiction in the animal model, a systematic review and meta-analysis. *Transl Psychiatry* **6**: e826–e826
- Benetka W, Koranda M, Maurer-Stroh S, Pittner F, Eisenhaber F** (2006) Farnesylation or geranylgeranylation? Efficient assays for testing protein prenylation in vitro and in vivo. *BMC Biochem* **7**: 6
- Berg RH** (2004) Evaluation of spectral imaging for plant cell analysis. *J Microsc* **214**: 174–181
- Berger BM, Kim JH, Hildebrandt ER, Davis IC, Morgan MC, Hougland JL, Schmidt WK** (2018) Protein Isoprenylation in Yeast Targets COOH-Terminal Sequences Not Adhering to the CaaX Consensus. *Genetics* **210**: 1301–1316
- Berndt N, Hamilton AD, Sebti SM, Sebti SM** (2014) Targeting protein prenylation for cancer therapy. 39
- Bhatnagar RS, Gordon JI** (1997) Understanding covalent modifications of proteins by lipids: where cell biology and biophysics mingle. *Trends Cell Biol* **7**: 14–20
- Biniossek ML, Schilling O** (2012) Enhanced identification of peptides lacking basic residues by LC-ESI-MS/MS analysis of singly charged peptides. *PROTEOMICS* **12**: 1303–1309
- Binzel ML, Hess FD, Bressan RA, Hasegawa PM** (1988) Intracellular Compartmentation of Ions in Salt Adapted Tobacco Cells. *Plant Physiol* **86**: 607–614
- Blanden MJ** (2018) Redefining The Scope Of Prenylation: Discovery Of “Forbidden” Substrate Recognition And Development Of Methods Utilizing Prenylated Proteins. Chemistry. Syracuse University
- Blasco B, Leroy D, Fidock DA** (2017) Antimalarial drug resistance: linking Plasmodium falciparum parasite biology to the clinic. *Nat Med* **23**: 917–928
- Bloch K, Chaykin S, Phillips AH, De Waard A** (1959) Mevalonic acid pyrophosphate and isopentenylpyrophosphate. *J Biol Chem* **234**: 2595–2604
- Bontinck M, Van Leene J, Gadeyne A, De Rybel B, Eeckhout D, Nelissen H, De Jaeger G** (2018) Recent Trends in Plant Protein Complex Analysis in a Developmental Context. *Front Plant Sci* **9**: 640
- Booden MA, Baker TL, Solski PA, Der CJ, Punke SG, Buss JE** (1999) A Non-farnesylated Ha-Ras Protein Can Be Palmitoylated and Trigger Potent Differentiation and Transformation. *J Biol Chem* **274**: 1423–1431
- Borrmann S, Lundgren I, Oyakhrome S, Impouma B, Matsiegui P-B, Adegnika AA, Issifou S, Kun JFJ, Hutchinson D, Wiesner J, et al** (2006) Fosmidomycin plus Clindamycin for Treatment of Pediatric Patients Aged 1 to 14 Years with Plasmodium falciparum Malaria. *Antimicrob Agents Chemother* **50**: 2713–2718
- Botta B, Delle Monache G, Delle Monache F, Bettolo GBM, Menichini F** (1986) Vismione H and prenylated xanthenes from vismia guineensis. *Phytochemistry* **25**: 1217–1219
- Boucher MJ, Yeh E** (2019) Plastid–endomembrane connections in apicomplexan parasites. *PLOS Pathog* **15**: e1007661
- Bracha-Drori K, Shichrur K, Katz A, Oliva M, Angelovici R, Yalovsky S, Ohad N** (2004) Detection of protein–protein interactions in plants using bimolecular fluorescence complementation. *Plant J* **40**: 419–427
- Bracha-Drori K, Shichrur K, Lubetzky TC, Yalovsky S** (2008) Functional Analysis of Arabidopsis Postprenylation CaaX Processing Enzymes and Their Function in Subcellular Protein Targeting. *Plant Physiol* **148**: 119–131
- Brady SM, Sarkar SF, Bonetta D, McCourt P** (2003) The *ABSCISIC ACID INSENSITIVE 3* (*ABI3*) gene is modulated by farnesylation and is involved in auxin signaling and lateral root development in *Arabidopsis*. *Plant J* **34**: 67–75
- Breitling R, Krisans SK** (2002) A second gene for peroxisomal HMG-CoA reductase? A genomic reassessment. *J Lipid Res* **43**: 2031–2036
- Brioschi M, Martinez Fernandez A, Banfi C** (2017) Exploring the biochemistry of the prenylome and its role in disease through proteomics: progress and potential. *Expert Rev Proteomics* **14**: 515–528
- Brown DA, London E** (2000) Structure and Function of Sphingolipid- and Cholesterol-rich Membrane Rafts. *J Biol*

Chem **275**: 17221–17224

**Bryon A, Kurlovs AH, Dermauw W, Greenhalgh R, Riga M, Grbić M, Tirry L, Osakabe M, Vontas J, Clark RM, et al** (2017) Disruption of a horizontally transferred phytoene desaturase abolishes carotenoid accumulation and diapause in *Tetranychus urticae*. *Proc Natl Acad Sci* **114**: E5871–E5880

**Buckley TN** (2019) How do stomata respond to water status? *New Phytol* **224**: 21–36

**Buddelmeijer N** (2012) N-Acylation of Lipoproteins: Not When Sour. *J Bacteriol* **194**: 3297–3298

**Butelman ER, Kreek MJ** (2015) Salvinorin A, a kappa-opioid receptor agonist hallucinogen: pharmacology and potential template for novel pharmacotherapeutic agents in neuropsychiatric disorders. *Front Pharmacol*. doi: 10.3389/fphar.2015.00190

**Caldelari D, Sternberg H, Rodríguez-Concepción M, Gruissem W, Yalovsky S** (2001) Efficient Prenylation by a Plant Geranylgeranyltransferase-I Requires a Functional CaaL Box Motif and a Proximal Polybasic Domain. *Plant Physiol* **126**: 1416–1429

**Camara B, Huguency P, d'Harlingue A, Quennemet J, Schantz R, Weil JH, Kuntz M** (1992) Carotenoid Biosynthesis and Regulation in Plants. In RJ Petroski, SP McCormick, eds, *Second.-Metab. Biosynth.* Metab. Springer US, Boston, MA, pp 337–347

**Camazine SM, Resch JF, Eisner T, Meinwald J** (1983) Mushroom chemical defense: Pungent sesquiterpenoid dialdehyde antifeedant to opossum. *J Chem Ecol* **9**: 1439–1447

**Cameron D, Edmonds J, Raverty W** (1976) Oxidation of emodin anthrone and stereochemistry of emodin bianthrone. *Aust J Chem* **29**: 1535

**Carden DE, Walker DJ, Flowers TJ, Miller AJ** (2003) Single-Cell Measurements of the Contributions of Cytosolic Na<sup>+</sup> and K<sup>+</sup> to Salt Tolerance. *Plant Physiol* **131**: 676–683

**Carretero-Paulet L, Ahumada I, Cunillera N, Rodríguez-Concepción M, Ferrer A, Boronat A, Campos N** (2002) Expression and Molecular Analysis of the Arabidopsis *DXR* Gene Encoding 1-Deoxy-d-Xylulose 5-Phosphate Reductoisomerase, the First Committed Enzyme of the 2- C -Methyl-d-Erythritol 4-Phosphate Pathway. *Plant Physiol* **129**: 1581–1591

**Casey PJ** (1992) Biochemistry of protein prenylation. *J Lipid Res* **33**: 1731–1740

**Casey PJ, Solski PA, Der CJ, Buss JE** (1989) p21ras is modified by a farnesyl isoprenoid. *Proc Natl Acad Sci* **86**: 8323–8327

**Casey PJ, Thissen JA, Moomaw JF** (1991) Enzymatic modification of proteins with a geranylgeranyl isoprenoid. *Proc Natl Acad Sci* **88**: 8631–8635

**Castaño-Cerezo S, Kulyk-Barbier H, Millard P, Portais J-C, Heux S, Truan G, Bellvert F** (2019) Functional analysis of isoprenoid precursors biosynthesis by quantitative metabolomics and isotopologue profiling. *Metabolomics* **15**: 115

**Castro RC de A, Fonseca BG, dos Santos HTL, Ferreira IS, Mussatto SI, Roberto IC** (2017) Alkaline deacetylation as a strategy to improve sugars recovery and ethanol production from rice straw hemicellulose and cellulose. *Ind Crops Prod* **106**: 65–73

**Chaimovitsh D, Shachter A, Abu-Abied M, Rubin B, Sadot E, Dudai N** (2017) Herbicidal Activity of Monoterpenes Is Associated with Disruption of Microtubule Functionality and Membrane Integrity. *Weed Sci* **65**: 19–30

**Chakrabarti\* D, Azam T, DelVecchio C, Qiu L, Park Y, Allen CM** (1998) Protein prenyl transferase activities of *Plasmodium falciparum*. *Mol Biochem Parasitol* **94**: 175–184

**Chakrabarti D, Da Silva T, Barger J, Paquette S, Patel H, Patterson S, Allen CM** (2002) Protein Farnesyltransferase and Protein Prenylation in *Plasmodium falciparum*. *J Biol Chem* **277**: 42066–42073

**Chappell J, Nable R** (1987) Induction of Sesquiterpenoid Biosynthesis in Tobacco Cell Suspension Cultures by Fungal Elicitor. *Plant Physiol* **85**: 469–473

**Charron G, Li MMH, MacDonald MR, Hang HC** (2013) Prenylome profiling reveals S-farnesylation is crucial for membrane targeting and antiviral activity of ZAP long-isoform. *Proc Natl Acad Sci* **110**: 11085–11090

**Chen D, Lv B, Kobayashi S, Xiong Y, Sun P, Lin Y, Genovese S, Epifano F, Hou S, Tang F, et al** (2016) Madagascine

Induces Vasodilatation via Activation of AMPK. *Front Pharmacol*. doi: 10.3389/fphar.2016.00435

**Chen J-C, Jiang C-Z, Reid MS** (2005) Silencing a prohibitin alters plant development and senescence: Prohibitins in development and senescence. *Plant J* **44**: 16–24

**Chen WJ, Andres DA, Goldstein JL, Brown MS** (1991) Cloning and expression of a cDNA encoding the alpha subunit of rat p21ras protein farnesyltransferase. *Proc Natl Acad Sci* **88**: 11368–11372

**Cheng W-Y, Lien J-C, Hsiang C-Y, Wu S-L, Li C-C, Lo H-Y, Chen J-C, Chiang S-Y, Liang J-A, Ho T-Y** (2009) Comprehensive evaluation of a novel nuclear factor- $\kappa$ B inhibitor, quinoxaline, by transcriptomic analysis. *Br J Pharmacol* **157**: 746–756

**Chenge-Espinosa M, Cordoba E, Romero-Guido C, Toledo-Ortiz G, León P** (2018) Shedding light on the methylerythritol phosphate (MEP)-pathway: long hypocotyl 5 (HY5)/phytochrome-interacting factors (PIFs) transcription factors modulating key limiting steps. *Plant J* **96**: 828–841

**Chiang Y-M, Szewczyk E, Davidson AD, Entwistle R, Keller NP, Wang CCC, Oakley BR** (2010) Characterization of the *Aspergillus nidulans* Monodictyphenone Gene Cluster. *Appl Environ Microbiol* **76**: 2067–2074

**Chinnusamy V, Jagendorf A, Zhu J-K** (2005) Understanding and Improving Salt Tolerance in Plants. *Crop Sci* **45**: 437–448

**Chinou I** (2005) Labdanes of Natural Origin-Biological Activities (1981-2004). *Curr Med Chem* **12**: 1295–1317

**Chiva C, Ortega M, Sabidó E** (2014) Influence of the Digestion Technique, Protease, and Missed Cleavage Peptides in Protein Quantitation. *J Proteome Res* **13**: 3979–3986

**Chowdhury I, Thompson WE, Thomas K** (2014) Prohibitins Role in Cellular Survival Through Ras-Raf-MEK-ERK Pathway: PROHIBITINS ROLE IN CELLULAR SURVIVAL. *J Cell Physiol* **229**: 998–1004

**Choy E, Chiu VK, Silletti J, Feoktistov M, Morimoto T, Michaelson D, Ivanov IE, Philips MR** (1999) Endomembrane Trafficking of Ras. *Cell* **98**: 69–80

**Christensen DG, Xie X, Basisty N, Byrnes J, McSweeney S, Schilling B, Wolfe AJ** (2019) Post-translational Protein Acetylation: An Elegant Mechanism for Bacteria to Dynamically Regulate Metabolic Functions. *Front Microbiol* **10**: 1604

**Christianson DW** (2017) Structural and Chemical Biology of Terpenoid Cyclases. *Chem Rev* **117**: 11570–11648

**Chung JA, Wollack JW, Hovlid ML, Okesli A, Chen Y, Mueller JD, Distefano MD, Taton TA** (2009) Purification of prenylated proteins by affinity chromatography on cyclodextrin-modified agarose. *Anal Biochem* **386**: 1–8

**Clapp KM, Ellsworth ML, Sprague RS, Stephenson AH** (2013) Simvastatin and GGTI-2133, a geranylgeranyl transferase inhibitor, increase erythrocyte deformability but reduce low O<sub>2</sub> tension-induced ATP release. *Am J Physiol-Heart Circ Physiol* **304**: H660–H666

**Clastre M, Goubard A, Prel A, Mincheva Z, Viaud-Massuart M-C, Bout D, Rideau M, Velge-Roussel F, Laurent F** (2007) The methylerythritol phosphate pathway for isoprenoid biosynthesis in coccidia: Presence and sensitivity to fosmidomycin. *Exp Parasitol* **116**: 375–384

**Colicelli J** (2004) Human RAS Superfamily Proteins and Related GTPases. *Sci Signal* **2004**: re13–re13

**Conéjéro G, Noirot M, Talamond P, Verdeil J-L** (2014) Spectral analysis combined with advanced linear unmixing allows for histolocalization of phenolics in leaves of coffee trees. *Front Plant Sci*. doi: 10.3389/fpls.2014.00039

**Cooper GM** (2019) *The cell: a molecular approach*, Eighth edition. Sinauer Associates, an imprint of Oxford University Press, Oxford ; New York

**Cordoba E, Porta H, Arroyo A, San Roman C, Medina L, Rodriguez-Concepcion M, Leon P** (2011) Functional characterization of the three genes encoding 1-deoxy-D-xylulose 5-phosphate synthase in maize. *J Exp Bot* **62**: 2023–2038

**Courdavault V, Burlat V, St-Pierre B, Giglioli-Guivarc'h N** (2009) Proteins prenylated by type I protein geranylgeranyltransferase act positively on the jasmonate signalling pathway triggering the biosynthesis of monoterpene indole alkaloids in *Catharanthus roseus*. *Plant Cell Rep* **28**: 83–93

- Courdavault V, Thiersault M, Courtois M, Gantet P, Oudin A, Doireau P, St-Pierre B, Giglioli-Guivarc'h N** (2005) CaaX-prenyltransferases are essential for expression of genes involved in the early stages of monoterpene biosynthetic pathway in *Catharanthus roseus* cells. *Plant Mol Biol* **57**: 855–870
- Coxon FP, Helfrich MH, Van't Hof R, Sebti S, Ralston SH, Hamilton A, Rogers MJ** (2000) Protein geranylgeranylation is required for osteoclast formation, function, and survival: inhibition by bisphosphonates and GGTI-298. *J Bone Miner Res Off J Am Soc Bone Miner Res* **15**: 1467–1476
- Croizy J-F** (1987) Oligomérisation linéaire régio et énantiosélective de diènes fonctionnalisés ou non sur catalyseurs au Nickel modifiés par des ligands aminophosphinites chiraux. Université de Lille
- Crowell DN** (2000) Functional implications of protein isoprenylation in plants. *Prog Lipid Res* **39**: 393–408
- da Cunha AR, Duarte EL, Lamy MT, Coutinho K** (2014) Protonation/deprotonation process of Emodin in aqueous solution and pKa determination: UV/Visible spectrophotometric titration and quantum/molecular mechanics calculations. *Chem Phys* **440**: 69–79
- Cunha SC, Faria MA, Fernandes JO** (2011) Gas Chromatography–Mass Spectrometry Assessment of Amines in Port Wine and Grape Juice after Fast Chloroformate Extraction/Derivatization. *J Agric Food Chem* **59**: 8742–8753
- Cutler S, Ghassemian M, Bonetta D, Cooney S, McCourt P** (1996) A Protein Farnesyl Transferase Involved in Abscisic Acid Signal Transduction in *Arabidopsis*. *Science* **273**: 1239–1241
- D'Addabbo T, Argentieri MP, Źuchowski J, Biazzi E, Tava A, Oleszek W, Avato P** (2020) Activity of Saponins from Medicago Species against Phytoparasitic Nematodes. *Plants* **9**: 443
- Dai X, Sun Y, Zhang T, Ming Y, Hongwei G** (2020) An overview on natural farnesyltransferase inhibitors for efficient cancer therapy. *J Enzyme Inhib Med Chem* **35**: 1027–1044
- Dai Y, Seeger M, Weng J, Song S, Wang W, Tan Y-W** (2016) Lipid Regulated Intramolecular Conformational Dynamics of SNARE-Protein Ykt6. *Sci Rep* **6**: 30282
- Dau T, Bartolomucci G, Rappsilber J** (2020) Proteomics Using Protease Alternatives to Trypsin Benefits from Sequential Digestion with Trypsin. doi: 10.1101/2020.01.30.927046
- Davies R, Graham DE, Vincent B** (1987) Water-cyclohexane-“Span 80”-“Tween 80” systems: Solution properties and water/oil emulsion formation. *J Colloid Interface Sci* **116**: 88–99
- Debierre-Grockiego F, Schwarz RT** (2010) Immunological reactions in response to apicomplexan glycosylphosphatidylinositols. *Glycobiology* **20**: 801–811
- Deracinois B, Flahaut C, Duban-Deweere S, Karamanos Y** (2013) Comparative and Quantitative Global Proteomics Approaches: An Overview. *Proteomes* **1**: 180–218
- Ding B-Y, Niu J, Shang F, Yang L, Chang T-Y, Wang J-J** (2019) Characterization of the Geranylgeranyl Diphosphate Synthase Gene in *Acyrtosiphon pisum* (Hemiptera: Aphididae) and Its Association With Carotenoid Biosynthesis. *Front Physiol* **10**: 1398
- Disch A, Schwender J, Müller C, Lichtenthaler HK, Rohmer M** (1998) Distribution of the mevalonate and glyceraldehyde phosphate/pyruvate pathways for isoprenoid biosynthesis in unicellular algae and the cyanobacterium *Synechocystis* PCC 6714. *Biochem J* **333**: 381–388
- Ditengou FA, Müller A, Rosenkranz M, Felten J, Lasok H, van Doorn MM, Legué V, Palme K, Schnitzler J-P, Polle A** (2015) Volatile signalling by sesquiterpenes from ectomycorrhizal fungi reprogrammes root architecture. *Nat Commun* **6**: 6279
- Dong X, Fu J, Yin X, Cao S, Li X, Lin L, Huyiligeqi, Ni J** (2016) Emodin: A Review of its Pharmacology, Toxicity and Pharmacokinetics. *Phytother Res* **30**: 1207–1218
- Dorey S, Baillieul F, Pierrel M-A, Saindrenan P, Fritig B, Kauffmann S** (1997) Spatial and Temporal Induction of Cell Death, Defense Genes, and Accumulation of Salicylic Acid in Tobacco Leaves Reacting Hypersensitively to a Fungal Glycoprotein Elicitor. *Mol Plant-Microbe Interactions* **10**: 646–655
- Dowil RT, Lu X, Saracco SA, Vierstra RD, Downes BP** (2011) *Arabidopsis* Membrane-anchored Ubiquitin-fold (MUB) Proteins Localize a Specific Subset of Ubiquitin-conjugating (E2) Enzymes to the Plasma Membrane. *J Biol Chem* **286**: 14913–14921



- Downes BP, Saracco SA, Lee SS, Crowell DN, Vierstra RD** (2006) MUBs, a Family of Ubiquitin-fold Proteins That Are Plasma Membrane-anchored by Prenylation. *J Biol Chem* **281**: 27145–27157
- Drummond CA, Molina MT, Taliansky S, Breidenbach CR, Fioravanti CF** (2014) Effects of Quinizarin and Five Synthesized Derivatives on Fifth Larval Instar Midgut Ecdysone 20-Monooxygenase Activity of the Tobacco Hornworm *Manduca sexta*. *Int J Zool* **2014**: 1–8
- Dudev T, Lim C** (2004) Monodentate versus Bidentate Carboxylate Binding in Magnesium and Calcium Proteins: What Are the Basic Principles? *J Phys Chem B* **108**: 4546–4557
- Dunford JE, Rogers MJ, Ebetino FH, Phipps RJ, Coxon FP** (2006) Inhibition of Protein Prenylation by Bisphosphonates Causes Sustained Activation of Rac, Cdc42, and Rho GTPases. *J Bone Miner Res* **21**: 684–694
- Durrant JD, Cao R, Gorfe AA, Zhu W, Li J, Sankovsky A, Oldfield E, McCammon JA** (2011) Non-Bisphosphonate Inhibitors of Isoprenoid Biosynthesis Identified via Computer-Aided Drug Design: Inhibitors of Isoprenoid Biosynthesis. *Chem Biol Drug Des* **78**: 323–332
- Dutilleul C, Ribeiro I, Blanc N, Nezames CD, Deng XW, Zglobicki P, Palacio Barrera AM, Atehortúa L, Courtois M, Labas V, et al** (2016) ASG2 is a farnesylated DWD protein that acts as ABA negative regulator in *Arabidopsis*: A farnesylated DWD protein linked to ABA responses. *Plant Cell Environ* **39**: 185–198
- Duval R, Duplais C** (2017) Fluorescent natural products as probes and tracers in biology. *Nat Prod Rep* **34**: 161–193
- Duval Saint M, Kyle DE** (2018) Phytohormones, Isoprenoids, and Role of the Apicoplast in Recovery from Dihydroartemisinin-Induced Dormancy of *Plasmodium falciparum*. *Antimicrob Agents Chemother* **62**: e01771-17, /aac/62/3/e01771-17.atom
- Dykema PE, Sipes PR, Marie A, Biermann BJ, Crowell DN, Randall SK** (1999) A new class of proteins capable of binding transition metals. *Plant Mol Biol* **41**: 139–150
- Eastman RT, White J, Hucke O, Bauer K, Yokoyama K, Nallan L, Chakrabarti D, Verlinde CLMJ, Gelb MH, Rathod PK, et al** (2005) Resistance to a Protein Farnesyltransferase Inhibitor in *Plasmodium falciparum*. *J Biol Chem* **280**: 13554–13559
- Eckstein A, Zięba P, Gabryś H** (2012) Sugar and Light Effects on the Condition of the Photosynthetic Apparatus of *Arabidopsis thaliana* Cultured in vitro. *J Plant Growth Regul* **31**: 90–101
- Elkazaz S, Jones PB** (2010) Photochemical Hydroxylation of 1-Methyl-9,10-anthraquinones: Synthesis of 9'-Hydroxyaloesaponarin II. *J Org Chem* **75**: 412–416
- Emmanouilidis L, Schütz U, Tripsianes K, Madl T, Radke J, Rucktäschel R, Wilmanns M, Schliebs W, Erdmann R, Sattler M** (2017) Allosteric modulation of peroxisomal membrane protein recognition by farnesylation of the peroxisomal import receptor PEX19. *Nat Commun* **8**: 14635
- Endo A, Kuroda M, Tanzawa K** (1976) Competitive inhibition of 3-hydroxy-3-methylglutaryl coenzyme a reductase by ML-236A and ML-236B fungal metabolites, having hypocholesterolemic activity. *FEBS Lett* **72**: 323–326
- Endo M, Druso JE, Cerione RA** (2020) The two splice variant forms of Cdc42 exert distinct and essential functions in neurogenesis. *J Biol Chem* **295**: 4498–4512
- Engeloch C, Schopfer U, Muckenschnabel I, Le Goff F, Mees H, Boesch K, Popov M** (2008) Stability of Screening Compounds in Wet DMSO. *J Biomol Screen* **13**: 999–1006
- Epand RM** (2008) Proteins and cholesterol-rich domains. *Biochim Biophys Acta BBA - Biomembr* **1778**: 1576–1582
- Epifano F, Genovese S, Fiorito S, Mathieu V, Kiss R** (2014) Lapachol and its congeners as anticancer agents: a review. *Phytochem Rev* **13**: 37–49
- Epstein WW, Lever D, Leining LM, Bruenger E, Rilling HC** (1991) Quantitation of prenylcysteines by a selective cleavage reaction. *Proc Natl Acad Sci* **88**: 9668–9670
- Epstein WW, Sweat FW** (1967) Dimethyl Sulfoxide Oxidations. *Chem Rev* **67**: 247–260
- Estévez JM, Cantero A, Reindl A, Reichler S, León P** (2001) 1-Deoxy-d-xylulose-5-phosphate Synthase, a Limiting Enzyme for Plastidic Isoprenoid Biosynthesis in Plants. *J Biol Chem* **276**: 22901–22909

- Fain VYa, Zaitsev BE, Ryabov MA** (2006) Tautomerism of anthraquinones: V. 1,5-Dihydroxy-9,10-anthraquinone and its substituted derivatives. *Russ J Org Chem* **42**: 1662–1667
- Farnsworth C, Casey P, Howald W, Glomset J, Gelb M** (1990a) Structural characterization of prenyl groups attached to proteins. *Methods* **1**: 231–240
- Farnsworth C, Gelb M, Glomset J** (1990b) Identification of geranylgeranyl-modified proteins in HeLa cells. *Science* **247**: 320–322
- Farnsworth CC, Wolda SL, GelbSa MH** (1989) Human Lamin B Contains a Farnesylated Cysteine Residue. **264**: 8
- Ferguson JJ, Durr IF, Rudney H** (1959) THE BIOSYNTHESIS OF MEVALONIC ACID. *Proc Natl Acad Sci U S A* **45**: 499–504
- Ferguson JJ, Rudney H** (1959) The biosynthesis of beta-hydroxy-beta-methylglutaryl coenzyme A in yeast. I. Identification and purification of the hydroxymethylglutaryl coenzymecondensing enzyme. *J Biol Chem* **234**: 1072–1075
- Fernandes CSM, Pina AS, Dias AMGC, Branco RJF, Roque ACA** (2014) A theoretical and experimental approach toward the development of affinity adsorbents for GFP and GFP-fusion proteins purification. *J Biotechnol* **186**: 13–20
- Fernando VCD, Schroeder DF** (2016) Role of ABA in Arabidopsis Salt, Drought, and Desiccation Tolerance. *Abiotic Biot Stress Plants - Recent Adv Future Perspect*. doi: 10.5772/61957
- Finkelstein R** (2013) Abscisic Acid Synthesis and Response. *Arab Book* **11**: e0166
- Flesch G, Rohmer M** (1988) Prokaryotic hopanoids: the biosynthesis of the bacteriohopane skeleton. Formation of isoprenic units from two distinct acetate pools and a novel type of carbon/carbon linkage between a triterpene and d-ribose. *Eur J Biochem* **175**: 405–411
- Fonrodona G, Ràfols C, Bosch E, Rosés M** (1996) Autoprotolysis in aqueous organic solvent mixtures. Water/alcohol binary systems. *Anal Chim Acta* **335**: 291–302
- Francis F, Vandermoten S, Verheggen F, Lognay G, Haubruge E** (2005) Is the (E)- $\beta$ -farnesene only volatile terpenoid in aphids?: (E)- $\beta$ -farnesene: the only volatile terpenoid in aphids. *J Appl Entomol* **129**: 6–11
- François G, Steenackers T, Assi LA, Steglich W, Lamottke K, Holenz J, Bringmann G** (1999) Vismione H and structurally related anthranoid compounds of natural and synthetic origin as promising drugs against the human malaria parasite *Plasmodium falciparum* : structure-activity relationships. *Parasitol Res* **85**: 582–588
- Frank A, Groll M** (2017) The Methylerythritol Phosphate Pathway to Isoprenoids. *Chem Rev* **117**: 5675–5703
- Friedman L, Miller JG** (1971) Odor Incongruity and Chirality. *Science* **172**: 1044–1046
- Friedman M, Jürgens HS** (2000) Effect of pH on the Stability of Plant Phenolic Compounds. *J Agric Food Chem* **48**: 2101–2110
- Fujii T, Mishima S, Tanaka N, Kawauchi O, Kodaira K, Nishikiori H, Kawai Y** (1997) Absorption and fluorescence spectra of 9-anthrol and its chemical species in solution. *Res Chem Intermed* **23**: 829–839
- FujiyamaSB A, Tamanoil F, Sakiyamall F** (1991) S-Farnesylation and MethylEsterification of C-terminal Domain of Yeast RASB Protein Prior to Fatty Acid Acylation. *JBC* **266**: 6
- Furumoto T, Jindai A** (2008) Isolation and Photoisomerization of a New Anthraquinone from Hairy Root Cultures of *Sesamum indicum*. *Biosci Biotechnol Biochem* **72**: 2788–2790
- G. Ricci C, Liu Y-L, Zhang Y, Wang Y, Zhu W, Oldfield E, McCammon JA** (2016) Dynamic Structure and Inhibition of a Malaria Drug Target: Geranylgeranyl Diphosphate Synthase. *Biochemistry* **55**: 5180–5190
- Gabriel HB, Azevedo MF, Kimura EA, Katzin AM** (2018) *Plasmodium falciparum* parasites overexpressing farnesyl diphosphate synthase/geranylgeranyl diphosphate synthase are more resistant to risedronate. *Mem Inst Oswaldo Cruz*. doi: 10.1590/0074-02760180174
- Galichet A, Hoyerová K, Kamínek M, Gruissem W** (2008) Farnesylation Directs AtIPT3 Subcellular Localization and Modulates Cytokinin Biosynthesis in Arabidopsis. *Plant Physiol* **146**: 1155–1164
- Galle J-B** (2015) Pharmacochimie d'anthranoïdes issus du genre *Psorospermum* (Hypericaceae): isolement,

activités antiparasitaires et synthèse d'analogues structuraux Jean-Baptiste Galle. Université de Strasbourg, Strasbourg

**Gans P** (2000) GLEE, a new computer program for glass electrode calibration. *Talanta* **51**: 33–37

**Garza RM, Tran PN, Hampton RY** (2009) Geranylgeranyl Pyrophosphate Is a Potent Regulator of HRD-dependent 3-Hydroxy-3-methylglutaryl-CoA Reductase Degradation in Yeast. *J Biol Chem* **284**: 35368–35380

**Gelb MH** (1997) Protein Prenylation, et cetera--Signal Transduction in Two Dimensions. *Science* **275**: 1750–0

**Gelb MH, Brunsveld L, Hrycyna CA, Michaelis S, Tamanoi F, Van Voorhis WC, Waldmann H** (2006) Therapeutic intervention based on protein prenylation and associated modifications. *Nat Chem Biol* **2**: 518–528

**Gelot A, Friesen W, Hamza HA** (1984) EMULSIFICATION OF OIL AND WATER IN THE PRESENCE OF FINELY DIVIDED SOLIDS AND SURFACE-ACTIVE AGENTS. *Colloids and Surfaces* **12**: 271–303

**des Georges A, Dhote V, Kuhn L, Hellen CUT, Pestova TV, Frank J, Hashem Y** (2015) Structure of mammalian eIF3 in the context of the 43S preinitiation complex. *Nature* **525**: 491–495

**Gerber E** (2005) Localisation cellulaire de protéines fluorescentes isoprénylables dans des cellules de tabac BY-2. Université de Strasbourg, Strasbourg

**Gerber E, Hemmerlin A, Hartmann M, Heintz D, Hartmann M-A, Mutterer J, Rodríguez-Concepción M, Boronat A, Van Dorsselaer A, Rohmer M, et al** (2009a) The Plastidial 2- C-Methyl-D-Erythritol 4-Phosphate Pathway Provides the Isoprenyl Moiety for Protein Geranylgeranylation in Tobacco BY-2 Cells. *Plant Cell* **21**: 285–300

**Gerber E, Hemmerlin A, Hartmann M, Heintz D, Hartmann M-A, Mutterer J, Rodríguez-Concepción M, Boronat A, Van Dorsselaer A, Rohmer M, et al** (2009b) The plastidial 2-C-methyl-D-erythritol 4-phosphate pathway provides the isoprenyl moiety for protein geranylgeranylation in tobacco BY-2 cells. *Plant Cell* **21**: 285–300

**Ghosh S, Singh UK, Meli VS, Kumar V, Kumar A, Irfan M, Chakraborty N, Chakraborty S, Datta A** (2013) Induction of Senescence and Identification of Differentially Expressed Genes in Tomato in Response to Monoterpene. *PLoS ONE* **8**: e76029

**Gilg AB, Bearfield JC, Tittiger C, Welch WH, Blomquist GJ** (2005) Isolation and functional expression of an animal geranyl diphosphate synthase and its role in bark beetle pheromone biosynthesis. *Proc Natl Acad Sci* **102**: 9760–9765

**Gill M** (2001) The Biosynthesis of Pigments in Basidiomycetes. *Aust J Chem* **54**: 721

**Gillette WK, Esposito D, Abreu Blanco M, Alexander P, Bindu L, Bittner C, Chertov O, Frank PH, Grose C, Jones JE, et al** (2015) Farnesylated and methylated KRAS4b: high yield production of protein suitable for biophysical studies of prenylated protein-lipid interactions. *Sci Rep* **5**: 15916

**Gisselberg JE, Herrera Z, Orchard L, Llinás M, Yeh E** (2017) A specific non-bisphosphonate inhibitor of the bifunctional farnesyl/geranylgeranyl diphosphate synthase in malaria parasites. doi: 10.1101/134338

**Giusti MM, Wrolstad RE** (2001) Characterization and Measurement of Anthocyanins by UV-Visible Spectroscopy. *Curr Protoc Food Anal Chem* **00**: F1.2.1-F1.2.13

**Glenn MP, Chang S-Y, Hornéy C, Rivas K, Yokoyama K, Pusateri EE, Fletcher S, Cummings CG, Buckner FS, Pendyala PR, et al** (2006) Structurally Simple, Potent, *Plasmodium* Selective Farnesyltransferase Inhibitors That Arrest the Growth of Malaria Parasites. *J Med Chem* **49**: 5710–5727

**Glennon EKK, Adams LG, Hicks DR, Dehesh K, Luckhart S** (2016) Supplementation with Abscisic Acid Reduces Malaria Disease Severity and Parasite Transmission. *Am J Trop Med Hyg* **94**: 1266–1275

**Glennon EKK, Torrevillas BK, Morrissey SF, Ejercito JM, Luckhart S** (2017) Abscisic acid induces a transient shift in signaling that enhances NF- $\kappa$ B-mediated parasite killing in the midgut of *Anopheles stephensi* without reducing lifespan or fecundity. *Parasit Vectors* **10**: 333

**Goalstone ML, Leitner JW, Golovchenko I, Stjernholm MR, Cormont M, Le Marchand-Brustel Y, Draznin B** (1999) Insulin Promotes Phosphorylation and Activation of Geranylgeranyltransferase II: STUDIES WITH GERANYLGERANYLATION OF Rab-3 AND Rab-4. *J Biol Chem* **274**: 2880–2884

**Golding AE, Visco I, Bieling P, Bement WM** (2019) Extraction of active RhoGTPases by RhoGDI regulates spatiotemporal patterning of RhoGTPases. *eLife* **8**: e50471

- Gomord V, Denmat L-A, Fitchette-Laine A-C, Satiat-Jeunemaitre B, Hawes C, Faye L** (1997) The C-terminal HDEL sequence is sufficient for retention of secretory proteins in the endoplasmic reticulum (ER) but promotes vacuolar targeting of proteins that escape the ER. *Plant J* **11**: 313–325
- González MA** (2015) Aromatic abietane diterpenoids: their biological activity and synthesis. *Nat Prod Rep* **32**: 684–704
- Goodman LE, Judd SR, Farnsworth CC, Powers S, Gelb MH, Glomset JA, Tamanoi F** (1990) Mutants of *Saccharomyces cerevisiae* defective in the farnesylation of Ras proteins. *Proc Natl Acad Sci* **87**: 9665–9669
- Goodman SR, Kurdia A, Ammann L, Kakhniashvili D, Daescu O** (2007) The Human Red Blood Cell Proteome and Interactome. *Exp Biol Med* **232**: 1391–1408
- Goritschnig S, Weihmann T, Zhang Y, Fobert P, McCourt P, Li X** (2008) A Novel Role for Protein Farnesylation in Plant Innate Immunity. *Plant Physiol* **148**: 348–357
- Gotch AJ, Loar GW, Reeder AJ, Glista EE** (2008) Formation of Single-Phase Microemulsions in Toluene/Water/Nonionic Surfactant Systems. *Langmuir* **24**: 4485–4493
- Greenspan P, Mayer EP, Fowler SD** (1985) Nile red: a selective fluorescent stain for intracellular lipid droplets. *J Cell Biol* **100**: 965–973
- Gregg EC** (1968) The hydrogenation of poly-2-alkylbutadienes: POLY-2-ALKYLBUTADIENES. *J Polym Sci Part C Polym Symp* **24**: 295–302
- Gu J-L, Tong H-F, Sun L-Y** (2017) Preparation and preliminary evaluation of macroporous magnetic agarose particles for bioseparation. *Biotechnol Bioprocess Eng* **22**: 76–82
- Guggisberg AM, Frasse PM, Jezewski AJ, Kafai NM, Gandhi AY, Erlinger SJ, Odom John AR** (2018) Suppression of Drug Resistance Reveals a Genetic Mechanism of Metabolic Plasticity in Malaria Parasites. *mBio* **9**: e01193-18, /mbio/9/6/mBio.01193-18.atom
- Guggisberg AM, Park J, Edwards RL, Kelly ML, Hodge DM, Tolia NH, Odom AR** (2014) A sugar phosphatase regulates the methylerythritol phosphate (MEP) pathway in malaria parasites. *Nat Commun* **5**: 4467
- Guida WC, Hamilton AD, Crotty JW, Sebti SM** (2005) Protein farnesyltransferase: flexible docking studies on inhibitors using computational modeling. *J Comput Aided Mol Des* **19**: 871–885
- Guo Z, Wu Y-W, Das D, Delon C, Cramer J, Yu S, Thuns S, Lupilova N, Waldmann H, Brunsveld L, et al** (2008) Structures of RabGGTase–substrate/product complexes provide insights into the evolution of protein prenylation. *EMBO J* **27**: 2444–2456
- Gutbrod K, Romer J, Dörmann P** (2019) Phytol metabolism in plants. *Prog Lipid Res* **74**: 1–17
- Ha YR, Hwang B-G, Hong Y, Yang H-W, Lee SJ** (2015) Effect of Farnesyltransferase Inhibitor R115777 on Mitochondria of *Plasmodium falciparum*; Korean J Parasitol **53**: 421–430
- Hagi T, Kobayashi M, Nomura M** (2015) Aerobic conditions increase isoprenoid biosynthesis pathway gene expression levels for carotenoid production in *Enterococcus gilvus*. *FEMS Microbiol Lett*. doi: 10.1093/femsle/fnv075
- Hála M, Žárský V** (2019) Protein Prenylation in Plant Stress Responses. *Molecules* **24**: 3906
- Han M, Heppel SC, Su T, Bogs J, Zu Y, An Z, Rausch T** (2013) Enzyme Inhibitor Studies Reveal Complex Control of Methyl-D-Erythritol 4-Phosphate (MEP) Pathway Enzyme Expression in *Catharanthus roseus*. *PLoS ONE* **8**: e62467
- Han Y-S, Van der Heijden R, Verpoorte R** (2001) Biosynthesis of anthraquinones in cell cultures of the Rubiaceae. *Plant Cell Tissue Organ Cult* **67**: 201–220
- Hancock JF, Cadwallader K, Marshall CJ** (1991) Methylation and proteolysis are essential for efficient membrane binding of prenylated p21K-ras(B). *EMBO J* **10**: 641–646
- Hancock JF, Magee AI, Childs JE, Marshall CJ** (1989) All ras proteins are polyisoprenylated but only some are palmitoylated. *Cell* **57**: 1167–1177
- Hancock JF, Paterson H, Marshall CJ** (1990) A polybasic domain or palmitoylation is required in addition to the CAAX motif to localize p21ras to the plasma membrane. *Cell* **63**: 133–139

- Hang HC, Wilson JP, Charron G** (2011) Bioorthogonal Chemical Reporters for Analyzing Protein Lipidation and Lipid Trafficking. *Acc Chem Res* **44**: 699–708
- Hannoush RN, Sun J** (2010) The chemical toolbox for monitoring protein fatty acylation and prenylation. *Nat Chem Biol* **6**: 498–506
- Harada H, Fujisawa M, Teramoto M, Sakurai N, Suzuki H, Shibata D, Misawa N** (2009) Simple functional analysis of key genes involved in astaxanthin biosynthesis using Arabidopsis cultured cells. *Plant Biotechnol* **26**: 81–92
- Harayama T, Riezman H** (2018) Understanding the diversity of membrane lipid composition. *Nat Rev Mol Cell Biol* **19**: 281–296
- Hartmann M, Gas-Pascual E, Hemmerlin A, Rohmer M, Bach TJ** (2015) Development of an image-based screening system for inhibitors of the plastidial MEP pathway and of protein geranylgeranylation. *F1000Research* **4**: 14
- Hassanpour SH, Dehghani M** (2017) Review of cancer from perspective of molecular. *J Cancer Res Pract* **4**: 127–129
- Hati S, Tripathy S, Dutta PK, Agarwal R, Srinivasan R, Singh A, Singh S, Sen S** (2016) Spiro[pyrrolidine-3, 3'-oxindole] as potent anti-breast cancer compounds: Their design, synthesis, biological evaluation and cellular target identification. *Sci Rep* **6**: 32213
- Hawes C** (2004) Cell biology of the plant Golgi apparatus. *New Phytol* **165**: 29–44
- Hawes C, Satiat-Jeunemaitre B** (2005) The plant Golgi apparatus—Going with the flow. *Biochim Biophys Acta BBA - Mol Cell Res* **1744**: 93–107
- Hazman M, Sühnel M, Schäfer S, Zumsteg J, Lesot A, Beltran F, Marquis V, Herrgott L, Miesch L, Riemann M, et al** (2019) Characterization of Jasmonoyl-Isoleucine (JA-Ile) Hormonal Catabolic Pathways in Rice upon Wounding and Salt Stress. *Rice* **12**: 45
- He B, Chen P, Chen SY, Vancura KL, Michaelis S, Powers S** (1991) RAM2, an essential gene of yeast, and RAM1 encode the two polypeptide components of the farnesyltransferase that prenylates a-factor and Ras proteins. *Proc Natl Acad Sci* **88**: 11373–11377
- Hemmerlin A** (2013) Post-translational events and modifications regulating plant enzymes involved in isoprenoid precursor biosynthesis. *Plant Sci* **203–204**: 41–54
- Hemmerlin A, Bach TJ** (2000) Farnesol-induced cell death and stimulation of 3-hydroxy-3-methylglutaryl-coenzyme A reductase activity in tobacco cv bright yellow-2 cells. *Plant Physiol* **123**: 1257–1268
- Hemmerlin A, Harwood JL, Bach TJ** (2012) A raison d'être for two distinct pathways in the early steps of plant isoprenoid biosynthesis? *Prog Lipid Res* **51**: 95–148
- Hemmerlin A, Hoeffler J-F, Meyer O, Tritsch D, Kagan IA, Grosdemange-Billiard C, Rohmer M, Bach TJ** (2003) Cross-talk between the Cytosolic Mevalonate and the Plastidial Methylerythritol Phosphate Pathways in Tobacco Bright Yellow-2 Cells. *J Biol Chem* **278**: 26666–26676
- Hepler PK** (2005) Calcium: A Central Regulator of Plant Growth and Development. *Plant Cell* **17**: 2142–2155
- Hightower KE, Casey PJ, Fierke CA** (2001) Farnesylation of Nonpeptidic Thiol Compounds by Protein Farnesyltransferase<sup>†</sup>. *Biochemistry* **40**: 1002–1010
- Hightower KE, Fierke CA** (1999) Zinc-catalyzed sulfur alkylation: insights from protein farnesyltransferase. *Curr Opin Chem Biol* **3**: 176–181
- Hildebrandt ER, Cheng M, Zhao P, Kim JH, Wells L, Schmidt WK** (2016) A shunt pathway limits the CaaX processing of Hsp40 Ydj1p and regulates Ydj1p-dependent phenotypes. *eLife* **5**: e15899
- Hippler H** (1993) Data Fitting in the Chemical Sciences. P. Gans. Wiley, Chichester, 1992. XII, 258 S., geb. 29.95 £. - ISBN 0-471-93412-7. *Angew Chem* **105**: 654–654
- Hjertén S** (1964) The Preparation Of Agarose Spheres For Chromatography Of Molecules And Particles. *Biochim Biophys Acta* **6**
- Hjertén S, Wu B-L, Liao J-L** (1987) An high-performance liquid chromatography matrix based on agarose cross-linked with divinyl sulphone. *J Chromatogr A* **396**: 101–113

- Hlasiwetz H, Grabowski A** (1867) Mittheilungen aus dem chemischen Laboratorium in Innsbruck. I. Ueber die Carminsäure; *Ann Chem Pharm* **141**: 329–345
- Ho C-L, Wang J-L, Lee C-C, Cheng H-Y, Wen W-C, Cheng HH-Y, Chen MC-M** (2014) Antroquinonol blocks Ras and Rho signaling via the inhibition of protein isoprenyltransferase activity in cancer cells. *Biomed Pharmacother* **68**: 1007–1014
- Hodge RG, Ridley AJ** (2016) Regulating Rho GTPases and their regulators. *Nat Rev Mol Cell Biol* **17**: 496–510
- Hoffman MD, Kast J** (2006) Mass spectrometric characterization of lipid-modified peptides for the analysis of acylated proteins. *J Mass Spectrom* **41**: 229–241
- Hohmann J, Molnár J** (2004) [Euphorbiaceae diterpenes: plant toxins or promising molecules for the therapy?]. *Acta Pharm Hung* **74**: 149–157
- Holstein SA, Hohl RJ** (2004) Isoprenoids: Remarkable diversity of form and function. *Lipids* **39**: 293–309
- Holstein SA, Hohl RJ** (2012) Is there a future for prenyltransferase inhibitors in cancer therapy? *Curr Opin Pharmacol* **12**: 704–709
- Holte D, Götz DCG, Baran PS** (2012) An Approach to Mimicking the Sesquiterpene Cyclase Phase by Nickel-Promoted Diene/Alkyne Cooligomerization. *J Org Chem* **77**: 825–842
- Hong G-J, Hu W-L, Li J-X, Chen X-Y, Wang L-J** (2009) Increased Accumulation of Artemisinin and Anthocyanins in *Artemisia annua* Expressing the Arabidopsis Blue Light Receptor CRY1. *Plant Mol Biol Report* **27**: 334–341
- Hooff GP, Wood WG, Müller WE, Eckert GP** (2010) Isoprenoids, small GTPases and Alzheimer's disease. *Biochim Biophys Acta BBA - Mol Cell Biol Lipids* **1801**: 896–905
- Horváth Gy, Bencsik T, Ács K, Kocsis B** (2016) Sensitivity of ESBL-Producing Gram-Negative Bacteria to Essential Oils, Plant Extracts, and Their Isolated Compounds. *Antibiot. Resist. Elsevier*, pp 239–269
- Hoshino Y, Gaucher EA** (2018) On the Origin of Isoprenoid Biosynthesis. *Mol Biol Evol* **35**: 2185–2197
- Hougland JL, Gangopadhyay SA, Fierke CA** (2012) Expansion of Protein Farnesyltransferase Specificity Using “Tunable” Active Site Interactions: DEVELOPMENT OF BIOENGINEERED PRENYLATION PATHWAYS. *J Biol Chem* **287**: 38090–38100
- Huchelmann A** (2013) Étude de l'implication des deux voies de biosynthèse des isoprénoïdes pour la spécificité et la régulation de la prénylation des protéines chez les plantes. Université de Strasbourg, Strasbourg
- Huchelmann A, Gastaldo C, Veinante M, Zeng Y, Heintz D, Tritsch D, Schaller H, Rohmer M, Bach TJ, Hemmerlin A** (2014) *S*-Carvone Suppresses Cellulase-Induced Capsidiol Production in *Nicotiana tabacum* by Interfering with Protein Isoprenylation. *Plant Physiol* **164**: 935–950
- Hussain H, Green IR** (2017) Lapachol and lapachone analogs: a journey of two decades of patent research(1997-2016). *Expert Opin Ther Pat* **27**: 1111–1121
- Hussain W, Khan YD, Rasool N, Khan SA, Chou K-C** (2019) SPrenylC-PseAAC: A sequence-based model developed via Chou's 5-steps rule and general PseAAC for identifying S-prenylation sites in proteins. *J Theor Biol* **468**: 1–11
- Ikram NKBK, Simonsen HT** (2017) A Review of Biotechnological Artemisinin Production in Plants. *Front Plant Sci* **8**: 1966
- Imlay L, Odom AR** (2014) Isoprenoid Metabolism in Apicomplexan Parasites. *Curr Clin Microbiol Rep* **1**: 37–50
- Ischebeck T, Zbierzak AM, Kanwischer M, Dörmann P** (2006) A Salvage Pathway for Phytol Metabolism in *Arabidopsis*. *J Biol Chem* **281**: 2470–2477
- Islam MT** (2017) Diterpenes and Their Derivatives as Potential Anticancer Agents: Diterpenes in Cancer. *Phytother Res* **31**: 691–712
- Jaffe AB, Hall A** (2005) RHO GTPASES: Biochemistry and Biology. *Annu Rev Cell Dev Biol* **21**: 247–269
- Jahnke W, Rondeau J-M, Cotesta S, Marzinzik A, Pellé X, Geiser M, Strauss A, Götte M, Bitsch F, Hemmig R, et al** (2010) Allosteric non-bisphosphonate FPPS inhibitors identified by fragment-based discovery. *Nat Chem Biol* **6**: 660–666
- Jalakas P, Huang Y-C, Yeh Y-H, Zimmerli L, Merilo E, Kollist H, Brosché M** (2017) The Role of ENHANCED RESPONSES

TO ABA1 (ERA1) in Arabidopsis Stomatal Responses Is Beyond ABA Signaling. *Plant Physiol* **174**: 665–671

Jang G, Chang SH, Um TY, Lee S, Kim J-K, Choi YD (2017) Antagonistic interaction between jasmonic acid and cytokinin in xylem development. *Sci Rep* **7**: 10212

Janosi L, Gorfe AA (2010) Segregation of Negatively Charged Phospholipids by the Polycationic and Farnesylated Membrane Anchor of Kras. *Biophys J* **99**: 3666–3674

Jarvis FG, Mesenko MT, Martin DG, Perrine TD (1967) Physicochemical properties of the Vi antigen before and after mild alkaline hydrolysis. *J Bacteriol* **94**: 1406–1410

Jennings BC, Danowitz AM, Wang Y-C, Gibbs RA, Distefano MD, Fierke CA (2016) Analogs of farnesyl diphosphate alter CaaX substrate specificity and reactions rates of protein farnesyltransferase. *Bioorg Med Chem Lett* **26**: 1333–1336

Jeong A, Suazo KF, Wood WG, Distefano MD, Li L (2018) Isoprenoids and protein prenylation: implications in the pathogenesis and therapeutic intervention of Alzheimer's disease. *Crit Rev Biochem Mol Biol* **53**: 279–310

Jiang H, Zhang X, Chen X, Aramsangtienchai P, Tong Z, Lin H (2018) Protein Lipidation: Occurrence, Mechanisms, Biological Functions, and Enabling Technologies. *Chem Rev* **118**: 919–988

Jin Y-X, Shi L-L, Zhang D-P, Wei H-Y, Si Y, Ma G-X, Zhang J (2019) A Review on Daphnane-Type Diterpenoids and Their Bioactive Studies. *Molecules* **24**: 1842

Johnson CD, Chary SN, Chernoff EA, Zeng Q, Running MP, Crowell DN (2005) Protein Geranylgeranyltransferase I Is Involved in Specific Aspects of Abscisic Acid and Auxin Signaling in Arabidopsis. *Plant Physiol* **139**: 722–733

Johnson JL, Erickson JW, Cerione RA (2012) C-terminal Di-arginine Motif of Cdc42 Protein Is Essential for Binding to Phosphatidylinositol 4,5-Bisphosphate-containing Membranes and Inducing Cellular Transformation. *J Biol Chem* **287**: 5764–5774

Jomaa H (1999) Inhibitors of the Nonmevalonate Pathway of Isoprenoid Biosynthesis as Antimalarial Drugs. *Science* **285**: 1573–1576

Jordão FM, Gabriel HB, Alves JM, Angeli CB, Bifano TD, Breda A, de Azevedo MF, Basso LA, Wunderlich G, Kimura EA, et al (2013) Cloning and characterization of bifunctional enzyme farnesyl diphosphate/geranylgeranyl diphosphate synthase from *Plasmodium falciparum*. *Malar J* **12**: 184

Jordão FM, Saito AY, Miguel DC, de Jesus Peres V, Kimura EA, Katzin AM (2011) *In Vitro* and *In Vivo* Antiplasmodial Activities of Risedronate and Its Interference with Protein Prenylation in *Plasmodium falciparum*. *Antimicrob Agents Chemother* **55**: 2026–2031

Junková P, Daněk M, Kocourková D, Brouzdová J, Kroumanová K, Zelazny E, Janda M, Hynek R, Martinec J, Valentová O (2018) Mapping of Plasma Membrane Proteins Interacting With Arabidopsis thaliana Flotillin 2. *Front Plant Sci* **9**: 991

Kakhniashvili DG, Bulla LA, Goodman SR (2004) The Human Erythrocyte Proteome: Analysis by Ion Trap Mass Spectrometry. *Mol Cell Proteomics* **3**: 501–509

Kale TA, Raab C, Yu N, Aquino E, Dean DC, Distefano MD (2003) Synthesis of high specific activity <sup>35</sup>S-labelled N-methanesulfonyl farnesylcysteine and a photoactive analog. *J Label Compd Radiopharm* **46**: 29–54

Kamiya Y, Sakurai A, Tamura S, Abe K, Tsuchiya E, Fukui S (1977) Isolation and Chemical Characterization of the Peptidyl Factor Controlling Mating Tube Formation in *Rhodospiridium toruloides*. *Agric Biol Chem* **41**: 1099–1100

Kamiya Y, Sakurai A, Tamura S, Takahashi N (1978) Structure of rhodotorucine A, a novel lipopeptide, inducing mating tube formation in *Rhodospiridium toruloides*. *Biochem Biophys Res Commun* **83**: 1077–1083

Kamuro Y, Kawai T, Kakiuchi T (1986) 73) Assignee: Fujisawa Pharmaceutical Co., Ltd., Japan 21 Appl. No.: 349,576. 4

Kanda Y, Nakamura H, Umemiya S, Puthukanoori RK, Appala VRM, Gaddamanugu GK, Paraselli BR, Baran P (2020) Two-Phase Synthesis of Taxol®. doi: 10.26434/chemrxiv.12061620.v1

Kasahara H, Hanada A, Kuzuyama T, Takagi M, Kamiya Y, Yamaguchi S (2002) Contribution of the Mevalonate and Methylerythritol Phosphate Pathways to the Biosynthesis of Gibberellins in *Arabidopsis*. *J Biol Chem* **277**: 45188–45194

- Kasahara H, Takei K, Ueda N, Hishiyama S, Yamaya T, Kamiya Y, Yamaguchi S, Sakakibara H** (2004) Distinct Isoprenoid Origins of *cis*- and *trans*- Zeatin Biosyntheses in *Arabidopsis*. *J Biol Chem* **279**: 14049–14054
- Kassai H, Aiba A, Nakao K, Nakamura K, Katsuki M, Xiong W-H, Yau K-W, Imai H, Shichida Y, Satomi Y, et al** (2005) Farnesylation of Retinal Transducin Underlies Its Translocation during Light Adaptation. *Neuron* **47**: 529–539
- Kavanagh KL, Dunford JE, Bunkoczi G, Russell RGG, Oppermann U** (2006) The Crystal Structure of Human Geranylgeranyl Pyrophosphate Synthase Reveals a Novel Hexameric Arrangement and Inhibitory Product Binding. *J Biol Chem* **281**: 22004–22012
- Kawamura S, Chu H, Felding J, Baran PS** (2016) Nineteen-step total synthesis of (+)-phorbol. *Nature* **532**: 90–93
- Kelly R, Card D, Register E, Mazur P, Kelly T, Tanaka K-I, Onishi J, Williamson JM, Fan H, Satoh T, et al** (2000) Geranylgeranyltransferase I of *Candida albicans*: Null Mutants or Enzyme Inhibitors Produce Unexpected Phenotypes. *J Bacteriol* **182**: 704–713
- Khan M, Singh I** (2019) Therapeutic exploitation of the S-nitrosoglutathione/S-nitrosylation mechanism for the treatment of contusion spinal cord injury. *Neural Regen Res* **14**: 973
- Khan MdA, Khan Z, Ahmad W, Paul B, Paul S, Aggarwal C, Akhtar MohdS** (2015) Insect Pest Resistance: An Alternative Approach for Crop Protection. In KR Hakeem, ed, *Crop Prod. Glob. Environ. Issues*. Springer International Publishing, Cham, pp 257–282
- Khanna C, Rosenberg M, Vail DM** (2015) A Review of Paclitaxel and Novel Formulations Including Those Suitable for Use in Dogs. *J Vet Intern Med* **29**: 1006–1012
- Kieber JJ, Schaller GE** (2014) Cytokinins. *Arab Book* **12**: e0168
- Kimple ME, Brill AL, Pasker RL** (2013) Overview of Affinity Tags for Protein Purification. *Curr Protoc Protein Sci*. doi: 10.1002/0471140864.ps0909s73
- Kishimoto S, Ohmiya A** (2006) Regulation of carotenoid biosynthesis in petals and leaves of chrysanthemum (*Chrysanthemum morifolium*). *Physiol Plant* **128**: 436–447
- Kohl NE, Diehl RE, Schaber MD, Rands E, Soderman DD, He B, Moores SL, Pompliano DL, Ferro-Novick S, Powers S** (1991) Structural homology among mammalian and *Saccharomyces cerevisiae* isoprenyl-protein transferases. *J Biol Chem* **266**: 18884–18888
- Kohli A, Sreenivasulu N, Lakshmanan P, Kumar PP** (2013) The phytohormone crosstalk paradigm takes center stage in understanding how plants respond to abiotic stresses. *Plant Cell Rep* **32**: 945–957
- Kolsrud H, Malerod H, Ray S, Reubsaet L, Lundanes E, Greibrokk T** (2012) A Critical Review of Trypsin Digestion for LC-MS Based Proteomics. *Integr Proteomics*. doi: 10.5772/29326
- Kopcsayová D, Vranová E** (2019) Functional Gene Network of Prenyltransferases in *Arabidopsis thaliana*. *Molecules* **24**: 4556
- Koyama FC, Carvalho TLG, Alves E, da Silva HB, de Azevedo MF, Hemerly AS, Garcia CRS** (2013) The Structurally Related Auxin and Melatonin Tryptophan-Derivatives and their Roles in *Arabidopsis thaliana* and in the Human Malaria Parasite *Plasmodium falciparum*. *J Eukaryot Microbiol* **60**: 646–651
- Koyama T** (1999) Molecular Analysis of Prenyl Chain Elongating Enzymes. *Biosci Biotechnol Biochem* **63**: 1671–1676
- Krengel F, Chevalier Q, Dickinson J, Herrera Santoyo J, Reyes Chilpa R** (2019) Metabolite Profiling of Anti-Addictive Alkaloids from Four Mexican *Tabernaemontana* Species and the Entheogenic African Shrub *Tabernanthe iboga* (Apocynaceae). *Chem Biodivers*. doi: 10.1002/cbdv.201800506
- Kruglyakov P** (1976) The HLB SYSTEM a time-saving guide to emulsifier selection. ICI Americas Inc.
- Kruh GD** (2003) Introduction to resistance to anticancer agents. *Oncogene* **22**: 7262–7264
- Kuchay S, Wang H, Marzio A, Jain K, Homer H, Fehrenbacher N, Philips MR, Zheng N, Pagano M** (2019) GGTase3 is a newly identified geranylgeranyltransferase targeting a ubiquitin ligase. *Nat Struct Mol Biol* **26**: 628–636
- Kumar SR, Rai A, Bomzan DP, Kumar K, Hemmerlin A, Dwivedi V, Godbole RC, Barvkar V, Shanker K, Shilpashree HB, et al** (2020) A plastid-localized *bona fide* geranylgeranyl diphosphate synthase plays a necessary role in monoterpene indole alkaloid biosynthesis in *Catharanthus roseus*. *Plant J* **103**: 248–265



- Kumari S, Priya P, Misra G, Yadav G** (2013) Structural and biochemical perspectives in plant isoprenoid biosynthesis. *Phytochem Rev* **12**: 255–291
- Kuzuguchi T, Morita Y, Sagami I, Sagami H, Ogura K** (1999) Human Geranylgeranyl Diphosphate Synthase: cDNA CLONING AND EXPRESSION. *J Biol Chem* **274**: 5888–5894
- Kuzuyama T, Shimizu T, Takahashi S, Seto H** (1998) Fosmidomycin, a specific inhibitor of 1-deoxy-d-xylulose 5-phosphate reductoisomerase in the nonmevalonate pathway for terpenoid biosynthesis. *Tetrahedron Lett* **39**: 7913–7916
- Kwon SJ** (2006) Proteomics studies of post-translational modifications in plants. *J Exp Bot* **57**: 1547–1551
- Lamphear CL** (2012) Molecular Recognition Of Substrates By Protein Farnesyltransferase And Geranylgeranyltransferase-I. University of Michigan
- Lane KT, Beese LS** (2006) *Thematic review series: Lipid Posttranslational Modifications*. Structural biology of protein farnesyltransferase and geranylgeranyltransferase type I. *J Lipid Res* **47**: 681–699
- Lavy M, Bracha-Drori K, Sternberg H, Yalovsky S** (2002) A Cell-Specific, Prenylation-Independent Mechanism Regulates Targeting of Type II RACs. *Plant Cell* **14**: 2431–2450
- Lee R, Chang SY, Trinh H, Tu Y, White AC, Davies BSJ, Bergo MO, Fong LG, Lowry WE, Young SG** (2010) Genetic studies on the functional relevance of the protein prenyltransferases in skin keratinocytes. *Hum Mol Genet* **19**: 1603–1617
- Lefèvre F, Fourmeau J, Pottier M, Baijot A, Cornet T, Abadía J, Álvarez-Fernández A, Boutry M** (2018) The *Nicotiana tabacum* ABC transporter NtPDR3 secretes O-methylated coumarins in response to iron deficiency. *J Exp Bot* **69**: 4419–4431
- Lell B, Ruangweeraayut R, Wiesner J, Missinou MA, Schindler A, Baranek T, Hintz M, Hutchinson D, Jomaa H, Kremsner PG** (2003) Fosmidomycin, a Novel Chemotherapeutic Agent for Malaria. *Antimicrob Agents Chemother* **47**: 735–738
- León IR, Schwämmle V, Jensen ON, Sprenger RR** (2013) Quantitative Assessment of In-solution Digestion Efficiency Identifies Optimal Protocols for Unbiased Protein Analysis. *Mol Cell Proteomics* **12**: 2992–3005
- Leung KF, Baron R, Seabra MC** (2006) *Thematic review series: Lipid Posttranslational Modifications*. Geranylgeranylation of Rab GTPases. *J Lipid Res* **47**: 467–475
- Li D, Halitschke R, Baldwin IT, Gaquerel E** (2020) Information theory tests critical predictions of plant defense theory for specialized metabolism. *Sci Adv* **6**: eaaz0381
- Li S, Balmain A, Counter CM** (2018) A model for RAS mutation patterns in cancers: finding the sweet spot. *Nat Rev Cancer* **18**: 767–777
- Lichtenthaler HK** (2007) Biosynthesis, accumulation and emission of carotenoids,  $\alpha$ -tocopherol, plastoquinone, and isoprene in leaves under high photosynthetic irradiance. *Photosynth Res* **92**: 163–179
- Ling Y, Li Z-H, Miranda K, Oldfield E, Moreno SNJ** (2007) The Farnesyl-diphosphate/Geranylgeranyl-diphosphate Synthase of *Toxoplasma gondii* Is a Bifunctional Enzyme and a Molecular Target of Bisphosphonates. *J Biol Chem* **282**: 30804–30816
- Liu J, Liu Y, Wang Y, Zhang Z-H, Zu Y-G, Efferth T, Tang Z-H** (2016) The Combined Effects of Ethylene and MeJA on Metabolic Profiling of Phenolic Compounds in *Catharanthus roseus* Revealed by Metabolomics Analysis. *Front Physiol*. doi: 10.3389/fphys.2016.00217
- Liu M, Masatani T, Adjou Moumouni PF, Lee S-H, Galon EM, Gao Y, Guo H, Li J, Li Y, Xuan X** (2019) Inhibitory effects of the phytohormone inhibitors fluridone and inabenfide against *Babesia gibsoni* in vitro. *Vet Parasitol* **265**: 19–23
- Liu X, Suh D-Y, Call J, Prestwich GD** (2004) Antigenic Prenylated Peptide Conjugates and Polyclonal Antibodies To Detect Protein Prenylation. *Bioconjug Chem* **15**: 270–277
- Liu Y, Cai Y, He C, Chen M, Li H** (2017) Anticancer Properties and Pharmaceutical Applications of Plumbagin: A Review. *Am J Chin Med* **45**: 423–441
- Lobell RB, Omer CA, Abrams MT, Bhimnathwala HG, Brucker MJ, Buser CA, Davide JP, deSolms SJ, Dinsmore CJ, Ellis-Hutchings MS, et al** (2001) Evaluation of farnesyl:protein transferase and geranylgeranyl:protein transferase

inhibitor combinations in preclinical models. *Cancer Res* **61**: 8758–8768

**Lois LM, Rodriguez-Concepcion M, Gallego F, Campos N, Boronat A** (2000) Carotenoid biosynthesis during tomato fruit development: regulatory role of 1-deoxy-D-xylulose 5-phosphate synthase. *Plant J* **22**: 503–513

**Long SB, Casey PJ, Beese LS** (2002) Reaction path of protein farnesyltransferase at atomic resolution. *Nature* **419**: 645–650

**López-Gallego F, Fernandez-Lorente G, Rocha-Martin J, Bolivar JM, Mateo C, Guisan JM** (2013) Stabilization of Enzymes by Multipoint Covalent Immobilization on Supports Activated with Glyoxyl Groups. In JM Guisan, ed, *Immobil. Enzym. Cells*. Humana Press, Totowa, NJ, pp 59–71

**Loreto F, Forster A, Durr M, Csiky O, Seufert G** (1998) On the monoterpene emission under heat stress and on the increased thermotolerance of leaves of *Quercus ilex* L. fumigated with selected monoterpenes. *Plant Cell Environ* **21**: 101–107

**Lu X, Malley KR, Brenner CC, Koroleva O, Korolev S, Downes BP** (2016) A MUB E2 structure reveals E1 selectivity between cognate ubiquitin E2s in eukaryotes. *Nat Commun* **7**: 12580

**Lundgren JG, Hesler LS, Tilmon K, Dashiell K, Scott R** (2009) Direct effects of soybean varietal selection and Aphid glycines-resistant soybeans on natural enemies. *Arthropod-Plant Interact* **3**: 9–16

**Luo Y** (1995) Hydrogenation of 1,3-butadiene and isoprene prepolymers having carboxyl end groups. *J Appl Polym Sci* **56**: 721–737

**Lynen F, Eggerer H, Henning U, Kessel I** (1958) Farnesyl-pyrophosphat und 3-Methyl- $\Delta^3$ -butenyl-1-pyrophosphat, die biologischen Vorstufen des Squalens. Zur Biosynthese der Terpene, III. *Angew Chem* **70**: 738–742

**MacArthur IC, Bei Y, Garcia HD, Ortiz MV, Toedling J, Klironomos F, Rolff J, Eggert A, Schulte JH, Kentsis A, et al** (2019) Prohibitin promotes dedifferentiation and is a potential therapeutic target in neuroblastoma. *JCI Insight* **4**: e127130

**de Macedo CS, Shams-Eldin H, Smith TK, Schwarz RT, Azzouz N** (2003) Inhibitors of glycosyl-phosphatidylinositol anchor biosynthesis. *Biochimie* **85**: 465–472

**Maeder Marcel, Zuberbuehler AD** (1990) Nonlinear least-squares fitting of multivariate absorption data. *Anal Chem* **62**: 2220–2224

**Majumder A, Gopalakrishna KN, Cheguru P, Gakhar L, Artemyev NO** (2013) Interaction of Aryl Hydrocarbon Receptor-interacting Protein-like 1 with the Farnesyl Moiety. *J Biol Chem* **288**: 21320–21328

**Maldonado-Mendoza IE, Burnett RJ, Lopez-Meyer M, Nessler CL** (1994) Regulation of 3-hydroxy-3-methylglutaryl-coenzyme A reductase by wounding and methyl jasmonate: Implications for the production of anti-cancer alkaloids. *Plant Cell Tissue Organ Cult* **38**: 351–356

**Maltese WA, Erdman RA** (1989) Characterization of Isoprenoid Involved in the Post-translational Modification of Mammalian Cell Proteins. *JBC* **264**: 5

**Manaswiyoungkul P, de Araujo ED, Gunning PT** (2020) Targeting prenylation inhibition through the mevalonate pathway. *RSC Med Chem* **11**: 51–71

**Mandal MK, Ahvari H, Schillberg S, Schiermeyer A** (2016) Tackling Unwanted Proteolysis in Plant Production Hosts Used for Molecular Farming. *Front Plant Sci*. doi: 10.3389/fpls.2016.00267

**Mandal MK, Fischer R, Schillberg S, Schiermeyer A** (2014) Inhibition of protease activity by antisense RNA improves recombinant protein production in *Nicotiana tabacum* cv. Bright Yellow 2 (BY-2) suspension cells. *Biotechnol J* **9**: 1065–1073

**Mansoori B, Mohammadi A, Davudian S, Shirjang S, Baradaran B** (2017) The Different Mechanisms of Cancer Drug Resistance: A Brief Review. *Adv Pharm Bull* **7**: 339–348

**Margueritte L** (2018) Développement d'une méthode de déconvolution pharmacophorique pour la découverte accélérée d'antipaludiques chez les Rhodophytes. *Pharmacognosie*. Université de Strasbourg, Strasbourg

**Margueritte L, Duciel L, Bourjot M, Vonthron-Sénécheau C, Delsuc M-A** (2019) Automated pharmacophoric deconvolution of plant extracts – application to *Cinchona* bark crude extract. *Faraday Discuss* **218**: 441–458

- Marquardt DW** (1963) An Algorithm for Least-Squares Estimation of Nonlinear Parameters. *J Soc Ind Appl Math* **11**: 431–441
- Martinière A, Bassil E, Jublanc E, Alcon C, Reguera M, Sentenac H, Blumwald E, Paris N** (2013) In Vivo Intracellular pH Measurements in Tobacco and *Arabidopsis* Reveal an Unexpected pH Gradient in the Endomembrane System. *Plant Cell* **25**: 4028–4043
- Martino E, Casamassima G, Castiglione S, Cellupica E, Pantalone S, Papagni F, Rui M, Siciliano AM, Collina S** (2018) Vinca alkaloids and analogues as anti-cancer agents: Looking back, peering ahead. *Bioorg Med Chem Lett* **28**: 2816–2826
- Mateo C, Abian O, Bernedo M, Cuenca E, Fuentes M, Fernandez-Lorente G, Palomo JM, Grazu V, Pessela BCC, Giacomini C, et al** (2005) Some special features of glyoxyl supports to immobilize proteins. *Enzyme Microb Technol* **37**: 456–462
- Mateo C, Palomo JM, Fuentes M, Betancor L, Grazu V, López-Gallego F, Pessela BCC, Hidalgo A, Fernández-Lorente G, Fernández-Lafuente R, et al** (2006) Glyoxyl agarose: A fully inert and hydrophilic support for immobilization and high stabilization of proteins. *Enzyme Microb Technol* **39**: 274–280
- Mathews ES, Jezewski AJ, Odom John AR** (2019) Protein prenylation and Hsp40 in thermotolerance of *Plasmodium falciparum* malaria parasites. doi: 10.1101/842468
- Maude RJ, Woodrow CJ, White LJ** (2009) Artemisinin antimalarials: preserving the “magic bullet.” *Drug Dev Res* n/a-n/a
- Maurer-Stroh S, Eisenhaber F** (2005) Refinement and prediction of protein prenylation motifs. *Genome Biol* **6**: R55
- Maurer-Stroh S, Koranda M, Benetka W, Schneider G, Sirota FL, Eisenhaber F** (2007) Towards Complete Sets of Farnesylated and Geranylgeranylated Proteins. *PLoS Comput Biol* **3**: e66
- McCormick F** (2019) Progress in targeting RAS with small molecule drugs. *Biochem J* **476**: 365–374
- McDonald K, Choe J, Elbaggari A, Zhu M, Albuero A** (2008) In-Gel Protein Quantitation Using the Criterion Stain Free™ Gel Imaging System. **6**
- McDonnell MM, Burkhardt SE, Stoddard JM, Wright ZJ, Strader LC, Bartel B** (2016) The Early-Acting Peroxin PEX19 Is Redundantly Encoded, Farnesylated, and Essential for Viability in *Arabidopsis thaliana*. *PLOS ONE* **11**: e0148335
- Mehrmohamadi M, Jeong SH, Locasale JW** (2017) Molecular features that predict the response to antimetabolite chemotherapies. *Cancer Metab* **5**: 8
- Melkonian KA, Ostermeyer AG, Chen JZ, Roth MG, Brown DA** (1999) Role of Lipid Modifications in Targeting Proteins to Detergent-resistant Membrane Rafts: MANY RAFT PROTEINS ARE ACYLATED, WHILE FEW ARE PRENYLATED. *J Biol Chem* **274**: 3910–3917
- Merzlyak EM, Goedhart J, Shcherbo D, Bulina ME, Shcheglov AS, Fradkov AF, Gaintzeva A, Lukyanov KA, Lukyanov S, Gadella TWJ, et al** (2007) Bright monomeric red fluorescent protein with an extended fluorescence lifetime. *Nat Methods* **4**: 555–557
- Mewis I, Schreiner M, Nguyen CN, Krumbein A, Ulrichs C, Lohse M, Zrenner R** (2012) UV-B Irradiation Changes Specifically the Secondary Metabolite Profile in Broccoli Sprouts: Induced Signaling Overlaps with Defense Response to Biotic Stressors. *Plant Cell Physiol* **53**: 1546–1560
- Michaelson D, Ali W, Chiu VK, Bergo M, Silletti J, Wright L, Young SG, Philips M** (2005) Postprenylation CAAX Processing Is Required for Proper Localization of Ras but Not Rho GTPases. *Mol Biol Cell* **16**: 1606–1616
- Miettinen K, Iñigo S, Kreft L, Pollier J, De Bo C, Botzki A, Coppens F, Bak S, Goossens A** (2018) The TriForC database: a comprehensive up-to-date resource of plant triterpene biosynthesis. *Nucleic Acids Res* **46**: D586–D594
- Mijimolle N, Velasco J, Dubus P, Guerra C, Weinbaum CA, Casey PJ, Campuzano V, Barbacid M** (2005) Protein farnesyltransferase in embryogenesis, adult homeostasis, and tumor development. *Cancer Cell* **7**: 313–324
- Millar AH, Heazlewood JL, Giglione C, Holdsworth MJ, Bachmair A, Schulze WX** (2019) The Scope, Functions, and Dynamics of Posttranslational Protein Modifications. *Annu Rev Plant Biol* **70**: 119–151
- Misaki R, Morimatsu M, Uemura T, Waguri S, Miyoshi E, Taniguchi N, Matsuda M, Taguchi T** (2010) Palmitoylated Ras proteins traffic through recycling endosomes to the plasma membrane during exocytosis. *J Cell Biol* **191**: 23–

- Mishra S, Ande SR, Nyomba BLG (2010) The role of prohibitin in cell signaling: PHB in cell signaling. *FEBS J* **277**: 3937–3946
- Missinou MA, Borrmann S, Schindler A, Issifou S, Adegnik AA, Matsiegui P-B, Binder R, Lell B, Wiesner J, Baranek T, et al (2002) Fosmidomycin for malaria. *The Lancet* **360**: 1941–1942
- Mitsuzawa H, Esson K, Tamanoi F (1995) Mutant farnesyltransferase subunit of *Saccharomyces cerevisiae* that can substitute for geranylgeranyltransferase type I (8 subunit. 5
- Mohamed A, Saavedra L, Di Pardo A, Sipione S, Posse de Chaves E (2012) -Amyloid Inhibits Protein Prenylation and Induces Cholesterol Sequestration by Impairing SREBP-2 Cleavage. *J Neurosci* **32**: 6490–6500
- Mohamed A, Viveiros A, Williams K, Posse de Chaves E (2018) A $\beta$  inhibits SREBP-2 activation through Akt inhibition. *J Lipid Res* **59**: 1–13
- Molina-Jiménez MF, Sánchez-Reus MI, Andres D, Cascales M, Benedi J (2004) Neuroprotective effect of fraxetin and myricetin against rotenone-induced apoptosis in neuroblastoma cells. *Brain Res* **1009**: 9–16
- Molnár G, Dagher M-C, Geiszt M, Settleman J, Ligeti E (2001) Role of Prenylation in the Interaction of Rho-Family Small GTPases with GTPase Activating Proteins<sup>†</sup>. *Biochemistry* **40**: 10542–10549
- Moncunill-Massaguer C, Saura-Esteller J, Pérez-Perarnau A, Palmeri CM, Núñez-Vázquez S, Cosialls AM, González-Gironès DM, Pomares H, Korwitz A, Preciado S, et al (2015) A novel prohibitin-binding compound induces the mitochondrial apoptotic pathway through NOXA and BIM upregulation. *Oncotarget* **6**: 41750–41765
- Moran NA, Jarvik T (2010) Lateral Transfer of Genes from Fungi Underlies Carotenoid Production in Aphids. *Science* **328**: 624–627
- Morimoto S, Tanaka Y, Sasaki K, Tanaka H, Fukamizu T, Shoyama Y, Shoyama Y, Taura F (2007) Identification and Characterization of Cannabinoids That Induce Cell Death through Mitochondrial Permeability Transition in *Cannabis* Leaf Cells. *J Biol Chem* **282**: 20739–20751
- Moudgil DK, Westcott N, Famulski JK, Patel K, Macdonald D, Hang H, Chan GKT (2015) A novel role of farnesylation in targeting a mitotic checkpoint protein, human Spindly, to kinetochores. *J Cell Biol* **208**: 881–896
- Mueller C, Schwender J, Zeidler J, Lichtenthaler HK (2000) Properties and inhibition of the first two enzymes of the non-mevalonate pathway of isoprenoid biosynthesis. *Biochem Soc Trans* **28**: 792–793
- Na S, Paek E, Choi J-S, Kim D, Lee SJ, Kwon J (2015) Characterization of disulfide bonds by planned digestion and tandem mass spectrometry. *Mol Biosyst* **11**: 1156–1164
- Nabi F, Arain MA, Rajput N, Alagawany M, Soomro J, Umer M, Soomro F, Wang Z, Ye R, Liu J (2020) Health benefits of carotenoids and potential application in poultry industry: A review. *J Anim Physiol Anim Nutr* jpn.13375
- Nagamune K, Xiong L, Chini E, Sibley LD (2008) Plants, endosymbionts and parasites: Abscisic acid and calcium signaling. *Commun Integr Biol* **1**: 62–65
- Nagata N, Suzuki M, Yoshida S, Muranaka T (2002) Mevalonic acid partially restores chloroplast and etioplast development in *Arabidopsis* lacking the non-mevalonate pathway. *Planta* **216**: 345–350
- Nagata T, Nemoto Y, Hasezawa S (1992) Tobacco BY-2 Cell Line as the “HeLa” Cell in the Cell Biology of Higher Plants. *Int. Rev. Cytol. Elsevier*, pp 1–30
- Nagegowda DA (2010) Plant volatile terpenoid metabolism: Biosynthetic genes, transcriptional regulation and subcellular compartmentation. *FEBS Lett* **584**: 2965–2973
- Nagel R, Bernholz C, Vranová E, Košuth J, Bergau N, Ludwig S, Wessjohann L, Gershenzon J, Tissier A, Schmidt A (2015) *Arabidopsis thaliana* isoprenyl diphosphate synthases produce the C<sub>25</sub> intermediate geranyl-farnesyl diphosphate. *Plant J* **84**: 847–859
- Nagel R, Schmidt A, Peters RJ (2019) Isoprenyl diphosphate synthases: the chain length determining step in terpene biosynthesis. *Planta* **249**: 9–20
- Nallan L, Bauer KD, Bendale P, Rivas K, Yokoyama K, Hornéy CP, Pendyala PR, Floyd D, Lombardo LJ, Williams DK, et al (2005) Protein Farnesyltransferase Inhibitors Exhibit Potent Antimalarial Activity. *J Med Chem* **48**: 3704–3713

- Nebenführ A, Gallagher LA, Dunahay TG, Frohlick JA, Mazurkiewicz AM, Meehl JB, Staehelin LA** (1999) Stop-and-Go Movements of Plant Golgi Stacks Are Mediated by the Acto-Myosin System. *Plant Physiol* **121**: 1127–1141
- Nguyen UTT, Goody RS, Alexandrov K** (2010) Understanding and Exploiting Protein Prenyltransferases. *ChemBioChem* **11**: 1194–1201
- Nishimura A, Linder ME** (2013) Identification of a Novel Prenyl and Palmitoyl Modification at the CaaX Motif of Cdc42 That Regulates RhoGDI Binding. *Mol Cell Biol* **33**: 1417–1429
- No JH, de Macedo Dossin F, Zhang Y, Liu Y-L, Zhu W, Feng X, Yoo JA, Lee E, Wang K, Hui R, et al** (2012) Lipophilic analogs of zoledronate and risedronate inhibit Plasmodium geranylgeranyl diphosphate synthase (GGPPS) and exhibit potent antimalarial activity. *Proc Natl Acad Sci* **109**: 4058–4063
- Nolan TM, Vukašinović N, Liu D, Russinova E, Yin Y** (2020) Brassinosteroids: Multidimensional Regulators of Plant Growth, Development, and Stress Responses. *Plant Cell* **32**: 295–318
- Noland CL, Kattke MD, Diao J, Gloor SL, Pantua H, Reichelt M, Katakam AK, Yan D, Kang J, Zilberleyb I, et al** (2017) Structural insights into lipoprotein N-acylation by *Escherichia coli* apolipoprotein N-acyltransferase. *Proc Natl Acad Sci* **114**: E6044–E6053
- Northey JGB, Liang S, Jamshed M, Deb S, Foo E, Reid JB, McCourt P, Samuel MA** (2016) Farnesylation mediates brassinosteroid biosynthesis to regulate abscisic acid responses. *Nat Plants* **2**: 16114
- Novoveská L, Ross ME, Stanley MS, Pradelles R, Wasiolek V, Sassi J-F** (2019) Microalgal Carotenoids: A Review of Production, Current Markets, Regulations, and Future Direction. *Mar Drugs* **17**: 640
- Ntantie E, Gonyo P, Lorimer EL, Hauser AD, Schuld N, McAllister D, Kalyanaraman B, Dwinell MB, Auchampach JA, Williams CL** (2013) An Adenosine-Mediated Signaling Pathway Suppresses Prenylation of the GTPase Rap1B and Promotes Cell Scattering. *Sci Signal* **6**: ra39–ra39
- Nussinov R, Tsai C-J, Jang H** (2019) Oncogenic KRas mobility in the membrane and signaling response. *Semin Cancer Biol* **54**: 109–113
- Ochocki JD, Distefano MD** (2013) Prenyltransferase inhibitors: treating human ailments from cancer to parasitic infections. *Med Chem Commun* **4**: 476–492
- Ochocki JD, Igbavboa U, Wood WG, Arriaga EA, Wattenberg EV, Distefano MD** (2014) Evaluation of Prenylated Peptides for Use in Cellular Imaging and Biochemical Analysis. *In* AE Nixon, ed, *Ther. Pept. Humana Press, Totowa, NJ*, pp 213–223
- Ohya Y, Caplin BE, Qadota H, Tibbetts MF, Anraku Y, Pringle JR, Marshall MS** (1996) Mutational analysis of the  $\beta$ -subunit of yeast geranylgeranyl transferase I. *Mol Gen Genet MGG* **252**: 1–10
- Ohya Y, Goebel M, Goodman LE, Petersen-Björn S, Friesen JD, Tamanoi F, Anraku Y** (1991) Yeast CAL1 is a structural and functional homologue to the DPR1 (RAM) gene involved in ras processing. *J Biol Chem* **266**: 12356–12360
- Okada A, Shimizu T, Okada K, Kuzuyama T, Koga J, Shibuya N, Nojiri H, Yamane H** (2007) Elicitor induced activation of the methylerythritol phosphate pathway toward phytoalexins biosynthesis in rice. *Plant Mol Biol* **65**: 177–187
- Okuhara M, Kuroda Y, Goto T, Okamoto M, Terano H, Kohsaka M, Aoki H, Imanaka H** (1980) Studies on new phosphonic acid antibiotics. III. Isolation and characterization of FR-31564, FR-32863 and FR-33289. *J Antibiot (Tokyo)* **33**: 24–28
- Okuyama E, Okamoto Y, Yamazaki M, Satake M** (1996) Pharmacologically Active Components of a Peruvian Medicinal Plant, Huanarpo (*Jatropha cillata*). *Chem Pharm Bull (Tokyo)* **44**: 333–336
- Olzmann JA, Carvalho P** (2019) Dynamics and functions of lipid droplets. *Nat Rev Mol Cell Biol* **20**: 137–155
- OMS** (2019) WORLD MALARIA REPORT 2019. World Health Organization
- Onono FO, Morgan MA, Spielmann HP, Andres DA, Subramanian T, Ganser A, Reuter CWM** (2010) A Tagging-via-substrate Approach to Detect the Farnesylated Proteome Using Two-dimensional Electrophoresis Coupled with Western Blotting. *Mol Cell Proteomics* **9**: 742–751
- Ormeño E, Mévy JP, Vila B, Bousquet-Mélou A, Greff S, Bonin G, Fernandez C** (2007) Water deficit stress induces different monoterpene and sesquiterpene emission changes in Mediterranean species. Relationship between terpene emissions and plant water potential. *Chemosphere* **67**: 276–284

- Osoba OA, Roberts MF** (1994) Methyltransferase activity in *Ailanthus altissima* cell suspension cultures. *Plant Cell Rep* **13**: 277–281
- Ossowski T, Goulart MOF, Abreu FC de, Sant'Ana AEG, Miranda PRB, Costa C de O, Liwo A, Falkowski P, Zarzeczanska D** (2008) Determination of the pKa values of some biologically active and inactive hydroxyquinones. *J Braz Chem Soc* **19**: 175–183
- Padhye S, Dandawate P, Yusufi M, Ahmad A, Sarkar FH** (2012) Perspectives on medicinal properties of plumbagin and its analogs: MEDICINAL PROPERTIES OF PLUMBAGIN. *Med Res Rev* **32**: 1131–1158
- Paetzold H, Garms S, Bartram S, Wieczorek J, Urós-Gracia E-M, Rodríguez-Concepción M, Boland W, Strack D, Hause B, Walter MH** (2010) The Isogene 1-Deoxy-D-Xylulose 5-Phosphate Synthase 2 Controls Isoprenoid Profiles, Precursor Pathway Allocation, and Density of Tomato Trichomes. *Mol Plant* **3**: 904–916
- Palsuledesai CC, Ochocki JD, Kuhns MM, Wang Y-C, Warmka JK, Chernick DS, Wattenberg EV, Li L, Arriaga EA, Distefano MD** (2016) Metabolic Labeling with an Alkyne-modified Isoprenoid Analog Facilitates Imaging and Quantification of the Prenylome in Cells. *ACS Chem Biol* **11**: 2820–2828
- Pamanes EL** (2017) Unveiling the role of DXS-Interacting (DXI) proteins in the regulation of plastidial isoprenoid biosynthesis. UNIVERSITAT DE BARCELONA
- Parish CA, Smrcka AV, Rando RR** (1996) The Role of G Protein Methylation in the Function of a Geranylgeranylated  $\beta\gamma$  Isoform<sup>†</sup>. *Biochemistry* **35**: 7499–7505
- Park HJ, Park HC, Lee SY, Bohnert HJ, Yun D-J** (2011) Ubiquitin and Ubiquitin-like Modifiers in Plants. *J Plant Biol* **54**: 275–285
- Park H-W** (1997) Crystal Structure of Protein Farnesyltransferase at 2.25 Angstrom Resolution. *Science* **275**: 1800–1805
- Parmryd I, Andersson B, Dallner G** (1999) Protein prenylation in spinach chloroplasts. *Proc Natl Acad Sci* **96**: 10074–10079
- Parmryd I, Shipton CA, Swiezewska E, Andersson B, Dallner G** (1995) Identification of Spinach Farnesyl Protein Transferase. Dithiothreitol as an Acceptor in Vitro. *Eur J Biochem* **234**: 723–731
- Parmryd I, Shipton CA, Swiezewska E, Dallner G, Andersson B** (1997) Chloroplastic prenylated proteins. *FEBS Lett* **414**: 527–531
- Patai S, ed** (1980) The chemistry of ethers, crown ethers, hydroxyl groups and their sulphur analogues. Supplement E,1: ... Chichester u.a
- Pei Z** (1998) Role of Farnesyltransferase in ABA Regulation of Guard Cell Anion Channels and Plant Water Loss. *Science* **282**: 287–290
- Pendyala PR, Ayong L, Eatrises J, Schreiber M, Pham C, Chakrabarti R, Fidock DA, Allen CM, Chakrabarti D** (2008) Characterization of a PRL protein tyrosine phosphatase from *Plasmodium falciparum*☆. *Mol Biochem Parasitol* **158**: 1–10
- Pérez-Palacios T, Barroso MA, Ruiz J, Antequera T** (2015) A Rapid and Accurate Extraction Procedure for Analysing Free Amino Acids in Meat Samples by GC-MS. *Int J Anal Chem* **2015**: 1–8
- Petersen J, Ludewig A-K, Michael V, Bunk B, Jarek M, Baurain D, Brinkmann H** (2014) Chromera velia, Endosymbioses and the Rhodoplex Hypothesis—Plastid Evolution in Cryptophytes, Alveolates, Stramenopiles, and Haptophytes (CASH Lineages). *Genome Biol Evol* **6**: 666–684
- Phillips M, Leon P, Boronat A, Rodriguezconcepcion M** (2008a) The plastidial MEP pathway: unified nomenclature and resources. *Trends Plant Sci* **13**: 619–623
- Phillips MA, D'Auria JC, Gershenzon J, Pichersky E** (2008b) The *Arabidopsis thaliana* Type I Isopentenyl Diphosphate Isomerases Are Targeted to Multiple Subcellular Compartments and Have Overlapping Functions in Isoprenoid Biosynthesis. *Plant Cell* **20**: 677–696
- Phuyal S, Farhan H** (2019) Multifaceted Rho GTPase Signaling at the Endomembranes. *Front Cell Dev Biol* **7**: 127
- Pichersky E, Lewinsohn E** (2011) Convergent evolution in plant specialized metabolism. *Annu Rev Plant Biol* **62**: 549–566

- Pichersky E, Raguso RA** (2018) Why do plants produce so many terpenoid compounds? *New Phytol* **220**: 692–702
- Pieterse CMJ, Van der Does D, Zamioudis C, Leon-Reyes A, Van Wees SCM** (2012) Hormonal Modulation of Plant Immunity. *Annu Rev Cell Dev Biol* **28**: 489–521
- Pinner AL, Mueller TM, Alganem K, McCullumsmith R, Meador-Woodruff JH** (2020) Protein expression of prenyltransferase subunits in postmortem schizophrenia dorsolateral prefrontal cortex. *Transl Psychiatry* **10**: 3
- Polier G, Neumann J, Thuaud F, Ribeiro N, Gelhaus C, Schmidt H, Giaisi M, Köhler R, Müller WW, Proksch P, et al** (2012) The Natural Anticancer Compounds Rocaglamides Inhibit the Raf-MEK-ERK Pathway by Targeting Prohibitin 1 and 2. *Chem Biol* **19**: 1093–1104
- Porath J, L»»s T, Janson J-C** (1975) Agar derivatives for chromatography, electrophoresis and gel-bound enzymes. *J Chromatogr A* **103**: 49–62
- Poulter CD, Wiggins PL, Le AT** (1981) Farnesylpyrophosphate synthetase. A stepwise mechanism for the 1'-4 condensation reaction. *J Am Chem Soc* **103**: 3926–3927
- Preisig-Muller R, Muster G, Kindl H** (1994) Heat shock enhances the amount of prenylated Dnaj protein at membranes of glyoxysomes. *Eur J Biochem* **219**: 57–63
- Prior IA, Lewis PD, Mattos C** (2012) A Comprehensive Survey of Ras Mutations in Cancer. *Cancer Res* **72**: 2457–2467
- Quinzii CM, Hirano M** (2010) Coenzyme Q and mitochondrial disease. *Dev Disabil Res Rev* **16**: 183–188
- Qureshi BM, Schmidt A, Behrmann E, Bürger J, Mielke T, Spahn CMT, Heck M, Scheerer P** (2018) Mechanistic insights into the role of prenyl-binding protein PrBP/ $\delta$  in membrane dissociation of phosphodiesterase 6. *Nat Commun* **9**: 90
- Rajalingam K, Wunder C, Brinkmann V, Churin Y, Hekman M, Sievers C, Rapp UR, Rudel T** (2005) Prohibitin is required for Ras-induced Raf-MEK-ERK activation and epithelial cell migration. *Nat Cell Biol* **7**: 837–843
- Randall SK, Crowell DN** (1999) Protein Isoprenylation in Plants. *Crit Rev Biochem Mol Biol* **34**: 325–338
- Randall SK, Marshall MS, Crowell DN** (1993) Protein isoprenylation in suspension-cultured tobacco cells. *Plant Cell* **5**: 433–442
- Ranjan A, Vadassery J, Patel HK, Pandey A, Palaparthi R, Mithöfer A, Sonti RV** (2015) Upregulation of jasmonate biosynthesis and jasmonate-responsive genes in rice leaves in response to a bacterial pathogen mimic. *Funct Integr Genomics* **15**: 363–373
- Reiss Y, Brown MS, Goldstein JL** (1992) Divalent cation and prenyl pyrophosphate specificities of the protein farnesyltransferase from rat brain, a zinc metalloenzyme. *J Biol Chem* **267**: 6403–6408
- Ren S, Xing Y, Wang C, Jiang F, Liu G, Li Z, Jiang T, Zhu Y, Piao D** (2020) Fraxetin inhibits the growth of colon adenocarcinoma cells via the Janus kinase 2/signal transducer and activator of transcription 3 signalling pathway. *Int J Biochem Cell Biol* **125**: 105777
- Resh MD** (2006) Trafficking and signaling by fatty-acylated and prenylated proteins. *Nat Chem Biol* **2**: 584–590
- Reuber TL, Ausubel FM** (1996) Isolation of Arabidopsis genes that differentiate between resistance responses mediated by the RPS2 and RPM1 disease resistance genes. *Plant Cell* **8**: 241–249
- Rivera-Perez C, Nyati P, Noriega FG** (2015) A corpora allata farnesyl diphosphate synthase in mosquitoes displaying a metal ion dependent substrate specificity. *Insect Biochem Mol Biol* **64**: 44–50
- Rocks O** (2005) An Acylation Cycle Regulates Localization and Activity of Palmitoylated Ras Isoforms. *Science* **307**: 1746–1752
- Rockwell NC, Lagarias JC, Bhattacharya D** (2014) Primary endosymbiosis and the evolution of light and oxygen sensing in photosynthetic eukaryotes. *Front Ecol Evol*. doi: 10.3389/fevo.2014.00066
- Rodriguez-Concepcion M** (1999) The prenylation status of a novel plant calmodulin directs plasma membrane or nuclear localization of the protein. *EMBO J* **18**: 1996–2007
- Rodríguez-Concepción M, Ahumada I, Diez-Juez E, Sauret-Güeto S, Lois LM, Gallego F, Carretero-Paulet L, Campos N, Boronat A** (2001) 1-Deoxy-d-xylulose 5-phosphate reductoisomerase and plastid isoprenoid biosynthesis during

tomato fruit ripening: DXR and plastid isoprenoid biosynthesis in tomato. *Plant J* **27**: 213–222

**Rodríguez-Concepción M, Boronat A** (2015) Breaking new ground in the regulation of the early steps of plant isoprenoid biosynthesis. *Curr Opin Plant Biol* **25**: 17–22

**Rodríguez-Concepción M, Forés O, Martínez-García JF, González V, Phillips MA, Ferrer A, Boronat A** (2004) Distinct Light-Mediated Pathways Regulate the Biosynthesis and Exchange of Isoprenoid Precursors during Arabidopsis Seedling Development. *Plant Cell* **16**: 144–156

**Rodríguez-Concepción M, Toledo-Ortiz G, Yalovsky S, Caldelari D, Gruissem W** (2000) Carboxyl-methylation of prenylated calmodulin CaM53 is required for efficient plasma membrane targeting of the protein: Plasma membrane targeting of prenylated CaM53. *Plant J* **24**: 775–784

**Rohmer M** (2003) Mevalonate-independent methylerythritol phosphate pathway for isoprenoid biosynthesis. Elucidation and distribution. *Pure Appl Chem* **75**: 375–388

**Rohmer M, Knani M, Simonin P, Sutter B, Sahm H** (1993) Isoprenoid biosynthesis in bacteria: a novel pathway for the early steps leading to isopentenyl diphosphate. *Biochem J* **295**: 517–524

**Rohmer M, Seemann M, Horbach S, Bringer-Meyer S, Sahm H** (1996) Glyceraldehyde 3-Phosphate and Pyruvate as Precursors of Isoprenic Units in an Alternative Non-mevalonate Pathway for Terpenoid Biosynthesis. *J Am Chem Soc* **118**: 2564–2566

**Rood D** (1999) *Gas Chromatography Problem Solving and Troubleshooting*. 37:

**Rosquete MR, Davis DJ, Drakakaki G** (2018) The Plant Trans-Golgi Network: Not Just a Matter of Distinction. *Plant Physiol* **176**: 187–198

**Rossi S, Tabolacci C, Lentini A, Provenzano B, Carlomosti F, Frezzotti S, Beninati S** (2010) Anthraquinones danthron and quinizarin exert antiproliferative and antimetastatic activity on murine B16-F10 melanoma cells. *Anticancer Res* **30**: 445–449

**Rothbauer U, Zolghadr K, Tillib S, Nowak D, Schermelleh L, Gahl A, Backmann N, Conrath K, Muyldermans S, Cardoso MC, et al** (2006) Targeting and tracing antigens in live cells with fluorescent nanobodies. *Nat Methods* **3**: 887–889

**Ruan Y-L** (2014) Sucrose Metabolism: Gateway to Diverse Carbon Use and Sugar Signaling. *Annu Rev Plant Biol* **65**: 33–67

**Ruan Y-L, Jin Y, Yang Y-J, Li G-J, Boyer JS** (2010) Sugar Input, Metabolism, and Signaling Mediated by Invertase: Roles in Development, Yield Potential, and Response to Drought and Heat. *Mol Plant* **3**: 942–955

**Rudney H** (1957) The biosynthesis of beta-hydroxy-beta-methylglutaric acid. *J Biol Chem* **227**: 363–377

**Rudney H, Ferguson JJ** (1959) The biosynthesis of beta-hydroxy-beta-methylglutaryl coenzyme A in yeast. II. The formation of hydroxymethylglutaryl coenzyme A via the condensation of acetyl coenzyme A and acetoacetyl coenzyme A. *J Biol Chem* **234**: 1076–1080

**Ruiz-Sola MÁ, Coman D, Beck G, Barja MV, Colinas M, Graf A, Welsch R, Rütimann P, Bühlmann P, Bigler L, et al** (2016) *Arabidopsis* GERANYLGERANYL DIPHOSPHATE SYNTHASE 11 is a hub isozyme required for the production of most photosynthesis-related isoprenoids. *New Phytol* **209**: 252–264

**Ruiz-Sola MÁ, Rodríguez-Concepción M** (2012) Carotenoid Biosynthesis in Arabidopsis: A Colorful Pathway. *Arab Book* **10**: e0158

**Running MP, Lavy M, Sternberg H, Galichet A, Gruissem W, Hake S, Ori N, Yalovsky S** (2004) Enlarged meristems and delayed growth in *plp* mutants result from lack of CaaX prenyltransferases. *Proc Natl Acad Sci* **101**: 7815–7820

**Russell RGG** (2011) Bisphosphonates: the first 40 years. *Bone* **49**: 2–19

**Ruzicka L** (1953) The isoprene rule and the biogenesis of terpenic compounds. *Experientia* **9**: 357–367

**Saladié M, Wright LP, Garcia-Mas J, Rodriguez-Concepcion M, Phillips MA** (2014) The 2-C-methylerythritol 4-phosphate pathway in melon is regulated by specialized isoforms for the first and last steps. *J Exp Bot* **65**: 5077–5092

**Santos JCS dos, Barbosa O, Ortiz C, Berenguer-Murcia A, Rodrigues RC, Fernandez-Lafuente R** (2015) Importance of the Support Properties for Immobilization or Purification of Enzymes. *ChemCatChem* **7**: 2413–2432



- dos Santos JCS, Rueda N, Barbosa O, Fernández-Sánchez JF, Medina-Castillo AL, Ramón-Márquez T, Arias-Martos MC, Millán-Linares MC, Pedroche J, Yust M del M, et al (2015) Characterization of supports activated with divinyl sulfone as a tool to immobilize and stabilize enzymes via multipoint covalent attachment. Application to chymotrypsin. *RSC Adv* **5**: 20639–20649
- Saravanakumar K, Fan L, Fu K, Yu C, Wang M, Xia H, Sun J, Li Y, Chen J (2016) Cellulase from *Trichoderma harzianum* interacts with roots and triggers induced systemic resistance to foliar disease in maize. *Sci Rep* **6**: 35543
- Sass G, Tsamo AT, Chounda GAM, Nangmo PK, Sayed N, Bozzi A, Wu JC, Nkengfack AE, Stevens DA (2019) Vismione B Interferes with *Trypanosoma cruzi* Infection of Vero Cells and Human Stem Cell-Derived Cardiomyocytes. *Am J Trop Med Hyg* **101**: 1359–1368
- Scaffidi A, Waters MT, Sun YK, Skelton BW, Dixon KW, Ghisalberti EL, Flematti GR, Smith SM (2014) Strigolactone Hormones and Their Stereoisomers Signal through Two Related Receptor Proteins to Induce Different Physiological Responses in Arabidopsis. *Plant Physiol* **165**: 1221–1232
- Schafer WR, Rine J (1992) Protein Prenylation: Genes, Enzymes, Targets, and Functions. *Annu Rev Genet* **26**: 209–237
- Schluttenhofer C, Pattanaik S, Patra B, Yuan L (2014) Analyses of *Catharanthus roseus* and *Arabidopsis thaliana* WRKY transcription factors reveal involvement in jasmonate signaling. *BMC Genomics* **15**: 502
- Schoberer J, Strasser R (2011) Sub-Compartmental Organization of Golgi-Resident N-Glycan Processing Enzymes in Plants. *Mol Plant* **4**: 220–228
- Schramek N, Wang H, Römisch-Margl W, Keil B, Radykewicz T, Winzenhörlein B, Beerhues L, Bacher A, Rohdich F, Gershenzon J, et al (2010) Artemisinin biosynthesis in growing plants of *Artemisia annua*. A <sup>13</sup>C<sub>2</sub> study. *Phytochemistry* **71**: 179–187
- Schwender J, Seemann M, Lichtenthaler HK, Rohmer M (1996) Biosynthesis of isoprenoids (carotenoids, sterols, prenyl side-chains of chlorophylls and plastoquinone) via a novel pyruvate/glyceraldehyde 3-phosphate non-mevalonate pathway in the green alga *Scenedesmus obliquus*\*. *Biochem J* **316**: 73–80
- Schymanski EL, Singer HP, Slobodnik J, Ipolyi IM, Oswald P, Krauss M, Schulze T, Haglund P, Letzel T, Grosse S, et al (2015) Non-target screening with high-resolution mass spectrometry: critical review using a collaborative trial on water analysis. *Anal Bioanal Chem* **407**: 6237–6255
- Scott Reid T, Terry KL, Casey PJ, Beese LS (2004) Crystallographic Analysis of CaaX Prenyltransferases Complexed with Substrates Defines Rules of Protein Substrate Selectivity. *J Mol Biol* **343**: 417–433
- Sedaira H, Idriss KA, Seleim MM, Abdel-Aziz MS (1998) Use of Quinizarin as a Spectrophotometric Reagent for MgO Content Analysis of Portland Cement and Cement Clinker. *Monatshefte Für Chem Chem Mon* **129**: 49–58
- Selmar D, Kleinwächter M (2013) Stress Enhances the Synthesis of Secondary Plant Products: The Impact of Stress-Related Over-Reduction on the Accumulation of Natural Products. *Plant Cell Physiol* **54**: 817–826
- Shah D, Sajjad N, Ali R, Nazir N, Hassan S, Shah S (2019) Sugar Regulates Plant Growth and Development Under In Vitro Conditions. *Plant Signal. Mol. Elsevier*, pp 257–268
- Shao F, Merritt PM, Bao Z, Innes RW, Dixon JE (2002) A *Yersinia* Effector and a *Pseudomonas* Avirulence Protein Define a Family of Cysteine Proteases Functioning in Bacterial Pathogenesis. *Cell* **109**: 575–588
- Shen J, Zeng Y, Zhuang X, Sun L, Yao X, Pimpl P, Jiang L (2013) Organelle pH in the Arabidopsis Endomembrane System. *Mol Plant* **6**: 1419–1437
- Shipton CA, Parmryd I, Swiezewska E, Andersson B, Dallner G (1995) Isoprenylation of Plant Proteins *in Vivo*: Soprenylated Proteins Are Abundant In The Mitochondria And Nuclei Of Spinach. *J Biol Chem* **270**: 566–572
- Shirakawa R, Goto-Ito S, Goto K, Wakayama S, Kubo H, Sakata N, Trinh DA, Yamagata A, Sato Y, Masumoto H, et al (2020) A SNARE geranylgeranyltransferase essential for the organization of the Golgi apparatus. *EMBO J*. doi: 10.15252/embj.2019104120
- Siegel RL, Miller KD, Jemal A (2020) Cancer statistics, 2020. *CA Cancer J Clin* **70**: 7–30
- Siepen JA, Keevil E-J, Knight D, Hubbard SJ (2007) Prediction of Missed Cleavage Sites in Tryptic Peptides Aids Protein Identification in Proteomics. *J Proteome Res* **6**: 399–408

- Simkin AJ, Guirimand G, Papon N, Courdavault V, Thabet I, Ginis O, Bouzid S, Giglioli-Guivarc'h N, Clastre M** (2011) Peroxisomal localisation of the final steps of the mevalonic acid pathway in planta. *Planta* **234**: 903–914
- Simonetti A, Brito Querido J, Myasnikov AG, Mancera-Martinez E, Renaud A, Kuhn L, Hashem Y** (2016) eIF3 Peripheral Subunits Rearrangement after mRNA Binding and Start-Codon Recognition. *Mol Cell* **63**: 206–217
- Singh AP, Zhang Y, No J-H, Docampo R, Nussenzweig V, Oldfield E** (2010) Lipophilic Bisphosphonates Are Potent Inhibitors of Plasmodium Liver-Stage Growth. *Antimicrob Agents Chemother* **54**: 2987–2993
- Sjogren A-KM, Andersson KME, Liu M, Cutts BA, Karlsson C, Wahlstrom AM, Dalin M, Weinbaum C, Casey PJ, Tarkowski A, et al** (2007) GGTase-I deficiency reduces tumor formation and improves survival in mice with K-RAS–induced lung cancer. *J Clin Invest* **117**: 1294–1304
- Sjögren L, Floris M, Barghetti A, Völlmy F, Linding R, Brodersen P** (2018) Farnesylated heat shock protein 40 is a component of membrane-bound RISC in *Arabidopsis*. *J Biol Chem* **293**: 16608–16622
- Šlechtová T, Gilar M, Kalíková K, Tesařová E** (2015) Insight into Trypsin Miscleavage: Comparison of Kinetic Constants of Problematic Peptide Sequences. *Anal Chem* **87**: 7636–7643
- Sorek N, Akerman A, Yalovsky S** (2013) Analysis of Protein Prenylation and S-Acylation Using Gas Chromatography–Coupled Mass Spectrometry. In MP Running, ed, *G Protein-Coupled Recept. Signal. Plants*. Humana Press, Totowa, NJ, pp 121–134
- Sorek N, Gutman O, Bar E, Abu-Abied M, Feng X, Running MP, Lewinsohn E, Ori N, Sadot E, Henis YI, et al** (2011) Differential Effects of Prenylation and S-Acylation on Type I and II ROPS Membrane Interaction and Function. *Plant Physiol* **155**: 706–720
- Sousa DP de, Júnior GAS, Andrade LN, Calasans FR, Nunes XP, Barbosa-Filho JM, Batista JS** (2008) Structure and Spasmolytic Activity Relationships of Monoterpene Analogues Found in Many Aromatic Plants. *Z Für Naturforschung C* **63**: 808–812
- Srinivas G, Babykutty S, Sathiadevan PP, Srinivas P** (2007) Molecular mechanism of emodin action: Transition from laxative ingredient to an antitumor agent. *Med Res Rev* **27**: 591–608
- Stanley L, Yuan Y-W** (2019) Transcriptional Regulation of Carotenoid Biosynthesis in Plants: So Many Regulators, So Little Consensus. *Front Plant Sci* **10**: 1017
- Steele WJ, Gurin S** (1960) Biosynthesis of  $\beta$ -Carotene in *Eugenia graciZis*. **235**: 9
- Steyaert J, Kobilka BK** (2011) Nanobody stabilization of G protein-coupled receptor conformational states. *Curr Opin Struct Biol* **21**: 567–572
- Storck EM, Morales-Sanfrutos J, Serwa RA, Panyain N, Lanyon-Hogg T, Tolmachova T, Ventimiglia LN, Martin-Serrano J, Seabra MC, Wojciak-Stothard B, et al** (2019) Dual chemical probes enable quantitative system-wide analysis of protein prenylation and prenylation dynamics. *Nat Chem* **11**: 552–561
- Stringlis IA, de Jonge R, Pieterse CMJ** (2019) The Age of Coumarins in Plant–Microbe Interactions. *Plant Cell Physiol* **60**: 1405–1419
- Suazo KF, Hurben AK, Liu K, Xu F, Thao P, Sudheer Ch, Li L, Distefano MD** (2018) Metabolic Labeling of Prenylated Proteins Using Alkyne-Modified Isoprenoid Analogues. *Curr Protoc Chem Biol* **10**: e46
- Suazo KF, Schaber C, Palsuledesai CC, Odom John AR, Distefano MD** (2016) Global proteomic analysis of prenylated proteins in *Plasmodium falciparum* using an alkyne-modified isoprenoid analogue. *Sci Rep* **6**: 38615
- Subramani PA, Narala VR, Michael RD, Lomada D, Reddy MC** (2015) Molecular docking and simulation of Curcumin with Geranylgeranyl Transferase1 (GGTase1) and Farnesyl Transferase (FTase). *Bioinformation* **11**: 248–253
- Sun C, Zhao W, Wang X, Sun Y, Chen X** (2020) A pharmacological review of dicoumarol: an old natural anticoagulant agent. *Pharmacol Res* **105**: 193
- Suprun EV** (2019) Protein post-translational modifications – A challenge for bioelectrochemistry. *TrAC Trends Anal Chem* **116**: 44–60
- Sussmann RAC, Angeli CB, Peres VJ, Kimura EA, Katzin AM** (2011) Intraerythrocytic stages of *Plasmodium falciparum* biosynthesize vitamin E. *FEBS Lett* **585**: 3985–3991
- Swiezewska E, Thelin A, Dallner G, Andersson B, Ernster L** (1993) Occurrence of Prenylated Proteins in Plant Cells.

Biochem Biophys Res Commun **192**: 161–166

**Szkopińska A, Płochocka D** (2005) Farnesyl diphosphate synthase; regulation of product specificity. *Acta Biochim Pol* **52**: 45–55

**Tadros TF** (2013) Emulsion Formation, Stability, and Rheology. *In* TF Tadros, ed, *Emuls. Form. Stab.* Wiley-VCH Verlag GmbH & Co. KGaA, Weinheim, Germany, pp 1–75

**Talamond P, Verdeil J-L, Conéjéro G** (2015) Secondary Metabolite Localization by Autofluorescence in Living Plant Cells. *Molecules* **20**: 5024–5037

**Tam SW, Worcel M, Wyllie M** (2001) Yohimbine: a clinical review. *Pharmacol Ther* **91**: 215–243

**Tang X, Demiray M, Wirth T, Allemann RK** (2018) Concise synthesis of artemisinin from a farnesyl diphosphate analogue. *Bioorg Med Chem* **26**: 1314–1319

**Tetali SD** (2019) Terpenes and isoprenoids: a wealth of compounds for global use. *Planta* **249**: 1–8

**Therrien M, Chang HC, Solomon NM, Karim FD, Wassarman DA, Rubin GM** (1995) KSR, a novel protein kinase required for RAS signal transduction. *Cell* **83**: 879–888

**Thissen JA, Casey PJ** (1993) Microsomal membranes contain a high affinity binding site for prenylated peptides. *J Biol Chem* **268**: 13780–13783

**Tissier A, Morgan JA, Dudareva N** (2017) Plant Volatiles: Going ‘In’ but not ‘Out’ of Trichome Cavities. *Trends Plant Sci* **22**: 930–938

**Tissier A, Ziegler J, Vogt T** (2014) Specialized Plant Metabolites: Diversity and Biosynthesis. *In* G-J Krauss, DH Nies, eds, *Ecol. Biochem.* Wiley-VCH Verlag GmbH & Co. KGaA, Weinheim, Germany, pp 14–37

**Tonhosolo R, D’Alexandri FL, Genta FA, Wunderlich G, Gozzo FC, Eberlin MN, Peres VJ, Kimura EA, Katzin AM** (2005) Identification, molecular cloning and functional characterization of an octaprenyl pyrophosphate synthase in intraerythrocytic stages of *Plasmodium falciparum*. *Biochem J* **392**: 117–126

**Tonhosolo R, D’Alexandri FL, de Rosso VV, Gazarini ML, Matsumura MY, Peres VJ, Merino EF, Carlton JM, Wunderlich G, Mercadante AZ, et al** (2009) Carotenoid Biosynthesis in Intraerythrocytic Stages of *Plasmodium falciparum*. *J Biol Chem* **284**: 9974–9985

**Toyama T, Tahara M, Nagamune K, Arimitsu K, Hamashima Y, Palacpac NMQ, Kawaide H, Horii T, Tanabe K** (2012) Gibberellin Biosynthetic Inhibitors Make Human Malaria Parasite *Plasmodium falciparum* Cells Swell and Rupture to Death. *PLoS ONE* **7**: e32246

**Tracewell CA, Vrettos JS, Bautista JA, Frank HA, Brudvig GW** (2001) Carotenoid Photooxidation in Photosystem II. *Arch Biochem Biophys* **385**: 61–69

**Tsai H-H, Rodríguez-Celma J, Lan P, Wu Y-C, Vélez-Bermúdez IC, Schmidt W** (2018) Scopoletin 8-Hydroxylase-Mediated Fraxetin Production Is Crucial for Iron Mobilization. *Plant Physiol* **177**: 194–207

**Tsiatsiani L, Heck AJR** (2015) Proteomics beyond trypsin. *FEBS J* **282**: 2612–2626

**Tuinman AA, Thomas DA, Cook KD, Xue C-B, Naider F, Becker JM** (1991) Mass spectrometric signature of S-prenylated cysteine peptides. *Anal Biochem* **193**: 173–177

**Twair A, Al-Okla S, Zarkawi M, Abbady AQ** (2014) Characterization of camel nanobodies specific for superfolder GFP fusion proteins. *Mol Biol Rep* **41**: 6887–6898

**Ueoka H, Sasaki K, Miyawaki T, Ichino T, Tatsumi K, Suzuki S, Yamamoto H, Sakurai N, Suzuki H, Shibata D, et al** (2020) A Cytosol-Localized Geranyl Diphosphate Synthase from *Lithospermum erythrorhizon* and Its Molecular Evolution. *Plant Physiol* **182**: 1933–1945

**Vallim MA, Fernandes L, Alspaugh JA** (2004) The RAM1 gene encoding a protein-farnesyltransferase  $\beta$ -subunit homologue is essential in *Cryptococcus neoformans*. *Microbiology* **150**: 1925–1935

**Vanstraelen M, Benková E** (2012) Hormonal Interactions in the Regulation of Plant Development. *Annu Rev Cell Dev Biol* **28**: 463–487

**Verebova V, Belej D, Joniova J, Jurasekova Z, Miskovsky P, Kozar T, Horvath D, Stanicova J, Huntosova V** (2016) Deeper insights into the drug defense of glioma cells against hydrophobic molecules. *Int J Pharm* **503**: 56–67

- Villette C, Zumsteg J, Schaller H, Heintz D** (2018) Non-targeted metabolic profiling of BW312 *Hordeum vulgare* semi dwarf mutant using UHPLC coupled to QTOF high resolution mass spectrometry. *Sci Rep* **8**: 13178
- Vranová E, Coman D, Gruissem W** (2013) Network Analysis of the MVA and MEP Pathways for Isoprenoid Synthesis. *Annu Rev Plant Biol* **64**: 665–700
- Vukašinović N, Russinova E** (2018) BRexit: Possible Brassinosteroid Export and Transport Routes. *Trends Plant Sci* **23**: 285–292
- Wagner H, Bladt S, Zgainski EM** (1984) *Plant Drug Analysis*. doi: 10.1007/978-3-662-02398-3
- Walsh CT, Garneau-Tsodikova S, Gatto GJ** (2005) Protein Posttranslational Modifications: The Chemistry of Proteome Diversifications. *Angew Chem Int Ed* **44**: 7342–7372
- Walter MH, Hans J, Strack D** (2002) Two distantly related genes encoding 1-deoxy-d-xylulose 5-phosphate synthases: differential regulation in shoots and apocarotenoid-accumulating mycorrhizal roots: DXS gene organization and regulation. *Plant J* **31**: 243–254
- Wang C, Gale M, Keller BC, Huang H, Brown MS, Goldstein JL, Ye J** (2005) Identification of FBL2 As a Geranylgeranylated Cellular Protein Required for Hepatitis C Virus RNA Replication. *Mol Cell* **18**: 425–434
- Wang H, Zou D, Xie K, Xie M** (2014a) Antibacterial mechanism of fraxetin against *Staphylococcus aureus*. *Mol Med Rep* **10**: 2341–2345
- Wang J, Xu C, Wong YK, Li Y, Liao F, Jiang T, Tu Y** (2019a) Artemisinin, the Magic Drug Discovered from Traditional Chinese Medicine. *Engineering* **5**: 32–39
- Wang J, Yao X, Huang J** (2017) New tricks for human farnesyltransferase inhibitor: cancer and beyond. *MedChemComm* **8**: 841–854
- Wang M, Casey PJ** (2016) Protein prenylation: unique fats make their mark on biology. *Nat Rev Mol Cell Biol* **17**: 110–122
- Wang Q, Quan S, Xiao H** (2019b) Towards efficient terpenoid biosynthesis: manipulating IPP and DMAPP supply. *Bioresour Bioprocess* **6**: 6
- Wang Y, Ries A, Wu K, Yang A, Crawford NM** (2010) The *Arabidopsis* Prohibitin Gene *PHB3* Functions in Nitric Oxide–Mediated Responses and in Hydrogen Peroxide–Induced Nitric Oxide Accumulation. *Plant Cell* **22**: 249–259
- Wang Y-C, Dozier JK, Beese LS, Distefano MD** (2014b) Rapid Analysis of Protein Farnesyltransferase Substrate Specificity Using Peptide Libraries and Isoprenoid Diphosphate Analogues. *ACS Chem Biol* **9**: 1726–1735
- Wang Z, Yang L, Yang X, Zhang X** (2014c) Advances in the Chemical Synthesis of Artemisinin. *Synth Commun* **44**: 1987–2003
- Wasser N** (2018) Synthèse et évaluation de l'activité anti-Leishmania d'anthranoïdes issus du genre *Psorospermum* (Hypericaceae) utilisé en médecine traditionnelle camerounaise. *Chimie médicinale*. Université de Strasbourg, Strasbourg
- Waters BM** (2011) Moving magnesium in plant cells: Commentary. *New Phytol* **190**: 510–513
- Wegner A, Weindl D, Jäger C, Sapcariu SC, Dong X, Stephanopoulos G, Hiller K** (2014) Fragment Formula Calculator (FFC): Determination of Chemical Formulas for Fragment Ions in Mass Spectrometric Data. *Anal Chem* **86**: 2221–2228
- Wennerberg K** (2005) The Ras superfamily at a glance. *J Cell Sci* **118**: 843–846
- Westendorf J** (1993) Anthranoid Derivatives — General Discussion. *In* PAGM De Smet, K Keller, R Hänsel, RF Chandler, eds, *Adverse Eff. Herb. Drugs 2*. Springer Berlin Heidelberg, Berlin, Heidelberg, pp 105–118
- Whyte DB, Kirschmeier P, Hockenberry TN, Nunez-Oliva I, James L, Catino JJ, Bishop WR, Pai J-K** (1997) K- and N-Ras Are Geranylgeranylated in Cells Treated with Farnesyl Protein Transferase Inhibitors. *J Biol Chem* **272**: 14459–14464
- Wilkins JA, Kaasik K, Chalkley RJ, Burlingame AL** (2020) Characterization of Prenylated C-terminal Peptides Using a Thiopropyl-based Capture Technique and LC-MS/MS. *Mol Cell Proteomics* **19**: 1005–1016

- Wills VS, Allen C, Holstein SA, Wiemer DF** (2015) Potent Triazole Bisphosphonate Inhibitor of Geranylgeranyl Diphosphate Synthase. *ACS Med Chem Lett* **6**: 1195–1198
- Wills VS, Metzger JI, Allen C, Varney ML, Wiemer DF, Holstein SA** (2017) Bishomoisoprenoid triazole bisphosphonates as inhibitors of geranylgeranyl diphosphate synthase. *Bioorg Med Chem* **25**: 2437–2444
- Wilson AL, Erdman RA, Castellano F, Maltese WA** (1998) Prenylation of Rab8 GTPase by type I and type II geranylgeranyl transferases. *Biochem J* **333**: 497–504
- Wotske M, Wu Y, Wolters DA** (2012) Liquid chromatographic analysis and mass spectrometric identification of farnesylated peptides. *Anal Chem* **84**: 6848–6855
- Wu J-R, Wang L-C, Lin Y-R, Weng C-P, Yeh C-H, Wu S-J** (2017) The Arabidopsis *heat-intolerant 5* (*hit5*)/*enhanced response to aba 1* (*era1*) mutant reveals the crucial role of protein farnesylation in plant responses to heat stress. *New Phytol* **213**: 1181–1193
- Xu N, Shen N, Wang X, Jiang S, Xue B, Li C** (2015) Protein prenylation and human diseases: a balance of protein farnesylation and geranylgeranylation. *Sci China Life Sci* **58**: 328–335
- Xu P, Zhao P-X, Cai X-T, Mao J-L, Miao Z-Q, Xiang C-B** (2020) Integration of Jasmonic Acid and Ethylene Into Auxin Signaling in Root Development. *Front Plant Sci* **11**: 271
- Xu Y, Chang Pfl, Liu D, Narasimhan ML, Raghothama KG, Hasegawa PM, Bressan RA** (1994) Plant Defense Genes Are Synergistically Induced by Ethylene and Methyl Jasmonate. *Plant Cell* 1077–1085
- Yahya MS, Syafiq M, Ashton-Butt A, Ghazali A, Asmah S, Azhar B** (2017) Switching from monoculture to polyculture farming benefits birds in oil palm production landscapes: Evidence from mist netting data. *Ecol Evol* **7**: 6314–6325
- Yalovsky S** (2011) Protein Prenylation CaaX Processing in Plants. *The Enzymes*. Elsevier, pp 163–182
- Yalovsky S, Rodriguez-Concepcion M, Bracha K, Toledo-Ortiz G, Grissem W** (2000) Prenylation of the Floral Transcription Factor APETALA1 Modulates Its Function. *Plant Cell* **12**: 1257
- Yalovsky S, Rodriguez-Concepcion M, Grissem W** (1999) Lipid modifications of proteins – slipping in and out of membranes. *Trends Plant Sci* **4**: 439–445
- Yang J, Chen Y-N, Xu Z-X, Mou Y, Zheng L-R** (2016) Alteration of RhoA Prenylation Ameliorates Cardiac and Vascular Remodeling in Spontaneously Hypertensive Rats. *Cell Physiol Biochem* **39**: 229–241
- Yang J, Duan G, Li C, Liu L, Han G, Zhang Y, Wang C** (2019) The Crosstalks Between Jasmonic Acid and Other Plant Hormone Signaling Highlight the Involvement of Jasmonic Acid as a Core Component in Plant Response to Biotic and Abiotic Stresses. *Front Plant Sci* **10**: 1349
- Yang J, Kulkarni K, Manolaridis I, Zhang Z, Dodd RB, Mas-Droux C, Barford D** (2011) Mechanism of Isoprenylcysteine Carboxyl Methylation from the Crystal Structure of the Integral Membrane Methyltransferase ICMT. *Mol Cell* **44**: 997–1004
- Yeh E, DeRisi JL** (2011) Chemical Rescue of Malaria Parasites Lacking an Apicoplast Defines Organelle Function in Blood-Stage Plasmodium falciparum. *PLoS Biol* **9**: e1001138
- Yokoyama K, Gillespie JR, Van Voorhis WC, Buckner FS, Gelb MH** (2008) Protein geranylgeranyltransferase-I of Trypanosoma cruzi. *Mol Biochem Parasitol* **157**: 32–43
- Yoshida T, Obata T, Feil R, Lunn JE, Fujita Y, Yamaguchi-Shinozaki K, Fernie AR** (2019) The Role of Abscisic Acid Signaling in Maintaining the Metabolic Balance Required for Arabidopsis Growth under Nonstress Conditions. *Plant Cell* **31**: 84–105
- Yurugi H, Marini F, Weber C, David K, Zhao Q, Binder H, Désaubry L, Rajalingam K** (2017) Targeting prohibitins with chemical ligands inhibits KRAS-mediated lung tumours. *Oncogene* **36**: 4778–4789
- Zadra C, Borgogni A, Marucchini C** (2006) Quantification of Jasmonic Acid by SPME in Tomato Plants Stressed by Ozone. *J Agric Food Chem* **54**: 9317–9321
- Zappey HW** (1991) Isomerization and Fragmentation of Aliphatic Thioether Radical Cations in the Gas Phase: Ion-Neutral Complexes in the Reactions of Metastable Ethyl Propyl Thioether Ions. *J CHEM SOC PERKIN TRANS* **6**
- Zeidler J, Schwender J, Müller C, Wiesnerb J** (1998) Inhibition of the Non-Mevalonate I-Deoxy-D-xylulose-5-phosphate Pathway of Plant Isoprenoid Biosynthesis by Fosmidomycin. **53**: 7

- Zeng Q, Wang X, Running MP** (2007) Dual Lipid Modification of Arabidopsis G  $\gamma$ -Subunits Is Required for Efficient Plasma Membrane Targeting. *Plant Physiol* **143**: 1119–1131
- Zengin G, Degirmenci N, Alpsoy L, Aktumsek A** (2016) Evaluation of antioxidant, enzyme inhibition, and cytotoxic activity of three anthraquinones (alizarin, purpurin, and quinizarin). *Hum Exp Toxicol* **35**: 544–553
- Zhang C-Y, Wu Y-L, Zhang P, Chen Z-Z, Li H, Chen L-X** (2019) Anti-inflammatory Lathyrane Diterpenoids from *Euphorbia lathyris*. *J Nat Prod* **82**: 756–764
- Zhang F, Liu W, Xia J, Zeng J, Xiang L, Zhu S, Zheng Q, Xie H, Yang C, Chen M, et al** (2018) Molecular Characterization of the 1-Deoxy-D-Xylulose 5-Phosphate Synthase Gene Family in *Artemisia annua*. *Front Plant Sci* **9**: 952
- Zhang H, Li Z-X** (2014) A Type-III Insect Geranylgeranyl Diphosphate Synthase with a Novel Catalytic Property. *Protein Pept Lett* **21**: 615–623
- Zhao J, Yao S, Lin D** (2009) Adsorbents for Expanded Bed Adsorption: Preparation and Functionalization. *Chin J Chem Eng* **17**: 678–687
- Zhou D, White RH** (1991) Early steps of isoprenoid biosynthesis in *Escherichia coli*. *Biochem J* **273**: 627–634
- Zhu JK, Bressan RA, Hasegawa PM** (1993) Isoprenylation of the plant molecular chaperone ANJ1 facilitates membrane association and function at high temperature. *Proc Natl Acad Sci* **90**: 8557–8561
- Zimbres FM, Valenciano AL, Merino EF, Florentin A, Holderman NR, He G, Gawarecka K, Skorupinska-Tudek K, Fernández-Murga ML, Swiezewska E, et al** (2020) Metabolomics profiling reveals new aspects of dolichol biosynthesis in *Plasmodium falciparum*. *Sci Rep* **10**: 13264
- Zucca P, Fernandez-Lafuente R, Sanjust E** (2016) Agarose and Its Derivatives as Supports for Enzyme Immobilization. *Molecules* **21**: 1577
- Zucca P, Sanjust E** (2014) Inorganic Materials as Supports for Covalent Enzyme Immobilization: Methods and Mechanisms. *Molecules* **19**: 14139–14194
- Zurzolo C, Simons K** (2016) Glycosylphosphatidylinositol-anchored proteins: Membrane organization and transport. *Biochim Biophys Acta BBA - Biomembr* **1858**: 632–639



# 10 ANNEXES





**Annexe 1 Compounds and molecular formula of the 346 compounds investigated in non-targeted metabolomic analysis by HPLC-QTOF-MS/MS**

Compounds	Molecular formula (M)	M - methyl (CH3)	M - CH3 + VIL	M - CH3 + VIM	M + palmitoyl	M + GSH	M + CoA	M + M
SVIL	C20H38N4O6							
CVIM	C19H36N4O5S2					C29H51N7O11S3	C40H70N11O20P3S3	C38H70N8O10S4
KCVIM	C25H48N6O6S2					C35H63N9O12S3	C46H82N13O21P3S3	C50H94N12O12S4
GQKCVIM	C32H59N9O9S2					C42H74N12O15S3	C53H93N16O24P3S3	C64H116N18O18S4
RGQKCVIM	C38H71N13O10S2					C48H86N16O16S3	C59H105N20O25P3S3	C76H140N26O20S4
KRGQKCVIM	C44H83N15O11S2					C54H98N18O17S3	C65H117N22O26P3S3	C88H164N30O22S4
CVIL peptide	C20H38N4O5S					C30H53N7O11S2	C41H72N11O20P3S2	C40H74N8O10S2
KCVIL	C26H50N6O6S					C36H65N9O12S2	C47H84N13O21P3S2	C52H98N12O12S2
GQKCVIL	C33H61N9O9S					C43H76N12O15S2	C54H95N16O24P3S2	C66H120N18O18S2
RGQKCVIL	C39H73N13O10S					C49H88N16O16S2	C60H107N20O25P3S2	C78H144N26O20S2
KRGQKCVIL	C45H85N15O11S					C55H100N18O17S2	C66H119N22O26P3S2	C90H168N30O22S2
S-geranyl-L-Cysteine methyl ester	C14H25NO2S	C13H23NO2S	C30H54N4O5S	C29H52N4O5S2	C29H53NO3S			
KS-geranyl-L-Cysteine methyl ester	C20H37N3O3S	C19H35N3O3S	C36H66N6O6S	C35H64N6O6S2	C35H65N3O4S			
GQKS-geranyl-L-Cysteine methyl ester	C27H48N6O6S	C26H46N6O6S	C43H77N9O9S	C42H75N9O9S2	C42H76N6O7S			
RGQKS-geranyl-L-Cysteine methyl ester	C33H60N10O7S	C32H58N10O7S	C49H89N13O10S	C48H87N13O10S2	C48H88N10O8S			
KRGQKS-geranyl-L-Cysteine methyl ester	C39H72N12O8S	C38H70N12O8S	C55H101N15O11S	C54H99N15O11S2	C54H100N12O9S			
S-farnesyl-L-cysteine methyl ester	C19H33NO2S	C18H31NO2S	C35H62N4O5S	C34H60N4O5S2	C34H61NO3S			
KS-farnesyl-L-Cysteine methyl ester	C25H45N3O3S	C24H43N3O3S	C41H74N6O6S	C40H72N6O6S2	C40H73N3O4S			
GQKS-farnesyl-L-Cysteine methyl ester	C32H56N6O6S	C31H54N6O6S	C48H85N9O9S	C47H83N9O9S2	C47H84N6O7S			
RGQKS-farnesyl-L-Cysteine methyl ester	C38H68N10O7S	C37H66N10O7S	C54H97N13O10S	C53H95N13O10S2	C53H96N10O8S			
KRGQKS-farnesyl-L-Cysteine methyl ester	C44H80N12O8S	C43H78N12O8S	C60H109N15O11S	C59H107N15O11S2	C59H108N12O9S			
S-geranylgeranyl-L-cysteine methyl ester	C24H41NO2S	C23H39NO2S	C40H70N4O5S	C39H68N4O5S2	C39H69NO3S			
KS-geranylgeranyl-L-Cysteine methyl ester	C30H53N3O3S	C29H51N3O3S	C46H82N6O6S	C45H80N6O6S2	C45H81N3O4S			
GQKS-geranylgeranyl-L-Cysteine methyl ester	C37H64N6O6S	C36H62N6O6S	C53H93N9O9S	C52H91N9O9S2	C52H92N6O7S			
RGQKS-geranylgeranyl-L-Cysteine methyl ester	C43H76N10O7S	C42H74N10O7S	C59H105N13O10S	C58H103N13O10S2	C58H104N10O8S			
KRGQKS-geranylgeranyl-L-Cysteine methyl ester	C49H88N12O8S	C48H86N12O8S	C65H117N15O11S	C64H115N15O11S2	C64H116N12O9S			
S-phytyl-L-cysteine methyl ester	C24H47NO2S	C23H45NO2S	C40H76N4O5S	C39H74N4O5S2	C39H75NO3S			
KS-phytyl-L-Cysteine methyl ester	C30H59N3O3S	C29H57N3O3S	C46H88N6O6S	C45H86N6O6S2	C45H87N3O4S			
GQKS-phytyl-L-Cysteine methyl ester	C37H70N6O6S	C36H68N6O6S	C53H99N9O9S	C52H97N9O9S2	C52H98N6O7S			
RGQKS-phytyl-L-Cysteine methyl ester	C43H82N10O7S	C42H80N10O7S	C59H111N13O10S	C58H109N13O10S2	C58H110N10O8S			
KRGQKS-phytyl-L-Cysteine methyl ester	C49H94N12O8S	C48H92N12O8S	C65H123N15O11S	C64H121N15O11S2	C64H122N12O9S			
S-geranylarnesyl-L-cysteine methyl ester	C29H49NO2S	C28H47NO2S	C45H78N4O5S	C44H76N4O5S2	C44H77NO3S			
KS-geranylarnesyl-L-cysteine methyl ester	C35H61N3O3S	C34H59N3O3S	C51H90N6O6S	C50H88N6O6S2	C50H89N3O4S			
GQKS-geranylarnesyl-L-cysteine methyl ester	C42H72N6O6S	C41H70N6O6S	C58H101N9O9S	C57H99N9O9S2	C57H100N6O7S			
RGQKS-geranylarnesyl-L-cysteine methyl ester	C48H84N10O7S	C47H82N10O7S	C64H113N13O10S	C63H111N13O10S2	C63H112N10O8S			
KRGQKS-geranylarnesyl-L-cysteine methyl ester	C54H96N12O8S	C53H94N12O8S	C70H125N15O11S	C69H123N15O11S2	C69H124N12O9S			
S-presqualene-L-cysteine methyl ester	C34H57NO2S	C33H55NO2S	C50H86N4O5S	C49H84N4O5S2	C49H85NO3S			
S-solanesyl-L-cysteine methyl esterA43	C49H81NO2S	C48H79NO2S	C65H110N4O5S	C64H108N4O5S2	C64H109NO3S			
S-palmitoyl-L-cysteine methyl ester	C20H39NO3S	C19H37NO3S	C36H68N4O6S	C35H66N4O6S2	C35H67NO4S			
KS-palmitoyl-L-cysteine methyl ester	C26H51N3O4S	C25H49N3O4S	C42H80N6O7S	C41H78N6O7S2	C41H79N3O5S3O5S			
GQKS-palmitoyl-L-cysteine methyl ester	C33H62N6O7S	C32H60N6O7S	C49H91N9O10S	C48H89N9O10S2	C48H90N6O8S			
RGQKS-palmitoyl-L-cysteine methyl ester	C39H74N10O8S	C38H72N10O8S	C55H103N13O11S	C54H101N13O11S2	C54H102N10O9S			
KRGQKS-palmitoyl-L-cysteine methyl ester	C45H86N12O9S	C44H84N12O9S	C61H115N15O12S	C60H113N15O12S2	C60H114N12O10S			
S-Heptaprenyl-L-cysteine methyl ester	C39H65NO2S	C38H63NO2S	C55H94N4O5S	C54H92N4O5S2	C54H93NO3S			
KS-Heptaprenyl-L-cysteine methyl ester	C45H77N3O3S	C44H75N3O3S	C61H106N6O6S	C60H104N6O6S2	C60H105N3O4S			
GQKS-Heptaprenyl-L-cysteine methyl ester	C52H88N6O6S	C51H86N6O6S	C68H117N9O9S	C67H115N9O9S2	C67H116N6O7S			

Compounds	Molecular formula (M)	M - methyl (CH3)	M - CH3 + VIL	M - CH3 + VIM	M + palmitoyl	M + GSH	M + CoA	M + M
RGQKS-Heptaprenyl-L-cysteine methyl ester	C58H100N10O7S	C57H98N10O7S	C74H129N13O10S	C73H127N13O10S2	C73H128N10O8S			
KRGQKS-Heptaprenyl-L-cysteine methyl ester	C64H112N12O8S	C63H110N12O8S	C80H141N15O11S	C79H139N15O11S2	C79H140N12O9S			
S-3,7-Dimethyl-2-octen-1-yl-L-cysteine methyl ester	C14H27NO2S	C13H25NO2S	C30H56N4O5S	C29H54N4O5S2	C29H55N3O3S			
KS-3,7-Dimethyl-2-octen-1-yl-L-cysteine methyl ester	C20H39N3O3S	C19H37N3O3S	C36H68N6O6S	C35H66N6O6S2	C35H67N3O4S			
GQKS-3,7-Dimethyl-2-octen-1-yl-L-cysteine methyl ester	C27H50N6O6S	C26H48N6O6S	C43H79N9O9S	C42H77N9O9S2	C42H78N6O7S			
RGQKS-3,7-Dimethyl-2-octen-1-yl-L-cysteine methyl ester	C33H62N10O7S	C32H60N10O7S	C49H91N13O10S	C48H89N13O10S2	C48H90N10O8S			
KRGQKS-3,7-Dimethyl-2-octen-1-yl-2-dodecen-1-yl-L-cysteine methyl ester	C39H74N12O8S	C38H72N12O8S	C55H103N15O11S	C54H101N15O11S2	C54H102N12O9S			
S-3,7,11-Trimethyl-2-dodecen-1-yl-L-cysteine methyl ester	C19H37NO2S	C18H35NO2S	C35H66N4O5S	C34H64N4O5S2	C34H65N3O3S			
KS-3,7,11-Trimethyl-2-dodecen-1-yl-L-cysteine methyl ester	C25H49N3O3S	C24H47N3O3S	C41H78N6O6S	C40H76N6O6S2	C40H77N3O4S			
GQKS-3,7,11-Trimethyl-2-dodecen-1-yl-L-cysteine methyl ester	C32H60N6O6S	C31H58N6O6S	C48H89N9O9S	C47H87N9O9S2	C47H88N6O7S			
RGQKS-3,7,11-Trimethyl-2-dodecen-1-yl-L-cysteine methyl ester	C38H72N10O7S	C37H70N10O7S	C54H101N13O10S	C53H99N13O10S2	C53H100N10O8S			
KRGQKS-3,7,11-Trimethyl-2-dodecen-1-yl-L-cysteine methyl ester	C44H84N12O8S	C43H82N12O8S	C60H113N15O11S	C59H111N15O11S2	C59H112N12O9S			
S-10,11-Dihydrofarnesyl-L-cysteine methyl ester	C19H35NO2S	C18H33NO2S	C35H64N4O5S	C34H62N4O5S2	C34H63N3O3S			
KS-10,11-Dihydrofarnesyl-L-cysteine methyl ester	C25H47N3O3S	C24H45N3O3S	C41H76N6O6S	C40H74N6O6S2	C40H75N3O4S			
GQKS-10,11-Dihydrofarnesyl-L-cysteine methyl ester	C32H58N6O6S	C31H56N6O6S	C48H87N9O9S	C47H85N9O9S2	C47H86N6O7S			
RGQKS-10,11-Dihydrofarnesyl-L-cysteine methyl ester	C38H70N10O7S	C37H68N10O7S	C54H99N13O10S	C53H97N13O10S2	C53H98N10O8S			
KRGQKS-10,11-Dihydrofarnesyl-L-cysteine methyl ester	C44H82N12O8S	C43H80N12O8S	C60H111N15O11S	C59H109N15O11S2	C59H110N12O9S			
S-3,7,11,15-Tetramethyl-2,6-hexadecadien-1-yl-L-cysteine methyl ester	C24H45NO2S	C23H43NO2S	C40H74N4O5S	C39H72N4O5S2	C39H73N3O3S			
KS-3,7,11,15-Tetramethyl-2,6-hexadecadien-1-yl-L-cysteine methyl ester	C30H57N3O3S	C29H55N3O3S	C46H86N6O6S	C45H84N6O6S2	C45H85N3O4S			
GQKS-3,7,11,15-Tetramethyl-2,6-hexadecadien-1-yl-L-cysteine methyl ester	C37H68N6O6S	C36H66N6O6S	C53H97N9O9S	C52H95N9O9S2	C52H96N6O7S			
RGQKS-3,7,11,15-Tetramethyl-2,6-hexadecadien-1-yl-L-cysteine methyl ester	C43H80N10O7S	C42H78N10O7S	C59H109N13O10S	C58H107N13O10S2	C58H108N10O8S			
KRGQKS-3,7,11,15-Tetramethyl-2,6-hexadecadien-1-yl-L-cysteine methyl ester	C49H92N12O8S	C48H90N12O8S	C65H121N15O11S	C64H119N15O11S2	C64H120N12O9S			
S-10,11-Dihydrogeranylgeranyl-L-cysteine methyl ester	C24H43NO2S	C23H41NO2S	C40H72N4O5S	C39H70N4O5S2	C39H71NO3S			
KS-10,11-Dihydrogeranylgeranyl-L-cysteine methyl ester	C30H55N3O3S	C29H53N3O3S	C46H84N6O6S	C45H82N6O6S2	C45H83N3O4S			
GQKS-10,11-Dihydrogeranylgeranyl-L-cysteine methyl ester	C37H66N6O6S	C36H64N6O6S	C53H95N9O9S	C52H93N9O9S2	C52H94N6O7S			
RGQKS-10,11-Dihydrogeranylgeranyl-L-cysteine methyl ester	C43H78N10O7S	C42H76N10O7S	C59H107N13O10S	C58H105N13O10S2	C58H106N10O8S			
KRGQKS-10,11-Dihydrogeranylgeranyl-L-cysteine methyl ester	C49H90N12O8S	C48H88N12O8S	C65H119N15O11S	C64H117N15O11S2	C64H118N12O9S			

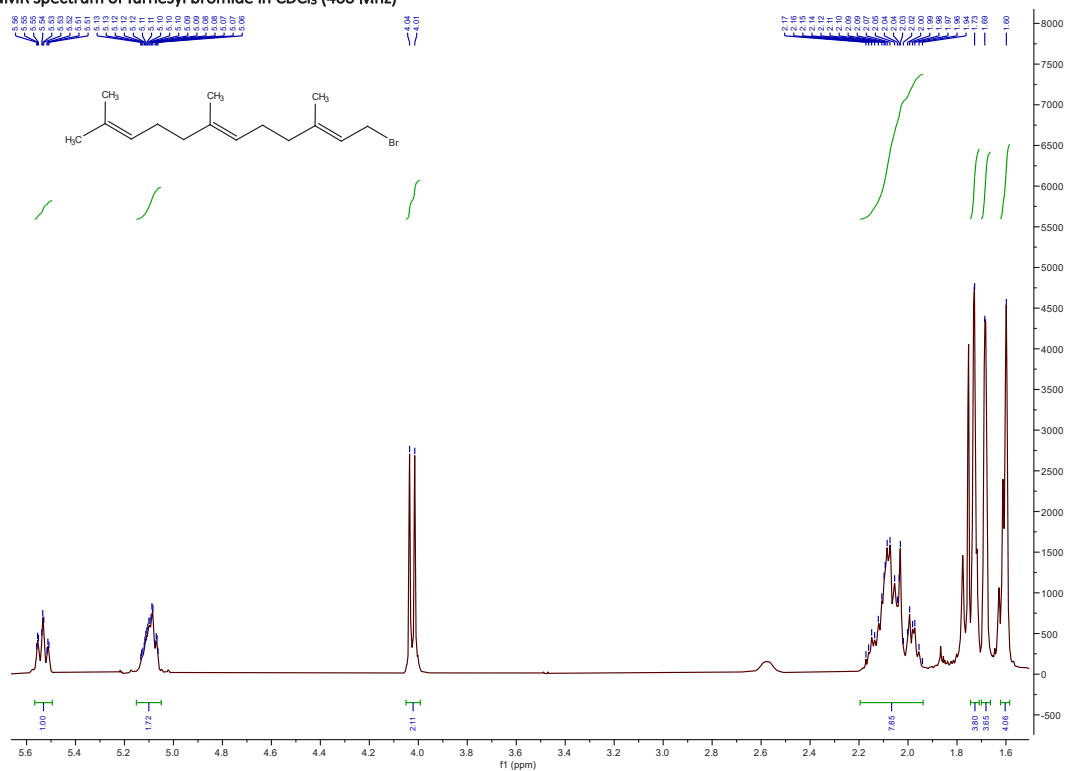
**Annexe 2 Examples of proteins found to be immunoprecipitated with our GFP-sensor expressed in tobacco plant or BY-2 cells.**

Stress proteins (red), chloroplast and photosynthesis associated proteins (green), isoprenoids biosynthesis or protein prenylation enzymes (orange) and other proteins (blue) increased specifically with the prenylated GFP-CVI (L/M) as compared to negative control (Ctr) or FOS-inhibited BY-2 cells expressing GFP-CVIL. Some examples of proteins illustrating the background (grey)

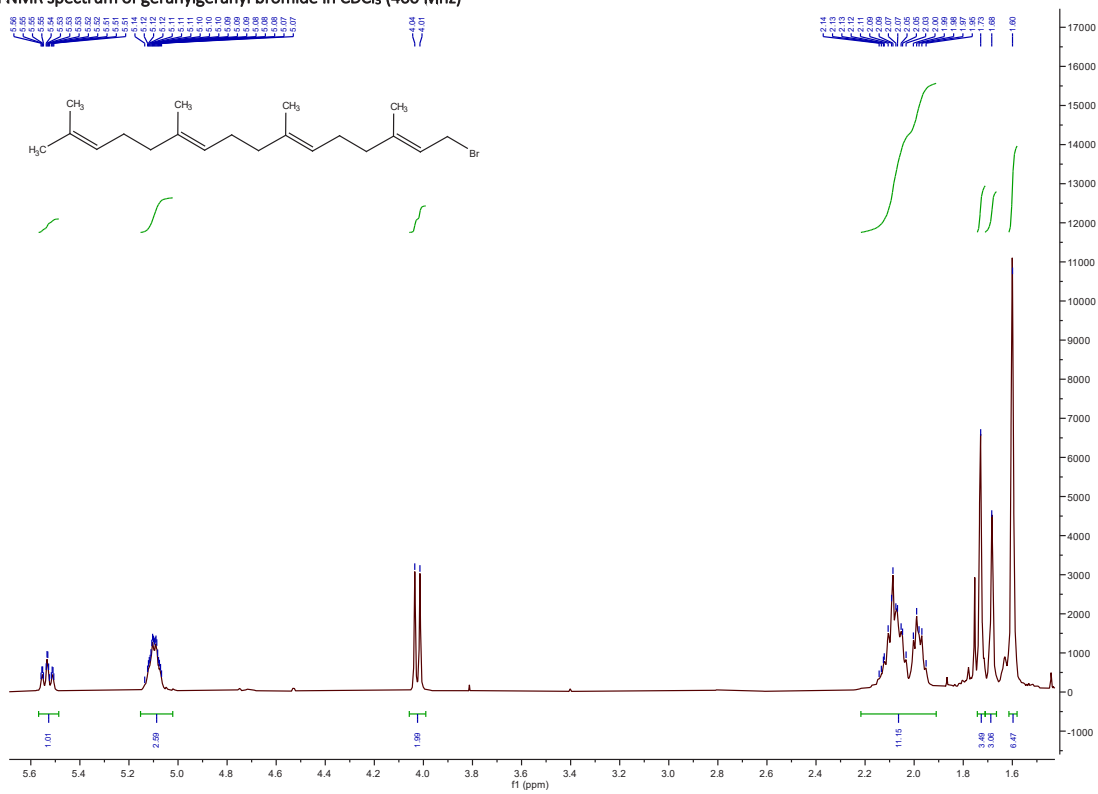
accession	description	protein_set_size	#sequences	#peptide_matches	750 mg leaf										2.5g leaf				2.5g BY-2 cells					
					GFP-Trap_MA					GFP-CVIM					GFP-SVIL		GFP-CVIL		FOSL		Incl.		Ctr	
					Ctr	GFP-CVIM	GFP-CVIM	GFP-CVIM	GFP-CVIM	GFP-CVIM	GFP-CVIM	GFP-SVIL	GFP-CVIL	GFP-CVIL	FOSL	Incl.	Incl.	Ctr	Ctr	Ctr	Ctr			
Nben1015f00449g06008.1	sp P02827 HSP70_XENLA*** Heat shock 70 kDa protein PR013126 (Heat	1963,29	26	30	2	48	34	26	25	25	30	83	33	65	20									
Nben1015f00992g01021.1	sp P17156 HSP72_MOUSE*** Heat shock-related 70 kDa protein 2 PR012	959,62	14	14	1	48	15	11	15	15	13	40	16	30	13									
Nben1015f12366g00008.1	sp Q07459 HSP71_BST*** Heat shock 70 kDa protein 1A/B PR013126 (H	247,757	31	38	6	22	34	41	41	38	36	139	52	99	35									
Nben1015f0488g05003.1	sp P17479 HST1B_MOUSE*** Heat shock 70 kDa protein 1B PR013126 (H	2447,227	33	37	5	22	31	43	37	37	42	112	44	81	28									
Nben1015f05389g00010.1	sp P34930 HST1A_PIG*** Heat shock 70 kDa protein 1A PR013126 (Heat	2338,27	32	37	5	22	47	37	35	33	47	103	46	81	26									
Nben1015f07272g02012.1	sp P17156 HSP72_MOUSE*** Heat shock-related 70 kDa protein 2 PR012	2248,041	29	30	6	22	52	39	37	34	50	113	47	83	27									
Nben1015f00449g00003.1	sp P34931 HST1L_HUMAN*** Heat shock 70 kDa protein 1-like PR01312	2334,331	29	30	5	22	46	34	30	27	47	104	44	77	28									
Nben1015f01655g01015.1	sp Q04888 HST1L_HKCSA*** Heat shock 70 kDa protein 1-like PR013126	1183,156	13	17	2	22	34	26	22	21	24	53	27	45	15									
Nben1015f02124g01003.1	sp P41753 HSP70_ACHIK*** Heat shock 70 kDa protein PR013126 (Heat	1064,80	14	15	4	22	22	26	21	19	17	22	52	22	39	18								
Nben1015f00119g03011.1	sp Q7Y0C6 HSP71_CANFA*** Heat shock 70 kDa protein 1 PR013126 (He	616,677	7	8	2	21	24	24	17	16	15	13	23	14	18	14								
Nben1015f11553g02038.1	sp Q07U33 HSP22_CAPH*** Heat shock-related 70 kDa protein 2 PR013	982,52	17	17	1	21	14	11	16	16	10	16	11	12	16									
Nben1015f0899g00005.1	sp P34932 HSP72_HUMAN*** Heat shock-related 70 kDa protein 2 PR012	957,28	18	19	1	21	15	11	16	15	10	16	11	12	16									
Nben1015f02972g00008.1	sp P27541 HSP70_BRUNJA*** Heat shock 70 kDa protein PR013126 (Hea	727,51	13	13	1	21	14	11	13	12	9	13	10	11	15									
Nben1015f13703g01006.1	sp P17066 HSP76_HUMAN*** Heat shock 70 kDa protein 6 PR013126 (H	322,29	4	4	4	21	13	9	9	9	8	13	6	9	6									
Nben1015f01091g00036.1	sp Q04903 FNTB_PEA*** Protein farnesyltransferase subunit beta 1 PR008	219,41	3	3			9																	
Nben1015f11530g00001.1	sp Q1G8B9 RL13_LACDA*** 50S ribosomal protein L15 PR005749 (Riboso	782,97	11	13				4	4	5	21	18												
Nben1015f01050g02008.1	sp Q3A705 RL15_CBRH*** 50S ribosomal protein L15 PR005749 (Riboso	710,25	10	12			5		3	4	18	16												
Nben1015f09517g02006.1	sp Q67561 RL15_AQUAE*** 50S ribosomal protein L15 PR005749 (Riboso	387,227	6	7			5		2	3	7	8												
Nben1015f06697g00014.1	sp Q5HQ15 CLPB_STAEK*** Chaperone protein Cpb1 PR001270 (CpbA/B fa	642,29	10	10			2				1		5	8	8									
Nben1015f15972g01024.1	sp Q8CKD0 CLPB_PASMU*** Chaperone protein Cpb1 PR001270 (CpbA/B fa	575,74	10	10			2				1		4	7	8									
Nben1015f00441g09016.1	sp Q8XG88 CLPB_CLDPE*** Chaperone protein Cpb1 PR001270 (CpbA/B fa	435,62	8	8			2				1		3	6	5									
Nben1015f00063g13005.1	sp A1547320.1*** malate dehydrogenase L1ENYH-403 PR001557 (L-acti	426,56	6	6	1		2	1					7	7	7									
Nben1015f02222g05009.1	sp Q8P6A0 CLPB_XANCP*** Chaperone protein Cpb1 PR001270 (CpbA/B fa	146,02	3	3	1		2		1					2										
Nben1015f00705g06002.1	sp B7H092 CLPX_ACIB3*** ATP-dependent Cbp binding subu	100,37	1	1						1														
Nben1015f01339g04007.1	sp P93227 FNTA_SOLLC*** Protein farnesyltransferase/geranylgerany	106,51	2	2			4																	
Nben1015f00116g01002.1	sp Q2R0H9 RECA_RH0H*** Protein RecA1 PR013765 (DNA recombina	61,4	1	1			2																	
Nben1015f02369g00003.1	sp Q08191 HSP71_ORYSA*** Heat shock 70 kDa protein 1 PR013126 (He	176,85	26	26	5		11	20	28	25	23	36	93	37	71	22								
Nben1015f01999g06011.1	sp Q08W82 DNAK_GIRAC*** Chaperone protein Dnak1 PR013126 (Heat s	1909,87	30	31	2		1	2	12	10	12	16	34	36	37									
Nben1015f03206g01008.1	sp Q653H7 ARFR_ORYS3*** Auxin response factor 18 PR003311 (AUX/AA	46,54	1	1			1					9	5	6	8									
Nben1015f02172g20008.1	sp A15661210.1*** soluble N-ethylmaleimide-sensitive factor adaptor	54,82	1	1			1																	
Nben1015f0808g04018.1	sp P27492 CB23_TOBAC*** Chlorophyll a-b binding protein 16, chloroplast	644,59	10	10	12		14	15	15	2	2		16											
Nben1015f01455g01031.1	sp P27493 CB23_TOBAC*** Chlorophyll a-b binding protein 21, chloroplast	585,18	9	9	8		11	15	1	2	1		12											
Nben1015f01548g00002.1	sp P27494 CB23_TOBAC*** Chlorophyll a-b binding protein 36, chloroplast	406,2	7	7	6		12	14	1				13											
Nben1015f0808g04005.1	sp P27495 CB24_TOBAC*** Chlorophyll a-b binding protein 40, chloroplast	153,68	2	2	6		7	6	1	2			6											
Nben1015f19423g00008.1	sp AQJ010 PSBA_AETGR*** Photosystem CII protein PR000484 (Photo	229	3	3			7	6	2	2			5											
Nben1015f00568g04011.1	sp B0L8M9 PSRC_GLIAB*** Photosystem II CP43 reaction center protein	473,23	6	7			8	9	1				4											
Nben1015f02104g00001.1	sp Q49L18 PSBA_EUCGG*** Photosystem CII protein PR000484 (Photo	217,63	3	3			6	5	2	2			3											
Nben1015f08973g01010.1	sp Q01667 CAB6_ABATH*** Chlorophyll a-b binding protein 6, chloroplast	286,83	5	5			6	4					2											
Nben1015f00417g20006.1	sp Q7NFWE PSAE_GLOW*** Photosystem I reaction center subunit I PR0	332,97	5	5			5	7					3											
Nben1015f00737g00003.1	sp Q78502 PSAD_GLUTH*** Photosystem I reaction center subunit II PR0	338,45	5	7	1		5	5	2	1			5											
Nben1015f01241g00003.1	sp Q3V513 PSRC_AOCLC*** Cytochrome b559 subunit alpha PR002217 (P	87,65	2	2			2	1					2											
Nben1015f00611g01005.1	sp Q25D11 POR_DALCA*** Protochlorophyllide reductase, chloroplast	212,45	4	4	4		1		1				4											
Nben1015f02351g07005.1	sp P27522 CB13_SOLLC*** Chlorophyll a-b binding protein 8, chloroplast	228,38	3	4			1						3											
Nben1015f0986g01021.1	sp QBYR22 ACS3_NOSS1*** Magnesium-protoporphyrin IX monomethy	132,87	3	3									2											
Nben1015f00044g02010.1	sp Q04616 CUTA_ABATH*** Protein CURVATURE THYLAKOID 1A, chlorop	297,14	5	5			11	10																
Nben1015f02606g01021.1	sp Q40459 PSB0_TOBAC*** Oxygen-evolving enhancer protein 1, chlorop	436,94	8	8			10	11																
Nben1015f02029g00004.1	sp Q40459 PSB0_TOBAC*** Oxygen-evolving enhancer protein 1, chlorop	435,56	8	8			10	11																
Nben1015f00027g040024.1	sp P51193 PSAF_PORPU*** Photosystem I reaction center subunit III PR0	83,28	2	2			3	2	2	1														
Nben1015f00304g05008.1	sp Q5SM84 PSB5_TOBAC*** Photosystem II 23 kDa protein, chloroplast	140,78	3	3			3	4																
Nben1015f00568g04011.1	sp Q3V513 PSRC_AOCLC*** Photosystem I P700 chlorophyll a apoprotein	132,03	2	2			3	3																
Nben1015f02972g01016.1	sp P27493 CB23_TOBAC*** Chlorophyll a-b binding protein 13, chloroplast	139,65	2	2									3											
Nben1015f00509g06001.1	sp Q7NFWE PSAE_GLOW*** Photosystem I reaction center subunit I PR0	114,42	2	2																				
Nben1015f01208g01014.1	sp A0A361 PSB8_COFAR*** Photosystem II CP47 reaction center protein I	58,99	1	1			1																	
Nben1015f01797g03034.1	sp Q9SLU5 PSAC_ABATH*** Photosystem I reaction center subunit psak d	44,45	1	1																				

accession	description	protein_set	seqs	#peptides	matrix	750 mg leaf						2.5g leaf			2.5g BY-2 cells			
						GFP-Trap MA			GFP-Trap v1			GFP-Trap v1			FOSL			
						Ctrl	GFP-CVIM	GFP-CVIM	GFP-CVIM	GFP-CVIM	GFP-CVIM	GFP-SVIL	GFP-CVIL	FOSL	Indl.	Ctrl		
Nben101Sc106249g03002.1	sp Q55087 CHLP_SVNY3 *** Geranylgeranyl diphosphate reductase I (PR003042)		541,78	9	5		10	5	1	1	1	1	1	1	1	1	1	1
Nben101Sc10070g00005.1	sp Q9LUE2 TPS18_ARATH *** Terpenoid synthase 18 (PR008930) (Terpenoid cycl)		306,92	5	9		1	1	3	1	1	1	1	1	1	1	1	1
Nben101Sc10071g02011.1	sp Q9LUE2 TPS19_ARATH *** Terpenoid synthase 19 (PR008930) (Terpenoid cycl)		260,06	5	5		1	1	3	1	1	1	1	1	1	1	1	1
Nben101Sc10531g02006.1	sp Q95071 ACD_1_EPDS *** Acyl carrier protein (PR002321) (Acyl carrier protein)		84,23	2	2		1	1	1	1	1	1	1	1	1	1	1	1
Nben101Sc100225g00008.1	sp AT5G54160.1 *** O-methyltransferase 1 (LENGTH=363) (PR016461) (O-methyltr		102,8	2	2		1	1	1	1	1	1	1	1	1	1	1	1
Nben101Sc103855g00003.1	sp AT5G27200.1 *** acyl carrier protein 5 (LENGTH=139) (PR003231) (Acyl carrier prote		75,15	1	1		1	1	1	1	1	1	1	1	1	1	1	1
Nben101Sc105206g03007.1	sp Q80642 PSTB1_ARATH *** Geranylgeranyl transferase type-1 subunit beta (PR		43,49	1	1		1	1	1	1	1	1	1	1	1	1	1	1
Nben101Sc12058g00007.1	emb CDX95231.1   *. * - BnaA02g296700 (Brassica napus)		832,23	12	12		1	3	1	27	30							
Nben101Sc10294g00020.1	emb CDY44410.1   *. * - BnaA02g296700 (Brassica napus)		539,23	8	8		1	2	1	17	21							
Nben101Sc100024g04006.1	sp P83970 PMAL_MHEAT *** Plasma membrane ATPase (PR001757) (P-type ATPa		183,36	3	3		2	1	1	1	1							3
Nben101Sc10308g01001.1	sp Q9N9W6 ANR53_MOUSE *** Ankyrin repeat domain-containing protein 42 (PR0		257,3	3	3		6	6	1	2	1	2						
Nben101Sc100216g00005.1	sp Q9N9W6 ANR53_HUMAN *** Ankyrin repeat domain-containing protein 53 (PR		228,68	3	3		5	5	1	1	1	2						
Nben101Sc103991g00007.1	sp Q9XKQ2 PRX28_ARATH *** Peroxiredoxin-28 (PR012336) (Thioredoxin-like fold)		201,65	3	3			1	1									
Nben101Sc117140g00001.1	sp Q94KU1 6PGD1_SPIOL *** 6-phosphogluconate dehydrogenase, decarboxyl		213,49	5	5	3												
Nben101Sc104673g00004.1	sp Q94KU1 6PGD1_SPIOL *** 6-phosphogluconate dehydrogenase, decarboxyl		177,85	4	4	2												
Nben101Sc100493g00020.1	sp P94040 GL31_ARATH *** Germin-like protein subfamily 3 member 1 (PR01192		133,66	3	3													
Nben101Sc116542g01003.1	sp Q5M8G4 LR040_XENTR *** Leucine-rich repeat-containing protein 40 (PR01216		94,83	2	2													
Nben101Sc101175g01018.1	sp Q61541 GL52_DRTS1 *** Germin-like protein 51 (PR001929) (Germin) (GO:003		48,89	1	1													
Nben101Sc108709g00009.1	sp Q06241 ASGL_BRANA *** L-ascorbate oxidase homologue		33,04	1	1													
Nben101Sc11178g01001.1	sp A02248 CYF_GOSBA *** Apocytochrome f (PR002325) (Cytochrome f) (PR0033		83,35	1	1		1	1	1	1	1	1	1	1	1	1	1	1
Nben101Sc102614g00017.1	sp Q95YM4 TPS1_ARATH *** Alpha-alpha-trehalose-phosphate synthase (UDP-Fo		246,17	4	4													5
Nben101Sc100426g02026.1	sp Q95U25 TZFA_ARATH *** Transcription initiation factor 1IF subunit alpha (PR00		160	3	3													2
Nben101Sc10091g00003.1	sp P45739 CATA_HELAN *** Catalase (PR011614) (Catalase core domain) (PR01180		1189,35	13	18	23		8	4	71	59	143	159	7	12	6		
Nben101Sc14996g00009.1	sp Q9M5L6 CATA_CAPAN *** Catalase (PR002226) (Catalase haem-binding site) (P		2983,91	33	47	163		84	59	188	193	299	241	4	6	3		
Nben101Sc11178g01008.1	sp Q9G9W4 RBL_DAUCA *** Ribulose biphosphate carboxylase large chain (PR000		2825,26	37	44	86		49	51	151	155	372	340					
Nben101Sc100173g09004.1	sp AG689 RBL_PHALU *** Ribulose biphosphate carboxylase large chain (PR002		2655,24	35	42	78		38	37	126	130	310	279					
Nben101Sc107103g01021.1	sp Q9G9W4 RBL_DAUCA *** Ribulose biphosphate carboxylase large chain (PR000		1152,58	17	18	47		29	26	62	69	188	163					
Nben101Sc12593g00016.1	sp Q49C11 RBL_CUSSA *** Ribulose biphosphate carboxylase large chain (PR000		560,64	8	8	31		17	20	45	47	132	121					
Nben101Sc101734g01047.1	sp Q06022 RBL_BETPA *** Ribulose biphosphate carboxylase large chain (PR000		1165,5	16	18	23		16	14	76	81	132	133					
Nben101Sc13103g01029.1	sp AT463870.1 *** fructose-biphosphate aldolase 2 (LENGTH=398) (PR000741) (Fru		1615,08	21	22	7		13	13	24	24	96	71					
Nben101Sc100197g02006.1	sp AT1G62020.1 *** Coatomer, alpha subunit (LENGTH=1216) (PR011048) (Cytochrom		6716,689	85	100	33		35	24	76	60	88	106	457	457	482		
Nben101Sc120652g01025.1	sp AT1G62020.1 *** Coatomer, alpha subunit (LENGTH=1216) (PR011048) (Cytochrom		4251,86	54	63	26		25	16	58	50	67	81	369	322	399		
Nben101Sc100628g00010.1	sp AT1G62020.1 *** Coatomer, alpha subunit (LENGTH=1216) (PR011048) (Cytochrom		5005,51	73	82	25		23	18	59	45	69	81	342	348	367		
Nben101Sc101777g03022.1	sp P30925 EF2_SUILO *** Elongation factor 2 (PR000640) (Translation elongation		3506,11	41	47	24		14	11	36	40	35	35	84	114	103		
Nben101Sc102360.2 *** Coatomer, beta' subunit (LENGTH=970) (PR016453) (Coatomer bet		4479,361	50	63	22		14	12	37	29	39	51	295	248	288			
Nben101Sc105044g01007.1	sp AT1G52360.2 *** Coatomer, beta' subunit (LENGTH=970) (PR016453) (Coatomer bet		4242,181	46	60	22		14	12	36	29	36	48	241	233	270		
Nben101Sc102461g09001.1	sp AT1G62020.1 * - Coatomer, alpha subunit (LENGTH=1216) (PR011048) (WD40/YVTN		2035,31	26	32	11		14	12	25	20	33	37	135	132	135		
Nben101Sc101998g03010.1	sp Q27131 EF2_METTH *** Elongation factor 2 (PR000640) (Translation elongation		3379,67	39	45	24		13	10	31	35	34	34	82	110	99		
Nben101Sc100127g01005.1	sp AT1G52360.2 *** Coatomer, beta' subunit (LENGTH=970) (PR016453) (Coatomer bet		3388,361	42	51	12		13	8	30	26	36	46	216	206	228		
Nben101Sc100646g04009.1	sp Q98418 RL3_PRRNA *** 50S ribosomal protein L3 (PR000597) (Ribosomal prote		2360,25	36	40	1		2	2	17	15	46	53	147	152	124		
Nben101Sc14636g01013.1	sp Q9M5W2 RL3_PRRNA *** 50S ribosomal protein L3 (PR000597) (Ribosomal prote		2365,04	34	38	1		2	2	15	15	45	55	141	149	131		
Nben101Sc100160g01005.1	sp Q9M3V8 RS6_ASPOF *** 40S ribosomal protein S6 (PR001377) (Ribosomal prote		1818,21	24	27			2	3	12	9	47	50	102	108	86		
Nben101Sc101779g05002.1	sp Q9M3V8 RS6_ASPOF *** 40S ribosomal protein S6 (PR001377) (Ribosomal prote		1740,43	24	27			2	3	14	9	39	43	88	92	85		
Nben101Sc100478g06002.1	sp Q9M3V8 RS6_ASPOF *** 40S ribosomal protein S6 (PR001377) (Ribosomal prote		1552,14	23	25			2	3	14	9	37	40	79	83	73		
Nben101Sc103113g02002.1	sp Q9HP88 RL6_HALSA *** 50S ribosomal protein L6 (PR000702) (Ribosomal prote		1514,41	17	19			2	1	16	19	37	36	129	172	123		
Nben101Sc14717g01000.1	sp P46300 RS4_SOLTU *** 40S ribosomal protein S4 (PR000876) (Ribosomal prote		1607,84	23	26			1	1	22	20	47	36	182	199	152		
Nben101Sc103156g00009.1	sp P46300 RS4_SOLTU *** 40S ribosomal protein S4 (PR000876) (Ribosomal prote		1585,29	23	25			1	1	22	18	48	36	173	190	125		
Nben101Sc132851g00036.1	sp P46300 RS4_SOLTU *** 40S ribosomal protein S4 (PR000876) (Ribosomal prote		1173,17	18	18			1	1	19	17	40	32	156	175	107		
Nben101Sc10898g02022.1	sp P46300 RS4_SOLTU *** 40S ribosomal protein S4 (PR000876) (Ribosomal prote		1194,79	18	18			1	1	20	17	41	32	150	167	101		
Nben101Sc100749g04008.1	sp A25700 RS7_METLZ *** 30S ribosomal protein S7 (PR000235) (Ribosomal prote		1375,36	18	22			1	1	3	4	46	40	91	111	76		
Nben101Sc104288g01012.1	sp B1L735 RS7_KORCO *** 30S ribosomal protein S7 (PR000235) (Ribosomal prote		1278,47	17	22			1	1	2	3	44	39	88	109	73		
Nben101Sc106848g10001.1	sp BOR8D0 RS7_HALS3 *** 30S ribosomal protein S7 (PR000235) (Ribosomal prote		1275,91	16	19			1	1	3	3	39	34	81	102	70		
Nben101Sc100294g03004.1	sp Q9NF97 RL4_PRLUA *** 60S ribosomal protein L4 (PR002136) (Ribosomal prote		2870,89	37	44	1		1	1	24	25	85	106	206	236	188		
Nben101Sc11023g00002.1	sp Q9NF97 RL4_PRLUA *** 60S ribosomal protein L4 (PR002136) (Ribosomal prote		2592,12	35	38	1		1	1	27	28	77	96	201	236	171		
Nben101Sc100496g01001.1	sp Q9NF97 RL4_PRLUA *** 60S ribosomal protein L4 (PR002136) (Ribosomal prote		2785,96	35	42	1		1	1	21	21	61	73	170	209	140		
Nben101Sc102473g01007.1	sp Q9SF40 RL4A_ARATH *** 60S ribosomal protein L4-1 (PR002136) (Ribosomal pr		1875,83	26	29	1		1	1	22	23	65	79	156	192	140		
Nben101Sc104418g12003.1	sp Q6UNT2 RL5_CUCSA *** 60S ribosomal protein L5 (PR005484) (Ribosomal prote		1916,82	21	26			1	1	17	17	36	59	139	134	101		
Nben101Sc103209g00029.1	sp P34091 RL6_MESCR *** 60S ribosomal protein L6 (PR000915) (60S ribosomal pr		1155,85	19	19			1	1	19	16	53	45	119	138	111		
Nben101Sc103977g01005.1	sp P34091 RL6_MESCR *** 60S ribosomal protein L6 (PR000915) (60S ribosomal pr		1099,35	18	19			1	1	12	11	45	36	101	120	84		

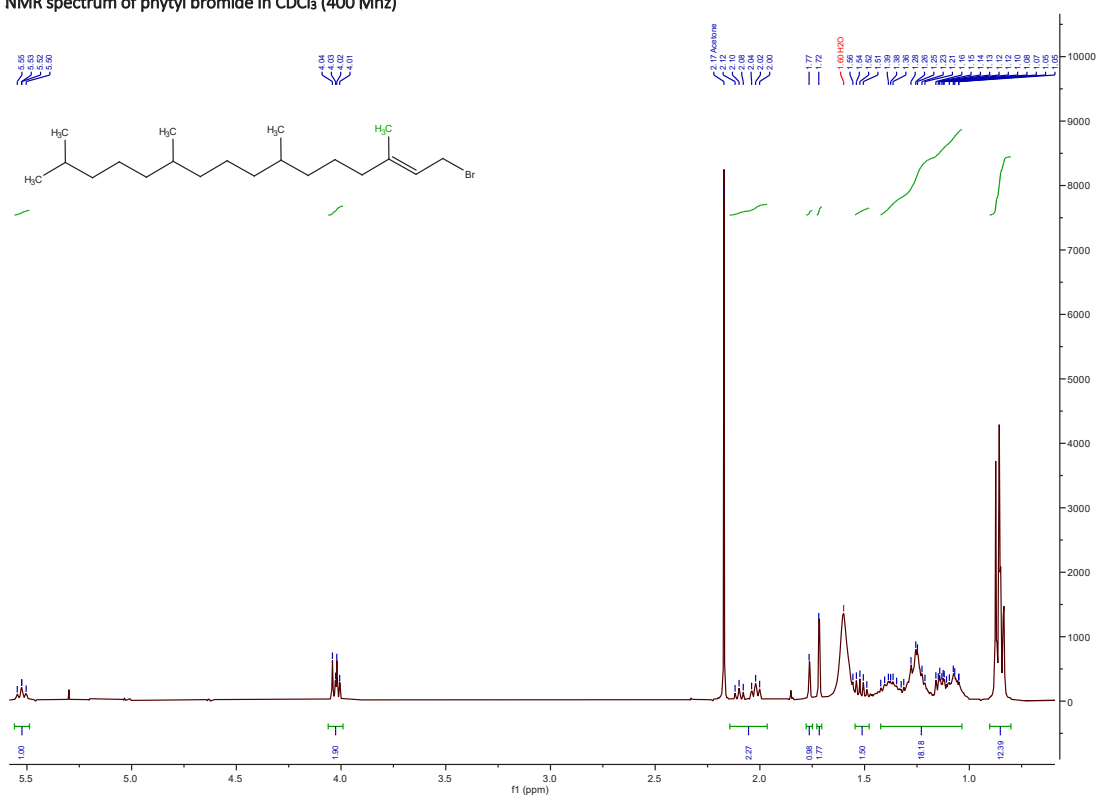
Annexe 3 <sup>1</sup>H NMR spectrum of farnesyl bromide in CDCl<sub>3</sub> (400 Mhz)



Annexe 4 <sup>1</sup>H NMR spectrum of geranylgeranyl bromide in CDCl<sub>3</sub> (400 Mhz)

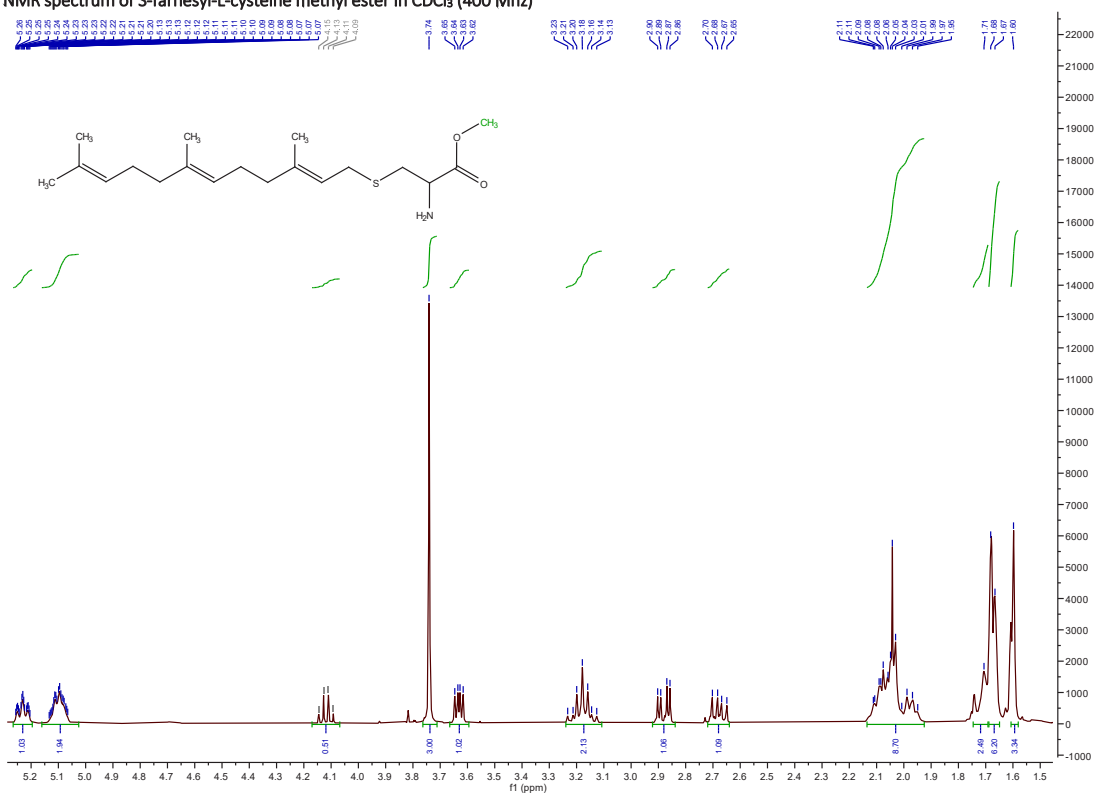


Annexe 5  $^1\text{H}$  NMR spectrum of phytol bromide in  $\text{CDCl}_3$  (400 Mhz)

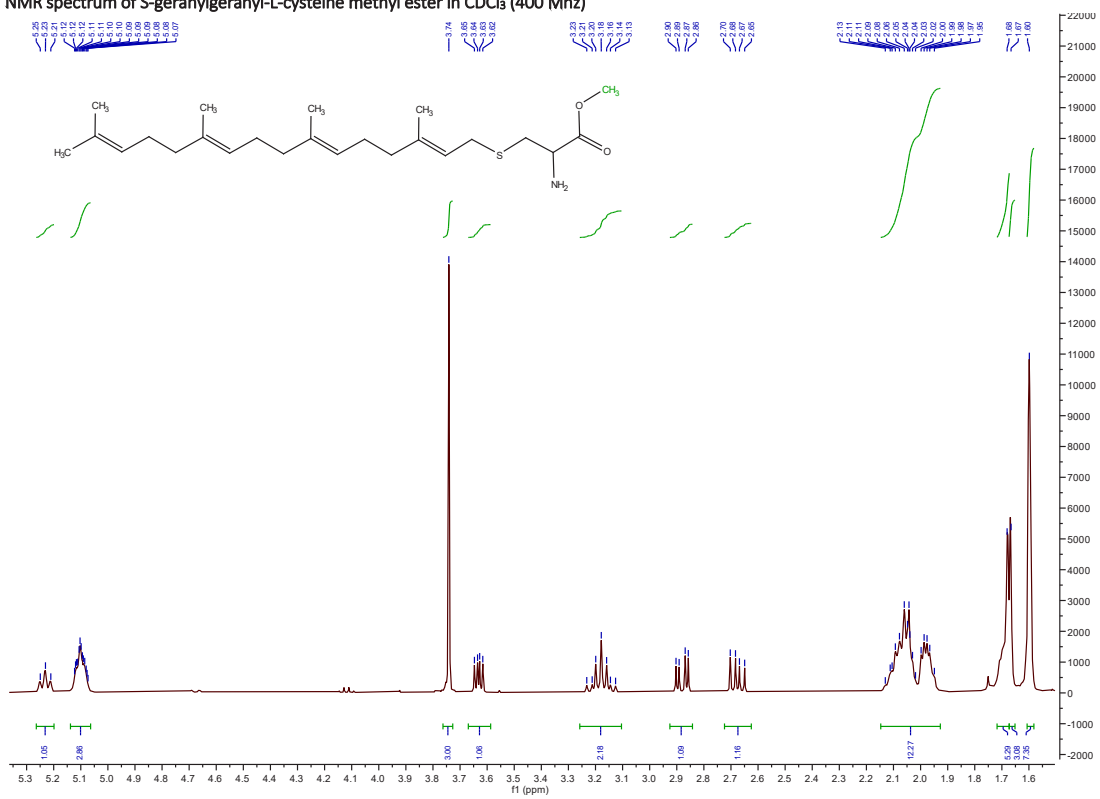




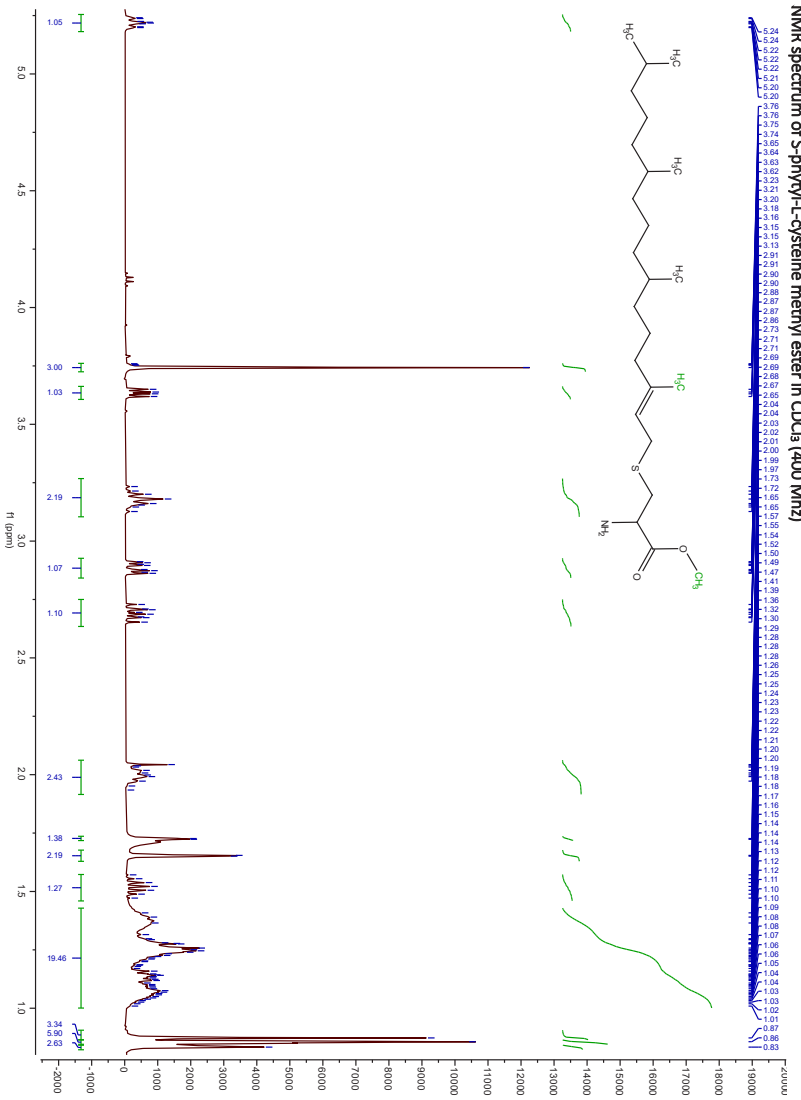
Annexe 6  $^1\text{H}$  NMR spectrum of S-farnesyl-L-cysteine methyl ester in  $\text{CDCl}_3$  (400 Mhz)



Annexe 7 <sup>1</sup>H NMR spectrum of S-geranylgeranyl-L-cysteine methyl ester in CDCl<sub>3</sub> (400 Mhz)

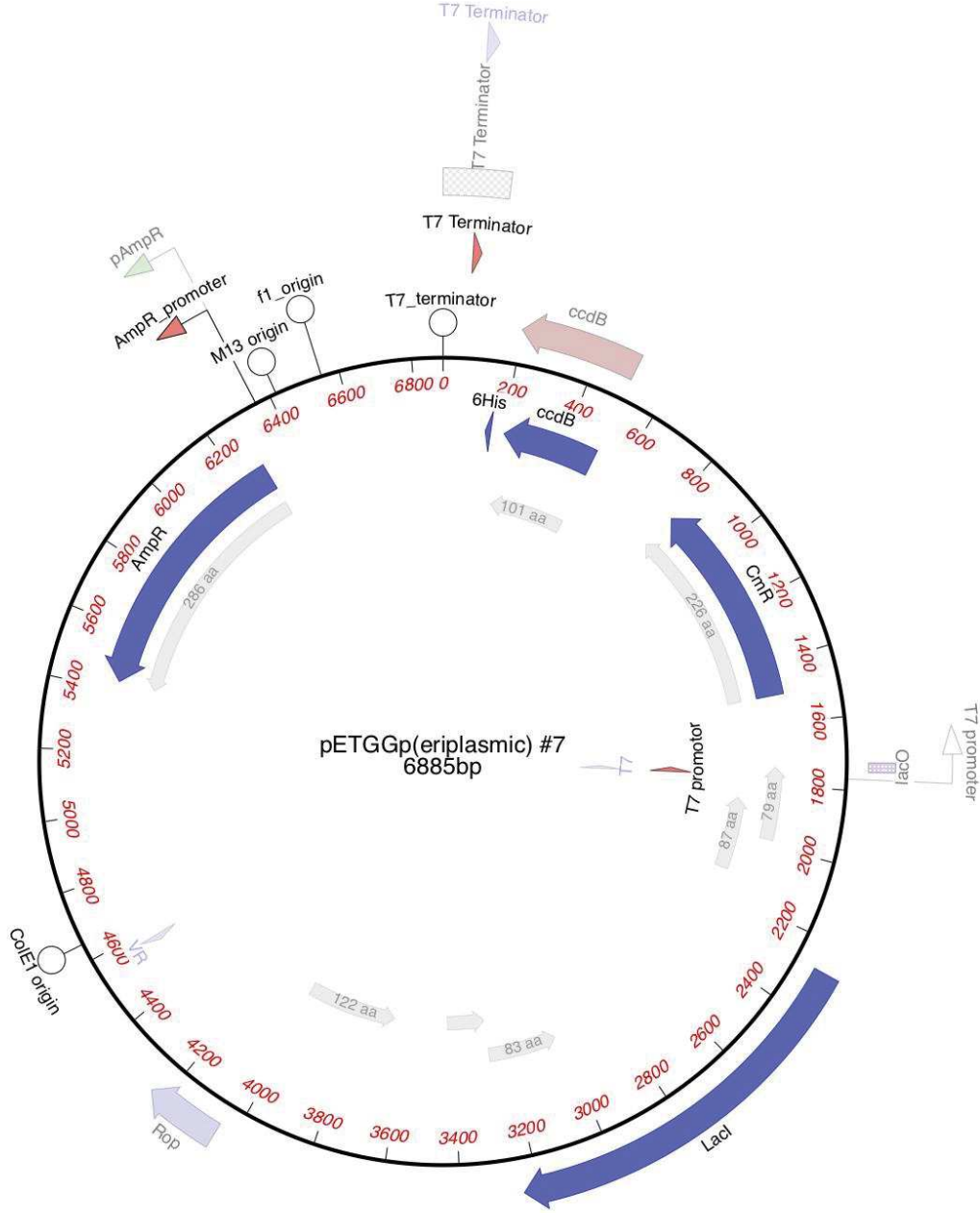


Annexe 8 <sup>1</sup>H NMR spectrum of S-phytyl-L-cysteine methyl ester in CDCl<sub>3</sub> (400 MHz)





ANNEXE 10 Map of the plasmid used for the periplasmic production of the Nbd@GFP in *E. Coli*



# 11 RESUME DE THESE EN FRANÇAIS



## 11.2 CONTEXTE GENERALE

Les isoprénoïdes ou terpènes constituent une vaste classe de molécules organiques hydrogénocarbonées appartenant à la famille des lipides et largement distribués dans l'empire eucaryote. Environ 50 000 isoprénoïdes ont été décrits, il s'agit de l'une des classes de métabolites la plus diversifiée ayant des fonctions importantes aussi bien dans la structure que dans la physiologie des organismes (Holstein and Hohl, 2004). Ils sont classés en fonction du nombre d'atomes de carbone qui les composent : monoterpènes (C10), sesquiterpènes (C15), diterpènes (C20), triterpènes (C30), tetraterpènes (C40), etc.

Mon travail de thèse s'inscrit dans le cadre plus global d'une étude de la régulation de la biosynthèse d'isoprénoïdes chez les plantes. Je m'intéresse plus particulièrement à la prénylation des protéines qui utilisent deux pools biosynthétiques pour assurer la modification post-traductionnelle de protéines avec un groupement prényle. Deux types de prénylation des protéines ont été caractérisées, la farnésylation et la géranylgéranylation des protéines (Casey, 1992; Wang and Casey, 2016). Ces réactions sont catalysées par des protéines prényltransférases (PPTs), la protéine farnésyl transférase (PFT) et la protéine géranylgéranyl transférase de type-I (PGGT-I). Des études préalables dans le laboratoire ont montré que chez les plantes, un pool de précurseurs d'origine plastidial (voie du MEP) est utilisé pour modifier des protéines à motifs de prénylation de type géranylgéranylation (CVIL ; (Gerber et al., 2009). Par ailleurs, il s'est avéré que des protéines possédant des motifs de type farnésylation pouvaient utiliser des pools d'origine cytosolique ou plastidiale. La prénylation des protéines représente donc un modèle d'étude de ce qui est décrit dans la littérature sous le terme de « cross-talk ». Dans ce modèle, les précurseurs d'isoprénoïdes sont échangés selon les besoins biosynthétiques (Hemmerlin et al., 2012). La question qui se posait était de savoir comment se fait le choix entre un pool ou un autre. L'hypothèse de départ suppose que ce sont les enzymes qui « choisissent » ou non un substrat prényle dipshosphate en fonction de l'état de la cellule dans son environnement. Mon travail consiste à élucider la régulation de protéine prényltransférases et d'observer comment elles sont capables de modifier leur « préférence » en substrats. Il a des implications dans des domaines de recherche médicaux comme la conception d'inhibiteurs de PPTs en tant qu'anticancéreux ou antipaludique pour éviter l'acquisition de résistance (Palsuledesai and Distefano, 2015)



## 11.3 PROBLEMATIQUE ET STRATEGIES

La double origine des substrats prényles chez les plantes est suspectée de conférer une flexibilité particulière à l'organisme notamment dans la prénylation des protéines. Chez *Arabidopsis thaliana*, les mutants perte de fonction des PPTs parviennent à se développer et à se reproduire contrairement aux animaux et à la levure pour qui, ces mutations sont souvent létales (He et al., 1991; Running et al., 2004; Charng et al., 2014). Comment les mutants *A. thaliana* parviennent-ils à se développer ? Quelle est l'implication du cross-talk des voies MVA/MEP dans la prénylation des protéines par les PPTs ? Comment l'activité des PPTs est-elle régulée *in vivo* pour s'adapter aux cross-talk qui régit la voie de biosynthèse des isoprénoïdes dépendante des conditions environnementales.

Mon travail de thèse consiste précisément à éclaircir ces zones d'ombre via l'étude de la flexibilité dynamique des activités des PPTs dans les plantes. Différents axes de recherches ont été parcouru pour répondre à cette problématique. Le modèle végétal a été sélectionné, car le métabolisme des isoprénoïdes des plantes englobe aussi bien celui de l'animale que ses parasites. Par ailleurs des mutants viables sont caractérisés chez *Arabidopsis thaliana*, permettant ainsi d'étudier l'absence d'activité des protéines prényltransférases de type-I.

### **Axe 1. Conditions induisant la flexibilité de l'activité des PPTs et analyse des protéines prénylées dans les plantes**

Dans la situation actuelle, une priorité est de comprendre les conditions physiologiques induisant la flexibilité dynamique des activités des protéines prényltransférases, mais aussi d'identifier sans ambiguïté les partenaires impliqués dans la prénylation des protéines. En utilisant le senseur GFP prénylable établi au laboratoire pour étudier la prénylation des protéines (Gerber et al., 2009), j'ai identifié les conditions induisant des changements *in vivo* dans les spécificités des substrats des PPTs. De plus, afin de caractériser ce changement en fonction des conditions environnementales, j'ai développé un protocole de purification et d'analyse systématique des parties prényles et protéiques permettant l'identification des protéines prénylées *in vivo*.

## Axe 2. Criblage d'inhibiteurs de la prénylation des protéines et applications

La prénylation des protéines ayant été proposée comme une cible clé pour le développement de nouveaux anticancéreux et antipaludiques, j'ai criblé un ensemble de composés synthétiques et naturels sur le modèle cellulaire végétal exprimant le senseur GFP développé au laboratoire. Ainsi, un ensemble d'inhibiteurs de prohibitines (PHB) qui présentent des propriétés anticancéreuses sur différentes lignées cellulaires humaines a été fourni par L. Desaubry (LIT, Strasbourg). Les PHB agiraient sur des protéines prénylées telles que K-RAS et C-RAS (Polier et al., 2012 ; Moncunill-Massaguer et al., 2015 ; Yurugi et al., 2017), ainsi les PHB ou les protéines en aval pourraient réguler la prénylation des protéines *in vivo*. En outre, des études avec des extraits d'algues rouges ont montré une activité prometteuse contre la forme intra-érythrocytaire de *P. falciparum*. Comme la voie du MEP est présente à la fois dans les plastes des algues rouges et dans l'apicoplaste de *P. falciparum*, j'ai criblé des extraits d'algues rouges étudiés par L. Margueritte (PhD 2018 - LIT ; (Margueritte, 2018)) pour évaluer si l'activité contre *P. falciparum* peut résulter de l'inhibition de la voie MEP. Enfin, de nombreux inhibiteurs de la MEP sont caractérisés par la présence d'un groupement prényle qui s'insère dans le site actif de l'enzyme mais ne peut être transféré. De manière intéressante, une étude préliminaire avec des cellules BY-2 exprimant la GFP-CVIL a donné lieu à un phénotype atypique après une inhibition avec l'acétylvismione-D, un anthranoïde prénylé (Hartmann et al., 2015).

A cet égard, j'ai poursuivi une investigation avec des vismiones extraites de *Psorospermum Glaberimum*, décrites par J.B. Gallé (PhD 2015 - LIT ; (Gallé, 2015)) et des analogues de dihydroanthracénone synthétisés par N. Wasser (PhD 2018 - LIT ; (Wasser, 2018)).

Par ailleurs, la stimulation des voies de biosynthèse des isoprénoïdes dans les plantes par élicitation (stimuli biotiques ou abiotiques) est jusqu'à présent rapportée pour ajuster les besoins en précurseurs prényles pour la biosynthèse de métabolites spécialisés. Différentes protéines prénylées ont été signalées comme intervenant directement dans la biosynthèse des hormones, des métabolites spécialisés et dans leur régulation. Ainsi, il a été décrit que la S-carvone inhibe la production de capsidiol induite après élicitation en interférant avec la prénylation des protéines (Huchelmann et al., 2014). En revanche, la production de MVA, son précurseur, reste fortement stimulée (Huchelmann et al., 2014). Ce résultat suggère que le contrôle de la prénylation de certaines protéines chez les plantes permettant d'orienter

l'utilisation de ce pool de MVA disponible pour produire des molécules d'intérêt. Est-il possible de monitorer le flux d'isoprénoïdes pour la production de métabolites spécialisés en combinant élévation et inhibiteurs de la prénylation des protéines ? Ainsi, pour comprendre l'origine des substrats prénylés et le rôle et des PPTs dans la production d'isoprénoïdes à haute valeur ajoutée, j'ai comparé l'effet de la lumière, de la *S*-carvone et de son énantiomère *R* sur des plantes de tabac élévitées et cultivées dans différentes conditions.

### **Axe 3. Caractérisation de la fluorescence *in vivo* et de la métabolisation de composés anthracéniques prénylés**

Une fluorescence particulière a été remarquée spécifiquement dans les cellules BY-2 traitées avec des composés anthracéniques prénylés et donc associée à une autofluorescence. Bien que la fluorescence des composés anthracéniques ait été rapportée, la fluorescence des vismiones n'a jamais été caractérisée *in vivo*. De plus, la dégradation des vismiones en anthrone, anthraquinones et dianthrones entraîne des changements de fluorescence. En combinant la microscopie à imagerie spectrale (SImaging) et l'analyse métabolomique non ciblée par HPLC-HRMS/MS, j'ai donc développé une approche pour observer la fluorescence des vismiones et des composés anthracéniques apparentés *in vivo*.

## **11.4 CONDITIONS INDUISANT LA FLEXIBILITE DE L'ACTIVITE DES PPTs ET ANALYSE DES PROTEINES PRENYLEES DANS LES PLANTES**

### **11.4.1 Flexibilité de l'activité des PPTs**

De nombreuses études ont contribué à la caractérisation des PPTs chez la levure et plus tard chez les animaux (Wang et Casey, 2016). La résolution des structures 3D des PPTs souligne une préférence de la PFT pour le FPP et de la PGGT-I pour le GGPP (Casey et al., 1991), mais il n'y a toujours pas de rapport publié sur les structures 3D des PPTs chez les plantes. En outre, l'analyse cristallographique de la PFT avec ses substrat a fourni une image moléculaire détaillée

de la cinétique de la réaction de prénylation des protéines (section 2.3.4, figure 25) (Lane et Beese, 2006 ; Jiang et al., 2018). En outre, les substrats canoniques des PPTs ont été confirmés par des essais enzymatiques *in vitro* utilisant des prényles diphosphates radiomarqués et des substrats portant des motifs CaaX (Goodman et al., 1990 ; Mitsuzawa et al., 1995 ; Gelb, 1997 ; Long et al., 2002 ; Scott Reid et al., 2004 ; Yokoyama et al., 2008 ; Wang et Casey, 2016).

Bien que la préférence de la PGGT pour le GGPP ait été confirmée chez les plantes, cette dernière semblait également capable de transférer la FPP sur le substrat de farnésylation -CVIM (Randall et al., 1993 ; Huchelmann, 2013). De plus, la PGGT-I était hautement sélective pour la GGPP, mais était également capable d'assurer son transfert sur des substrats avec motif de géranylgéranylation CVIL ou -CVIM. Il a été constaté que les inhibiteurs de prénylation développés comme médicaments anticancéreux n'ont pas atteint les résultats escomptés malgré leur efficacité *in vitro* (Whyte et al., 1997 ; Holstein et Hohl, 2012 ; Wang et al., 2017). En fait, les PPT employées dans les études *in vitro* étaient produites en système hétérologue, elles ne tenaient donc pas compte des régulations possibles *in vivo*. En conséquence, il est devenu plus suspect que l'activité de la PFT soit versatile et puisse être régulée par des mécanismes cellulaires eucaryotes tels que les PTMs ou les interactions protéine-protéine.

Des expériences réalisées avec des extraits acellulaires isolés de cellules BY-2 ont montrés que les protéines portant un motif de géranylgéranylation de la CVIL peuvent être marquées avec du [<sup>3</sup>H]FPP (Randall et al., 1993 ; Gerber et al., 2009a ; Huchelmann, 2013). Il est intéressant de noter qu'aucune des enzymes purifiées, produites dans *E. coli*, n'a pu utiliser cette combinaison de substrats, ce qui met en évidence une possible régulation de l'activité de la PFT dans les cellules eucaryotes. Étant donné que les plantes produisent du FPP par la voie du MVA et du GGPP par la voie du MEP (section 2.4.3, 2.2.2), le modèle végétal semble particulièrement adapté à l'étude des mécanismes de prénylation des protéines qui se produisent chez tous les eucaryotes (Yalovsky, 2011 ; Hemmerlin et al., 2012 ; Hemmerlin, 2013). De plus, des mutants *A. thaliana* viables et mutés dans les gènes codants pour les sous-unités  $\beta$ -F (era1),  $\beta$ -GG (ggb-2) ou  $\alpha$  (plp) ont été caractérisés et permettent d'étudier l'implication de chaque PPT dans la prénylation de substrats protéiques spécifiques (Cutler et al., 1996 ; Running et al., 2004 ; Johnson et al., 2005).

Ainsi, un modèle cellulaire végétal exprimant le senseur-GFP de la prénylation des protéines a été utilisé au laboratoire pour évaluer la flexibilité dynamique des activités des protéines

prényltransférases *in vivo*. Tout d'abord, des expériences menées avec des cellules BY-2 exprimant le senseur-GFP inhibées par la MV et la FOS ont montré qu'en effet, il est possible de restaurer la prénylation d'une protéine GFP-CVIL, en utilisant des substrats prényles externes tels que le Fol, le GGol, ou le précurseur MVA. Ensuite, des études similaires avec des disques foliaires de tabac ont indiqués que la lignée exprimant la GFP-CVIM contient des formes prénylées (membrane) et non prénylées (noyau) dans des conditions de croissance standard, sauf pour les cellules BY-2 où seule la membrane est marquée (Huchelmann, 2013). À l'opposé des racines de tabac et des cellules BY-2, la prénylation de la GFP-CVIM dans les feuilles de tabac n'a pas pu être entravée, même avec le MV et la FOS à des concentrations allant jusqu'à 20 et 200  $\mu\text{M}$ , respectivement. De plus, bien qu'une inhibition complète de la prénylation de GFP-CVIL ait été obtenue avec 300  $\mu\text{M}$  de FOS, les mêmes résultats ont été obtenus avec la combinaison de 5  $\mu\text{M}$  de MV et 50  $\mu\text{M}$  de FOS, ce qui suggère que la voie du MVA contribue également à la prénylation des protéines géranylgeranylées. De façon remarquable, des essais de complémentation avec le phytol ont démontré sa capacité à restaurer la prénylation des protéines dans les feuilles de tabac, alors que dans les cellules BY-2, ce composé n'avait aucun effet (Huchelmann, 2013). Ces résultats sont compatibles avec une hypothétique mobilisation du phytol provenant du catabolisme chlorophyllien comme c'est le cas pour la biosynthèse du tocophérol (Ischebeck et al., 2006 ; Gutbrod et al., 2019). Cela suggère également que les phytol kinases requises pour activer le phytol en phytyl diphosphate pourraient être exclusivement fonctionnelles dans les tissus photosynthétiques. De même, l'inhibition avec 50  $\mu\text{M}$  de FOS et 1  $\mu\text{M}$  de MV d'un substrat protéique GFP-CVIL exprimé dans des cellules BY-2 a pu être complétement par l'élicitation avec la cellulase (Huchelmann, 2013 ; Huchelmann et al., 2014).

Ces résultats indiquent que l'élicitation module non seulement le flux métabolique des isoprénoïdes par l'induction de la biosynthèse de MVA, mais aussi la capacité de prénylation des protéines. Étant donné que l'élicitation des plantes de tabac induit une expression de *hmgr* (Chappell et Nable, 1987), on peut supposer qu'une augmentation des concentrations de MVA fournit un signal qui active la flexibilité de l'activité PFT (Huchelmann, 2013). D'autres expériences ont confirmé cette hypothèse, car le GGTi-2133 seul n'a pas conduit à un arrêt total de la production de capsidiol induite par la cellulase, alors que le phénotype est totalement supprimé avec 2 mM de *S*-carvone (Huchelmann et al., 2014). En conséquence, il a

été suggéré que la PFT remédie au manque d'activité de la PGGT-I et qu'au moins une protéine géranylgeranylée est impliquée dans la cascade de signalisation induite par la cellulase. Pour cette raison, la flexibilité de l'activité de la PFT pourrait fournir une issue de secours lorsque la géranylgeranylation des protéines ou la biosynthèse de GGPP sont inhibés, par exemple dans le cadre d'une interaction entre la plante et des espèces de *Streptomyces* qui synthétisent la FOS. Cette étude a mis en évidence une interconnexion entre le stress et la prénylation des protéines, proposant que la flexibilité des activités de la PFT doit être essentielle pour les interactions biotiques impliquant l'inhibition de la prénylation des protéines. Cependant, ces propriétés physiologiques sont encore sujettes à débat car la quantité de produit utilisée pour réaliser les expériences peut différer des concentrations physiologiques. Nous nous sommes donc intéressés à la recherche de signaux de stress déclenchant une telle flexibilité dans un contexte cellulaire. De plus, dans la mesure où la glycolyse fournit des précurseurs pour la biosynthèse des isoprénoïdes, on peut supposer que la concentration de saccharose dans le milieu de culture a un impact sur la prénylation des protéines. Également, il est bien décrit que l'ajout de sucre externe améliore la croissance des plantes et la teneur en chlorophylle (Eckstein et al., 2012 ; Shah et al., 2019). Dans ce contexte, la prénylation des protéines est-elle déjà influencée dans les cellules BY-2 cultivées en milieu MS avec du sucre ? Ainsi, des feuilles de tabac de plantes cultivées sur des milieux de culture enrichis en saccharose ou non ont été comparées, afin d'évaluer l'influence du sucre sur la capacité de prénylation des protéines dans les plantes.

Dans ce chapitre nous avons mis en évidence la flexibilité des activités des protéines prényltransférases dans les plantes. Nous avons observé que les mécanismes physiologiques dépendant de la signalisation des hormones de défense comme le JA et l'éthylène induisent une flexibilité de la PFT pour pallier l'absence GGPP ou d'activité PGGT-I dans la prénylation des protéines avec des motifs -CaaL. Dans ces conditions, nos résultats indiquent que la voie du MVA est utilisée pour fournir le substrat prényle nécessaire à la prénylation des protéines. De plus, l'utilisation du senseur GFP dans le mutant *era1-9* a permis d'obtenir un aperçu du processus de prénylation des protéines en l'absence d'activité PFT *in vivo*. Contrairement au mutant *ggb2, era1-9* possède un niveau minimal mais uniforme de prénylation des protéines, quel que soit le motif CaaX qui doit être modifié. On peut spéculer que cet état de prénylation homogène est probablement orchestré par la plante pour assurer simultanément au moins les

fonctions essentielles, impliquant les protéines prénylées dans le développement mais aussi la défense.

Bien que la PFT joue un rôle central, il semble que la PGGT-I puisse reprendre partiellement sa fonction dans le mutant *era1*. La capacité de prénylation du senseur GFP-CaaM a été augmentée par le GGol alors que celle du Fol ne l'a pas été, ce qui suggère que l'activité de la PGGT-I est également flexible et peut assurer le transfert d'un substrat lié au GGPP sur la protéine avec un motif -CaaM plutôt que -CaaL. Il serait intéressant de réaliser des expériences où les lignées *era1-9::GFP-CVI* (M/L) sont traitées avec de la MeJA. Dans un tel contexte, nous serions en mesure de voir si la PGGT-I peut prendre en charge la prénylation de la GFP-CVIL dans des conditions de stress. De plus, la lignée *plp* mutantes d'*Arabidopsis* transformées pourraient être essentielles pour déchiffrer l'ensemble de la machinerie de prénylation des protéines, y compris la PFT, la PGGT-I et d'autres partenaires inconnus déclenchant la flexibilité dynamique de la PPT *in vivo*. Cependant, comme le mutant *plp* est difficile à cultiver et que les lignées *era1-9* exprimant le senseur GFP ont été obtenues tardivement, ces essais n'ont pas été réalisés. Par ailleurs, même si les croisements ont été rigoureusement réalisés et le génotype *era1-9* validé, le séquençage de la séquence terminale CaaX insérée dans l'ADN génomique n'a pas encore été effectué. Il devra donc être réalisé à l'avenir pour s'assurer qu'aucune inter-conversion n'a été faite lors de la manipulation des lignées.

#### **11.4.2 Analyse des protéines prénylées dans les plantes**

Depuis la découverte de la prénylation des protéines en 1975, et plus tard du rôle des protéines prénylées telles que les membres de la famille RAS dans le cancer humain ou la lamine B dans la progéria, plusieurs méthodes ont été développées pour purifier et caractériser les prényles portés par ces protéines (section 2.2.1). Néanmoins, la preuve de la flexibilité des substrats prényles ainsi que des protéines CaaX a poussé à reconsidérer les approches développées pour étudier la prénylation des protéines *in vivo*. L'une des raisons est que de nombreuses expériences ont été réalisées *in vitro* avec des substrats purifiés et des PPTs recombinantes, ce qui ne reflète évidemment pas la réalité *in vivo*. Une autre raison est que des inhibiteurs et/ou des substrats radiomarqués, ou leurs précurseurs, ont été ajoutés pour les expériences *in vivo*, induisant ainsi une adaptation du mécanisme cellulaire aux conditions fixées par l'expérimentateur dans les études chez l'Homme. Bien que des solutions analytiques aient été

proposées dans les études sur les protéines prénylées, elles ont révélé certaines limites (figure 52, tableau 3). Par exemple, le nickel de Raney et l'iodométhane ont été définis comme des standards pour cliver les prényls avant les analyses CCM, GC-FID, radiométrie HPLC-UV ou GC-MS. Néanmoins, ces réactions comportent des risques d'explosion car l' $H_2$  est nécessaire pour l'hydrogénation sur platine avant le clivage, et le nickeli de Raney sec est également auto-inflammable. Même si ces approches ont permis de libérer et de détecter les prényls, aucune corrélation directe entre les protéines et les prényls ne peut être établit sans ambiguïté, notamment *in vivo*. De plus, si l'analyse était effectuée avec du matériel végétal, le phytyl et le GG se transformeraient tous deux en phytane après l'étape d'hydrogénation.

En conséquence, de nouveaux protocoles utilisant la HPLC-MS/MS ou la RMN ont été proposés pour déterminer sans ambiguïté l'état de prénylation sans clivage des prényls, mais leur utilisation a longtemps été limitée aux protéines ou aux peptides prénylés *in vitro*. Récemment, des supports pour la purification par affinité, la chimie biorthogonale et l'analyse de protéines marquées fournissent de nouvelles caractéristiques sur le prénylome de certains organismes (Chung et al., 2009 ; Hannoush et Sun, 2010 ; Onono et al., 2010). Cependant, la plupart de ces approches nécessitent de nourrir les cellules avec des substrats synthétiques pour une purification ultérieure, ce qui entraîne une possible prénylation artéfactuelle des protéines. En fait, le principal défi reste l'analyse des protéines prénylées modifiées *in vivo* avec des substrats prénylés disponibles dans des conditions physiologiques. Même si elles sont surexprimées, les protéines prénylées restent peu abondantes par rapport aux sous-unités ribosomales ou aux protéines structurelles comme l'actine ou la tubuline. Ainsi, d'autres stratégies ont été proposées pour la purification des protéines prénylées sans ajout d'analogues de prényl. Par exemple, un modèle de piège à protéines farnésylées a été proposé en fonction de l'affinité de la protéine Aryl Hydrocarbon-Receptor-interacting-protein-like-1 (AIP1) pour le fragment farnésyl de la sous-unité de la phosphodiesterase-6A (Majumder et al., 2013). Cependant, cette approche pourrait également être limitée par la taille, la conformation et la composition des protéines prénylées. En outre, le partage de phase utilisant le triton X-114 est assez bien documenté pour la purification des protéines acylées et prénylées (Goalstone et al., 1999 ; Mohamed et al., 2012 ; Yang et al., 2016 ; Akula et al., 2019). Mais, cette approche ne correspond pas à la perspective d'une protéine putative interagissant avec des protéines prénylées car une variabilité de la polarité des protéines interactantes induirait une séparation



différentielle. De plus, une étude préliminaire a été réalisée avec des cellules BY-2 exprimant His-GFP-CVIL (Gerber et al., 2009a), mais la plupart de la protéine GFP a été retenue sur la colonne de purification His-tag (Données non publiées). Enfin, certains articles rapportent une purification par affinité avec des inhibiteurs de dissociation du GDP fusionnés à la glutathion-S-transférase (GST), mais la quantité de protéine purifiée reste relativement faible et spécifique des Small GTPases (Mohamed et al., 2018). Nous nous sommes donc intéressés à développer une procédure pour l'analyse non biaisée des protéines senseur GFP prénylée *in vivo* dans des conditions physiologiques de prénylation des protéines. Puisque plusieurs matrices d'immunoprécipitation (IP) pour les protéines GFP sont disponibles et décrites (Fernandes et al., 2014), cette stratégie a été mise en œuvre pour la purification des senseur GFP.

Au cours de cette longue phase de développement, nous avons mis au point une approche durable pour purifier les protéines du senseur GFP exprimés et prénylés dans les plantes. En outre, une méthode de digestion ciblée a été mise au point pour optimiser l'analyse de l'extrémité C-ter non structurée, y compris le domaine basique et la cystéine prénylée. Nous avons également montré que la S-Pre-L-cys OMe et les tétrapeptides CaaX sont détectés principalement avec  $m/z = 1$  après séparation et analyse par HPLC-HRMS/MS. L'analyse métabolomique non ciblée a confirmé la farnésylation de la protéine GFP-CVIM dans *N. tabaccum* dans des conditions standard. Cependant, nos résultats indiquent que l'ester méthylique de la S-prényl-L-cystéine est possible instable et se dégrade au niveau de la fonction carboxyméthyle. Il n'a donc pas été possible de confirmer l'état de carboxyméthylation de la cystéine terminale de la GFP-CVIM prénylée. Enfin, bien que la protéomique n'ait pas permis d'identifier les prényles sur les senseurs GFP dans nos conditions, certaines protéines pertinentes pour le métabolisme des isoprénoïdes et la photosynthèse ont été annotées de manière récurrente et explicite dans les échantillons dans lesquels les capteurs sont prénylés. Malgré l'absence de fonction de notre protéine senseur GFP, ces résultats suggèrent que des interactions avec d'autres protéines liées à la photosynthèse ou à la biosynthèse des isoprénoïdes se produisent.

## 11.5 CRIBLAGE D'INHIBITEURS DE LA PRENYLATION DES PROTEINES ET APPLICATIONS

Depuis les années 1990, la prénylation des protéines est considérée comme une cible prometteuse pour le traitement de pathologies humaines telles que la progéria et le cancer (section 2.6). Cette étude vise à trouver de nouveaux composés agissant sur des cibles non conventionnelles. Ainsi, nous avons criblé 20 composés purs et 13 extraits en utilisant le modèle de cellules BY-2 exprimant la protéine GFP-CVIL. Notre collaboration avec C. Vonthron-Sénécheau (LIT, Strasbourg), travaillant sur des molécules antiprotozoaires naturelles, a permis de cribler des extraits d'algues rouges et des composés anthracéniques actifs contre *P. falciparum*. Par ailleurs, L. Desaubry (ex chercheur au LIT), travaillant en cardio-oncologie et chimie médicinale, nous a permis de tester une série de ligands des prohibitines (PHB) efficaces sur des lignées cellulaires cancéreuses de mammifères.

D'un autre point de vue, des études chez *Catharanthus roseus* et *N. tabacum* ont montré que l'inhibition de la prénylation des protéines influence la biosynthèse de métabolites spécialisés. Par exemple, les alcaloïdes monoindoloterpéniques (MIA) tels que la vinblastine, la vincristine sont des composés anticancéreux à succès que l'on trouve dans *C. roseus* et d'autres espèces d'Apocynaceae. Ces molécules sont issues de la condensation de tryptophane et de sécologanine (sesquiterpène). Il est intéressant de noter que sous l'effet de l'inhibition avec des inhibiteurs de la PFT tels que la Manumycine A, l'acide Chaetomelic A ou l'extinction des gènes de CrPFT et CrPGGT-I par ARNi, la biosynthèse des MIA chez *C. roseus* est appauvrie (Courdavault et al., 2005 ; Courdavault et al., 2009 ; Kumar et al., 2020). De même, des expériences avec la *S*-carvone et le GGTi-2133 ont montré que l'inhibition de la prénylation des protéines arrête la production de capsidiol dans les disques foliaires de tabac (Huchelmann et al., 2014). Ces deux métabolites spécialisés sont régulés par la signalisation MeJA, dont la transduction du signal dépend de protéines prénylées, en particulier dans des conditions de stress. Bien que le capsidiol n'ait pas un tel intérêt pour une application humaine, les MIAs comme anticancéreux sont très précieux, et la production de ces molécules reste extrêmement dépendante de l'approvisionnement en plantes (Martino et al., 2018). Un intérêt moindre mais non négligeable existe pour plusieurs autres MIAs tels que l'ibogaïne, la yohimbine étant également utilisés pour le traitement des addictions et des dysfonctionnements érectiles respectivement (Tam et al., 2001 ; Belgers et al., 2016 ; Kregel et al., 2019). De plus, certaines

protéines prénylées ont été caractérisées dans la biosynthèse ou la signalisation hormonale des réponses au stress, mais aussi dans le développement comme le CYP85A2 (2.3.3). Si l'on considère que de nombreux autres terpènes sont utiles non seulement en pharmacie, mais aussi en agronomie ou en cosmétique, les inhibiteurs de prénylation des protéines peuvent-ils trouver leur application dans l'agronomie ? En conséquence, ce chapitre traite également des applications possibles des inhibiteurs de la prénylation des protéines dans la production de métabolites spécialisés à haute valeur ajoutée dans les plantes, tels que les caroténoïdes. En effet, les caroténoïdes, en raison de leurs propriétés antioxydantes, sont largement utilisés dans l'agro-industrie pour la conservation et la qualité des aliments (Novoveská et al., 2019 ; Nabi et al., 2020). Néanmoins, leur production reste extrêmement limitée et coûteuse. L'augmentation récente des demandes de céto-caroténoïdes plus actifs tels que l'astaxanthine ou la canthaxanthine pour la production d'aliments destinés aux animaux de compagnie a poussé la recherche de nouvelles alternatives d'approvisionnement. En 2018, le marché de l'astaxanthine représentait 600 millions USD et devrait atteindre plus de 800 millions d'ici 2026. Dans ce contexte, nous avons évalué l'inhibition de la prénylation des protéines dans la production de caroténoïdes dans les plantes de tabac.

Nous avons identifié le composé synthétique IN2 comme un nouvel inhibiteur de la prénylation des protéines dont le mécanisme d'action diffère des inhibiteurs conventionnels de la voie du MEP ou des protéines prényltransférases. Bien que la cible et les mécanismes d'action impliqués dans son activité n'aient pas encore été caractérisés, les résultats obtenus dans notre modèle cellulaire BY-2 ont démontré que son efficacité est au moins 10 fois supérieure à celle de notre composé de référence, la fosmidomycine. De plus, contrairement aux vismiones testées et aux dihydroanthracénones (DHA) synthétiques, les essais sur les extraits d'algues rouges efficaces contre *P. falciparum* ont montré qu'ils contiennent probablement aussi des molécules capables d'inhiber la prénylation des protéines. L'héritage de la voie du MEP d'une Rhodophyte à Apicomplexa est une hypothèse intéressante pour identifier de nouveaux inhibiteurs de la prénylation des protéines ayant une activité antipaludique. Néanmoins, l'activité obtenue était faible et les expériences ne permettent pas de conclure sur la nature commune des molécules impliquées dans l'activité sur la pLDH de *P. falciparum* et l'inhibition de la prénylation des protéines.

Par ailleurs, nous avons démontré que la teneur en caroténoïdes et autres métabolites dans les feuilles de tabac peut être modifiée en utilisant la *S*-carvone identifiée comme un inhibiteur de la prénylation des protéines dans le tabac (Huchelmann et al., 2014). De manière remarquable, ces expériences fournissent également des preuves que le MVA joue un rôle clé dans la régulation ou la biosynthèse des caroténoïdes, bien que la voie du MEP soit décrite depuis longtemps pour la biosynthèse des caroténoïdes dans les plantes (Steele et Gurin, 1960 ; Disch et al., 1998 ; Lichtenthaler, 2007 ; Vranová et al., 2013)). Pour la première fois, nous avons observé les effets des isoprénoïdes sur les alcaloïdes de type azine, comme le montre l'influence sur la production ou l'excrétion de nicotine à partir de feuilles de tabac élicitées par la cellulase et traitées avec de la *S*-carvone et la MVA. Enfin, la comparaison des effets de la *S*-carvone et de la *R*-carvone sur les plantes de tabac élicitées a montré que les plantes comme les animaux répondent spécifiquement à la stéréochimie des monoterpènes. Dans l'ensemble, ces résultats confirment que la recherche sur les inhibiteurs de la prénylation des protéines fournit des composés thérapeutiques ainsi que des outils puissants pour comprendre le métabolisme et sa régulation dans les plantes dans le contexte d'applications telles que l'ingénierie métabolique de composés d'intérêt.

Bien que les composés anthracéniques n'aient eu aucun effet sur l'inhibition de la prénylation des protéines, nous avons pu démontrer que ces composés sont en réalité autofluorescents et sont responsables du phénotype particulier rapporté dans la littérature (Hartmann et al., 2015).

## **11.6 CARACTERISATION DE LA FLUORESCENCE *IN VIVO* ET DE LA METABOLISATION DE COMPOSES ANTHRACENIQUES PRENYLES**

Le règne végétal est une source de ~200.000 métabolites spécialisés identifiés. Parmi ceux-ci, ~10.000 composés phénoliques (ou polyphénols) sont utilisés comme ingrédients dans les industries pharmaceutiques, cosmétiques et agroalimentaires en raison de leurs diverses propriétés bioactives (Pichersky et Lewinsohn, 2011 ; Tissier et al., 2014). Pourtant, la biosynthèse et les mécanismes d'action de nombreux polyphénols et notamment des composés anthracéniques restent flou (Figure 112). Traditionnellement, les anthraquinones

comme l'émodyne (Emo) sont utilisées comme pigments et constituants essentiels de nombreuses plantes purgatives.

Aujourd'hui, plus d'une douzaine d'activités thérapeutiques différentes ont pu être attribuées à l'Emo, allant des propriétés laxatives aux propriétés antinéoplasiques (Srinivas et al., 2007 ; Dong et al., 2016). Même si les mécanismes d'action de l'Emo ne sont pas entièrement compris, les propriétés laxatives des anthraquinones ont été bien décrites et nécessitent la présence de groupes hydroxyles en position 1 et 8 (Figure 112). Par ailleurs, certains composés anthracéniques prénylés tels que les vismiones ont montré une activité antipaludique prometteuse, mais leurs cibles moléculaires sont encore inconnues et leur biosynthèse à partir de l'atrichrysonne reste hypothétique (François et al., 1999 ; Galle, 2015).

La biosynthèse des composés anthracéniques se fait par deux voies distinctes chez les plantes (Figure 112) : la voie des polykétides est présente chez les Rhamnaceae, Fabaceae, Aloeaceae, Polygonaceae et la voie shikimate/o-succinylbenzoïque est présente chez les Rubiaceae (Han et al., 2001). L'enzymologie de ces voies de biosynthèse chez les plantes est très peu connue, notamment pour la voie des polykétides dont seule la première étape assurée par une polykétide synthase a été décrite (Han et al., 2001). Cette dernière aboutit à la formation d'un octakétide à partir de l'addition de sept malonyl-CoA sur l'Acétyl-CoA. Avec les sporophores de *Cortinarius sanguineus* (Syn. *Dermocybe sanguinea*), des expériences d'incorporation avec de la [<sup>14</sup>C]endocrocine, un précurseur des formes acide carboxylique des anthraquinones "neutres" ont été réalisées (Gill, 2001). Les résultats suggèrent que la 8-hydroxyméthylation et la 4-hydroxylation peuvent se produire pour donner la dermolutéine et la dermorubine mais pas les anthraquinones "neutres" comme l'Emo et la dermoglaucine qui nécessitent une décarboxylation en position C2 (Gill, 2001). De plus, l'incorporation de [2,4-<sup>3</sup>H<sub>2</sub>]émodyne 6-O-β-D-glucopyranoside dans les sporophores de *Cortinarius semisanguineus*. a montré que l'Emo peut être 6-hydroxyméthylée et aussi 5- ou 7-hydroxylée comme le radiomarquage a été trouvé dans la dermoglaucine et la dermocybine (Gill, 2001). De plus, des expériences similaires ont suggéré que les dihydroanthracénones telles que la torosachrysonne et l'atrichrysonne sont des intermédiaires clés dans la biosynthèse des anthraquinones susmentionnées, en raison de leur structure, elles émettent également une fluorescence vive dans l'eau. Une autre étude a proposé une voie de biosynthèse pour les dérivés des monodictyphénones et de l'émodyne en accord avec l'analyse génomique et la caractérisation d'intermédiaires de biosynthèse dans des

souches d'*Aspergillus niger* (Chiang et al., 2010). Cependant, ces expériences indiquent que la O-méthylation, l'oxydation, l'hydroxylation, la dimérisation et la glycosylation peuvent être réalisées par des enzymes, tandis que d'autres peuvent résulter de réactions chimiques telles que la tautomérisation, la photoisomérisation et l'hydroxylation photochimique (Fain et al., 2006 ; Furumoto et Jindai, 2008 ; Elkazaz et Jones, 2010). Ainsi, en conditions oxydatives comme dans le DMSO, la VH isolée de *Psorospermum glaberimum* est soumise à une dégradation rapide aboutissant à la forme anthrone, qui est ensuite oxydée en sa forme anthraquinone madagascine (Mad) ou alternativement dimérisée en bianthrone (Galle, 2015). Dans la mesure où la fluorescence des composés anthracéniques a été partiellement décrite, ces propriétés pourraient-elles être utilisées pour comparer si des événements similaires se produisent dans des cellules végétales vivantes ?

Dans l'ensemble du spectre UV-Vis, plus de 300 composés fluorescents naturels ont été rapportés avec des rendements quantiques allant de 0,01% à 100% *in vitro* (Duval et Duplais, 2017). De manière intéressante, les composés anthracéniques sont fluorescents et malgré leurs similitudes structurales, leurs propriétés de fluorescence diffèrent les unes des autres, permettant leur différenciation par une analyse fine de leur fluorescence. Ainsi, l'acétylvismione D solubilisée dans MeOH émet une fluorescence verte ( $\lambda_{Em} = 534$  nm) avec un faible rendement quantique d'environ 2% (Galle, 2015), alors que les anthrones/anthranols émettent une lumière bleue ( $\lambda_{Em} = 458$  nm) dans l'alcool et une forte fluorescence jaune-vert dans l'eau ( $\lambda_{Em} = 539$  nm) (Fujii et al., 1997). De leur côté, les anthraquinones comme la Qui et l'hypericine présentent de bonnes propriétés de fluorescence dans la fenêtre orange à rouge lointain (570-675 nm) avec un rendement quantique pouvant atteindre 30 % (Fujii et al., 1997 ; Verebova et al., 2016 ; Duval et Duplais, 2017). Malgré ces connaissances et l'intérêt porté aux composés anthracéniques, les vismiones n'ont jamais été observées *in vivo* et la fluorescence particulière des composés anthracéniques n'a jamais été utilisée pour comprendre en profondeur leur comportement au sein des cellules.

De même, peu d'informations sur la biosynthèse des composés anthracéniques dans les plantes ont été rapportées et des différences entre les activités biologiques de ces composés sont observées. Par conséquent, nous nous sommes intéressés au suivi des vismiones et des composés anthracéniques apparentés dans les cellules en utilisant leur fluorescence particulière pour identifier chacune des formes vismiones et des anthrones ou anthraquinones

putatives à une échelle subcellulaire. La microscopie à fluorescence a été utilisée comme un outil fondamental pour suivre des sondes fluorescentes *in cellula* pour la recherche biomédicale ou pour comprendre les voies métaboliques. Bien que les propriétés spectrales de plusieurs composés anthracéniques en solution aient été décrites, les conditions physiologiques ne sont jamais idéalement simulées *in vitro*. En effet, le métabolisme, le catabolisme et le stockage des métabolites peuvent avoir lieu dans plus de trois compartiments cellulaires et tissus différents (Han et al., 2001). Il a également été démontré que le nombre et la position des substituants, en particulier des hydroxyles sur les anthranoïdes, influencent largement leurs propriétés physico-chimiques (c'est-à-dire les propriétés de protonation) et de fluorescence. Par conséquent, si les paramètres biochimiques et physicochimiques ne sont pas pris en compte et bien évalués, les propriétés de fluorescence des composés anthracéniques et d'autres composés phénoliques en solution peuvent être omises dans la description de leur comportement dans un contexte cellulaire. Le SImaging est un outil approprié pour observer et identifier avec précision chez les plantes plusieurs composés phénoliques auto-fluorescents tels que les phénols simples, la vanilline et la mangiférine (Conéjéro et al., 2014 ; Talamond et al., 2015). En fait, cette méthode permet de détecter le signal de fluorescence de l'échantillon dans plusieurs canaux indépendants avec une résolution < 10 nm. Par conséquent, le SImaging offre un avantage considérable pour discriminer les signaux de fluorescence apparentés par rapport à l'approche classique employée en microscopie de fluorescence. À cet égard, nous avons utilisé la méthode SImaging pour analyser et comparer la fluorescence de la VH, des anthranoïdes apparentés (Mad, Emo, Qui) et d'une naphthoquinone prénylée (Lap) dans des cellules BY-2 de tabac traitées. Ce dernier a été choisi comme modèle végétal car il est bon marché, sûr, facile à manipuler et exempt de composés autofluorescents dans des conditions standard (Nagata et al., 1992). Par ailleurs, la fraxétine (Fra) a été utilisée comme contrôle positif, car sa fluorescence et sa biosynthèse sont rapportées dans les cellules BY-2 (Tsai et al., 2018). La comparaison des spectres de référence à ceux enregistrés par l'observation SImaging a permis d'identifier le signal des produits naturels observés dans différents compartiments cellulaires à un même moment. Pour caractériser les molécules sur la base de leur fluorescence observée par SImaging, nous avons comparé nos résultats de SImaging à ceux d'une analyse spectrofluorométrique de composés références en solution modèle. D'un autre point de vue, nous avons réalisé une analyse métabolomique des extraits de cellules traitées BY-2 afin de fournir une annotation non ambiguë des métabolites fluorescents.

Cet article décrit la mise en œuvre du SImaging en tant qu'outil efficace pour étudier la fluorescence ainsi que les processus de métabolisation des composés anthracéniques et d'autres molécules d'origine naturelle dans des cellules vivantes. Notre approche, qui combine l'analyse SImaging et la métabolomique non ciblée, permet d'identifier et de caractériser facilement les empreintes spectrales des composés de références et des métabolites apparentés. De plus, en raison de son faible coût, de sa faible autofluorescence et de son métabolisme hétérogène, le modèle cellulaire BY-2 est particulièrement intéressant pour cette preuve de concept et pourrait sans aucun doute contribuer à de nouvelles recherches. Étant donné que des composés anthracéniques et d'autres composés fluorescents d'origine naturelle ont une valeur ajoutée importante, il serait intéressant d'étendre cette étude réalisée sur le modèle BY-2 à d'autres plantes afin d'étudier les voies de biosynthèse et l'influence de certains facteurs sur le métabolisme des composés d'origine naturelle. D'un autre point de vue, l'approche développée offre des perspectives intéressantes dans le domaine médical, car la VH et des composés similaires ont été décrits pour leurs propriétés antipaludiques et les cibles biologiques et les mécanismes d'action restent inconnus.

Enfin, il serait intéressant de comparer les résultats obtenus avec les cellules BY-2 à ceux de globules rouges infectés par *P. falciparum* traités par VH et analogues, ouvrant ainsi une voie à des études de localisation de fluorescence/rerelations structure/activité.

## 11.7 CONCLUSION GÉNÉRALE

Au final, je considère cette thèse comme réussie car nous avons acquis de nouveaux éléments pertinents, le stress a été défini comme une condition physiologique induisant la flexibilité des PPTs, dans le mutant *era1* d'*Arabidopsis*. Par ailleurs, la flexibilité des PPTs a été spécifiée et une nouvelle méthode d'identification non ambiguë des protéines prénylées a été mise en place et optimisée pour la durabilité et l'investigation de la flexibilité de l'activité des PPTs. En outre, nous avons identifié un puissant inhibiteur de la géranylgéranylation des protéines, au moins 10 fois plus efficace que la fosmidomycine (composé de référence), et agissant *via* un mécanisme d'action atypique et inconnu. En outre, nous avons mis en évidence pour la première fois la fluorescence des vismiones dans les organismes végétaux et développé une nouvelle méthode pour étudier les processus de métabolisation et le transport des composés fluorescents naturels.



Je pense que l'un des plus grands défis pour l'avenir est le développement de méthodes efficaces pour l'étude *in vivo*. Jusqu'à présent, de nombreuses études préliminaires et précliniques étaient réalisées *in vitro* car moins coûteuses et plus faciles à contrôler, mais aujourd'hui, ces approches se heurtent à d'importantes difficultés concernant le développement des médicaments et plus particulièrement leur administration. En effet, de nombreux paramètres sont impliqués dans les mécanismes physiologiques et sont influencés par plusieurs facteurs qui ne sont pas pris en compte dans les modèles *in vitro* classiques.

Aujourd'hui, de nouvelles techniques et équipements sont disponibles et permettent l'observation et l'analyse de mécanismes complexes dans les organismes vivants. La clé de voûte de cette thèse était de combiner ces techniques et de développer des méthodes pour l'observation de la prénylation des protéines mais plus généralement des mécanismes physiologiques *in vivo*.



# Dynamic flexibility of protein prenyltransferase activities

## Résumé

La prénylation des protéines est une modification post-traductionnelle essentielle pour le développement, la signalisation et l'adaptation à l'environnement des cellules eucaryotes. Bien que de nombreux inhibiteurs actifs et spécifiques des protéine-prenyltransférases aient été isolés à ce jour, la méconnaissance des bases biologiques contrôlant les modifications des protéines par des groupements isopréniques rend leur utilisation inefficace dans le traitement de cancer ou du paludisme. Pour caractériser la modification des protéines prénylées, nous avons utilisé un modèle cellulaire unique permettant de visualiser ces changements *in vivo*. De plus, des techniques de capture des protéines modifiées ont été développées afin d'analyser les mécanismes au niveau moléculaire par des approches protéomiques et métabolomiques. Dans un criblage d'inhibiteurs potentiels, une molécule efficace *in vivo* a été identifiée. Par ailleurs, le criblage a permis d'observer *in vivo* la fluorescence de vismiones (composés anthracéniques prénylé) extraites de plantes et décrites pour leurs propriétés antipaludiques. Une méthode ingénieuse associant l'imagerie spectrale et l'analyse métabolomique a été développée pour tracer et caractériser le métabolisme associé aux vismiones dans des cellules de plantes.

**Mots clés :** Plantes, protéines prénylées, *in vivo*, métabolisme, microscopie confocale, imagerie spectrale, métabolomique, protéomique, cancer, paludisme

## Abstract

The protein prenylation is a key post-translational modification for the development, signaling and environmental adaptation of eukaryotic cells. Although many active and specific inhibitors of protein prenyltransferases have been isolated, the lack of knowledge on the biological mechanisms controlling protein modification by isoprenic groups makes their use inefficient in the treatment of cancer or malaria. To characterize the modification of prenylated proteins, we used a unique cell model to visualize these changes *in vivo*. In addition, techniques to capture the modified proteins were developed to analyze the mechanisms at the molecular level by using proteomics and metabolomics approaches. In a screening of potential inhibitors, an effective drug *in vivo* was identified. Moreover, the screening allowed to observe in living cells a fluorescence of vismiones (prenylated anthranoids) extracted from plants and described for their antimalarial properties. An ingenious method combining spectral imaging microscopy and metabolomic analysis was developed to track vismiones *in vivo* and to characterize the related metabolism in plant cells.

**Keywords:** Plants, prenylated proteins, *in vivo*, metabolism, confocal microscopy, spectral imaging, metabolomics, proteomics, cancer, malaria